SERI/TP-214-4135 • UC Category: 270 • DE91002149

Annual Report

Photovoltaic Subcontract Program FY 1990

K.A. Summers, Editor

Solar Energy Research Institute
1617 Cole Boulevard
Golden, Colorado 80401-3393
A division of Midwest Research Institute
operated for the U.S. Department of Energy
under contract No. DE-AC02-83CH10093

Prepared under task No. PV040101

March 1991

NOTICE: This report was prepared as an account of work sponsored by an agency of the United States government. Neither the United States government nor any agency thereof, nor any of their employees, makes any warranty, express or implied, or assumes any legal liability or responsibility for the accuracy, completeness, or usefulness of any information, apparatus, product, or process disclosed, or represents that its use would not infringe privately owned rights. Reference herein to any specific commercial product, process, or service by trade name, trademark, manufacturer, or otherwise does not necessarily constitute or imply its endorsement, recommendation, or favoring by the United States government or any agency thereof. The views and opinions of authors expressed herein do not necessarily state or reflect those of the United States government or any agency thereof.

Printed in the United States of America

Available from:
National Technical Information Service
U.S. Department of Commerce
5285 Port Royal Road
Springfield, VA 22161

Price: Microfiche A01, Printed Copy A14

Codes are used for pricing all publications. The code is determined by the number of pages in the publication. Information pertaining to the pricing codes can be found in the current issue of the following publications which are generally available in most libraries: *Energy Research Abstracts (ERA)*; *Government Reports Announcements and Index (GRA and I)*; *Scientific and Technical Abstract Reports (STAR)*; and publication NTIS-PR-360 available from NTIS at the above address.

PREFACE

This report summarizes the progress of the subcontracted photovoltaic (PV) research and development (R&D) performed under the Photovoltaics Program at the Solar Energy Research Institute (SERI). The SERI subcontracted PV research and development represents most of the subcontracted R&D that is funded by the U.S. Department of Energy (DOE) National Photovoltaics Program. The DOE program is managed by the Photovoltaics Division under the Office of Solar Energy Conversion, which is under the Office of Utility Technologies within DOE's Conservation and Renewable Energy organization. This report covers fiscal year (FY) 1990: October 1, 1989, through September 30, 1990. During FY 1990, the SERI PV program started to implement a new DOE subcontract initiative, entitled the "Photovoltaic Manufacturing Technology (PVMaT) Project." Excluding PVMaT because it was in a start-up phase, in FY 1990 there were 54 subcontracts with a total annualized funding of approximately $11.9 million. Approximately two-thirds of those subcontracts were with universities, at a total funding of over $3.3 million. Cost sharing by industry added another $4.3 million to that $11.9 million of SERI PV subcontracted R&D. The six technical sections of this report cover the previously ongoing areas of the subcontracted program: the Amorphous Silicon Research Project, Polycrystalline Thin Films, Crystalline Silicon Materials Research, High-Efficiency Concepts, the New Ideas Program, and the University Participation Program. Technical summaries of each of the subcontracted programs discuss approaches, major accomplishments in FY 1990, and future research directions. Another section introduces the PVMaT project and reports the progress since its inception in FY 1990. Highlights of technology transfer activities are also reported.

Approved for the SOLAR ENERGY RESEARCH INSTITUTE

Thomas Surek, Manager
Photovoltaic Program

Jack L. Stone, Director
Solar Electric Research Division

Notice: This publication was reproduced from camera-ready copy submitted by the individual subcontractors. The efficiency values reported by the subcontractors may not have been independently confirmed by SERI or Sandia.

SUMMARY

The Solar Energy Research Institute's (SERI) subcontracted photovoltaic (PV) research and development (R&D) represents most of the subcontracted R&D funded by the U.S. Department of Energy (DOE) National Photovoltaics Program. That DOE program is managed by DOE in the Photovoltaics Division under the Office of Solar Energy Conversion, which is under the Office of Utility Technologies within DOE's Conservation and Renewable Energy organization. During fiscal year (FY) 1990 (October 1, 1989, through September 30, 1990), the SERI PV program started to implement a new DOE subcontract initiative entitled the "Photovoltaic Manufacturing Technology (PVMaT) Project." Excluding PVMaT because it was in a start-up phase, there were 54 subcontracts in FY 1990 with a total, annualized funding of approximately $11.9 million. Cost sharing by industry added another $4.3 million to that $11.9 million of SERI PV subcontracted R&D.

The SERI PV program subcontracted R&D was conducted in the following, previously ongoing task areas: the Amorphous Silicon Research Project (ASRP), Polycrystalline Thin Films, Crystalline Silicon Materials Research, High-Efficiency Concepts, the New Ideas Program, and the University Participation Program. In the new area of PVMaT, planning was completed and a solicitation was started.

Major program redirections in FY 1990 were continued to have been implemented based on prior competitive solicitations. We initiated all planned FY 1990 subcontract procurements in the ongoing task areas, and we awarded 75% of that planned $11.9 million as of the end of FY 1990. The PVMaT project was another program redirection that DOE funded at an additional amount of $1.7 million and assigned SERI to manage and implement. During FY 1990, PVMaT Phase I solicitations were received, evaluations were performed, and negotiations were begun with awards expected in early FY 1991. Another program redirection included system studies for high-value applications and subcontract partnership arrangements between SERI and utilities/companies.

Amorphous Silicon Research Project (ASRP)

The objectives of research in amorphous silicon are to improve and to understand the optoelectronic properties of amorphous-silicon-based alloy materials and to improve the conversion efficiency and stability of single-junction and multijunction solar cells and submodules. The research is directed toward achieving FY 1990 goals, which are 10% efficiency for single-junction and 13% efficiency for multijunction submodules of 900 cm^2 aperture area.

The technical plan of the ASRP is divided into two principal activities: (1) multidisciplinary research activities and (2) fundamental research activities. Multidisciplinary activities involve government/industry cost-shared programs made up of broad-based research teams, located at individual companies' facilities, performing directed research that covers starting materials to demonstrations of proof-of-concept cells and submodules. The cost-shared multidisciplinary programs address issues concerning single- and multijunction cells and submodules. Fundamental

research activities involve basic, higher-risk, and supporting research at universities and research laboratories that aids industry in advancing the technology base. Research is performed to advance the conversion efficiency and stability of cells and submodules fabricated by plasma-enhanced chemical vapor deposition. Stability issues encompass both intrinsic aspects, such as light-induced effects, and extrinsic aspects, such as diffusion or corrosion, as a result of the environment. Efficiency improvement involves work on better light trapping, higher conductivity of interconnectors, and minimizing area losses due to interconnections.

Polycrystalline Thin Films

The objective of the Polycrystalline Thin Films Program is to develop thin-film, flat-plate modules that meet DOE's long-term goals of reasonable efficiencies (15%-20%), very low cost (near $\$50/m^2$), and long-term reliability (30 years). The approach relies on developing solar cells based on highly light-absorbing, compound semiconductors such as $CuInSe_2$ and CdTe and their alloys. These semiconductors are fabricated as thin films (1-3-μm thick) with minimal material and processing costs.

Polycrystalline devices require continued development to achieve 15%-20% conversion efficiencies. Two strategies are being used: one to develop single-junction cells and another, smaller effort on two-junction cascade cells. Improvement in the single-junction technologies has been steady and reliable. This strategy remains the major focus of the task. Potentially achievable module efficiencies exceed 15% at costs under $\$50/m^2$.

Developing scalable, low-cost fabrication methods is important in providing industry with a foundation for future large-area, high-throughput commercial processes. Within the SERI program, methods for fabricating polycrystalline cells include a selenization method (for $CuInSe_2$), a sputtering method (for CdTe), close-spaced sublimation, evaporation, electrodeposition, sputtering, metal-organic chemical vapor deposition, and spraying.

Crystalline Silicon Materials Research

The emphasis of the SERI Silicon Materials Research Program is to develop a coordinated effort between industry, university, and SERI to study basic mechanisms pertaining to the kinetics of defects and synergistic effects related to defect-impurity interactions. Of particular interest is to identify the effects of post-growth processing on photovoltaic properties of low-cost silicon and methods for passivating electrically active defects in silicon.

Although silicon solar cells fabricated on low-cost substrates have already demonstrated efficiencies exceeding 15%, the technology to commercially produce cells of such high efficiency on low-cost substrates does not exist. Some of the reasons for the lack of such a technology are related to our inadequate understanding of the roles that many defects and impurities play in cell performance. Furthermore, it is not well understood how the characteristics of silicon, containing defects/impurities, change under various thermal processes; this makes it difficult to design cell fabrication processes that can ameliorate the deleterious effects of defects/impurities.

High-Efficiency Concepts

The objective of the High-Efficiency Concepts Task is to evaluate and develop advanced PV technologies capable of energy conversion efficiencies in excess of 20% for flat-plate configurations and 30% for concentrator systems. Because of the demonstrated performance of crystalline III-V semiconductors, the task has become synonymous with III-V compound semiconductor research.

SERI's program of research in High-Efficiency Concepts has approached the terrestrial PV goals from the direction of first demonstrating the feasibility of exceeding these efficiency targets to ensure that production engineering trade-offs between performance and cost can be accommodated. Recent advancements by the community researching high-efficiency technologies provide a high level of confidence that the efficiency goals can readily be met.

Research supported by this program benefits future development efforts by strengthening the understanding of basic mechanisms that affect the uniformity of doping, composition, and thickness over large-area wafers, from wafer to wafer and from run to run. Efficiently utilizing source materials and evaluating potentially superior sources (cost, purity, control, safety, and other factors) are also important topics for research. Continued improvement in cell efficiency is also a critical factor in reaching cost-effectiveness for the technology.

The basic issues that form the focus of research supported under this program have been summarized. Technology for deposition of III-V compound semiconductors by potentially low-cost processes that provide excellent uniformity, purity, and crystallographic quality is clearly the key factor for achieving the near-term PV program goals through the high-efficiency path. Research on characterizing materials and cells, analyzing loss mechanisms in cells, demonstrating improved cell designs, and improving the monitoring, control, and safety of the processes also contribute greatly to the technology base.

New Ideas Program

The objective of the New Ideas Program is to identify new PV materials, device configurations, and concepts, and to conduct preliminary research and development in the areas that show the most promise. Subcontracted New Ideas research that shows significant potential is transferred into the appropriate major task area within the DOE PV program for continued support.

The New Ideas Program provides public solicitations for new and innovative research ideas that are relevant under the PV program guidelines to perform high-risk, long-term, and potentially high-payoff R&D. These solicitations for new and innovative research ideas are submitted by universities, businesses, and non-profit organizations. Subcontracts are awarded to study the most promising concepts associated with these solicitations. These subcontracts are reviewed, and successful concepts are selected for renewal with a second year of funding.

University Participation Program

The objective of this program is to maximize the contribution of universities to the future of PV technology by focusing on the traditional needs and strengths of that community. Thus, it provides a forum in which the university researchers identify research topics critical to advancing the PV technology with minimal influence from the current programmatic interests.

The selected participants are then permitted to pursue the proposed basic and applied research ideas in an environment designed to foster creativity by limiting the requirements for delivering reports and samples, and achieving specific goals. Reporting is limited to annual reports and journal publications. Research symposia organized by the participants are held periodically and are open to all students, program participants, and outside researchers. The intent of the initiative is to provide continuity of funding over a minimum three-year period, which will allow universities to build and support interdisciplinary teams with specialized expertise that can be applied to furthering the technology base of PV. Such a program is expected to attract the most highly qualified university research teams to the national PV program. The University Participation Program also supports the PV industry through technology transfer; this occurs through publishing research results in the technical literature but also through enhanced student awareness of PV technology and educating future professionals.

Technology Transfer

The prompt and effective transfer of research results is a key element of the PV program strategy. Close working relationships are maintained with the academic, university, and electric utility communities, through simple subcontracts and through the unique government/industry partnership approaches, such as in the amorphous silicon and polycrystalline thin films areas. Another primary means of information transfer is through review meetings and subcontractor reports. These reports are made available to the entire PV community, and the review meetings are open to subcontractors as well as all relevant outside interests. Frequent discussions with university and industry researchers and utility planners assisted task managers in assessing future research needs and directions.

During FY 1990, over 450 researchers participated in various review meetings, conferences, and workshops organized or co-organized by the PV program staff. The participants included subcontractors, SERI in-house researchers, invited individuals from outside the program (including the international PV community), and PV program personnel. The meetings held or planned in FY 1990 included: (1) the 21st IEEE Photovoltaic Specialists Conference, (2) the Workshop on Amorphous Silicon-Germanium, (3) the Workshop on Defects in Crystalline Silicon, (4) the 10th Review of the SERI Photovoltaic Project (held in October 1990), (5) the Photovoltaic Module Reliability Workshop (held in October 1990), and (6) the Workshop on Defects, Hydrogen and Metastability in Crystalline and Amorphous Silicon (also held in October 1990). These meetings are selected examples of the extensive SERI cooperation with DOE, other laboratories, the private sector, and international groups to foster enhanced opportunities for further development of PV science and technology. Other significant examples of technology transfer include assisting in developing the Interim Qualification Tests and Procedures

for Thin Film Modules document, collaborating on module materials reliability studies, participating in the Photovoltaics for Utility-Scale Applications (PVUSA) project, and supporting numerous professional societies and meetings. With DOE and Sandia National Laboratories, we also participated in visits to several utilities to discuss their potential interest in PV technology.

The Photovoltaic Manufacturing Technology (PVMaT) Project

The Photovoltaic Manufacturing Technology (PVMaT) Project is being developed as a group of government/industry partnerships between the Federal government (through the U.S. Department of Energy) and U.S. industry. Its planned major impacts over a five-year period are to improve manufacturing processes, accelerate manufacturing cost reductions for PV modules, increase commercial product performance, and generally lay the groundwork for substantial scale-up of U.S.-based manufacturing plant capabilities.

The project goal is to ensure that U.S. industry retains and extends a world leadership role in the manufacture and commercial development of PV components and systems. Most of the R&D will be done by industrial participants that will be selected through competitive procurements and that have strong commitments to improve their manufacturing lines and products, reduce manufacturing costs, and increase their manufacturing capacities.

PVMaT is being implemented in two phases. Phase 1 is a problem identification phase of about three months duration. Subcontracts were being negotiated for Phase 1 as of the end of FY90. Approximately 20 subcontracts of up to $50,000 each will be issued. In this phase SERI is seeking to characterize the status and needs of the U.S. photovoltaic manufacturing industry. Phase 2 is the solution phase expected to be initiated shortly after the Phase 1 subcontracts are underway.

TABLE OF CONTENTS

Page

1.0 Introduction 1

1.1 Background 1
1.2 Key Accomplishments 4
1.2.1 Amorphous Silicon 4
1.2.2 Polycrystalline Thin Films 5
1.2.3 Crystalline Silicon Materials Research 8
1.2.4 High-Efficiency Concepts 8
1.2.5 New Ideas 9
1.2.6 University Participation 10
1.2.7 PV MaT 10
1.3 Technology Transfer 11
1.4 Conclusions 12

2.0 Amorphous Silicon Research Project 13

Research on Stable High-Efficiency Large-Area Amorphous Silicon-Based Submodules; ***Chronar Corporation*** 15

Research on High-Efficiency, Multiple-Gap, Multijunction Amorphous Silicon-Based Alloy Thin Film Solar Cells; ***Energy Conversion Devices, Inc.*** 21

Material Properties of Device Quality Amorphous Silicon Deposited at High Deposition Rates Using Higher Order Silanes; ***Glasstech Solar, Inc.*** 24

Optimization of Transparent and Reflecting Electrodes for Amorphous Silicon Solar Cells; ***Harvard University*** 29

Structural and Electronic Studies of a-SiGe:H Alloys; ***Harvard University*** 32

Photochemical Vapor Deposition of Amorphous Silicon Alloy Materials and Devices; ***Institute of Energy Conversion, University of Delaware*** 36

Amorphous Silicon Deposition Research with In Situ Diagnostics; ***Jet Propulsion Laboratory*** 42

Diagnostics of Glow Discharges Used to Produce Hydrogenated Amorphous Silicon Films; ***National Institute of Standards and Technology*** 48

Research on Amorphous-Silicon-Based Thin Film Devices; ***Solarex Thin Film Division*** 50

TABLE OF CONTENTS (continued)

Page

Studies on the Relative Effects of Charged and Neutral Defects in Hydrogenated Amorphous Silicon; ***University of North Carolina*** 57

Investigations of the Origins of Light-Induced Changes in Hydrogenated Amorphous Silicon; ***University of Oregon*** 61

Structure of Amorphous Silicon Alloy Films; ***Washington University*** 64

Research on the Structural and Electronic Properties of Amorphous Silicon Alloys; ***Xerox PARC*** 70

3.0 Polycrystalline Thin Films 76

Investigations of $CuInSe_2$ Thin Films and Contacts; ***California Institute of Technology*** 78

Role of Polycrystallinity in CdTe and $CuInSe_2$ Photovoltaics; ***Colorado State University*** 88

Development of High-Efficiency CdTe and CdZnTe Solar Cells; ***Georgia Institute of Technology*** 91

Polycrystalline Thin-Film Materials and Devices; ***Institute of Energy Conversion*** 96

High Efficiency Copper Ternary Thin Film Solar Cells; ***International Solar Electric Technology*** 102

High-Efficiency, Large-Area CdTe Panels; ***Photon Energy, Inc.*** 108

Development of Computer Model for Polycrystalline $CuInSe_2$ and CdTe Solar Cells; ***Purdue University*** 113

Novel Thin Film $CuInSe_2$ Fabrication; ***University of Colorado*** 119

Alternative Fabrication Techniques for High-Efficiency $CuInSe_2$ and $CuInSe_2$-Alloy Films and Cells; ***University of Illinois*** 125

Thin Film Cadmium Telluride, Zinc Telluride, and Mercury Zinc Telluride Solar Cells; ***University of South Florida*** 131

Thin Film Cadmium Telluride Photovoltaic Cells and Submodules Fabrication; ***The University of Toledo*** 137

TABLE OF CONTENTS (continued)

Page

4.0 Crystalline Silicon Materials Research 143

Basic Studies of Point Defects and Their Influence on Solar Cell Related Electronic Properties of Crystalline Silicon; ***Duke University*** 144

Impurity and Defect Characterization in Silicon; ***Georgia Institute of Technology*** 150

The Effectiveness and Stability of Impurity/Defect Interaction and Their Impact on Minority Carrier Time; ***North Carolina State University*** 155

Passivation and Gettering Studies in Solar Cell Silicon; ***The University at Albany*** 161

Electrical Characterization Support for a Crystalline Silicon; ***University of Southern California*** 170

5.0 High-Efficiency Concepts 176

Arsine and Hydride Radical Generation for MOCVD Growth; ***Colorado State University*** 177

High-Efficiency, Thin-Film Solar Cells; ***Kopin Corporation*** 180

Basic Studies of II-V High-Efficiency Cell Components; ***Purdue University*** 185

Research on Semiconductors for High-Efficiency Solar Cells; ***Rensselaer Polytechnic Institute*** 191

Low-Cost, High-Efficiency Solar Cells Utilizing GaAs-on Si Technology; ***Spire Corporation*** 197

Advanced High-Efficiency Concentrator Cells; ***Varian Research Center*** 202

6.0 New Ideas Program 206

The Avalanche Heterostructure and Superlattice Solar Cells; ***Georgia Tech Research Institute*** 207

Novel Ways of Depositing ZnTe Films by a Solution Growth Technique; ***Institute of Energy Conversion*** 213

Low-Cost Technique for Producing CdZnTe Devices for Cascade Cell Application; ***International Solar Electric Technology*** 217

TABLE OF CONTENTS (concluded)

Page

Advanced Studies of Solar Photovoltaic/Electrolytic Hydrogen Systems; ***Princeton University*** 223

Hydrogen Radical Enhanced Growth of Solar Cells; ***Rensselaer Polytechnic Institute*** 230

An Inverted AlGaAs/BaAs Patterned Tunnel Junction Cascade Concentrator Solar Cell; ***Research Triangle Institute*** 236

High Efficiency Epitaxial Optical Reflector Solar Cells; ***University of Southern California*** 242

7.0 University Participation Program 247

Improvement of Bulk and Epitaxial III-V Semiconductors for Solar Cells by Creation by Creation of Denuded Recombination Zones; ***Carnegie-Mellon University*** 248

New Approaches for High-Efficiency Solar Cells: Role of Strained Layer Superlattices; ***North Carolina State University*** 253

Fundamental Studies of Defect Generation in Amorphous Silicon Alloys Grown by Remote Plasma-Enhanced Chemical-Vapor Deposition (Remote PECVD); ***North Carolina State University*** 259

Photon and Ion Assisted Doping and Growth of II-VI Compound Thin Films; ***Stanford University*** 265

Defects and Photocarrier Processes in Hydrogenated Amorphous Silicon Alloys; ***Syracuse University*** 270

Atomic Layer Epitaxy for High Efficiency Solar Cells; ***University of Southern California*** 276

Electronic Processes in Thin Film PV Materials; ***University of Utah*** 279

8.0 The Photovoltaic Manufacturing Technology (PVMaT) Project 285

9.0 List of Active Subcontracts 290

10.0 Photovoltaic Program Branch FY 1990 Bibliography 296

Subcontractor Reports and Publications 296

Photovoltaic Program Branch Reports and Publications 301

1.0 INTRODUCTION

This report reviews subcontracted research and development activities under the SERI Photovoltaic Program from October 1, 1989, to September 30, 1990.

1.1 Background

Under the U.S. Department of Energy (DOE) National Photovoltaics (PV) Program, the SERI Photovoltaic Program sponsors high-risk, potentially high-payoff research and development (R&D), manufacturing development, and systems and marketing development in photovoltaic energy technology. The program also provides services to industry and electric utilities or other users, and it leads the National Photovoltaics Program for DOE. DOE's aim is to provide a technology base from which the private sector can choose options for further development and competitive application in U.S. electrical markets. The SERI PV program is responsible for most of the R&D, manufacturing technology development, and some of the systems and market development task areas under the national PV program. The implementation of these programs is based on cooperative research partnerships among the federal government, private industries, universities, and electric utilities, as outlined in the DOE draft "Photovoltaics Program Plan (Fiscal Year 1991 - 1995)."

SERI's specific PV activities include managing subcontracted R&D projects as well as internal research. The primary research activities are conducted in advanced photovoltaic material technologies, including amorphous silicon thin-film materials; polycrystalline thin films, such as copper indium diselenide, cadmium telluride, and their alloys; and high-efficiency crystalline cells, including silicon and gallium arsenide and their alloys. The PV Manufacturing Technology (PVMaT) Project is a new subcontracted activity, separate from the above research activities. PVMaT focuses on improving manufacturing processes and products, accelerating manufacturing cost reduction, and laying the foundation for increased production capacity. Transferring the R&D results to private industry in a timely and effective manner is a major objective of SERI's PV program.

Subcontracted R&D is a significant part of the PV program; more than 50% of the project's budget is allocated yearly to subcontracts. Excluding PVMaT, which was just being initiated in FY 1990, the program managed 54 subcontracts with a total annualized funding of approximately $11.9 million. Approximately two-thirds of those subcontracts were with universities, with a total funding of over $3.3 million. Cost-sharing by industry added over $4.3 million to that $11.9 million of SERI subcontracted PV research and development. In addition to the advanced materials technologies listed above, subcontracted research is conducted under both the New Ideas for PV Conversion and the University Participation programs. Table 1-1 shows how the subcontract budget is distributed among the various task areas for FY 1990 and prior years. Figure 1-1 shows the distribution of subcontract funds by business category. Table 1-2 shows the SERI contacts for the PV subcontracts.

This report summarizes the R&D activities of the subcontracted portion of the SERI PV program. The research is described under the following headings: Amorphous Silicon Research Project (Section 2.0), Polycrystalline Thin Films (Section 3.0), Crystalline Silicon Materials Research (Section 4.0), High-Efficiency Concepts (Section 5.0), New Ideas Program (Section 6.0), University Participation Program (Section 7.0), and the PV Manufacturing Technology Project

(Section 8.0). The reports in each section are preceded by a brief overview of the task objectives and approaches, as well as some of the key developments of FY 1990. The overviews are followed by technical summaries of each of the subcontractors' activities in FY 1990. These sections were provided by the subcontractors themselves or were derived from various project reports submitted by the subcontractors. Section 9.0 provides a list of active subcontracts in FY 1990, and Section 10.0 provides a list of major subcontractor reports.

Table 1-1. Subcontract Budget History of the SERI Photovoltaic Program[a]

	Fiscal Year			
Task Area	**1978-1987 ($M)**	**1988 ($M)**	**1989 ($M)**	**1990 ($M)**
Research and Development				
Amorphous Silicon Thin Films	52.5	6.7	7.7	6.0
Polycrystalline Thin Films	34.9	2.2	3.7	4.6
High-Efficiency Concepts	27.6	3.0	2.0	1.9
Crystalline Silicon	21.5	0.6	0.6	0.5
New Ideas	17.5[b]	0.1	0.4	0.4
University Participation	3.5	1.3	0.9	0.4
Subtotal	157.5	13.9	15.3	13.8
Manufacturing Technology Development				
PV Manufacturing Technology Project[c]	N/A	N/A	N/A	1.7
Total	**157.5**	**13.9**	**15.3**	**15.5**

[a]Includes approximately 15% for program management, fees, etc.
[b]Includes $9 million for photoelectrochemical cell research.
[c]Initiated in FY 1990 (awards planned for early FY 1991).

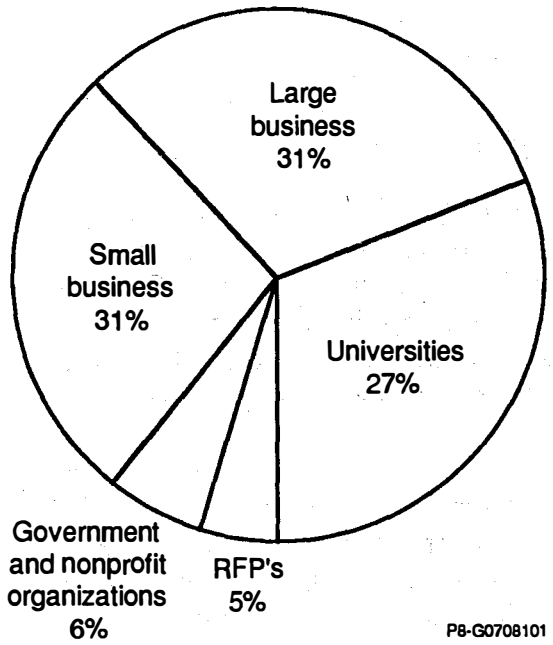

Figure 1-1. Business category distribution of FY 1990 research and development subcontract funds.

Table 1-2. SERI Photovoltaic Program Subcontract Personnel

Task Area	Contact Name	Telephone[a]
PV Program	Thomas Surek, Manager	231-1371
	Kathy Summers, Admin. Assist.	231-1395
	Thomas S. Basso	231-7035
	William Wallace	(202) 586-7326
Amorphous Silicon Research Project	Werner Luft, Manager	231-1823
	Byron Stafford	231-7126
	Bolko von Roedern	231-1380
High-Efficiency Concepts, Crystalline Silicon Materials, and University Program	John Benner, Manager	231-1396
	Bhushan Sopori	231-1383
	Cecile Leboeuf	231-1066
Polycrystalline Thin Films	Kenneth Zweibel, Manager	231-7141
	Richard Mitchell	231-1379
	Harin Ullal	231-1841
New Ideas Program	Richard Mitchell, Manager[b]	231-1379
PV Manufacturing Technology	Ed Witt, Manager	231-1402

[a]Area code (303), FTS number 327-xxxx.
[b]FY 1991 contact is Thomas S. Basso.

1.2 Key Accomplishments

1.2.1 Amorphous Silicon Research Project

Four companies were awarded contracts in 1987 under the second government/industry 50% cost-shared partnership for amorphous silicon research: ARCO Solar; Chronar Corporation; Energy Conversion Devices, Inc.; and Solarex Corporation. The primary goal of this three-year, nearly $36 million program (cost shared 50% by the industrial partners) is to achieve efficiencies of 10% for single-junction and 13% for multijunction submodules with aperture areas of about 900 cm^2. The key accomplishments during the third year of that joint program are described hereafter.

Upon completion of the current three-year program (in the FY 1990 timeframe), research priorities will be devoted to all-amorphous-silicon alloy, two-terminal multijunction cells and modules. For that purpose, a new three-year Government/Industry Partnership Program was started in the February-March (1990) timeframe with funding from the FY 1990 budget. The principal objectives of this research are to (1) conduct research on semiconductor materials and non-semiconductor materials to enhance two-terminal, multijunction, thin-film, large-area, all-amorphous-silicon-alloy device performance; (2) develop high-efficiency, *stable, reproducible*, and *low-cost* multijunction PV modules (of at least 900 cm^2 in area) based on all-amorphous materials; (3) demonstrate in FY 1993 a stable 12% [air mass (AM) 1.5] aperture-area solar conversion efficiency for different-band-gap modules; and (4) demonstrate in FY 1993 a stable 10% (AM 1.5) aperture-area solar conversion efficiency for same-band-gap modules.

- ARCO Solar achieved aperture-area efficiencies of 9.4% for amorphous silicon modules with white back reflectors and an area of 844 cm^2, and they reported 8.4% for an area of 3,970 cm^2. For semitransparent amorphous silicon modules without the current gain from the back-reflected light, the corresponding efficiencies are 9.7% and 7.6%, respectively. Stand-alone $CuInSe_2$ modules were reported to have 11.2% and 9.7% efficiency over areas of 938 cm^2 and 3,970 cm^2 , respectively. Preliminary demonstrations of 1 x 4 ft, four-terminal tandem modules with an air gap separating the two module circuits gave a 10.5% aperture-area efficiency. Chronar has fabricated 1.1-m^2 single-junction amorphous silicon modules with 4.4% efficiency verified by SERI.

- In addition to the government/industry program, progress has been made in the fundamental research on amorphous silicon. Glasstech Solar, Inc., has produced single-junction, 1-cm^2 cells of 9.7% efficiency, in which the intrinsic layer was deposited at a rate of 2 nm/s from disilane. Solarex has fabricated single-junction and triple-junction submodules with aperture-area (>900 cm^2) efficiencies of 9.7% and 9.3%, respectively.

- A. Gallagher of the National Institute for Standards and Technology has found the surface reaction probability in silane, disilane, and silane/germanium discharge deposition to be in the range of 0.3 to 0.4. These results have led to the recognition that the key film-quality growth characteristic is the surface diffusion of radicals before incorporation in the film, combined with preferential incorporation in atomic-scale valleys.

- The Jet Propulsion Laboratory has deposited a-C:H and a-SiC:H films by electron cyclotron resonance microwave plasma chemical vapor deposition. The electron cyclotron resonance (ECR)-deposited a-SiC:H films have a slightly higher optical band gap than RF-deposited films. The deposition rate as a function of hydrogen dilution demonstrates that hydrogen etching plays an important role in a-SiC:H film deposition by ECR chemical vapor deposition (CVD).

- R. Gordon of Harvard University has developed fluorine-doped zinc oxide produced by atmospheric pressure CVD. The highest electrical conductivity (1200 S/cm) and light transmission were found for films containing 0.5 atomic percent fluorine deposited at 450°C.

- D. Cohen of the University of Oregon unambiguously confirmed that there is a significant deleterious role of carbon impurities in amorphous silicon films. Samples were prepared with a modulated carbon profile and were then characterized by drive-level capacitance profiling in the annealed and light-soaked states.

- Excellent agreement has been obtained on multijunction cell efficiency measurements between SERI, Energy Conversion Devices, and Solarex. While the measurement techniques and equipment may vary, agreement within 3% has been achieved on the same multijunction cells measured at the three different locations.

- Extensive studies of amorphous germanium films deposited by plasma-enhanced CVD at Harvard University have confirmed that the optoelectronic properties are poor. It appears the preparation conditions need to be adjusted to enhance surface bombardment during deposition.

- Xerox Corporation developed a chemical equilibrium model for plasma-enhanced CVD of amorphous silicon films. Studies from the incorporation of arsenic and phosphorus impurities indicate that chemical reactions at the growth surface, rather than kinetic reactions in the plasma, determine the impurity incorporation.

- Xerox demonstrated that the rate of defect creation is dependent on the thermal history of the amorphous silicon film and cannot be the direct result of the specific hydrogen bonding structure (e.g., dihydride).

- The Institute of Energy Conversion at the University of Delaware demonstrated a band-gap-graded device with 40% quantum efficiency at 800 nm using a "front loaded" SiGe alloy 40 nm thick. A device model incorporating spatially dependent mobilities was developed to analyze the performance of band-gap-graded devices.

1.2.2 Polycrystalline Thin Films

Significant progress has been made in FY 1990 in the subcontracted research of polycrystalline thin films. The key accomplishments in both CdTe and $CuInSe_2$ solar cells and modules are listed below.

- Awards from the Polycrystalline Thin Film Module Development RFP (19019) were partially completed during FY 1990. Three-year awards to Photon Energy, ISET, Solarex, and the University of Toledo have been signed. Two others are in final negotiations.

- Siemens Solar reported achieving a power output of 37.8 W from an unlaminated 4-ft^2 $CuInSe_2$ module. The power of 37.8 W corresponds to a reported aperture-area efficiency of approximately 9.7%. This is the highest efficiency for any thin film of this size. SERI has continued outdoor stability tests of Siemens' CIS modules. The results of the tests were continued stability, with final efficiencies at the end of almost two years being within 5% of their initial values.

- Photon Energy has completed their final report on a three-year subcontracted effort on high-efficiency, large-area CdTe and CdHgTe panels. The research effort described in this report covers the developments and achievements of Photon Energy CdTe technology. This includes fabrication of an over 7.3% aperture-area efficient module (929 cm^2), the proof-of-feasibility of producing a 4 ft^2 CdS/CdTe module, and the achievement of 12.3% small-area cell efficiencies. As a result of the recent competitive solicitation in Polycrytalline Thin Films, Photon Energy is continuing their efforts in this area under their new three-year subcontract entitled "Module Process Optimization and Device Efficiency Improvement for Stable, Low-Cost, Large-Area CdTe-Based Photovoltaic Module Production."

- We have met an internal AOP milestone in polycrystalline thin films. The milestone ("demonstrate less than 5% degradation of CdTe after 4 months outdoors" - September 1990) was met by test devices from Photon Energy. Two of three such devices have been tested outdoors at SERI for over 6 months without measurable degradation. As a follow up, Photon Energy has delivered six 1-ft^2 CdTe modules to SERI for a second round of outdoor tests.

- The Environmental Protection Agency (EPA) recently revised its test for hazardous materials, adopting a Toxicity Characteristics Leading Procedure (TCLP). The test replaces the EP Toxicity Test. Michael King of ASARCO has now tested Siemens Solar Industries CIS Modules using the TCLP. As with the previous EP toxicity test, the CIS modules passed the new TCLP. Measured quantities and limits (in parenthesis follow: Se: under 0.1 (1.0); Cd: 0.15 (1.0); Pb 3.8 (5). Note that both selenium and cadmium were well under the limit. Only lead was near the limit, because of lead solder.

- The Polycrystalline Thin Film task completed (ahead of schedule) an FY90 AOP Control Milestone to publish a report on cadmium safety issues. The joint SERI/Brookhaven National Labs report "Health, Safety, and Environmental Issues Relating to Cadmium Usage in PV Energy Systems," (Moskowitz, Zweibel, Fthenakis) explores the manufacturing, use, and disposal issues associated with cadmium. The report concludes that ongoing attention to the management and amelioration of Cd-related issues is needed and would provide a good basis on which to continue the successful development of CdTe PV modules. As a follow-up to the report, we plan a discussion with ASARCO, a cadmium producer, on the feasibility of recycling "spent" CdTe modules. It appears that no technological barriers exist to such a strategy.

- Efforts to understand contact degradation issues for CdTe devices continued to suggest that the p-CdTe/p-ZnTe/metal contact achieves both high performance and excellent stability. Ametek developed several encapsulation schemes for their 3" x 6" thin film CdS/CdTe/ZnTe submodules. Preliminary tests were encouraging. In one particular test, the CdTe submodule while immersed under water, was illuminated with approximately 100 mW/cm^2 intensity. No change in electrical performance was observed. Typically, CdTe modules are sensitive to the presence of moisture, as is the case with most thin film modules. The Institute of Energy Conversion at the University of Delaware reported fabricating thin film CdTe devices with efficiency over 11%. One such device had a V_{oc} of 805 mV. IEC is also doing stability testing of these devices. Their data suggests that cells with the ZnTe/metal contacts demonstrate the most stable device performance, thus confirming earlier reported results of Ametek. Au contacts, on the other hand, have demonstrated contact problems presumably because of Au diffusion, resulting in lower V_{oc} and FF. The ZnTe/metal contact appears to be a viable solution to the contact stability problem for thin film CdTe devices and major contribution of the previously supported R&D program at Ametek.

- Ametek submitted their draft final report entitled, "Polycrystalline Thin Film n-i-p Solar Cells" under subcontract #ZL-7-06031-2. The major accomplishments under this subcontract were the following: 1) developed and improved a unique n-i-p cell design that has resulted in a SERI verified, total-area, single-junction, AM1.5 global efficiency of 11.2% for 1.07 cm^2 device (the efficiency was about 9% at the start of the subcontract); 2) developed capabilities to dip-coat "thin CdS" up to areas of 6" x 6" and 1 ft^2 , 3) demonstrated reported stability of submodules (100 cm^2) for over 5000 hours of indoor testing; 4) developed simplified module processing techniques; 5) addressed issues of environment, health, and safety for Cd-based manufacturing; and 6) developed cost-estimates for manufacturing capacity of 500 KW ($2.88/W), 10 MW ($0.64/W), 50 MW ($0.36/W) based on realistic module power output of 8 W/ft^2. Furthermore, in their analysis projected efficiency of 17%-18% are possible in 3-5 years based on refining existing cell design. This is consistent with the analysis of Jim Sites of CSU. Also, Ametek has had several collaborative research efforts with the following groups: BNL, CSU, IEC, GIT, JPL, USF, and SERI. Many of the groups have achieved near 10% efficiency for polycrystalline thin film CdTe solar cells fabricated by various methods, because of the close interaction with Ametek (e.g. IEC (PVD), GIT (MBE, MOCVD), JPL (MOCVD)).

- The Institute of Energy Conversion (IEC), at the University of Delaware, investigated novel methods for depositing thin ZnTe films using solution growth techniques. Using a room temperature aqueous solution, IEC has successfully deposited ZnTe films on 7059-glass/ITO/CdS/CdTe substrates. These films were grown using a cathodic process, a Zn electrode (connected to the CdTe sample without an external voltage source) in a solution of $ZnCl_2$, TeO_2, and NaOH. Additional efforts by IEC in the solution growth area have also resulted in depositing a thin film of ZnSe on a $CuInSe_2$ substrate. The aqueous solution involved in this growth process was $ZnCl_2$, NH_3, N_2H_4, and Na_2SeSO_3. To date, these latter devices have shown a low V_{oc}(0.25 volts). So far, this is believed to result from discontinuities in the ZnSe film layer. Current efforts at IEC are under way to investigate both the Cu doping of the ZnTe films deposited by solution growth and increasing the thickness of the solution grown ZnSe layers.

- SERI has verified a total-area, single-junction, AM1.5 global efficiency of 11.1% for 4 cm^2 thin-film $CuGaInSe_2$ solar cells fabricated by Boeing. The cell parameters are J_{sc} = 31.13 mA/cm^2, V_{oc} = 0.5419, and FF = 0.659. The Ga content in the film is 26% (In:Ga, 74:26). The cell structure is ZnO/thin CdZnS/$CuGaInSe_2$/Mo/Alumina. The ZnO and the "thin CdZnS" was deposited by sputtering and dip-coating, respectively. This is the highest efficiency achieved for a 4-cm^2 device with 25% Ga content in the CIS.

1.2.3 Crystalline Silicon Materials Research

SERI has actively worked with subcontractors in several research areas and facilitated interactions among subcontracts as well as with the industry. Development of a basic facility for optical processing and availability of SERI expertise for hydrogenation have led to formation of a nucleus for a collaborative program.

Major accomplishments of this program are:

- A method, based on optical processing, has been developed to produce texturing on the back-side of a solar cell. This "dry texturing" technique works on all crystal orientations.

- Formation of hydrogen damage and the associated defect structure has been identified. A back-side hydrogenation technique has been developed for defect passivation of solar cells.

- Efficiency of dislocations as sinks for point defects has been determined for commercial low-cost silicon.

- Diffusion of hydrogen in silicon has been modelled using experimental data.

- Influence of dissolved oxygen on minority carrier lifetime in silicon was studied.

- A technique for fabrication of optically reflecting low-resistivity ohmic contacts on silicon has been developed.

1.2.4 High-Efficiency Concepts

Seven new subcontracts were awarded during FY1990 as a result of this solicitation. These include:

- Colorado State University; Professor G. Collins will investigate plasma deposition of GaAs and in situ generation of arsine for improved safety and reduced growth temperatures.

- Purdue University; Professors M. Lundstrom and M. Melloch continue analysis, design and preparation of high-efficiency GaAs solar cells with new emphasis on thin-cell designs employing optical confinement and high-efficiency designs tolerant of lower quality materials properties.

- Research Triangle Institute; Dr. M. Timmons will initiate the study of the GaInAsP quaternary system for GaAs-lattice matched, high-bandgap cells in tandem structures.

- University of Southern California; Prof. P. D. Dapkus will investigate atomic layer epitaxy for large-area, lower temperature solar growth. Large-area-uniformity is expected to be enhanced due to surface kinetic control of growth in the Atomic Layer Epitaxy (ALE) regime.

- Kopin Corporation; Dr. R. Gale will apply Kopin's unique CLEFT process for preparation of thin, crystalline GaAs films for evaluation of potential efficiency improvements resulting from optical confinement in thin-cell structures. Related materials research will investigate lateral epitaxial overgrowth using chlorinated metalorganic sources.

- Spire Corporation; S. Vernon will evaluate the potential improvement in film quality resulting from use of atomic layer epitaxy for nucleation of GaAs films on silicon substrates. New cell structures specifically designed for the materials properties encountered in the GaAs/Si system will be developed and tested.

- Rensselaer Polytechnic Institute; Professors S. Ghandhi and J. Borrego will design and analyze gas flow regimes and reaction chemistry for new chemical vapor deposition technology.

1.2.5 New Ideas Program

The following is a list of key accomplishments in the New Ideas Program in FY 1990.

- Work was concluded on these three concepts: the avalanche heterostructure and superlattice solar cell developed by Georgia Tech Research Institute; the low-cost techniques for producing CdZnTe devices for cascade cell applications, researched by International Solar Electric Technology; and hydrogen radical enhanced growth of solar cells, at Rensselaer Polytechnic Institute.

- Three new subcontract awards were initiated: novel ways of depositing ZnTe films by solution, researched by the Institute of Energy Conversion (IEC) at the University of Maryland; development of an inverted AlGaAs/GaAs patterned tunnel junction cascade concentrator cell, at the Research Triangle Institute (RTI), and; development of high efficiency epitaxial optical reflector cells, at the University of Southern California (USC). These awards were based on the FY 1988 solicitation for New Ideas for Photovoltaic Conversion.

- Scientists at the RTI have reported they fabricated planar GaAs tunnel junctions, using atmospheric pressure organo-metallic vapor phase epitaxy, that are comparable in resistivity (~3.3 x 10^{-3} ohm-cm^2) to the lowest reported resistivity (~3.0 x 10^{-3} ohm-cm^2) tunnel junctions for GaAs produced by molecular beam epitaxy. This was achieved by lowering the growth temperature to 650°C, with their "cycled" growth for the p++ GaAs. Their tunnel junction should be suitable for 400-sun AM1.5 operation of an AlGaAs/GaAs cascade.

- Researchers at USC, in collaboration with Varian Associates researchers, developed the computer models for USC's "epitaxial optical reflector" (EOR) solar cell. Designs based on the models show EOR cells will have higher efficiency (up to 31.5%) than conventional cells over an order of magnitude in doping. The preferred EOR cell design requires the growth of as many as 100 layers with precisely controlled layer-thickness. Growth of reproducible Bragg reflectors was achieved, and this technique is being applied to grow cell structures.

1.2.6 University Participation Program

- Professors S. Bedair and N. El-Masry provided a major contribution to the understanding of ordering in $Ga_{0.5}In_{0.5}P$ crystals by growing samples using atomic layer epitaxy. Spontaneous ordering has been observed using MOCVD growth of this alloy. ALE, with its self-limiting monolayer growth, was expected to enhance the ordering processes. Electron diffraction patterns indicated that the theoretically predicted CuPt type ordering was occurring. Photoreflectance measurements gave a room temperature bandgap of 1.77eV, far lower than the 1.9 eV predicted for the metastable alloy.

- Professor G. Lucovsky's studies in remote plasma enhanced chemical vapor deposition of micro crystalline silicon made a break-through in the deposition of low-conductivity, $6x10^{-8}$ S/cm, lightly boron-doped, near-"intrinsic" material. These samples display photoconductivity comparable to device grade a-Si:H and show no Staebler-Wronski effect in initial measurements under $50mW/cm^2$ for up to 10 hours.

1.2.7 PV Manufacturing Technology (PVMaT) Project

The Photovoltaic Manufacturing Technology (PVMaT) Project is being developed as a group of government/industry partnerships between the Federal government (through the U.S. Department of Energy) and U.S. industry. Its planned major impacts over a five-year period are to improve manufacturing processes, accelerate manufacturing cost reductions for PV modules, increase commercial product performance, and generally lay the groundwork for substantial scale-up of U.S.-based manufacturing plant capabilities.

The project goal is to ensure that U.S. industry retains and extends a world leadership role in the manufacture and commercial development of PV components and systems. Most of the R&D will be done by industrial participants that will be selected through competitive procurements and that have strong commitments to improve their manufacturing lines and products, reduce manufacturing costs, and increase their manufacturing capacities.

PVMaT is being implemented in two phases. Phase 1 is a problem identification phase of about three months duration. Subcontracts were being negotiated for Phase 1 as of the end of FY90. Approximately 20 subcontracts of up to $50,000 each will be issued. In this phase SERI is seeking to characterize the status and needs of the U.S. photovoltaic manufacturing industry. Phase 2 is the solution phase expected to be initiated shortly after the Phase 1 subcontracts are underway.

1.3 Technology Transfer

The prompt and effective transfer of research results is a key element of the PV Project strategy. Close working relationships are maintained with the academic, university, and electric utility communities, through simple subcontracts and through the unique government/industry partnership approaches, such as in the amorphous silicon, and in the polycrystalline thin films areas. Another primary means of information transfer is through subcontractor reports and review meetings. These reports are made available to the entire PV community, and the review meetings are open to all relevant outside interests as well as to subcontractors. During FY 1990, over 22 subcontractor reports were widely distributed. Frequent discussions with university and industry researchers and utility planners assisted task managers in assessing future research needs and directions. SERI subcontract managers made nearly 35 site visits to subcontractor facilities in FY 1990 to review research progress.

The following is a list of some key FY 1990 accomplishments in the area of technology transfer.

- The results of the DOE Office of Energy Research (OER), Office of Program Analysis review of the National PV Program ranked the PV program as among the best programs assessed by OER. The OER comments were evaluated and used to develop the FY 1990 and FY 1991 PV Program plans. SERI subcontractors were responsible for 49 of the total 129 presentations given to 17 panels of OER expert reviewers. The OER review was conducted during August to December, 1989.

- Over 450 researchers participated in various conferences, meetings, or workshops held or planned in FY 1990 that were organized or co-organized by the PV Program. That included: the 21st IEEE PV Specialists Conference, the Workshop on Amorphous Silicon-germanium, the Workshop on Defects in Crystalline Silicon, the 10th Review of the PV AR&D Project (held October 1990), the PV Module Reliability Workshop (held October 1990), the Workshop on Defects, Hydrogen and Metastability in Crystalline and Amorphous Silicon (held October 1990). Other activities that SERI subcontracted researchers participated in included: developing the Interim Qualification Tests and Procedures for Thin Film Modules document, collaborating on module materials reliability studies, the PVUSA project. These meetings and activities are selected examples of the extensive SERI cooperation with DOE, other laboratories, the private sector, and international groups, to foster enhanced opportunities for further development of PV science and technology. Other significant examples include participating in (FY89 -- Sandia's Crystalline PV Technology Review, hosting the Interagency Power Group) Meeting, and supporting numerous professional societies and meetings.

- The Solar Energy Research and Education Foundation (SEREF) subcontract supported DOE in the GM Sunrayce USA competition, the first major PV car race in the U.S. The event stressed energy, education, and the environment, was competitively open to all university teams, and was cosponsored by General Motors Corporation (GM), the Chevrolet Division, the Society for Automotive Engineers, and DOE. SEREF provided photovoltaic and renewable energy education information to news media and educators along the race route from Kissimmee, Florida to Warren, Michigan. The top three finishers of the race were sponsored by GM to participate in the "World Solar Challenge" (PV solar car race), held in

Australia in November, 1990. SERI also supported this race in material, measurements and time.

1.4 Conclusions

More than 50% of SERI's PV Program involves subcontracted research and development with industry, universities, and nonprofit laboratories. Significant technical advances were made in all areas of the subcontracted PV program during FY 1990. Research progress was assessed through site visits, task review meetings, and topical workshops. That research progress is expected to continue during FY 1991 while expanding in the areas of manufacturing development, and systems and marketing development, to help achieve the long-term goals of the U.S. DOE National PV Program.

2.0 AMORPHOUS SILICON RESEARCH PROJECT

Werner Luft (Manager), Byron Stafford, and Bolko von Roedern

The objectives of this research in amorphous silicon are to improve and understand the optoelectronic properties of amorphous-silicon based alloy materials, and to improve the conversion efficiency and stability of single-junction and multijunction solar cells and submodules. The research is directed toward the achievement of goals in DOE's Five Year Research Plan which are 10% efficiency (900 cm^2) for single-junction submodules, and 13% efficiency (900 cm^2 aperature area) for multijunction submodules. A transition in research emphasis is occuring from single-junction cell and submodule research to multijunction module research.

The technical plan of the Amorphous Silicon Research Project (ASRP) is divided into two principal activities - (1) multidisciplinary activities, and (2) fundamental research activities. The multidisciplinary activities involve government/industry cost-shared programs composed of broad-based research teams located at the facilities of the individual companies. These teams perform directed research that covers aspects from starting materials to development of modules. Fundamental research, on the other hand, involves basic, higher-risk, and supporting research as done by academia and research laboratories to aid the industry groups' advance of the technology base. The cost-shared multidisciplinary programs address issues related to all aspects of 2-terminal multijunction cells and modules using same-bandgap or different-bandgap device structures. Research is performed to advance the conversion efficiency and the stability of both small-area multijunction cells and of multijunction modules having areas of about 900 cm^2 and greater using glow discharge deposition as the primary method of fabricating the amorphous silicon films. The stability of these devices is examined for fundamental changes in the bulk material properties, for temperature effects such as diffusion, for fabrication and area-related defects (interfaces), and for extrinsic degradation related to module encapsulation and framing issues. The transparent conductor was studied to improve the electrical conductivity while achieving optical transmissions greater than 85%. The quality and controlled texturing of ZnO transparent conductors based on low-cost processes is emphasized. The opto-electronic properties of a-SiGe:H and a-SiC:H alloy materials is investigated to determine the limits of these materials with regard to their use in practical multijunction devices. The a-SiGe:H material is constantly being improved. Now, good 1.40 eV material is being produced and the research for FY 1990 did continue to improve material of less than 1.40 eV bandgap. Improved open-circuit voltage was addressed by the development of high conductivity, highly transparent, microcrystalline p^+ and n^+ layers. The interconnection of cells in a series-connected module configuration was a major issue to be studied since it impacts conversion efficiency through the inactive area losses, influences stability through changes over time in the contact resistance, and influences cost through its impact on yield and the number and type of processing steps. Research was continued to reduce the patterning process from three to two steps.

The a-Si:H technology is moving toward modules and system development. Issues relating to module reliability and system development which are now being confronted by the module manufacturers will be addressed in the future. The government's role in these two areas will be

limited in scope and will be guided by the overall ASRP program objective of aiding U.S. industry in choosing the most effective route to cost competitiveness by helping industry advance the a-Si:H R&D base. In the module reliability area (module reliability excludes studies of light-induced stability), the environmental effects on module performance will be studied with direct interaction with the module development programs of U.S. industry. With respect to systems containing a-Si:H technology, a few small systems will be built for the purpose of getting hands-on experience and thus maintaining technology expertise. This will enable the government to be better capable of gathering, cataloging, and assessing data for future system technology transfer from systems being built under the DOE supported PV USA project and also from systems operating under privately-funded efforts. In both areas, these support research activities will be carried out under the guidance of the Amorphous Silicon Research Project.

The second 3-year Government/Industry Partnership Program was completed. The Government/Industry Program has been highly successful and significant advances have been made in cell/submodule performance. At the end of the current Government/Industry Program, different-bandgap multijunction cell and submodule efficiencies were 13% (active area) and 9.3% (aperature area), respectively. In addition, 9.8% efficient single-junction submodules were demonstrated. Research priorities will now be devoted to all-amorphous silicon, two-terminal multijunction modules.

A new 3-year Government/Industry Partnership Program was started in May 1990 with funding from the FY 1990 budget. The principal objectives of this research are: i) to conduct research on semiconductor materials and non-semiconductor materials to enhance two-terminal, multijunction, thin-film, large-area, all-amorphous-silicon-alloy device performance, ii) to develop high-efficiency, *stable, reproducible*, and *low-cost* multijunction photovoltaic modules based on all-amorphous materials, iii) to demonstrate in FY 1993 stable 12% (AM 1.5) aperture area solar conversion efficiency for different-bandgap modules, and iv) to demonstrate in FY 1993 stable 10% (AM 1.5) aperture area solar conversion efficiency for same-bandgap modules. The modules will be at least 900 cm^2 in area and consist of at least two integrally stacked devices using all-amorphous-silicon alloy materials.

In the fundamental research activity, the following general areas were addressed in support of the multidisciplinary activities - light-induced stability, alternative material deposition approaches, amorphous silicon alloy materials, material deposition rate, and plasma and material characterization. Summaries of these studies follow.

Title: **Research on Stable, High Efficiency, Large Area, Amorphous Silicon Based Submodules**

Organization: Chronar Corporation, Princeton, NJ 08542

Contributors: J. Macneil, program manager; A.E. Delahoy, and T. Tonon, principal investigators; J.A. Cambridge, F.B. Ellis, Jr., M. Ghosh, C. Huang, F.J. Kampas, C. Kothandaraman, X. Li, R. Liu, T. Liu, W. Stroud, J. Xi.

Objectives

The primary objective of this subcontract is to develop the technology for same bandgap, amorphous silicon tandem junction photovoltaic modules having an area of at least 900 cm^2 with the goal of achieving an aperture area efficiency of 9%. A further objective is to demonstrate modules that retain 95% of their power output under standard light soaking conditions.

Approach

Chronar's approach to the attainment of these objectives is based on the following distinctive technologies; a) in-house deposition of SiO_2/SnO_2:F onto soda lime glass by APCVD to provide a textured, transparent electrode, b) single chamber r.f. glow discharge deposition of the a-Si:H layers onto vertical substrates contained with high packing density in a "box carrier" to which the discharge is confined, c) sputter deposition of highly reflecting, ZnO-based back contacts, and d) laser scribing of the a-Si:H and electrodes with real-time scribe tracking to minimize area loss.

Results

Continued development of single junction amorphous silicon was aggressively pursued as a proving ground for various optical enhancement schemes, new p-layers, and i-layer quality. The culmination of this effort was the measurement of a 1.05 cm^2 p-i-n cell at 11.3% efficiency. The I-V curve and structure of this cell are shown in Figure 1. The high short circuit current density (18 mA/cm^2) results from the use of an MgF_2 AR coating, a low-absorption p-layer, and a highly reflective back contact consisting of ZnO backed with Ag. The excellent fill factor for this 1 cm^2 cell (72%) is testimony to the high quality and good transport properties of the i-layer. The cell was isolated from a 1 ft^2 substrate coated in an a-Si:H deposition system capable of simultaneous deposition on 4 1 ft^2 substrates. Diborane was used as the p-layer dopant gas.

In a smaller research system, the development of high efficiency p-i-n cells has been undertaken using trimethylboron (TMB) as the p-layer dopant gas. Figure 2 shows the relationship between conductivity and Tauc gap for a-$Si_{1-x}C_x$:H p-layers using B_2H_6 and TMB as dopant. It can be seen that in the neighborhood of 2 eV bandgap, higher

conductivities have been achieved using TMB. Using a cell structure identical to that in Figure 1, but with no transitional i-layer (i_t), an efficiency of 10.5% has been attained using the TMB p-layer.

The I-V curve of our best (9.3%) tandem cell is shown in Fig. 3. The cell features a graded-index glass surface to eliminate front surface reflection, and a TiO_x interstack recombination layer to improve voltage and fill factor [1]. The optimized second stack p and i_t layers differ somewhat from those of single junction devices. It may be noted that all devices described in this review employ carbon-graded p and i_t layers.

High quality amorphous silicon material layers and cells have also been produced in a new research deposition system. This system is load-locked, and is designed to produce extremely high purity layers with good thickness uniformity right up to the edges of the 1 ft^2 substrates. The system is intended for module development.

Several studies of deposition uniformity have been conducted. Some possible sources of thickness variation across a large substrate are a) gas distribution effects, b) r.f. effects, and c) change of gas composition in the direction of flow. The last effect is particularly noticeable for a-$Si_{1-x}C_x$:H p-layers; it has been found that the spatial variation of H, C, and B concentrations in the deposited film along the direction of gas flow act in concert to increase bandgap and decrease conductivity. For example, it is possible to observe a change in p-layer conductivity from 3.4×10^{-5} S/cm to 3.0×10^{-7} S/cm over a gas flow distance of 25 inches. Based on these studies, the uniformity of both p and i layer properties have been improved.

New records have also been set for single and tandem junction modules of various sizes. The successful development of a process for incorporating back reflectors into 1 ft^2 modules, including critical annealing schedules, has allowed the attainment of an aperture area efficiency of 7.55% for a 1 ft^2 single junction module with a ZnO/Al back contact. This module has an aperture area of 873 cm^2 and generates 6.59 W. A new, high-precision X-Y table for laser patterning has allowed scribe related area losses to be reduced to 3%.

In Chronar's Eureka project, the application of many of the techniques mentioned above has resulted in the achievement of a world record power output for a monolithic thin film PV module of 74.4 W [2]. This single junction module (approximately 155 cm x 79 cm) has an aperture area of 11,900 cm^2, generates 61 V open circuit, 1.85 A short circuit, and possesses the remarkable fill factor of 66% (see Fig. 4). The back contact is Al.

With tandem junction silicon, aperture area efficiencies of 7.17% and 6.42% have been achieved for 1 x 1 ft^2 and 1 x 3 ft^2 modules, corresponding to powers of 6.04 W and 16.4 W, respectively. These modules were metallized with Al; back reflectors have not yet been applied to tandem junction modules.

In the all-important area of stability we have not made any attempt to better a previously announced achievement of only 11% power loss from an encapsulated 1 x 1 ft^2 tandem junction module during a period of over 140 days outdoor exposure [3]. However, some

new results have been obtained, and other studies are underway in preparation for an assault on this record. We have rigorously demonstrated, for example, that the introduction of a transitional i-layer does not impair stability, and that the initial gain in performance is retained. We have also demonstrated a small improvement in cell stability through a post-fabrication treatment consisting of multiple, intense light flashes followed by sufficient annealing [3]. Finally, while some experiments have indicated that stability can be improved by overcoating of the SnO_2 with ZnO, others have not, and further work is necessary to understand the various factors at work.

Conclusions

Performance data for single and tandem junction cells and modules are summarized in Table I. Good progress has been made in single junction technology, as evidenced by the performance of the 1.2 m^2 Eureka modules, 900 cm^2 modules with ZnO/Al reflectors, and 1 cm^2 cells. However, additional efforts are required to realize corresponding advances in tandem junction cells and modules in order to improve stabilized efficiency. It is clear that improvements in the amorphous silicon layers will continue to be a major factor in achieving these goals, and that techniques for obtaining deposition uniformity over large areas, and for obtaining novel doped layers with higher transparency and conductivity, must be brought into the mainstream. Module performance is still diminished relative to cell performance by problems related to patterning and to defects of various origin. These issues must be understood and brought under control. With the emphasis on stabilized efficiency and increased outdoor testing, encapsulation issues must be faced within these research programs, and encapsulation materials and processes developed so that environmental effects do not contribute to power loss [4]. Until this is accomplished, it will remain difficult to separate observed long term power loss into contributions from the Staebler-Wronski effect and/or possible materials problems at cell interfaces.

References

1. A.E. Delahoy, "Recent Developments in Amorphous Silicon Photovoltaic Research and Manufacturing at Chronar Corporation." Solar Cells, 27(1989) 39-57.

2. J. Macneil, A.E. Delahoy, F.J. Kampas, E. Eser, A. Varvar, and F.B. Ellis, Jr., "A 10 MWp A-Si:H Module Processing Line." Proc. 21st IEEE Photovoltaic Specialists Conference, Orlando, Florida, May 21-25, 1990 (IEEE, NY, 1990) pp. 1501-1505.

3. A.E. Delahoy, F.B. Ellis, Jr., C. Kothandaraman, H. Schade, T. Tonon, and H. Weakliem, Semi-Annual Subcontract Report 16 March 1989-30 November 1989, Subcontract No. ZB-7-06003-1 (SERI/TP-211-3667. Available NTIS: Order No. DE90000320).

4. J. Grez, J. Kolesar, and F. Kampas, "Reliability Studies of Eureka Modules" SERI PV Module Reliability Workshop, October 25-26, 1990, Lakewood, CO, and to be published in Solar Cells.

Table I. Performance of amorphous silicon cells and modules (single and tandem junction)

Device type	Power (W)	Area (cm^2)	Efficiency (%)	V_{oc} (V)	J_{sc} or I_{sc} (mA/cm^2 or mA)	FF (%)	AR	Metallization	Meas. at
1J cell	-	1.05	11.3	0.854	18.3	72.2	MgF_2	ZnO/Ag	Chronar
1J cell (TMB, no i_t)	-	0.072	10.5	0.823	17.4	73.7	MgF_2	ZnO/Ag	Chronar
1J module (1x1)	6.59	873	7.55	24.2	404	67.0	-	ZnO/Al	SERI
1J module (Eureka)	74.4	11,900	6.23	61.0	1848	66.0	-	Al	SERI
2J cell	-	0.08	9.30	1.65	7.47	75.6	G.I.	Al	Chronar
2J cell	-	1.00	8.70	1.64	7.41	71.6	-	Al	Chronar
2J module (1x1)	6.04	842	7.17	48.3	189	66.1	-	Al	Chronar
2J module (1x3)	16.4	2,555	6.42	46.7	548	64.1	-	Al	SERI

Notes: For modules, the efficiency quoted is aperture area efficiency
J_{sc} given for cells, I_{sc} given for modules
G.I. denotes graded-index glass

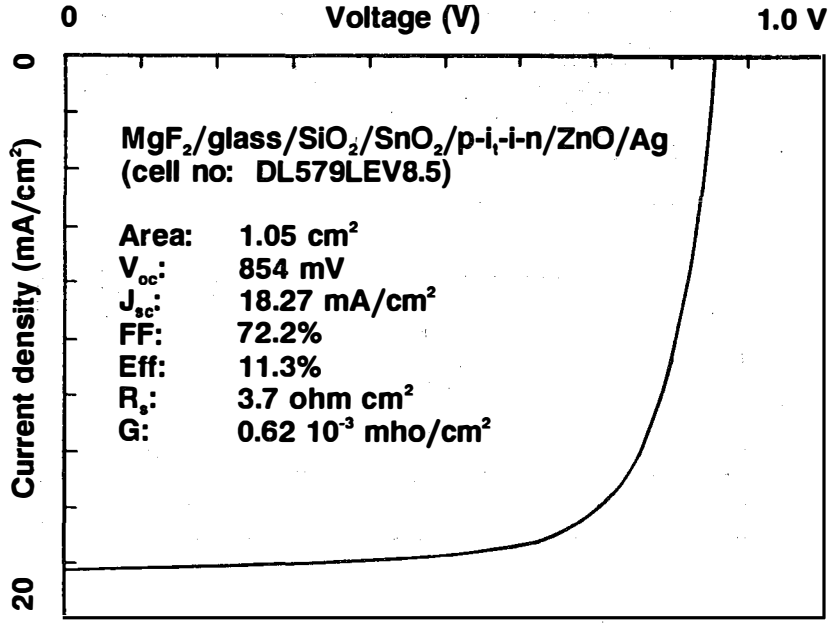

Fig. 1. J-V curve for a 11.3% efficient 1 cm^2 single junction cell with ZnO/Al reflector.

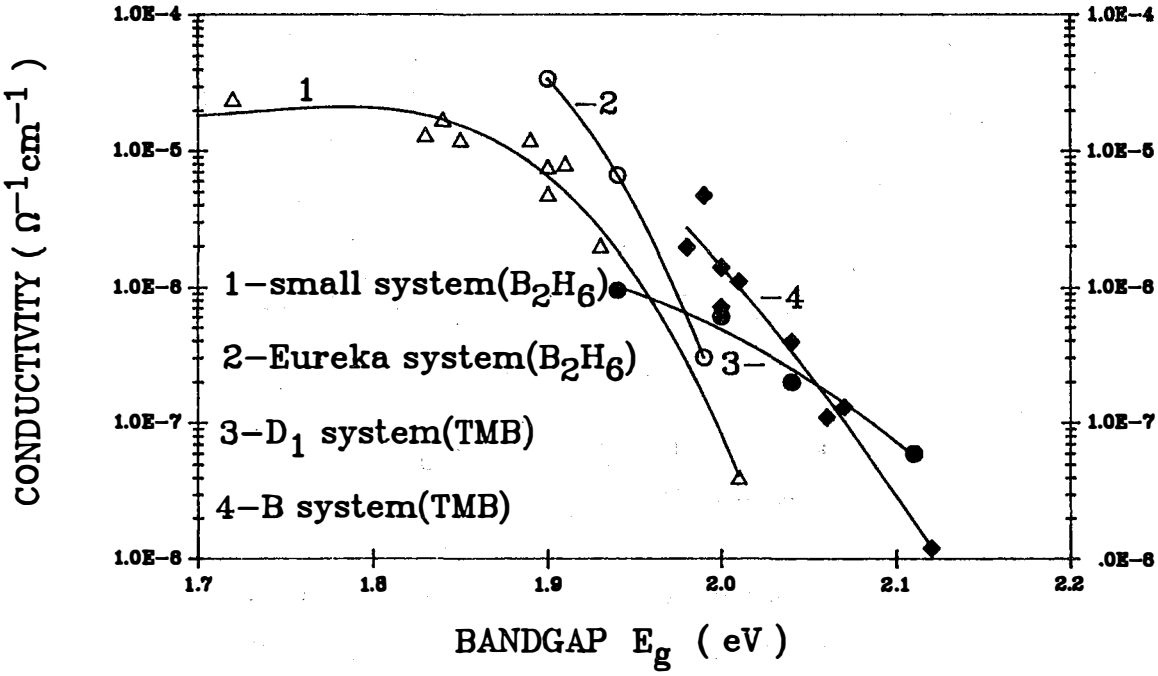

Fig. 2. Conductivity versus bandgap for a-$Si_{1-x}C_x$:H p-layers prepared using either B_2H_6 or TMB as dopant gas.

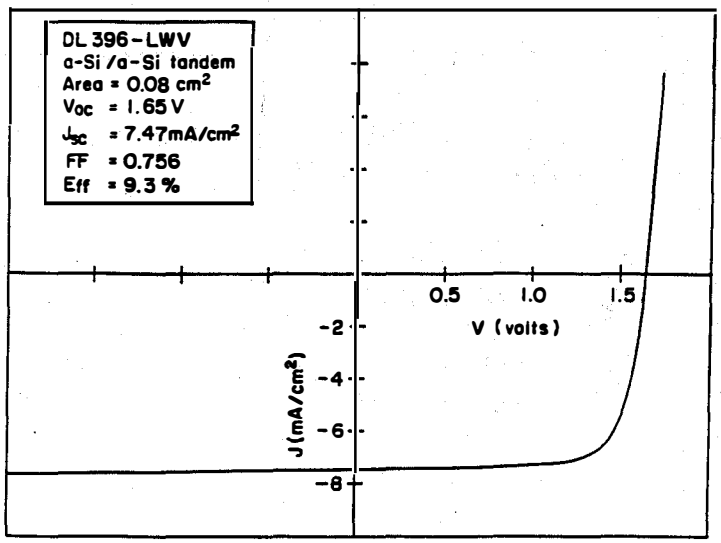

Fig. 3. J-V curve for a 9.3% efficient tandem junction cell with TiO_x interstack recombination layer.

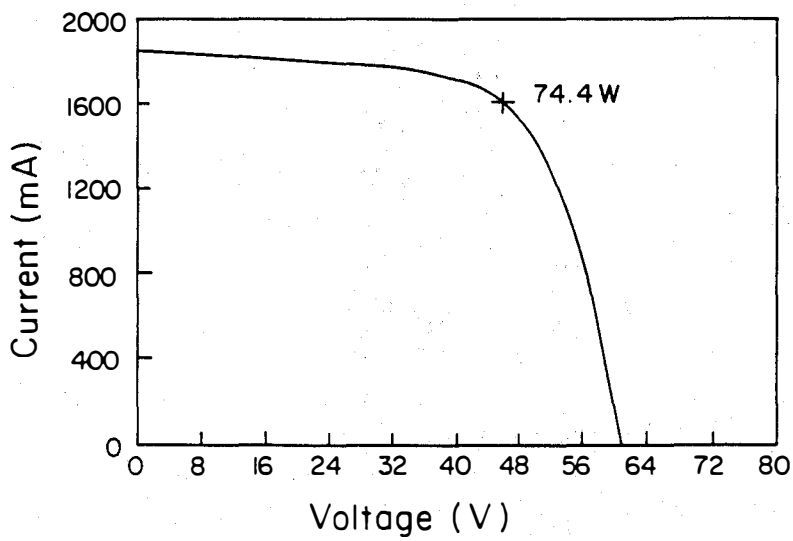

Insolation = 1004 W/m²	Vm = 46.4 V
Temp = 32.6°C	Im = 1602 mA
V_{oc} = 61.0 V	Pm = 74.4 W
I_{sc} = 1848 mA	Aperture area = 11,900 cm²
FF = 66.0%	Ap. area efficiency = 6.23%

Fig. 4. Outdoor measurements on a 1.2 m^2 Eureka module; power output 74.4 W, a world record for a monolithic thin film module. (Data acquired on April 6, 1990 at the SERI PV module testing and performance facility).

Title: **Research on High-Efficiency, Multiple-Gap, Multi-Junction Amorphous Silicon-Based Alloy Thin Film Solar Cells**

Organization: Energy Conversion Devices, Inc., Troy, Michigan

Contributors: S. Guha, principal investigator; A. Banerjee, C. Bernotaitis, J. Burdick, E. Chen, T. Glatfelter, G. Hammond, M. Hopson, T. Laarman, M. Lycette, R. Mohr, P. Nath, A. Pawlikiewicz, I. Rosenstein, R. Ross, D. Wolf, J. Yang, and K. Younan.

The research program is directed toward advancing the understanding of amorphous silicon-based alloys and their use in small area, multi-junction, multi-bandgap solar cells. The principal objectives are (1) to develop a broad scientific base for the chemical, structural, optical, and electronic properties of amorphous silicon-based alloys; (2) to determine the optimum properties of alloy materials as they relate to high-efficiency cells; (3) to determine the optimum device configuration for multi-junction cells; and (4) to demonstrate by February 1990 the proof-of concept, multi-junction amorphous silicon alloy-based solar cells having an efficiency of 16% under standard AM1.5 global insolation conditions and having an area of at least 1 cm^2.

Approach/Present Tasks

Energy Conversion Devices has been using rf glow-discharge decomposition approach to deposit amorphous silicon alloy materials (a-Si:H:F, a-Si:Ge:H:F). In order to obtain high efficiency with good stability, a multi-junction triple cell configuration has been used in which different bandgap materials are used to capture the wide spectrum of solar photons. The different bandgap materials are being optimized for incorporation in the cells. Novel cell designs are also being investigated to obtain higher efficiency with good stability. The tasks of the subcontract relate to materials, single-junction cell and multi-junction cell research.

Status/FY 1990 Accomplishments

During the period October 1989 to February 1990, work was continued on improving the efficiency of multi-junction devices by optimizing the low bandgap material, back reflector and cell design. High quality a-Si:Ge alloys were developed with optical bandgap of 1.25 eV with an Urbach edge slope of less than 50 meV. The mid-gap state density was, however, higher than that of 1.5 eV alloys. With increasing Ge-concentration, the majority carrier $\mu\tau$ product was found to decrease faster than the increase in mid-gap state density, indicating that the electron mobility also decreases with increasing germanium concentration.

Theoretical analysis showed that further enhancement in the red response for a given cell should be achievable with a more optimized back reflector. Extensive studies were made on a variety of back reflector combinations with different reflectivity and microstructures. Ag/ZnO_x back reflector gave the best performance. Improvement of the Ag/ZnO_x interface and reduction of transmission losses of ZnO_x is expected to give further improvement in the long wavelength response of the devices.

Computer simulation studies have been extended to investigate triple-cell structures with a-Si:C alloy in the top cell. Even with a small amount of carbon incorporation so that the bandgap of the alloy is 1.85 eV, an enhancement in efficiency has been predicted. This is because the top cell now captures shorter wavelength of the spectrum, allowing more of the green photons to enter the middle cell, thereby increasing its current for a given cell thickness.

We have investigated the light-induced degradation rates of high efficiency triple-junction cells. Degradation rates of 12%-17% after 300 hours illumination (100 mW/cm^2 AM1.5) have been measured in triple-junction cells with initial efficiencies 11%-12%. A triple-junction cell with an initial efficiency of 13% degraded 13% after 240 hours of illumination. These degradation rates of 12%-17% are significantly better than degradation rates of 25%-40% observed in single-junction cells of comparable efficiencies.

Degradation of solar cells at high light intensities has been investigated. Degradation is found to obey a $(time)^{1/3}$ law, and at high intensities (5 W/cm^2), saturation is observed beyond 5.10^3 sec.

Using outdoor measurements and simulated spectra, it has been demonstrated that multi-junction devices exhibit similar time-of-day performance as single-junction cells. There has been concern in the past that the efficiency of multi-junction devices would be affected by changes in the spectra which would affect current matching between cells in multi-junction devices leading to current losses. The advantage of multi-junction devices is the higher efficiency which leads to greater total power generated in a day as compared to lower efficiency single-junction devices.

References

1. Picosecond Electron Drift-Mobility Measurements in Hydrogenated Amorphous Silicon. E. A. Schiff, R. I. Devlen, H. T. Grahn, J. Tauc, and S. Guha, Appl. Phys. Lett., 54, 1911 (1989).

2. Numerical Modeling of an Amorphous-Silicon-Based p-i-n Solar Cell. A. Pawlikiewicz and S. Guha, IEEE Trans. on Electron Devices, 37 No. 2, 403 (February 1990).

3. Outdoor Performance Studies of a-Si Alloy Multi-junction Solar Cells Using Simulated Solar Illumination. J. Burdick and T. Glatfelter, 21st IEEE PVSC, Kissimee, FL, (May 1990); to be published.

4. Improved Blue Response of Amorphous Silicon Alloy Solar Cells. A. Banerjee and S. Guha, Mat. Res. Soc. Symp. Proc. (April 1990).

5. Performance Comparison of Triple and Tandem Multi-junction a-Si:H Solar Cells: A Numerical Study. A. Pawlikiewicz and S. Guha, IEEE Trans. on Electron Devices, 37 No. 7 (July 1990).

6. Study of Back Reflectors for Amorphous Silicon Alloy Solar Cell Application. A. Banerjee and S. Guha, J. of Appl. Physics; to be published.

7. Tandem Type Amorphous Silicon Alloy Solar Cells. S. Guha, Optoelectronics-Devices and Technologies (Japan); to be published.

Title: Material Properties of Device Quality Amorphous Silicon Deposited at High Deposition Rates Using Higher Order Silanes

Organization: Glasstech Solar, Inc., 6800 Joyce Street, Golden, CO 80403

Contributors: D.S. Shen, Program Manager; P.K. Bhat, Principal Investigator, H. Chatham, C. Matovich, A. Benson

Objective:

The major objective of the research during this period was to demonstrate p-i-n devices with intrinsic layers deposited at a rate of 2 nm/s having initial efficiency higher than 10%, to improve the stability of the high deposition rate devices, and to obtain an 8% stable efficiency cell after 200 hrs. of light soaking.

GSI Approach:

The work was organized in two major tasks: materials research and device research. The goal of materials research was developing high quality a-Si:H materials at high-deposition-rates. Various techniques were used to improve the film quality. The properties of the films deposited from Si_2H_6 and SiH_4 have also been compared. For the device research, the major effort was to improve the p-layer and the p/i interface. An ITO/Ag back reflector has also been studied. Study on tandem cells with high-deposition-rate i-layers was carried out to compare the stability of single junction cells versus tandem-juntion cells.

Research results:

By using high excitation frequency (110 MHz) and optimization of deposition conditions, the electronic properties of i-layers deposited from Si_2H_6 or SiH_4 at ~2 nm/s approached the properties of low deposition rate films.

Table 1 shows the properties and deposition conditions of optimized i-layers deposited from Si_2H_6 or SiH_6 at 2 nm/s.

Table 1 Properties and Deposition Conditions of High Deposition Rate (2 nm/s) i-layer

Source Gas	E_g eV	α_{600} cm^{-1}	σ_{ph} Scm^{-1}	σ_d Scm^{-1}	γ red	γ AM1.5	T_{sub} °C	Power mW/cm^3
Si_2H_6	1.82	$2.4x10^4$	$1x10^{15}$	$2x10^{-11}$	0.90	0.86	240	46
SiH_4	1.79	$2.9x10^4$	$3x10^{-5}$	$4x10^{-11}$	0.88	0.82	210	385

$B(CH_3)_3$ was used as an alternative p-layer doping gas. The results show that $B(CH_3)_3$ is a better doping gas than B_2H_6, due to its better thermal stability, and produces a film with better electro-optical properties [1].

Figure 1 shows the conductivity versus Tauc's band gap of p-layers deposited from $B(CH_3)_3$, SiH_4 and CH_4.

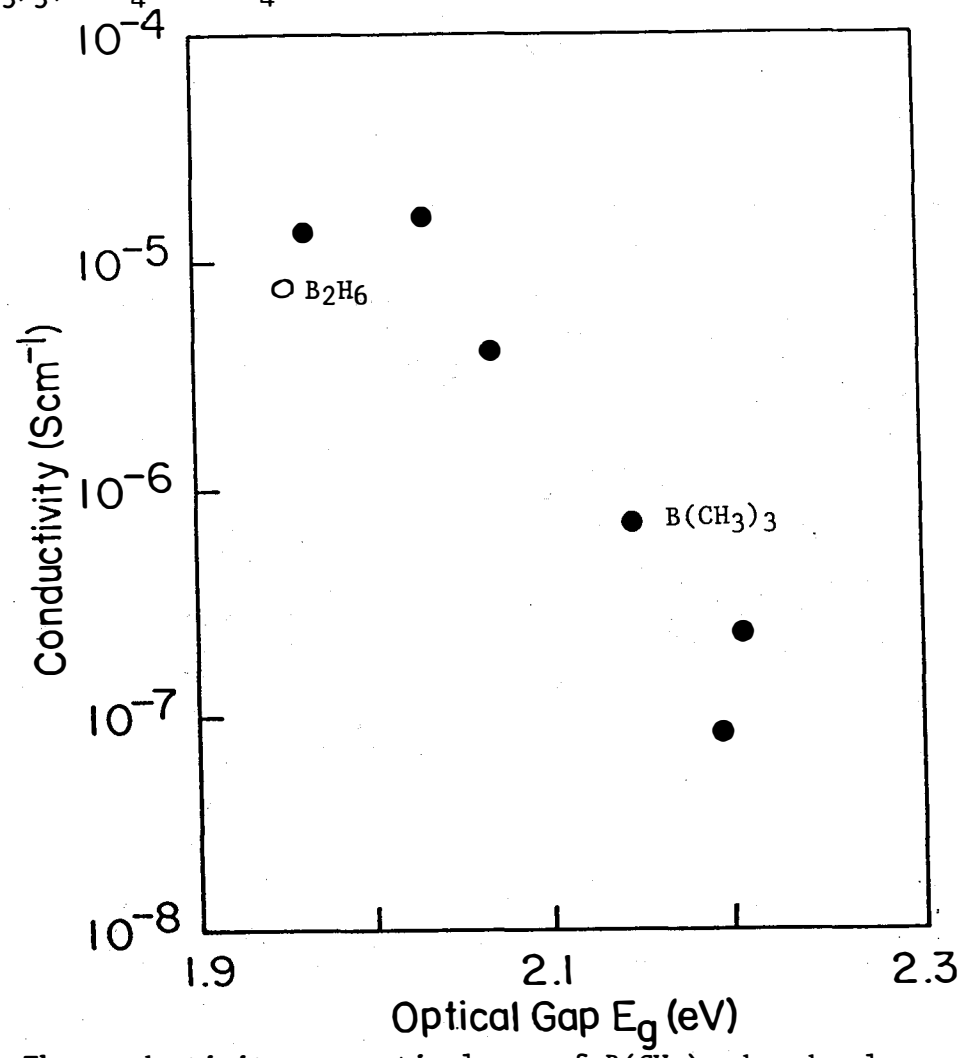

Figure 1 The conductivity vs. optical gap of $B(CH_3)_3$ doped p-layers

The open-circuit voltage, V_{oc}, of the devices has been improved by using a $B(CH_3)_3$ p-layer and a better p/i interface layer. The short circuit current density, J_{sc}, has been improved by using an ITO/Ag back reflector. For thin cells (~300 nm), the current density using ITO/Ag back reflector can be increased by about 1.5 mA/cm^2 compared with those using Ag back reflector. The key for fabricating high-deposition-rate SiH_4 devices has been found to be the p/i interface. Figure 2 shows the quantum efficiency of SiH_4 single junction cells; one deposited at low-rate, one at high-rate, and one at high-rate but with a low-power interface layer [2]. As a result, high-deposition-rate cells deposited from both Si_2H_6 and SiH_4 source gases reached 10% efficiencies. A 1 cm^2 cell deposited at 2 nm/s from Si_2H_6 reached 10.1% initial efficiency, as measured by SERI (Figure 3).

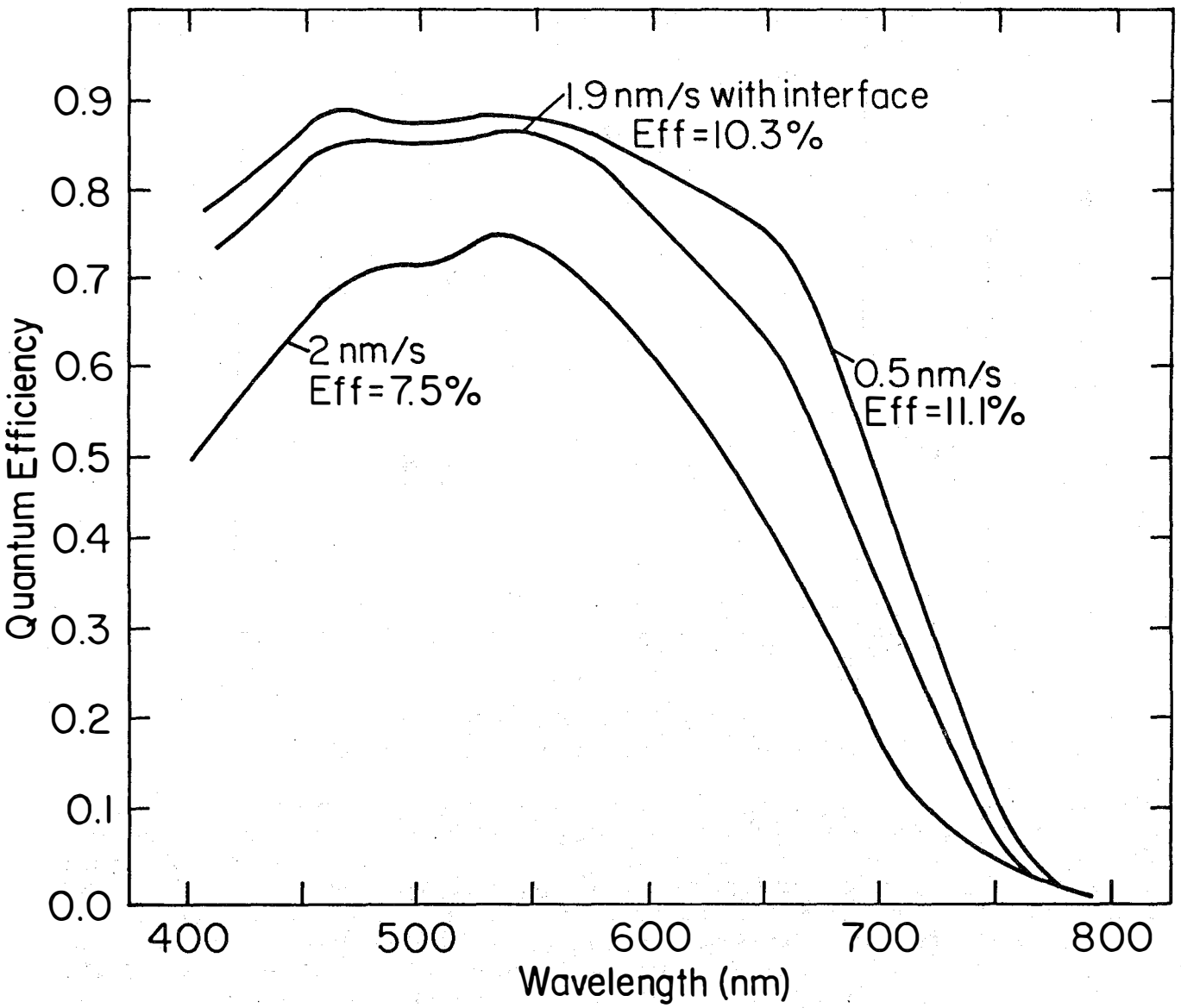

Figure 2 Quantum efficiency of SiH_4 devices for various i-layer deposition rates.

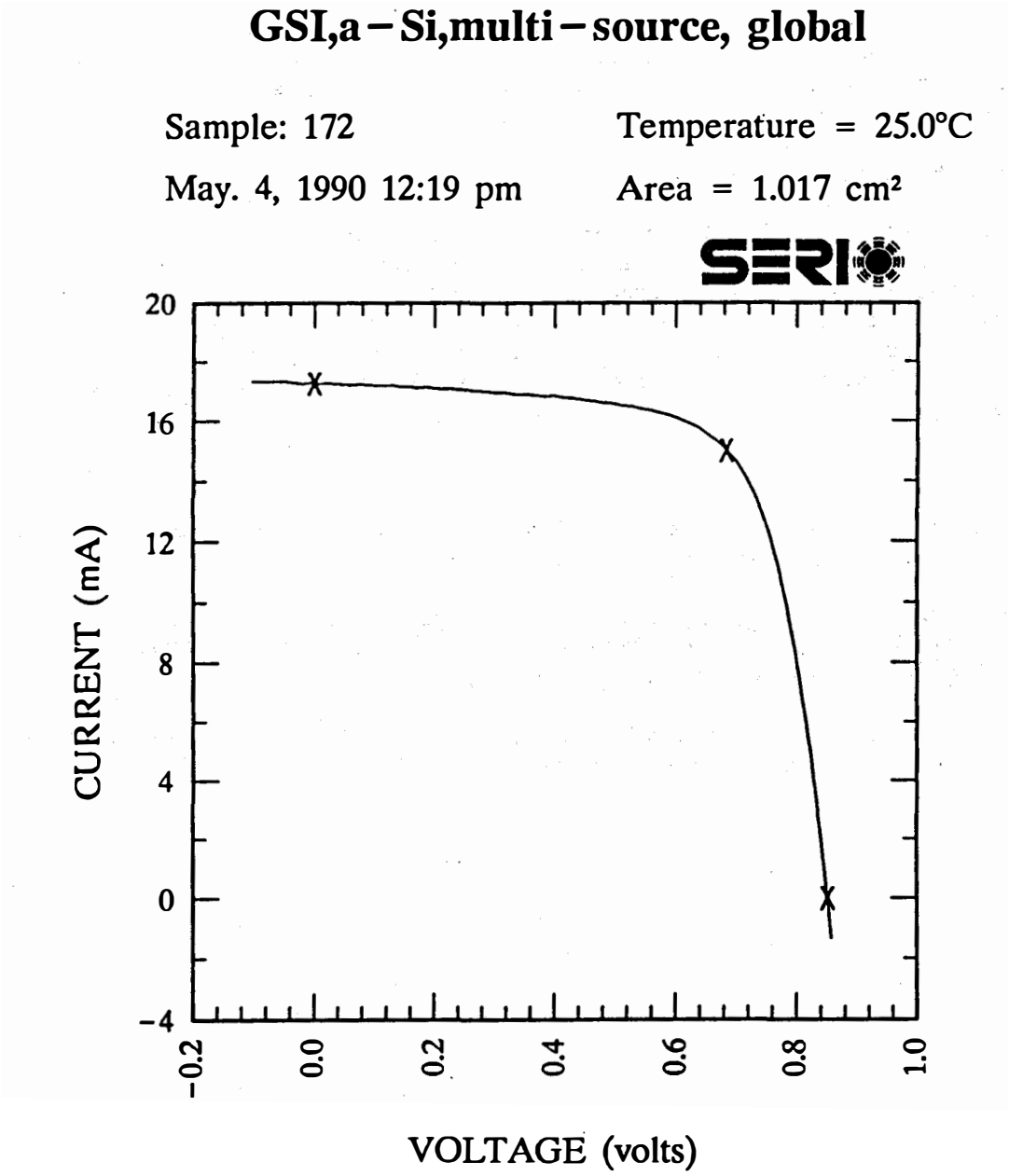

V_{oc} = 0.8523 volts	I_{sc} = 17.26 mA
J_{sc} = 16.98 mA/cm²	P_{max} = 10.27 mW
Fill factor = 69.78 %	I_{max} = 15.01 mA
Efficiency = 10.1 %	V_{max} = 0.6841 V

Figure 3 I-V curve of Si_2H_6 high-deposition-rate (2 nm/s) device.

An attempt to reduce the hydrogen concentration in the film while keeping the deposition rate high was not successful. Due to the high hydrogen concentration in the i-layer, the stability of the high deposition rate device is inferior to the low deposition rate device.

Conclusions and Further Research:

The electronic properties of i-layers deposited at 2 nm/s approached those of low-deposition-rate material. Devices with 10.1% initial efficiency have been fabricated, using i-layers deposited at 2 nm/s. This is the highest efficiency reported to date for this category. The instability seems linked to hydrogen concentration in the film. Tandem cells are more stable than single junction cells. Further experiments should be conducted to reduce hydrogen in a-Si:H films deposited at 2 nm/s deposition rates.

References:

1. D.S. Shen, H. Chatham, and R.E.I. Schropp, "$B(CH_3)_3$ as P Layer Doping Gas," MRS Symp. Proc,. Vol. 192, p. 523, 1990.

2. D.S. Shen, H. Chatham and P.K. Bhat, "High-Deposition-Rate Amorphous Silicon Solar Cells: Silane or Disilane?," presented at the SERI 10th PV AR&D Meeting, to be published in Solar Cells.

3. D.S. Shen and P.K. Bhat, "Amorphous Silicon Solar Cells Prepared at High Deposition Rates," Annual Report, FY1990 (June 1990).

Title: Optimization of Transparent and Reflecting Electrodes for Amorphous Silicon Solar Cells

Organization: Department of Chemistry, Harvard University, Cambridge, MA.

Contributors: R. G. Gordon, Principal Investigator; J. Hu; J. Musher; Carmen Giunta

SUMMARY

OBJECTIVES

Transparent conducting materials are essential components of many kinds of solar cells, in which they serve as front-surface electrodes. In tandem cells, back surface electrodes also need to be transparent. Finally, some designs for highly reflective back contacts also call for a transparent conducting layer. The compositions of these transparent conducting layers are usually based on oxides of tin, indium and/or zinc, and are hence referred to as transparent conducting oxides (TCO). In addition to having low electrical resistance and low optical absorption, the structure of a TCO must minimize reflection losses. The TCO must also resist degradation during cell fabrication and use. Finally, the method for making the TCO must be inexpensive and safe.

Our general objectives are to improve the performance of TCO materials and the methods for their production. We aim to reduce their electrical resistance, optical absorption and reflection losses, and to avoid degradation of the materials. For the production method, the prime consideration is to deposit the TCO layers at a high rate with relatively simple apparatus. The method chosen is chemical vapor deposition at atmospheric pressure (APCVD), since it has been demonstrated, in the glass-coating industry, to be the most cost-effective method for making large areas of TCO coatings.

RESULTS

Textured Zinc Oxide Films

Zinc oxide is a promising material for forming less expensive TCO layers, since zinc metal is much less expensive than tin or indium. Also, zinc is much more abundant in the earth's crust, than is tin or indium, so that even large-scale use of solar cells would not lead to any shortage of zinc.

Also, zinc is widely distributed on earth, and is mined in many countries, so continuity of supply is assured in any kind of political situation. In contrast, tin is mined in large quantities in only a few countries. Another advantage of zinc oxide is its greater stability toward hydrogen plasmas used to deposit amorphous silicon solar cells.We discovered that fluorine can also be used to dope zinc oxide to high electrical conductivity. Fluorine is an ideal dopant for zinc oxide, since it is known to be electrically inactive, or even beneficial, in hydrogenated amorphous silicon. An additional benefit of the fluorine doped zinc oxide is its higher electron mobility, which results in greater transparency.

The fluorine-doped zinc oxide is produced by CVD from diethyl zinc, ethanol and hexafluoropropylene at atmospheric pressure, in the temperature range 375° to 450°C. Films deposited under these conditions show good adhesion to the glass substrates (Scotch tape test). The highest electrical conductivity and light transmission are found for films deposited at the highest temperatures (450°C), and containing about 0.5 atomic percent fluorine. With this material, we could produce a TCO with a sheet resistance of 5 ohms per square and a visible transmission of about 87%, at growth rates up to 2500Å/minute.

We discovered that the amount of texture (roughness) of the zinc oxide films depends dramatically on the amount of water vapor in the growth atmosphere. Small amounts of water vapor (about 1% of the ethanol concentration) produce smooth films, but decreasing the water content to less than 0.25% of the ethanol content produces textured (rough) zinc oxide films suitable for efficient light-trapping in solar cells. Eliminating the water entirely, however, almost completely eliminates film growth, so a small, controlled source of water vapor is essential to control of film texture[1].

Growth Rate of Zinc Oxide films

In order to produce zinc oxide films at high growth rates, the reactant system dimethylzinc plus oxygen was explored. When excess oxygen is used, the growth rate increases linearly with dimethylzinc concentration. Values up to 6000Å/minute were measured at a substrate temperature of 460°C. These films were, however, smooth under all growth conditions tried, and therefore were not suitable for efficient light-trapping in solar cells[2].

Low Temperature Deposition of Zinc Oxide

Zinc oxide films were deposited on substrates at temperatures from 300°C to 450°C. using diethylzinc, tertiary-butanol and hexafluoropropene. All the films were found to contain about the same amount of fluorine (0.5 ± 0.2 atomic per cent). However, the sheet resistances of the films varied by many orders of magnitude (from about 8 ohms per square at 450°C to 80,000 ohms per square at 300°C). Thus the fluorine is incorporated in an electrically ineffective form at the lower temperatures.

Titanium Nitride Diffusion Barriers

Titanium nitride is a metallic conductor with high reflectivity in the red and infrared parts of the spectrum. TiN has outstanding chemical and mechanical stability. It contains inexpensive and abundant elements. Thus TiN is a good candidate for forming durable and inexpensive back contacts to solar cells. It may also be used as a diffusion barrier between metals, such as aluminum or silver, and the amorphous silicon in a solar cell.

Recently we discovered how to chemically vapor deposit titanium nitride at low enough temperatures (≈200°C) to preserve amorphous silicon. Tests were carried out to see if the CVD material also forms a good barrier to diffusion of metals. Gold was used as the test metal because RBS is very sensitive to gold. Gold/titanium nitride/silicon structures were

annealed at temperatures up to 500°C, and showed no interdiffusion by RBS. At higher temperatures, 550°C or above, the titanium nitride barriers fail, and the gold diffuses into the silicon.

The failure temperatures are much higher than any encountered in use of solar cells. Thus the CVD TiN films should be effective as diffusion barriers at the normal temperatures of operation of solar cells[3].

Optical Tuning of Front and Back Contacts

Samples of textured, fluorine-doped zinc oxide films on glass were sent to Dr. Anthony Catalano at Solarex Corporation. They prepared amorphous silicon solar cells on these substrates, and found very high (~90%) peak quantum efficiencies for these cells. These results show that the texture of these zinc oxide films gives high light-trapping efficiency, and also confirm that the absorption of light in the zinc oxide is very small, not more than a few per cent. The open circuit voltages and fill factors of these cells were, however, low; this means that some other aspects of cell fabrication on these substrates need optimization in order to make high efficiency cells[1].

CONCLUSIONS

- Textured fluorine-doped tin oxide films with high electrical conductivity (5 ohms/square) and high transparency (87%) were produced by chemical vapor deposition at atmospheric pressure (APCVD) on glass substrates at about 450°C, at moderate deposition rates (up to 2500 Angstroms per minute).

- Amorphous silicon solar cells grown on these textured films show very high quantum efficiencies, which demonstrates the high light-trapping ability of this texture, and the high transparency of the zinc oxide film.

- Transparent, conductive fluorine-doped zinc oxide films were grown by APCVD at high deposition rates (up to 6000 Ansgtroms/minute), but these films are smooth, not textured, and thus are not suited to make high efficiency solar cells.

- Fluorine-doped zinc oxide films were grown at temperatures below 300°C, but they have low conductivity and are not suitable for back contacts to solar cells.

References

1. Jianhua Hu and Roy Gordon, accepted for publication in Solar Cells, 1990.

2. Jianhua Hu and Roy Gordon, Materials Research Society, Fall Meeting, 1990 (to be published).

3. Roy Gordon, Annual Report, SERI Subcontract XG-0-19121-1 (1990).

Title: **Structural and Electronic Studies of a-SiGe:H Alloys**

Organization: Division of Applied Sciences, Harvard University, Cambridge, MA

Contributors: William Paul, principal investigator; Warren A. Turner, Scott J. Jones, Francisco C. Marques, Dawen Pang, Anna E. Wetsel, and Paul Wickboldt

Objectives

The principal objectives of this research have been (1) to carry out a detailed study of the structural, electrical and optical properties of a-Ge:H, the end-component of the a-SiGe:H alloy series, in order to determine the values of deposition parameters optimizing the properties relevant to photovoltaic devices, (2) to continue a collaboration with Professor Richard Norberg of Washington University to prepare films of a-Si and a-Ge containing deuterium, so that the Norberg laboratory can study deuteron magnetic resonances (DMR), which may be interpreted to give information on the microstructure of films on a 100 Å scale, (3) to continue a collaboration with Dr. M.L. Theye of the Laboratoire d'Optique, University of Paris, to explore low photon energy absorption spectra determined by photothermal deflection spectroscopy or steady state photoconductivity, (4) to continue a collaboration with Professor J.H. Chen of Boston College to study the electron spin resonance spectra of hydrogenated amorphous semiconductors, (5) to continue a collaboration with Professor I. Chambouleyron of the University of Campinas to compare the properties of a-Ge:H prepared by reactive sputtering (Campinas) and plasma-enhanced CVD (Harvard), and (6) to carry out a collaboration with Dr. Y.M. Li of Solarex Corporation to study minority carrier properties of a-Ge:H using the photocarrier grating technique.

Approach

Our research has been guided by the philosophy that insight into the difficulties surrounding the preparation of acceptable low band-gap a-SiGe:H alloy material may be obtained through a detailed understanding of the deposition conditions necessary for the preparation of high-quality a-Ge:H. The typical experimental gambit used in the production of such low band-gap alloy materials is to start from conditions which produce high-quality a-Si:H, add some form of germanium to the deposition plasma, and to then perturb the conditions of deposition slightly from those used to produce a-Si:H until the properties of the resulting material are empirically optimized. It is not unreasonable to suggest that the properties of such alloy materials should be at least as sensitive, if not more so, to conditions which produce high-quality germanium, as a-Ge:H is typically found to be notoriously bad. It is our contention that the conditions necessary for the preparation of high-quality a-Ge:H are significantly different from those used to produce high-quality silicon.

The films required were prepared by r.f. glow discharge and reactive sputtering at Harvard and Campinas, respectively. These films were subjected to an extensive battery of structural, optical and electrical characterizations in our laboratory and, in some instances, those of our collaborators. The measurements made included conductivity *versus* temperature, optical absorption in the sub-band-gap region of the spectrum, optical vibrational absorption in the infrared region, photoconductivity spectra, ambipolar diffusion length, Raman spectra, gas evolution, transmission and scanning electron microscopy, differential scanning calorimetry, isothermal calorimetry, and deuteron and electron magnetic resonance.

Discussion

Significant progress has been made during the past year on a number of fronts. High density, non-porous, highly photoconductive films of a-Ge:H showing minimal microstructure have been deposited using the r.f. glow discharge method out of a gas plasma of GeH_4 and H_2. These films, deposited on substrates mounted on the powered electrode of a diode reactor, show

remarkable improvement over co-deposited material taken from the unpowered electrode. Films were prepared under the systematic variation of substrate temperature, discharge power and dilution of the plasma by H_2.

This state-of-the-art material has been extensively characterized both at Harvard and by our collaborators. The optical and electrical properties are all consistent with material containing a low density of defect related states in the energy gap. This material typically has an $\eta\mu\tau = 3 \times 10^{-7}$ cm^2V^{-1} and ratio of photocurrent to dark current of 1-2 x 10^{-1} measured using photoconductivity, a $\mu\tau = 4 \times 10^{-8}$ cm^2V^{-1} measured using time of flight, an ambipolar diffusion length of 550 Å measured using the photocarrier grating technique, an Urbach energy of approximately 50 meV and α at 0.7 eV below 10 cm^{-1} measured using photothermal deflection spectroscopy, a dangling bond spin density of 5 x 10^{16} cm^{-3} measured using electron spin resonance, photoluminescence with a peak energy position of 0.81 eV and full width at half maximum of 0.19 eV, activation energy of 0.50 -0.55 eV and σ_0 nearly 10^{-4} $(\Omega cm)^{-1}$ measured using dark conductivity, and an E_{04} band-gap of 1.24 eV measured by optical absorption. Structural measurements indicate a homogeneous material lacking any island/tissue and columnar structure when investigated using transmission and scanning electron microscopy, respectively. Hydrogen concentrations calculated from infrared and gas evolution measurements can only be reconciled by postulating a large quantity of unbonded hydrogen whose presence is confirmed using deuteron magnetic resonance. The bonded deuterium component, as seen in a film using DMR, has a spin-lattice relaxation time of the order of 4000 s. The differential calorimetry measurement shows rapid crystallization occurring near 421 °C and the presence of large compressive stresses have been confirmed using a bending-beam method. A complete account of the results of the characterization of this material has been published.

Our collaborations have resulted in a number of other publications, as well as the unified collaborative effort involved in the characterization of our recently prepared, high-quality a-Ge:H. In addition to these collaborations, we have continued to make advances in the understanding of the structure of a-Ge:H using electron microscopy, x-ray, and Raman techniques as well as the special tools (GE and DSC) we have developed. We have confirmed substrate dependent structural differences found for low-quality a-Ge:H prepared at low substrate temperatures. These differences appear to be strongly linked to the yield strength of the underlying substrate. A detailed discussion of these results may be found elsewhere.

Conclusions

State-of-the-art material produced on the powered electrode has an electron $\eta\mu\tau$ and ratio of photo to dark conductivity which are at least comparable to any reported in the literature to date. They are orders of magnitude better than those of samples co-deposited on the unpowered electrode, even though they have similar activation energies with Fermi levels located near mid-gap. The measurement of the ambipolar diffusion length indicates that this improvement does not come at the expense of the mobility of the minority carrier. The material produced on the powered electrode is environmentally stable while material produced in our deposition system on the unpowered electrode at similar temperatures becomes contaminated when exposed to the atmosphere as noted in the infrared spectra and photoconductivity as functions of exposure time. The infrared spectra and DMR suggest different hydrogen bonding configurations as well as a significant amount of unbonded hydrogen in the sample produced on the powered electrode. We speculate that the remarkable improvement of the photoresponse of the material produced on the powered electrode is directly linked to the significant structural differences observed in the material. Many of the characterizations suggest a significantly lower density of states in the band-gap of this material which we correlate with the increased homogeneity of the structure observed in the TEM micrographs. The material lacks a low-density, highly defected tissue network and hence the density of states in the gap, which might otherwise be heavily influenced by a high density of defects from the tissue material, is dominated by a relatively high-quality island material containing few defects.

It is difficult to compare our material with any other material having comparable photoconductive properties due to insufficient information contained in the literature. However, judging from the conditions quoted for the production of the best material, it would appear that the deposition conditions are indeed different from those needed to produce high-quality a-Si:H. We have not undertaken an optimization of a-Si:H produced on the powered electrode, so we cannot state that such material produced on the powered electrode is inherently inferior under all conditions. Possibly more significant to our work is the observation that, unlike a-Si:H produced on the unpowered electrode, the conditions for the production of high-quality a-Ge:H may be extremely sensitive to the exact geometry and flow conditions which exist in the reactor. They may also depend strongly on the exact plasma conditions at different points in the deposition chamber and on the concentrations of the different radicals which finally reach the growing surface.

We are currently undertaking further optimization of the deposition parameters used in the production of a-Ge:H. It is our intention to exploit the region of parameter space producing optimized a-Ge:H to attempt to produce improved alloy material with high germanium concentrations, focusing on germanium concentrations which would produce alloys with band-gaps in the region of 1.3 to 1.5 eV. We also intend to conduct studies of the plasma to address the question of why our depositions on the powered electrode produce such improved material.

References

1. W.A. Turner, S.J. Jones, D. Pang, B.F. Bateman, J.H. Chen, Y.-M. Li, F.C. Marques, A.E. Wetsel, P. Wickboldt, W. Paul, J. Bodart, R.E. Norberg, I. El Zawawi, and M.L. Theye, Structural, optical, and electrical characterization of improved amorphous hydrogenated germanium, J. Appl. Phys. **67**, 7430 (1990).

2. W.A. Turner, S.J. Jones, Y.-M. Li, A.E. Wetsel, J.H. Chen, and W. Paul, Optimization of the properties of undoped a-Ge:H, to be published in the Proceedings of the Spring 1990 meeting of the Materials Research Society, San Francisco.

3. M.P. Volz, P.A. Fedders, R.E. Norberg, W.A. Turner, and W. Paul, Deuteron magnetic resonance in a-Ge, J. Non-Cryst. Solids **114**, 546 (1989).

4. P. Santos-Filho, M.P. Volz, R.L. Corey, Y.W. Kim, P.A. Fedders, R.E. Norberg, W.A. Turner, and W.Paul, Molecular HD and D_2 in amorphous semiconductors, J. Non-Cryst. Solids **114**, 235 (1989).

5. M.P. Volz, P. Santos-Filho, M.S. Conradi, P.A. Fedders, W.A. Turner, and W. Paul, Unique deuteron spin echoes from HD and ortho-D_2 in large crystal fields, Phys. Rev. Letters **63**, 2582 (1989).

6. D. Fournier, J.P. Roger, A.C. Boccara, M.L. Theye, L. Chahed, W.A. Turner, and W.Paul, Subgap amorphous silicon photothermal deflection spectroscopy; spatial absorption localization, Proceedings of the 6th International Meeting on Photoacoustic and Photothermal Phenomena, Baltimore, Maryland, 1989.

7. L. Chahed, M.L. Theye, D. Fournier, J.P. Roger, A.C. Boccara, Y.-M. Li, W.A. Turner, W. Paul, Studies of surface effects in hydrogenated amorphous silicon by photothermal deflection experiments, submitted to Phys. Rev. B (1990).

8. A.E. Wetsel, S.J. Jones, W.A. Turner, W. Paul, I. El Zawawi, L. Chahed, Y. Bouziem, M.L. Theye, F.C. Marques, and I Chambouleyron, Comparison of the properties of sputtered and glow discharge a-Ge:H, to be published in the Proceedings of the Spring 1990 meeting of the Materials Research Society, San Francisco.

9. S.J. Jones, S.M. Lee, W.A. Turner, and W. Paul, Substrate temperature dependence of the structural properties of glow discharge produced a-Ge:H, Mater. Res. Soc. Symp. Proc. **149**, 45 (1989).

10. S.J. Jones, W.A. Turner, D. Pang, and W. Paul, The effect of sample substrate on the structural properties of co-deposited films, J. Non-Cryst. Solids **114**, 546 (1989).

11. S.J. Jones, W.A. Turner, and W. Paul, The effect of sample substrate on the structural properties of co-deposited films of a-Ge:H, to be published in the Proceedings of the Spring 1990 meeting of the Materials Research Society, San Francisco.

12. W. Paul, S.J. Jones, and W.A. Turner, Studies on the structure of a-Ge:H using DSC, GE and TEM techniques, (Spear Festschrift) Phil. Mag. (1990) to be published.

13. S.J. Jones, W.A. Turner, D. Pang, and W. Paul, An electron microscopy study of the effects of deposition conditions on the growth of glow discharge prepared a-Ge:H films, to be published in the Proceedings of the Fall 1990 meeting of the Materials Research Society, Boston.

14. W. Paul, Brief survey of narrow-gap semiconductors, with particular reference to a-Sn and a-SnGe alloys, Semicond. Sci. Technol. **5**, (1990).

Title: **Photochemical Vapor Deposition of Amorphous Silicon Alloy Materials and Devices**

Organization: Institute of Energy Conversion
University of Delaware
Newark, Delaware 19716

Contributors: B.N. Baron, Project Director;
C.M. Fortmann and S.S. Hegedus, Principal Investigators; W.A. Buchanan and T.X. Zhou, Research Contributors

Objectives:

The project is a continuation of research on photochemical vapor deposition of amorphous silicon materials in order to determine and understand the limits of material preparation and to demonstrate proof-of-concept solar cells. The present objectives are to develop low band gap a-SiGe:H cells for use in high efficiency, stable multijunction thin film solar cells and to determine and understand the origin of Staebler-Wronski effect degradation in a-Si:H cells.

Technical Approaches:

Theoretical studies of multi-junction a-Si:H alloy solar cells project conversion efficiencies greater than 20%. Presently, the performance of these cells is limited by electronic transport in a-SiGe:H. Studies of the relationships between electronic transport, composition and deposition conditions are integrated with investigations of device behavior. The a-SiGe:H materials are prepared in a photo-CVD deposition system that has demonstrated state-of-the-art a-Si:H materials and devices.

Stable, high efficiency cells also require more stable a-Si:H. The origins of the defects involved in the Staebler-Wronski effect in a-Si:H are being investigated. a-Si:H p-i-n cells are degraded by high temperature current injection and room temperature light soaking. Samples are also prepared for analysis of annealed state and light induced defect densities by capacitance and ESR measurements performed by collaborating laboratories. Photo-CVD is used to prepare a-Si:H films and solar cells with a range of H content.

Significant Results

a-SiGe:H Materials

The relationships between C_H, C_{Ge}, and electronic transport were investigated in a-SiGe:H with band gaps ranging from 1.2 to 1.45 eV(1). The excess photoconductivity of a-SiGe:H decreases with increasing C_{Ge}, reaching a minimum at C_{Ge}=60%. Analysis of the photo and dark conductivities showed that electron mobility decreases with increasing C_{Ge}. The observed decrease in photoconductivity was found to be predominantly a decrease in electron mobility. Figure 1 shows photoconductivity decreasing as C_H increases from 2% to 8% for films with C_{Ge} = 55%-65%. The same films showed an increase in photoconductivity

with decreasing a band gap. Lifetime and C_H were unrelated. The decrease in photoconductivity with increasing C_H is attributed to decreasing mobility.

a-SiGe:H Solar Cells

Electron and hole collection as well as performance under red illumination were investigated using p-i-n solar cells with a-SiGe:H i-layers. All cells contained at least a 250Å thick layer of 1.3 eV a-SiGe:H alloy. Front loaded cells had the 1.3 eV a-SiGe:H alloy in the region of the i-layer nearest the p/i interface. Back loaded cells had the a-SiGe:H alloy nearest the n/i contact. Ungraded i-layer devices using 700Å of 1.3 eV a-SiGe:H were also fabricated. All devices had at least 150Å of a-Si:H buffer layer at the n/i and p/i interfaces to reduce recombination. Short wavelength quantum efficiency (SWQE) as a function of bias voltage was measured to investigate limiting cases where recombination is predominantly controlled by a single carrier.

Previously we used SWQE measured through the p-layer to identify the electron mobility as a major factor controlling the performance of graded a-SiGe:H solar cells (2). The greater SWQE of front loaded solar cells compared to back loaded solar cells for illumination through the p-layer (Figure 2) is consistent with the effect of grading on the electron transport.

Hole transport was probed by SWQE measured through the n-layer of solar cells with transparent ITO back contacts. Figure 2 also shows the SWQE for n-layer illumination as a function of bias voltage for front and back loaded cells. The SWQE for n-layer illumination shows relatively little dependence on grading scheme with both front and back loaded solar cells having the same zero bias collection efficiency.

These results indicate similar hole collection lengths in a-SiGe:H and a-Si:H. Moreover, hole and electron collection lengths in a-SiGe:H may be of comparable magnitude.

High reflectivity ITO/Ag contacts were applied to the front loaded, back loaded and ungraded p-i-n solar cells. These cells were evaluated under white light (AM1.5, 100 mW/cm^2) and filtered (red) illumination through the p-layer. Table 1 shows that all cells had greater than 5% efficiencies under white light, the front loaded cell and the ungraded cell had 2% efficiency under the red light and the ungraded cell had QE@800nm of 40%.

a-Si:H Stability and C_H

Photo-CVD a-Si:H i-layers with low (7%) and high (11%) C_H were investigated. Deposition conditions and film properties for low and high C_H materials are given in Table 2. Note that the deposition temperature was the same for both films. Powder formation during deposition of the C_H = 11% material indicated gas phase polymerization. The IR absorption spectra showed structure associated with dihydride and polyhydride bonding only in the high C_H material.

The stability of p-i-n cells with low and high C_H i-layer thicknesses from 0.5 to 0.9 μm thick was investigated. Both low and high C_H solar cells had good

fill factors (~67%) in the annealed state. After light exposure the low C_H cell had better performance than the high C_H cell. For example, after 100 hours of light exposure, a 0.5 μm i-layer low C_H solar cell degraded from 6.2% efficiency to 4.6% while the high C_H solar cell degraded from 5.2% to 3.4% after the same light exposure. Initial efficiencies were not systematically related to C_H.

The effect of C_H on stability was also investigated by current injection at high temperature. P-i-n cells were current-injected at 100-300 mA/cm^2 at 175°C for 1 hour and the steady state defect density determined from measurements of short wavelength quantum efficiency (3). The change in SWQE was much larger in the high C_H sample. This indicates that the steady state density of current injection-induced dangling bonds increases with increasing C_H. Since high C_H p-i-n solar cells also degraded at a faster rate under illumination at room temperature, it is likely that the weak bond sites are directly related to C_H.

Conclusions

As a result of these efforts, we have shown that the addition of hydrogen and germanium reduces the electron mobility in a-SiGe:H i-layer films. The principal effect of Ge in a-SiGe:H solar cells is to reduce collection of electrons. However, using thin compositionally graded i-layers, a-SiGe:H cells with promising performance characteristics for use as the red sensitive component in multijunction solar cells have been achieved. Further improvements in a-SiGe:H cell efficiency are expected from continued investigation of materials and devices with reduced H content. Future work on a-SiGe:H should focus on deposition and characterization of 1.3-1.4 eV materials and devices with i-layer C_H<2%.

From our investigations of the SW effect in a-Si:H solar cells, we found that H content is strongly linked to stability. Future work should focus on a-Si:H with i-layer C<6% in order to quantify the relationships between stabilized cell efficiency and hydrogen content.

References

1. C.M. Fortmann, et al., Mat. Res. Soc. Symp. Proc. Vol. 164, p. 315, MRS, Pittsburgh (1989).

2. C.M. Fortmann, et al., Journal of Non-Crystalline Solids, 115, p. 21-23 (1989).

3. C.M. Fortmann, et al., J. Appl. Phys., 64, p. 4219 (1988).

Table 1

Performance of Graded Cells with ITO/Ag contacts (0.105 cm^2)

Grading	Illumination	V_{oc} (V)	J_{sc} (mA/cm^2)	FF (%)	Eff (%)	QE (800 nm) (%)
Front	White*	0.60	16.0	57	5.4	28
	Red**	0.56	6.2	58	2.0	
Back	White	0.63	15.0	55	5.2	24
	Red	0.60	5.5	51	1.7	
Uniform	White	0.57	17.9	49	5.0	40
	Red	0.54	7.3	52	2.0	

* AM1.5 @ 100 mW/cm^2
**AM1.5 with 630 nm sharp cut on filter

Table 2

Photo-CVD Deposition Conditions and Properties of High and Low C_H a-Si:H Materials

C_H (%)	T_{sub} (°C)	P (torr)	Dep. Rate (A/sec)	Gas Composition	N_s* (cm^{-3})	$\mu\tau$ (cm^2/V)	E_G (eV)
7	205	5	0.52	1:9 SiH_4:He	$<4x10^{15}$		1.73
11	205	10	0.58	pure SiH_4	$<4x10^{15}$	$8x10^{-7}$	1.77

*dangling bond densities from ESR measurements by Prof. P.C. Taylor, Univ. Utah

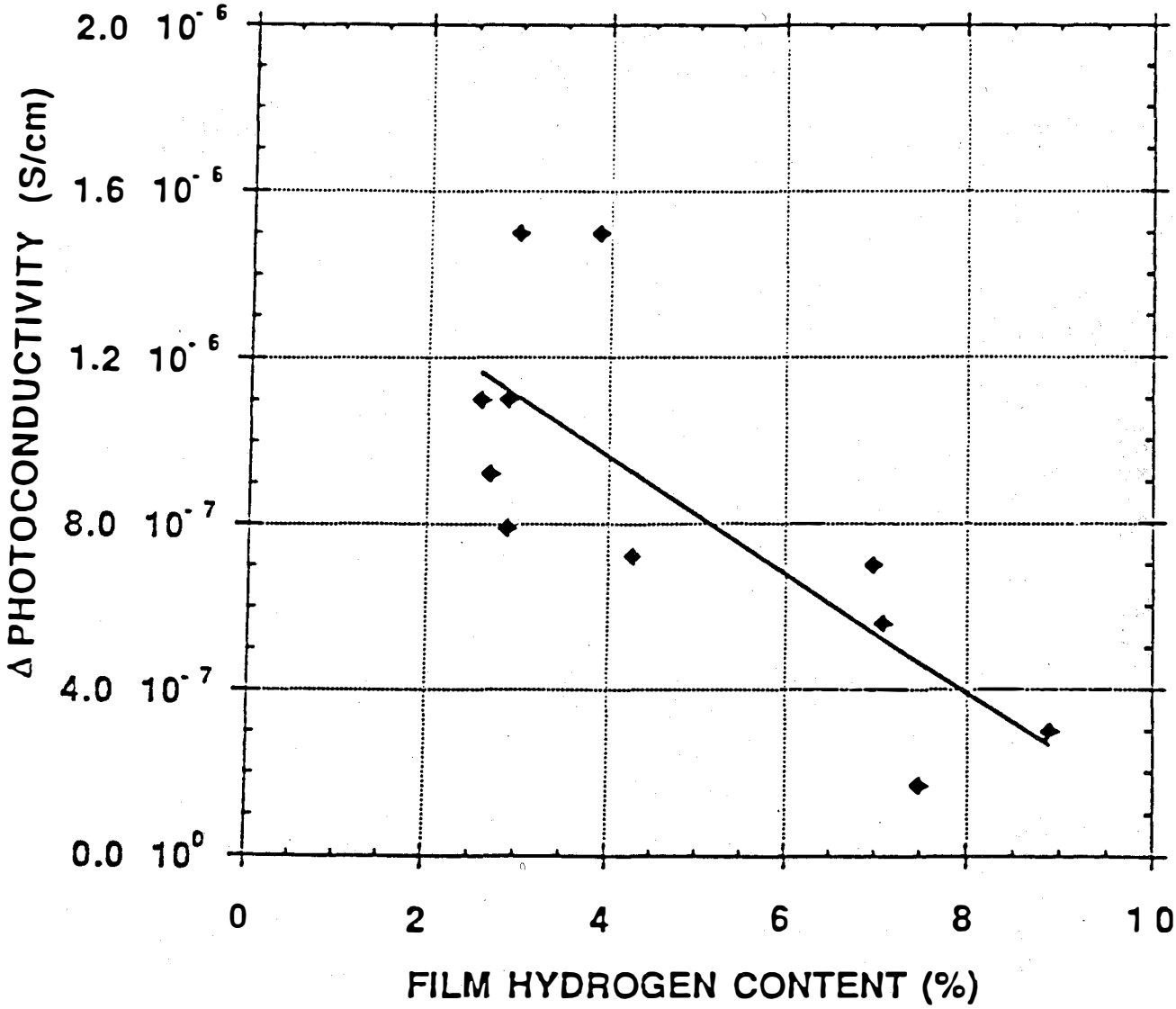

Figure 1. Excess photoconductivity (@100mW/cm^2) vs hydrogen content for a-SiGe:H films with C_{Ge} = 55-65%.

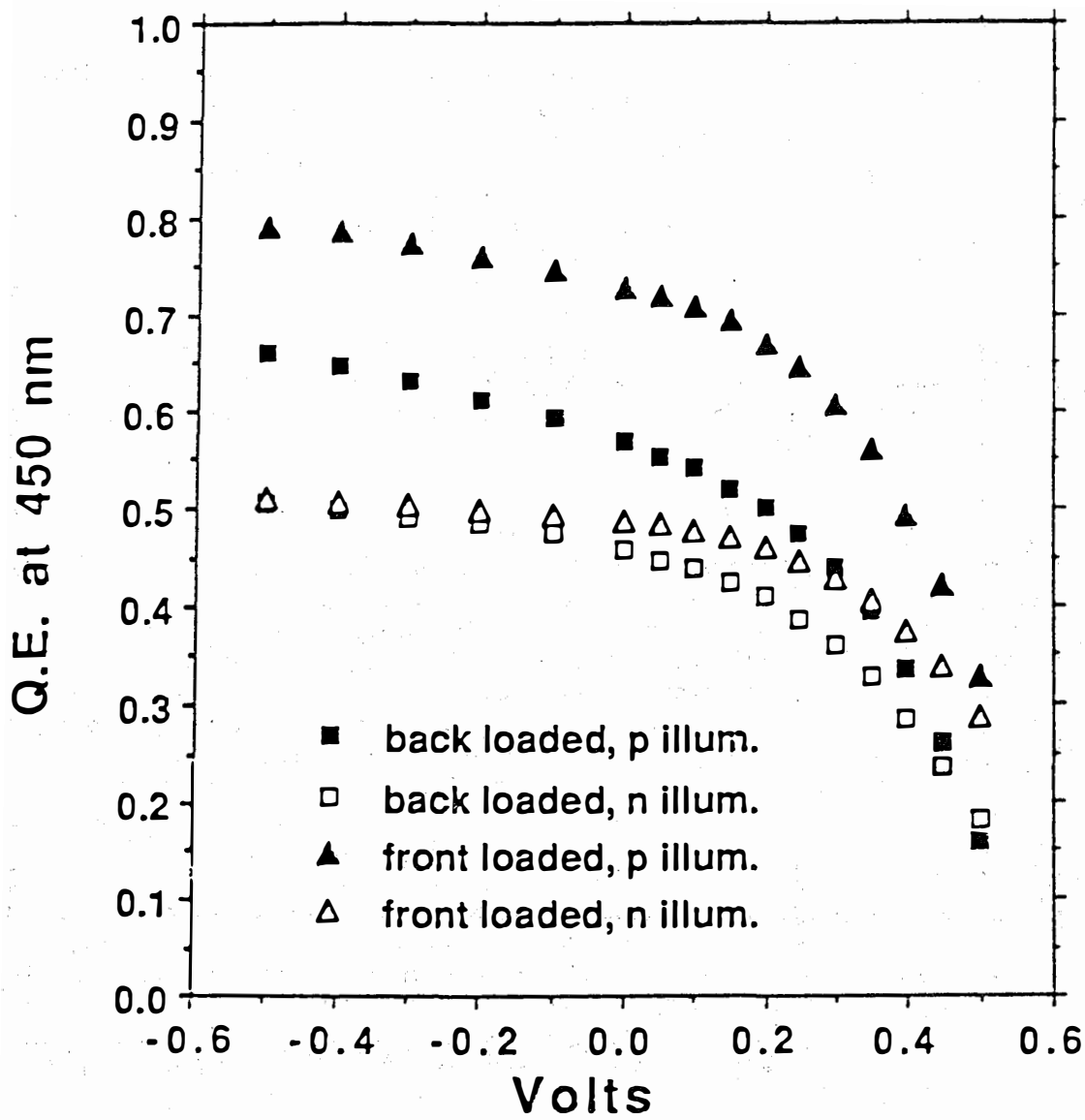

Figure 2. Voltage bias dependence of Q.E. at 450 nm for illumination through p and n-layers of front and back loaded a-SiGe:H solar cells.

Title: **Amorphous Silicon Deposition Research with In Situ Diagnostics**

Organization: Jet Propulsion Laboratory, California Institute of Technology, Pasadena, California

Contributors: Y. H. Shing, Principal Investigator; F. S. Pool, C. E. Allevato and J. M. Essick (Occidental College)

Objective

The objective of this research program is to develop electron cyclotron resonance (ECR) microwave plasma technology for the deposition of hydrogenated amorphous silicon (a-Si:H) and silicon carbon alloy thin films (a-SiC:H) for photovoltaic device applications.

Approach

A state-of-the-art electron cyclotron resonance (ECR) microwave (2.45 GHz) plasma deposition system has been developed at JPL for depositing amorphous silicon (a-Si:H) and binary alloy thin films. The JPL ECR deposition system has unique capabilities of depositing films at high substrate temperatures up to 1000°C and of performing in situ plasma diagnostic experiments. The high substrate temperature and plasma diagnostics are employed to develop necessary process conditions for depositing stable, device-quality a-Si:H and a-SiC:H alloy thin films. Photosensitive a-Si:H, diamond-like and polymer-like amorphous carbon (a-C:H), amorphous and microcrystalline silicon carbon alloy (μc-SiC:H) thin films have been deposited using the JPL ECR deposition system [1-4]. The RF bias applied to the sample stage is found to play a critical role in modifying the mechanical and optoelectronic properties of ECR-deposited films [1-2]. The substrate bias effect is attributed to the control of the low energy ion bombardment during the film growth. Photovoltaic applications of ECR-deposited films are pursued by incorporating these films in a-Si:H p-i-n a-Si:H solar cells. The optical, electrical and morphological properties of ECR-deposited a-Si:H and a-SiC:H films are characterized by infrared, visible transmission, Raman spectroscopy, light and dark conductivity measurements. Junction capacitance and constant photocurrent measurements are employed to determine the defect density and the Urbach slope for further analyzing the film quality. Diagnostic-device evaluations of ECR-deposited films are implemented by comparing the performance of ECR and RF glow discharge deposited a-Si:H p-i-n solar cells.

ECR-Deposited, Photosensitive and Conductive a-Si:H Films

The ECR deposition of photosensitive a-Si:H films has been investigated in the parameter space of substrate temperature, deposition pressure, microwave power, magnetic field profile and hydrogen dilution. It is found that microwave mode variations in ECR plasmas can produce significant changes in the ECR deposition process. Within similar ECR deposition conditions, the a-Si:H deposition rates can be varied by a factor of ten owing to the microwave mode variations. The high deposition rate of greater than 1000 Å/min can be obtained with ECR plasmas operated in the pressure region of 1 to 10 mTorr[4]. The resonant nature of ECR plasma deposition rates is demonstrated in Figure 1 as a function of the magnetic field strength. In these experiments, a-Si:H films are

deposited using hydrogen diluted silane plasmas with a hydrogen flow rate of 45 sccm and a silane flow rate of 15 sccm. The deposition rate of a-Si:H films has shown a resonant peak at the ECR condition with a magnetic field of 875 Gauss. The resonant enhancement of the ECR deposition rate is a direct result of the high plasma density under the ECR condition.

The photoconductivity of ECR-deposited a-Si:H films has a typical value of 7×10^{-5} $(\Omega\text{-cm})^{-1}$ with a photosensitivity (light to dark conductivity ratio) of 1×10^{6}; these values are comparable to the best results of RF glow discharge deposited a-Si:H films. In addition to the photosensitive a-Si:H films, ECR plasmas can also produce a new type of conductive a-Si:H film, which may contain a microcrystalline silicon phase. The ECR-deposited, conductive a-Si:H films have shown a photoconductivity up to 3×10^{-4} $(\Omega\text{-cm})^{-1}$ and a dark conductivity of 2×10^{-4} $(\Omega\text{-cm})^{-1}$. The p-type doping of the conductive a-Si:H films with a B_2H_6/SiH_4 gas phase ratio of 0.3% has produced a conductivity of 5×10^{-2} $(\Omega\text{-cm})^{-1}$.

The material properties of ECR-deposited, photosensitive a-Si:H films have been characterized by the constant photocurrent method (CPM) and the junction capacitance measurements. Figure 2 shows the spectral dependence of the uncalibrated optical absorption of a photosensitive, ECR-deposited a-Si:H film, as derived from the CPM measurements. The characteristic slope of the Urbach exponential absorption tail is determined to be 48 meV, which is comparable to the Urbach slope of device-quality, RF glow discharge deposited a-Si:H films. Junction capacitance measurements have been performed on 1 to 2 μm thick a-Si:H films deposited on heavily doped p-type Si substrates. The capacitance-temperature measurements have shown that the Fermi level of typical ECR-deposited a-Si:H films is located at about 0.72 - 0.85 eV from the conduction band mobility edge. Figure 3 shows the drive level defect density determined by AC capacitance measurements at various temperatures as a function of the depletion width. The integrated defect density of an ECR-deposited a-Si:H film with a photoconductivity of 6×10^{-6} $(\Omega\text{-cm})^{-1}$, as derived from the drive level defect density, is found to be in the range of 1 to 2×10^{16} $(\text{cm})^{-3}$. The optical bandgap of ECR-deposited a-Si:H films is determined by Tauc plots to be in the range of 1.75 to 1.85 eV. The infrared spectrum of ECR-deposited, photosensitive a-Si:H films has shown the same Si-H bonding configurations and similar hydrogen content as those of RF glow discharge deposited, device-quality a-Si:H films. However, the infrared spectrum of ECR-deposited, conductive a-Si:H films, as shown in Figure 4, indicates that the total hydrogen content is about a factor of ten less than that in the photosensitive a-Si:H film.

ECR-Deposited a-SiC:H and μc-SiC:H Films

The dependence of the ECR deposition rate of a-SiC:H films as a function of the hydrogen flow rate is similar to that of the RF deposition rate, in which a large decrease in the deposition rate is caused by a small fraction of hydrogen dilution. This behavior is quite different from the linear dependence of the deposition rate on hydrogen dilution that has been observed for a-Si:H and a-SiGe:H films. The hydrogen dilution effect in SiH_4 and CH_4 mixed gas plasmas suggests that the hydrogen etching plays an important role in depositing a-SiC:H films. The ECR deposition of μc-SiC:H films has been performed under a pressure of 15-30 mTorr, substrate temperature of 500°C to 600°C, hydrogen dilution ratio (H_2/SiH_4+CH_4) of 10-30, and microwave power of 300-400 W. The formation of an intense ECR plasma beam at the center of the plasma chamber is found to be the critical condition for depositing μc-SiC:H films. An x-ray diffraction (XRD) pattern of an ECR-deposited μc-SiC:H film is shown in Figure 5. The diffraction peak at a two-theta angle of 38.1 degrees identifies the (101) plane of hexagonal

SiC (polymorph 2H); the broad peak, centered around two-theta of 25.5°, is related to the amorphous network structures. The microstructure of μc-SiC:H films has been examined by scanning electron microscopy (SEM). Both SEM and XRD show that ECR-deposited μc-SiC:H film is a two-phase material consisting of SiC microcrystallites of about 1000Å embedded in the amorphous network. Infrared spectra of a-SiC:H films have shown broad absorption peaks of CH_n, SiH_n and SiC stretching modes. These absorption peaks indicate that bonded hydrogen in a-SiC:H films is preferentially associated with bonds to carbon. In contrast to a-SiC:H films, Figure 6 shows an infrared spectrum of an ECR-deposited μc-SiC:H film in which strong SiH_n rocking (630 cm^{-1}) and SiH stretching (2000 cm^{-1}) modes are observed. These infrared absorption features suggest that the bonded hydrogen in ECR-deposited μc-SiC:H film is shifted to silicon bonds. The infrared absorption features are also consistent with the two-phase nature of the ECR-deposited μc-SiC:H film.

Conclusions and Future Plans

Highly photosensitive a-Si:H films deposited by ECR plasmas show a light conductivity of 7×10^{-5} $(\Omega\text{-cm})^{-1}$, and a photosensitivity of 1×10^{6}. Optical bandgaps of ECR-deposited a-Si:H films are in the range of 1.75 to 1.85 eV. The integrated defect density in the mobility gap and the Urbach slope of photosensitive a-Si:H films are determined by the junction capacitance and the CPM measurements to be about $1 \times 10^{16}/cm^3$ and 48 meV, respectively. These material properties of ECR-deposited a-Si:H films are comparable to device-quality RF-PECVD deposited a-Si:H films. A new type of conductive a-Si:H films, which may contain a microcrystalline phase, has also been deposited by ECR-PECVD. The p-type doping of ECR-deposited, conductive a-Si:H films has shown a conductivity of 5×10^{-2} $(\Omega\text{-cm})^{-1}$. Infrared spectroscopy reveals that the bonded hydrogen content in the conductive a-Si:H film is about a factor of ten less than that in the photosensitive a-Si:H film.

Amorphous and microcrystalline SiC:H films have been deposited by ECR microwave plasmas using SiH_4, CH_4, and H_2 gas mixtures. Hydrogen dilution in the ECR plasma with a dilution ratio up to 5 has shown no significant effect on the optical bandgap of a-SiC:H films. The hydrogen dilution effect on the deposition rate indicates that the etching in ECR hydrogen plasmas plays an important role in the deposition of a-SiC:H films. The microcrystallinity of ECR-deposited μc-SiC:H films has been demonstrated by XRD and Raman spectroscopy. The two-phase nature of μc-SiC:H films is shown by both XRD and SEM to consist of 1000 Å SiC microcrystallites and amorphous network structures.

In our future research, the photodegradation of ECR-deposited a-Si:H films will be investigated as a function of the ECR deposition conditions. The ECR deposition of μc-Si:H films will be developed using hydrogen dilution and low-energy ion bombardment. The density and energy distribution of low-energy ions in ECR plasmas will be studied using Langmuir probe measurements. The low-energy ion bombardment effect in the ECR deposition process will be evaluated by varying the substrate bias and the magnetic field profile. Diagnostic p-i-n a-Si:H solar cells incorporating ECR-deposited and RF-deposited films will be fabricated to provide a comparative, device-oriented evaluation of the ECR deposition process.

References:

1. Y. H. Shing and F. S. Pool, Vacuum, 41, 1368 (1990).
2. F. S. Pool and Y. H. Shing, J. Appl. Phys. 68, 62, (1990).
3. Y. H. Shing and F. S. Pool, Proc. 21st IEEE PVSC, 1574 (1990).
4. Y. H. Shing and F. S. Pool, Solar Cells (submitted) (1990).

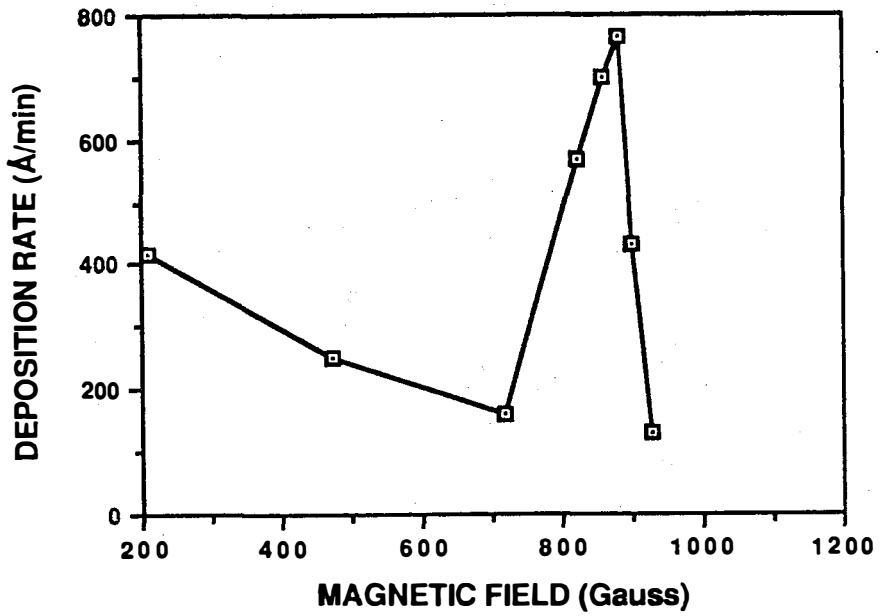

Figure 1. ECR deposition rate of a-Si:H films as a function of the magnetic field strength.

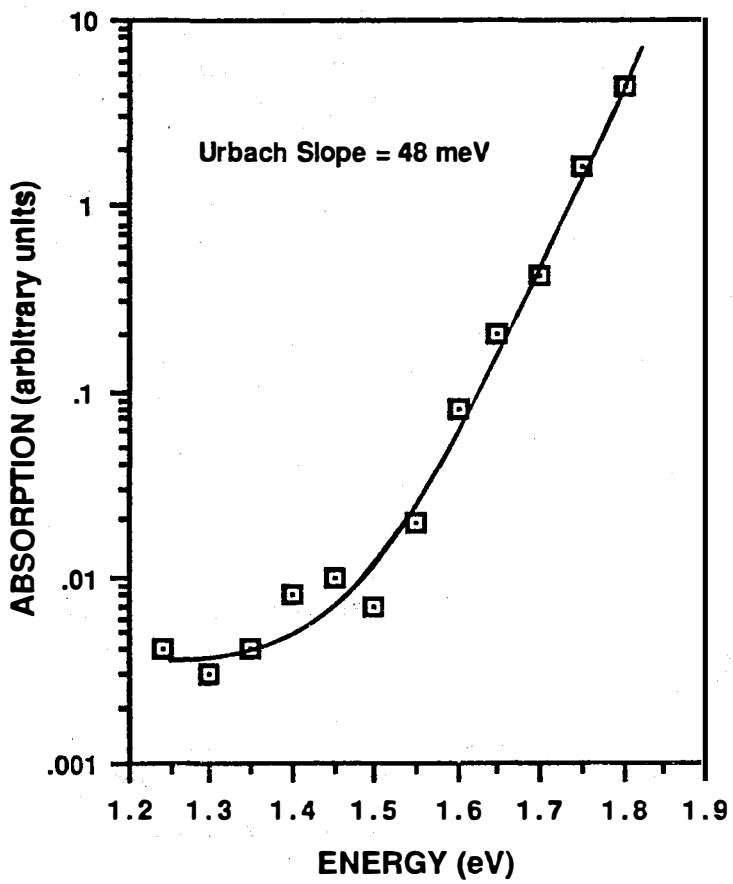

Figure 2. Spectral dependence of the uncalibrated optical absorption of a photosensitive, ECR-deposited a-Si:H film, as derived from the CPM measurements.

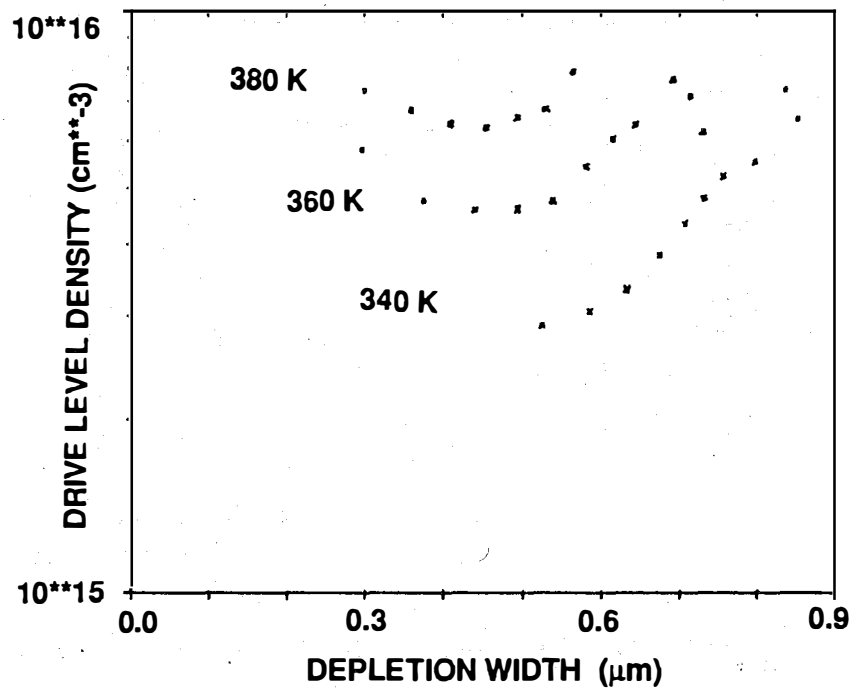

Figure 3. Drive level defect density of an ECR-deposited a-Si:H film determined by junction capacitance measurements at various temperatures.

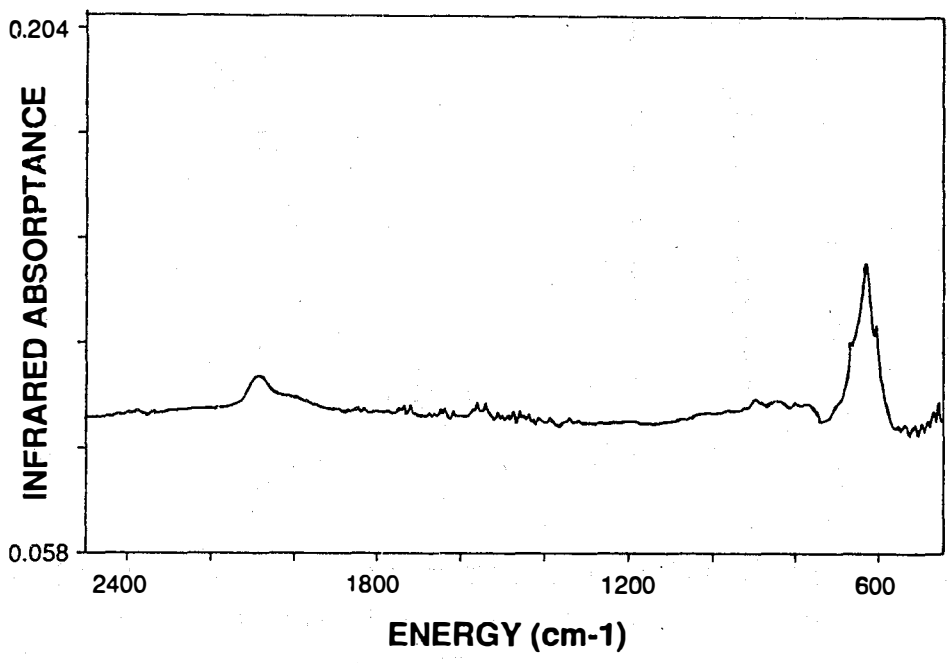

Figure 4. Infrared absorption spectrum of an ECR-deposited, conductive a-Si:H film.

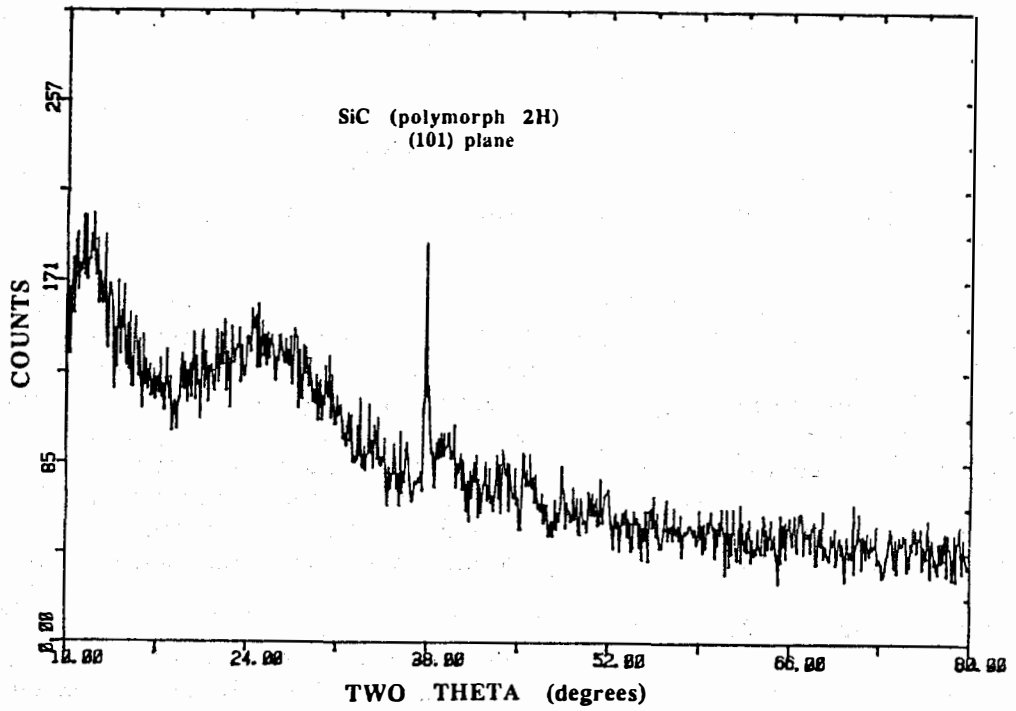

Figure 5. X-ray diffraction pattern of an ECR-deposited μc-SiC:H film.

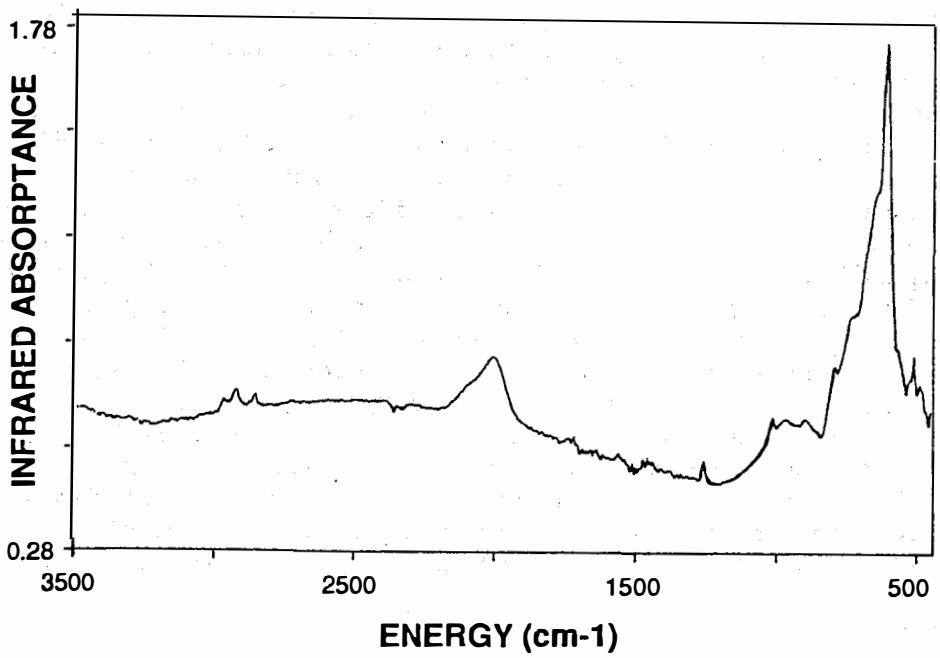

Figure 6. Infrared absorption spectrum of an ECR-deposited μc-SiC:H film.

Title: **Diagnostics of Glow Discharges Used to Produce Hydrogenated Amorphous Silicon Films**

Organization: National Institute of Standards and Technology, Boulder, Colorado

Contributors: A. Gallagher, D. A. Doughty, J. Doyle, R. Ostrom

The overall objective of this work is to explain causes of glow-discharge produced a-Si:H, a-Ge:H and a-Si:Ge:H film quality, and its dependence on deposition discharge conditions. During this contract period this involved: (1) diagnosing and preparing for publication a large array of data regarding the chemical and physical properties of rf and dc discharges used to deposit hydrogenated amorphous silicon, germane, and silicon-germane films (a-Si:H, a-Ge:H, a-Si:Ge:H), (2) designing, constructing, trouble-shooting, improving and utilizing a new film-diagnostic apparatus. This apparatus provides detailed pictures of the freshly-deposited film surfaces with individual-atom resolution.

Diagnosis of Germane Discharge Data

The production of high quality lower band-gap a-Si:Ge:H films, for use in tandem with a-Si:H, would be aided by an improved understanding of pure germane plasma chemistry and of the conditions that produce optimum a-Ge:H film quality. We have therefore applied to germane discharges many of the measurement techniques previously used on silane discharges. These include measurement of the spatial distribution of light emission I(x) and of film deposition D(x) between the electrodes, stable gas and film-growth stoichiometry, and surface reaction probability (β) of the depositing radicals. The I(x) results indicate that the pure germane rf discharge at typical pressures and electrode gap is in a different self-sustaining regime than for a silane discharge. This produces more asymmetry in the electrode ion bombardment in germane, which can be important but is not the major cause of poor a-Ge:H film quality. The D(x) data demonstrate that deposition is dominated by a radical that diffuses to the electrodes without reacting, as occurs in silane discharges. Fewer higher germanes are produced, compared to higher silanes, but again this cannot directly explain the large film-quality difference. β for a-Ge:H deposition at 200°C is 0.60, compared to 0.37 for a-Si:H deposition. This difference indirectly supports the following proposed cause of the poorer a-Ge:H quality. The initial radical deposition produces a very H-rich surface layer that must spontaneously undergo Ge-Ge bonding with H_2 release to produce the subsurface and bulk film. From enthalpies it can be shown that this H_2 elimination reaction is much more exothermic for germane than for silane, hence the resulting Ge-Ge bonding in the film tends to be much more disordered. Thus, some form of Ge-Ge bond strengthening during growth is needed. This occurs in post-deposition shakeup by energetic ion bombardment, in etching by H atoms in H_2 mixtures, or by F in fluorinated gases. A detailed report has been prepared for publication.

Diagnosis of Silane dc Discharge Data

Comparison of I(x) and D(x) data in silane dc discharges shows that almost all depositing radicals are produced very close to the cathode, where there is very little light emission. The light emission is concentrated in the center of the discharge and tracks the energetic electron collisions that also cause silane dissociation into depositing radicals. This implies that most dissociation in the dc discharge is not a result of electron collisions. Energetic ion collisions are clearly implicated, as ion energies rapidly increase near the

cathode. These impact on silane, causing showers of energetic radicals that induce further dissociations. Typical dc silane discharges operate at 600 V, whereas normal rf deposition discharges work at 100-200 V peak-to-peak, and the ions do not obtain sufficient energy in the rf cathode sheath to cause this. However, when very high powers are used to obtain high deposition rates or when pressures are lowered this can occur in rf discharges as well, leading to a different mix of depositing species as well as frequent energetic surface bombardments. Details are scheduled for publication in Physical Review A.

Diagnosis of Mixed Silane, Disilane, and Germane Discharge Data

In silane discharges a large fraction of initial silane decomposition produces higher silanes, most of which are subsequently dissociated. Similarly, discharges in disilane produce large amounts of silane which will be subsequently decomposed at high power/flow. Thus, the discharge chemistry of disilane and of disilane-silane mixtures also occurs in normal silane discharges. Analysis of our measurements of stable gas stoichiometry in disilane and mixed silane disilane discharges has thus provided a picture for the dominant plasma chemistry in these as well as normal silane discharges. In all cases H atom and SiH_2 radical reactions dominate the gas chemistry, while SiH_3 plus some disilane radicals dominate the film deposition. In mixed SiH_4/GeH_4 and Si_2H_6/GeH_4 we conclude that H atoms, GeH_2 and SiH_2 dominate the gas chemistry, while SiH_3 and GeH_3 dominate film deposition. Details are in preparation for publication.

Construction and Operation of Scanning Tunneling Microscope for Film Analysis

During this contract period we have constructed an ion and titanium pumped UHV chamber, containing a scanning tunneling microscope (STM), a low energy electron diffraction (LEED) apparatus, plus sample and tunneling-tip annealing and cleaning setups. This is attached through a gate valve to a turbomolecular-pumped chamber, which operates as a load-lock for sample entry as well as a discharge chamber where the a-Si:H and a-Si:Ge:H films are deposited. After film deposition, the discharge chamber is evacuated and the substrate is cooled to room temperature in ~1 minute, then transferred into the UHV chamber for surface analysis.

In order to measure the shape and chemical character of the film surface with individual-atom resolution, it is very helpful to deposit the film on a large area that is initially atomically-flat and clean. We have achieved this so far by cleaving GaAs crystal wafers in vacuum; areas of many square microns without steps and containing at most a few above-plane atoms are now regularly obtained in this way. We have also annealed Si(111) wafers to ~1200°C in UHV, but so far have not achieved equivalent atomically-flat Si surfaces for film deposition studies. The entire vacuum system is vibration isolated above 1 Hz, and the STM is isolated inside the vacuum above 3 Hz. Surface height resolution of ~0.2Å is thereby achieved. The etched W probe tips are oxide-free and produce appropriately rapid dependence of tunneling current on height. However, their atomic-scale tip shape is not controllable or reproducible, and the image of the sample surface can change any time during operation by the addition or removal of individual atoms or molecules from the probe tip. This remains a primary problem in carrying out and in interpreting STM measurements. Nonetheless, we now often obtain ostensibly correct atomic images of crystal substrates, and we are preparing to deposit a-SiH on these.

Title: **Research on Amorphous-Silicon-Based Thin Film Photovoltaic Devices****

Organization: Solarex Corporation, Thin Film Division
826 Newtown-Yardley Rd., Newtown, PA 18940

Contributors: A. Catalano, Program Manager; L. Yang, Task I Project Leader; J. Newton, Task II Project Leader; J. Morris, Task III Project Leader; R.R. Arya, M. Bennett, Y. Li, B. Fieselmann, S. Wiedeman, K. Rajan, G. Wood, C. Poplawski, B. Goldstein

Introduction

Multijunction cells and modules offer the potential for achieving high conversion efficiency while overcoming the principal shortcoming of a-Si:H, namely the light-induced degradation. Amorphous silicon based devices are attractive because they are simply fabricated at low temperature from abundant non-toxic, low cost materials, have very high absorption coefficients which permits useful devices of submicron thickness, and the processes are environmentally responsible in keeping with the spirit of renewable energy.

In order to achieve the goal of developing low cost, stable, high efficiency modules, we have undertaken a program consisting of three tasks that address the important technological issues required to meet the program's first year (FY91) goal of obtaining 8.8% efficient, stable modules*. These tasks are 1) semiconductor materials research, 2) non-semiconductor materials research, and 3) module research.

Notable accomplishments within these tasks are:

- The demonstration of aperture area conversion efficiencies of 9.27% (SERI verified) in modules with an area > 900 cm^2, and 98% area utilization.
- The demonstration of excellent long-term stability in triple junction cells and modules.
- The development of an "ad hoc" model that relates the time dependent performance of triple junction devices to device design, and operating temperature.
- An understanding of the relationship between the structural properties of the a-SiGe:H alloys, their relationship to preparation conditions, and the influence on device performance and stability.

---

* 600 hrs., AM1.5 exposure, 50°C; area ≥ 900 cm^2.

** This work was supported under Solar Energy Research Institute ZB-7-06003-2 and ZM-19033-1.

- The development of a comprehensive model detailing optical losses within triple junction devices.

The following is a review of progress on a task-by-task basis.

Task I. Semiconductor Materials Research

Work performed within Task I has focused on developing 1) improved a-SiGe:H alloy materials and devices, 2) useful microcrystalline doped layers, 3) a model to predict optical losses in the complex multijunction devices, and 4) a useful working model of the degradation of multijunction devices.

a-SiGe:H alloys and devices have been prepared by dc or rf glow discharge decomposition of either silane or disilane, and germane feedstocks. Photothermal Deflection Spectroscopy (PDS), light and dark conductivity and Steady State Photoconductive Grating (SSPG) measurements have been the primary tools used for the characterization of transport properties. The structure of the materials have been inferred from FTIR and Raman Spectroscopy measurements.

We have previously shown that amorphous alloys between Si and Ge exhibit a preference for homonuclear bonding (1). Hydrogen dilution has been shown to ameliorate this condition, improving the diffusion length. Infrared transmission measurements have shown that a-SiGe:H films prepared from the undiluted feedstock contain a high concentration of dihydride bonds. The dihydride bonding is seen to occur only in the alloys and even for a small addition of germane. 5:1 (reactants + hydrogen:reactants) hydrogen dilution acts to reduce the concentration of the dihydride bonds and improve the stability. Figure 1 plots the normalized efficiency after

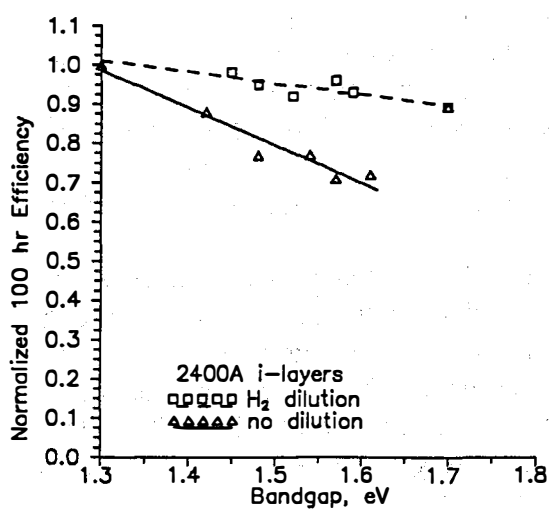

Figure 1. Normalized efficiency of a-SiGe:H devices as a function of the optical bandgap of the i-layer.

100 hrs. of AM1.5 light exposure for single junction a-SiGe:H devices as a function of the optical bandgap of the 2400Å thick i-layer. A substantial decrease in the rate of degradation occurs as germanium is added to reduce the optical bandgap of the alloy in both the undiluted and diluted case. However, a much higher rate of degradation is seen in the case of films prepared without hydrogen dilution as is expected for films with a higher dihydride content. In all cases, the hydrogen diluted alloy is more stable than a-Si:H.

SSPG measurements of the minority carrier diffusion length, L, in the alloys are a good indicator of device performance. For the most part the SSPG measured values of L scale with the fill factor for hydrogen diluted a-SiGe:H alloys. However, caution should be used when comparing the values of L determined by the method from different laboratories since surface states and trace level doping appear to considerably influence the measurements. As an illustration of the importance of surface states, a series of films of identical composition were prepared with thicknesses varying from on the order of several thousand Angstroms up to two microns. The value of L increases with thickness and appears to approach a limiting value above 2 microns. The Urbach Energy, E_0, likewise, decreases with film thickness. Although one may consider this phenomenon to be the result of structural improvements as the film becomes thicker, quantitative analysis by ourselves (2) and others (3), (4) suggest surface effects are primarily responsible for the effect. Although the minority carrier diffusion length decreases with optical bandgap, satisfactory devices can be prepared even at bandgaps as low as 1.22 eV where device fill factors of over 0.5 have been obtained. In addition to the germanium content of the i-layer, bandgap profiling can influence performance as demonstrated in several references (5), (6). The reader is referred to these references for further information.

Modeling of the optical absorption in multijunction device structures has been performed to identify the major current losses in such devices. An important feature of this modeling is the quantitative treatment of scattering and reflection occurring at interfaces within these complex multilayer structures. This includes contributions from the front and rear contacts as well as absorption by each of the many layers within the device. The three most important losses in the device occur in the tin oxide front contact (4.1 mA/cm^2), the rear contact (ITO-1.67 mA/cm^2, Ag 4.04 mA/cm^2) and the tunnel junction between the first and second junction (1.14 mA/cm^2).

By combining the results of stability measurements of a-SiGe devices with our previous model for the behavior of amorphous silicon devices, we have derived an "ad hoc" model for the time dependent behavior of tandem and triple junction devices. All amorphous silicon p-i-n devices we have examined to date, with the exception of those with trace doping in the i-region, exhibit a semilogarithmic decrease of efficiency with time (7). This dependence has also been extended (8) to include the operating temperature and the thickness of the i-region to give a fairly complete expression for the time dependent performance. Bennett and Rajan (9), comparing the degradation of mechanically interconnected and vertically interconnected cells have observed that the overall rate of degradation is simply the arithmetic average of the individual single junction components. By combining the stability data of Figure 1, and assuming the thickness and temperature dependence of a-Si:H devices holds for the a-SiGe:H alloy devices allows one to model performance of a triple junction device.

$$\eta(t) / \eta(0) = \frac{1}{3}\sum_{i=1}^{3} [1.1 - (K_i (d_i)^{0.54} \exp (0.19/kT)) \log t] \quad (1)$$

where $\eta(t)$ and $\eta(0)$ are the efficiencies after time t, d_i is the thickness of the i th junction, T is temperature and K_i is rate constant for the i th junction. Several important conclusions emerge from this model. First and foremost is that the overall stability of a triple junction device is far better than the comparable single junction solar cell. Secondly, the most important factor governing the rate of degradation is the thickness of the middle junction cell. Figure 2 summarizes the thickness dependence expected for triple junction devices with 1.7eV/1.7eV/1.45eV optical bandgaps for i_1,i_2 and i_3, respectively. At a typical operating temperature of 50°C, the model predicts a degradation of only 9% after 1000 hrs., the equivalent of approximately one year outdoors. One somewhat surprising result of the model is the relative lack of importance of the optical bandgap of the rear cell to stability. For lower bandgaps, the thinner bottom junction coupled with the lower degradation rate of these alloys might be expected to lead to improved stability. Although there is an improvement, the effect is seen to be small because the rate of degradation of the bottom cell is low and remains low over the range of meaningful thicknesses, compared to the far larger rate of the middle junction cell.

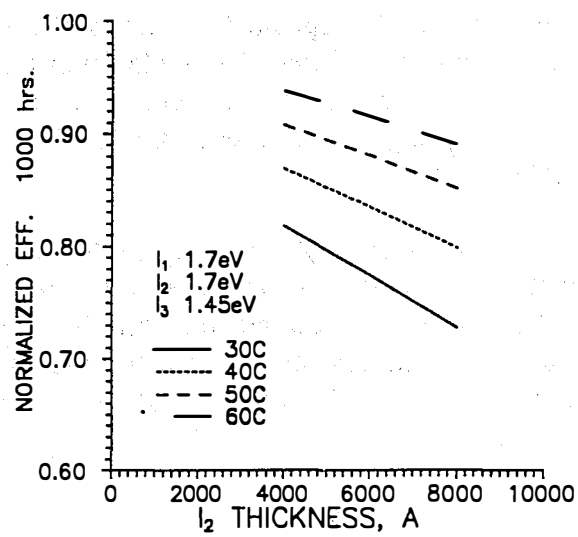

Figure 2. Calculated values of normalized efficiency after 1000 hrs. of AM1.5 exposure for triple junction devices as a function of middle junction thickness.

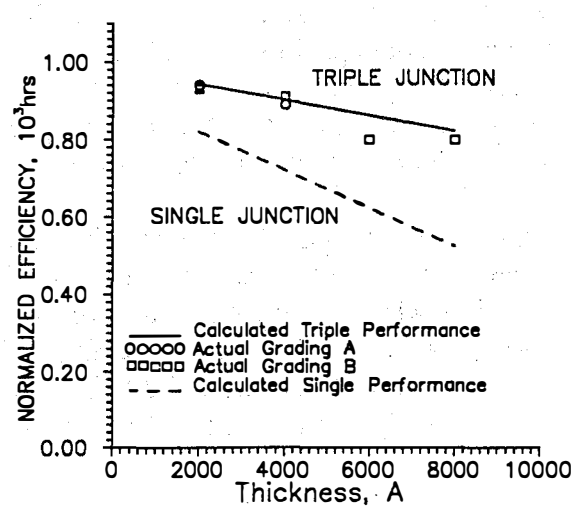

Figure 3. Comparison of the calculated efficiencies with experiment. Also shown for comparison is the behavior expected for single junction cells.

Figure 3 compares the calculated rate of degradation for a series of triple junction cells with the values found experimentally. The devices are plotted as a function of the thickness of the middle junction i-layer. Very good agreement with the model is found. Of special importance is the fact that devices with a 4000Å thick middle junction i-layer have been prepared with a 9.6% initial that retain 90% of their initial efficiency after 1000 hrs. light exposure. Also shown for comparison are the model results expected for single junction cells. The comparable 4000Å thick single junction, 1.7eV device is expected to retain only 70% of its initial efficiency.

Task 2. Non Semiconductor Materials

As discussed in the previous section, the front and rear contacts of the device account for the majority of the optical losses in the device. The front contact of a superstrate device performs the functions of electrical contact as well as light transmission and scattering. These functions are somewhat contradictory, since, in general, the thicker film will be more conductive and scatter light more effectively at long wavelength, but will of course have a lower transmission. The rear contact of the device dominates the long wavelength response of the device. The reflectivity of the rear contact is of special importance in multijunction cells since a limitation in the red must be compensated for by adding additional germanium to the i-layer, resulting in a lower performance for the device overall.

The baseline front contact we have employed is textured tin oxide deposited by atmospheric chemical vapor deposition (CVD). As an alternative, we have also explored zinc oxide deposited by atmospheric and low pressure CVD (LP-CVD). For the rear contact reactively sputtered ITO/Ag has been selected as a baseline process with work having begun on both sputtered and LP-CVD ZnO/Ag as a low cost alternative to the baseline process.

Specular or textured ZnO films have been prepared by organometallic LP-CVD using diethyl zinc as a feedstock. Typical specular films with 0.8 micron thickness have an absorbance of 0.05 over the visible with a sheet resistance of 60-100 ohms/sq. The temperatures required for the deposition are generally less than 200°C. The material is satisfactory for ohmic rear contacts. Devices made with textured ZnO for the front contact show an impressive peak quantum efficiency as high as 0.9 with a 700 nm response of 0.65.

The ITO/Ag rear contact has been scaled to cover substrate areas greater than 900 cm^2. Although the method is sensitive to process conditions such as temperature and flow rate the greatest difficulty associated with the contact may be an interfacial reaction between ITO and silver. Although a reflectivity of 95% would be expected from such a combination, actual measurements on textured surfaces yield much lower values. The use of a diffusion barrier between the ITO and Ag films yields a major improvement in reflectivity.

Task 3. Modules

Amorphous silicon triple junction modules have been fabricated using the device structures a-SiC:H/ a-Si:H/ a-SiGe:H and a-Si:H/ a-Si:H/ a-SiGe:H. In all cases, an ITO/Ag rear contact

was used to enhance red response in conjunction with the textured tin oxide front contact. Laser patterning of all three layers was performed to provide the monolithic interconnections between adjacent segments. Reduction of laser spot size to a diameter of approximately 0.001" and the use of high precision positioning systems allowed compression of the adjacent tin oxide, semiconductor, and ITO/Ag scribes, yielding an overall active area/aperture area ratio of 98%. The segment width was chosen to maximize efficiency as per Gupta, et al. (10). One of the immediate problems encountered when fabricating interconnected modules was a problem of low shunt resistance. The origin of the low resistance path appears to be associated with the laser patterning of the ITO/metal layer. Isolated defects occur due to conducting particulate debris that is ejected by the laser. Another shunt path was found to be crystallization of the semiconductor layers at the edge of the trench created by the laser. This was disclosed by microscopic laser Raman spectroscopy which clearly disclosed a narrow border usually on the order of only a few microns. The crystallization of the region was decreased to acceptable levels by lowering laser power.

The uniformity of the performance of modules was examined by using laser patterning to divide the entire surface of the module into roughly 1 cm^2 devices which then were automatically accessed and measured to arrive at a topographic map of V_{oc}, FF, I_{sc}, etc.

The best triple junction submodule employed an a-Si:H/a-Si:H/a-SiGe:H configuration and had a SERI measured aperture area efficiency of 9.27% for the 939.6 cm^2 device. Table 1 summarizes the test data. A similar efficiency was obtained from outdoor measurements performed at Solarex. It is noteworthy that the active area/aperture area ratio was 98% in this module.

Table I

Operating Parameters of Record Setting Triple Junction Module.
Measurements performed at 25°C at SERI.

V_{oc}, Volts	I_{sc}, mA	V_{mp}, Volts	I_{mp}, mA	Power, Watts	Efficiency, % Aperture Area	Aperture Area, cm^2
66.75	206.4	52.48	166.	8.712	9.27	939.6

References

1. L. Yang, A. Catalano, R.R. Arya, M. Bennett, I. Balberg, "Effect of Low Level Boron Doping on Transport Properties of a-Si:H and a-SiGe:H Alloys", Mat. Res. Soc. Symp. Proc., Vol. 149 (MRS, Pittsburgh, 1989), pp. 563-568.

2. L. Yang, I Balberg, A. Catalano and M. Bennett, "Strong Thickness Dependence of Photoelectronic Properties in Hydrogenated Amorphous Silicon", Presented at the MRS Spring Meeting 1990.

3. H. Fritzche, in Semiconductors and Semimetals, Vol. 21, part C, edited by J. Pankove, Academic Press, Orlando, 1984, p. 309.

4. H. Curtins and M. Favre in Advances in Disordered Semiconductors - Vol. 1: Amorphous Silicon and Related Materials, Vol. A, edited by H. Fritzche, World Scientific, Teaneck, N.J., 1989, p. 329.

5. S. Guha, J. Yang, A. Pawlikiewicz, T. Glatfelter, R. Ross, S.R. Ovshinsky, "Band-Gap Profiling for Improving the Efficiency of Amorphous Silicon Alloy Solar Cells", Appl. Phys. Lett. **54** (23), 5 June 1989, pp. 2330-2332.

6. R.R. Arya, M.S. Bennett, K. Rajan, A. Catalano, "Role of Interfaces on the Performance and Stability of a-SiGe:H P-I-N Solar Cells", Proceedings of the 9th E.C. Photovoltaic Solar Energy Conference (Freiburg, Germany, 1989), pp. 251-254.

7. A. Catalano, M. Bennett, R. Arya, K. Rajan, J. Newton, "Impurity and Temperature Effects on the Rate of Light-Induced Degradation in a-Si:H p-i-n Devices: Implications to Device Design", Proceedings of the 18th IEEE Photovoltaic Specialists Conference (IEEE, N.Y., 1985), pp. 1378-1382.

8. A. Catalano, "Advances in a-Si:H Alloys for High Efficiency Devices", Proceedings of the 21st IEEE Photovoltaic Specialists Conference (IEEE, N.Y., 1990), to be published.

9. M. Bennett and K. Rajan, "Stability of Multi-Junction a-Si Solar Cells", Proceedings of the 20th IEEE Photovoltaic Specialists Conference (IEEE, N.Y., 1988), pp. 67-72.

10. Y. Gupta, H. Liers, S. Woods, S. Young, R. DeBlasio, L. Mrig, "Optimization of a-Si Solar Cell Current Collection", Proceedings of the 16th IEEE Photovoltaic Specialists Conference (IEEE, N.Y., 1982), pp. 1092-1101.

Major Project Reports

"Progress on High Performance Multijunction a-Si:H Alloy Based Solar Cells and Modules", A. Catalano, R.R. Arya, M. Bennett, L. Yang, Y. Li, B. Fieselmann, S. Wiedeman, J. Newton, J. Morris, K. Rajan, G. Wood, C. Poplawski, B. Goldstein, Presented at the 10th SERI PV AR&D Review Meeting (SERI/CP), Denver, Colorado, 1990.

"Research on High-Efficiency, Large Area, Amorphous Silicon Based Solar Cells", A. Catalano, Final Subcontract Report for Period 1 February 1989 - 28 February 1990, Contract No. ZB-7-06003-2, Report No. SERI/TP-211-3906, Solarex Thin Film Division.

Title: **Studies on the Relative Effects of Charged and Neutral Defects in Hydrogenated Amorphous Silicon**

Organization: Department of Physics and Astronomy
University of North Carolina
Chapel Hill, North Carolina 27599-3255

Contributors: Professor M. Silver; Drs. Dashing Han, Keda Wang, M. E. Zvanut and Mr. M. Kemp

The objectives of our research program were to evaluate the relative effects of neutral and charged defects by theoretical and experimental means. In this endeavor, we collaborated with many other groups. Our most extensive work was with Howard Branz of S.E.R.I. We also worked closely with Professor Bassler of the University of Marburg FRG and were kindly supplied with samples from Alan Deahoy of Chronar.

Experimentally we have concentrated on electroluminescence in p/i/n devices of a-Si:H as a function of Temperature, Voltage and Photodegradation. We also have studied transient space charge limited currents before and after photodegradation in a-Si:H n/i/n structures. These results show that both the radiative and non-radiative life-times are temperature dependent giving insight into the recombination mechanisms. Further, the transient space charge limited currents show little capture by deep states other than the band tails but after photodegradation, capture by the deep photogenerated states is apparent. Theoretically we have developed a simple model to explain the E.L. results. Further, we have shown that the long range coulomb potential has a great effect upon the recombination rate constant.

Experimental Research

In figure 1 we show the transient space charge limited current before and after photodegradation. In state A, before degradation the decay of the current with time is small indicating little capture by deep states. On the other hand in state B, after degradation, there is a larger decay followed by flat regions. This result indicates that a deep state is being generated by the photodegradation process. We estimate that these states lie only 0.45 e.v. below the conduction band. If these new states are T_3^0 then the double occupied state T_3^- is relatively shallow.

The logarithm of the E.L. signal divided by the forward bias current vs. T should be a straight line providing that the radiative life-time is independent of T. Our results shown in figure 2 show that at high temperature, the radiative life-time is constant but increases as T decreases at lower temperature. These results show that a pure distant pair-tunneling model cannot work.

Theoretical Research

Most theories on hopping do not take into account the modification of the density of states near a coulomb center. Simple models for the density of band tail states are

$$1)\ g(\varepsilon) = g_c \exp\left[(\varepsilon - \varepsilon_c)/kT_o\right]$$

where g_c is the density of states at the band edge ε_c and kT_o characterizes the width of the tail. We showed that near an oppositely charged coulomb center, $g(\varepsilon)$ must be modified to:

2) $g(\varepsilon,r) = g_c \exp[(\varepsilon - \varepsilon_c + e^2/4\pi\varepsilon r)/kT_o$

where r is the distance between a tail state and the coulomb center. Since hopping depends upon $g(\varepsilon,r)^{-1/3}$ the hopping transport toward the coulomb center is greatly enhanced and the recombination life-time shortened compared with what occurs far from a charged center.

Publications

"Current-Voltage Characteristics - What do Experiments Really Tell Us?" (with Finley Shapiro), MRS 149, 315 (1989).

"Electronic Transport at Low Temperatures in Amorphous Silicon" (with W. E. Spear) MRS 149, 351 (1989).

"Zinc Oxide Varistor Time Response" (with F. A. Modine and R. W. Major - Oak Ridge National Laboratory; L. B. Bergman and S.-I. Choi - UNC/Chapel Hill), Advances in Varistor Technology 3, 176-185 (1989).

"A Unified Model for Exponential Band Tails, Optoelectronic Properties and Metastabililty in A-Si:H Based on Charged Dangling Bonds" (with G. Winborne - UNC/Chapel Hill; H. Branz - S.E.R.I.; L. Pautmeier and H. Bassler - Philipps University), Journal of Non-Crystalline Solids 114, 244-246 (1989).

"Experimental Determination for the Transition Temperature Between Ballistic and Hopping Controlled Recombination in a-Si:H (with M. E. Avanut, K. Wang and D. Han) MRS 192, 305 (1990).

"Defect Thermodynamics, Inhomogeneity and the Density of Gap States in Hydrogenated Amorphous Silicon." (with H. M. Branz) MRS 192, 261 (1990).

Papers Submitted for Publication

"Potential Fluctuation Due to Inhomogeneity in Hydrogenated Amorphous Silicon and the Resulting Charged Dangling-Bond Defects," with H. Branz. To be published Phys. Rev. B 1990.

"Temperature and Current Dependence of Electroluminescence (with K. Wang, D. Han and M. E. Zvanut) Phil. Mag. 61 (to be published 1990).

"Electroluminescence Studies of Recombination in Hydrogenated Amorphous Silicon p-i-n devices. To be published Solar Cell. 1990.

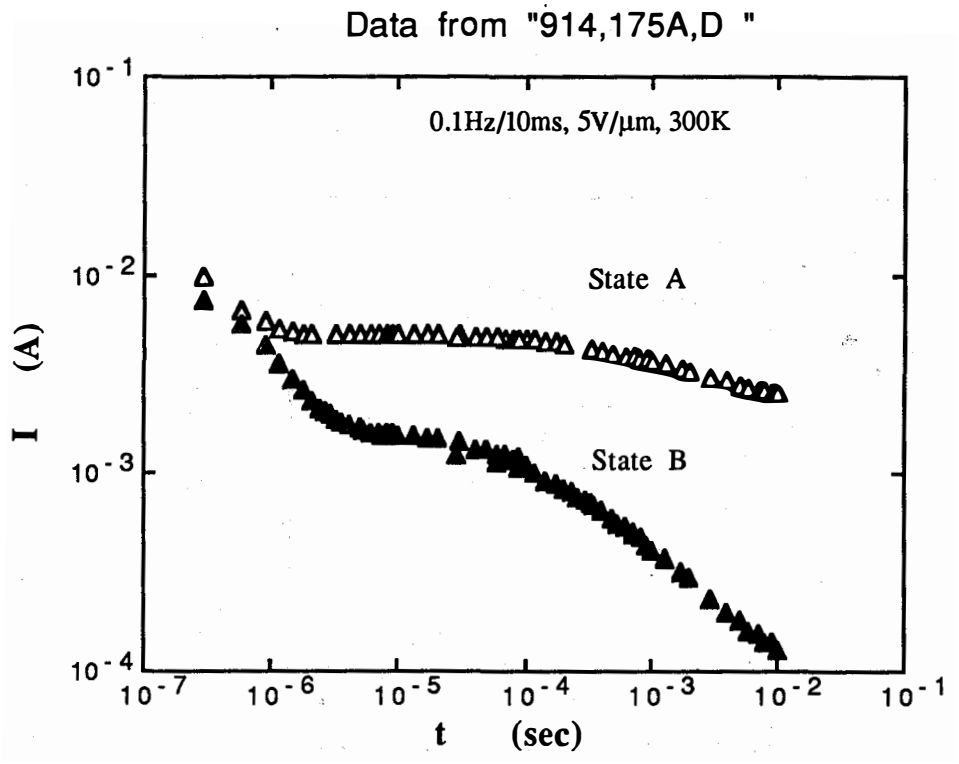
Data from "914,175A,D "
0.1Hz/10ms, 5V/μm, 300K
State A
State B
I (A)
t (sec)
10-1
10-2
10-3
10-4
10-7
10-6
10-5
10-4
10-3
10-2
10-1

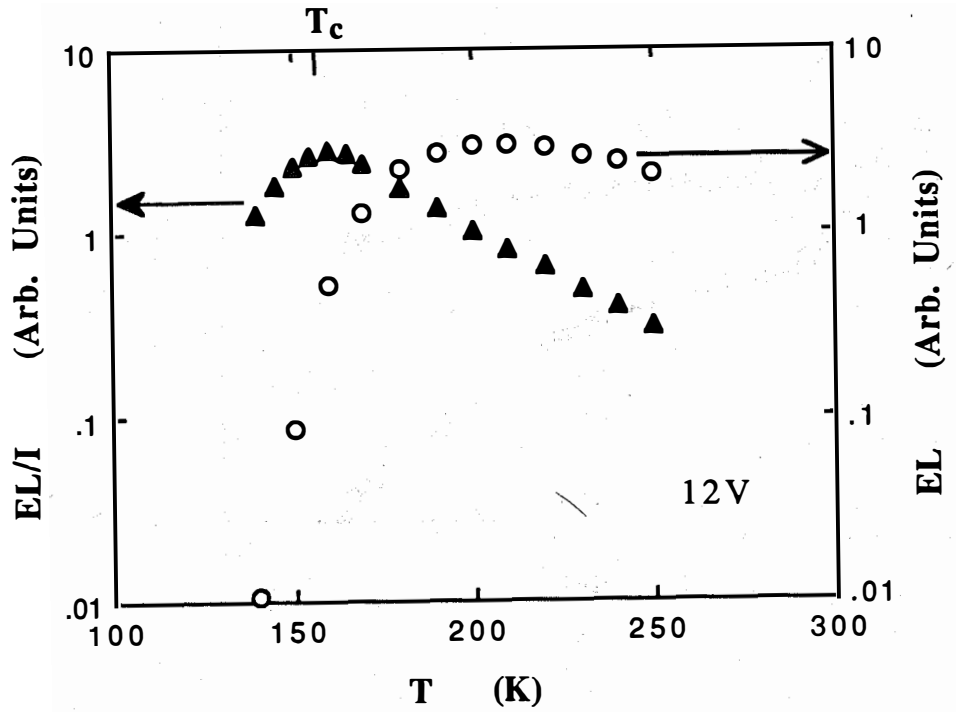
Tc
10
1
.1
.01
EL/I (Arb. Units)
10
1
.1
.01
EL (Arb. Units)
12V
100
150
200
250
300
T (K)

Title: **Investigations of the Origins of Light-Induced Changes in Hydrogenated Amorphous Silicon**

Organization: University of Oregon, Eugene, Oregon

Contributors: J. David Cohen (Principal Investigator), Tom Leen, Randy Rasmussen, Thomas Unold

The primary research goals of this project are to elucidate the basic mechanisms by which a-Si:H degrades with long term light exposure. During the past year this work has been concentrated on a finer assessment of the role of extrinsic carbon impurities on enhancing such degradation.

The Carbon Impurity Dependence of Light-Induced Metastable Effects in Undoped a-Si:H

We have continued to study samples in which a particular impurity is periodically modulated spatially during growth by switching the gas phase mixture during growth in a glow discharge reactor. Switching such gas mixtures every 10 to 15 minutes results in a spatial variation within the sample on a 1000-3000Å distance scale. These samples are then SIMS analyzed[1] to deduce the actual impurity profiles, and are also profiled using the drive-level capacitance technique[2,3] to determine the spatial variation of deep defects before and after light soaking.

We have continued to focus this work on the effects of *carbon* impurities which have been incorporated in our samples by small admixtures of methane gas to the discharge. In Fig. 1(a) we see a representative SIMS profile on one such sample. The carbon impurity concentration is seen to vary between roughly 0.9at.% to less than 0.1at.% in the two regions, respectively. The hydrogen concentrations are also observed to vary slightly. However, by growing films with and without a 50% Ar dilution, the relative concentrations of carbon and hydrogen could be varied so that we could resolve any possible ambiguity between these two cases in our results.

The capacitance profiles obtained for this sample before and after light soaking are shown in Fig. 1(b) and both show a periodic variation exactly matching the period of the carbon profile in Fig. 1(a). The variation in the light-soaked state B, however, is much larger, indicating a much larger increase in defects after light-soaking in the carbon-rich regions than in the carbon-poor regions.

While the curves in Fig. 1(b) appear saw-tooth like in contrast to the more square-wave dependence of the SIMS impurity profiles, this is actually an artifact due to the finite spatial resolution of the capacitance method. By numerically modeling the capacitance profiling data assuming a particular defect density for each region we were able to reproduce the experimental curves quite accurately [Fig. 1(d)] with the nearly square-wave spatial variation of deep defects displayed in Fig. 1(c). To get this level of agreement, however, we found it was necessary to include a parameter specifying the abruptness with which the electronic properties changed between the two spatial regions. The value of this abruptness parameter for this sample was 450±50Å in state B but somewhat longer (650±100Å) in state A. This indicated a smoother variation of electronic properties in the dark annealed state than after light soaking.

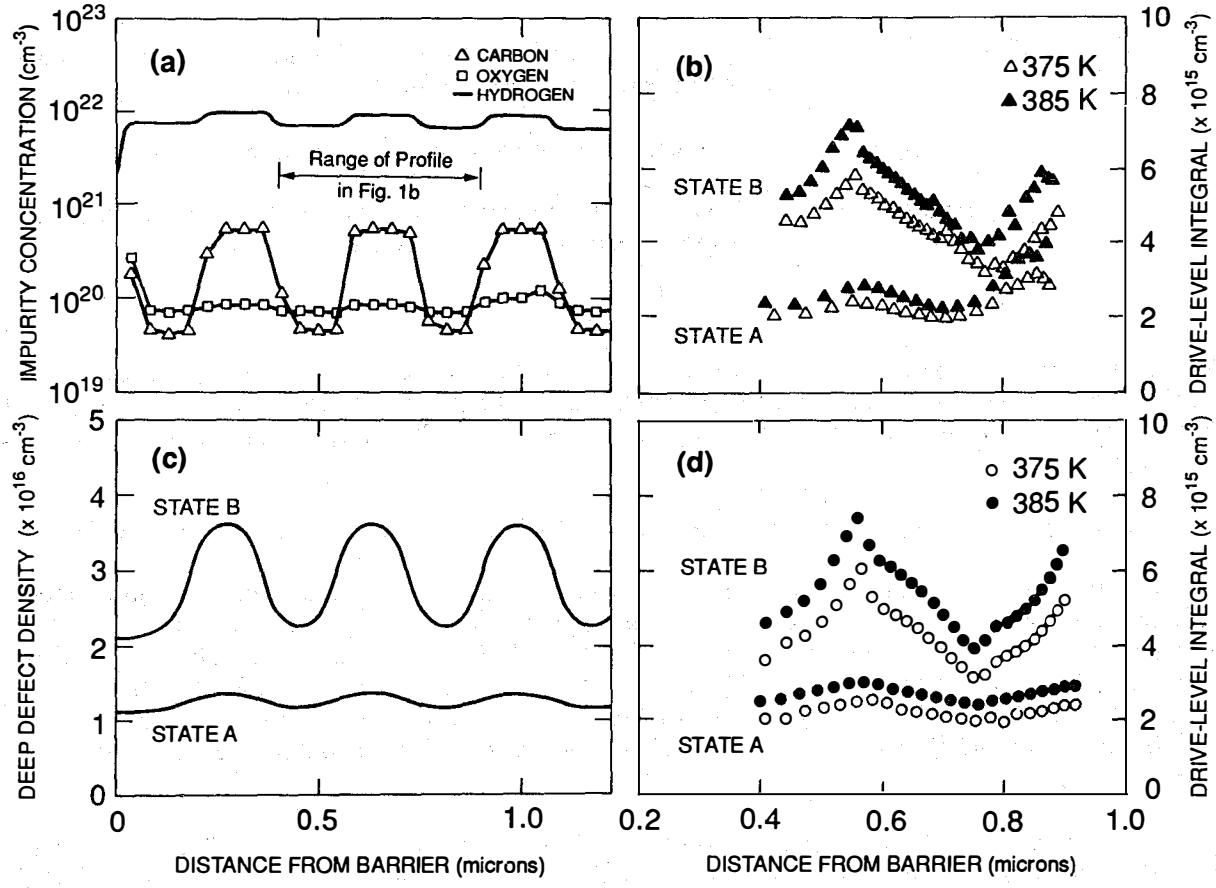

FIG. 1. (a) SIMS deduced profiles for C, O, and H in sample 1 showing the spatially varying carbon concentration within the sample.
(b) Drive-level capacitance profiling data reflecting the spatial variation of deep states for state A and state B.
(c) Spatial variation of the total deep defect density in states A and B as deduced by numerical modeling of the profiling data of Fig. 1(b).
(d) Calculated drive-level capacitance profiles using the spatial variation of deep defects shown in Fig. 1(c).

Our analysis for this sample indicated that light-soaking resulted in almost twice as many defects in the carbon-rich regions compared to the carbon-poor regions, thus indicating a significantly higher degradation for those regions. Figure 2(a) summarizes the variation in defect densities as a function of carbon content before and after light-soaking for several samples. We see that while there is a slight increase in defect densities for state A with increasing carbon, the larger slope in state B indicates a much larger degradation for regions of higher carbon content. Roughly speaking, our results indicate an additional increase of 1 to 2 x 10^{16} cm^{-3} light-induced defects for a carbon level of 0.5at.%. To test whether the increased degradation is due to the above mentioned increased hydrogen content in the carbon-rich regions we have also plotted the defect densities for the same samples as a function of the SIMS determined hydrogen content. From Fig. 2(b), however, we see no significant correlation between total hydrogen content and light-induced metastable degradation in our samples. These data thus leave no doubt that a strong correlation exists between light-induced degradation and the carbon concentrations at levels between 0.1 and 1at.%.

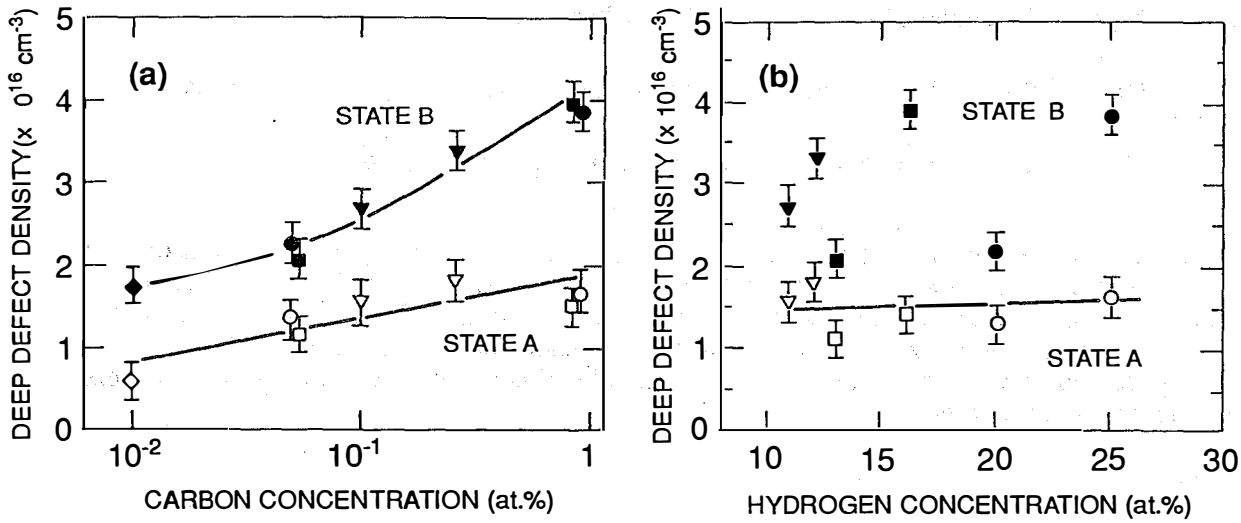

FIG. 2. (a) Total deep defect densities in state A and B deduced for several films as a function of carbon content. For each spatially modulated film the defect density is given for both the carbon-rich and the carbon-poor regions using an identical symbol. The data points displayed at the lowest carbon content sample were obtained for an *unmodulated* sample.
(b) Defect densities as in Fig. 2(a), however now displayed as a function of total hydrogen content.

Our results are inconsistent with earlier conclusions that have ruled out any such correlation for impurity levels below 5at.%.[4,5] We believe this difference is a result of the higher sensitivity of our method to bulk a-Si:H properties as compared to electron spin resonance and photothermal deflection spectroscopy (PDS) techniques employed in the earlier studies. While we do not propose a specific microscopic model for this enhanced degradation, it seems obvious that impurities will generally add more configurational degrees of freedom to the amorphous network, so that it is quite reasonable that this will increase the possible routes to metastable gap state (dangling bond) formation.

References

1. SIMS performed by Sally Asher, SERI, and also Charles Evans and Associates, Redwood City, CA.

2. C.E. Michelson, A.V. Gelatos, and J.D. Cohen, Appl. Phys. Lett. 47, 412 (1985).

3. K.K. Mahadavi, K. Zellama, J.D. Cohen, and J.P. Harbison, Phys.Rev.B35, 7776 (1987).

4. M. Stutzmann, W.B. Jackson, and C.-C. Tsai, Phys.Rev.B32, 23 (1985).

5. A. Skumanich and N.M. Amer, Phys.Rev. B37, 8465 (1988).

Title: **Structure of Amorphous Silicon Alloy Films**

Organization: Department of Physics, Washington University, St. Louis, Missouri

Contributors: R. E. Norberg and P. A. Fedders, principal investigators

The principal objective of this work has been to improve our understanding, at the microscopic level, of the structure of amorphous silicon-germanium alloy films by means of joint theoretical and experimental approaches to the correlation of results of nuclear magnetic resonance, electron spin resonance, transmission electron microscopy, and other measurements. A major focus of the work is the examination of significant rearrangements that take place under photoillumination, dark anneal, and various deposition and postdeposition conditions.

Approach

Deuteron magnetic resonance (DMR) at 30.7 and 46.0 MHz in magnetic fields of 4.7 and 7.0 Tesla has been used to examine a series of film samples of a-Si:D,H; a-Si:D; and a-Ge:D,H prepared at Harvard by the group of W. Paul. The results have been compared with DMR data obtained in samples provided by other laboratories including Xerox PARC (J. B. Boyce, et al.) and Xerox Webster (S. Kaplan, F. Jansen, and M. Machonkin). DMR spectroscopy of these systems is particularly important because it has been demonstrated that DMR can provide detailed structural information on hydrogen (deuterium) in amorphous Si and Ge, including hydrogen rearrangements under various conditions. DMR determines resolved components for tightly bound deuterium (TBD), weakly bound deuterium (WBD), void-contained molecular deuterium (D_2 or DH), rotating silyl groups (SiD_xH_{3-x}), and isolated D_2 and HD trapped in the semiconductor matrix. Thus DMR offers the particular opportunity to examine connections between hydrogen arrangements and electrical properties in amorphous silicon and germanium and in their alloys.

In the past year we have learned a great deal about a-Si from molecular dynamics simulations using the *ab-initio* total energy/MD scheme of Sankey and Niklewski [1]. In earlier work we have shown that forces generated by various angular dependent potentials give substantial errors [2]. These errors are serikous enough to cast doubt on most of the simulations using these methods. Using the first principles code of Sankey, we have generated a-Si samples of 32 and 64 atoms that contain as few as two geometrical defects. Although this is still a far greater fraction of defects than is found in good quality material, it is far less that the 15-20% defects that one gets from other methods. Thus we have produced "samples" with various numbers of types of defects. These samples are characterized by bond angle distributions and pair correlation functions that are very close to those measured on good laboratory grown material. These samples form a body of data on which one can test various theoretical techniques.

Amorphous Silicon and Germanium

We have shown that several resolvable features of the deuteron magnetic resonance (DMR) spectra in a-Ge:D,H and a-Si:D,H films show systematic correlations with transport measurements of photovoltaic quality. These correlations indicate a structural basis for the changes in photovoltaic quality. Figure 1 shows an example of such a correlation between the relative fraction of the DMR signal which is attributable to tightly-bonded Ge-D and Si-D configurations and the corresponding photoresponse products $\eta\mu\tau$ measured in William Paul's laboratories. The percentage of the tightly-bound DMR doublet increases systematically with $\eta\mu\tau$ for a series of a-Ge:D,H samples and one high quality a-Si:D,H sample. Similar correlations exist for other DMR features. Large $\eta\mu\tau$ is associated with a small DMR fraction from microvoid-contained molecular HD and D_2, but is associated with an increased fraction of nanovoid-trapped HD.

Atomic Rearrangements and the Light-Induced Metastability

We have begun to compare DMR signals for films dark-annealed with those after exposure to light. The experiments are difficult because the anticipated participating hydrogen fraction is about 10^{-5}. We have constructed a DMR sample probe designed for *in situ* dark anneal and light soak sequences without otherwise disturbing the film sample. Controlled illumination is conveyed to the sample via dual optical fibers. With this geometry we have observed a reasonable Staebler-Wronski effect as monitored by electron spin resonance (ESR) intensity. Robert Corey has begun careful measurements of DMR difference signals for light soak/dark anneal sequences. Our exploratory measurements have proved promising. Figure 2 shows DMR difference spectra, recently obtained at 30 K, between a light-soaked and 150°C dark annealed high quality a-Si:D,H film sample. The repetition interval between rf pulse sequences is short compared to the spin-lattice relaxation time for D tightly-bonded to Si. Thus the difference spectra reflect faster-relaxing weakly-bound D components. The results are preliminary and not yet fully analyzed. Nevertheless it is clear that we have reproducible DMR difference spectra associated with illumination and dark-anneal sequences. We propose to examine these difference spectra for various a-Si and a-Ge film samples, for a variety of DMR spectroscopic parameters, and as a function of illumination characteristics. We hope to characterize any detectable hydrogen-silicon rearrangements associated with the light-induced metastability. A tentative interpretation of the difference spectrum in Fig. 2 is that it reflects an approximately 50 kHz quadrupolar doublet associated with a distinct strained-bond Si-D configuration.

Role of Topology and Distortions on Dopants and Band Tailing

We have recently finished calculations of the energy levels in the band gap of a-Si for Si, B, and P as a function of the coordination number and the strain or topological environment. This work shows that one can easily get both deep electron and hole traps from a variety of sources.

For example, conventional wisdom or elementary theory assumes that 3-fold coordinated B and 3-fold or 5-fold coordinated P are electrically inert when incorporated into a-Si while 4-fold coordinated B and P form shallow acceptors and donors respectively. Using tight binding and the Bethe-lattice used earlier when analyzing dangling and floating bonds, we have shown that the elementary theory is far too restrictive. In particular we have shown that both 3-fold coordinated P and B can form a deep level in the gap if the topology is right. These results are summarized in Figs. 3 and 4. We have further showed that conduction band tailing due to strained bonds is considerably less than valence band tailing as was shown by the experimental work of Alhishi, Cohen, Jin, and Ley[3]. Finally, 4-fold coordinated dopant atoms can produce deep levels in the gap with only modest strains.

Molecular Dynamics

We have collaborated with a number of different investigators in first principles molecular dynamics simualtions in a-Si and in a critical analysis of angular dependent potentials used by other investigators.

More specifically we compared forces generated by various angular dependent potentials and by *ab initio* band structure calculations with a limited number of k-points. We found that all of the angular dependent force models yielded forces for badly disordered samples that are in error by about the magnitude of the forces. In terms of absolute error, these methods were much better for samples that are nearer to equilibrium but they are still only qualitatively correct. It is highly unlikely that these potentials can yield reliable defect structures for a-Si samples. We also found with supercells of 32 or 64 atoms, that using only the point $k = 0$ gave substantial errors in the forces and that one must use many more k points in order to obtain accurate forces.

Conclusions

- Hydrogen structural changes accompany variations of photovoltaic quality among differently-prepared plasma-deposited a-Si:D,H and a-Ge:D,H films. Improved photovoltaic quality is accompanied by increased relative populations of hydrogen tightly bonded to Si or Ge and of molecular hydrogen trapped on nanovoid surfaces. The molecular hydrogen contained in microvoids decreases monotonically with increasing film quality.

- Reversible atomic rearrangements accompany the light-induced metastability in device-quality a-Si:D,H.
- The low doping efficiency of a-Si probably is associated with the fact that many dopants can act as either acceptors or donors.
- Comparison with *ab initio* band structure calculations shows that reported angular dependent force models yield poor defect structure results for highly disordered a-Si samples.

References

1. O. F. Sankey and D. J. Niklewski, Phys. Rev. B **140**, 3979 (1989).
2. D. A. Drabold, J. D. Dow, P. A. Fedders, A. E. Carlsson, and O. F. Sankey, Phys. Rev. B, to be published.
3. S. Alhishi, J. D. Cohen, S. Jin, and L. Ley, Phys. Rev. Lett. **64**, 2881 (1990).

Table 2-1 Characterization Parameters for Pairs of Deuterated and Non-Deuterated Films

Sample	T_S (°C)	Power* (watts)	Pressure (Torr)	Flow SiH_4 or GeH_4 (sccm)	Flow H_2 or D_2 (sccm)	$\eta\mu\tau$ (cm^2V^{-1})
H489 Si:H H541 Si:D,H	232 230	10 10	0.70 0.70	4 4	76 76 D_2	1.6×10^{-5}
H510 Ge:D,H H511 Ge:D,H H521 Ge:H	261 260 250	8 8 8	0.95 0.95 0.95	1 1 1	40 D_2 40 D_2 40	1.0×10^{-10} 1.7×10^{-10}
H522 Ge:H H643 Ge:D,H	298 301	8 8	0.95 0.95	1 1	40 40 D_2	2.5×10^{-10}
H680 Ge:H H686 Ge:D,H	250 250	8 8	0.95 0.95	1 1	40 40 D_2	7×10^{-10}
H519 Ge:H H642 Ge:D,H	151 151	8 8	0.95 0.95	1 1	40 40 D_2	9.3×10^{-9}
H680A Ge:H H686A Ge:D,H	150 150	8 8	0.95 0.95	1 1	40 40 D_2	3.2×10^{-7}

*The average power densities for the depositions were 0.12 W/cm^2 (10W) and 0.096 W/cm^2 (8W).

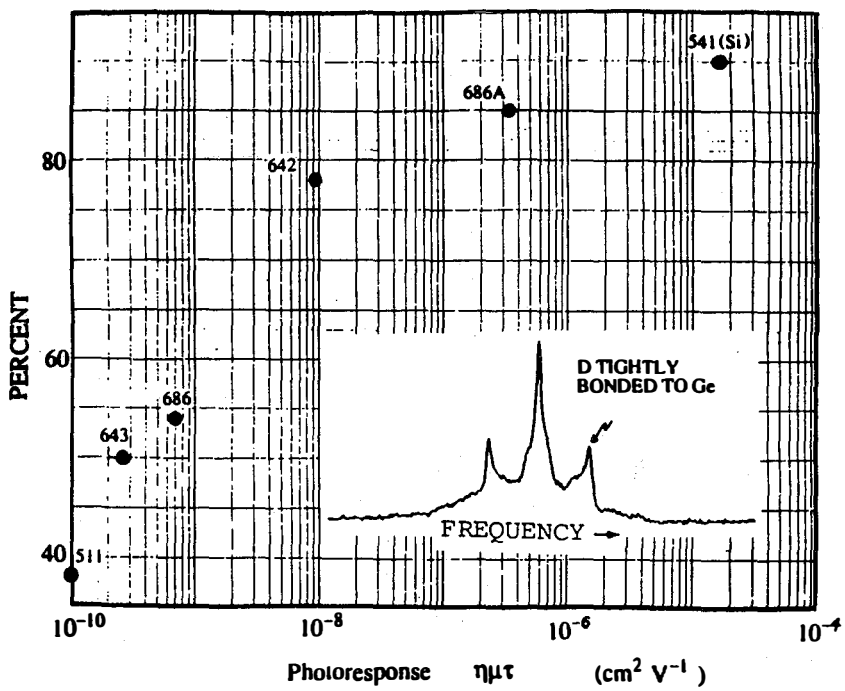

Fig. 1. Comparison of tightly bonded Ge-D relative content with ημτ products for a-Ge films.

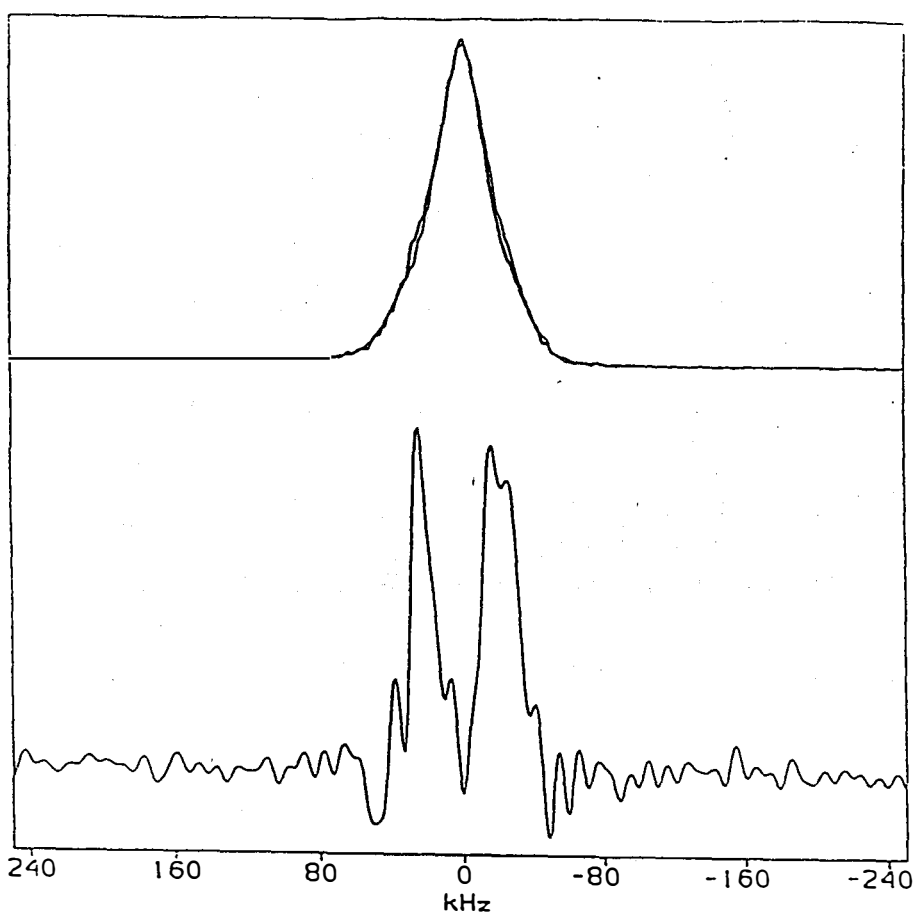

Fig. 2. (Top) DMR spectra at 30 K for light-soaked and 150°C dark-annealed a-Si:D,H.
(Bottom) Difference spectrum light-soaked minus dark-annealed.

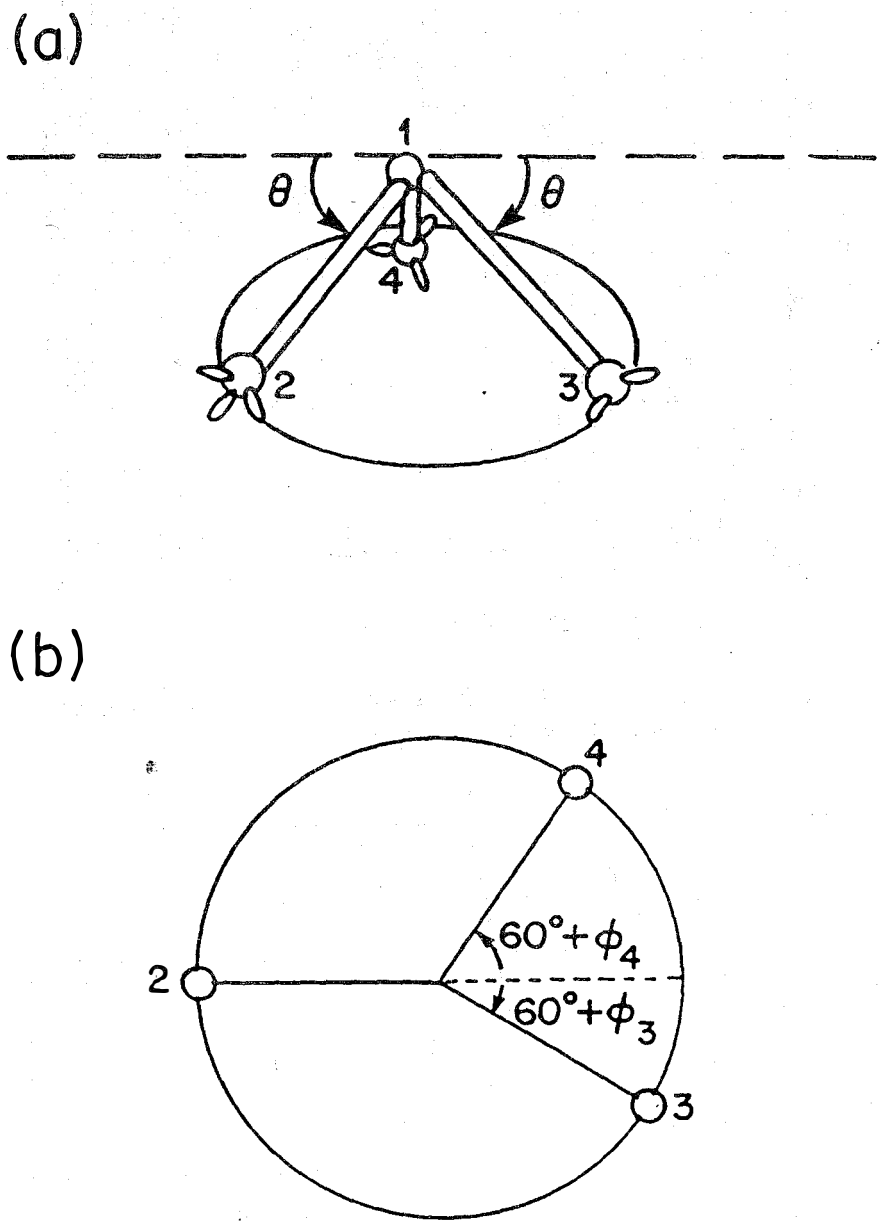

Fig. 3. The geometry of the most general dangling bond. The angles θ, ϕ_3, and ϕ_4 yield a complete description.

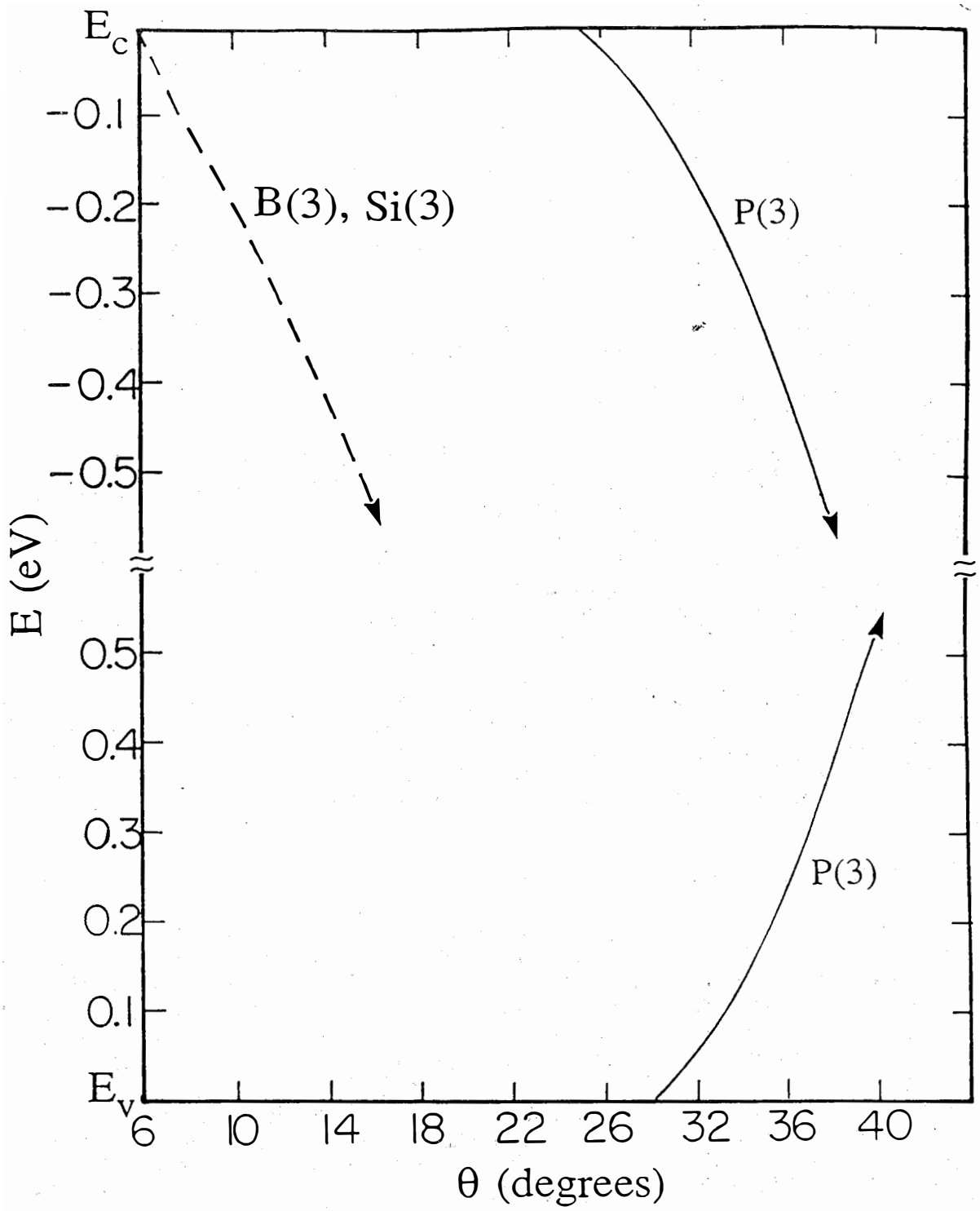

Fig. 4. Energies of states in the gap of three-fold coordinated B, Si, and P as a function of the angle θ.

Title: **Research on the Structural and Electronic Properties of Amorphous Silicon Alloys**

Organization: Xerox Palo Alto Research Center, Palo Alto, CA 94304

Contributors: W. B. Jackson, N. M. Johnson, P. Santos, R. A. Street (Principal Investigator), K. Stevens, R. Thompson, C. C. Tsai.

The aim of this research project is to improve the performance of a-Si:H-based solar cells through the understanding of metastability, doping and growth.

Saturation of Light Induced Defects

The constant photoconductivity method (CPM) has been used to study the kinetics of light induced defect creation in a-Si:H, in particularly the saturation at temperatures up to 550K. Defect creation and saturation were explored over a wide range of light intensities, using illumination from a filtered tungstem lamp or a krypton laser. The saturated defect density is weakly temperature dependent and also weakly intensity dependent. Equilibration of the unilluminated defect density is observed above about 400K and at sufficiently high temperature the annealed and illuminated defect densities become equal.

The saturation of the light-induced defects is analysed using an extension of the explanation for the equilibrium defect density in doped a-Si:H. The model assumes that the steady state defect density depends on the quasi-Fermi energy during illumination, and is able to account for the data. A close similarity is found between the light-induced and doping-induced defects, which will be studied in further exeriments.

Hydrogen bonding configurations in silicon

Many experiments suggest that metastability is induced by the motion of bonded hydrogen. Several models of hydrogen-induced metastability have been proposed, mostly based on chemical reactions between different hydrogen bonding species. The chemical reaction approach has been successful, but does not easily deal with the distributions of possible hydrogen bonding states which are expected in an amorphous semiconductor. An alternative approach is to describe the hydrogen reactions in terms of a hydrogen density of states (HDOS) distribution, analogous to the usual description of the electronic states. We have developed a qualitative model for the HDOS which is shown in Fig. 1. The HDOS contains the Si-H bonds, hydrogen in interstitial sites including weak Si-Si bonds, and the energy of hydrogen migration, E_M. The metastability is explained by the redistribution of hydrogen following illumination, annealing or a shift of the Fermi energy. Irreversible changes are related to structural reconstructions which change the shape of the distribution, while the reversible changes correspond to a redistribution of hydrogen within an approximately constant density of states.

We have also calculated the energy of different Si-H configurations using the local density approximation. We have discovered a low energy paired complex (denoted H_2^*), in which one the hydrogen atoms occupies a bond center site and a second occupies a nearest neighbor interstitial site as shown in Fig. 2. This complex has a

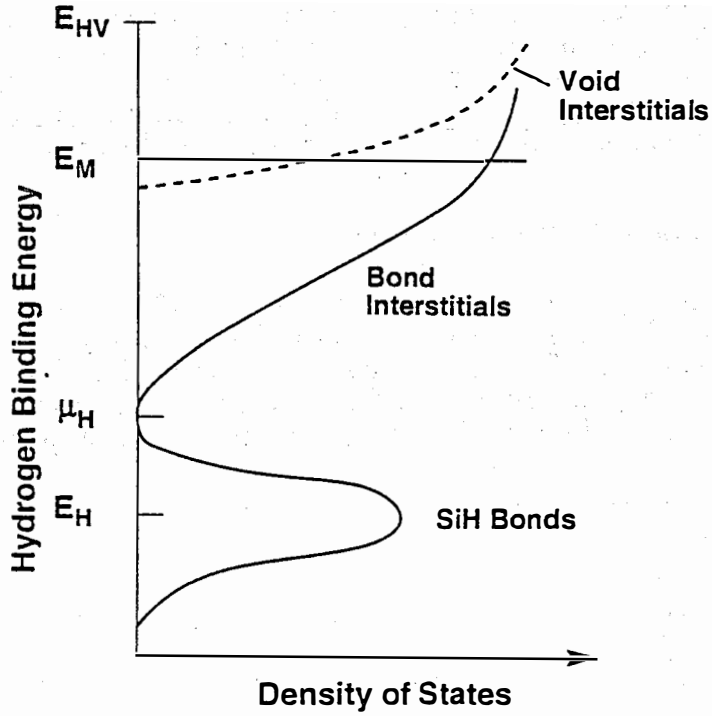

FIG. 1. The hydrogen density of states distribution showing the Si-H states, the distribution of interstitial states and the hydrogen migration energy.

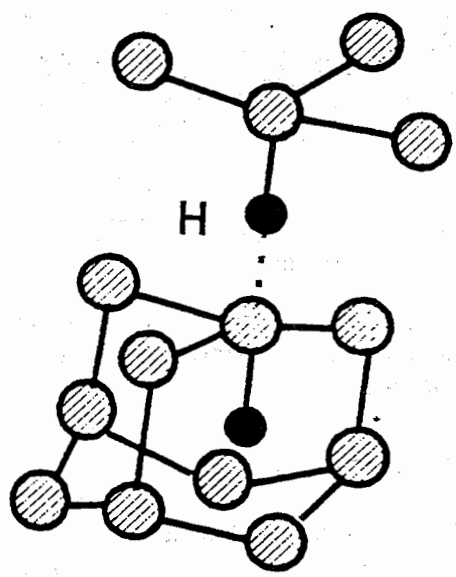

FIG. 2. The structure of the H_2* complex.

much lower energy than a pair of hydrogen atoms in bond center sites, and has only a small excess energy compared to a pair of isolated ideal Si-H bonds. This complex is a possible source for the metastable defect creation, through a mechanism of light-induced dissociation of the hydrogen pair. The calculated energies agree well with the measured activation energies of defect creation and annealing, and hydrogen diffusion.

Conduction and metastability in p-i-n devices

A detailed knowledge of the electronic properties of p-i-n devices is needed for solar cell modelling. The time dependence of the reverse bias current has been studied at different voltages. The reverse current changes for about 20 minutes after a voltage is applied at room temperature. The current decays due to depletion of deep trapped charge, as shown in Fig. 3. The depletion charge of about 6×10^{14} cm^{-3}

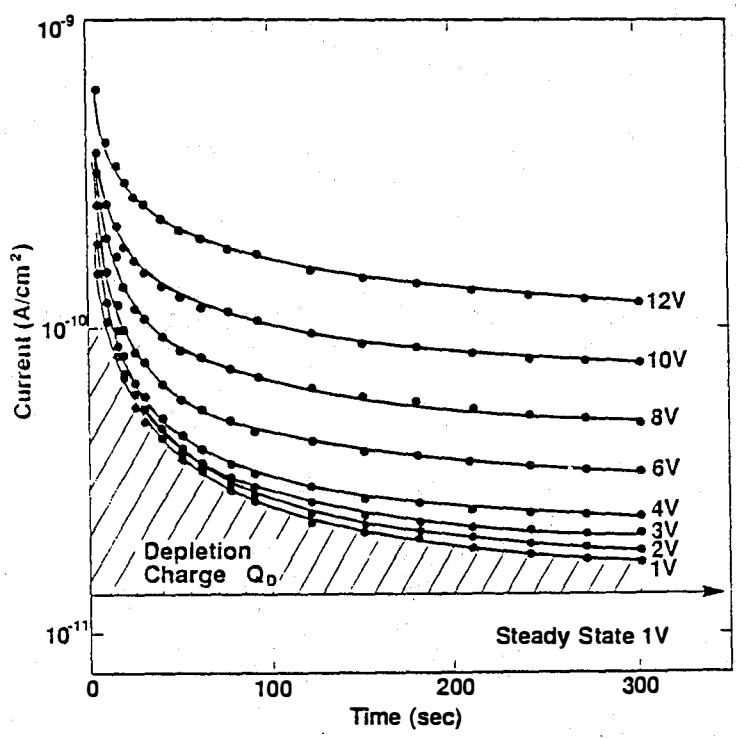

FIG. 3. The time dependence of the current after a reverse bias is appplied. The shaded region represents the depletion charge.

reflects the density and energy of mid-gap states.

When the p-and n-type layers are not optimized, there is a metastable current injection mechanism in reverse bias. The current increases slowly with time, in some cases continuing for more than 24 hours. The bias causes a metastable change in the material, which is manifested by the larger reverse current which is present upon subsequent applications of the voltage. The high current is removed by annealing at temperatures from 100-200°C, as for the other metastable phenomena. The current is identified as arising from contact injection over the barrier created by the doped

layer, and is interpreted in terms of bias-induced defect or dopant effects near the p-i interface. However, the details of the structural changes are as yet unclear.

Remote plasma deposition and ESR diagnostics

A remote hydrogen plasma reactor is used to grow novel a-Si:H films and alloys. The study of solid source doping has continued with a survey of many dopants including Group III acceptors and Group VI chalcogens. Studies are also in progress of the doping efficiency of arsenic, compared to the usual rf plasma reactors, and of high temperature deposition. The remote plasma reactor is able to make high quality films at a growth tempersature of 400°C, which is above the optimum temperature range for rf plasma reactors.

In addition, we have developed a miniature microwave plasma reactor for electron spin resonance (ESR) studies of the plasma chemistry during growth. Gas radicals are generated in the plasma and passed through the cavity of an ESR spectrometer, which allows a direct measurement of the radical concentration. For example, atomic hydrogen has a pair of sharp resonance lines split by the atomic hyperfine interaction. We have measured the dependence of the atomic hydrogen concentration on the gas flow rate, the pressure and the microwave power. Further, the atomic hydrogen concentration is reduced when it is mixed with silane, as shown in Fig. 4. The reaction,

$$SiH_4 + H \rightarrow SiH_3 + H_2$$

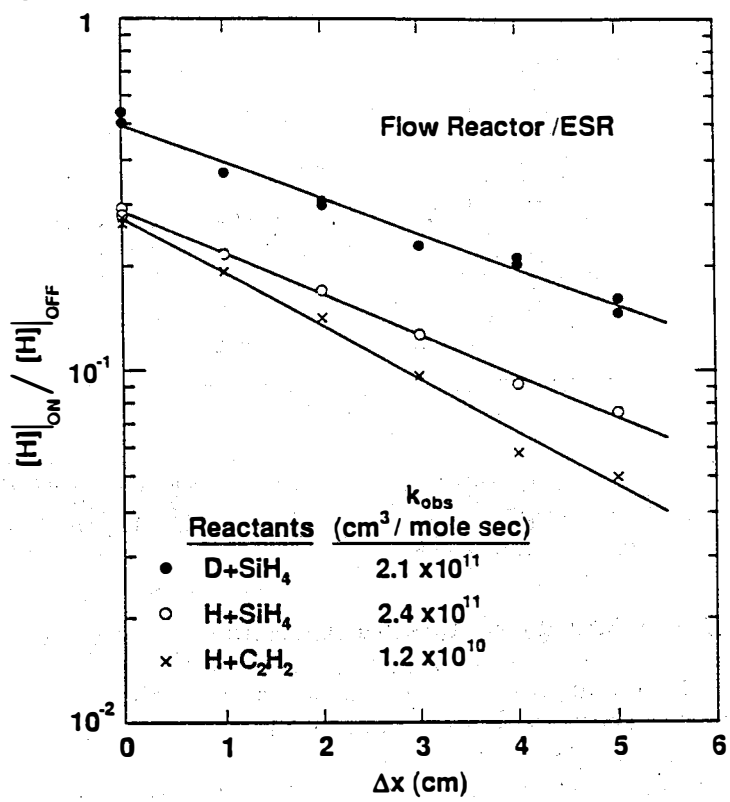

FIG. 4. The decay of the atomic hydrogen concentration due to mixing with SiH_4, SiD_4 and C_2H_2. The deduced reaction rates are indicated.

initiates growth of a-Si:H and the evaluation of its rate is important for all a-Si:H deposition processes. The decay of the hydogen concentration versus distance from the mixing point in Fig. 3, allows the evaluation of the reaction rate which is shown in the figure. The similar reaction of deuterium with SiH_4 and hydrogen with C_2H_2 is also shown.

Potential fluctuations in compensated a-Si:H

The role of long range potential fluctuations of the band edges on the electronic properties of a-Si:H has received much attention. Compensated a-Si:H has a high doping efficiency, but almost complete dopant ionization, and so should have strong fluctuations. To investigate this possibility we have studied the drift mobility and optical absorption in compensated samples. The drift mobility of both electrons and holes in the compensated samples drops rapidly with doping up to about 10^{-4}, but decreases more slowly at higher doping levels. The reduced mobility is accompaied by an increase in the activation energy to about 0.6 eV. In contrast, the slope of the optical absorption edge hardly changes for doping levels up to 10^{-4} and then increases rapidly, as shown in fig. 5.

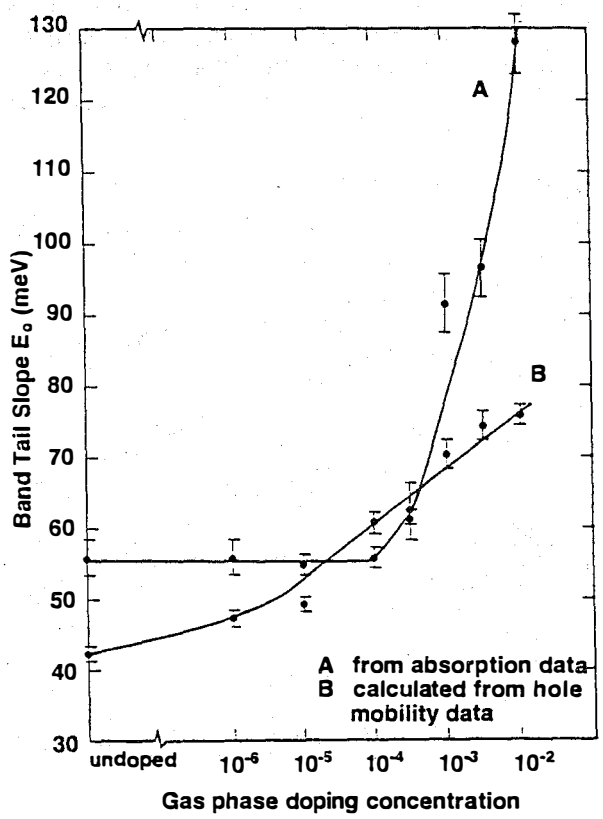

FIG. 5. The slope of the valence band edge in compensated a-Si:H deduced from time-of-flight and optical absorption.

The data is consistent with the presence of potential fluctuations, but cannot be explained by broadened band tails. If a reduction in drift mobility is caused by a broadening of the band tails, then the same broadening should be observed in the optical absorption. However if potential fluctuations reduce the mobility then the absorption edge is unchanged. The increase in the slope of the absorption at high

doping levels is explained by the large internal electric field as the dopant concentration increases, causing a Franz-Keldysh shift of the absorption.

Hydrogen in the growth of a-Si:H

The mechanisms determining the structure of PECVD a-Si:H films are still not well understood. We have developed a model which relates the chemical potential of hydrogen in the growth plasma to the structural disorder of the films. The model proposes that the hydrogen near the growth surface is in equilibrium, because it can move freely in and out of the surface. Hydrogen interacts with the silicon network to optimize the local bonding structure, by removing silicon dangling bonds and weak bonds which overlap the chemical potential. We deduce that the distribution of bonding states has a minimum at the hydrogen chemical potential (see Fig. 1), and hence that the disorder of the film also depends on this parameter. It is further proposed that the transition to microcrystalline growth occurs because hydrogen dilution raises the chemical potential to the point that the disordered film is not stable.

Bibliography

J. A. Howard and R. A. Street, *Evidence for potential fluctuations in compensated a-Si:H,* to be published

N. M. Johnson, J. Walker, and K. Stevens, *Characterization of a remote hydrogen plasma reactor with electron spin resonance,* (1990) submitted for publication.

W. B. Jackson, *Role of hydropgen complexes in the metastability of hydrogenated amorphous silicon,* (1990) Phys. Rev. B41, 10257.

W. B. Jackson, *Microscopic mechanism for dopant activation in hydrogenated amorphous silicon,* (1990) Phys. Rev. B41, 12323.

S. E. Ready, J. B. Boyce, N. M. Johnson, J. Walker and K. S. Stevens, *Hydrogen bondiing in a-Si:H prepared by remote hydrogen plasma deposition,* (1990) MRS Symp. Proc. 192, 127.

R. A. Street, *Thermal generation currents in hydrogenated amorphous silicon p-i-n structures,* (1990) Appl. Phys. Lett. 57, 1334.

R. A. Street, *Long time transient conduction in a-Si:H p-i-n devices,* (1991) Philos. Mag. in press.

R. A. Street, *The hydrogen chemical potential and the structure of a-Si:H,* (1990) Phys. Rev. in press.

R,. A. Street, *The density of states distribution of bonded hydrogen in a-Si:H,* (1990) Solar Cells, in press

K. Winer and R. A. Street, *Impurity incorporation and doping efficiency in a-Si:H,* (1990) Phys. Rev. B42, 3120.

S. B. Zhang, W. B. Jackson and D. J. Chadi, *Diatomic hydrogen-complex dissociation: A microscopic model for metastable defect generation in Si.* (1990) Phys. Rev. Lett. in press.

3.0 POLYCRYSTALLINE THIN FILMS

Kenneth Zweibel (Manager), Harin Ullal, and Richard Mitchell

The objective of the Polycrystalline Thin Film Program is to develop thin-film, flat-plate modules that meet DOE's long-term goals of reasonable efficiencies (15%-20%), very low cost (near $\$50/m^2$), and long-term reliability (30 years). The approach relies on developing PV devices based on highly light-absorbing compound semiconductors such as $CuInSe_2$, CdTe, and their alloys. These semiconductors are fabricated as thin films (1-3 μm thick) with minimal material and processing costs.

Very high efficiencies have been achieved by these promising materials. $CuInSe_2$ cells made by ARCO Solar and by Boeing were measured at SERI at 13.1% and 12.9% efficiency (active area: 11.3% and 12.5% total area), respectively. Others surpassing 10% efficiency in $CuInSe_2$ are SERI, International Solar Electric Technology, and Institute of Energy Conversion. Larger area $CuInSe_2$ devices have also been fabricated with very high efficiencies. ARCO Solar has made a 938-cm^2 (aperture area) $CuInSe_2$ module with 11.1% efficiency (10.4 W), and an 8.7% (4-ft^2) module, both measured at SERI. ARCO Solar reports achievement of a 14.1% cell efficiency (active area) and a 9.7% 4-ft^2 module efficiency (aperture area).

$CuInSe_2$ shows good proven stability under controlled conditions (9000 hours of illumination), and initial outdoor tests (ARCO) are also promising. We have conducted over a year of outdoor testing on two ARCO Solar $CuInSe_2$ panels with very little change in their efficiencies (under 4%). These are the first such tests on $CuInSe_2$ by an independent agency and show the great potential stability of $CuInSe_2$ panels.

Three U.S. laboratories (University of South Florida, Ametek, and Photon Energy) report CdTe cell efficiencies between 10.5% and 12.5%. Photon Energy has fabricated near-square-foot CdTe submodules measured outdoors at SERI at 7.3% efficiency (aperture area). They also have the world record in CdTe cell efficiency (12.3%), measured at SERI. BP Solar has reported 9.5% efficient square-foot CdTe (not SERI measured). Innovative designs are now addressing past difficulties in contacting CdTe. We have recently begun testing encapsulated CdTe submodules provided by Photon Energy. After nine months, they show no degradation. As with the $CuInSe_2$, these are the first independent tests of encapsulated devices made from this material. Both Matsushita and BP Solar have reported similar stability for their own CdTe modules. Since stability has been an identified issue with CdTe, these initial results are considered very favorable.

The improved efficiencies and larger areas of $CuInSe_2$ and CdTe devices, and their apparent stability, are the major recent advances in these technologies. But polycrystalline thin film cells require continued development to achieve 15%-20% conversion efficiencies. Two strategies are being used: development of single-junction cells and an innovative effort on two-junction cascade cells. Improvement of the single-junction technologies has been steady and reliable. This strategy remains the major focus of the task. Potentially achievable cell efficiencies approach 20%, and projections indicate the likelihood of fabricating modules of more than 15% efficiency. Developing two-junction, $CuInSe_2$-based cascade cells permits even more ambitious

long-term efficiency goals. The materials being investigated for the top cells include CdTe and ZnTe alloyed with Mn, Mg, Zn, and Hg.

Developing scalable, low-cost fabrication methods is important in providing industry with a foundation for future large-area, high-throughput commercial processes. Research methods for fabricating polycrystalline cells include, for $CuInSe_2$, an e-beam evaporation (with selenization) methods (International Solar Electric Technology and Solarex), a reactive-sputtering and hybrid sputtering/evaporation method (University of Illinois), and evaporation (Boeing); for CdTe, close-spaced sublimation and CVD (Solar Cells Inc. and USF), evaporation (Institute of Energy Conversion), metal-organic chemical vapor deposition (MOCVD) (Georgia Tech and University of South Florida), and spraying (Photon Energy).

An initiative in the Polycrystalline Thin Film Program was begun with the release of an RFP in FY 1989. The objective of the solicitation was to stimulate progress in $CuInSe_2$ and CdTe submodule development and to deepen the U.S. participation in these promising technologies. The research community responded favorably, as reflected in the many excellent technical proposals received in response to the solicitation. Several new cost-shared contracts have resulted from the RFP.

Title: **Investigations of $CuInSe_2$ Thin Films and Contacts**

Organization: California Institute of Technology
Division of Engineering and Applied Science
Pasadena, California 91125

Contributors: M.A. Nicolet

1. Introduction

$CuInSe_2$ (CIS) polycrystalline thin films with molybdenum as metal contacts has been one of the most promising configurations for thin-film heterojunction solar cells.[1] The first part of this work is to study the contact stability by a systematic investigation of thermally induced bilayer reactions of Mo with Cu, In and Se individually.[2] Influence of oxygen in Mo layer on interdiffusion of metal couples is simulated by a Cu/Mo/Au trilayers system.[3] As to the $CuInSe_2$, since selenization has become a successful process used to fabricate CIS thin films for photovoltaic cells,[4,5] the second part of this work is to investigate how the morphologies, phases and reactions of pre-selenization Cu-In structure are affected by the deposition process and subsequent heat treatments.[6]

2. Approach

To investigate the interaction between Mo and $CuInSe_2$, the binary thin-film couples Mo/Cu, Mo/In and Mo/Se were deposited on oxidized Si wafers by e-beam evaporation or rf magnetron sputtering. All couples were annealed in the vacuum furnace (Mo/Cu) or an Ar-flowing furnace (for Mo/In, Mo/Se) at temperatures ranging from 100°C to 600°C for 10 minutes to 1 hour. All samples were analyzed by RBS and x-ray diffraction before and after annealing.

Influence of oxygen on diffusion is studied by using the polycrystalline Cu/Mo/Au trilayers deposited on oxidized Si wafers by rf magnetron sputtering in two systems with different base pressures (System #1: 9×10^{-8} torr; System #2: 5×10^{-6} torr) such that the oxygen content in Mo films are different. Annealings were performed in a vacuum furnace at 600°C for 30 minutes. Analyses of the films have been carried out using RBS and X-ray diffraction.

For the study of pre-selenization Cu-In structures, bilayers of slightly Cu-rich overall composition of Cu and In prepared on oxidized Si wafers at room temperature by vacuum evaporation electroplating and rf sputtering have been analyzed by RBS, SEM and x-ray diffraction before and after annealing at 400°C in vacuum for 1 hour.

3. Results

3.1 Interactions of Mo Contact with Cu, In and Se

3.1.1 Mo/Cu

Figure 1(a) shows 3 MeV $^4He^{++}$ normal incidence RBS spectra obtained before and after annealing at 600°C for 1 hour of a trilayer of Cu/Mo/Cu. It is clear that no reaction occurs. No reaction either is observed with samples formed by e-beam evaporation.

3.1.2 Mo/In

The 4.7 $^4He^+$ normal incidence RBS spectra of Fig. 1(b) are for a Mo layer deposited by e-beam evaporation and covered by an In layer.

Up to 200°C annealing, the RBS spectra of annealed samples are practically identical to the as-deposited spectrum. After 600°C and 10 min, the signal peaks decrease slightly and we observe a non-zero count between peaks. At the small thicknesses of our samples (thickness of In about 20 nm, thickness of Mo about 30 nm), the RBS system resolution is inadequate to display the full height of the signals. A small difference in thickness would thus be reflected in a difference in signal heights. The non-zero count between the peaks is not due to an interdiffusion between the layers, but to a non-uniform thickness of the top layer due to a balling up effect of the In which has melted at this annealing temperature. Optical microscope observation of the surface reveals the presence of innumerable tiny In balls on the surface.

3.1.3 Se/Mo

The Se/Mo bilayer was prepared by e-beam evaporation of a Se film on an oxidized Si wafer, followed by a Mo layer deposition. Figure 1(c) shows 4.7 MeV $^4He^+$ normal incidence RBS spectrum of the bilayers before and after annealing at 600°C. A detailed analysis of the as-deposited spectrum indicates that the Se has probably already penetrated into the Mo layer during deposition though the system resolution combined with the small thickness of the films preclude any definitive conclusion. No change was detected after annealing at 150°C and 30 min. After annealing at 200°C for 30 min, we observe a slight decrease in the Se signal, and a slight shift to higher energy. This evolution becomes pronounced after annealing at 600°C for 10 min and is attributed to a complete intermixing of the Se and the Mo layers. The x-ray analysis of

this sample performed with a Read camera reveals the existence of small amounts of $MoSe_2$. The total number of counts of the Se signal decreases, suggesting a loss of Se by evaporation at the surface.

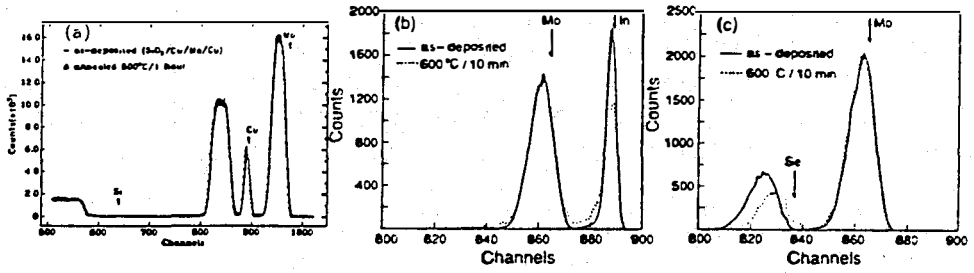

Fig. 1
(a) 3 MeV $^4He^{++}$ normal incidence RBS spectrum of Cu/Mo/Cu as-deposited and after annealing in vacuum at 600°C for 1 hour, (b) 4.7 MeV $^4He^+$ normal incidence RBS spectrum of Mo/In as-deposited and after annealing in flowing argon at 600°C for 10 min, (c) 4.7 MeV $^4He^+$ normal incidence RBS spectrum of Se/Mo as-deposited and after annealing in flowing argon at 600°C for 10 min.

3.2 Influence of Oxygen on Diffusion in the Cu/Mo/Au System

The Cu/Mo/Au trilayers were deposited on a thermally oxidized Si wafer sequentially together with a carbon substrate for each deposition of metal layer. We evaluated the oxygen concentration in the films deposited on carbon substrates using backscattering spectrometry. No impurities were detected in any of the Cu or Au films, or in the Mo layer deposited in system #1 (Fig. 2(a)). According to the sensitivity limit of our backscattering system, we estimate that the impurity concentration is below 2% for elements heavier than carbon. A uniform concentration of 5.5 at% of oxygen is measured in the Mo film from system #2 as shown in Fig. 2(b).

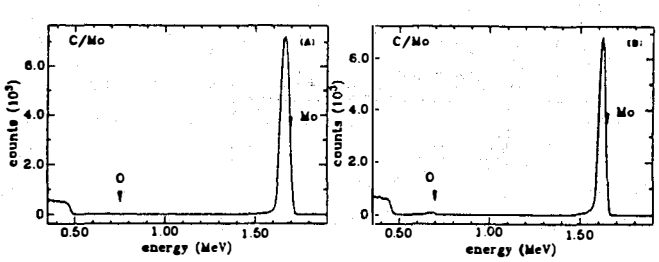

Fig. 2.
2.0 MeV He^+ normal incidence backscattering spectra of a Mo layer (a) deposited in system #1, (b) deposited in system #2, on a carbon substrate.

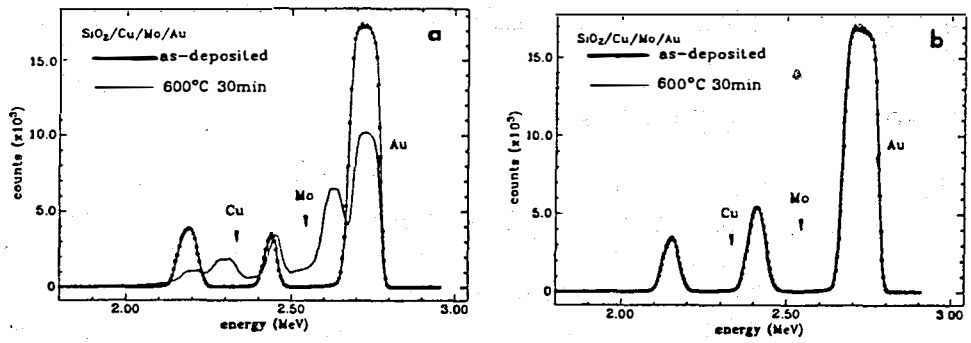

Fig. 3
3.0 MeV He^{2+} normal incidence backscattering spectra of the Cu/Mo/Au trilayer (a) deposited in system #1 (not containing detectable amount of oxygen in Mo), (b) deposited in system #2 (with 5.5 at% of oxygen in Mo) as-deposited and after annealing in vacuum at 600°C for 30 min.

Fig. 3 shows backscattering spectra of two sets of Cu/Mo/Au samples before and after annealing at 600°C for 30 min. It is clear that a rapid diffusion of Cu and Au across Mo film after annealing when no impurities are detected in the as-deposited polycrystalline Mo layer (Fig. 3(a)). When oxygen is introduced in the as-deposited Mo layer, the two spectra overlap perfectly (Fig. 3(b)) which indicates that no detectable intermixing occurs during heat treatment.

X-ray diffraction using the theta 2-theta technique reveals the formation of AuCu compound after annealing for the sample without impurities in the Mo film (Fig. 4). The spectra taken from the samples with oxygen contamination before and after annealing are both similar to the spectrum of the as-deposited sample without oxygen contamination. No molybdenum oxide compound was detected in all of the samples.

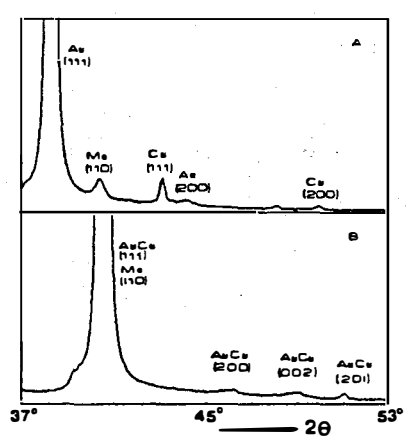

Fig. 4
X-ray diffraction spectra of a Cu/Mo/Au trilayer without detectable amounts of oxygen in Mo layers (a) as-deposited and (b) after annealing in vacuum at 600°C for 30 min.

3.3 Morphology, Phases and Reactions in the Pre-Selenized Cu-In Samples

3.3.1 As-Deposited Samples

The Cu-In bilayers were prepared by different deposition techniques. That the deposition process affects the surface morphology is apparent. Fig. 5 shows representative scanning electron micrographs of the three types of samples, as well as their $^4He^{2+}$ backscattering spectra. The sample deposited by e-beam evaporation of both Cu and In (Fig. 5(a)) consists of many distinct grains about 1 um in size. Energy dispersive X-ray analysis reveals that the grains are In-rich. The picture suggests a melting and island forming process of the In. The surface layer of the samples deposited by e-beam evaporation of Cu and electrodeposition of In is bumpy, but remains singly connected (Fig 5(b)). The surface roughness of the samples deposited by low-power rf sputtering is several orders of magnitude finer in scale than for the previous two cases, and essentially flat, except for a few bubble-like shallow protrusions (as shown in Fig. 5(c)) of an approximate areal density of $10^4/cm^2$.

The drooping low-energy edge of the In and Cu signals in the backscattering spectra of the first two samples are characteristic of laterally nonuniform layers, consistent with the scanning electron micrographs. The spectra further shows that Cu is present on the sample surface and that the shape of the In and Cu signals are similar, all of which is highly suggestive of a fully intermixed Cu-In layer with a laterally varying thickness. In the spectrum of the low-power sputtered sample, the Cu signal position is clearly shifted below the energy of a surface Cu signal (arrow labeled Cu). This fact proves that the Cu and In layers are distinct; but the non-symmetric shape of both the Cu and In signals reveals that some slight interfacial mixing may exist.

X-ray diffraction shows that all the as-deposited samples contain the Cu fcc phase and CuIn compound. The In diffraction lines of the low power sputtered sample are consistent with ASTM file; but for the samples with electroplated In, the most intensive In diffraction line is shifted by + 2% comparing to the ASTM file.

3.3.2 Annealed Samples

After vacuum annealing (400°C, 1h) scanning electron micrographs and backscattering spectra indicate that the initially rough samples have smoothened much (shrinking low energy tails of Cu and In signals in backscattering spectra, Fig. 6(a) and (b)).

The surface morphology of low-power sputtered samples hardly changes, except for a collapse of the small bubble-like features, as shown in Fig. 6(c). The widening of the backscattering signals of Cu and In in that figure and the shift of the Cu signal to its surface energy position reveal that Cu and In are now intermixed.

By X-ray diffraction analysis, the Cu and CuIn phases have disappeared from the samples and some Cu-rich compounds (Cu_9In_4 and Cu_7In_4) appear; the In phase remains.

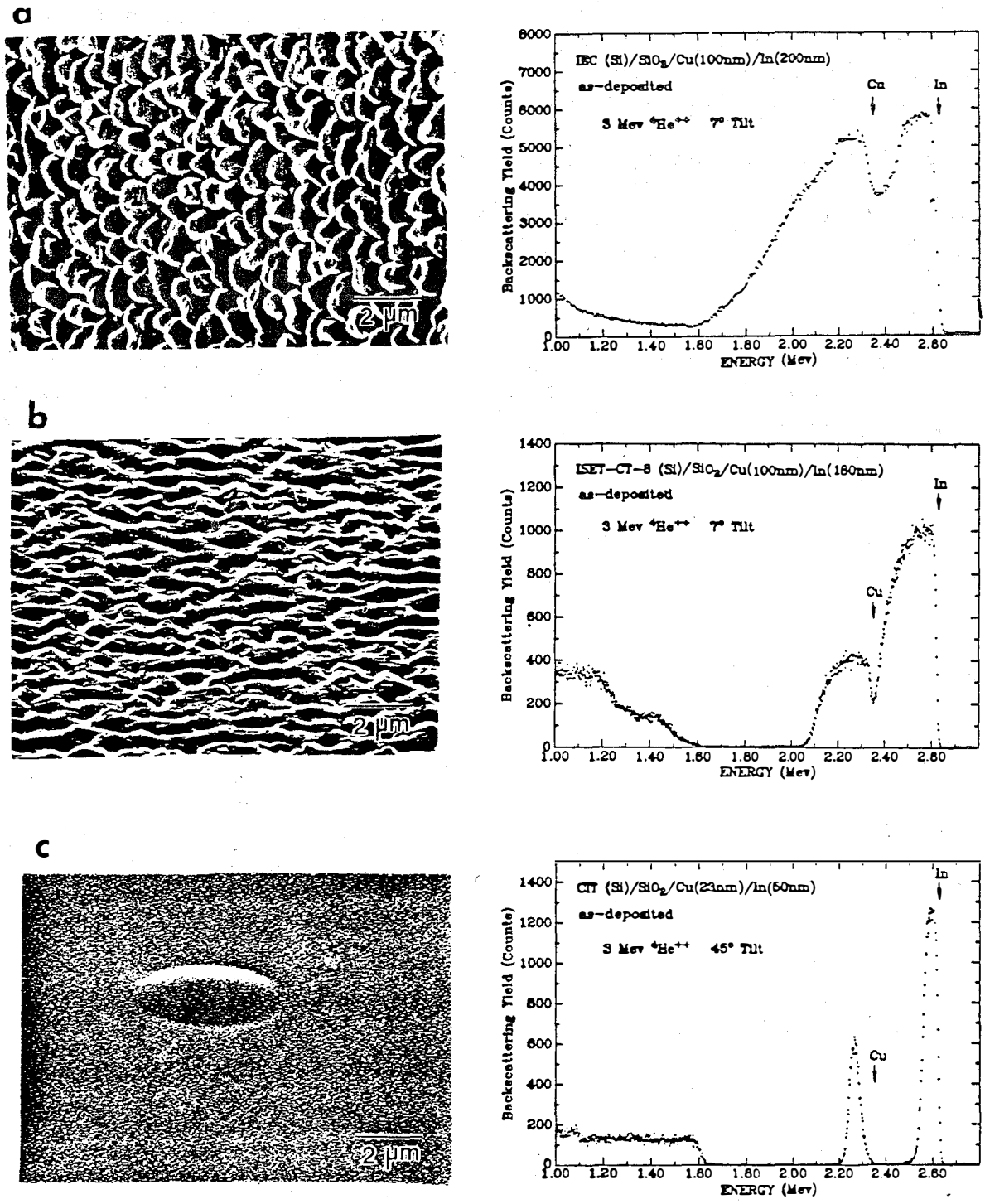

Fig. 5
Scanning electron micrographs and 3 MeV $^{4}He^{++}$ backscattering spectra (with scattering angle of detected particles: 170°) of Cu/In bilayers before annealing, deposited by (a) e-beam evaporation of both layers, (b) e-beam evaporation of Cu and electrodeposition of In (c) rf sputtering of both layers.

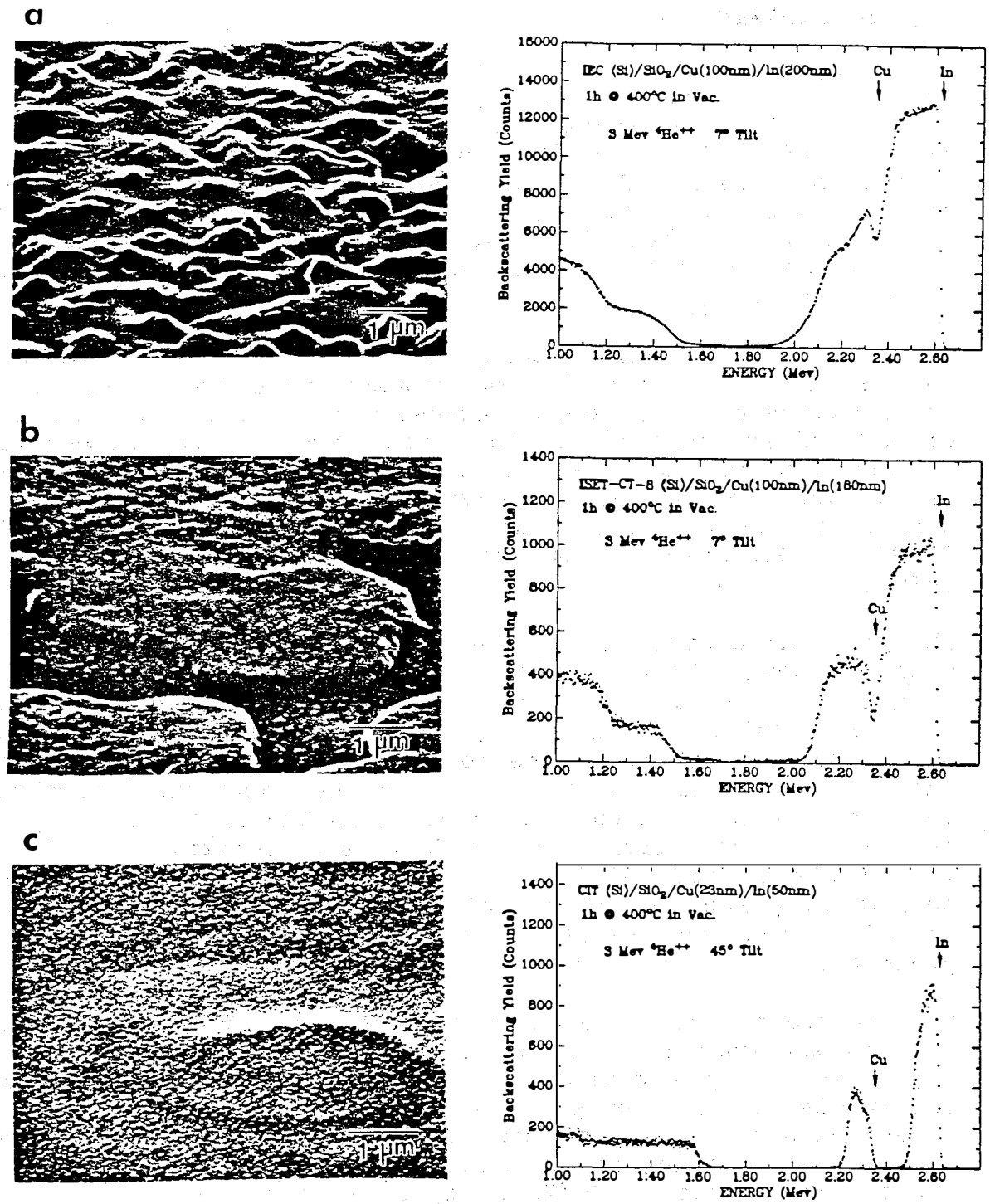

Fig. 6
Scanning electron micrographs and 3 MeV $^4He^{++}$ backscattering spectra of Cu/In bilayers after annealing for 1 h at 400°C, in vacuum, deposited by (a) e-beam evaporation of both layers (b) e-beam evaporation of Cu and electrodeposition of In (c) rf sputtering of both layers.

4. Discussion

According to the phase diagrams, no compounds exist in the Mo-Cu and Mo-In systems and the mutual solid solubilities are quite small[7]. Our experiments show insignificant interaction between bilayers of Mo/Cu and Mo/In, up to 600°C annealing. This absence of interdiffusion and compound formation is advantageous from the point of view of contacting CIS layers. However, impurities such as oxygen may be decisively involved in limiting interdiffusion. Indeed, the oxygen concentration in all Mo films is at least 5 at%, as measured by RBS.

Cu, In and Au are all mutually immiscible with Mo. According to the results of interdiffusion studies in Cu/Mo/Au trilayers, a rapid diffusion of Cu and Au across the Mo film and the formation of AuCu after annealing at 600°C for 30 min in vacuum occurs only when no impurity is present in the Mo layer. The Au-Cu interaction is impeded when 5.5 at% of oxygen is introduced to the Mo layer during deposition. The results of this investigation are relevant in the application of Mo thin films used as the contacts to $CuInSe_2$.

The phase diagram of the Mo-Se[7] system indicates the existence of $MoSe_2$ and Mo_3Se_4 below 1150°C. The atomic ratio of molybdeium to selenium, estimated from the RBS spectra of the as-deposited bilayer sample, suggests that the equilibrium in this bilayer system can be reached by the formation of a Mo_3Se_4 compound accompanied by an excess of Mo. However the Mo_3Se_4 was not observed. Instead, the $MoSe_2$ phase was detected in the Se/Mo sample annealed at 600°C by X-ray diffraction.In fact, some intermixing between the layers takes place already in the as-deposited sample. During subsequent annealing the reaction proceeds further and after 600°C annealing the two layers are completely intermixed, with the Se present on the sample surface.

For the pre-selenized Cu-In structures, every Cu/In bilayer sample we analyzed contained the CuIn phase in the as-deposited state, regardless of the deposition process employed. This phase is metastable at room temperature and must form by virtue of a fast interdiffusion mechanism. Probably related to that mechanism, and possibly associated with an actual melting of the In, is the observation that a planar Cu/In bilayer is an unstable configuration which breaks up easily into heavily intermixed lumps of about 1 um in size. The details of the sample morphology depend sensitively on the deposition technique. Annealing tends to smoothen out this initial roughness and to induce the formation of Cu-rich compounds.

5. Future Plan

We will further clarify the influence of the microstructure, surface morphology and different phases in the pre-selenized Cu-In samples on the performance of the $CuInSe_2$ after selenization. An investigation of diffusion in Cu/Mo/In trilayers will be undertaken to seek the correlation of diffusion with the contact stability on $CuInSe_2$. Substitution of Mo contacts by some other low diffusivity, stable metal compounds is studied with the collaboration of the Institute of Energy Conversion, University of Delaware.

C. REFERENCES

1. K. Mitchell, C. Eberspacher, J. Ermer, and D. Pier, Proc. 20th IEEE PV Specialists Conf., p. 1384, (1988).

2. S. Raud, Q.T. Vu, M-A. Nicolet, G.A. Pollock, K.W. Mitchell, J.A. Leavitt, M.D. Ashbaugh and L.C. McIntyre, MRS Symp. Proc. Spring Meeting, 1990 (in press).

3. S. Raud, J-S. Chen and M-A. Nicolet, Appl. Phys. A52, (in press).

4. T.L. Chu, S.S. Chu, S.C. Lin and J. Yue, J. Electrochem. Soc. 131, 2182 (1984).

5. V.K. Kapur, B.M. Basol and E.S. Tseng, Proc. 7th Intl. Conf. Ternary and Multinary Compounds, Snowmass, Co., Sept. 10-12, 1986 (Mat.Res.Soc. 1987), P. 219.

6. J.S. Chen, E. Kolawa and M-A. Nicolet, Solar Cells (in press).

7. L. Brewer and R.H. Lamoreaux, Molybdenum: Physico-Chemical Properties of its Compounds and Alloys, International Atomic Energy Agency Vienna, (1989).

Title:	**Role of Polycrystallinity in CdTe and $CuInSe_2$ Photovoltaics**
Organization:	Department of Physics, Colorado State University, Fort Collins, Colorado
Contributors:	J. R. Sites, principal investigator; R. A. Sasala, X. X. Liu, H. Tavakolian, and J. M. Nash

Objectives

The objectives of this program are quantitative separation of individual loss mechanisms and characterization of extraneous electron states responsible for excessive forward recombination current in polycrystalline thin-film cells.

Loss Mechanisms

Techniques for extraction of individual loss mechanisms have become relatively routine and quantitative [1-4]. The input required for current losses is quantum efficiency and reflection as a function of wavelength. For voltage losses, light and dark current-voltage curves are required.

Fig. 1 shows the lost photon fraction, one minus the quantum efficiency, for two CdTe cells. The independently measured reflection is nearly wavelength independent and accounts for nearly all the lost photons in the 600-700 nm range. Lower wavelength losses are attributed to window absorption, and lower wavelength ones to photons that penetrate too deeply to be collected. Integration of the lost photon fraction, normalized to the photon current of the spectrum gives the current loss for each mechanism. The dashed-curve cell in Fig. 1 has a thinner CdS window and also better collection of the more penetrating photons. Hence it has the superior photocurrent.

Voltage losses are found by comparison of a cell's forward current curve with that of a single-crystal cell of comparable bandgap. The polycrystalline forward current is generally 2-4 orders of magnitude larger, as illustrated in Fig. 2. Horizontal differences at a fixed current give the losses. For V_{OC} losses the forward current $J + J_L$ is equal to the photocurrent J_L; for V_{MP} the appropriate forward current is about 4 mA/cm^2. In this case the dark GaAs/polycrystalline CdTe difference is 170 mV at V_{MP}, the dark/light CdTe difference is 180 mV, and the series resistance reduction is 4 mA/cm^2. The total effect at maximum power, a loss of nearly 400 out of 920 mV, is substantial.

The individual current and voltage losses are shown in Fig. 3. The size of these losses will of course vary from cell to cell. The dashed-line cell of Fig. 1 has smaller window and deep photon absorption losses; one Ametek cell studied has about 80 mV less V_{MP} loss. For $CuInSe_2$ cells, the voltage loss is generally smaller, but the advantage is offset by a less optimum bandgap. For intermediate bandgap $CuGaInSe_2$, the forward current enhancement, and hence the voltage loss tends to be intermediate, and the resulting efficiency is similar to both CdTe and $CuInSe_2$.

Recombination Current

Three approaches are being taken to the problem of understanding excessive forward recombination current. One is a theoretical modeling study, basically making the question of what configuration of recombination states is required to fit the experimental current-voltage-temperature data. The second is continued analysis of capacitance data which gives a semi-quantitative measure of densities and energies of extraneous states with time constants in the 1 μs to 1 ms range. The third, which is new, is the extension of time response to much longer intervals through the digital record of current following an abrupt change in voltage or illumination.

References

1. Sites, J. R., "Analysis of Loss Mechanisms in Polycrystalline Thin-Film Solar Cells, SERI/TP-211-3950 (August 1990).

2. Sites, J. R., H. Tavakolian, and R. A. Sasala, "Analysis of Apparent Quantum Efficiency," Solar Cells 29, 39 (1990).

3. Sites, J. R., "Effect of Granularity on $CuInSe_2$ Solar Cell Response," Proc. of April 1990 MRS Symposium S.

4. Tavakolian, H., and J. R. Sites, "Individual Losses in Thin-Film CdTe Solar Cells," Proc. 21st IEEE Photovoltaics Specialists Conf. (1990), p. 556.

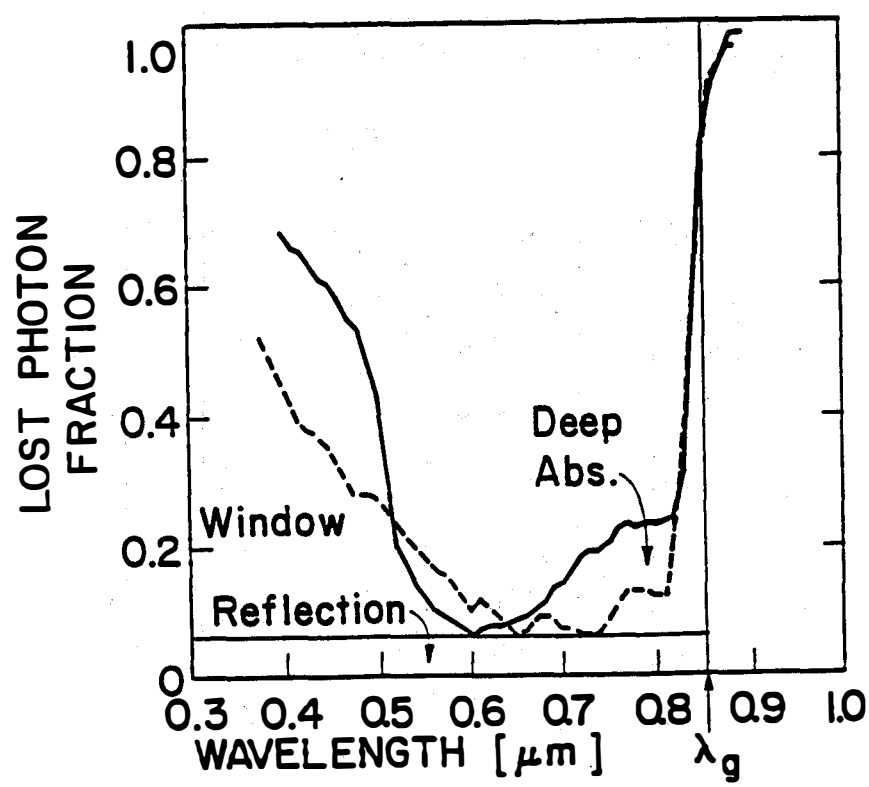

Figure 1. Use of quantum efficiency to separate CdTe photon losses. Solid line is a 9% Ametek cell, dashed is Photon Energy's best (12.3%) cell.

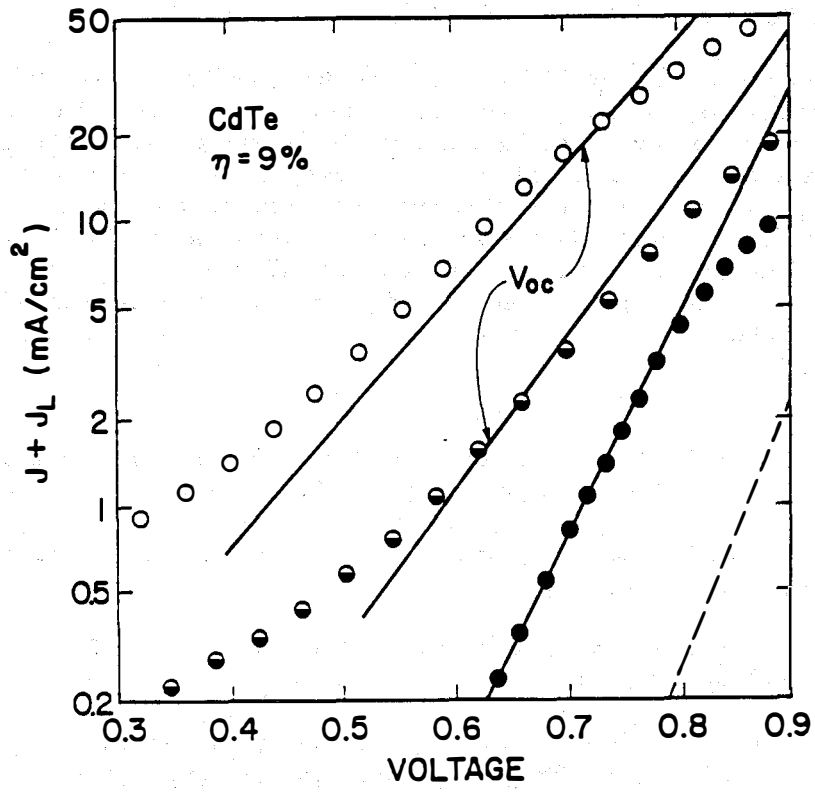

Figure 2. Forward current in dark, 6 mW/cm^2 light, and 60 mW/cm^2 light. Solid lines are fits for zero leakage or series resistance. Dashed line is crystalline GaAs forward current.

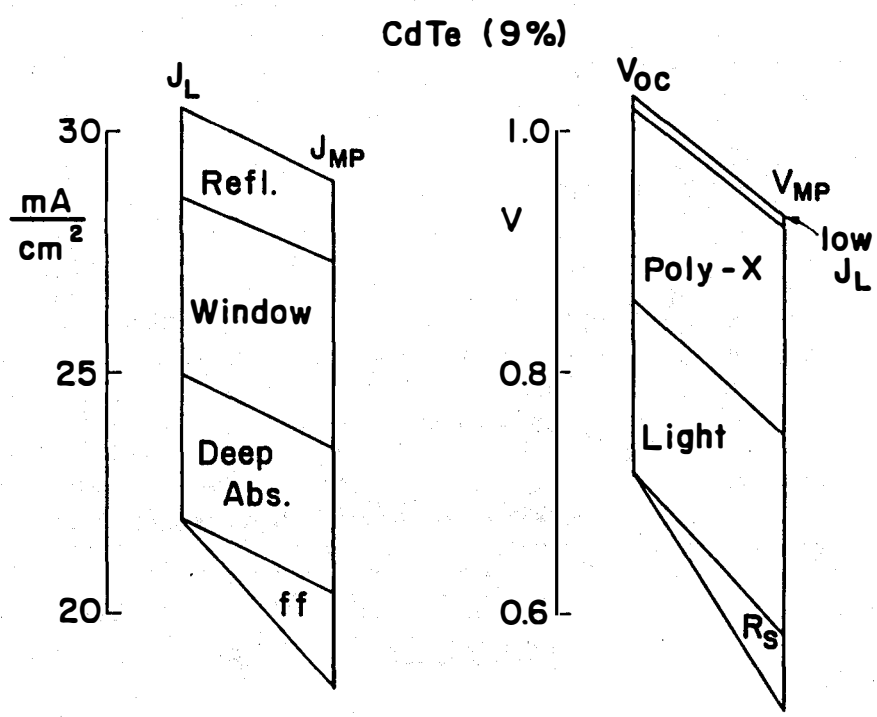

Figure 3. Individual current and voltage losses. Intercept values are shown to the left, maximum power losses to the right. Optimum values are at the top, actual ones at the bottom.

Title: **Development of High Efficiency CdTe and CdZnTe Solar Cells**

Organization: School of Electrical Engineering, Georgia Institute of Technology, Atlanta, Georgia.

Contributors: A. Rohatgi, R. Sudharsanan, S. A. Ringel, M. H. MacDougal, and A. Erbil

Objective:

The objective of this program is to improve the polycrystalline CdTe cell efficiency to ~15% and wide bandgap (1.7 eV) CdZnTe cell efficiency to ~10%.

Film growth:

CdTe films were grown on CdS/SnO_2/glass substrates by MOCVD and MBE. The Cd/Te ratio in the growth ambient was varied from 0.4 to 4.0. MBE CdTe and CdZnTe films were grown using a Varian Gen II MBE system.

Cell Fabrication:

P-i-n front-wall solar cells were fabricated at AMETEK applied materials laboratory [1]. P-n CdTe cells were fabricated by treating the CdTe films with $CdCl_2$ followed by an air anneal at 400°C for 30 minutes. Contact to the p-CdTe was made by a sequential evaporation of 100 Å Cu and 400 Å Au followed by an anneal at 150° C in argon atmosphere for 90 minutes. Finally, bromine-methanol etch was performed on the entire structure to etch off any residual Cd and Te oxides.

Material and device characterization:

Electrochemical surface photovoltage (SPV) measurement, Auger electron spectroscopy (AES), X-ray photoelectron spectroscopy (XPS), and transmission measurements were used for optical, physical and chemical characterization of the films. J-V-T, frequency dependent C-V, and bias dependent spectral response measurements were used to characterize device properties.

Results and Discussion:

MOCVD grown polycrystalline p-n CdTe solar cells with efficiencies of ~10% were demonstrated using an in-house cell fabrication facility (figure 1). The cell parameters of p-n CdTe cell are similar to p-i-n CdTe cells fabricated earlier by AMETEK [1]. Also, the spectral response of both cells show a strong wavelength independent bias dependence, suggesting the defects at the CdTe/CdS interface are limiting the performance of these cells. Attempts were made to improve the interface quality by (a) controlling CdTe film deposition conditions, (b) adjusting CdTe stoichiometry and (c) varying the in-situ preheat treatment of CdS in hydrogen atmosphere prior to CdTe deposition. In-situ preheat treatment of glass/SnO_2/CdS substrates at 450° C for 15 minutes prior to CdTe deposition was found to be essential for high performance devices it removes oxygen and related defect states. The heat treatment also simultaneously makes the CdS surface Cd-deficient resulting in Cd vacancy-related interface states. Since Cd deficiency in CdS is a potential source of interface defects, one way of reducing such defects is to grow CdTe in Cd-rich conditions. This was attempted by gradually increasing the Cd/Te ratio in the vapor from 0.4 to 4.0. The 10% cells were grown with Cd/Te ratio of 0.4, in a Cd deficient ambient. The SPV responses of these films were measured with light incident on the CdTe film side. Figure 2 shows SPV spectra of CdTe films grown on CdS with various Cd/Te ratios. It is interesting to note that the Cd-rich films show a significant increase in the surface photovoltage suggesting that the excess Cd in the CdTe film is eliminating the Cd deficiency at the CdS/CdTe interface. Since SPV response is an indicator of V_{oc}, it is possible to expect

higher V_{oc} on films grown under Cd-rich condition compared to 9.7% efficient CdTe cells grown in Te-rich ambient. If the higher SPV response is maintained throughout the cell processing, then we should be able to attain a higher V_{oc} and efficiency compared to the 10% efficient cells. Preliminary model calculations suggest that the removal of these defects can increase the cell efficiency from 10% to 13.5%.
Further improvement in efficiency can be achieved by eliminating the loss due to absorption of high energy photons in the thick (1500 Å) CdS window layer. Attempts are being made to deposit thin CdS films by the chemical immersion method. We have successfully grown CdS films in the thickness range of 400 to 1400 Å by controlling the immersion time and have found an appreciable improvement in the transmission of 400 Å CdS film in the short wavelength range [2].

CdZnTe Solar Cells:

Polycrystalline CdZnTe films with a 1.7 eV bandgap were successfully deposited by MBE on CdS/SnO_2/glass substrates. However, CdZnTe solar cells fabricated by the identical process sequence used successfully for high efficiency CdTe cells gave efficiencies of only ~ 4.4%. In addition, the CdZnTe bandgap shifted from 1.7 eV to 1.55 eV and the series resistance (~ 2-6 ohm-cm^2) was 3-5 times higher than in the counterpart CdTe solar cells. Detailed investigations were conducted to understand and remove the source of these problems.

ESCA analysis and AES profiles show that without any post-anneal chemical etch, a significant amount of Cd-O, Te-O and Zn-O are present at and below the CdZnTe surface. After an etch in Br_2:CH_3OH, which was used in the standard cell fabrication prior to ZnTe/Ni back contact deposition, both Cd and Te oxides were removed from the surface but the Zn-O remained at and below the surface, responsible in part for the high series resistance. In an attempt to remove the Zn-O and make the CdZnTe surface Te rich, various chemical etchants were investigated. A post-anneal saturated pottasium dichromate ($K_2Cr_2O_7O_7$:H_2SO_4) etch removed the near surface region that contained Zn-O and yielded a ~0.15 um Te-rich surface layer with little or no detectable trace of Cd, Zn, or oxygen (figure 3). This should eliminate the contribution from high contact resistance to the measured high series resistance [3].

The next step was to investigate the process-induced bandgap shift observed in processed CdZnTe films. AES depth profiles shown in figure 4 and the SPV spectra in Figure 5 after the standard air anneal, with and without the $CdCl_2$ treatment, clearly demonstrate that it is not the air anneal itself, but the $CdCl_2$ treatment coupled with the air anneal that is responsible for the bandgap shift. $CdCl_2$ treatment is bypassed to preserve the bandgap, a very weak photoresponse is observed, resulting in only 1-2% efficient cells. However, the SPV data clearly show that incorporation of $CdCl_2$ during the processing of CdZnTe cells resulted in much higher photovoltages but the cutoff edge (or bandgap) shifted from 1.7 eV to 1.55 eV. The $CdCl_2$ treatment was also found to reduce the series resistance of the CdZnTe/CdS cells by a factor of ~ 10.
In order to investigate both the need and beneficial effects of the $CdCl_2$ treatment on CdTe-based polycrystalline solar cells, experiments were first conducted on p-i-n CdTe solar cells fabricated with and without the $CdCl_2$ treatment to eliminate the complication due to the presence of Zn. It is shown that $CdCl_2$ is essential for high efficiency CdTe solar cells because it promotes grain growth which improves bulk collection, reduces interface state density, and eliminates the tunneling of carriers through the interface to improve V_{oc}, J_{sc}, and efficiency [2].

Conclusions:

In-situ pre-heat treatment of glass/SnO_2/CdS substrates at 450° C for 15 minutes prior to CdTe deposition was found to be essential for high performance devices because it removes oxygen and related defect states. The heat treatment also simultaneously makes the CdS surface Cd-deficient resulting in Cd vacancy-related interface states. Preliminary model calculations suggest that the removal of these states can increase the cell efficiency from 10% to 13.5 %. Photon absorption in the CdS film also limits the cell performance and elimination of this loss mechanism can result in efficiencies in excess of 18%. Thus a combination of optimum preheat treatment, proper Cd/Te ratio, and thin CdS films should yield a significant

improvement in the MOCVD CdTe cell efficiency.

The CdTe process sequence cannot be used to fabricate efficient CdZnTe cells because it results in high resistance and a bandgap shift from the desired value of 1.7 eV to 1.55 eV. The contribution to the high series resistance from non-ohmic back-contact was solved by using a saturated dichromate instead of the Br:CH_3OH post-anneal etch. It is shown that $CdCl_2$ is essential for high efficiency CdTe solar cells because it promotes grain growth which improves bulk collection, reduces interface state density, and eliminates the tunneling of carriers through the interface to improve V_{oc}, J_{sc} and efficiency. However, the use of a $CdCl_2$ dip prior to air anneal was established to be the main source of the observed bandgap shift in CdZnTe due to $ZnCl_2$ formation by substitution of Cd for lattice Zn. This also resulted in incomplete grain growth in CdZnTe since much of the $CdCl_2$ was consumed by this process. Development of an alternative sintering aid, which induces grain growth but prevents the bandgap shift, is the key to the success of widegap polycrystalline CdZnTe solar cells for tandem cell applications.

References:

1. R. Sudharsanan and A. Rohatgi, Solar Cells, 1990.
2. A. Rohatgi, R. Sudharsanan, S. A. Ringel, and M. H. MacDougal, Solar Cells (In Print).
3. Annual Report, Photovoltaic Program Branch, FY 1989. (March 1990).

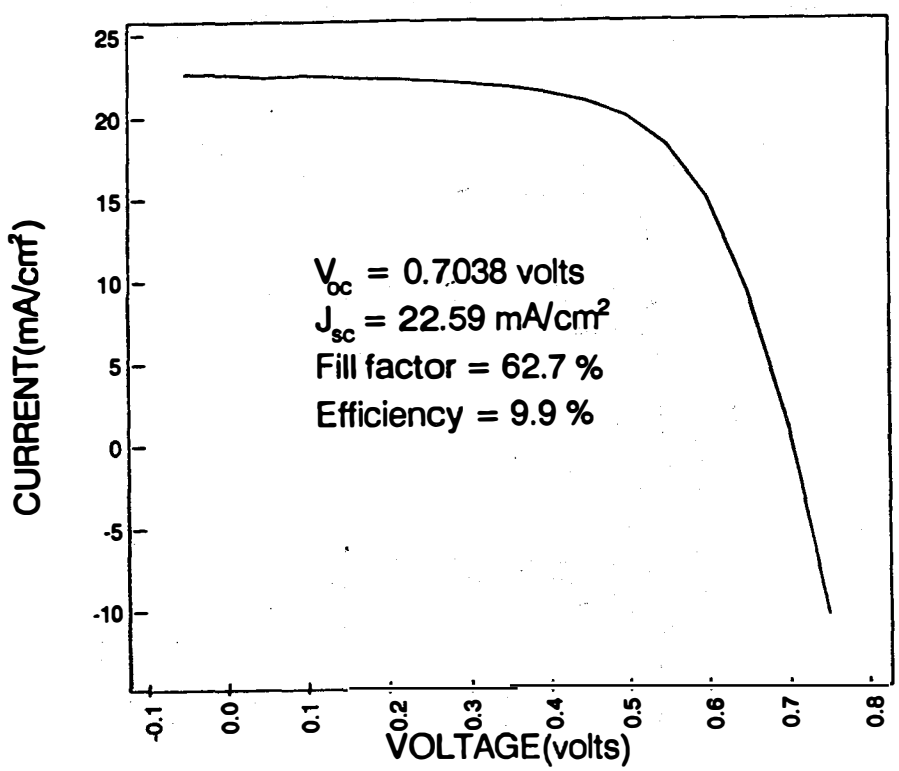

Figure 1. Light I-V data of 9.9% p-n MOCVD-grown CdTe/CdS solar cells.

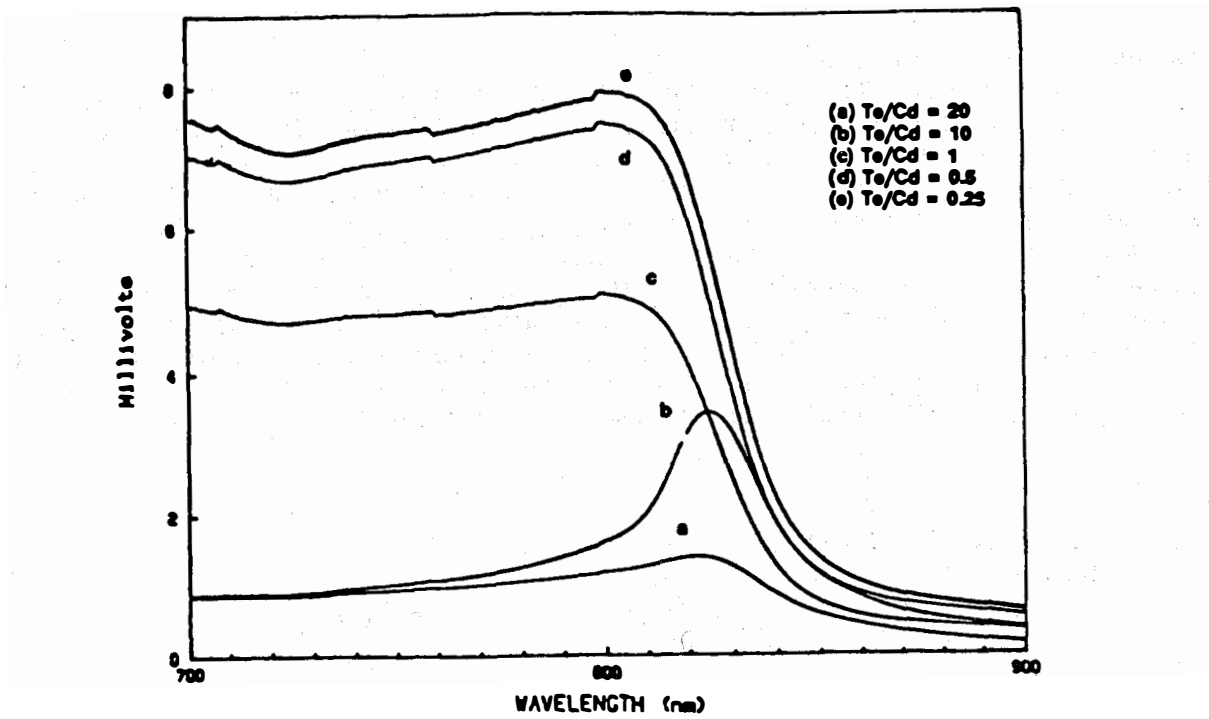

Figure 2. SPV spectra of CdTe films grown by MOCVD on CdS/SnO_2/glass substrates with different Cd/Te ratios.

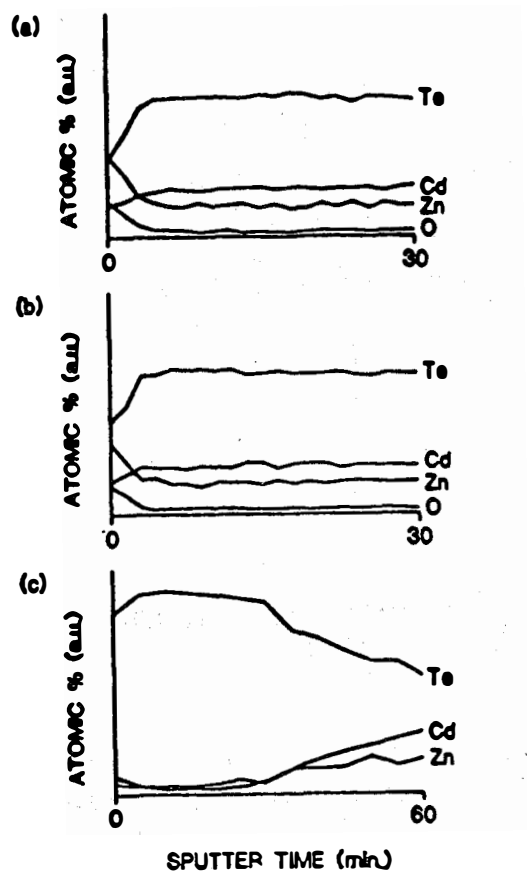

Figure 3. Auger depth profiles of air annealed CdZnTe films after (a) no post-anneal etch, (b) Br_2:CH_3OH etch, and (c) saturated pottasium dichromate etch.

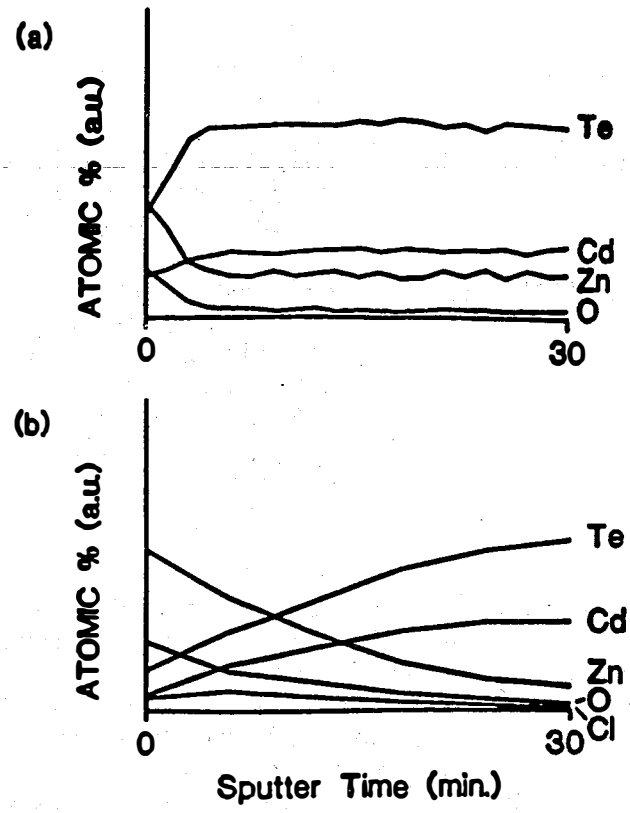

Figure 4. Auger depth profiles of air annealed CdZnTe films (a) without $CdCl_2$ treatment and (b) with $CdCl_2$ treatment.

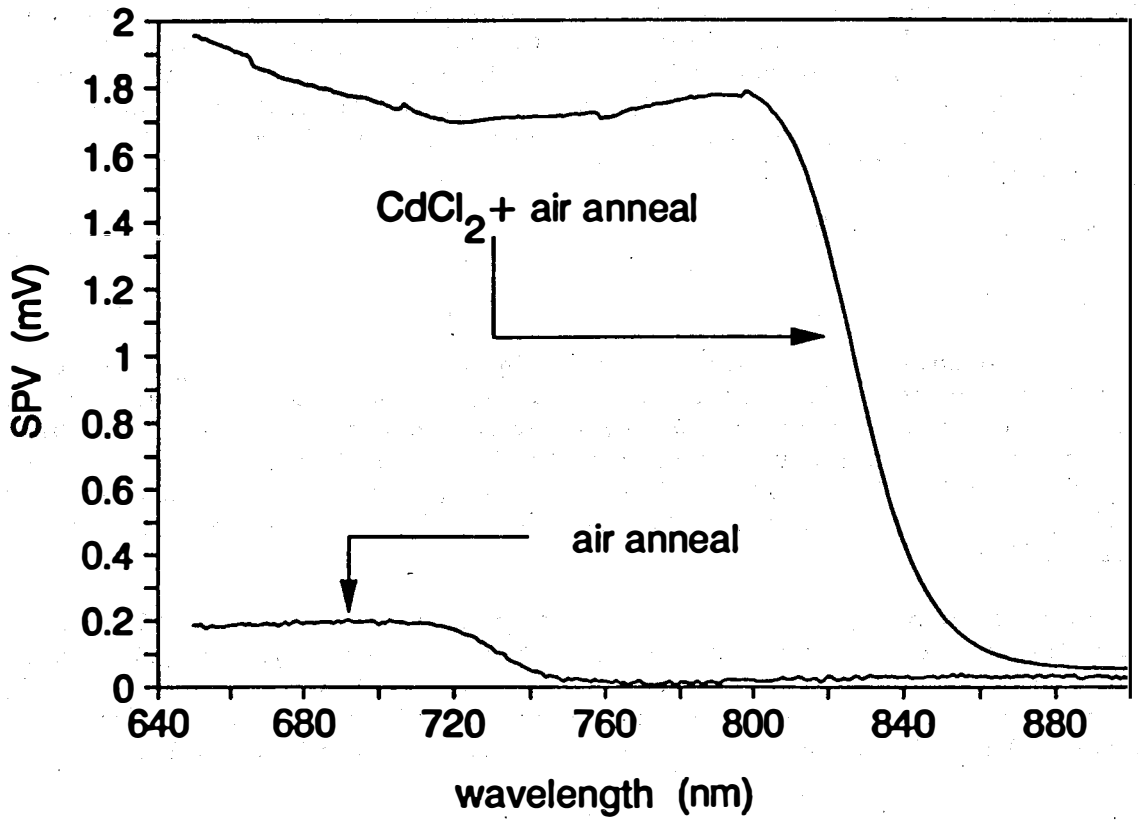

Figure 5. Electrochemical surface photovoltage spectra of air annealed CdZnTe/CdS structures with and without the $CdCl_2$ treatment.

Title: **Polycrystalline Thin-Film Materials and Devices**

Organization: Institute of Energy Conversion
University of Delaware
Newark, Delaware 19716

Contributors: B.N. Baron, Projector Director; R.W. Birkmire and J.E. Phillips, Principal Investigators; B.E. McCandless, M. Roy, W.N. Shafarman, S.S. Hegedus, R.D. Varrin, Jr., D.A. Fardig and T.I. Yokimcus, Research Contributors

Objectives

The objectives of this research are to obtain the understanding of the materials processing, properties and performance of polycrystalline $CuInSe_2$ and CdTe thin-film solar cells needed to achieve the goals for efficiency, reliability and cost for flat plate thin-film photovoltaic systems set by DOE for the National Photovoltaics Program. A further objective of this program is to support the development of a competitive U.S. photovoltaic industry through collaboration with other research groups and the training of photovoltaic engineers and scientists.

Technical Approach

Issues for $CuInSe_2$ addressed in this work are development of a process for forming $CuInSe_2$ films by the selenization of Cu and In layers and improving V_{oc} of $CuInSe_2$/CdS solar cells by modifying the bandgap of the space charge region in the $CuInSe_2$ with a thin layer of $Cu(InGa)Se_2$. Research on CdTe is concerned with post-deposition processing used to fabricate high efficiency CdTe/CdS solar cells with evaporated CdS and CdTe.

Significant Results

$CuInSe_2$ Film Growth

The formation of $CuInSe_2$ by selenization of Cu/In layers in flowing H_2Se is being investigated as a process which is expected to be scalable for large area cells and modules. The Cu and In layers are sequentially deposited by electron beam evaporation with Cu/In atomic ratios of 0.85-0.95 and fixed relative thicknesses to produce 2 μm thick $CuInSe_2$ films. The Cu/In ratio and In surface morphology, which is affected by the deposition rate, are critical for achieving homogeneous single phase $CuInSe_2$.

Selenization in flowing H_2Se has been done at temperatures from 380-450°C in a quartz reaction tube using from 2-8% H_2Se by weight in an Ar balance (1). Total flow rates from 35-100 sccm and reaction times from 30-120 min. have been used. Composition measurements of samples selenized for different times show that single phase $CuInSe_2$ is formed within 30 min. The formation of $CuInSe_2$ takes

more than 10 times longer when just the Cu/In substrates are heated compared to when the entire reactor is heated. This suggests that the Cu/In surface reacts primarily with Se_x species formed by the pyrolysis of the H_2Se. XRD analysis of partially reacted films indicates that the selenization proceeds primarily via reaction of the Se_x species with the Cu/In to form $Cu_{2-x}Se$ and In_2Se_3 compounds which then form $CuInSe_2$. The best cell made to date using $CuInSe_2$ from this process had V_{oc}=0.404V, J_{sc}=36.1 mA/cm^2, FF=67.7% and 9.9% efficiency.

An alternative to H_2Se for forming $CuInSe_2$ is the direct reaction of layers of Cu/In/Se. E-beam evaporated Cu/In bi-layers were coated with Se by thermal evaporation in a bell-jar. The Cu/In/Se layers were heated <u>in situ</u> under a background of Se vapor. Single phase $CuInSe_2$ was observed and $CuInSe_2$/CdS cells with efficiencies over 7% were obtained.

V_{oc} Enhancement in $CuInSe_2$ Cells

Analysis of $CuInSe_2$/(CdZn)S cells has shown that the diode mechanism is dominated by Shockley-Read-Hall (SRH) recombination in the space charge region, where p~n, and the barrier height is equal to the bandgap of $CuInSe_2$ (2).

An approach to improving V_{oc} is to increase the bandgap in the space charge region, using Cu(InGa)Se_2. When the Cu(InGa)Se_2 layer is thin compared to the depletion width, loss in J_{sc} should be minimal. Cu(InGa)Se_2 layers were deposited by thermal evaporation using four elemental effusion sources as thin discrete layers on two step evaporated $CuInSe_2$ films (3).

I-V results are shown in Table 1 for cells with three thicknesses of 1.15 eV bandgap Cu(InGa)Se_2 layers. With the thickest layer, V_{oc} is close to that of a cell with uniform Cu(InGa)Se_2 but J_{sc} is smaller. As the Cu(InGa)Se_2 layer thickness is reduced, V_{oc} decreases and J_{sc} increases. In each case, spectral response curves show collection out to 1.0 eV, the $CuInSe_2$ band edge. However, the collection is strongly voltage dependent, particularly in the long wavelength response, resulting in low J_{sc} and FF. This may be due to a reduced diffusion length when Ga is present or a barrier in the conduction band which increases as the Cu(InGa)Se_2 thickness increases.

V_{oc} may also improve by decreasing the space charge width if the diffusion length is sufficiently large to collect the photogenerated minority carriers. The diffusion length and absorption coefficient of the $CuInSe_2$ in a completed high efficiency cell fabricated with a semi-transparent, 400Å, Mo back contact has been determined by analysis of the bi-facial spectral response (4). Figure 1 shows the absorption coefficient determined from the best fit at several voltage biases along with data from a compilation of results on single crystal and thin film $CuInSe_2$. The same data gave a diffusion length $\approx$1.5 μm and a space charge collection length $\leq$0.1 μm under normal operating conditions of the solar cell. Thus, the minority carriers are primarily collected by diffusion and reducing the space charge width should not decrease J_{sc}. Experiments are underway to investigate this method for improving V_{oc}.

CdTe Cell Processing

A post-deposition and contacting process has been developed and used to fabricate high efficiency, ~10%, CdS/CdTe solar cells with evaporated CdTe and CdS films deposited on ITO coated glass with Cu/Au contacts. After the CdTe deposition, a 0.5 μm $CdCl_2$ coating is applied and the sample heat treated in dry air at 400°C for 30 min. and rinsed in DI water. XRD analysis showed improved (111) orientation of the CdTe, with the grain size increased to ~1 μm, and a shift in the lattice parameter. Auger and SIMS depth profiles showed interdiffusion of Te and S. Also, a 20 meV red shift in the CdTe optical absorption edge was observed. These results suggest formation of a CdS_xTe_{1-x} layer with x~0.01-0.02 which would result in narrower bandgap (5).

I-V and SR measurements were made with illumination through glass/ITO/CdS and through a semi-transparent Cu/Au back contact. The SR curves measured before and after 150°C heat treatment in air for 0.5-2 hr. are shown in Figure 2. Initially, the device had low V_{oc} and J_{sc}~8 mA/cm^2 and the SR showed significant collection over the entire wavelength range for illumination from either side. After heat treatment, J_{sc} increased to 19 mA/cm^2. The SR increased uniformly when illuminated through the CdS while it decreased, with the maximum response near the CdTe absorption edge, when illuminated through the Cu/Au. This change in the SR indicates a change from p-i-n to p-n heterojunction operation which may have resulted from diffusion of Cu into the bulk CdTe, doping its p-type.

A final chemical treatment by immersion in 0.01% Br_2-CH_3OH, for 5 s. increases V_{oc} by 50-150 mV, and improves fill factor due to the contact becoming more ohmic, as seen by a change in the forward bias region of the I-V curve. J_{sc} and the spectral response do not change. Auger and XPS analysis show the formation of a Te-rich region near the CdTe surface. The excess Te can form Cu_2Te and $AuTe_2$ which make ohmic contact to p-type CdTe. The increase in V_{oc} may result from a chemical interaction at the grain boundary resulting in a reduction in Jo. The highest efficiency cell had V_{oc}=0.764V, J_{sc}=18.0 mA/cm^2, FF=73.4%, and 10.1% efficiency, measured under ELH illumination at 32°C and J_{sc} normalized to AM1.5.

I-V data as a function of temperature were used to determine barrier height and diode A-factor of CdS/CdTe/Cu/Au cells. The barrier height was 1.3-1.4 eV, slightly less than the bandgap of CdTe. This may be due to recombination from band tail states in the CdTe, which were also observed in the spectral response, or from a narrower bandgap in the junction region of the CdTe due to interdiffusion of S and Te. A-factors were 1.5 to 2.0. These results are consistent with SRH.

Conclusions

An apparatus and procedure for fabricating 10% $CuInSe_2$/CdS thin-film solar cells by reacting Cu/In layers with H_2Se has been developed. Characterization of the mechanisms of $CuInSe_2$ film growth by selenization revealed that initial reactions involve liquid-solid-vapor formation of Cu_xSe and In_2Se and that the initial reaction rate is limited by transport of gas phase Se_x species to the substrate. Final formation of device quality $CuInSe_2$ is governed by solid state reaction between Cu_2Se and In_2Se_3. The initial results on the formation of $CuInSe_2$ films

by selenization of Cu/In/Se layers indicate that this may be a viable alternative to selenization using H_2Se. Future research is aimed at continued optimization and analysis of the growth process, and investigation of alternatives to H_2Se.

Experiments with band gap modified $CuInSe_2$ devices utilizing a thin layer of $Cu(InGa)Se_2$ showed that V_{oc} can be increased while generating carriers out to the $CuInSe_2$ band edge, although the bandgap modified layer needs to be further optimized to reduce losses in J_{sc} and FF. Deposition of bandgap modified layers by selenization will be investigated.

A process consisting of post-deposition heat treatment contacting steps has been develop to fabricate high efficiency CdTe/CdS solar cells using CdTe films deposited by vacuum evaporation. Future research will be directed to improving CdTe/CdS cell efficiency by developing improved window and contact layers.

References

1. R.D. Varrin, Jr., et al., Proc. 21st IEEE Photovoltaic Specialists Conf. (1990) 529-534.

2. M. Roy et al., Proc. 20th IEEE Photovoltaic Specialists Conf. (1988), 1618-1623.

3. R.W. Birkmire et al., Proc. 21st IEEE Photovoltaic Specialists Conf. (1990) 550-555.

4. J.E. Phillips, Proc. 21st IEEE Photovoltaics Specialists Conf. (1990) 782-786.

5. K. Ohata et al., Jpn. J. Appl. Phys. **12** (1973), 1198.

Table 1

$CuInSe_2/Cu(InGa)Se_2$ Cell Results

$Cu(InGa)Se_2$ thickness (μm)	V_{oc} (V)	J_{sc} (mA/cm^2)	FF (%)
0.4	0.49	22	48
0.2	0.47	24	38
0.1	0.45	31	33

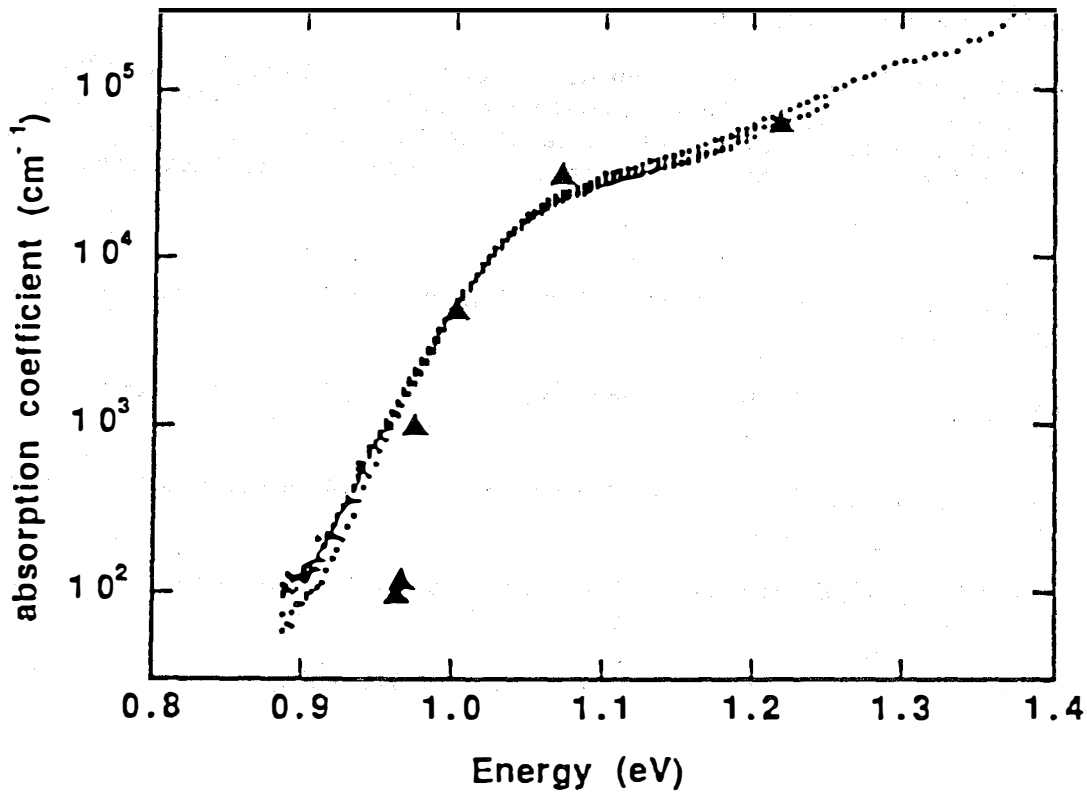

Figure 1. The absorption coefficient of $CuInSe_2$ determined from the bi-facial SR compared to a compilation of optical data from literature (▲).

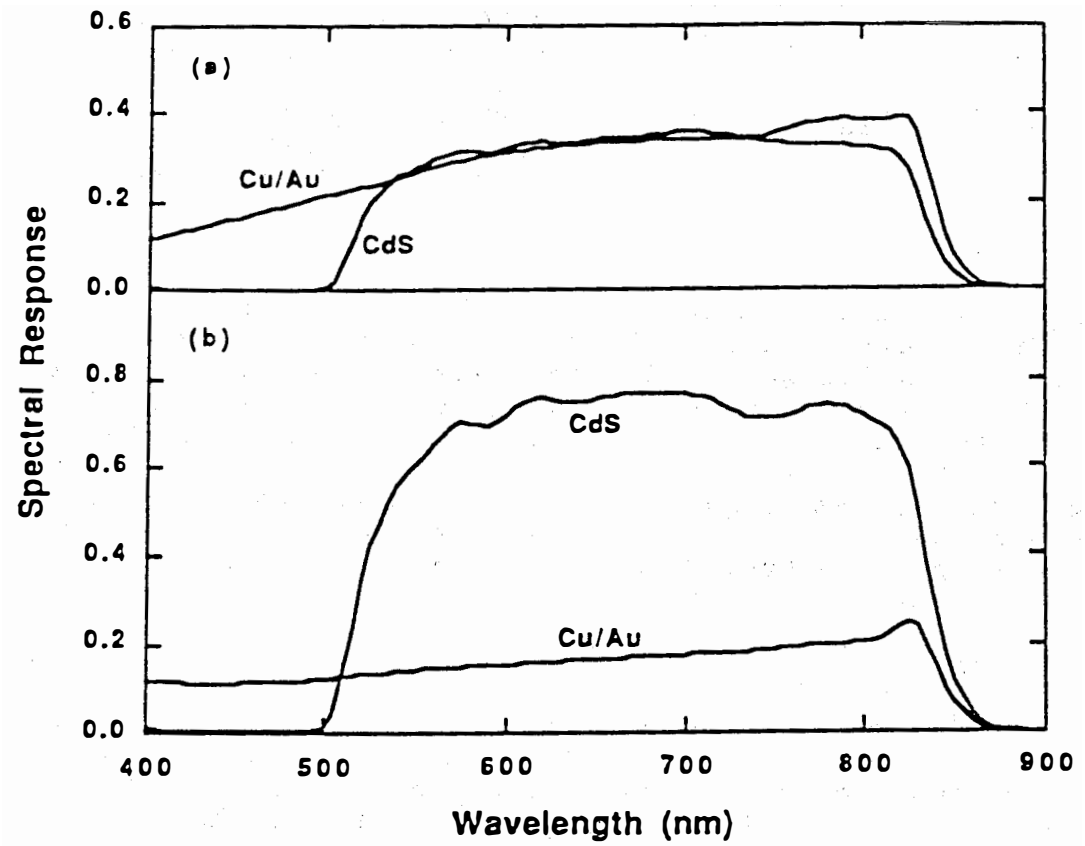

Figure 2. The SR of a CdS/CdTe cell measured with illumination through the CdS or Cu/Au contact; (a) after Cu/Au deposition, (b) after 150°C air heat treatment.

Title: **High Efficiency Copper Ternary Thin Film Solar Cells**

Organization: International Solar Electric Technology (ISET), 8635 Aviation Blvd., Inglewood, CA 90301

Contributors: B.M. Basol and V.K Kapur, principal investigators; A. Halani, W. Ragland and C. Leidholm

The objective of this program is to develop high efficiency thin film $CuInSe_2$ (CIS) solar cells and sub-modules using a two-stage process. The two-stage process involves first deposition of a Cu-In layer of controlled stoichiometry (Cu-to-In ratio) on a substrate and then selenization of this Cu-In film to form CIS.

During the present contract period we have continued our development work on the evaporation/selenization approach that utilized evaporated Cu-In precursors for selenization.

Cu-In Layers

Cu and In layers were deposited on Mo coated glass substrates using an E-beam evaporator. The effect of the deposition parameters and the deposition sequence on the nature of the Cu-In films were studied. It was discovered that unlike the electro-deposited Cu/In stacks which mostly consist of two separate elemental phases (Cu and In), Cu-In layers evaporated on uncooled substrates were, to a large extent, alloyed. The degree of alloying depended upon the deposition conditions and the deposition sequence. Fig. 1 shows the XRD data taken from two samples prepared on Mo/glass substrates. Sample A was obtained by evaporating an In layer over the Cu film which was previously deposited on the Mo layer. The evaporation sequence was reversed for Sample B. The Cu-to-In ratio in both of these films was 0.9. The XRD data of Samples A and B show many peaks which are not associated with the pure Cu and In peaks. These extra reflections are due to Cu-In alloys some of which have been identified in Fig. 1. In the case of In-on-Cu film (Sample A), there are peaks belonging to the CuIn phase as well as to the Cu phase. An additional set of peaks (labeled as ?) could not be identified using the JCPDS sets 1-38, but they were tentatively attributed to a cubic phase with a lattice parameter of a=4.657 Å. In addition to the alloy peaks seen in Sample A, Sample B also exhibits peaks associated with the Cu-rich phases of Cu-In alloys (Cu_4In and Cu_7In_4).

The sequence of deposition for the Cu and In films also affects the morphology of the resulting layer. Films obtained by evaporating In over Cu layers are generally better in terms of their surface micro-structure compared to those obtained by

evaporating Cu over In. Poor wetting of the Mo surface by the In film is thought to give rise to a non-uniform Cu-In layer with a rough surface morphology in samples prepared by evaporating Cu over In. Selenization of such non-uniform Cu-In films results in non-uniform CIS morphology.

CIS Films

After the evaporation step, the Cu-In layers were placed into a furnace for selenization. Selenization was typically carried out for 1 hour at 400 °C in a 5-10% H_2Se (in Ar) atmosphere. The nature of the selenized compound layers were found to strongly depend on the nature of the Cu-In precursors. Specifically, the microstructure of a CIS film was, to a large extent, determined by the processes and procedures used in depositing the Cu-In layers. Fig. 2 is a SEM picture of a CIS film obtained by selenizing a Cu-In film obtained by evaporating Cu over In. The non-uniformity of the grain structure observed in Fig. 2 is a result of the non-uniformities in the precursor film and it can be directly translated into the stoichiometric non-uniformities in the grains of this film. It should be noted that solar cells fabricated on such non-uniform films display poor fill factors and open circuit voltages due to the shorting effect by the Cu-rich grains which most probably contain Cu-selenide phase.

The deposition technique of the Cu-In layers also affects the grain structure of the CIS films. The film of Fig. 3 was obtained by selenizing an electrodeposited Cu/In stacked layer. The film of Fig. 4, on the other hand, was prepared using an evaporated (therefore, alloyed) Cu-In film. It is observed that the electrodeposited and selenized CIS film has well defined grains that are 2.0-3.0 um in size. The evaporated/selenized film, on the other hand, has a sub-micron grain size. This observation can be explained by the fact that the selenization of a Cu/In stacked layer gets initiated at the surface of the In film which is in the form of a liquid at above 157 °C. Therefore, during the early stages of the selenization period both the selenization of In and the diffusion of Cu takes place into a liquid medium. As a result, large grains are formed. In the case of the evaporated and alloyed Cu-In films with high melting points there is no liquid medium and the alloy film is transferred into CIS by the gas/solid reactions and solid/solid diffusion processes. As a result, the grain size is smaller.

Alloying of the evaporated Cu-In layers may have another effect on the CIS film properties. As we had previously reported, one of the problems associated with the electrodeposited/selenized CIS films is their poor adhesion to the Mo coated substrates. The reason for the poor adhesion is believed to be the nearly 3-fold volume expansion caused by the incorporation of Se into the Cu/In layers during the selenization process. This volume expansion exerts considerable stress on the already weak Mo/CIS interface and causes the films to peel. Measurements made on the evaporated Cu-In layers showed that the density of the alloyed layers was

much less than the individual densities of the Cu and In films. An alloy film obtained by evaporating a 0.2 um thick Cu film and a 0.4 um thick In layer, for example, had a thickness of 1.1 um. This corresponds to a volume expansion of almost 2-fold and Se can be more easily incorporated into these films without exerting much stress on the Mo/CIS interface.

Device Fabrication

Both evaporated and chemically deposited CdS layers were used as junction partners to the CIS films. The evaporated CdS films had the commonly used two-layer structure that was obtained by first evaporating a 0.4-0.8 um thick undoped layer and then depositing on top of it a 0.8-1.0 um thick In-doped region. Chemically deposited CdS layers were 500-3000 Å thick and they were obtained by the solution growth method. Chemical deposition (also known as dip-coating or solution growth) is a technique that is known to yield thin layers of near-stoichiometric, highly transparent CdS films. In our work we have used a solution with cadmium acetate, ammonium hydroxide and TEA. These reagents were mixed with deionized water and warmed up to 65 °C. A CIS coated substrate was placed in the container with the above solution mixture, and a thiourea solution was then added into the container with stirring. After 5-20 minutes, a coating of CdS that was 500-3000 Å was obtained.

Because of their excessive sheet resistance values the chemically deposited CdS films need to be contacted by TCO layers. We have used both ITO and ZnO films for this purpose. ZnO layers were deposited by the magnetron sputtering technique. The target material was doped with 2 wt% Al_2O_3 and the deposition rate was around 5 Å/sec. The surface of the target was first conditioned by sputtering onto the shutter in a 10% O_2 + 90 % Ar plasma. The oxygen flow was then cut off and the shutter was opened for deposition over the substrates. We were able to obtain films with resistivity values as low as $1x10^{-3}$ ohm-cm by this technique.

The illuminated I-V characteristics one of the most efficient CIS solar cells prepared using thick, evaporated CdS layers is given in Fig. 5a. This cell has the solar cell parameters of V_{oc} = 0.47 V, J_{sc} = 30.50 mA/cm^2, FF = 71.50 % and Eff. = 10.26%. The active area efficiency of this device was 10.8 %. It should be noted that the current density values in cells with thick CdS window layers are rather low. Improvement of these values to over 35 mA/cm^2, which is our near term goal, will improve the efficiency to over 12 %.

Fig.5b belongs to a cell with an ITO/ZnO/CdS window layer where the thickness of the chemically deposited CdS film was about 0.1 um. The active area of this device was 0.075 cm^2. The solar cell parameters of Fig.5b are: V_{oc}= 0.4627 V, J_{sc}= 35.36 mA/cm^2, FF= 66.59% and Eff.= 10.89 % (active area). Reduction of the CdS thickness below 1000 Å is expected to further improve the short circuit current value of these cells. The best solar cell

parameters observed during this period of research were; V_{oc} 0.49 V, J_{sc} 36.36 mA/cm^2 and FF = 71.59 %. These results clearly demonstrate the near term potential of the two-stage process.

During this period we have also achieved deposition of up to 50 cm^2 area CIS films by the evaporation/selenization technique. Having achieved this , we have initiated work on the sub-module integration procedures. The sub-module fabrication process consisted of 5 major steps: a) Substrate preparation, b) metals deposition, c) selenization, d) device interconnection scribe, e) CdS deposition, and f) device isolation scribe. Using this approach we have fabricated several sub-modules with areas of 20-50 cm^2. One of these samples contained twenty interconnected cells of about 3.5 cm wide and 2.5 mm length and it gave an open circuit voltage of 8.8 Volts. Low resistivity ZnO should be deposited over the CdS layer of step e) for efficiency improvement in these preliminary sub-modules.

Conclusions

In this work we have successfully developed a two-stage process for the deposition of CIS thin films. We have studied the correlation between the micro-structural characteristics of the CIS layers and the nature of the Cu-In precursors. We have fabricated solar cells with better than 10% efficiency using the CIS films deposited by this very promising method. We have demonstrated the integration steps on preliminary sub-modules. Small improvements in the device design, especially in the window layers, will provide cells with over 12% efficiency in the very near future. Our work during FY91 will concentrate on the fabrication of large area (1 ft^2) sub-modules and high efficiency (14-15 %) cells.

List of papers and reports published on our process since the FY 1989 PV Branch Annual Report are given below.

References

1. V. K. Kapur, B. M. Basol and R. C. Kullberg, "High Efficiency Cu-Ternary Thin Film Solar Cells," Annual Report on SERI Contract XL-7-06031-6, July 1989.
2. B. M. Basol and V. K. Kapur, "High Efficiency Cu-Ternary Thin Film Solar Cells," Final Report on SERI Contract XL-7-06031-6, November, 1990.
3. B. M. Basol and V. K. Kapur, Appl. Phys. Lett., 54 (1989) 1918.
4. B. M. Basol, V. K. Kapur and R. C. Kullberg, Solar Cells, 27 (1989) 299.
5. B. M. Basol and V. K. Kapur, IEEE Trans. Electron. Dev., 37 (1990) 418.
6. B. M. Basol and V. K. Kapur, Proc. 21st IEEE Photovoltaic Specialists Conf., Florida, 1990, IEEE, New York, 1990,

p. 546.
7. V. K. Kapur and B. M. Basol, Proc. 21st IEEE Photovoltaic Specialists Conf., Florida, 1990, IEEE, New York, 1990, p. 467.
8. B. M. Basol and V. K. Kapur, Solar Cells, 1990 (in press).

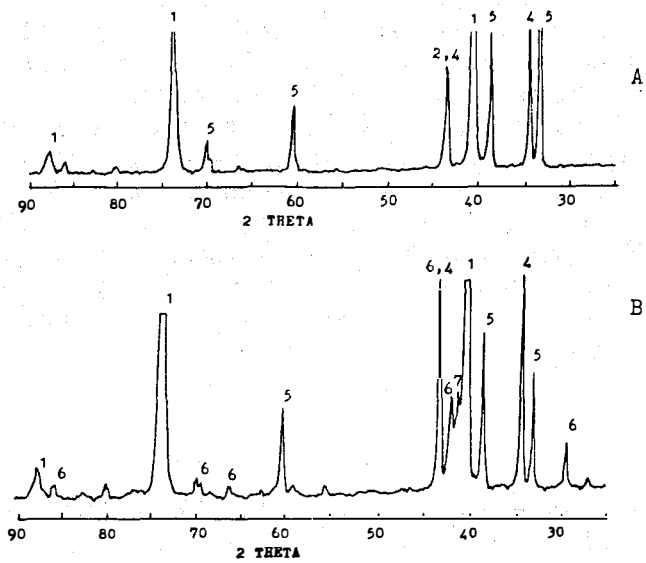

Fig. 1. XRD data taken from two Cu-In films. Film A: In/Cu/Mo/glass, Film B: Cu/In/Mo/glass.(1:Mo,2:Cu,4:CuIn,5:?,6:Cu_4In and 7:Cu_7In_4).

Fig. 2. SEM of a CIS film obtained by selenizing a Cu/In/Mo/glass structure.

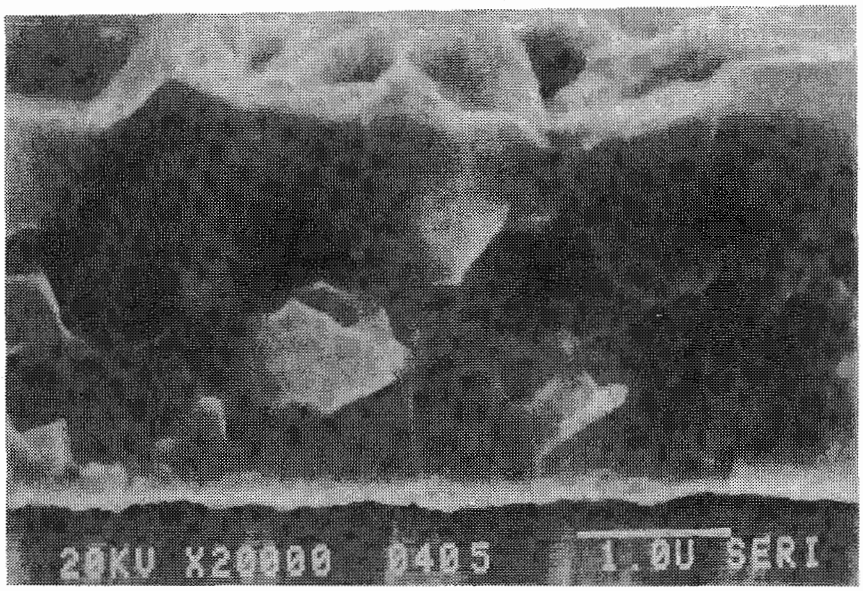

Fig. 3. SEM of an electrodeposited/selenized film.

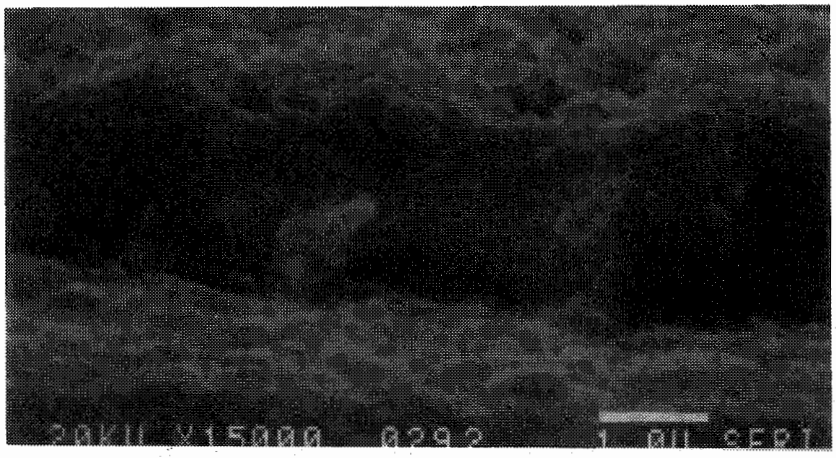

Fig. 4. SEM of an evaporated/selenized film.

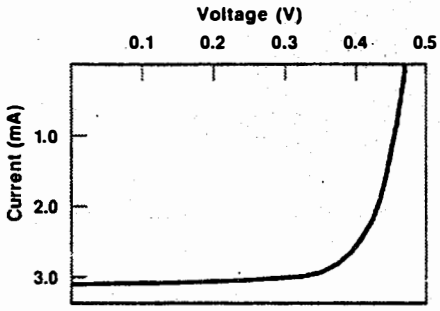

CdS / CIS / Mo / Glass
V_{OC} = 0.470 V
J_{SC} = 30.50 mA / cm^2
FF = 71.50%
Eff = 10.26%
Eff(Active Area) = 10.80%

a)

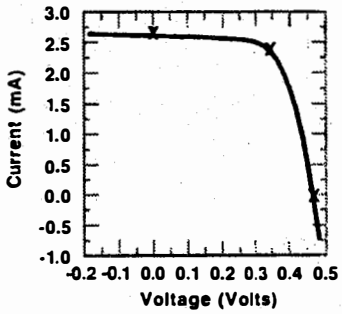

ITO / ZnO / CdS / CIS / Mo / Glass
V_{OC} = 0.463 V
J_{SC} = 26.52 mA / cm^2
FF = 66.59%
Eff = 8.18%
Eff(Active Area) = 10.89%

b)

Fig. 5. Illuminated I-V characteristics of two cells.

Title: **High-Efficiency, Large-Area CdTe Panels**

Organization: Photon Energy, Inc., El Paso, Texas

Contributors: S.P. Albright, R.R. Chamberlin, J.F. Jordan

Introduction and Objectives

Photon Energy Inc.(PEI) has been involved with the development of CdS/CdTe devices and modules since 1984. Since 1987 a three(3) year subcontract under SERI has contributed to progress toward the common objectives between PEI and the Department of Energy(DOE). In mid 1990 a second three(3) year subcontract was begun in order to better address the manufacturing objectives of the PEI and DOE goals.

The PEI objectives in Photovoltaics are succinctly covered through continuing advancement in four(4) major areas:

* Modules efficiency
* Module size
* Module reliability
* Module cost

The CdTe technology at PEI offers the capability to achieve significant advancement toward satisfactory attainment of the goals established in each of these areas. Specifically, the three-year goals of the present three-year subcontract are:

* to achieve efficiencies greater than 14% on small cells

* to achieve aperture area efficiencies of greater than 12.5% on 4 ft^2 modules

* to achieve greater than 20 year extrapolated module life with no greater than 10% efficiency degradation

Experimental

In order to meet the goals and milestones within this project at least five(5) basic tasks have been specified. They include:

TASK I: Windows, Contacts and Substrates (external device optimization)

* Improved CdS window layers will be evaluated using various methods of deposition, including deposition from solution.

* The tin oxide window layer-electrode resistivity and uniformity will be addressed.

* Improved electroding techniques will be explored.

* Reduction of optical losses due to module division will be addressed.

TASK II: Absorber Material (Internal device optimization)

* The deposition, characterization and evaluation of CdTe alloys will be pursued.

* The effect of morphology of the CdTe will be characterized, evaluated and improved.

TASK III: Optimization of Device Structure

* Electronic characterization and modeling of device will be explored.

* The development of improved device structures will continue.

TASK IV: Encapsulation

* Present methods will be analysed and optimized.

* Hermetic sealing techniques will be explored.

* Long term corrosion issues will be isolated and addressed.

TASK V: Process Optimization

* The diffusions and reaction kinetics involved during the process will be more thoroughly explored.

* Heat transfer issues will be explored and solved.

Much of this is to be done at PEI. However, the solution depositions, and the majority of the alloy depositions are to be done by Dr. T.L.Chu and his group at the University of South Florida. The majority of the modelling work on the device structure is to be done by Dr. V.P Singh and his group at the University of Texas at El Paso.

Results and Projections

Laboratory devices with areas approximately 0.3 cm^2 cut from 1 ft^2 substrates have shown efficiencies as high as 12.3% (with a fill factor of 63%) as measured at SERI [1]. Fill factors as high as 72% have also been achieved. Through an increase from 63% to 72% fill factor, 14% efficiencies are expected to be realized in the reasonably near future. The potential for reaching significantly greater than 63% fill factor on the improved current devices lies primarily in the reduction of this diode quality factor and not in the ohmic contact to the CdTe.[2] Table 1 indicates a conservative estimate for the efficiency potential of this technology.

One foot square modules have attained active-area efficiencies of 8.1% as measured at SERI. An aperture area of 838 cm^2 for the same module results in a 7.3% aperture area efficiency. The current-voltage parameters for a 6.1 watt module include a short circuit current of 0.519 amps; an open circuit voltage of 20.5 volts; and a fill factor of 57%.[3]

Four square foot modules have also been made. The first sizable demonstration project for the 4 ft^2 substrates is a 20 KW installation to be installed in Davis, CA for the Photovoltaics for Utility Scale Application (PVUSA) project. The 4 ft^2 module to be produced at PEI will be 2' x 2' and will yield 23 to 28 watts in the early stages.

An efficiency of 14% over the active area will be able to produce approximately 50 watts output from a 4 ft^2 module at 1000 watts/m^2 insolation. This corresponds to 135 watts per m^2 and is expected to be achieved in the mid 1990's. 150 Watts per square meter is a longer-term goal.

Table 1. Device Efficiency Projections

	Present Cell	Ideal Device	Best Observed Single Parameter	Optimized Device
V_{oc}	0.78 V	0.95	0.83	0.85
J_{sc}	25 mA/cm²	29	25	27
FF	0.627	0.80	0.72	0.75
Eff	12.3%	22.0%	12.3% 14.9% if all together	17.2%

Long-term outdoor and accelerated life testing at SERI and PEI has shown the CdS/CdTe technology to be inherently stable, when adequately encapsulated. Outdoor lifetesting at the SERI Outdoor Measurement and Reliability Testing Laboratory have shown no measurable degradation after 270 days so far on the majority of samples. The data from this life testing is shown in Figure 1.[4] In addition, accelerated lifetesting of laboratory cell samples, at elevated temperatures, is an ongoing part of process parameter studies, and helps substantiate the inherent stability of the device. Further accelerated and real time lifetesting continues.

It has been shown by the SERI Reliability and Testing Laboratory that the structural integrity of a modules are adequate regarding expansion coefficient issues. A 4 ft² dummy module was thermally cycled from -40 °C to 90 °C for over 200 cycles with no indications of any type of delamination.[4] Water permeability has been measured through accelerated and real time life testing in the range between 2 and 50 mg per year per linear foot of edge.[5]

Conclusions

The efficiency and stability objectives at PEI on CdS/CdTe modules are being addressed. To summarize:

* Efficiencies of 12.3% have been achieved.
* 14% efficient devices are predicted in the relatively near future.
* 16-18% efficiencies are expected in the longer term.
* One square foot modules have achieved over 8% efficiency (aperture = 7.3%)
* Four square foot modules are expected to produce 24 watts in the near term, greater than 50 watts in the longer term.
* Life testing at SERI (and PEI) shows no inherent stability problems with the CdTe technology.

As one can see from the task outline, there still remain substantial areas for achievement with this technology. However, the major issues have been identified and further advancements are forthcoming.

References

1 K.Emery,SERI Measurement Laboratory, Personal Communication, 1989.

2 J.Sites, Colorado State University, Private Communications, 1989.

3 R.DeBlasio, S.Rummel, SERI PV Module Testing and Performance Facility, Test Report #8910, 1988.

4 Laxmi Mrig, SERI Outdoor Measurement and Reliability Testing Laboratory, Private Communication, 1989-1990.

5 S.P.Albright, R.R.Chamberlin, J.F.Jordan, "Cadmium Telluride Module Development", Presented at PVAR&D meeting in Lakewood,CO, October 1990. (To be Published in *Solar Cells*).

OUTDOOR LIFE TESTING DATA MEASURED AT SERI

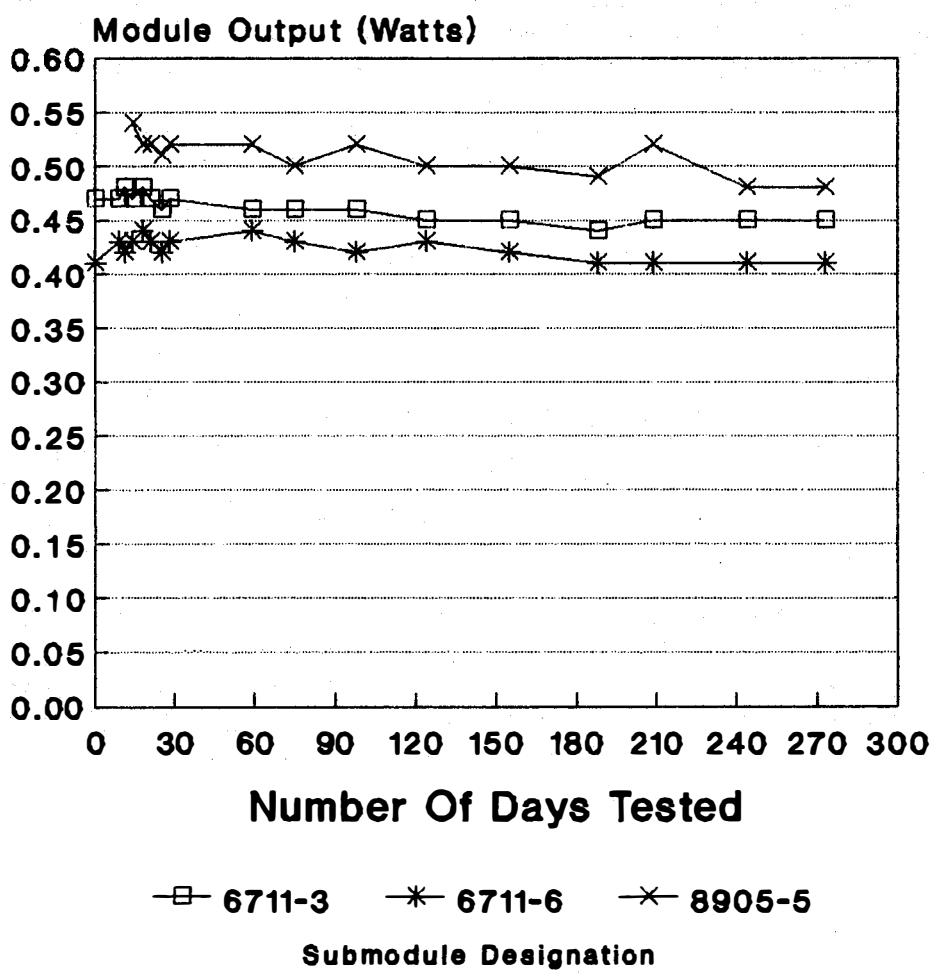

Figure 1: Outdoor Life Testing Data Measured At SERI

Title: **Development of a Computer Model for Polycrystalline Thin-Film $CuInSe_2$ and CdTe Solar Cells**

Organization: School of Electrical Engineering
Purdue University
West Lafayette, IN 47907

Contributors: R. J. Schwartz and J. L. Gray, principal investigators; Y. J. Lee, graduate student

Objective

The purpose of this research program is to develop an accurate numerical model for $CuInSe_2$ (CIS) and CdTe based solar cells. A computer model for thin film Si:H solar cells previously developed at Purdue [1] is being modified for this purpose. This code will be used to analyze and aid in the design of CIS and CdTe based solar cells.

Approach

An accurate numerical model depends on precise knowledge of a variety of material and device parameters. The first phase of this research has been to obtain published values for materials parameters and state-of-the-art CIS and CdTe solar cells. Models for absorption, recombination, carrier transport, band structure, and carrier profiles suitable for implementation in the code are being developed based on this information.

The numerical code being developed for this program is based on a general purpose code, ADEPT (A Device Emulation Program and Toolbox). Customized versions of this code designed specifically for the simulation of CIS and CdTe based solar cells capable of running on a personal computer will be released to SERI subcontractors and in-house researchers. The final versions of these codes will include a menu driven GUI (graphical user interface) and a plotting package for displaying the spatial dependence of internal parameters. These plots are invaluable aids in interpreting device operation.

Finally, the customized ADEPT codes will be used to undertake an exhaustive study of CIS and CdTe based solar cell operation and design. This study will include interpretation of material parameter measurements, device design optimization, performance projections, and identification of performance limiting mechanisms. This phase will involve extensive interaction with SERI researchers and subcontractors.

Results

Much of the parameter study for CIS has been completed and appropriate models implemented into the code. In particular, absorption models for several forms of CIS have been developed and implemented based on measured values. In addition, parameter studies for CdS (a typical CIS window layer) and CdTe are well underway.

Parameter studies for other related materials (such as CuGaInSe) will be undertaken as needed.

A customized version of ADEPT for CIS based cells, ADEPT/1D for CIS, will be the first code released under this program. This code runs in a Apple Macintosh II environment. Future releases will also include an IBM compatible version.

Figure 1 shows a Mac IIci display of a typical CIS solar cell analysis using ADEPT/1D for CIS. Typical execution time for a complete solar cell analysis is approximately 10 minutes on a Mac IIci. The user is able observe the progress of the simulation in the status window. The solution for each bias point is obtained via a Newton iteration method. The Newton Error bar graph shows the size of the estimated error at each iteration. The I-V characteristic is plotted as it is being generated so that the user can better gage the progress of the simulation. A complete summary of the analysis is contained in the summary file (in this case CIS.sum, as shown in Figure 1). A data file containing information on the spatial dependence of all the internal parameters at each bias point is also stored. This information will be used by the plotting package.

ADEPT has already been used to make some initial investigations into CIS cell performance [2-3]. Rather than discuss these results in this report, a brief example of some of the capabilities of the simulation code will be given instead.

A simple CdS/CIS structure is shown in Figure 2 [4]. Figure 3 shows a simulated I-V characteristic for the device illuminated using a one sun AM1.5 global spectrum. This device is not optimized and the specific material parameters have not been precisely determined. Simulations such as this will be used during this research program to better understand the role of individual parameters and to help determine what their specific values are.

Recombination is a primary factor in determining the performance of solar cells. Knowledge of where carriers recombine gives crucial information pertaining to the design of more efficient cells. Figure 4 shows the spatial distribution of recombination and its contribution to the total recombination current in the cell of Figure 1.

Conclusions

Numerical simulation has already proved its usefulness in analyzing and designing a variety of semiconductor devices, including solar cells. Initial modeling of CIS cells has already improved the understanding of the performance of these cells. As the specific models relevant to absorption, recombination, transport, etc. are improved, the ability of the code to analyze and design CIS and CdTe based solar cells is expected to be an invaluable tool for PV researchers.

References

1. J. L. Gray, "Computer Simulation of Thin-Film Silicon-Hydrogen Alloy Solar Cells," IEEE Trans. Electron Devices, Vol. 36, No. 5, 1989, pp. 906-912.

2. G. B. Turner, R. J. Schwartz, and J. L. Gray, "Band Discontinuity and Bulk vs. Interface Recombination in Cd/$CuInSe_2$ Solar Cells," Conference Record of the Twentieth IEEE Photovoltaic Specialists Conference, Las Vegas, Nevada, September 1988, pp. 1457-1460.

3. R. J. Schwartz and J. L. Gray, "The use of $CuIn_{1-x}Ga_xSe_2$ Layers to Improve the performance of $CuInSe_2$ Cells," Conference Record of the Twenty-First IEEE Photovoltaic Specialists Conference, Kissimmee, Florida, May 1990, pp. 570-574.

4. John R. Tuttle, Solar Energy Research Institute, *personal communication.*

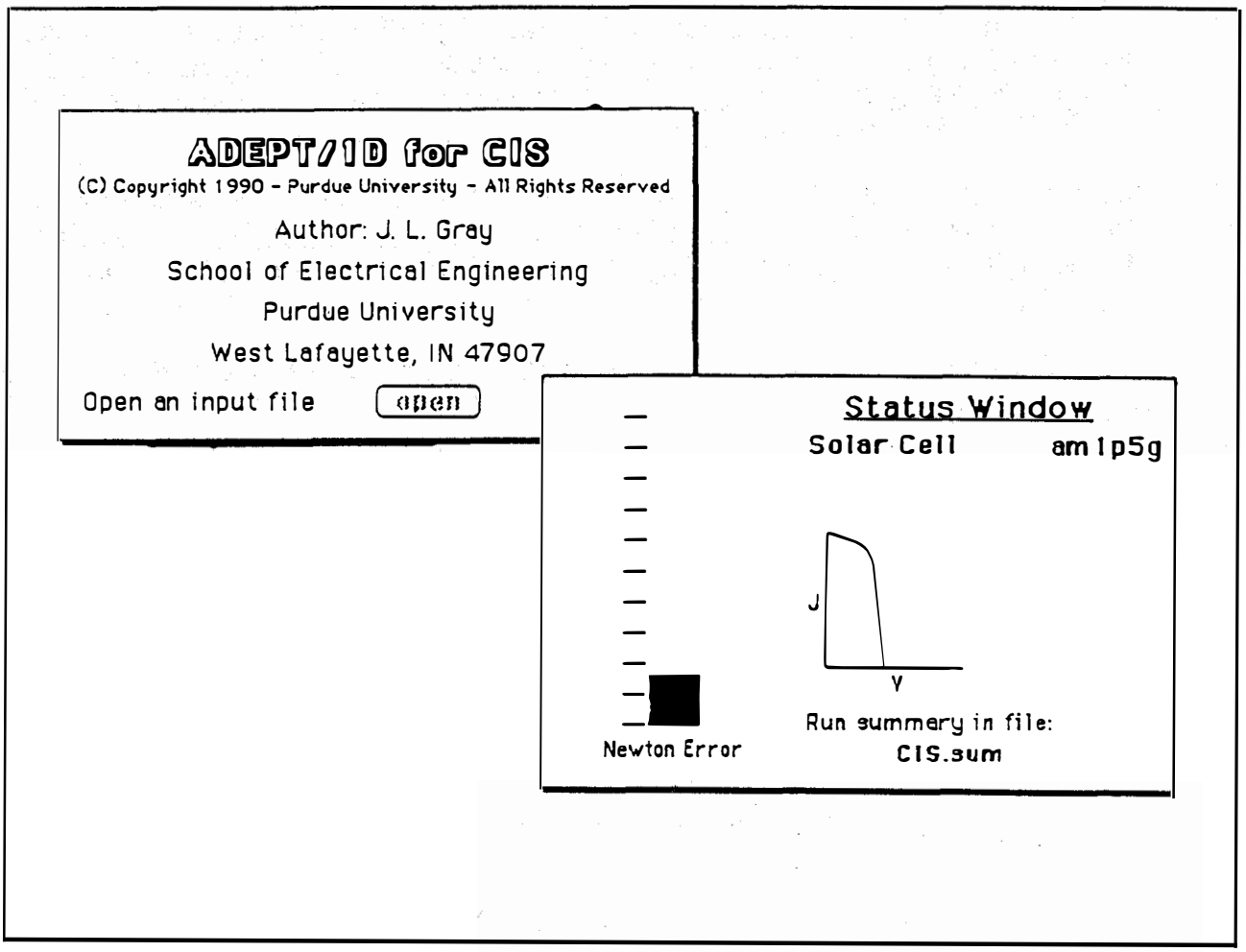

Figure 1.
Apple Macintosh II display of a typical solar cell analysis using ADEPT/1D for CIS

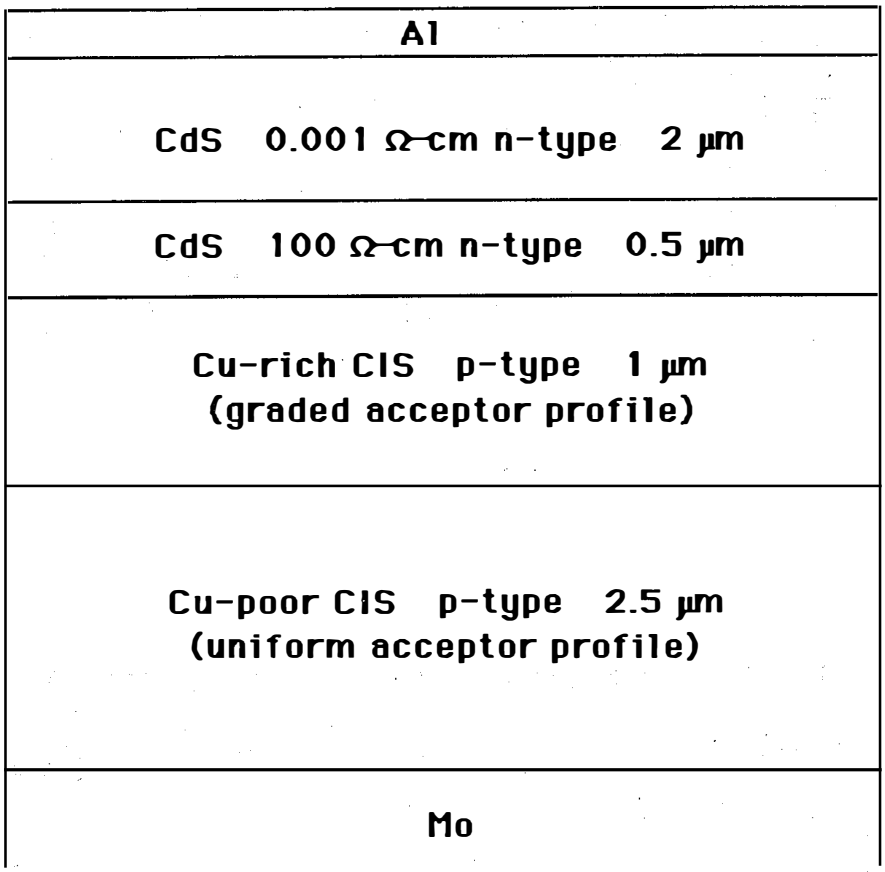

Figure 2.
Simple CdS/CIS solar cell

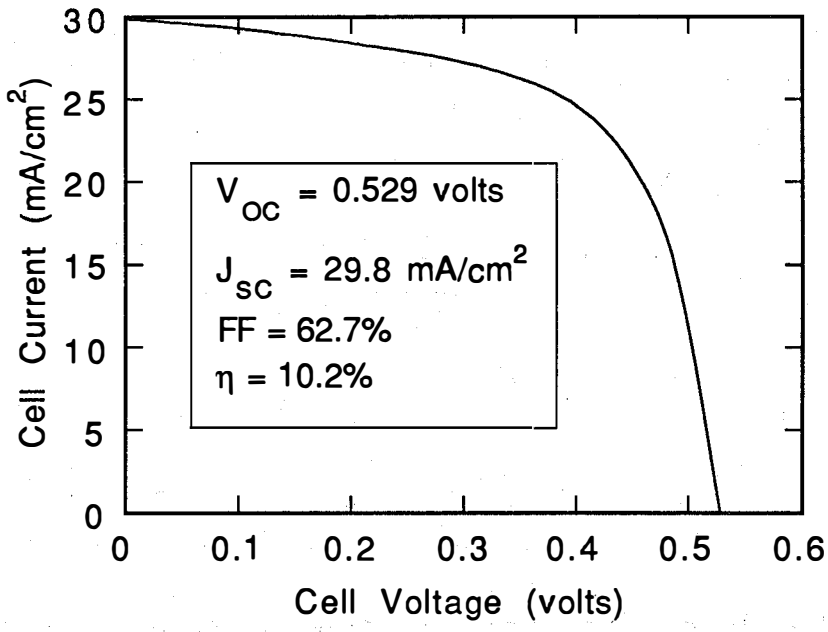

Figure 3.
Simulated 1 sun, AM1.5 global, I-V characteristic for cell of Figure 2.

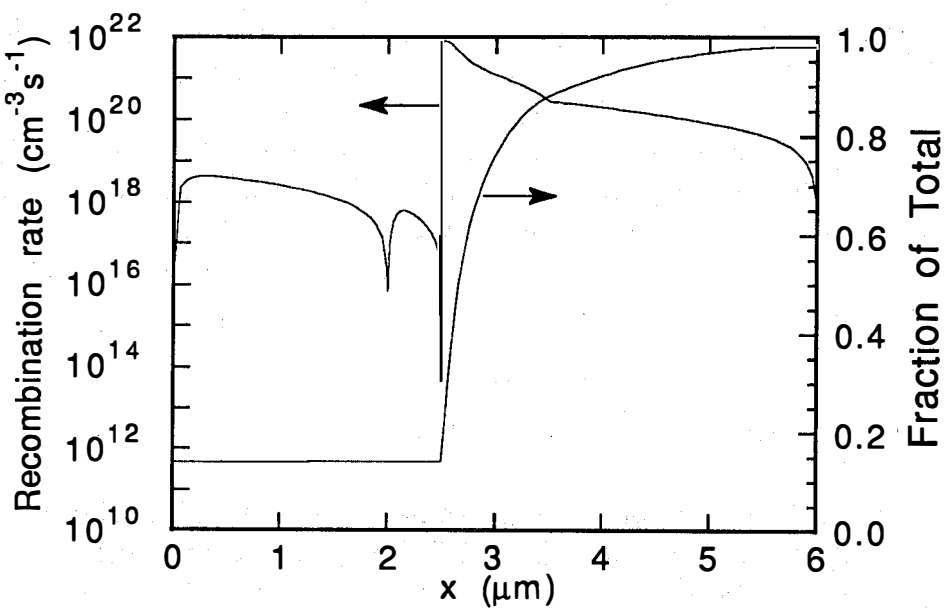

Figure 4.
Plot of spatial dependence of recombination in the cell of Figure 2.
The CdS layer starts at x=0.

Title: **Novel Thin Film CuInSe2 Fabrication**

Organization: Department of Physics, University of Colorado, Boulder, Colorado

Contributors: A. M. Hermann and G. D. Mooney, Principle Investigators

Objective

The objective of this work is to study the feasibility of fabricating $CuInSe_2$ (CIS) for use in photovoltaic cells by rapid annealing processes in inert atmospheres. Presently, the chalcopyrite phase of the best device quality CIS is obtained by more conventional thermal anneals in a highly toxic atomosphere of H_2Se. Our objective is to explore methods that may be more attractive for large scale production by studing techniques to form CIS thin films by annealing samples use rapid thermal processing (RTP).

Summary

Formation of polycrystalline thin-film $CuInSe_2$ has been achieved by the rapid thermal processing of vacuum co-deposited Cu, In, and Se. Films were fabricated and characterized in three composition regions – Cu-poor (~20 atomic % Cu), stoichiometric (25 atomic %) and Cu rich (~28 atomic %). Characterization results including X-ray diffraction analysis, electron probe for microanalysis, scanning electron microscopy, and optical reflection and transmission measurements are presented. Results show nearly single phase material has been formed from co-deposited precursors with a post-deposition annealing time of less than two minutes. The films have smooth morphologies amenable for photovoltaic device fabrication, optical absorption coefficients in the high 10^4 cm^{-1} range, and an optical band-gap of 1.0 eV.

Rapid Thermal Processing of Co-Deposited Precursor Thin Films

To conduct our post-deposition processing, we have used an AET ADDAX®, computer-interfaced rapid thermal processor. The RTP heats the sample using a bank of 18 halogen quartz lamps. With the computer, the operator has control of the processing temperature, processing time, the rate of temperature increase, and the atmosphere in which the sample is annealed. The temperature is controlled by a thermocouple that is in direct thermal contact with the sample. The output of the thermocouple controls the power output of the lamps via a closed loop with the computer software based on the desired temperature input by the operator. The sample is enclosed in a sealed quartz

chamber where process gases are introduced using mass flow controllers. The processing of all of our samples was performed in an argon atmosphere.

We have chosen initially to anneal the precursors using a three-dimensional matrix approach varying the post-deposition anneal parameters as described in Figure 1. Only the experiments at the corners of the cube of Figure 1 were performed in this initial study. The temperature during the ramp and anneal was maintained to within ± 2 °C. The precursors were 2.5 μm thick co-deposited films fabricated on Mo-coated polycrystalline alumina substrate (Al_2O_3/Mo/Cu+In+Se) in a vacuum of 10^{-6} Torr. The substrate temperatures were held above the In melting point(156 °C) at 225 °C.

We have performed experiments within this parameter space in three different composition regions – Cu poor (20 at. % Cu), stoichiometric (25 at. % Cu), and Cu rich (28 at. % Cu). These compositions were studied in detail because previous studies of CIS/CdS devices have utilized materials with these compositions [1]. Table 1 shows the precursor and post-annealed compositions for films in the three regions of interest.

The three annealed samples were processed using the conditions at corner 7 of Figure 1. Because of In and Se re-evaporation during the anneal, the films become relatively more Cu rich (i.e. the ratio of at. % Cu to at. % In increased) in all three regions. This occurred at all annealing conditions and resulted in a need to compensate the composition of the precursors to obtain the desired post-annealed stoichiometry.

Verification of the desired phase of CIS was accomplished by X-ray diffraction (XRD) measurements. Figure 2 shows the XRD pattern of a stoichiometric post-annealed film processed under the conditions of corner 6 of Figure 1. As is seen, the film is mostly single phase CIS with the only binary compound detected being the copper selenide peak at a 2θ value of 14°. The inset shows a comparison of the same film's (112) peak to that of its precursor. In order to meaningfully compare X-ray peak intensities, intensity corrections were performed based on an alumina standard measured before each sample. Analysis of the (112) integrated peak intensities for stoichiometric samples processes under the RTP conditions of Figure 1 indicates the general trend to be higher temperatures, longer anneals and slower temperature ramp rates result in larger volume recrystallization. This trend was also evident in recrystallized Cu-poor and Cu-rich films.

XRD results for recrystallized Cu-poor and Cu-rich films also indicate a majority of CIS formation. Present in the Cu-poor film XRD data were the signature peaks of Cu_2Se at 14°, In_2Se_3 at 25°, $Cu_{.22}In_{1.25}Se_{3.5}$ at 39°, and the ordered vacancy compound (OVC). The XRD data for the Cu-rich films show the excess Cu concentrations result in a large volume of Cu_2Se and $Cu_{2-x}Se$ formation as well as CIS. It should be noted that the XRD results from all three composition regions agree with published data [2] for vacuum deposited films reacted *in-situ* at elevated substrate temperatures.

Optical reflection and transmission measurements were also taken on stoichiometric, Cu-poor, and Cu-rich films co-deposited on glass to a thickness of 5000Å and processed under the conditions of Figure 1. The measurements were conducted using a Beckman 5240 spectrophotometer equipped with an integrating sphere. From this data, the absorption coefficient α, was calculated [3] and for the processed films was on the order of 5×10^4 cm^{-1}. A plot of the log of alpha versus photon energy is shown in Figure 3 for a stoichiometric film and its precursor. The anneled sample was processed under the conditions of corner 8 in Figure 1. As is seen, the processed stoichiometric film has very little sub-gap absorption and the transition is very sharp, indicating a minimum of allowed impurity states in the gap. The Cu-poor samples showed slightly more sub-gap absorption indicating the existence of states in the gap, while the Cu-rich sample has sub-gap absorption on the order of 3×10^4 cm^{-1} indicating the existence of many impurity states in the gap. This data is consistent with the XRD findings with the large amount of sub-gap absorption in the Cu-rich sample attributable to Cu-Se impurity incorporation into the film. The inset of the figure is a plot of alpha squared versus photon energy for the processed sample. The band-gap was determined by extrapolating the linear portion of the α^2 curve to the photon energy axis intercept. The primary transitions for all samples was around 1.0 eV except for films processed under the conditions of corner 3 of Figure 1. Films processed under the conditions of this corner had optical properties similar to that of its precursor indicating that these annealing conditions do not fully recrystallize the film. The optical data also agrees with published data [3] for films vacuum deposited and reacted *in-situ* by elevated substrate temperatures. All results discussed above are presented in more detail in referene 4.

Conclusions and Future Directions

In conclusion, we have demonstrated that polycrystalline thin films of CIS can be synthesized using RTP with a variety of processing conditions. We have shown that rapid thermal anneal times of less than two minutes produce mostly single phase CIS with morphologies suitable for photovoltaic devices. The materials have good optical properties exhibiting an optical band-gap of 1 eV, an absorption coefficient of 5×10^4 cm^{-1} at energies above the band-gap.

Experiments to further refine the parameter space for co-deposited precursors as well as experiments processing sequentially deposited, elemental layered precursors are now under way. Fabrication of CIS/CdS photovoltaic devices using RTP is also being explored with preliminary results yielding a device with Jsc = 30 mA/cm2, Voc = 200 mv, and FF = 54 percent, yielding a 3 percent efficent cell.

References

1. Rommel Noufi and John Dick, *J. Appl. Phys.*, **58**, 3884 (1985).

2. John R. Tuttle, *An Optical and Microstructural Characterization Study and Microstructural Model of Co-Evaporated Polycrystalline Thin Film $CuInSe_2$ For Photovoltaic Applications*, Ph.D. Dissertation, 1990.

3. J. R. Tuttle, D. Albin, R. J. Matson, and R. Noufi, *J. Appl. Phys.*, **66**, 4408(1989).

4. G. D. Mooney, A. M. Hermann, J. R. Tuttle, D. S. Albin, and R. Noufi, to be published in *Solar Cells.*

Table 1. Compositions of Precursor and Annealed Films In The Three Regions of Interest

Composition Region	Precursor Composition (at.% Cu/at.% In/at.% Se)	Annealed Composition (at.% Cu/at.% In/at.% Se)
Cu poor	20.33/27.32/52.35	20.44/27.38/52.04
Stoichiometric	24.36/24.68/50.96	24.94/24.74/50.17
Cu rich	27.03/22.94/50.03	28.81/22.79/48.40

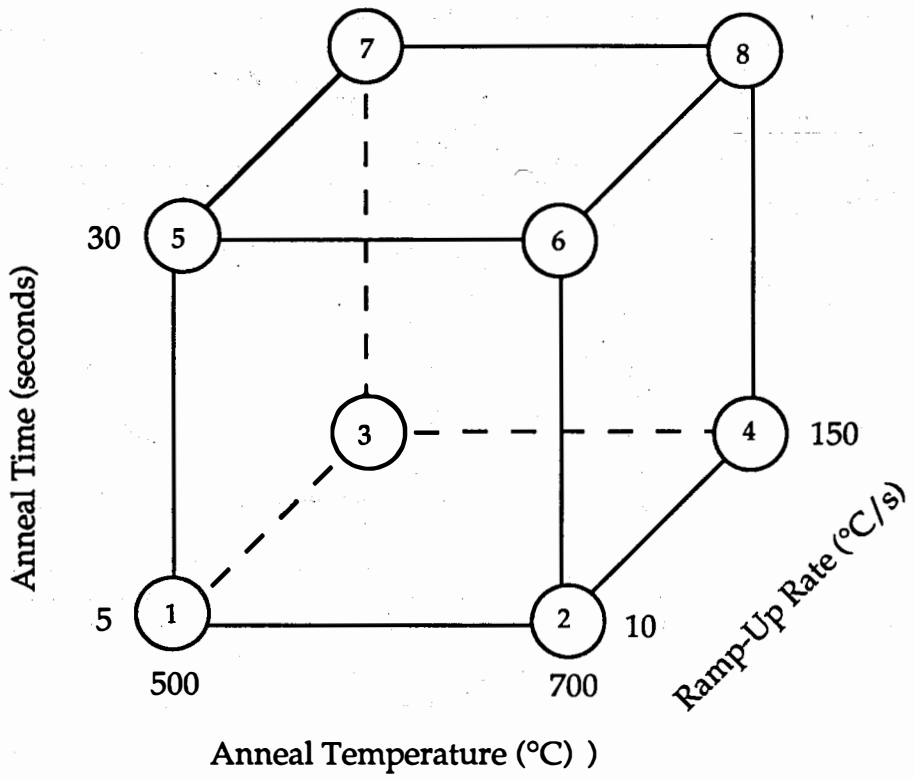

Figure 1. Experimental matrix for RTP study of co-deposited CIS thin films. The numbers in the corner positions are for reference.

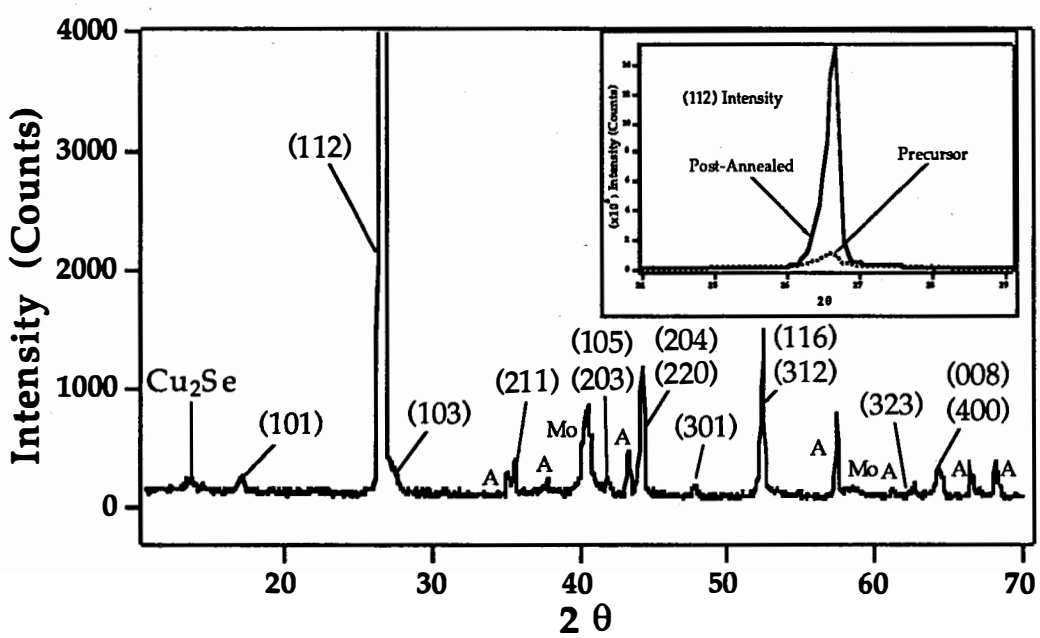

Figure 2. XRD pattern of a co-deposited, stoichiometric thin film. The inset is a comparison of the primary (112) peak of the same film and its precursor demonstrating significant recrystallization. The "A"s designate the alumina peaks.

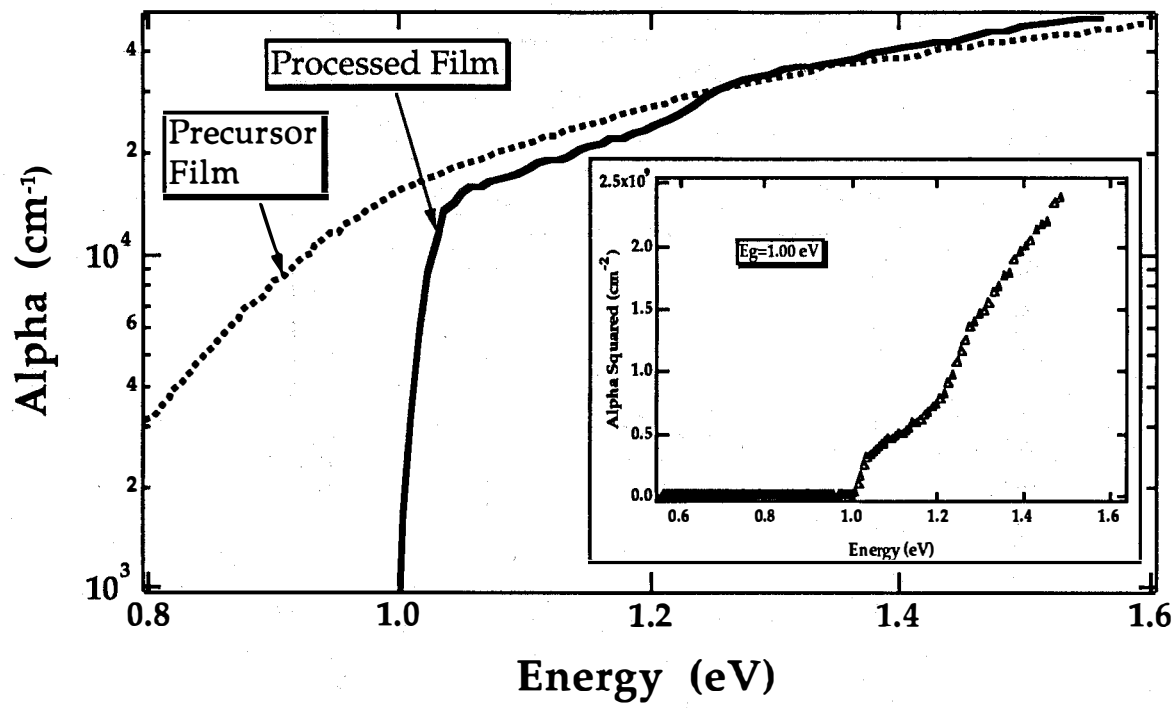

Figure 6. Optical absorption data of a stoichiometric sample processed under the conditions of position 8 of the experimental matrix compared to its precursor film. The inset shows the alpha squared data of the processed sample.

Title: **Alternative Fabrication Techniques for High-efficiency $CuInSe_2$ and $CuInSe_2$-alloy Films and Cells**

Organization: Department of Materials Science, University of Illinois, Urbana, Illinois

Contributors: A. Rockett, principal investigator; E. Banda, G. Kenshole, L. Chung Yang, T. Bales, and A. Feen.

Objectives

The objective of this project is to demonstrate a $CuInSe_2$ thin film deposition technique which is clearly scalable to large areas and capable of producing material suitable for solar cell applications. To achieve efficient use and scale up of any such technology it is essential to understand the fundamental behavior of the principal materials involved.[1] Hence, the program seeks to characterize the structure/processing/cell-performance relationships for $CuInSe_2$. This will serve to improve the processes under development, optimize deposition conditions, and ultimately to accelerate the return of large deposition facilities to service after periods of maintenance.

Technical Approach

The $CuInSe_2$ deposition method considered by this project is a hybrid of sputtering and evaporation. Cu and In are sputtered with Ar gas while Se is supplied to the growing film by a conventional effusion cell.[2] The substrate temperature is controlled between room temperature and 450°C. The process has been shown to be straightforward to control with a linear relationship between the ion current ratio at the targets and the film composition established by previous results.[3] The experiments underway focus development of a reasonably high efficiency $CuInSe_2$/CdS heterojunction solar cell, and on understanding the fundamental properties of $CuInSe_2$. Cell development efforts are primarily directed at demonstration not only of control capability but also of reproducible results from the hybrid process.[4,5] The current research on materials involves characterization of bulk $CuInSe_2$ single crystals and thin films (deposited by the hybrid process and by other methods) in the transmission electron microscope (TEM) and by chemical analysis techniques.

Results for FY 90

Hybrid Process

The principal effort during this contract period has been characterization of the hybrid process. This has focused on determining and improving the reproducibility of the growth of $CuInSe_2$ suitable for device production. To assist this effort we have established a capability to fabricate simple devices at the University of Illinois. Although transparent conducting oxides as top contacts and antireflection coatings are not yet available on site, the basic devices should be of reasonable performance. The capability to produce repeatably active devices at the University of Illinois has been demonstrated during this contract period. We have shown that in order to obtain reproducible performance from the hybrid process it is necessary to design or operate the vacuum system in a mode which maintains the sputtering targets reasonably free of Se. This was achieved by maintaining slow sputtering of the targets during heating and cooling of the Se source from its operating temperature before and after film growth. Finally, we have demonstrated that composite Cu/In targets can be produced and operated satisfactorily in the hybrid system. Hence, Cu/Ga alloys can be produced and inserted as chunks into Cu or In targets to yield the desired Ga content in deposited films.

To better asses and improve the performance of these cells we have begun a simulation using the SPICE device modelling program. It has been found that adhesion of the $CuInSe_2$ layer to the back contact is not always good. This may reduce device performance by shorting the CdS window/contact to the back contact. Using SPICE we have simulated the effect of pinhole shorts through the $CuInSe_2$ and have shown that an optimal resistance for the CdS layer exists. For a given resistivity of the CdS this translates to an optimal thickness or, for fixed thickness, an optimal resistivity. An example of preliminary results of this calculation is shown in Figure 1.

Materials Characterization

Slightly In-rich single crystals grown by Tomlinson using the vertical Bridgeman technique and hybrid-sputtered polycrystalline films were analyzed by TEM and XPS. TEM results included plan-view and cross-sectional electron micrographs as well as selected area diffraction.[6,7] After an extensive search comparing compositions of individual grains in $CuInSe_2$ to the bulk composition, analyzing selected area diffraction patterns, and characterizing the structure of grains and grain boundaries, it is clear that second phases are not common in the material studied.[6] From this we conclude that point defects on more than one sublattice of $CuInSe_2$ must (to maintain low carrier density) be present. In spite of this, devices can still operate satisfactorily. Hence, to find the microstructural defects limiting device performance we have begun to examine line and planar defects in more detail.[7] We have characterized the structure of dislocations in the $CuInSe_2$. Both a[110] perfect edge-type dislocations and dislocations dissociated into paired partials have been observed. An example of the latter is shown in Figure 2. Single partial dislocations have been observed at the intersection of stacking faults which are common growth defects in polycrystalline films. Finally, we have observed misfit dislocation arrays at low-angle grain boundaries.

It is important to determine the changes in band structure as a function of film composition if one is to understand how solar cells can operate efficiently over a broad range of Cu/In ratios without regard to heterointerface structure. X-ray photoelectron spectra for films with average In/Cu atom ratios as determined by EDX between 1.82 and 0.71 were recorded and a series of valence band spectra for several average compositions are shown in Figure 3.[3] These spectra can be adequately fitted with five peaks. The results of the fits indicate a weak peak at ~ 1 eV, a stronger peak at ~ 3eV, a peak at ~5 eV which appeared to increase strongly with bulk In content above stoichiometry, and weak peaks at 7 and 9 eV. The 7 and 9 eV peaks were strongest in samples deviating significantly from stoichiometry. The changes in valence band spectrum were also reflected in concurrent variations in higher binding energy satellites of the main Cu LVV Auger transition. The results agree well with ultraviolet photoelectron spectroscopy results.[8]

Conclusions and Future Research

The current results demonstrate that the hybrid process is a viable method for production of device-quality $CuInSe_2$. While some issues remain concerning reproducibility and total device performance, it is clear that no "show-stoppers" limit the technique. The microanalysis results indicate a remarkable robustness of the material allowing high-performance solar cells to be fabricated in spite of large numbers of point, line and planar defects. Future efforts will pursue these issues by demonstration of more and higher performance solar cells, continued device simulations, and microanalysis to aid in optimization and design of $CuInSe_2$/CdS cells and modules.

Relationship to Other Contracts

The research program described above is funded by SERI for development of high-performance photovoltaic devices based on $CuInSe_2$ deposited by sputtering-based techniques. The development of the hybrid sputtering and evaporation process itself is funded by the Electric Power Research Institute. Both agencies fund the materials characterization with additional direct support from the Department of Energy.

References

[1] A. Rockett and R.W. Birkmire, "$CuInSe_2$ for Photovoltaic Applications," submitted to Applied Physics Reviews.

[2] A. Rockett, T.C. Lommasson, P. Campos, L.C. Yang, and H. Talieh, "Growth of $CuInSe_2$ by Two Magnetron Sputtering Techniques", Thin Solid Films **171**, 109 (1989).

[3] A. Rockett, T.C. Lommasson, L.C. Yang, H. Talieh, P. Campos, and John A. Thornton, "Deposition of $CuInSe_2$ by the Hybrid Sputtering and Evaporation Method", Proceedings of the 20th IEEE Photovoltaic Specialists Conference, Las Vegas, September 26-30, 1988 (Institute of Electrical and Electronics Engineers, New York, 1988), p. 1505.

[4] H. Talieh and A. Rockett, "Device-Quality $CuInSe_2$ Produced by the Hybrid Process," Solar Cells **27**, 321 (1989).

[5] A. Rockett, G. Kenshole, L. Chung Yang, H. Talieh, L.C. Yang, P. Campos, E. Banda and A. Agarwahl, "Characterization of CuInSe2 Deposited by the Hybrid Sputtering and Evaporation Method and Heterojunction Solar Cell Performance", 21st IEEE Photovoltaic Specialists Conference, Orlando, May 21-25, 1990 (Institute of Electrical and Electronics Engineers, New York, 1990), p. 764.

[6] B.-H. Tseng, A. Rockett, T.C. Lommasson. L.C. Yang, C.A. Wert, and John A. Thornton, "Chemical and Structural Characterization of Physical-Vapor Deposited $CuInSe_2$ for Solar Cell Applications", J. Appl. Phys. **67**, 2637 (1990).

[7] C.J. Kiely, R.C. Pond, G. Kenshole, and A. Rockett, "A TEM Study of the Crystallography and Defect Structures of Single Crystal and Polycrystalline Copper Indium Diselenide", Phil. Mag. **A**, in press.

[8] Art J. Nelson, Steven Gebhard, Angus Rockett, Elio Colavita, Mike Engelhardt and Hartmut Höchst, "Synchrotron Radiation Photoemission Study of $CdS/CuInSe_2$ Heterojunction Formation," Phys Rev. **B**, in press.

Figures

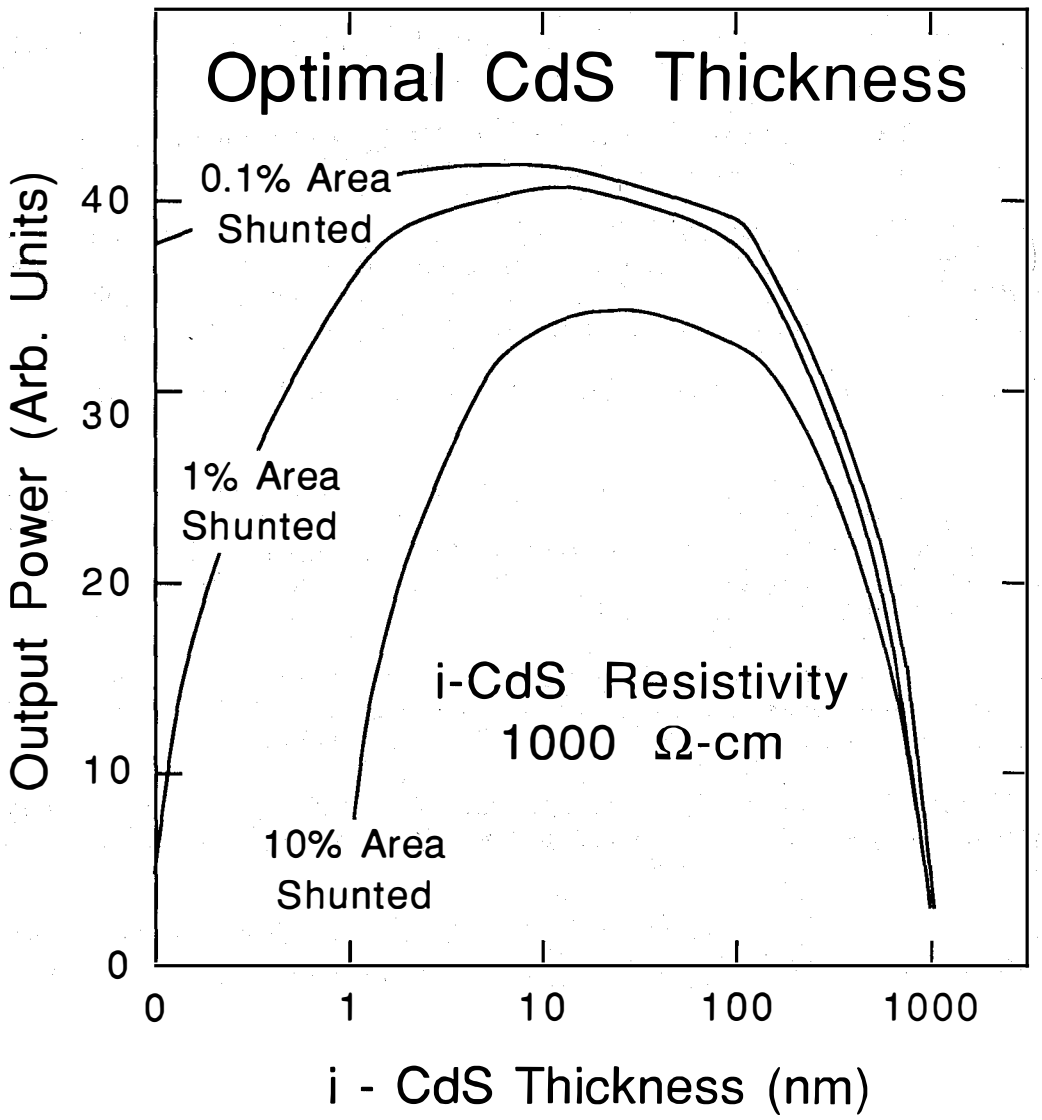

Figure 1. Shows the results of SPICE simulations of $CuInSe_2$/CdS devices with shunts across the $CuInSe_2$ layer. It is clear that for a fixed CdS resistivity there is an optimal CdS thickness which increases with shunt area (ignoring losses due to CdS absorption).

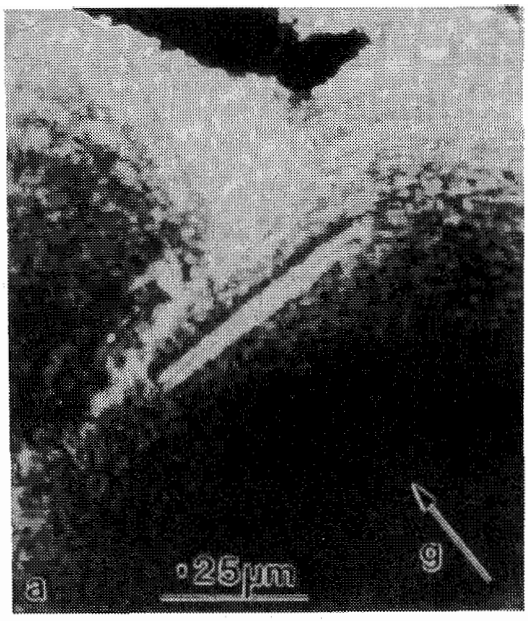

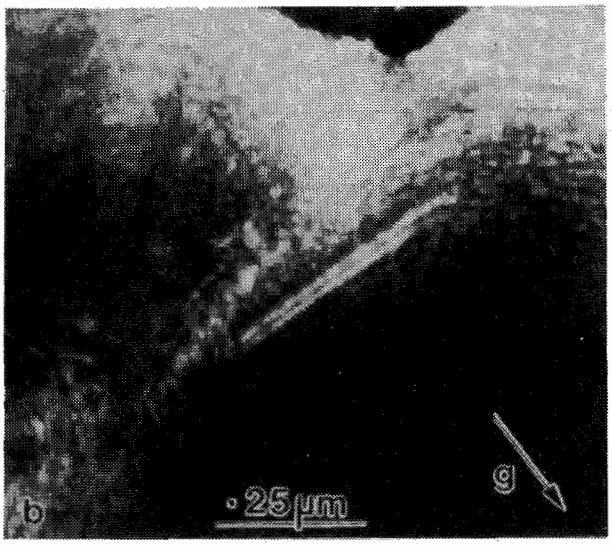

Figure 2. A TEM micrograph showing a perfect edge dislocation dissociated into two partial dislocations. The dislocations are separated by a region of antiphase.

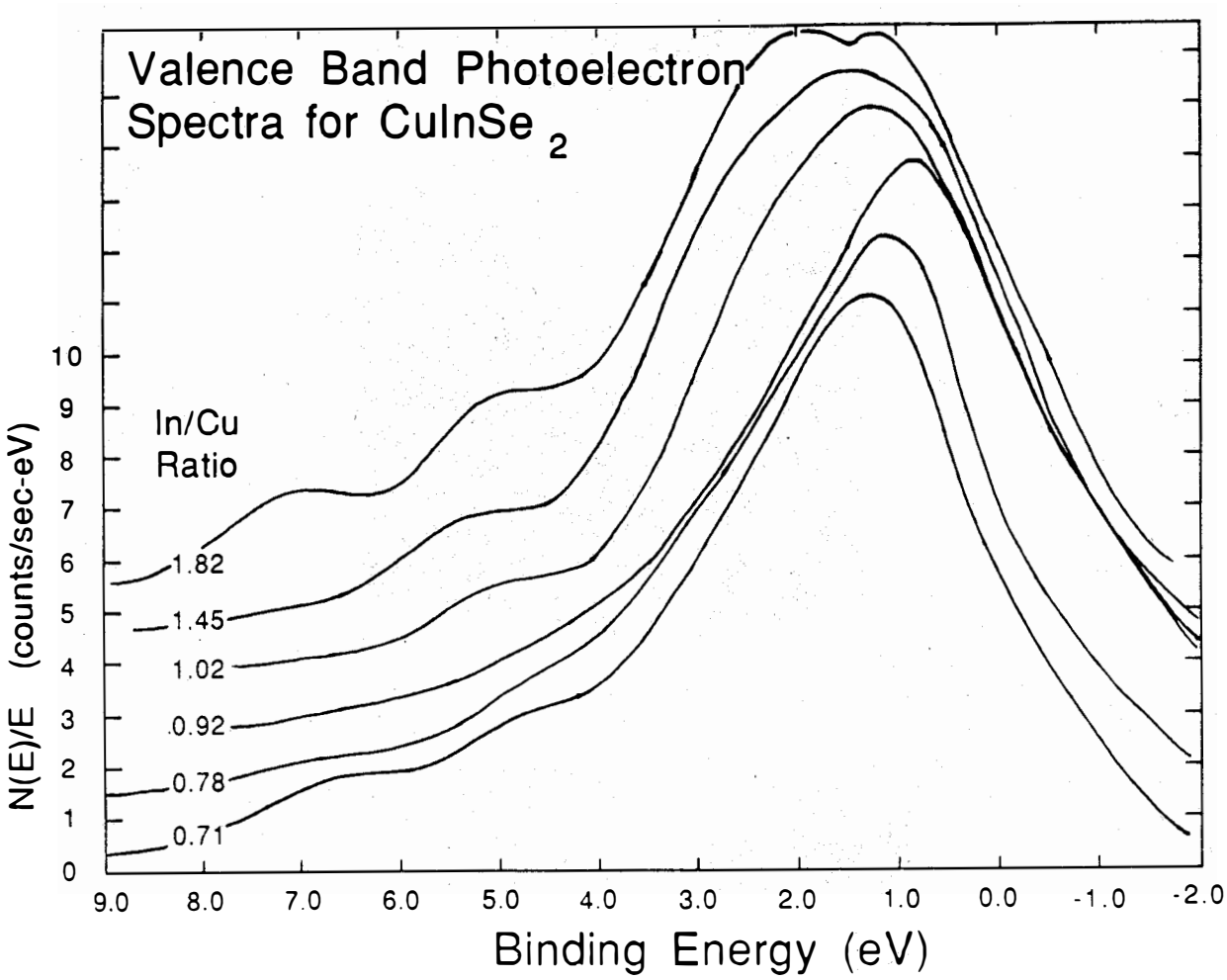

Figure 3. A series of valence band X-ray photoelectron spectra obtained on a number of $CuInSe_2$ samples as a function of composition as well as one single crystal sample (In/Cu ratio = 1.02)

Title: **Thin Film Cadmium Telluride, Zinc Telluride, and Mercury Zinc Telluride Solar Cells**

Organization: University of South Florida, Tampa, Florida

Contributors: T. L. Chu and S. S. Chu, Principal Investigators; J. Britt, G. Chen, C. Ferekides, N. Schultz, and C. Wu

The major objective of this program is to investigate the preparation, characterization, and optimization of thin-film solar cells of II-VI compounds and alloys with emphasis on cadmium telluride (CdTe), cadmium zinc telluride ($Cd_xZn_{1-x}Te$), and mercury zinc telluride ($Hg_xZn_{1-x}Te$). Thin film CdTe solar cells are of the homojunction and heterojunction configurations in order to demonstrate a quantum efficiency of 75% at 0.44 μm and a photovoltaic conversion efficiency of 11.5% or greater. Thin film $Cd_xZn_{1-x}Te$ and $Hg_xZn_{1-x}Te$ with bandgap energy of 1.65-1.75 eV are suitable as the top members in two-cell cascade structures. The solar cells are of the heterojunction configuration in order to demonstrate a transparency to sub-bandgap radiation of 65% and a photovoltaic conversion efficiency of 8% or greater. The technical approach consists of (1) the deposition of transparent conducting semiconductor (TCS) films from aqueous solutions and by metalorganic chemical vapor deposition (MOCVD), (2) the deposition of CdTe films by MOCVD with emphasis on doping and the characterization and processing of these films with emphasis on contact formation, (3) the deposition and characterization of $Cd_xZn_{1-x}Te$ and $Hg_xZn_{1-x}Te$ films, and (4) the formation and characterization of thin film junctions and solar cells.

Transparent Conducting Semiconductors

Cadmium sulfide (CdS) is best suited as the heterojunction partner to CdTe. Vacuum evaporation and growth from aqueous solutions were used in the prior years. During the past year, the reaction between dimethylcadmium (DMCd) and propanethiol (C_3H_8S) has been used for the deposition of CdS films on glass and SnO_2:F/glass substrates at 350°C - 400°C. The resistivity of deposited films without intentional doping is higher than 10^6 ohm-cm. Using triethylaluminum (TEAℓ) as a dopant, the resistivity of CdS films can be controlled over a wide range, 1 - 10^3 ohm-cm for example.

Zinc sulfide (ZnS) and cadmium zinc sulfide ($Cd_xZn_{1-x}Se$) films have also been deposited by MOCVD using diethylzinc (DEZn) as the zinc source. ZnS has a large bandgap energy (about 3.6 eV); however, the doping of ZnS films with B or Aℓ has not been successful. The composition of $Cd_xZn_{1-x}S$ films can be readily controlled by controlling the composition of the reaction mixture. The resistivity of $Cd_xZn_{1-x}S$ films with $x \geq 0.6$ has been controlled by using TEAℓ as a dopant.

Cadmium Telluride Films - Deposition and Doping

CdTe films have been deposited on glass, SnO_2:F/glass, and CdS/SnO_2:F/glass substrates at 350°C - 400°C using DMCd and diisopropyltellurium (DIPTe) in a hydrogen atmosphere. Using fixed flow rates of hydrogen and DIPTe, Fig. 1 shows the dependence of the deposition rate of CdTe on the DMCd/DIPTe molar ratio in

the reaction mixture. The deposition rate increases initially with increasing DMCd/DIPTe molar ratio and levels off at a DMCd/DIPTe ratio higher than about 0.7, indicating the greater stability of DIPTe. All CdTe films deposited on glass substrates have high electrical resistivity. The conductivity type of CdTe films was deduced from junction photovoltage spectra by using films of 2-3μm thickness deposited on SnO_2:F/glass substrates. Graphite paste was applied to the surface of the CdTe film to form a graphite/CdTe/SnO_2:F/glass structure. The junction photovoltage spectrum was then measured by illuminating the glass surface with a tungsten-halogen lamp. The graphite/n-CdTe and p-CdTe/SnO_2 junctions are know to be rectifying, and the n-CdTe/SnO_2 and p-CdTe/graphite junctions are essentially ohmic. Thus, the graphite/p-CdTe/SnO_2:F/glass structures show considerable better response in the short wavelength region than graphite/n-CdTe/SnO_2:F/glass structures, as illustrated in Fig. 2. Using this technique, all films deposited at 400°C with a DMCd/DIPTe molar ratios of about 0.51 or lower have been found to be p-type. The deposited films are n-type at higher DMCd/DIPTe ratios.

The lateral resistivity of CdTe films on glass substrates was measured by the conventional potential probe technique using graphite contacts. The dark lateral resistivity of all CdTe films has been found to be 10^7 - 10^8 ohm-cm, essentially independent of the DMCd/DIPTe molar ratio in the reaction mixture. Under illumination with ELH lamps at 100 mW/cm^2, the lateral resistivity is reduced by a factor of 100-300. CdTe films deposited on glass and CdS/SnO_2:F/glass substrates have been heated at 350°-400°C in He and He - O_2 atm. All films on glass substrates showed no measurable changes in resistivity and microstructure after heat treatment. Intrinsic CdTe films of n-type conductivity on CdS/SnO_2:F/glass substrates showed no changes in junction photovoltage spectrum after heating in He, but changed to p-type after heating in a He - O_2 atm. One may conclude that during the heating process, oxygen has diffused into CdTe films where oxygen acts as an acceptor.

To reduce the resistivity of intrinsically-doped CdTe films, triethylgallium (TEGa) and arsine (AsH_3) have been used as the n- and p-type dopant, respectively, during the MOCVD process. Since Ga occupies the Cd position in the CdTe lattice, the incorporation of Ga will be facilitated by using a reaction mixture with a small DMCd/DIPTe molar ratio, and a large DMCd/DIPTe molar ratio should be used for the deposition of As-doped CdTe films. Figures 3 and 4 show the dark and illuminated lateral resistivity of Ga-doped and As-doped CdTe films as a function of the concentration of dopant in the reaction mixture. The resistivity of CdTe films is significantly reduced by the addition of TEGa into the reaction mixture. However, the capacitance-voltage and SIMS profile measurements indicated that a major fraction of incorporated Ga atoms is electrically inactive. The incorporation of As into CdTe appears to be highly ineffective as compared with the Ga incorporation.

Cadmium Telluride Films - Contact and Homojunction

The formation of a stable, low resistance contact to p-CdTe films is a difficult problem, particularly to high resistivity films deposited by MOCVD. Low resistivity HgTe and ZnTe films have been shown to form ohmic contacts to p-CdTe films due to their large work functions. ZnTe is better suited for MOCVD CdTe films because of the ease of deposition by in-situ MOCVD. ZnTe films of 1-5 ohm-cm resistivity have been deposited on glass and TCS-coated glass substrates at

300°-400°C in a H_2 atmosphere using DEZn, DIPTe, and AsH_3 as source materials. These films have been used successfully as low resistance contacts to p-CdTe.

Preliminary work on thin film CdTe homojunctions has been carried out. Films of n-CdTe, p-CdTe, and p^+-ZnTe were deposited successively in-situ on SnO_2:F/glass substrates, and Ni contacts applied to p^+-ZnTe by electron beam evaporation. Figure 5 shows the dark current-voltage characteristics of an as-deposited homojunction, while the diode quality factor (1.8) is reasonable, the saturation current density is relatively high (10^{-8} A/cm^2). Under illumination with ELH lamps at 100 mW/cm^2, the V_{oc}, J_{sc}, and FF, are 0.52V, 18 mA/cm^2, and 51%, respectively (Fig. 6) corresponding to an efficiency of about 4.8%. The series resistance of the homojunction is about 1.2 ohm-cm^2. It is believed that as-deposited MOCVD CdTe films have high defect concentrations contributing to recombination current in the space charge region. Post deposition treatments are under study.

Cadmium Zinc Telluride and Mercury Zinc Telluride Films

Preliminary work on the MOCVD of $Cd_xZn_{1-x}Te$ and $Hg_xZn_{1-x}Te$ films has been carried out to determine the bandgap energy-composition relations, optimum deposition conditions, doping, etc. $Cd_{0.7}Zn_{0.3}Te$ and $Hg_{0.2}Zn_{0.8}Te$ films with bandgap energy in the range of 1.65 - 1.75 eV have been characterized and heterojunctions prepared. As an example, Figures 7 and 8 show the dark and illuminated current-voltage characteristics of a $Hg_{0.15}Zn_{0.85}Te/Cd_{0.7}Zn_{0.3}S/SnO_2$:F/glass heterojunction, where both shunting and series resistance are apparent. The high series resistance is due mainly to the uncontrolled doping in the window and absorber.

Conclusions and future Research

MOCVD has been shown to be a flexible technique for the deposition of thin films of II-VI compounds (such as CdTe, ZnTe, and CdS) and their solid solutions (such as $Cd_xZn_{1-x}Te$, $Hg_xZn_{1-x}Te$, and $Cd_xZn_{1-x}S$). The MOCVD of CdTe films has the advantages that n- and p- type dopants can be incorporated during deposition for the preparation of homojunctions and that low-resistance contact to p-CdTe can be formed by in-situ deposition of p^+-ZnTe. However, the as-deposited CdTe films appear to have high defect density, and techniques for post-deposition treatment must be developed.

The current efforts are directed to (1) the post-deposition treatment of MOCVD CdTe films, (2) the optimization of thin film CdTe homojunction solar cells, (3) the incorporation of information from MOCVD CdTe into the inorganic CVD processes, (4) the deposition and characterization of TCS films, such as $Cd_xZn_{1-x}S$, ZnSe, etc., and (5) the preparation and characterization of thin film TCS/$Cd_xZn_{1-x}Te$ and TCS/$Hg_xZn_{1-x}Te$ solar cells.

References

1. T. L. Chu, Shirley S. Chu, J. Britt, and C. Ferekides, "Zinc Telluride Films for Photonic Devices," presented at the 176th National Meeting of the Electrochemical Society. Hollywood, FL, October 15-20, 1989.

2. T. L. Chu, Shirley S. Chu, J. Britt, and C. Ferekides, "Transparent conducting Semiconductor/Zinc Telluride Heterojunction by MOCVD," presented at the March 1990 Meeting of the American Physical Society, Anaheim, CA, March 12-16, 1990.

3. T. L. Chu, Shirley S. Chu, C. Ferekides, J. Britt, and C. Q. Wu, "Thin Film CdTe Homojunctions by MOCVD." Conference Record of the Twenty-First IEEE Photovoltaic Specialists Conference, p.777 (1990).

4. T. L. Chu, Shirley S. Chu, C. Ferekides, J. Britt, and C. Q. Wu, "Zinc Telluride and Cadmium Telluride Photovoltaic Devices by MOCVD," presented at the International Conference on Electronic Materials, Newark, N. J., September 17-19, 1990. Proceedings in press.

5. T. L. Chu and Shirley S. Chu, "Degenerate Cadmium Oxide Films for Electronic Devices," J. Electronic Materials, 19, 1003 (1990).

6. T. L. Chu, Shirley S. Chu, C. Ferekides, J. Britt, and C. Q. Wu," Cadmium Telluride Films by Metalorganic Chemical Vapor Deposition, "J. Appl, Physics, submitted for publication.

7. T. L. Chu, Shirley s. Chu, J. Britt, C. Ferekides, and C. Q. Wu, "Zinc Telluride Films by Photoenhanced Metalorganic chemical Vapor Deposition," J. Appl. Phys, submitted for publication.

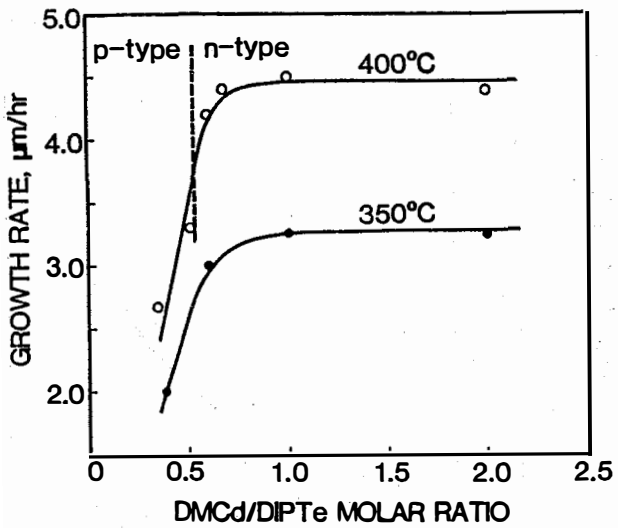

Fig. 1. The deposition rate of CdTe films as a function of DMCd/DIPTe molar ratio in the reaction mixture.

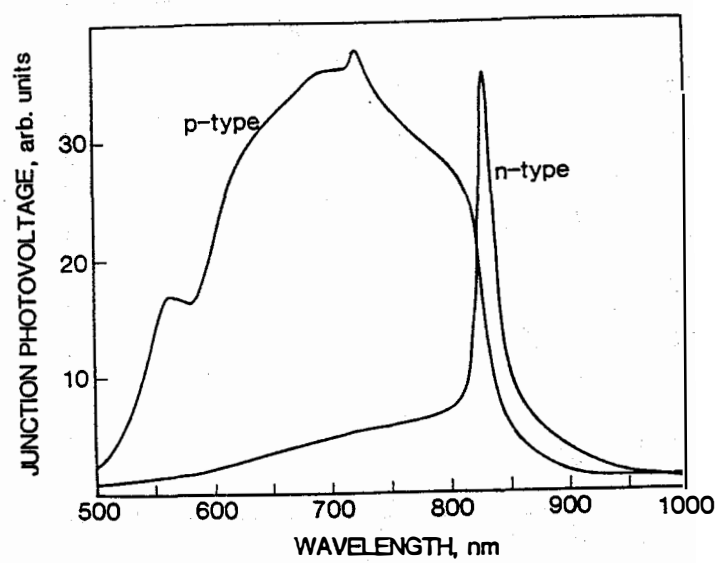

Fig. 2. Junction photovoltage spectra of graphite/n-CdTe/SnO_2:F/glass and graphite/p-CdTe/SnO_2:F/glass structures.

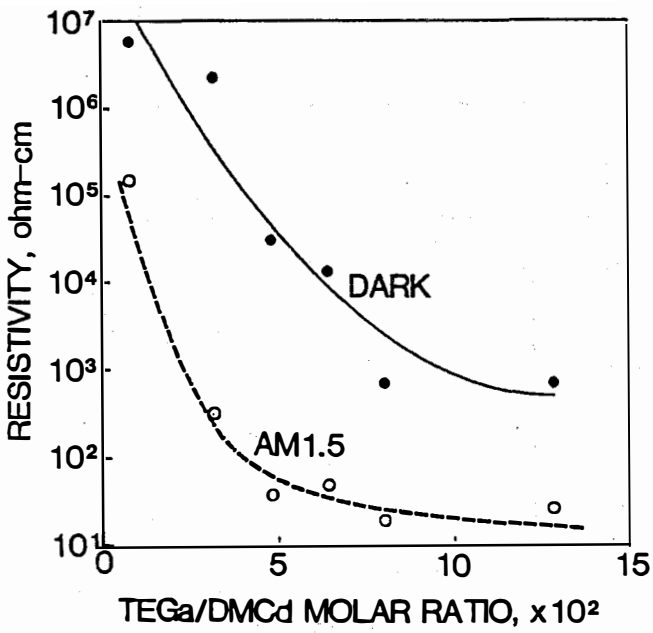

Fig. 3. Lateral resistivity of Ga-doped CdTe films.

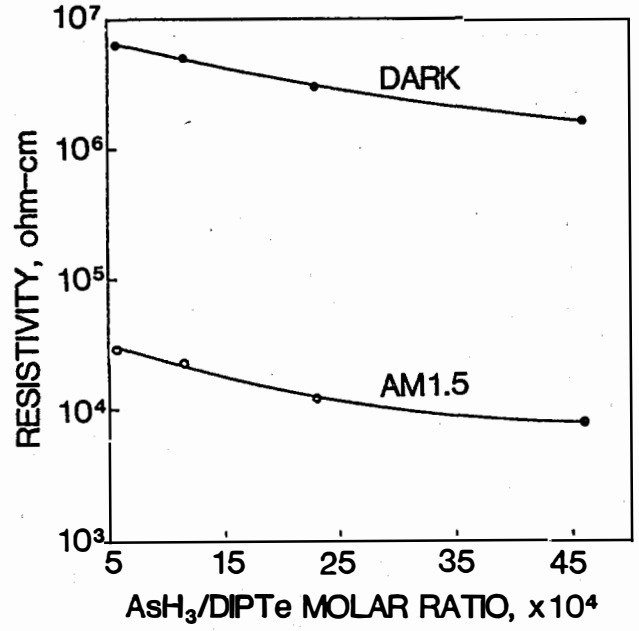

Fig. 4. Lateral resistivity of As-doped CdTe films.

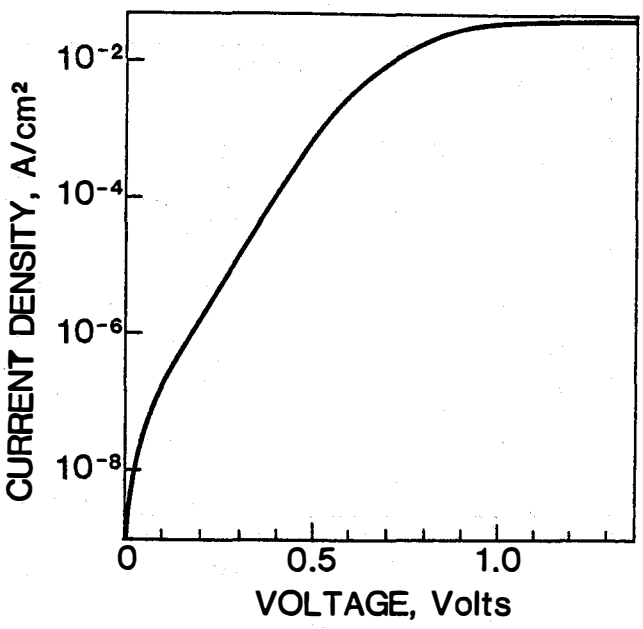

Fig. 5 Dark current-voltage characteristics of a thin film CdTe homojunction

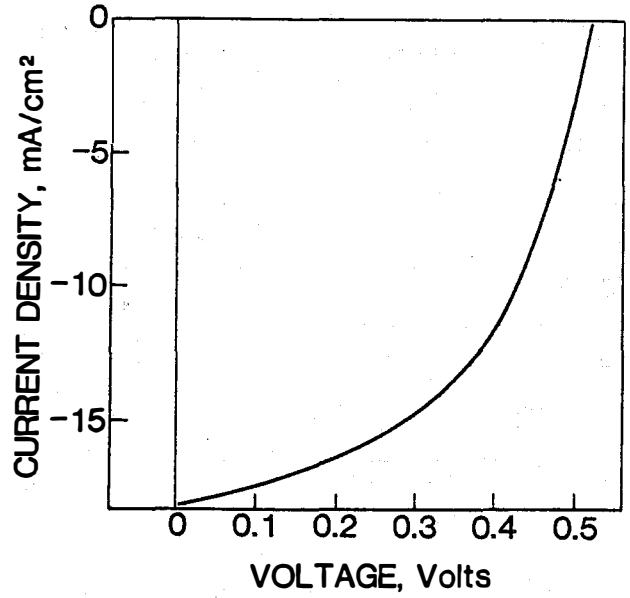

Fig. 6 Illuminated current-voltage characteristics of a thin film CdTe homojunction.

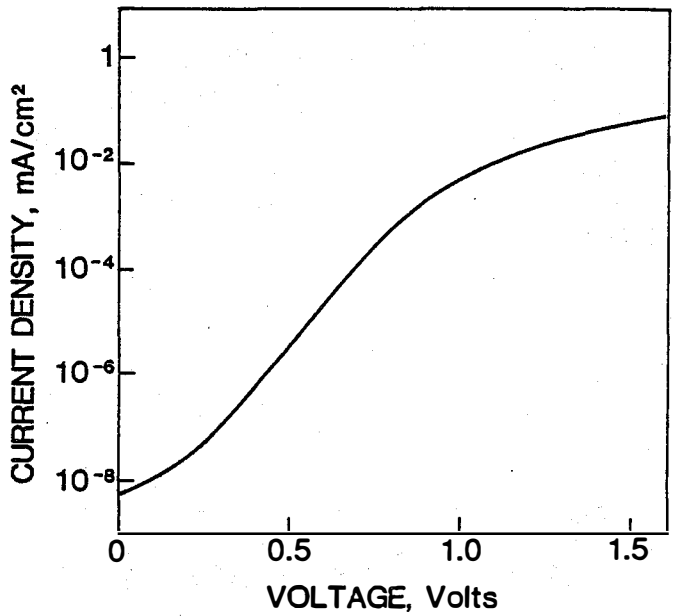

Fig. 7 Dark current-voltage characteristics of a thin film $Hg_{0.15}Zn_{0.85}Te/Cd_{0.7}Zn_{0.3}S$ heterojunction.

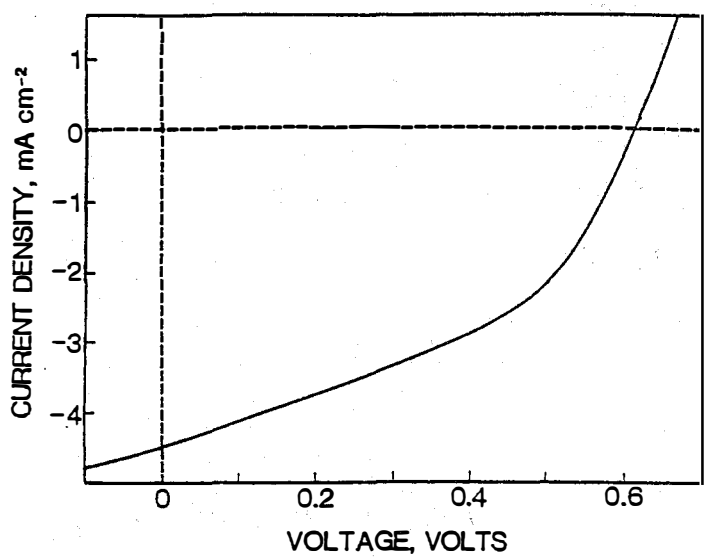

Fig. 8 Illuminated current-voltage characteristics of a thin film $Hg_{0.15}Zn_{0.83}Te/Cd_{0.7}Zn_{0.3}S$ heterojunction.

Title: **Thin Film Cadmium Telluride Photovoltaic Cells and Submodules Fabrication**

Organization: Department of Physics and Astronomy
The University of Toledo
Toledo, Ohio 43606

Contributors: Alvin D. Compaan, principal investigator; Randy G. Bohn, co-investigator; Atilla Aydinli, Ajit Bhat, Li-Hua Tsien, Shuzhen Liu, Zhifang Chen, Charles Tabory

Lower-Tier Subcontractors: Glasstech Solar Inc., Golden, CO
Pawan Bhat, C. DeHart, A. Benson, M. Landry

Glasstech Inc., Perrysburg, OH, and
Solar Cells Inc., Toledo, OH
James F. Nolan

Objectives

This new program which began at the end of July 1990, is designed to develop alternative vacuum-based growth techniques for CdTe-related thin-film solar cells and submodules. The program will seek to develop three new techniques for deposition of CdTe polycrystalline thin films and related window materials: laser-driven physical vapor deposition (LDPVD), plasma-enhanced chemical vapor deposition (PECVD) of organometallics, and reactive sputtering involving organometallics. The program emphasizes fundamental understanding of the physical mechanisms underlying these growth processes as well as the related device performance. Considerable effort will be applied to understand the effects of post-growth treatment on the structural, optical and electronic film properties. Ultimate goals after three years include the development of 4 cm^2 cells with AM1.5 efficiency of 13% and a large-area fabrication system based on one of the above deposition methods.

Technical Approach

This program involves close collaboration of the group at The University of Toledo with the lower-tier subcontractors. Glasstech Solar is principally responsible for the development of the techniques of PECVD and reactive sputtering with organometallic gases as well as a comprehensive examination of the effects of post-growth treatment on CdTe and related materials prepared by a variety of methods. Glasstech, Solar Cells, and Glasstech Solar are primarily responsible for the scaling up of the deposition methods to large areas and the optimization of the associated tasks of submodule fabrication. A particular focus of Solar Cells is the modification/development of a continuous, in-line production system for thin-film CdTe deposition on large-area substrates. At The University of Toledo, the emphasis is on the development and optimization of excimer-laser-driven physical vapor deposition of CdS, CdTe, ZnTe and related compounds and the basic physical understanding of the laser-driven process. A wide variety of materials characterization and device characterization is being performed at UT and GSI. These include optical absorption, x-ray diffraction, scanning electron microscopy, Raman scattering and photoluminescence, current-voltage measurements in the dark and with AM1.5 illumination, Hall measurements, and spectral quantum

efficiency. These are supplemented with measurements such as Auger electron spectroscopy and energy- or wavelength-dispersive spectroscopy at SERI.

Laser-Driven Physical Vapor Deposition

Studies of the LDPVD process were begun at UT prior to the start of support from the SERI Polycrystalline Thin Films Initiative. This work was supported by the State of Ohio's Thomas Edison Program, Solar Cells Inc., and The University of Toledo. Highlights of some results obtained to date are presented here.

The system for film growth is shown in Fig. 1. The 308 nm beam from the XeCl excimer laser (or 532 nm beam from the Nd:YAG) is weakly focussed with a 50 cm lens onto the pressed powder target. Target powders from Alpha Chemicals (five nines purity) were pressed in atmosphere to ~$3x10^8$ Pascals before loading into the chamber. To prevent pitting and grooving of the target, the target holder was rotated in an oscillatory motion with a stepper motor from below. The laser spot was also moved in a radial oscillation using the mirror M1. An interior window W2 was heated to ≥350 °C to protect the laser entrance window from gradual accumulation of deposits. The elevated temperature and the high laser power density effectively prevent deposition on the inner window.

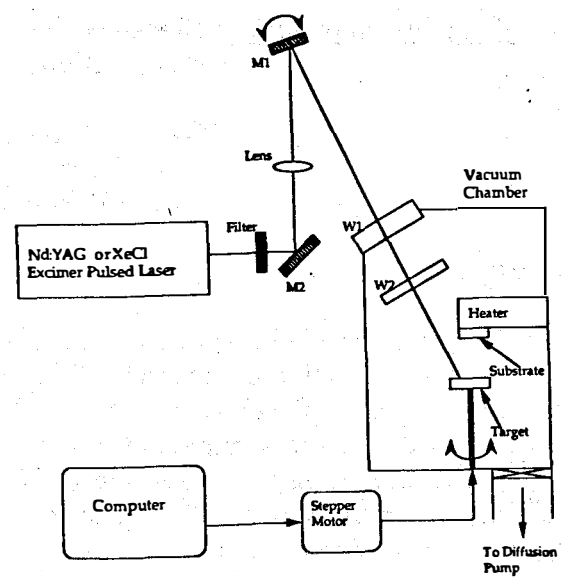

Figure 1. System used for the laser-driven physical vapor deposition. Target holder and mirror are rotated with stepper motors and window W2 is heated to ≥350° C.

At focal power densities above ~3 J/cm^2, the laser pulse generates a plume of vapor oriented normal to the target surface with a half-width of about 9 degrees. The as-grown films were optically very smooth and usually free of pinholes. Because of the thickness variation away from the point normal to the target laser interaction spot, it was convenient to obtain the film thickness profile simply by scanning a focussed AlGaAs laser spot (λ=840 nm) along the films and recording the reflected intensity. Figure 2 translates the interference fringe results for a CdS film into an angular dependence for the laser-driven plume. Note that the results are displayed for two scans--one parallel and one perpendicular to the plane of incidence of the excimer laser and the target. The film thickness has circular symmetry and follows a Gaussian shape over the central 70% but falls more slowly in the wings of the deposition.

The efficiency of target utilization was measured by directly weighing the target and substrate before and after a deposition. We find that at the typical substrate growth temperature of 260°C, 40% of the target mass loss appears on the two-inch square substrate. For a room temperature substrate, about 55% of the target mass loss appears as deposited film. The above results were obtained for a target-substrate separation of 55mm, a laser

power density of ~5J/cm^2, and a vacuum pressure of ~5 x 10^{-6} Torr. At laser power densities of ~5 J/cm^2 for CdTe, the growth rate at the center of the deposition was about 1 Å per pulse.

Film Characterization

The most important growth parameter determining film quality is the substrate deposition temperature. During the past year, we have made preliminary observations of the materials properties of the as-grown films by x-ray diffraction, optical absorption, Raman scattering, and by electrical measurements.

X-ray diffraction showed a predominant polycrystalline grain orientation of <111> for growth temperatures of 180°C and above. Typical results are given in ref. 1. SEM studies show that the grains are columnar with lengths extending through the typically 1 μm film thickness and with diameters ~300Å prior to annealing.

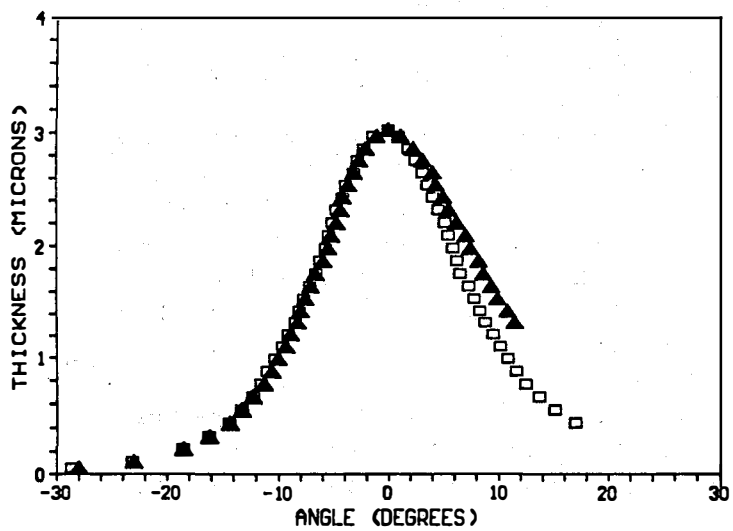

Figure 2. Thickness profile of a CdS film plotted vs. angle relative to target normal for x-direction (triangles) and y-direction (squares).

Optical absorption measurements obtained on a Varian DMS300 double beam spectrometer for films deposited on Corning 7059 glass indicated absorption edges (extrapolated from plots of $(\alpha h\nu)^2$ vs $h\nu$) typical of crystalline films as reported in the literature[2] for both CdS and CdTe. The optical absorption was found not to be as sensitive to the crystal quality as the other measurements discussed here.

Raman scattering was performed on both CdS and CdTe films and provided results which were quite sensitive to the film quality. For CdS the Raman scattering was obtained with an argon laser (λ = 457.9 nm) which has a photon energy slightly above the CdS band gap. In this case the (resonance) Raman effect is similar to a resonance photoluminescence process[3,4] in which the photoexcited carriers may scatter from one optical phonon (first order Raman) or from two or more optical phonons (Raman overtones) before undergoing radiative recombination. However, the photoexcited carriers (electrons or holes) may also scatter from impurities or recombine nonradiatively. These competing processes will decrease the intensity of the higher order Raman lines relative to the first order Raman process. This behavior is seen in Fig. 3 in which we have compared the room temperature first, second, and third-order Raman lines from a bulk single crystal, and from two polycrystalline CdS thin films grown at 215°C and 260°C. Note that the results from the 260°C film deposition are significantly better than for deposition at 215°C but still show less overtone intensity than the bulk single crystal. (The background at the larger frequency shifts arises from the near-band-edge photoluminescence due to thermalized carriers.) Similar results were obtained for CdTe utliizing a krypton ion laser which has transitions near resonance with the band edge of CdTe.

The substrate temperature during deposition has a strong effect also on the electrical properties of the films. Results for in-plane resistivity on CdS films grown using the Nd:YAG laser are shown in Fig. 4. The resistivity was measured using a Van der Pauw contact geometry for the sample in darkness and under room light illumination. Note that the resistivity of these films grown from undoped CdS powder *increases* with increasing deposition temperature. Our SEM results have shown that in general the grain size increases with deposition temperature and thus one might expect grain boundary scattering to decrease in importance and yield *lower* resistivity. The opposite occurs. Similar results have been obtained recently by Figueroa and Sanchez-Sinencio on polycrystalline CdTe who found that the mobility of electrons and holes decreases with increase in grain size for their polycrystalline films grown by close-spaced vapor transport.[5] These results are consistent with the model of stronger trapping at the boundaries of large grains as discussed by Kazmerski.[6] Figure 4 displays also the effects of adding a small amount of metallic In powder to the target powder. The film resistivity is lowered by about three orders of magnitude clearly indicating that the In is doping the film.

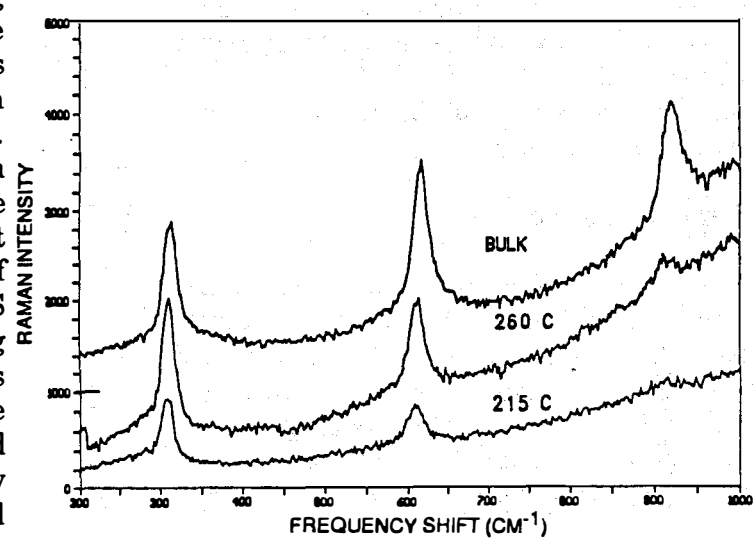

Figure 3. Raman scattering spectra showing the first order LO phonon at ~300 cm^{-1} and two overtones for bulk single crystal (baseline shifted by 1000 counts) and for two polycrystalline films with different growth temperatures.

Device properties

Solar cells were fabricated by a two-step deposition of CdS and then CdTe on SnO_2-coated glass substrates obtained from Glasstech Solar Inc. The SnO_2 coating was textured with a 20% haze. Other SnO_2-coated glass substrates were also used successfully. Auger electron spectroscopy was used to profile the film composition in the as-deposited structures. The results indicated no observable interdiffusion across the SnO_2/CdS and CdS/CdTe interfaces within the resolution limits of the measurement.

Following deposition the structures were dipped in a saturated $CdCl_2$ solution and annealed at 400°C for 30 min. Our SEM studies showed that the grain size typically increased so that the columnar grain structures reached 0.1 to 0.2 μm in diameter. Gold dots were then evaporated on the films and wires bonded with Ag paint to the Au contacts and to the SnO_2 to provide access for electrical characterization.

A current-voltage measurement obtained from one of the dots on a recent solar cell structure is presented in ref. 1. Under approximate AM1.5 illumination from a tungsten-halogen lamp the cell gave I_{SC} = 20.9 mA/cm^2 and V_{OC} = 5.2 V. The fill factor FF is ~50%. In comparison with state-of-the-art CdS/CdTe cells the open circuit voltage is low (best $V_{oc} \cong 0.78$ V) and the fill factor is low (best FF ≅ 0.80). Work is in progress to improve these values.

The spectral quantum efficiency (See Fig. 5) indicates a nearly flat response over the range from the CdS window layer absorption near 500 nm to the band edge of CdTe at about 830 nm. At 1 and 2 volts reverse bias the response is slightly improved probably due to improved carrier collection across the junction.

Future Work

Research at UT will continue toward optimizing the laser deposition process including a comprehensive understanding of the physics in the laser-driven evaporation or ablation plume and its dependence on laser wavelength, pulse energy density, and pulse repetition rate. Efforts are also being made toward optimizing the growth of doped CdS and ZnTe and the enhancement of grain size in the as-grown films. At GSI efforts will focus on studies of plasma-enhanced growth of CdTe and reactive sputtering for CdTe growth. Hybrid processing will continue to be studied. This involves cells prepared both by plasma-enhanced processing and by laser-driven deposition. A considerable effort will be placed on materials characterization and device analysis throughout this project. The choice of methods of film growth is designed to provide a smooth interface with existing technologies presently being utilized by GSI and SCI for photovoltaic structures. The studies of alternative methods of film growth are structured to provide information for a choice at the end of two years, of the optimum growth process for each deposited layer of the photovoltaic structure.

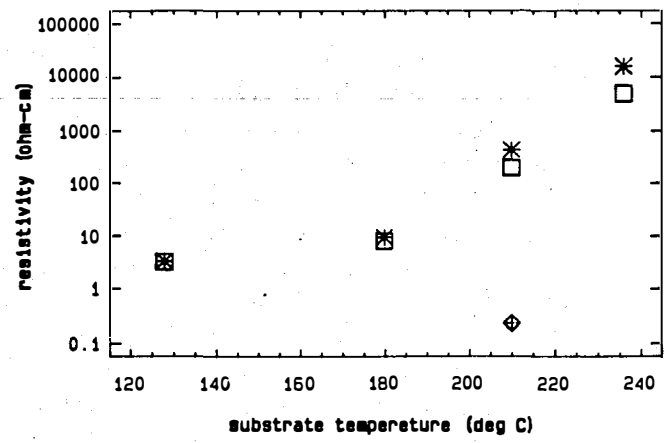

Figure 4. Resistivity of CdS grown by Nd:YAG LDPVD as a function of growth temperature. Data taken with room lights on (squares) and in the dark (asterisks) on undoped films. Diamond represents data (light and dark) from film grown with $1x10^{20}$ In/cm^3 powder mixed into the target CdS power.

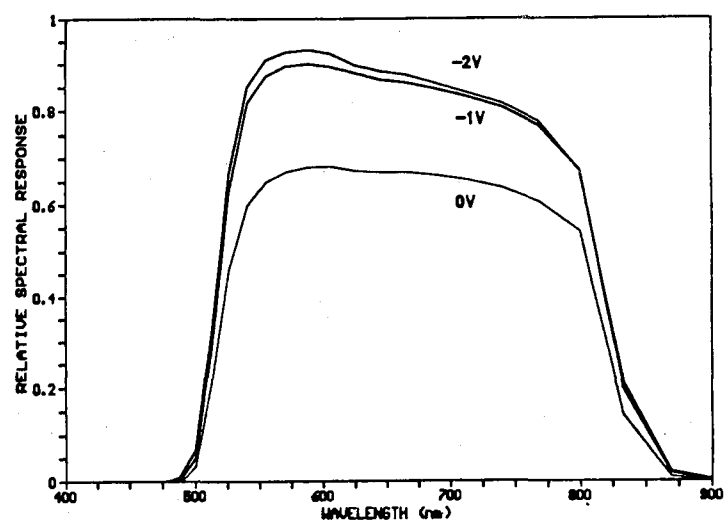

Figure 5. Spectral quantum efficiency as a function of bias voltage.

References

1. A. Compaan, A. Bhat, C. Tabory, S. Liu, M. Nguyen, A. Aydinli, L-H. Tsien, and R.G. Bohn, Solar Cells (in press). [Procedings of the 10th Photovoltaic Advanced Research and Development Symposium, Golden, CO., Oct 22-25, 1990.]
2. Landolt-Bornstein, Numerical Data and Functional Relationships in Science and Technology, vol. 17B [Physics of II-VI and I-VII Compounds, Semimagnetic Semiconductors] (Springer-Verlag, Berlin, 1982).
3. M. Cardona, in Light Scattering in Solids I, 2nd ed., edited by M. Cardona, p. 1 (Springer-Verlag, Berlin 1982).
4. A. Compaan, Appl. Spectroscopy Reviews, 13, 295 (1977).
5. J. M. Figueroa, F. Sanchez-Sinencio, J. G. Mendoza-Alvarez, O. Zelaya, G. Contreras-Puente, and A. Diaz-Gongora, J. Crystal Growth (in press).
6. L. L. Kazmerski, Polycrystalline and Amorphous Thin Films and Devices, (Academic Press, 1980), p. 84.

4.0 CRYSTALLINE SILICON MATERIALS RESEARCH

John Benner (Manager), Bhushan Sopori

Although crystalline silicon technologies for material growth and device processing are considered to be mature for a variety of applications, there remain a host of issues about which the current understanding is only marginal. These issues pertain to the role of defects and impurities in altering the properties of silicon and silicon solar cells. It is generally recognized that the presence of impurities/defects in the substrate can degrade the cell performance; however, recent data show that in the presence of crystal defects, the influence of impurities on the cell performance is somewhat mitigated. It is also known that some defects can be passivated by presence of hydrogen or oxygen, although a detailed knowledge of these effects is certainly lacking. Clearly, these issues are critical to photovoltaic technology based on use of low-cost substrates which contain high concentrations of impurities and/or defects. The current research program was developed in collaboration with industry representatives to ensure that the industry research needs, pertaining to basic material issues, are adequately addressed. In this coordinated research effort between industry, universities and SERI, the SERI role is primarily to support the area of test device fabrication/analysis in order to relate material characteristics directly to solar cell performance.

This research program is aimed at developing understanding of basic mechanisms related to influence of impurities and defects on the important photovoltaic parameters in silicon. In particular, emphasis is towards development of post-growth processes that can be applied to low-cost substrates, preferably as a part of solar cell fabrication process, in order to improve subcontracts that are supported by SERI in-house research participation. Major areas of research are: (1) mechanisms of hydrogen, oxygen interaction in low-cost silicon; (2) mechanisms of hydrogen passivation and kinetics of hydrogen diffusion; (3) effects of hydrogen on solar cells containing different types of crystal defects; (4) development of techniques for impurity characterization in silicon containing crystal defects; and (5) nondestructive testing of the photovoltaic parameters of commercial material. In the coming year an effort will be made to develop some low-cost cell processing techniques that incorporate the knowledge obtained from this research, to fabricate high-efficiency cells on commercial solar cell silicon.

Title: **Basic Studies of Point Defects and Their Influence on Solar Cell Related Electronic Properties of Crystalline Silicon**

Organization: School of Engineering, Duke University, Durham, North Carolina

Contributors: U.M. Goesele, principal investigator; W.J. Taylor, and W.S. Yang

I. Introduction

The goal of this work is to establish a relationship between precipitate-generated strain in the matrix and the electrical properties of solar-grade polycrystalline silicon. Precipitates involving oxygen and carbon are suspected to affect the minority carrier diffusion length[1]. Unsatisfied atomic bonds at the interface between the precipitate and the silicon matrix act as traps or recombination centers for the carriers. Evidence from surface oxide layers[2] indicates that strain influences the electrical behavior of these traps. We assume that the strain surrounding a precipitate buried in a matrix can similarly influence the electrical behavior, and that by tailoring the precipitation processes to minimize strain, one can minimize deleterious effects of these traps. This year we have made considerable advances in our understanding of precipitation processes and the associated strains.

The formation of precipitates involving volume changes is strongly influenced by the point defects involved[3]. We consider self-interstitials as the dominant point defect. These self-interstitials, in turn, can be affected by dislocations in the matrix. Analytical work this year has led to surprising results in two areas: the effect of dislocations on self-interstitial supersaturations (Section III), and the effect of self-interstitial supersaturations on precipitate nucleation (Section IV). Since the self-interstitials play such an important role in precipitation processes, knowledge of their diffusivity (D_I) is vital. This will affect how quickly self-interstitial supersaturations can flow to/from the sinks/sources. Unfortunately, D_I is a poorly known quantity at temperatures of 900°C and below, where many cell manufacturing processes occur. Therefore we are studying diffusivity at these temperatures (Section II).

In the next year we plan to combine results of these investigations and form a coherent model for strain around precipitates of oxygen and carbon in polycrystalline silicon. Then we intend to qualitatively relate these strains to the minority carrier diffusion length of the material.

II. Studies of Self-Interstitial Diffusivity (D_I)

We measure the diffusivity of self-interstitials by generating them at one side of a wafer and observing their arrival at a given depth via enhanced diffusion of a marker species. High concentration phosphorus is diffused at 900°C into a highly carbon-doped (3×10^{17} cm^{-3}) silicon wafer. The in-diffusing phosphorus creates silicon self-interstitials , which subsequently rapidly diffuse across the wafer and assist the carbon to diffuse into an undoped 5 μm epitaxial layer on the opposite side. The enhanced carbon diffusion profile acts as a marker for the arrival of the self-interstitials, allowing evaluation of the diffusivity of self-interstitials. This year, two

rounds of experiments were performed. In the first, the samples were etched to a variety of thicknesses prior to diffusion to reduce the self-interstitial diffusion distances and allow a better determination of the diffusivity. Large variations in results obtained from these samples indicated that the etched samples were not perfectly flat, causing scatter of the detection ions in Secondary Ion Mass Spectroscopy (SIMS) analysis. In addition, the data showed very little enhancement, even for the thinnest samples, which suggests possible loss of self-interstitials as they diffuse through the highly carbon-doped silicon wafer. This observation is in line with our hypothesis that a self-interstitial supersaturation favors co-precipitation of carbon and self-interstitials.

More recent experiments avoided both problems: the possible consumption of self-interstitials in the highly carbon-doped bulk and the data scatter due to uneven samples. This was achieved by diffusing the phosphorus from the front side into the non-carbon doped epitaxial layer. Figure 1 shows the carbon profile after 16 hours at 900°C with no phosphorus enhancement, along with the computer simulation model. Figure 2 clearly shows the effect of the phosphorus-generated self-interstitials on the carbon diffusion profile. After only 1 hour at 800°C, the profile shows carbon diffusivity enhancement of 50-100x, which correlates as expected with the enhancement displayed by the tail of the in-diffusing phosphorus profile (which is also directly related to the self-interstitial supersaturations). These tests showed that our approach is capable of producing repeatable results, and have provided a lower boundary on the self-interstitial diffusivity (3×10^{-11} cm^2/sec at 800°C). This estimate is still considerably lower than that anticipated (1×10^{-8} to 10^{-7} cm^2/sec at 800 to 900°C). Experiments continue in this area, including variation of etch procedures, etch depths and diffusion times. Currently several samples are being investigated by Sally Asher of the SIMS group at SERI.

III. Effect of Dislocations on Self-Interstitial Supersaturations

It will be shown in the next section that supersaturations of self-interstitials can drastically decrease nucleation and precipitation rates. However, it is known that precipitation occurs, and it is also quite reasonable to expect supersaturations to occur during processing. One must answer the question of how these supersaturations are eliminated. In polycrystalline silicon, which is known to contain dislocations in densities of 10^4 to 10^7 cm^{-2}, it is commonly expected that these act as sinks to easily absorb self-interstitial supersaturations. However, the following analysis shows that this can be true only under certain circumstances.

We begin with two assumptions which should assist a material in absorbing self-interstitials. We assume that the material has a very high dislocation density ($\rho = 10^7$ cm^{-2}) and that these dislocations are perfectly efficient at absorbing self-interstitials ($\alpha = 1$). Additionally, we note that due to the exponential dependence of C_I^{eq} on temperature, supersaturations of magnitude 10 or higher are not unreasonable. The equation describing the decrease of a self-interstitial supersaturation of magnitude $C_I - C_I^{eq}$ is

$$dC_I/dt = -\alpha \rho D_I (C_I - C_I^{eq}) \qquad (1)$$

where t is time and D_I is the self-interstitial diffusivity. The quantity $(C_I - C_I^{eq})$ may be approximated by C_I for sufficiently high self-interstitial supersaturations. This means that if the dislocations are to significantly affect C_I during a time period Δt, the following relationship must hold:

$$\alpha \rho D_I \Delta t \approx 1 \qquad (2)$$

If $\alpha \rho D_I \Delta t$ were significantly less, such as .01, then very little change in C_I would occur. The relationship between these parameters is given in Figure 3. The range of the x-axis covers the various estimates proposed for D_I at 900°C. Note that only for the higher diffusivities are significant decreases in self-interstitial supersaturations possible. Note also that the times are only that required for the dislocations to absorb a quantity of self-interstitials of magnitude C_I. If C_I is initially supersaturated by a factor of 10, then it would require roughly 10 times as long for C_I to decrease to close to C_I^{eq}.

IV. Precipitation Modeling

Progress has been made in several areas concerning precipitation. First, we investigated the effect of a self-interstitial supersaturation (C_I/C_I^{eq}) on oxygen nucleation rate. We have used the relationship[4]

$$r_{crit} \approx 2\sigma\Omega \,/\, (kT \ln [(O_i/O_i^{eq})(C_I^{eq}/C_I)^{1/2}]) \qquad (3)$$

for the critical radius and the expression

$$\dot{N} = O_i \exp[-\frac{4\pi\sigma}{3(kT)} r_{crit}^2] \cdot O_i 4\pi r_{crit}^2 \frac{D}{d} \qquad (4)$$

for the nucleation rate. Here O_i/O_i^{eq} is the oxygen supersaturation, σ is the surface energy, Ω is the molecular volume of SiO_2, and D/d is the ratio of oxygen diffusivity to lattice parameter, we plot nucleation rate versus self-interstitial supersaturation in Figure 4. This shows that even for a self-interstitial supersaturation of 2, nucleation is essentially eliminated. This leads to the important conclusion that if nucleation of oxygen precipitation is to occur at all, $C_I \approx C_I^{eq}$ must be true.

On another front, we have obtained an expression for the critical radius of an oxygen precipitate which includes the effect of matrix stress. The volume of the precipitate is expressed solely in terms of the incorporated oxygen atoms. The volume provided by the matrix is expressed in terms of oxygen atoms and self-interstitials. The ratio of these volumes provides an expression for the strain energy in the matrix, analogous to the results of Mott and Nabarro[5]. This is incorporated into the free energy equation for the system, and a minimum is found. The result is an expression similar to (3) above, with an additional term in the exponent for the self-interstitials. The strain energy in the matrix is controlled by the self-interstitial supersaturation. We are currently working on the incorporation of the effects of carbon into this

strain equation. This procedure should allow us to express the resulting precipitation strain in terms of oxygen, carbon, and self-interstitial supersaturations, which in turn would give a guide on how to minimize these strains using proper oxygen and carbon concentrations and cooling conditions.

The strong effects of carbon[6] on oxygen precipitation must be investigated, since it has been shown[7] that simultaneous high oxygen and high carbon concentrations lead to low matrix strain. Carbon precipitating alone would tend to decrease the strain in the matrix (and absorb self-interstitials). Oxygen precipitating alone would tend to increase the strain in the matrix (and generate self-interstitials). The carbon and oxygen may either precipitate independently and communicating via self-interstitials, or they may precipitate together. Our analysis concerning the surface energy of a SiC precipitate indicate that this energy is too high to allow for significant nucleation of SiC precipitates. This means that the carbon and oxygen are most likely precipitating together (C-0 complexes), and not independently.

V. Summary

In this past year significant advances in our understanding of precipitation have been made. Self-interstitial supersaturations dramatically affect nucleation rates, according to both a simple approach and a more elaborate approach which incorporates the strain energy of the matrix. We now have reason to believe that carbon precipitates predominantly together *with* oxygen, in oxygen-carbon containing precipitates, and not independently as SiC precipitates. Finally, a lower bound on D_I at low temperatures has been obtained and will be refined. In the coming year.we will combine this information with tests on minority carrier diffusion length to form a model correlating precipitation to electrical properties.

References

[1] S. Pizzini, A. Sandrinelli, M. Beghi, D. Narducci, F. Allegretti, S. Torchio, G. Fabbri, G.P. Ottaviani, F. Demartin, and A. Fusi, J. Electrochem. Soc., **135**, 155 (1988)

[2] C.H. Bjorkman, J.T. Fitch, and G. Lucovsky, Appl. Phys. Lett., **56**, 1983 (1990)

[3] N.B. Urli and B. Pivac, Rad. Eff. and Def. Sol., **111&112**, 449 (1989)

[4] U. Gösele and T.Y. Tan, Appl. Phys. **A28**, 79 (1982)

[5] N.F. Mott and F.R.N. Nabarro, Proc. Phys. Soc. **52**, 80,(1940)

[6] Q. Sun, K.H. Yao, J. Lagowski, and H.C. Gatos, J.Appl. Phys., **67**, 4313 (1990)

[7] S. Hahn, M. Arst, K.N. Ritz, S Shatas, H.J. Stein, Z.U. Rek, W.A. Tiller, J. Appl. Phys. **64**, 849 (1988)

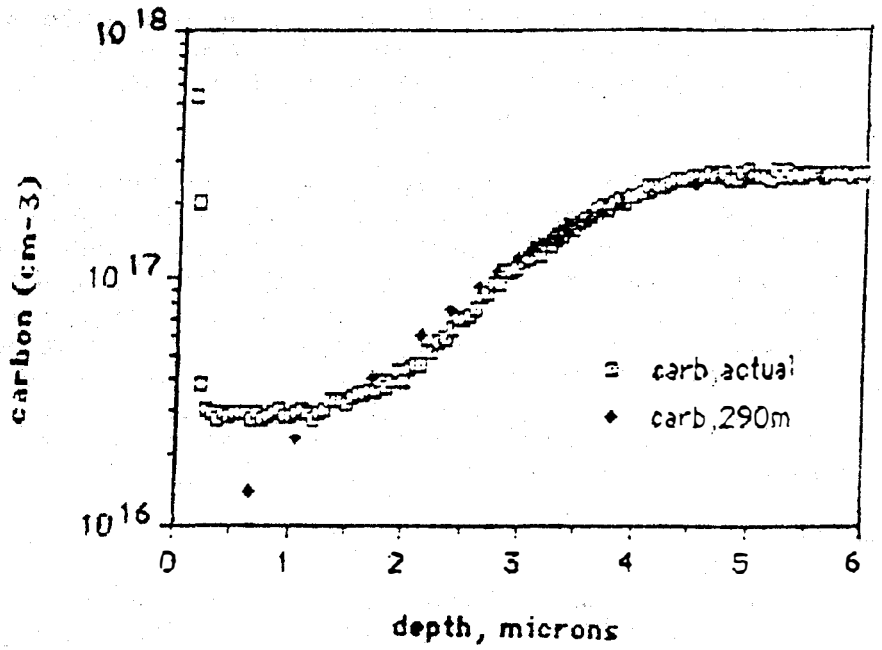

Figure 1 : Actual data and computer simulation (carb,290) for carbon diffusing into the epitaxial silicon layer for 16 hours at 900°C. SIMS background for carbon in silicon has been around $2x10^{16}$ cm^{-3} in these experiments.

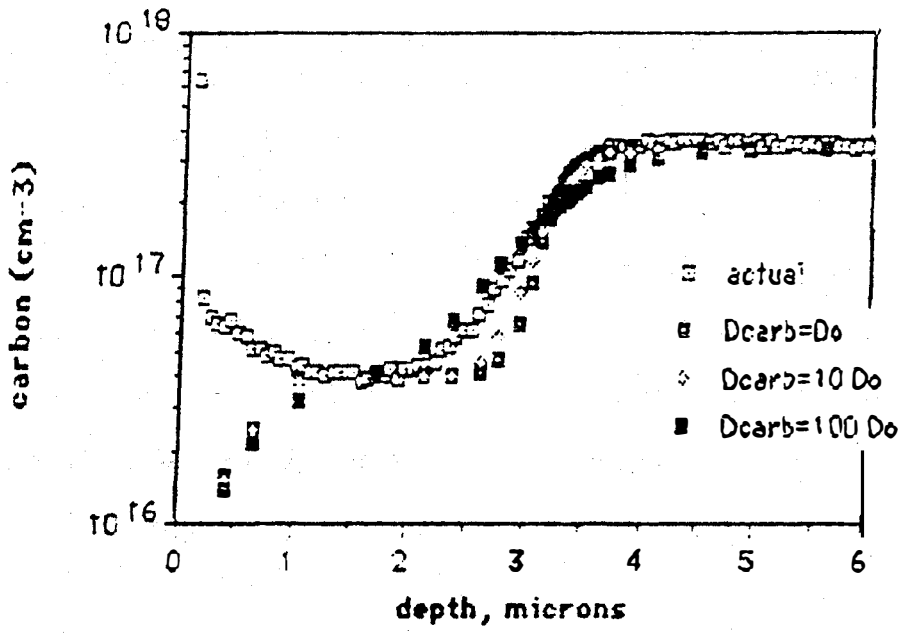

Figure 2: Actual data for carbon diffusing into the epitaxial layer for 1 hour at 800°C with phosphorus-generated self-interstitials coming in from x=0. Computer simulations indicate a diffusivity enhancement of near 100x ($D=100xD_o$ curve).

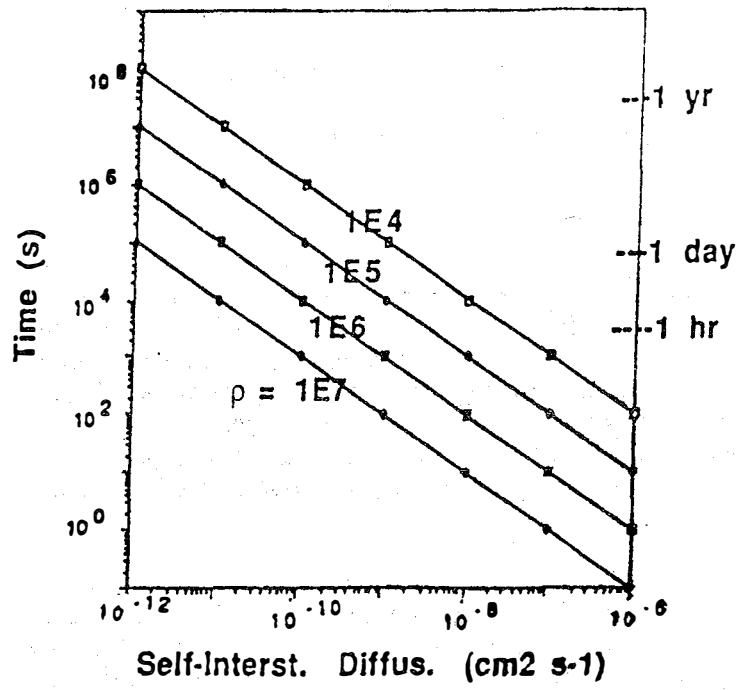

Figure 3: The time required for dislocations to reduce self-interstitial supersaturations by 1. The parameter is dislocation density in cm^{-2}. To reduce a supersaturation of 10x would take 10 times as long.

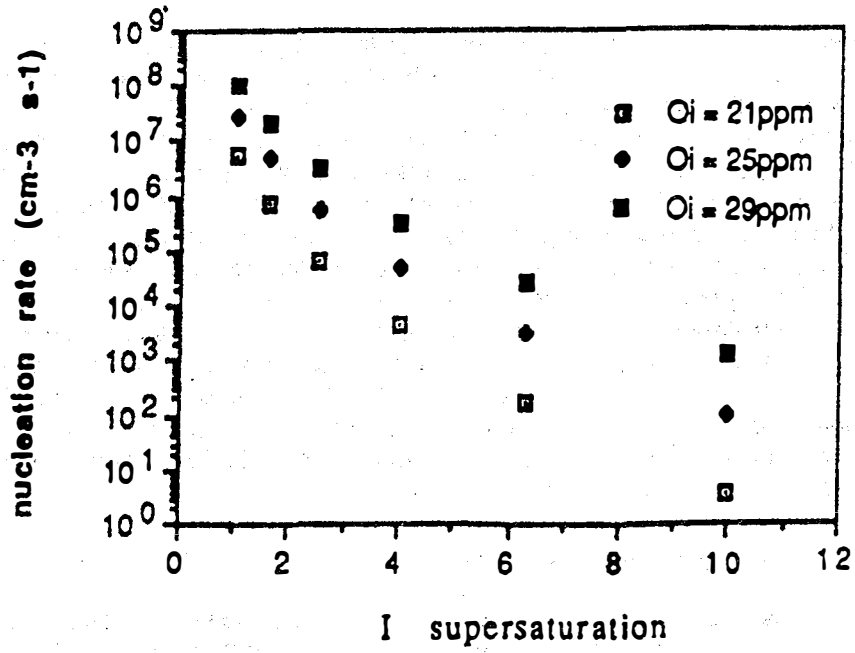

Figure 4: The effect of a self-interstitial supersaturation (C_I/C_I^{eq}) upon nucleation rate of SiO_2 precipitates in silicon at 700°C. Parameter is oxygen concentration.

Title: **Impurity and Defect Characterization In Silicon**

Organization: Georgia Institute of Technology, Atlanta Ga. 30332

Contributors: A. Rohatgi and W. A. Doolittle

Introduction:

The effect of oxygen on minority carrier lifetime and defects has been an area of active investigation, but there is still no consensus about the exact role of oxygen. Generally, single crystal silicon with high oxygen content is considered more vulnerable to lifetime degradation. Some investigators believe [1] there may be an optimum oxygen concentration for high lifetime in polycrystalline silicon. Polycrystalline silicon has recently become a strong contender for cost-effective photovoltaic cells but the role of oxygen in these cells, is at best, poorly understood. The objective of this program is to improve the fundamental understanding of the effect of oxygen on promising photovoltaic, polycrystalline silicon materials.

Experimental:

Mobil EFG Material: Several EFG nanogans were grown with controlled oxygen. Nanogans were doped with boron with target resistivities ranging from 0.5 to 5.0 ohm-cm. In select cases, oxygen was introduced into the these ribbons by controlling the CO_2 concentration around the meniscus [2]. Standard n+ -p-p+ solar cells were fabricated with single layer Si_3N_4 antireflection coatings using phosphorus on the front and Al sintering on the back. In all cases, cells were hydrogen passivated to improve the performance. The as grown ribbons were analyzed by SPV, FTIR and DLTS measurements and the solar cells were characterized by lighted and dark I-V, spectral response and OCVD lifetime measurement. In order to investigate electrically active defects in finished devices, the cells were first subdivided into 50 mil diameter mesa diodes and then DLTS and J-V-T measurements were performed.

Solarex CDS Material: Substitutional carbon and interstitial oxygen concentrations in wafers cut from various positions in the ingot were determined by FTIR. Using a PC based imaging system [3] , the grain size statistics and etch pit densities were also measured on these wafers. This data is summarized in Table 1. Standard n+ p cells with three different base dopings were fabricated on wafers cut from similar ingot positions, 1.8 to 15.5 cm, in order to investigate the role of dopants. No hydrogen passivation was used in these cells. The Voc, Isc, and fill factor were measured and are summarized in Table 2. The grid lines and AR coatings of the high and low resistivity cells were then removed and small area, 0.44 mm^2 and 0.05 mm^2 , Ti/Au mesa diodes were fabricated on the front with Au back contacts. Deep level transient spectroscopy, using forward bias injecting pulses, was performed to determine majority and minority carrier trap levels. When two DLTS peaks overlapped, the correct peak location and height was determined by a combination of Least squares fit [4] and Levenburg-Marquardt [5] fit routines. Current versus temperature measurements at fixed reverse bias were performed in order to support that the levels detected by DLTS were indeed the device limiting levels. Due to the random nature of defects in these materials, several locations on each wafer were analyzed to obtain a statistical variation of deep levels. The levels obtained are summarized in Table 3 along with the average trap concentrations.

Effect of Oxygen on the Polycrystalline Solar Cells:

The effect of oxygen was investigated on two promising polycrystalline photovoltaic materials: Mobil Solar EFG ribbon and Solarex semicrystalline silicon. EFG ribbon is pulled through a graphite die from a silicon melt contained in a graphite crucible. This results in about $1x10^{18}$ atoms/cc carbon but less than $2x10^{16}$ atoms/cc oxygen. In order to investigate the effect of oxygen, EFG ribbon was grown in a CO_2 rich ambient which resulted in about 5 ppm oxygen in the ribbon. Table 2 shows that oxygenated cells were about 1-2% more efficient than the non-oxygenated cells. The addition of a small amount of oxygen increased Voc, Isc,

spectral response and the bulk lifetime. Attempts to explain this improvement on the basis of defects or DLTS measurements failed because DLTS spectra did not reveal any distinct peaks in the finished devices. In addition to that, the DLTS detection limit was $10^{11}/cm^3$ for these samples. Therefore, reverse bias J-V-T measurements were performed which do not suffer from the detection limit and if done properly, such that the reverse current is dominated by generation of carriers from the trap, can reveal deep levels. Ln(J) vs. 1/T plots in figure 1 shows that non-oxygenated cells had two deep levels, at 0.54 and 0.75 eV, but oxygenated cells showed only a 0.54 ev trap. Incorporation of oxygen resulted in the passivation or elimination of the 0.75 eV trap which was responsible for the lower cell efficiency of the non-oxygenated EFG cells. Thus, a small amount of oxygen can be beneficial in some polycrystalline materials. However, the addition of too much oxygen can begin to degrade the cell performance due to the possibility of oxygen precipitation and/or oxygen related defect complexes. Attempts to incorporate more oxygen in EFG indeed resulted in lower lifetime and cell efficiencies.

Solarex semicrystalline cast-silicon is another promising photovoltaic material that routinely gives efficiencies of 12-13% in large area production and has recently produced small area cell efficiencies of 17% . Attempts were made to investigate the reason for about 2% lower absolute efficiency of the cells made from the bottom part of the ingot compared to the top (see figure 2). Comparisons were made between cell performance and variations in oxygen, carbon, grain size, etch pit density and deep levels as a function of ingot position. No correlation was found between etch pit density and cell performance. The top wafers that gave the best cell performance had lower oxygen (15.7 ppm) and larger grains (0.85 cm^2) compared to the bottom cells which showed 24 ppm oxygen and small grain size (0.15 cm^2). Both grain boundaries and oxygen precipitates are classified as extended defects and can be a source of distributed states. DLTS measurements confirmed that the lower end of the ingot has a considerable amount of distributed states in contrast to the top cells where DLTS peaks were more well defined (see figure 3). This suggests that Solarex semicrystalline silicon may be suffering from an excess amount of oxygen which can precipitate and as a result, degrade the cell performance. Although all measurements were performed on intragrain locations far away from the grain boundaries, at this point , the role of the smaller grain size at the bottom cannot be completely ruled out in forming the distributed states.

Summary:

Moderate amounts of oxygen (about 5 ppm) in polycrystalline materials like EFG ribbon can improve cell performance by passivating harmful defects. An excess amount of oxygen (> 15 ppm) can hurt the performance of polycrystalline materials by forming distributed states via oxygen precipitation.

References:

1. B. L. Sopori, "Influence of oxygen on the Performance of Silicon Solar Cells", Proc. 20th IEEE PVSC, p. 591, 1988.
2. B. Macintosh, et. al. E. C. Photovoltaic Solar Energy Conference, Ed. W. Palz, D. Reidel and Dordrecht, p. 553, 1981.
3. R. Brenneman, D. Ramsey and D. Angell, "Automated Defect, Inclusion and Morphological Analysis of Solarex Polycrystalline Silicon", Proc. of the 21st PVSC, Orlando Fl., May, 1990.
4. R. Langfeld, Appl. Phys. A, **44** (1987) 107.
5. W. H. Press, B. P. Flannery, S. A. Teukolsky, W. T. Vetterling, Numerical Recipes: The Art of Scientific Computing, Cambridge University Press, 1986.

Table 1

Wafer Position from Bottom of Ingot (cm)	Grain Area Avg.± S. D. (cm^2)	Average O_i (ppm)	Average C_s (ppm)	Average Etch Pit Density (cm^{-2})
1.8 *	0.15 ± 0.03	24.1	0.7	5109
4.4	0.47 ± 0.14	22.2	1.0	6644
7.1	0.64 ± 0.11	22.7	0.9	5763
11.6	0.70 ± 1.09	17.4	1.6	3348
14.5**	0.85 ± 0.25	15.7	2.5	7512
17.0	1.24 ± 0.29	17.1	4.0	4547
19.6***	1.33 ± 0.44	05.2	8.3	79,587

* Resulted in the worst cell performance.
** Resulted in the best cell performance.
*** This wafer is from material considered unusable.

Table 1: Ingot position vs. grain size, oxygen and carbon concentrations and etch pit density for Solarex CDS polycrystalline silicon.

Table 2

Sample Id	Oxygen Content (ppm)	Voc (mV)	Jsc (mA/cm^2)	Efficiency
EFG-1	< 0.5	550	28.4	11.7
EFG-2	≈ 5.0	570	29.7	13.1
CAST-1	24.0	572	24.5	10.1
CAST-2	15.7	595	28.0	12.5

Table 2: The oxygen dependence of two types of polycrystalline silicon solar cells.

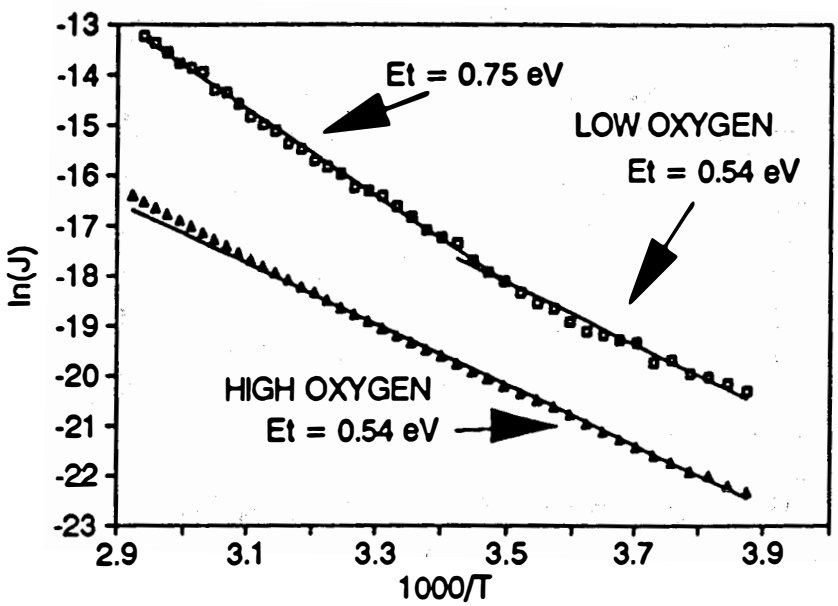

Figure 1: Ln(J) vs. 1/T for non-oxygenated (top) and oxygenated (bottom) EFG cells, showing two traps in the non-oxygenated case but only one in the oxygenated material.

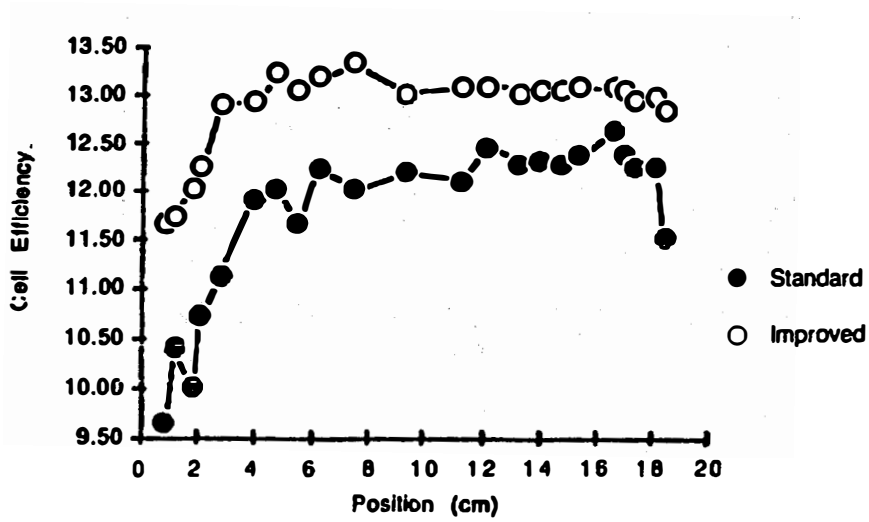

Figure 2: Variations in cell efficiency vs. ingot position for Solarex CDS polycrystalline silicon (both the standard and improved processes).

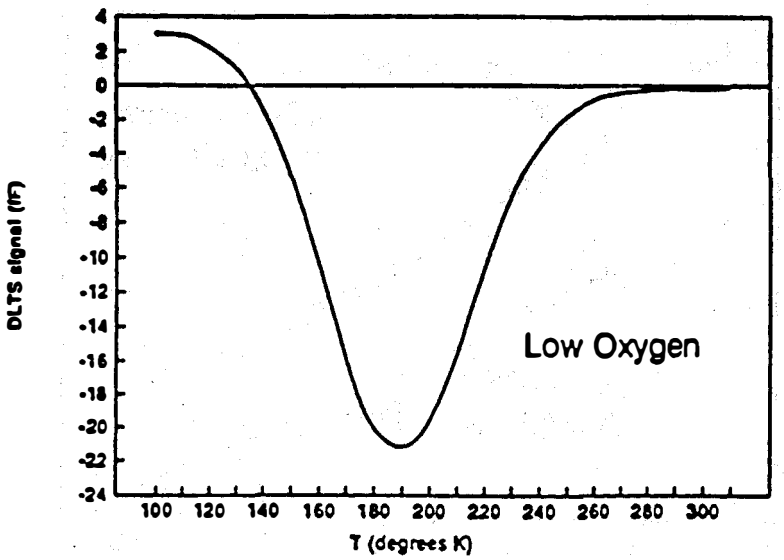

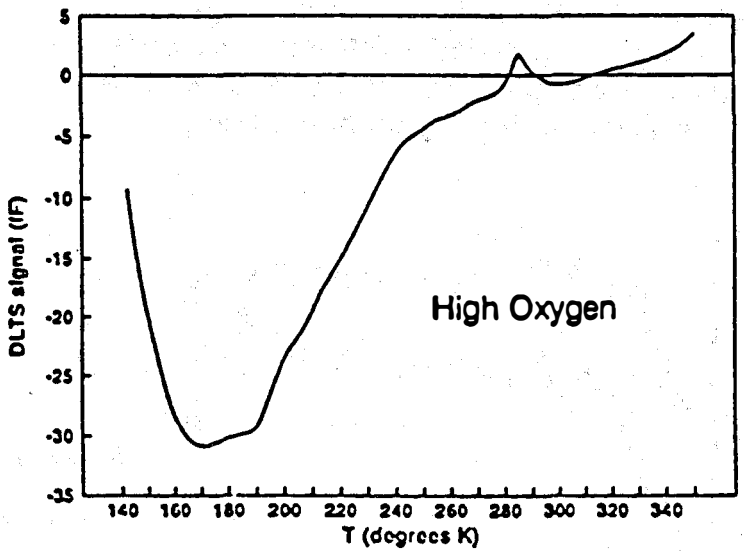

Figure 3: DLTS signal for the low resistivity, Solarex cell showing distributed peaks in the high oxygen sample (bottom) that are not present in the low oxygen cell (top).

The Effectiveness and Stability of Impurity/Defect Interactions and Their Impact on Minority Carrier Lifetime

Organization: Materials Science and Engineering Department, North Carolina State University, Raleigh, North Carolina

Contributors: G. A. Rozgonyi, Program manager; F. Shimura, principal investigator, A. Buczkowski, research associate; T.Q. Zhou, graduate student

The project is focused on the study of the electrical activity of metal impurities and extended defects such as dislocations, precipitates and grain boundaries; as well as the subsequent hydrogenation of those recombination centers. Metal impurity doped Czochralski silicon and extrinsically gettered (XG) silicon-silicon germanium epitaxial heterostructures were selected as representative subtrates for this study. The XG wafers were used as a model system for defect property and impurity gettering studies since they have a well defined and controlled defect density and location. Several different electrical measurements have been developed and applied to the above materials. These measurements are a convenient way to estimate the relative importance of defects, impurities and their complexes. In order to determine recombination lifetime values in solar cell materials and to relate changes to specific defect and fabrication procedures we developed and computerized the diode pulse recovery (PR) technique. This technique, when applied in conjunction with a varying substrate temperature, can supply information not only about carrier lifetime, but also about the properties of traps introduced into the forbidden gap during device processing. We will also present data on the application of contactless microwave recombination lifetime spectroscopy in the temperature varying mode, which has enabled us to perform noncontact laser/microwave deep level transient spectroscopy (LM-DLTS). In addition, imaging of the electrical activity of interfacial misfit dislocations in silicon has been performed using the electron beam induced current (EBIC) technique in a scanning electron microscope[1]. Clean dislocations formed during high temperature Si(Ge) chemical vapor epitaxy were studied. These defects were subsequently decorated with known metallic impurities (Au and Ni) by diffusion (in a rapid thermal annealer) from a back side evaporated layer, and also with unknown residual processing contaminants. From our previous TEM studies[2-5], it is known that misfit dislocations in epitaxial Si(Ge) samples are effective for gettering metal impurities and hydrogen. So, such a system allows us to focus on an individual defect, misfit dislocation in our case, and simple impurity-defect complexes.

An EBIC examination of the as grown Si on Si(Ge) on Si structure used in this work, see Fig. 1a, did not reveal any misfit dislocation contrast at all. However, surface traces of the misfit

dislocations were visible on the top surface of the same sample using Nomarski optical microscope, as shown in Fig. 1b. At this stage of the experiment we conclude that the electrical activity of as grown misfit dislocations is very low, below the detection limits of EBIC performed at room temperature. Metal Ni and Au were chosen for the gettering study since they are well known lifetime killers. Significant differences in the electrical activity of Au and Ni decorated dislocations have been observed. According to the literature gold decorated dislocations introduce a deep level into band gap, which is a strong recombination center. However, the Au decorated misfit dislocations become active only after over 1000°C annealing and appear as continues dark lines indicating that the dislocations are active recombination centers as shown in Fig. 1c. Very different observations occur for Ni decorated dislocations. The dislocation-nickel complexes are active as shown in Fig. 1d, and also the contrast is not uniform along Ni decorated dislocation as it was for Au decoration. The fact that Ni forms silicides with silicon may explain the formation of large precipitates which result in non-uniform EBIC contrast along dislocations. The dislocations are still not visible between the precipitated segments what indicates that non-decorated dislocations are probably inactive, as they were before the decoration process. The formation of precipitates has been observed on EBIC images after annealing at temperature as low as 400°C. The density of precipitates increases with annealing temperature and a continuous line contrast appears if the samples are annealed at temperatures above 1100°C. Impurities can also diffuse into samples from contaminated chambers of processing equipment. In order to illustrate this, a sample which initially had a non-detectable EBIC contrast was oxidized in an oxidation furnace at 1100°C for 15 minutes. After oxidation, the oxide was stripped and a Schottky contact deposited without any additional annealing. An EBIC examination of this sample revealed the presence of dislocations in the form of continuous lines indicating that unknown contaminants were gettered by the dislocations thereby increasing their recombination activity.

In addition to the EBIC study, a separate set of Czochralski silicon wafers doped during crystal pulling was used to study the impact of impurities on recombination lifetime. The silicon wafers used in this study were p-type <100> CZ silicon crystals grown from the melt with or without doping of metallic impurities in addition to the dopant boron. A pulse recovery (PR) technique for recombination lifetime measurements was used since it does not require any complicated equipment and can be easily computerized. For this study a 1 μm deep n^+/p junction was fabricated by phosphorus diffusion. The measurement system consists of a Model K 2609 MMR® cold stage functioning as a N_2 refrigerator covering the temperature range from 80K to 373K (a separate hot plate can be used to reach 523K). The lifetime value is calculated from the experimental recovery phase of the current-time response of a diode pulsed from forward to reverse bias. For better accuracy, it is fed into a simulation procedure working as a feedback loop which selects a value yielding the best agreement between theory and experiment. The theoretical

simulation is based on voltage-time relations, describing the recovery and reverse phases, respectively. These non-analytical equations are solved numerically for theory-experiment comparison. Theoretical calculations illustrate the influence of voltage bias, load resistance and forward current on normalized reverse current decay.

Additional information about trap properties within the forbidden gap of the Si sample were obtained from the temperature influence on the pulse recovery signal. Figure 2 presents a theoretical prediction of the influence of the location of an energy trap within the band gap on a lifetime vs temperature curve. The value of midgap energy E_i was arbitrarily chosen equal to zero (reference level). Depending on the trap location E_T within the gap one can observe different shapes of this curve. For relatively deep traps, located near the midgap reference level, the lifetime values are low, and are temperature independent up to ~350 K. Shallower traps (closer to valence or conductance bands), result in a higher τ, which is more temperature sensitive. The lifetime vs temperature measurement was performed on chromium, iron and gold CZ silicon and the results are showed in Fig. 3. Fe, Cr and Au related defects were deep traps. Comparing with theoretical calculation, we obtained an energy level (E_T-E_V) on the order of 0.4eV to 0.5eV for chromium and iron related traps, while gold related traps had an energy level (E_T-E_V) about 0.35eV. However, we shall note that the electrical properties of metallic impurities in silicon greatly depend on their states, e.g., atomic lattice site (interstitial or substitutional), or precipitate, etc.

For material characterization, a noncontact method which requires no specific sample preparation is desired since electrical properties such as lifetime in finished devices is very sensitive to process conditions. Noncontact laser/microwave spectroscopy based on the measurement of microwave reflection power as a function of temperature has been developed and applied to the measurement of minority-carrier recombination lifetime (LM-τ) and the identification of energy levels (LM-DLTS)[6] in p-type CZ silicon crystals grown with metallic impurity doping. The decay of minority carriers generated by laser irradiation at λ=910 or 830nm is measured by analyzing the decay of microwave reflection power in the temperature range from room temperature to 250°C[7], as shown in Fig. 4. The effect of different metallic impurities on the lifetime is clearly shown. The contrasting behavior of the lifetime as a function of temperature is shown for Fe-doped and Cr-doped silicon crystals. Iron-doping greatly reduces the lifetime in the entire temperature range. Although Cr-doping also shows a reduction at room temperature, the degradation effect completely disappears at elevated temperatures. Doping with Na, Ni, Cu, and W shows little effect on lifetime; Na-doping results in a rather higher lifetime compared with that of un-doped silicon. Additional lifetime measurements as a function of holding time at an elevated temperature also clearly distinguishes un-contaminated silicon from metal-doped silicon. That is, the lifetime increases with holding time in un-contaminated silicon, while it does not change in contaminated silicon.

Next, LM-DLTS using a laser/microwave system was applied to identify energy levels in the CZ-Si wafers. Although the principle of conventional DLTS and our LM-DLTS are different. It was shown that information about energy levels can be obtained from the temperature dependent microwave decay signal. Both techniques are based on the temperature dependent occupancy of traps; however, conventional DLTS analyzes filling and emptying traps within the depletion region, while LM-DLTS analyzes the trap recombination process for excess carriers generated by laser irradiation. The activation energy levels can be obtained from the Arrhenius plots with the noncontact LM-DLTS method for each metallic impurity.

In conclusion, from EBIC study it has been found that the recombination activity of clean dislocations is very low, below the detection limits of this technique. The activity, however, increases significantly in the presence of metallic impurities as well as unknown contaminates introduced into the sample during thermal processing. The lifetime study of metallic impurity doped silicon showed that the lifetime depended on the specific impurity and its contamination levels. Both pulse recovery technique and LM-DLTS can yield the information about the energy level of individual impurities. Future work will also examine the influence of hydrogen on pure and contaminated defects.

Reference

1. Z. J. Radzimski, T. Zhou, A. Buczkowski, G.A. Rozgonyi, D. Finn, L. Hellwig and J. Ross, submitted to Appl. Phys. Lett. (1990)
2. A. Salih, H.J. Kim, R.F. Davis and G.A. Rozgonyi, Appl. Phys. Lett. **46**, 419 (1985)
3. D.M. Lee, J. Posthill, F. Shimura and G. Rozgonyi, Appl. Phys. Lett., **53**, 370 (1988)
4. T. Zhou, Z. Radzimski, Z. Xiao, B. Sopori and G. A. Rozgonyi, *Impurity, Defect and Diffusion in Semiconductor: Bulk and Layer Structures*, MRS Proceeding, vol. **163**, Boston, MA (1989)
5. T. Zhou, Z. Radzimski, B. Patnaik, G. A. Rozgonyi and B. Sopori, submitted to Appl. Phys. Lett. (1990)
6. Y. Kirino, A. Buczkowski, Z.J. Radzimski, G.A. Rozgonyi and F. Shimura, submitted to Appl. Phys. Lett. (1990)
7. F. Shimura, T. Okui and T. Kusama, J. Appl. Phys., **67**, 7168 (1990)

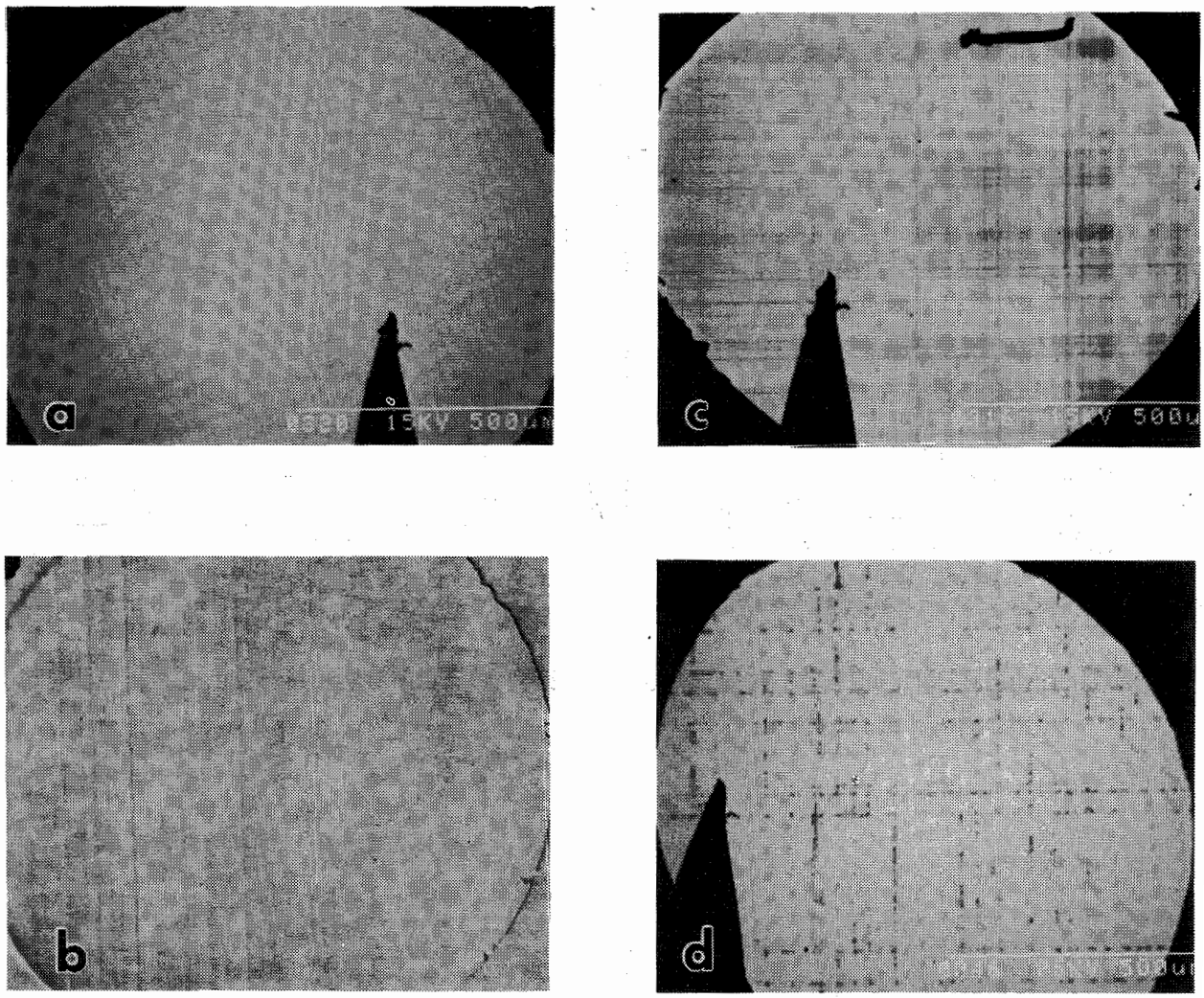

Fig.1 EBIC/SEM image of as grown heteroepitaxial structure showing no contrast from interfacial misfit dislocations buried at 4 μm depth. Electron beam energy = 25 keV(a), (b) Nomarski micrograph of the area shown in (a), and EBIC/SEM image of the heterostructure with misfit dislocations decorated with gold (c) and nickel (d) at temperature 1000°C

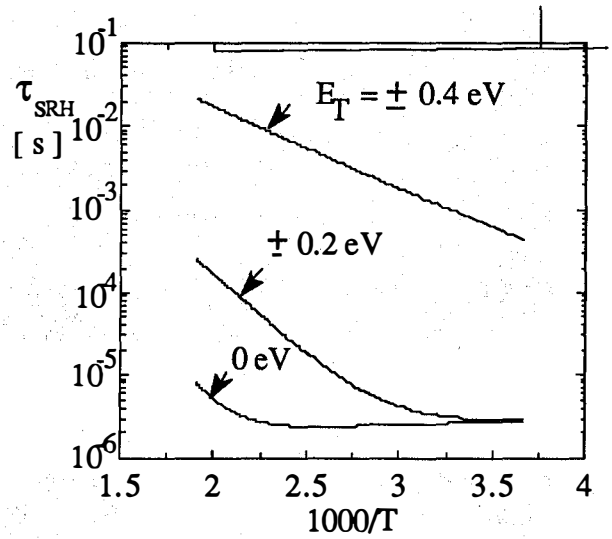

Fig.2 Theoretical influence of energy trap location within the bandgap.

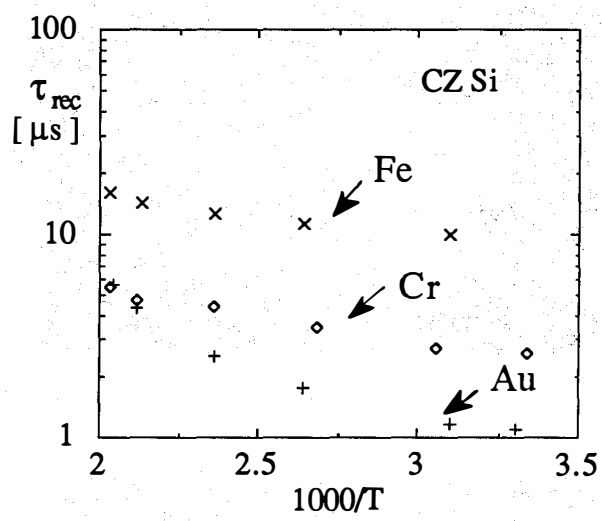

Fig. 3 Lifetime vs temperature data for Cr, Fe and Au doped samples.

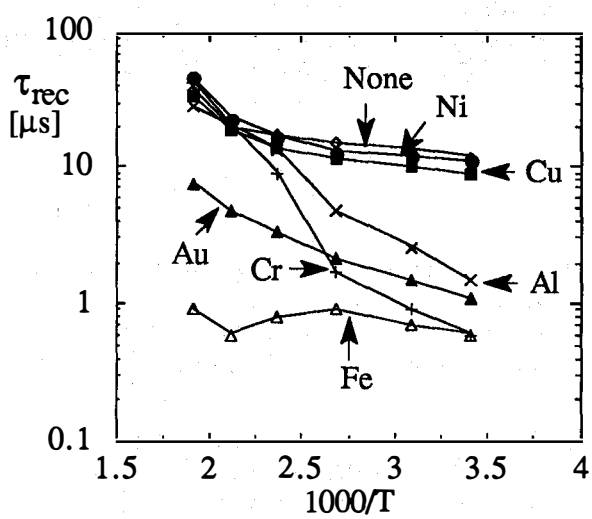

Fig. 4 Temperature dependence of lifetime for metal doped CZ Si

Title: **Passivation and Gettering Studies in Solar Cell Silicon**

Organization: Institute for the Study of Defects in Solids, Physics Department, The University at Albany, Albany, N. Y. 12222

Contributors: J. W. Corbett, principal investigator; D. Angell, O. O. Awadelkarim, Kajoli Banerjee, C. Barbero, B. Baufeld, H. Bakhru, T. D. Bestwick, J. T. Borenstein, J.-Y. Chen, M. A. Chubnikov, J. C. Corelli, G. Davies, P. Deák, S. K. Estreicher, Y. P. Feng, V. V. Frolov, N. N. Gerasimenko, N. L. Grigorenko, W. M. Gibson, M. Gong, G. L. Gutsev, P. Hadizad, A. Hallén, M. Heinrich, P. L. Jones, A. E. Kaloyeros, L. Korpás, W. A. Lanford, J. L. Lindström, J. Liu, F. Lu, T.-M. Lu, B. Mohadjeri, B. Monemar, G. C. Myaken'kaya, G. S. Oehrlein, C. Ortiz, A. Owusu, S. J. Pearton, R. B. Rizk, W. L. Roth, G. J. Scilla, R. K. Singh, Vijay A. Singh, L. C. Snyder, A. Sólyom, U. F. Stas', S.A. Suliman, B. G. Svensson, J. Svensson, A. J. Tavendale, P. J. Toscano, D. A. Tulchinsky, I. V. Verner, P. W. Wang, G.O. Williams, R.-Zh. Wu, Q. Xiao, Y. Zhang, A. S. Yapsir, Z.-P. You, J.-Z. Yuan, Y. Zhang, and B. Zheng. (Not all receive support from the contract.)

This research program has two major aspects: 1) The study of hydrogen in crystalline silicon; and 2) The study of gettering in crystalline silicon. In the hydrogen studies are concerned with all aspects of hydrogen in silicon: how hydrogen is introduced into silicon (by wet-etching, boiling, plasma treatment, injection from a Kaufman source, etc.); its configurations and diffusion mechanisms; and the nature of its interactions with defects; the quantitative modeling of the diffusion profiles. The gettering studies are concerned with mechanism by which deleterious impurities are introduced into silicon and the mechanism by which these impurities can be removed from the device region, e. g., removal at an external surface or at a precipitate. Using studies on radio-active copper we have established that copper can permeate into and diffuse in silicon at room temperature, and have begun studies of gettering of this element. Following a visit to Mobil Solar, we have begun parallel studies of slow diffusers (e. g., Ti) and fast diffusers (e. g., Co, which may form a silicide which is commensurate with the silicon lattice, and Cu, which forms silicides which disrupt the silicon lattice). There are a variety of related studies being carried on in which we have enlisted many co-workers, hence the list of contributors above.

Hydrogen-Related Studies.

The mechanisms by which hydrogen is introduced into silicon are not fully established [1-8]. Implantation of hydrogen into silicon is well understood, although the resultant damage is not [9]. The other means of introducing hydrogen into silicon are even less understood; some of our work is directed at improving this understanding. We have carried out, and are continuing, studies of the interactions of hydrogen with a silicon surface [10-12] of the role of hydrogen in the etching of silicon [13, 14] (such as may occur in a gas or in a liquid), and plasma- and reactive-ion-etching [15-17]. We are continuing our studies of the mechanisms by which hydrogen interacts with defects and impurities [18-26] We also are continuing our studies of the influence of hydrogen during processing on the properties of systems, e. g., Schottky barrier heights and leakage currents [27-29].

We have studied the configuration of the hydrogen once it is introduced into silicon, and its diffusion mechanisms, the latter studies necessarily including the study of the inter-

actions of hydrogen with defects [30-40]. Our theoretical work and that of others[41-45] have argued that the bond-centered (BC) site is the lowest energy configuration for isolated hydrogen in silicon, and that the anti-bonding (AB) site is a higher energy local minimum. The BC-site is clearly indicated in the EPR results of Gorelkinskii *et al.*[46] for the AA-9 center, and by the correlative results for the anomalous muon [47]; channeling studies [48,49] also support this ordering of sites.

Infra-red[50-52], channeling [49, 53, 54] and theoretical [55, 56] studies supported by perturbed angular correlation studies [57-59] have established that the hydrogen de-activating a shallow acceptor is essentially at the BC-site as proposed by Pankove *et al.* [60] as that for the shallow donor is at an AB-site as proposed by Johnson *et al.*[35]. We have found that there remain some complexities [61] in the As-H vs Sb-H sequence which we are studying using Rutherford Back-Scattering, channeling, and standing- wave x-ray measurements. In the normal boron-deactivation experiment the hydrogen is introduced at ca. 125°C and the boron activity is restored by annealing at ca. 200°C; we have found [15] that introducing hydrogen at ca. 50°C results in hydrogen that remains relatively free so that it can move deeper into the material upon annealing at ca. 125°C; this is distinct from the field-induced migration found by Tavendale et al.[62]; the deactivation observed following mechanical-polishing [63] in which the boron recovers upon annealing to ca. 100°C. The process which anneals at ca. 170°C we attribute to the hydrogen at the BC-site; that at ca. 70°C to the AB-site, with a small energy barrier between the two sites; and we argue that both sites deactivate the hydrogen. Even so this does not explain the relative mobile hydrogen which can migrate deeper into the crystal without an applied field; since the boron is not reactivated as Tavendale found, we must assume that this hydrogen is an extra hydrogen, such as might occur if a boron could trap two (or more) hydrogens at AB-sites, the first one being most strongly bound. Studies of the introduction of hydrogen from water are underway to try to elucidate this process.

The model which appears to describe the diffusion processes in p-type silicon includes the following reactions:

$$H^+ + B^- \rightarrow (H \bullet B), \quad (1)$$

$$H + (H \bullet B) \rightarrow (B \bullet H \bullet H), \quad (2)$$

$$(n-2)\,H + (B \bullet H \bullet H) \rightarrow (B \bullet H_n). \quad (3)$$

Equation 1 reflects the Coulombic interaction between the charged boron and a charged hydrogen; the diffusion profiles suggest that the (0/+) level for hydrogen is at ca. (E_V + 0.3 ±0.1 eV). Equations 2 & 3 describe the capture of additional hydrogens by a boron; the diffusion profiles suggest this additional capture with n ~ 8--16, and as we mentioned we have found direct evidence for an additional, slightly bound hydrogen in C-V experiments[15]. Theoretical studies [33, 34, 64-66] have suggested that hydrogen may agglomerate without forming hydrogen molecules.; we are carrying out theoretical studies [67] on the agglomeration process (for n < 8) at a boron in silicon. It is not clear if the {111} and {100} platelet formation observed by Johnson *et al.*[68] and by Jeng *et al.*[69] occurs heterogeneously or homogeneously. Although the {111} planar defects observed could be due to the partially dissociated multi-vacancy defects that we have discussed earlier [70], we are inclined to the view proposed by Johnson *et al.*[48] that a number of hydrogens in BC-sites interact through their associated distortions to form an extended planar defect. We have performed calculations [65,66] on such a defect, and find that the strain interaction will stabilize a planar defect; we further find that subsequent hydrogens will bond in the same bond axis, i.e., one on each silicon, without forming a molecule, and thereby form an

incipient crack, a prototype of a defect causing the brittleness [65,66] of silicon grown in hydrogen gas.

The model which appears to describe the diffusion processes in n-type silicon includes the following reactions:

$$H^- + P^+ \rightarrow (H \bullet P), \quad (4a)$$

$$H + P \rightarrow (H \bullet P), \quad (4b)$$

$$H + (H \bullet P) \rightarrow P + (H \bullet H), \quad (5)$$

$$(n)H + P \rightarrow P + (H \bullet H)_n \quad (6)$$

Equations 4 show the reaction of a single hydrogen with the donor phosphorus; Eq. 4a describes the possibility of a Coulombic interaction. Our diffusion data does not require this reaction, i. e., we see no evidence of a negatively charged hydrogen in the range of resistivities of 100- to 0.1 Ω-cm silicon; more specifically these diffusion profiles do not exhibit the abrupt change in character found in p-type material. Johnson et al.[71] and Tavendale *et al.*[72] have found evidence of H^- in drift experiments, so the Coulombic reaction should occur. Equation 5 indicates that a second hydrogen may reactivate the phosphorus, a process which we use to explain the the "partial deactivation" of the phosphorus and the fact that the diffusion profile does not show the plateau associated with impurity trapping (a plateau observed for boron-doping); we must note as well that the "partial deactivation" may simply be due to the thermal instability of the phosphorus-hydrogen complex as suggested by Seager[73]. The diffusion profile for 100 Ω-cm silicon (both n-type and p-type) shows the shape which is characteristic of diffusion limited by molecule formation. As the phosphorus concentration increases the slope of the profile steepens, which we interpret as reflecting impurity-mediated molecule formation. There is also at shallow depths a peak in the profile which tends to increase with the impurity concentration and it is for that reason we invoke the multi-hydrogen agglomeration at a phosphorus shown in Eq. 6. It does seem from the work of Stavola and co-workers[74-76] that a high percentage (e. g., >80%) of phosphorus can be deactivated with sufficient hydrogen.

The diffusion profiles for both p-type and n-type silicon near the surface both tend to exhibit a steep exponential drop such as one would find for an unsaturable trap [39,40]. It is the presumption that the {111} and {100} platelets mentioned above act as unsaturable traps for the hydrogen. As shown in these papers, these traps tend to limit the penetration of hydrogen into silicon, and account for the log (time) dependence observed by Seager and Anderson [77, 78].

We find that we can fit the simple diffusion profiles (e.g., 1 Ω-cm p-type and 100 Ω-cm n-type) with physically reasonable parameters, for example, with a 40 Å capture radius for the process in Eq. 1, and a 4 Å capture radius for those in Eqs. 2 and 3, and a similar 4 Å radius for direct "molecule" formation (where the quotations indicate that the equations do not require an actual molecule--merely a di-hydrogen reaction) :

$$H + H \rightarrow (H \bullet H). \quad (7)$$

We have also found[79], however, that these parameters are not unique! For example, we have found that we can fit the molecule-formation data with comparable success for the range of variables described by the following equations:

$$R\,D\,H_o^2 = C_1, \quad (8)$$

$$R\,H_o = C_2; \quad (9)$$

and for the impurity-trapping regime for the range of variable described by the equation:

$$D\,H_o = C3. \quad (10)$$

In these equations D is the diffusion coefficient, R the corresponding capture radius, and H_o the (unknown) concentration of hydrogen at the surface of the silicon; C1, C2, and C3 are constants. There are "invariants" associated with conservative systems [80] described by non-linear equations, but we know of none such as these "invariants" for non-conservative systems such as these. We have been unable to derive these "quasi-invariants" with any generality from our equations, but .we have challenged our Russian co-workers, who are experts in such analysis, to seek them. We do not despair of establishing our diffusion parameters unambiguously, in particular since some of the parameters may well be the same in different processes.

As we have discussed before [1-8], there is considerable scatter in the published data for diffusion of hydrogen in silicon. Part of this results from the common presumption that the diffusion profile is described by the conventional erfc profile and that the Einstein relationship holds:

$$D\,t = \overline{\mathbf{X}}^2 \quad (11)$$

with D -- the diffusion coefficient, t --the time of diffusion and $\overline{\mathbf{X}}$ --the mean distance (suitably defined) in the diffusion profile. But the profiles for the molecule-forming regime and the impurity-trapping regime is not an erfc profile, nor is Eq. 11 an accurate measure of the diffusion of hydrogen in silicon. The breakdown of Eq. 11 is a manifestation of a broader phenomenon, namely, diffusion in a fractal lattice. Equation 11 holds for diffusion in one-, two- and three-dimensional lattices. As Gefen *et al.* have shown [81] it does not hold for diffusion in a fractal lattice where the appropriate result is

$$D\,t^R = \overline{\mathbf{X}}^2 \quad (12)$$

with

$$R = 2/(2+d) \quad (12)$$

with d -- a parameter equal to zero for one-dimension, equal to 0.8 for two, and equal 1.5 for three, in their results [81]. Gefen *et al.* define an "effective dimensionality", d_{rw}, of the process as

$$d_{rw} = (2+d). \quad (13)$$

The origin of this deviation from Eq. 11 is the hindered motion of the random walk. A hindered motion also occurs in hydrogen diffusion in silicon. For example, a random array of impurities at which the hydrogen can be trapped presents a hindrance to penetration into the lattice; similarly a random distribution of diffusing hydrogen with which a hydrogen can form molecules also forms a hindrance. We have not found a derivation of the expres-

sion corresponding to Eq. 12 for these cases, and have explored that dependence using numerical computations [39, 40].

For the unsaturable-trap case, such as pertains near the surface, the profiles fall exponentially with depth with the slope of successive profiles increasing until the later profiles become parallel to each other. The fact that they are parallel means that, however one defines it, $\overline{X}$ does *not* change with time, i. e., in Eq. 12, R = 0, or d_{rw} is *infinite*. The profile does penetrate deeper and deeper into the sample, but the mean penetration distance does not change, because the surface concentration is also rising. That d_{rw} is infinite here, and *negative* for the di-hydrogen case, suggests that terming it an "effective dimensionality," is infelicitous, but this parameter does characterize the impediment to the penetration of hydrogen into the lattice.

For the di-hydrogen ("molecule") formation case, the scaling yielded a d_{rw} which is negative and approximately equal to a negative 2.3. (We have challenged out theorist colleagues to see if this scaling is in fact exactly 9/2.) The diffusion profile does continue to move into the material, but at a relatively slower and slower pace as the density of traps at the surface increases, hence the negative scaling.

For the saturable-trap case, such as occurs with the formation of the boron-hydrogen complex), the scaling, or the d_{rw}, is not constant. It depends on the trap concentration, the hydrogen concentration, and depends on how $\overline{X}$ was defined. Although choosing $\overline{X}$ the normal way at (1/2) the surface value of hydrogen yields a scaling of *about* two, i. e., the normal scaling, the shallower part of the profile may have a scaling of three, while the deeper part the value may fall to 1.5. Further the slope of log (D t) versus log $\overline{X}$ is not linear, i. e., the highly non-linear equations for this system do not exhibit any more than an approximately constant scaling at any hydrogen concentration.

Gettering-Related Studies

It is well known that oxygen precipitates act as gettering sites for the iron-group transition elements, i.e., for the major "fast diffusers." We have completed several studies[82-84] related to these problems, including identifying [84] the defect created when a vacancy interacts with an iron atom. A major problem in gettering studies is the indirect nature of the measurement studying the transition element, e.g., EPR can identify the transition element if it is in the proper charge state, DLTS can identify an electrical level which may be associated with a transition element. We have begun studies using radioactive tracers to better follow the introduction and history of the transition elements. Another aspect of gettering at oxygen defects is identifying the oxygen defects of which there are a plethora of varieties[85]. We have carried out a number of studies[86- 96] helping to clarify the nature of the electrical properties of the 450°C thermal donors, the new shallow donors, the anomalous oxygen diffusion mechanism, and the nature and structure of the core of the thermal donors, and of the thermal donors, and oxygen-related recombination centers. We anticipate exploiting this knowledge in our gettering studies.

It has been found by a number of authors [4, 63, 97-103], that chemo-mechanical polishing of silicon results in changes in the resistivity of the material, and Schnegg et al.[6], using secondary ion mass spectrometry, showed directly the penetration of hydrogen into silicon during polishing. It is well known that hydrogen passivates deleterious defects in semiconductors, and it is now known that in silicon the shallow acceptors can be deactivated by hydrogen, as can the shallow donors. It was the perturbed angular

correlation studies by Wichert *et al.*[58, 59], however, which suggested that another defect was also entering the silicon during polishing, and suggested that it was copper[104]. Following these leads we investigated the permeation of radio-active copper (^{64}Cu) into silicon wafers at room temperature. These results show that copper does indeed enter silicon in routine room temperature processing. A preliminary account of this work has been published [4], but further work is required.

Following a visit to Mobil Solar we have reoriented our passivation-gettering studies to discriminate among the various types of impurities. We have studies under way of two fast-diffusers: cobalt, which may form a silicide which is commensurate with the silicon lattice, and Cu, which forms silicides which disrupt the silicon lattice); and we are studying slow diffusers such as titanium. Our studies include Rutherford-back-scattering and channeling studies to establish the lattice location of the impurities (a point that has compromised many of the past studies) and the associated electrical properties. We also are doing hydrogen passivation and gettering studies on these elements.

References

1 S. J. Pearton, J. W. Corbett, and T.-S. Shi, *Appl. Phys. A* **43** (1987) 153.

2 J. W. Corbett J. L. Lindström, L. C. Snyder, and S. J. Pearton in Defects in Electronic Materials, eds. M. Stavola, S. J. Pearton, and G. Davies (MRS, Pittsburgh, 1988) pp. 229-239.

3 S. J. Pearton, M. Stavola, and J. W. Corbett in *Defects in Semiconductors 15*, ed. G. Ferenczi (Trans Tech, Switzerland, 1989) 25-37.

4 J. W. Corbett, S. J. Pearton, and M. Stavola in *Control of Defects in Semiconductors*, ed. K. Sumino, in press.

5 *Hydrogen in Semiconductors*, S. J. Pearton, J. W. Corbett, and M. Stavola (Springer Verlag, Berlin, 1990) in press.

6 J. W. Corbett, P. Deak, U. Desnica, and S. J. Pearton in *Hydrogen in Semiconductors*, eds., J. I. Pankove and N. M. Johnson (Academic Press, N. Y. 1990), in press.

7 S. J. Pearton, M. Stavola, and J. W. Corbett, *Rad. Eff. & Defects in Solids*, **111/112** (1989) 323-344.

8 S. J. Pearton, J.W. Corbett, and J.T. Borenstein in *Proc. Trieste Conf. on Hydrogen in Semiconductors*, Aug. 1990.

9 J. W. Corbett, P. Deák, U. Desnica, and S. J. Pearton in *Hydrogen in Semiconductors*, eds. J. I. Pankove and N. M. Johnson (Academic Press, NY 1990).

10 G.S. Oehrlein, J.L. Lindström and J.W. Corbett, *Phys. Letters A* **81**, 246-248 (1981).

11 J. W. Corbett, D. Peak, S. J. Pearton, and A. Sganga in *Hydrogen in Disordered and Amorphous Solids*, eds. G. Bambakidis and R. C. Bowman (Plenum, N.Y. 1986) p. 61.

12 T.S. Shi, S.N. Sahu and J.W. Corbett, *Surface Science*, **130**, L289-290 (1983).

13 F. Lu, J. W. Corbett, and L. C. Snyder, *Phys. Lett.* **133** (1988) 249.

14 B. Zheng and J. W. Corbett, to be published.

15 J. L. Lindström, G. S. Oehrlein, G. J. Scilla, A. S. Yapsir, and J. W. Corbett, *J. Appl. Phys.*, **65** (1989) 3297.

16 T. Bestwick, G. S. Oehrlein, D. Angell, P. Jones, and J. W. Corbett, *Appl. Phys. Lett.* **54** (1989) 2321.

17 G. S. Oehrlein, T. D. Bestwick, P. L. Jones, and J. W. Corbett, to be published.

18 N.N. Gerasimenko, M. Rolle, L.J. Cheng, Y.H. Lee, J.C. Corelli and J.W. Corbett, *Phys. Stat. Sol. B* **90**, 689-696 (1979).

19 V.A. Singh, J.W. Corbett, C. Weigel and L.M. Roth, *Phys. Stat. Sol. (b)* **81**, 637 (1977).

20 Vijay A. Singh, J.W. Corbett, C. Weigel and L.M. Roth, *Phys. Letters A* **65**, 261-263 (1978).

21 R.L. Kleinhenz, Y.H Lee, Vijay A. Singh, P.M. Mooney, A. Jaworowski, L.M. Roth, J.C. Corelli and J .W. Corbett in *Defects and Radiation Effects in Semiconductors*, 1978, ed. J.H. Albany (Inst. of Phys., Bristol-London, 1979) pp. 200-204.
22 T.S. Shi, S.N. Sahu, G.S. Oehrlein, A. Hiraki and J.W. Corbett, *Phys. Stat. Sol.* (a) **74**, 329-341 (1982).
23 J.W. Corbett, S.N. Sahu, T.S. Shi and L.C. Snyder, *Phys. Letters* **93**, 303-304 (1983).
24 Shi Tian-sheng, S.N. Sahu, J. W. Corbett, and L.C. Snyder, *Scientia Sinica*, Series A, **27**, 98-112 (1984).
25 R.J. Pflueger, J.C. Corelli, and J.W. Corbett, Int'l Conf. on Triple Beams, Portland Oregon, May 29-31, 1985.
26 A. S. Yapsir, P. Deak, R. K. Singh, L. C. Snyder, J. W. Corbett, and T.-M. Lu, *Phys. Rev. B* **38** (1988) 9936.
27 A. S. Yapsir, P. Hadizad, T.-M. Lu, J. C. Corelli, J. W. Corbett, W. A. Lanford, and H. Bakhru, *Phys. Rev. B* **37** (1988) 8982.
28 A. S. Yapsir, P. Deák, R. K. Singh, L. C. Snyder, J. W. Corbett, and T.-M. Lu, *Phys. Rev. B* **38** (1988) 9936.
29 J. Liu and J. W. Corbett, to be published.
30 P. Deák, J. L. Lindström, J. W. Corbett, S. J. Pearton, and A. J. Tavendale, *Phys. Lett. A* **126** (1988) 427.
31 P. Deák, L. C. Snyder, and J. W. Corbett, *Phys. Rev. B* **37** (1988) 6887.
32 P. Deák, L. C. Snyder, and J. W. Corbett in *New Developments in Semiconductor Physics*, eds. G. Ferenczi and F. Beleznay (Springer Verlag, Berlin, 1988) 163.
33 P. Deák, M. Heinrich, L. C. Snyder, and J. W. Corbett in EMRS Proc. 1989, in press.
34 P. Deák, L. C. Snyder, M. Heinrich, and J. W. Corbett, to be published.
35 J.W. Corbett, J.L. Lindström, S.J. Pearton, and A.J. Tavendale, Solar Cells **24** (1988) 127-133.
36 J. T. Borenstein, D. Angell, and J. W. Corbett in *Characterization of the Structure and Chemistry of Materials*, eds., B. C. Larson, M. Rühle, and D. N. Seidman (Materials Research Society, Pittsburgh, 1989) 209.
37 P. Deák, L. C. Snyder, and J. W. Corbett, Phys. Rev. B. in press.
38 P. Deák, L. C. Snyder, M. Heinrich, C. R. Ortiz, and J. W. Corbett, 6th Trieste Symposium on Hydrogen in Semiconductors, 1990 in press.
39 D. A. Tulchinsky, J. W. Corbett, J. T. Borenstein, and S. J. Pearton, Phys. Rev. B 1990 in press.
40 D. A. Tulchinsky, J. W. Corbett, J. T. Borenstein, and S. J. Pearton, to be published.
41 C. G. DeLeo, M. Doragi, and W. B. Fowler, *Phys. Rev. B* (1988), in press.
42 A. A. Bonapasta, A. Lapiccirella, N. Tomassini, and M. Capizzi, *Europhys. Lett.* **7** (1988) 145.
43 C. G. Van der Walle, Y. Bar-Yam, and S. T. Pantelides, *Phys. Rev. Lett.* **60** (1988) 2761.
44 C. G. DeLeo and W. B. Fowler, *Phys. Rev. B* **31** (1985) 6861.
45 C. G. DeLeo and W. B. Fowler, *Phys. Rev. Lett.* **56** (1986) 402.
46 Yu. V. Gorelkinskii and N. N. Nevinnyi, *Pis'ma Zh. Tekh. Fiz.* **13** (1987) 105.
47 R. Kiefl, M. Celio, T. L. Estle, G. M. Luke, S. R. Kreitzman, J. H. Brewer, D. R. Noakes, E. J. Ensaldo, and K. Nishiyama, *Phys. Rev. Lett.* **58** (1987) 1780.
48 S. T. Picraux and F. Vook, *Phys. Rev. B* **18** (1978) 2066.
49 B. Bech Nielsen, *Phys. Rev. B* **37** (1988) 6353.
50 M. Stavola, S.J. Pearton, J. Lopata, and W.C. Dautremont-Smith, *Appl. Phys. Lett.* **50** (1987) 1086-1088.
51 K. Bergman, M. Stavola, S.J. Pearton, and T. Hayes, *Phys. Rev. B* **38** (1988) 9643.
52 B. Pajot, A. Chari, M. Aucouturier, M. Astier, and M. Chantre, Solid State Comm. (1988) in press.
53 A.D. Marwick, G.S. Oehrlein, and N.M. Johnson, *Phys. Rev. B* **36** (1987-1) 4539-4542.
54 A.D. Warwick, G.S. Oehrlein, J.H. Barrett, and N.M. Johnson, Phys. Rev. **B 36** (1987) in press.
55 N. M. Johnson, C. Herring, and D. J. Chadi, *Phys. Rev. Lett.* **56** (1986) 769.

56 K.J. Chang and D.J. Chadi, Phys. Rev. Lett. **60** (1988) 1422-1425.
57 M. Deicher, G. Grübel, E. Recknagel, and T. Wiechert, in *Defects in Semiconductors*, ed. H.J. von Bardeleben (Trans Tech Publ., Zürich, 1986) 1141-1146.
58 T. Wichert, H. Skudlik, M. Deicher, G. Grübel, R. Keller, E. Recknagel, and L. Song, *Phys. Rev. L.ett.* **59** (1987) 2087.
59 T. Wichert, M. Deicher, G. Grübel, R. Keller, N. Schulz and H. Skudlik, *Appl. Phys. A* (1988) in press.
60 J.J. Pankove, P.J. Zanucchi, C.W. Magee, and G. Lukovsky, *Appl. Phys. Lett.* **46** (1985) 421.
61 Y. Zhang, J. W. Corbett, Q. Xiao, and W. M. Gibson,to be published.
62 A.J. Tavendale, A.A. Williams, D. Alexiev, and S.J. Pearton, in *Oxygen, Carbon, Hydrogen, and Nitrogen in Crystalline Silicon*, eds., J. C. Mikkelsen, S. J. Pearton, J. W. Corbett, and S. J. Pennycook, (Materials Res. Soc. Pittsburgh, 1986) p. 469.
63 A. Schnegg, H. Prigge, M. Grundner, P.O. Hahn, and H. Jacob in *Defects in Electronic Materials*, eds. M. Stavola, S. J. Pearton, and G. Davies, (MRS, Pittsburgh, 1988) p. 291.
64 K. J. Chang and D. J. Chadi, *Phys. Rev. Lett.* **62** (1989) 937.
65 J. W. Corbett, P. Deák, C. Ortiz, and L. C. Snyder, *J. Nucl. Materials*, in press.
66 C. Ortiz, D. Deák. L. C. Snyder, and J. W. Corbett, to be published.
67 L. Korpás, S. K. Estreicher, J. W. Corbett, and L. C. Snyder, to be published.
68 N.M. Johnson, F.A. Ponce, R.A. Street, and R.J. Nemanich, *Phys. Rev. B* **35** (1987-1) 4166.
69 S.-J. Jeng, G.S. Oehrlein, and G.J. Scilla, *Appl. Phys. Lett.* **53** (1988) 1755.
70 J. W. Corbett, J. P. Karins, and T.-Y. Tan, *Nucl. Instr. & Meth.* **182/183** (1981) 457.
71 N. M. Johnson and C. Herring in Defects in Semiconductors 15, ed. G. Ferenczi (Trans Tech, Switzerland, 1989) p. 961.
72 S. J. Pearton, private communication.
73 C. H. Seager, personal communication.
74 M. Stavola, S.J. Pearton, J. Lopata, and W.C. Dautremont-Smith, Appl. Phys. Lett. **50** (1987) 1086-1088.
75 K. Bergman, M. Stavola, S.J. Pearton, and J. Lopata, *Phys. Rev. B* **37** (1988) 2770.
76 K. Bergman, M. Stavola, S.J. Pearton, and T. Hayes, *Phys. Rev. B* **38** (1988) 9643.
77 C. H. Seager and R. H. Anderson, Appl. Phys. Lett. 53 (1988) 1181.
78 C. H. Seager and R. H. Anderson, to be published.
79 J. T. Borenstein, D. A. Tulchinsky, and J. W. Corbett in Proc. Fall-MRS-89, to be published.
80 See, for example, R. Z. Sagdeev, D. A. Usikov, and G. M. Zaslavsky, *Nonlinear Physics: From the Pendulum to Turbulence and Chaos* (Harwood Academic Publishers, New York, 1988).
81 Y. Gefen, A. Aharony, and S. Alexander, *Phys. Rev. Lett.* **50** (1983) 77.
82 P. W. Wang, H. S. Cheng, W. M. Gibson, and J. W. Corbett, *J. Appl. Phys.* **60** (1986) 1336.
83 P.W. Wang, Y. P. Feng, W. L. Roth, and J. W. Corbett, *J. Non-Cryst. Solids* **104** (1988) 81.
84 Zh.P. You, M. Gong, J.-Y. Chen, and J. W. Corbett, *J. Appl. Phys.* **63** (1988) 324.
85 See the several pertinent review articles in *Oxygen, Carbon, Hydrogen and Nitrogen in Crystalline Silicon*, eds. J. C. Mikkelsen, Jr., S. J. Pearton, J. W. Corbett, and S. J. Pennycook (MRS, Pittsburgh, 1986) and in *Defects in Electronic Materials*, eds. M. Stavola, S. J. Pearton, and G. Davies, (MRS, Pittsburgh, 1988).
86 J. T. Borenstein, J. W. Corbett, M. Herder, S. N. Sahu, and L. C. Snyder, *J. Phys. C: Solid State Phys*, **19** (1986) 2893.
87 J. T. Borenstein, D. Peak, and J. W. Corbett, in *Oxygen, Carbon, Hydrogen and Nitrogen in Crystalline Silicon*, eds. J. C. Mikkelsen, Jr., S. J. Pearton, J. W. Corbett, and S. J. Pennycook (MRS, Pittsburgh, 1986)
88 J. A. Griffin, H. Navarro, J. Weber, L. Genzel, J. T. Borenstein, J. W. Corbett, and L. C. Snyder, *J. Phys. C: Solid State Phys.* **19** (1986) L579.
89 L. C. Snyder, J. W. Corbett. P. Deák, and R.-Zh. Wu in *Defects in Electronic Materials*, eds. M. Stavola, S. J. Pearton, and G. Davies (MRS, Pittsburgh, 1988) p. 179.

90 K. Banerjee, V. A. Singh, and J. W. Corbett, *Semicond. Sci. & Tech.* **3** (1988) 542.

91 L. C. Snyder, J. W. Corbett, P. Deák, and R.-Zh.Wu in *New Developments in Semiconductor Physics,* eds. G. Ferenczi and F. Beleznay (Springer Verlag, Berlin 1988) 147-156.

92 P. Deák, L. C. Snyder, J. W. Corbett, R.-Zh. Wu and A. Sályom in *Defects in Semiconductors 15,* ed. G. Ferenczi (Trans Tech, Switzerland 1989) 281.

93 L.C. Snyder, P. Deák, R.-Zh. Wu, and J. W. Corbett in *Defects in Semiconductors 15,* ed. G. Ferenczi (Trans Tech, Switzerland 1989) 329.

94 L. C. Snyder, P. Deák, R.-Zh. Wu, and J. W. Corbett in *Proc. Shallow Donor Conf., Linköping, Sweden, 1988,* in press.

95 L. C. Snyder, R.-Z. Wu, P. Deák, and J. W. Corbett, in *"Impurities, Defects, and Diffusion in Semiconductors: Bulk and Layered Structures,"* eds. J. Bernholc, E. E. Haller, and D. J. Wolford (Materials Research Soc., Pittsburgh, 1990) in press.

96 P. Deák, L. C. Snyder, and J. W. Corbett, to be published 1990.

97 J. Reichel and S. Sevcik, *Phys. Stat. Sol.* **103** (1987) 413-420.

98 A. Schnegg, M. Grunder, and H. Jacob in *Semiconductor Silicon/1986,* ed. H.R. Huff, T. Abe, and B. Kolbesen (Electrochem. Soc., Pennington, NJ 1986) p. 186.

99 S. J. Pearton, A. J. Tavendale, A. A. Williams, and D. Alekiev in *Semiconductor Silicon/1986,* ed. H.R. Huff, T. Abe, and B. Kolbesen (Electrochem. Soc., Pennington, NJ 1986) p. 826.

100 A. Chantre, L. Bouchet, and E. Andre, *J. Electrochem. Soc.* **135** (1988) 2867-2869.

101 T. Zundel, J. Weber, B. Benson, P. O. Hahn, A. Schnegg, and H. Prigge, *Appl. Phys. Lett.* **53** (1988) 1426-1428.

102 A. Schnegg, H. Prigge, M. Grunder, P. O. Hahn, and H, Jacob, in *Proc. ICDS-15,* in press.

103 M. Deicher, G. Grübel, R. Keller, E. Recknagel, N. Schulz, H. Skudlik, Th. Wichert, H. Prigge, and A. Schnegg, Proc. 3rd Conf. on Shallow Impurities in Semiconductors, Linköping, Sweden, 1988, in press.

104 Th. Wichert, private communication.

TECHNICAL REPORT

Title: **Electrical Characterization Support for a Crystalline Silicon Program**

Organization: University of Southern California
Department of Electrical Engineering
Los Angeles, CA 90089-0241
(213) 740-4345

Contributors: S. R. Forrest, principal investigator; V. Prabhakar and E. Haskal

The objectives of this program were to develop methods of using the non-destructive organic-on-inorganic (OI) semiconductor heterojunction to fully characterize Si and other materials useful for PV cell technology. In past work, we have shown that vacuum deposition of a thin layer (1000Å - 3000 Å) of a crystalline organic compound such as 3,4,9,10 perylenetetracarboxylic dianhydride (PTCDA) onto the surface of either n or p-type semiconductors forms a rectifying heterojunction at the organic/inorganic semiconductor interface [1]. After deposition of the organic, ohmic metal contact dots are then applied to the surface of the organic layer, and the entire device is reverse-biased.

Due to the nature of the OI heterojunction, reverse bias voltages as large as the avalanche breakdown voltage of the inorganic substrate under study can be applied. This allows for the determination of a wide range of materials properties in the inorganic material such as free carrier concentration, heterojunction offsets, trap densities, leakage current processes, and the distribution in values of these parameters around the wafer surface. Principally, the OI heterojunction is used to apply a bias across the inorganic semiconductor to obtain these materials parameters via standard techniques such as measuring the capacitance- and current-voltage characteristics of the OI heterojunction. Since biases equal to the breakdown voltage of the underlying substrate can be applied, these wafer properties can be determined to very extended distances from the wafer surface. Once the testing is complete, the organic layer and contacts can be removed without damage to the wafer by immersion in a dilute, aqueous base solution.

During this segment of the research, we concentrated on developing techniques for simplifying the process of applying the OI contacts, and to making the OI devices more versatile in their analysis capabilities.

In one segment of the research, we have devised means to increase the spatial and temporal resolution of the OI technique. To this end, we used a high speed turbo pumped vacuum system to allow for rapid deposition of the organic films onto cooled substrate test wafers. The cooled substrate allows for the deposition of very smooth films such that they can be made very thin. Here, we observed that deposition of the thin films on room temperature substrates results in the deposition of polycrystalline thin films of PTCDA, with a grain size of from 2000 Å - 1 μm in diameter. While such polycrystalline films are useful for most OI analysis measurements such as for obtaining free carrier concentration and current-voltage characteristics, their existence decreases the mobility of the carriers transiting the organic material from the ohmic contact to the semiconductor surface. Thus, the temporal response of the diodes can limit their utility in such frequency-dependent experimental techniques as DLTS and other transient capacitance and transient photoresponse analysis measurements which require diode response times of < 5 ns.

On the other hand, deposition on substrates cooled to less than 100 K results in a single crystalline thin film extending across the entire wafer surface [2]. In this case, we have found the mobility of the device to be significantly increased, and also the thickness of the film can be reduced by virtue of its perfection. The turbo-pumped system used for these systems was modified to include a simple substrate holder which could be cooled to low temperature during deposition using a continuous flow of liquid nitrogen. We have succeeded in depositing relatively high mobility (> 3 cm^2/V-s) single crystalline films in our lab to a thickness of 10 Å, with continuous films to 50 Å. This implies a device switching speed of approximately 100 ps, which is adequate for the analysis of most recombination processes of interest in solar cell applications.

In separate work directed at increasing the spatial resolution of the technique, we have successfully applied a photolithographic patterning process to the fabrication of OI diodes. In the past, the size of the device was limited by the size of the opening in a shadow mask which determined the diameter of the metal contact pad to the diode. Typically, the size of the diode is >60 μm which ultimately determined the spatial resolution of the technique. By using photolithographic techniques, diodes with contacts as small as 20 - 30 μm in diameter are easily achieved for use with automated wafer probe systems. Thus, the areal spatial resolution of the technique has increased by a factor of 4 - 9.

Details of the process sequence used in photolithographic patterning of the devices are shown in Fig. 1 [3]. In particular, it relies on the deposition, by pyrolitic CVD, of a SiO_2 mask onto the organic thin film to provide protection of the organic material from the photoresist layer.

As shown in Fig. 2, the I-V characteristics of the PTCDA/p-Si diode are excellent over a broad range of voltage in both the forward and reverse bias directions. It appears that the dark current of the diodes (with areas of 5.4 x 10^{-4} cm^2 for these data) is limited by generation and recombination in the Si bulk, and is not affected by the patterning process. This bulk current limitation is due to the very low leakage across the OI heterojunction. The relatively high barrier energy (> 0.5 eV) coupled with the "self guarding" nature of the OI contact results in the observed barrier leakage currents. By self-guarding, we imply that the extremely large asymmetries in the conductivity of the organic film confines the charge (and electric field lines) to be uniformly distributed beneath the ohmic contact metal pad. Here, the conductivity perpendicular to the wafer surface is found to be more than 10^6 times higher than parallel to the wafer surface.

We also demonstrated that PTCDA/InSb heterojunctions are useful for rectification purposes even at room temperature, in spite of the fact that the room temperature band gap of InSb is only 0.17 eV. We were able to accomplish routine C-V analysis on InSb wafers at room temperature since the OI barrier height was a relatively large 0.12 eV. The room temperature reverse bias applied to the InSb substrate (with a doping of 5 x 10^{16} cm^{-3}) was -6V prior to breakdown. Thus, the OI analysis technique has been extended to an additional family of materials: semiconductors with very small band gaps.

One of the goals of this research has also been to use the OI contact as a means for understanding the carrier surface recombination dynamics at the organic/inorganic heterojunction (HJ). It is our ultimate goal to use the OI-HJ as a tool for doing non-destructive analysis of PV materials, and in particular to measure the surface recombination velocity of such materials with a thin organic overlayer deposited on their surfaces. The motivation for this experiment arises largely from the ability of the OI-HJ to form a large rectifying barrier, and hence optical DLTS data generated by high energy light incident on the semiconductor surface may give detailed information regarding the surface recombination velocity of the underlying semiconductor, provided that the surface of the semiconductor is not strongly perturbed by the deposition of the organic film.

To begin these investigations of surface recombination, we measured the time-resolved flourescence of the PTCDA films themselves. This information is crucial to our understanding of the behavior of the OI-HJ, since light emitted from the film and then reabsorbed in the underlying semiconductor must be separated from the data ultimately obtained from the more complicated OI-HJ. In our experiments with the luminescence of PTCDA, therefore, we pumped the thin films (2000Å - 4000Å thick deposited on glass substrates) with an Ar-ion laser in the center of the

PTCDA 0-1 exciton line (approximately 4500Å wavelength). The resulting luminescence band occurs at wavelengths between 6500Å to 8000Å, and is quite intense at both room and low (20K) temperatures.

Time resolved flourescence measurements were made using a photomultiplier tube in conjunction with a 5 ns time constant photon counter. Our results show that the low temperature flourescence of PTCDA has a radiative lifetime of approximately 11 ns. This time can be reduced to approximately 6 ns by growing multi-layer stacks of PTCDA and NTCDA with layer thicknesses of 20Å or less [4]. These multilayer structures can therefore prove useful in measuring the luminescence of very high surface recombination velocity semiconductors.

In conclusion, we have extended both the spatial and temporal resolution of the non-destructive organic/inorganic semiconductor analysis technique to allow for expanded capabilities of the method for use in PV materials analysis applications. Junction response times of 100 ps with spatial resolution of < 30 μm are now possible. This technique has been used to measure the intrinsic current and capacitance-voltage characteristics of the underlying PV cell materials under study, and is completely non-destructive to that material. These results open up a wide range of possibilities for the use of organic thin films for the high resolution optical and electronic characterization of solar cell material.

References

1. "Organic thin films for semiconductor wafer diagnostics", S. R. Forrest, M. L. Kaplan and P. H. Schmidt, Ann. Rev. Mater. Sci., 17, 189 (1987).

2. "Growth and characterization of organic semiconductor heterojunctions and multiple quantum wells" F. F. So, L. Y. Leu and S. R. Forrest, SPIE, 1285, 95 (1990).

3. "A patterned and passivated organic-inorganic semiconductor heterojunction diode", V. Prabhakar, S. R. Forrest, J. P. Lorenzo and K. Vaccaro, IEEE Photon. Technol. Lett., 2, 724 (1990).

4. "Quasi-epitaxial growth of organic multiple quantum well structures by organic molecular beam deposition", F. F. So, S. R. Forrest, Y. Q. Shi and W. H. Steier, Appl. Phys. Lett., 56, 674 (1990).

Fabrication of Organic/Inorganic HJ Diodes - 1

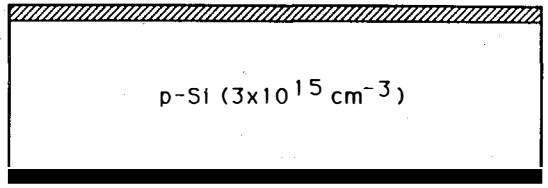

1. Deposit back metal contact (2000 Å In)
2. Deposit 1500 Å PTCDA

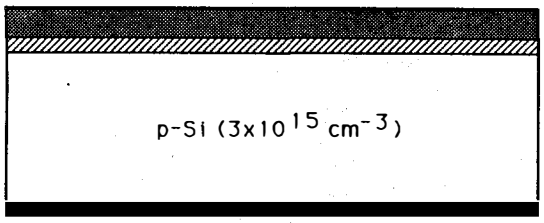

3. Deposit 3000 Å SiO_2
(Pyrolytic CVD, 125 ^{o}C)

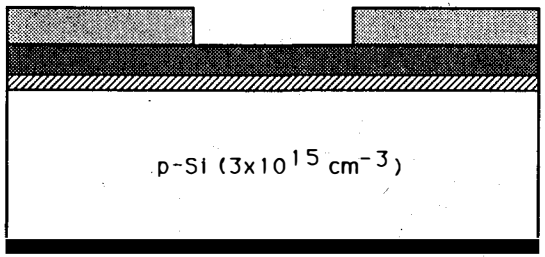

4. Deposit and pattern HNR 120

Fabrication of Organic/Inorganic HJ Diodes - 2

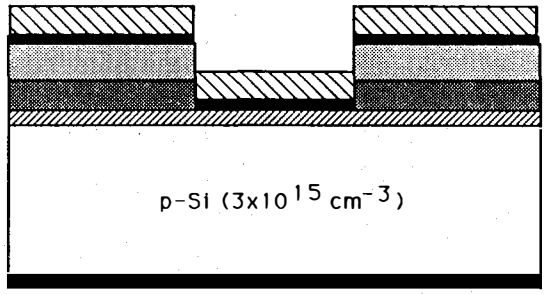

5. Etch SiO_2 in 10:1 H_2O:HF
6. Deposit Metal (Ti/Au or In)

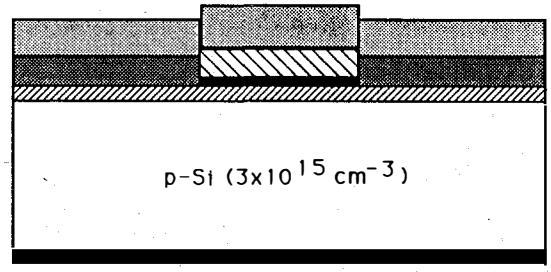

7. Deposit PR and etch back metals

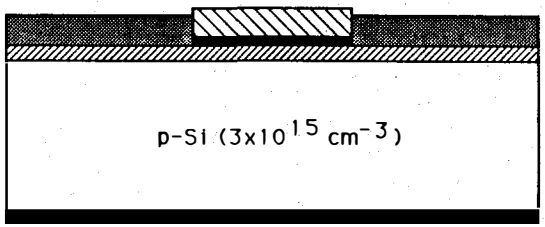

8. Remove PR (Oxygen plasma)

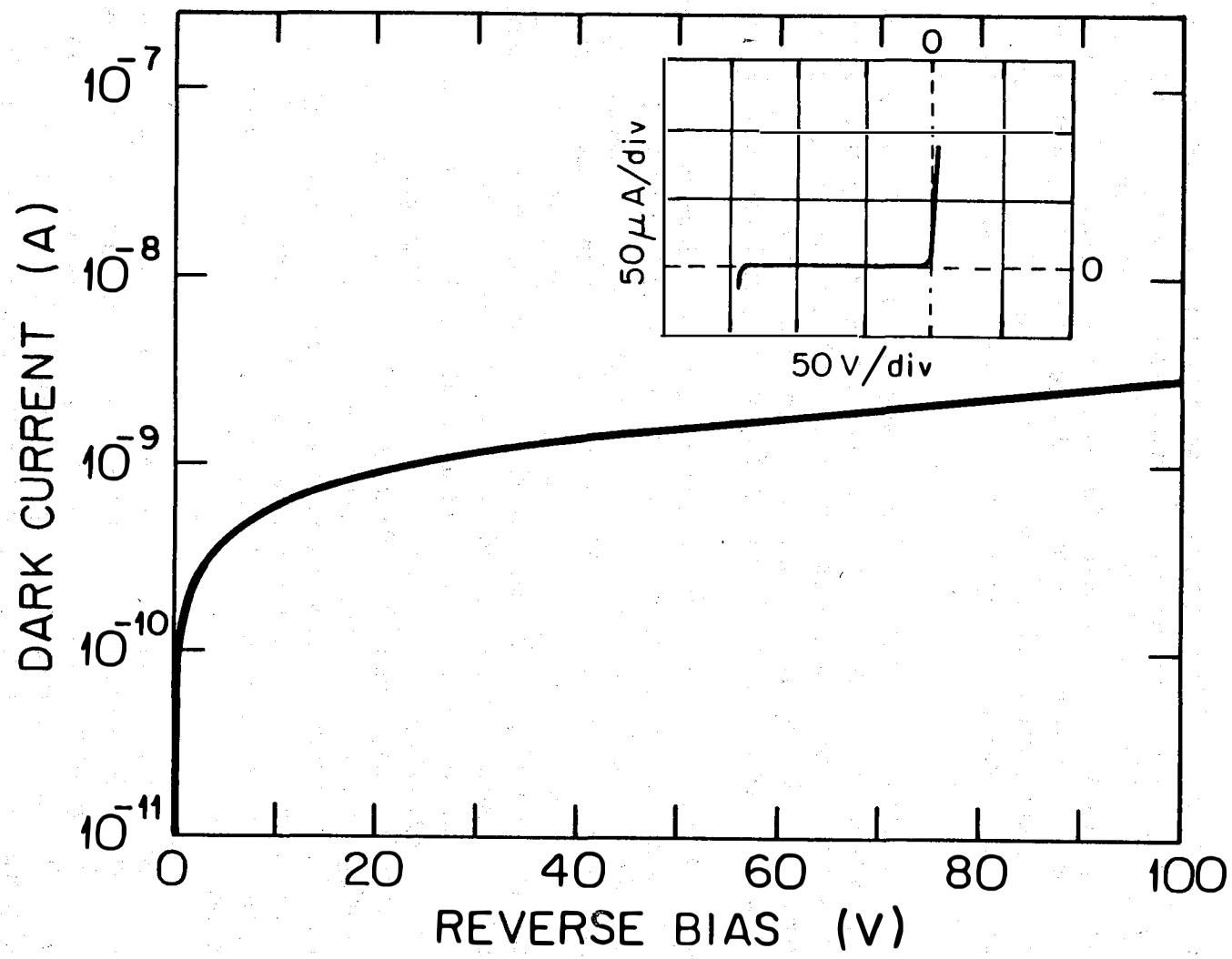
DARK CURRENT (A)
10^{-7}
10^{-8}
10^{-9}
10^{-10}
10^{-11}
0
20
40
60
80
100
REVERSE BIAS (V)
0
50 μA/div
0
50 V/div

5.0 HIGH-EFFICIENCY CONCEPTS

John Benner, (Manager) and Cecile Leboeuf

The objective of the High Efficiency Concepts Task is to evaluate and develop advanced photovoltaic technologies capable of energy conversion efficiencies in excess of 20% for flat-plate configurations and 30% in concentrator systems. These goals are discussed in the DOE Five-Year Research Plan as technology targets for the late 1990s. Even on this longer term horizon, it is difficult to envision a technology capable of achieving such high efficiencies without incorporating the demonstrated performance of crystalline III-V semiconductors. Thus, the High Efficiency Concepts task has become synonymous with III-V compound semiconductor research.

SERI's program of research in High Efficiency Concepts has approached the terrestrial photovoltaic goals from the direction of first demonstrating the feasibility of exceeding the efficiency targets to assure that production engineering trade-offs between performance and cost can be accommodated. Recent advancements by the community researching high efficiency technologies provide a high level of confidence that the efficiency goals can readily be met.

The achievement of 25% efficiency in commercial concentrator modules will likely require production cells having more than 29% efficiency. The system cost target for that efficiency corresponds to cell costs less than $\$10/cm^2$. At least three organizations have demonstrated that a single-junction GaAs cell at approximately this efficiency level. Recent successes in multiple-junction devices or through technologies show encouraging progress toward fulfilling the theoretical promise of providing commercial cells with more than 35% efficiency. However, a fivefold reduction in processing costs would be needed to meet the cell cost target for concentrator cells. Much of this reduction can be achieved through use of larger wafers and higher through-put deposition systems. Research supported by this program benefits future development efforts by strengthening the understanding of basic mechanisms which affect uniformity of doping, composition, and thickness over large area wafers, from wafer-to-wafer and from run-to-run. Efficient utilization of source materials and evaluation to potentially superior sources (cost, purity, control, safety, and other factors) are also important topics for research. Continued improvement in cell efficiency is also a critical factor in reaching cost-effectiveness for the technology.

Flat-plate technologies have several advantages relative to concentrator technologies because the ability to utilize both the direct and diffuse components of the solar energy resource increases the geographical range of operation, simplifies system design and operation, and opens a variety of market opportunities for small installations. High-efficiency modules can be achieved either through development of multiple junction and/or development of processes for low-cost deposition of single crystal thin films. Two technologies have already reached performance levels consistent with the efficiency goals. One approach, which produces thin-crystalline-films, separated from a reusable substrate in a process called CLEFT, has reached efficiencies of 22.4%. Thin films of GaAs grown on silicon substrates are rapidly closing in on the 20% efficiency target, having improved from 11% to 19.9% efficiency in the last two years.

Title: **Arsine and Hydride Radical Generation for MOCVD Growth**

Organization: Electrical Engineering Department, Colorado State University, Fort Collins, Colorado

Contributors: G. J. Collins, principal investigator; B. G. Pihlstrom, L. R. Thompson, and T. Sheng

The objective of this program is to develop capabilities to generate in-situ arsine and hydride radicals from lower toxicity solid and gas precursor sources of arsenic. These techniques will then be applied to the deposition of arsenic containing semiconductors. The emphasis will be on the reduction of toxicity of the starting material as well as the reduced deposition temperature due to the reactivity of the hydride radicals. These hydrogenated species can be generated with either large area DC generated disc plasmas or microwave plasmas. To date, the results for epitaxial material has been limited to the use of trimethylarsenic as the low toxicity group V precursor and the report of this work is listed in Ref. [1].

Plasma Source Development

This research has resulted in the deposition of epitaxial GaAs at low temperature (300 °C) utilizing trimethylgallium and trimethylarsenic with a remote DC hydrogen plasma. However, the trust will be the use of solid sources of arsenic as the group V precursor. Disc shaped DC plasmas were explored as a means to provide volatile arsenic species from solid arsenic to transport the material to the deposition region of the reactor. However, the ability to delivery adequate quantities for the growth of III-V material was limited. The further evolution of the arsine and arsine radical source lead to the development of a microwave generated plasma that is compatible with the present plasma assisted OMVPE deposition as far as absolute pressure and other reactor parameters. The low pressure used in the deposition will aid in extending the life times of the radicals by reducing there chances of interaction with other gas phase species.

Details of the Microwave Plasma Source

The experimental setup is a microwave generator with a 8mm I.D. quartz tube. Downstream from the plasma approximately 5cm is the solid arsenic source. The byproducts of the plasma source are analyzed with a mass spectrometer. The signal shown in Figure 1 is from the plasma generated hydride and approximates the mass spectrometeric signature of arsine with the established spectrum. Figure 2 shows the intensity of the arsine signal with respect to the microwave power indicating the saturation of the signal with higher plasma intensities.

Conclusions and Future Work

Homoepitaxial GaAs has been deposited via a remote hydrogen plasma assisted technique at both low temperature and low pressure utilizing trimethylarsenic as the group V precursor. An alternative delivery technique for the arsenic has been developed with the use of a microwave

plasma that generates from solid arsenic arsine. This source is presently being further explored with future application for material growth.

Reference

1. B. G. Pihlstrom, L. R. Thompson, and G. J. Collins, "Low Temperature Growth of Homoepitaxial GaAs by Dissociating Trimethylgallium and Trimethylarsenic in a Remote Hydrogen Plasma," to be published in Solar

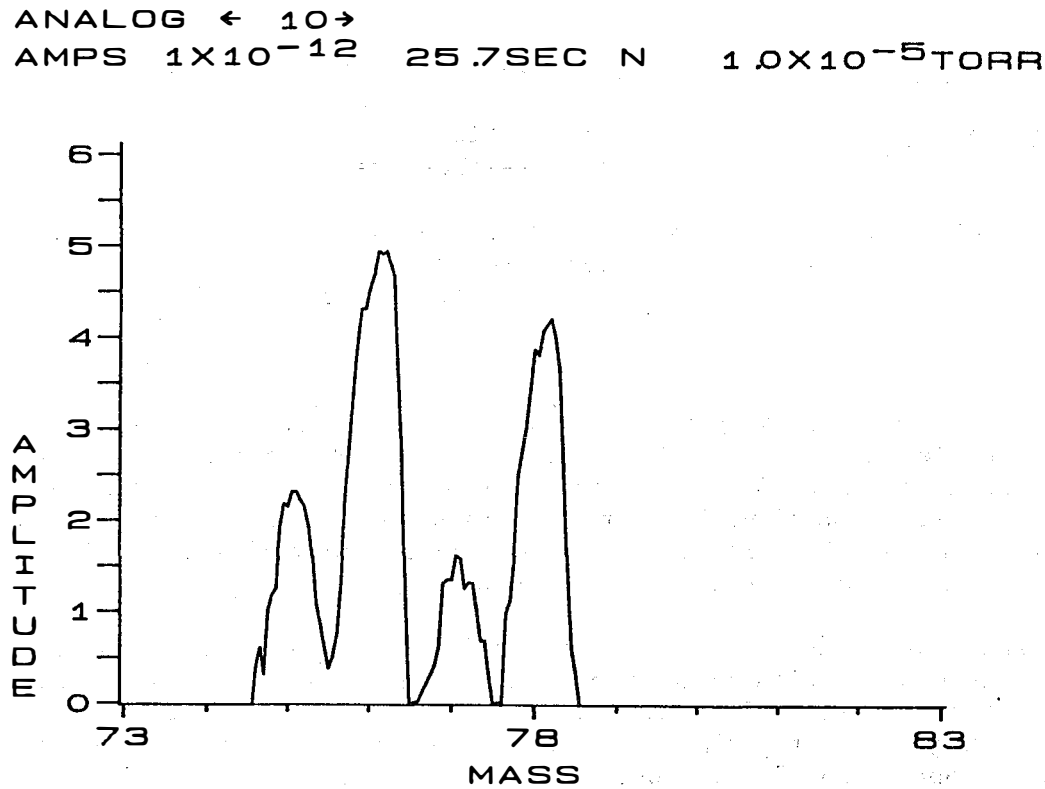

Figure 1. The mass spectrum of the byproducts of the microwave generated plasma with solid arsenic placed down stream of the plasma.

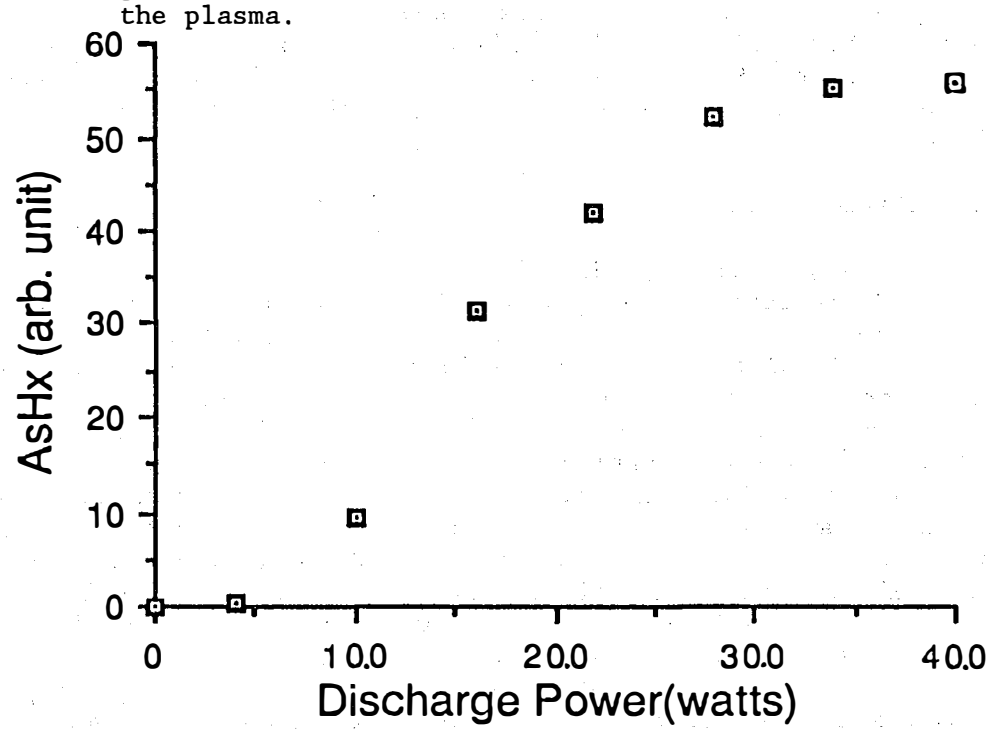

Figure 2. Mass spectrometer intensity of the mass 76 signal from the arsine spectrum as a function of microwave power.

Title:	**High-Efficiency Thin-Film Solar Cells**
Organization:	Kopin Corporation Taunton, Massachusetts
Contributors:	Ronald P. Gale and John C. C. Fan, Coprincipal Investigators; Robert W. McClelland, Brenda D. Dingle.

Objectives

The objectives of this research program are to demonstrate large areas and high efficiencies in thin-film III-V solar cells. Kopin's approach is to use a thin-film technique (CLEFT[1]) to produce high-efficiency single-crystal GaAs/AlGaAs cells less than 5 um thick. This very effective use of material coupled with the multiple reuse of the GaAs substrate will allow this approach to meet the Department of Energy's cell cost targets.

Several significant advances were achieved in FY90. We have demonstrated the monolithic interconnection of multiple thin-film AlGaAs/GaAs solar cells from a single wafer. We have shown that the CLEFT process is capable of producing large area, high efficency thin-film submodules less than 5 um thick and over 21% AM1.5 global, total submodule area. The area of the thin-film GaAs submodules was increased to 16 cm^2, making them the largest GaAs solar devices produced at that time. We have also demonstrated the versatility of our interconnection approach by fabricating submodules with various voltages and areas. We have extended our materials research to include GaInP, in order to produce even higher efficiency thin-film cells. Along with this new material, we have introduced tertiarybutylphosphine (TBP) as our group 5 source for more efficient chemical utilization and safer operation as compared to phosphine, the industry standard.

Monolithic Interconnection

An important feature of any thin-film solar technology is the ability to monolithically interconnect individual cells. The monolithic interconnection reduces external wire connections between cells, and the associated array-assembly costs. It also allows for simple scale up to larger submodule areas, as the cell design can remain constant while the number of cells on a submodule is increased. Since no cell structure changes are required upon scaleup, the submodule fabrication processes need only be modified to handle the larger wafer areas's. This may only be a matter of fixture enlargement. These advantages and more have been realized by the thin-film amorphous and polycrystalline industries, and can now be used for high-efficiency thin-film GaAs solar cells as well. Monolithic interconnection of thin-film GaAs cells allows the simple fabrication of GaAs submodules with a choice of output voltage and current. Each submodule is produced from a single wafer, where the area can be broken down into numbers of series and parallel-connected cells. These monolithically interconnected thin-film GaAs cells are fabricated using the CLEFT process.

Using this attribute of the GaAs thin films, monolithic interconnection of four thin-film single crystal GaAs cells on a single wafer has been demonstrated. We have succeeded in fabricating 16 cm2 monolithically series-intercon-

nected thin-film four-cell strings exhibiting V_{oc} of 4.04 V, and a total-area submodule efficiency of 21.0% under AM1.5 global illumination at 26°C. In addition, an eight-cell string was produced which had a V_{oc} of 7.96V, an AM1.5 efficiency of 21.2%, and a total submodule area of 2 cm^2.

Fabrication and Testing

Thin films are prepared using the CLEFT process, a mechanical separation of a layer from its substrate. The process has been described elsewhere[1,2]. In the CLEFT process, the substrate wafer is recovered and reused; therefore many thin-film cells can be obtained from one substrate. For this reason, the CLEFT technique makes possible a large reduction in material usage and cost.

The cell structure is an AlGaAs/GaAs double heterostructure[3] deposited onto CLEFT substrates by OMCVD. The submodule[4] structure is shown in Fig. 1. All front side processing, including metallization and AR coating, is completed prior to separation of the thin-film from the substrate. The cell is then bonded to an AR coated coverglass and the epitaxial layers are mechanically separated from their substrate using the CLEFT process. After separation, the rear side of the film is accessible for backside processing, consisting of interconnect plating and cell isolation. These process steps all depend on accurate front-to-back registration, which is easily accomplished by way of infrared alignment through the thin GaAs film.

Two different cell strings were fabricated using the above monolithic interconnection processing sequence. One string consisted of four 4 cm^2 interconnected cells connected in series for a total submodule area of 16 cm^2. The second string had eight .25 cm^2 interconnected cells also connected in series for a total submodule area of 2 cm^2. The cells were designed for operation at one sun. Measurements on both the 16 cm^2 and the 4 cm^2 submodules were made under at the Solar Energy Research Institute (SERI) courtesy of Dr. K. Emery.

Submodule Performance

The illuminated I-V characteristics of the 16 cm^2 thin-film submodule are shown in Figure 2. The total area of each individual cell was about 4.0 cm^2, and the four cells were connected in series. The four cell string exhibited a Voc of 4.04V, an Isc of 104.9 mA, and a fill factor of 80% for a submodule efficiency of 21.0% under AM1.5 global illumination. This efficiency number is based on the total submodule area of 16 cm^2. This performance is comparable to our single 4 cm^2 GaAs thin-film cells, and demonstrates area scaleup without loss of performance.

The current 16 cm^2 submodule design minimizes coverage losses due to interconnecting and packing the four cells close together. Since the cells are connected in series, the device runs at low current, high voltage conditions, allowing for a low grid coverage. The inter-cell interconnects and grid coverage account for a 2.5% and a 2% coverage loss respectively. The packing factor for the individual cells in the submodule is also very high. The cell areas add up to over 98% of the total submodule area. This area utilization can be maintained or improved in the design of other submodules.

The illuminated I-V curve for another submodule is shown in Figure 3. This string consists of eight .25 cm^2 cells monolithically interconnected in

series. The submodule shows a V_{oc} of 7.96 V, an I_{sc} of 6.26 ma, and a fill factor of 85%, for a total-area efficiency of 21.2%, AM1.5 global illumination as measured at SERI. The voltages can again be seen to add in the predicted manner.

Growth of GaInP

Investigation into the use of the ternary compound GaInP for thin-film cells was initiated. Growth experiments were carried out using tertiarybutylphosphine (TBP) as the group 5 source. TBP is significantly less hazardous than phosphine, the phosphorus source typically used in OMCVD. Phosphine also requires high temperatures to decompose, and in low-pressure systems such as ours at Kopin, exhibits extremely low chemical utilization. Using TBP, we can grow at both lower temperatures and lower V/III ratios with reasonable chemical utilization.

GaInP layers were grown latticed matched to GaAs. Using double-crystal X-ray diffraction, peak separations of less than 100 arc-sec were reproducibly achieved. This corresponds to lattice mismatch ($\Delta a/a$) of 0.0005 or less. The layers had good surface morphology and exhibited strong room-temperature photoluminescence (PL). Interface recombination between GaAs and GaInP layers was measured by R. Ahrankiel and B. Keyes of SERI using the PL decay technique. Although GaAs bulk lifetimes appeared to be close to theoretical limits, the interfaces needed improvement before being useful for solar cells.

Summary

Several significant advances were achieved in FY90. We have demonstrated the monolithic interconnection of multiple thin-film AlGaAs/GaAs solar cells from a single wafer. The CLEFT process produced large area, high efficency thin-film submodules less than 5 um thick and over 21% AM1.5 global, total submodule area. The area of the GaAs thin-film submodules was increased to 16 cm^2. We have also demonstrated the versatility of our interconnection approach by fabricating submodules with various voltages and areas. We have extended our materials research to include GaInP, in order to produce even higher efficiency thin-film cells. Along with this new material, we have introduced tertiarybutylphosphine (TBP) for our group 5 source as part of a more manufacturable process for solar cell production.

Future work will be centered around improving the cell efficiencies further using GaInP, and addressing process improvements in order to demonstrate lower cost cells. Thin-film cell efficiencies well over 25% are achievable, and improvements in deposition, processing, and substrate reuse costs are needed to reach DOE cost goals for these high-efficiency cells.

References

1. R.W. McClelland, C.O. Bozler, and J.C.C. Fan, Appl.Phys.Lett.**37**(1980)560.

2. J.C.C. Fan, R.W. McClelland, and B.D. King, Proc. 17th IEEE Photovoltaic Specialists' Conf., Kissimmee FL, 1984(IEEE, New York, 1984) p. 31.

3. R.P. Gale, R.W. McClelland, B.D. King, and J.V. Gormley, Proc. 20th IEEE Photovoltaic Specialists' Conf., Las Vegas NE, 1988(IEEE, New York, 1989) p. 446.

4. R.W. McClelland, B.D. Dingle, R.P. Gale, and J.C.C. Fan, Proc. 21st IEEE Photovoltaic Specialists' Conf., Kissimemee FL, 1990(IEEE, New York, 1990) p. 168.

FOUR-CELL SUBMODULE SCHEMATIC

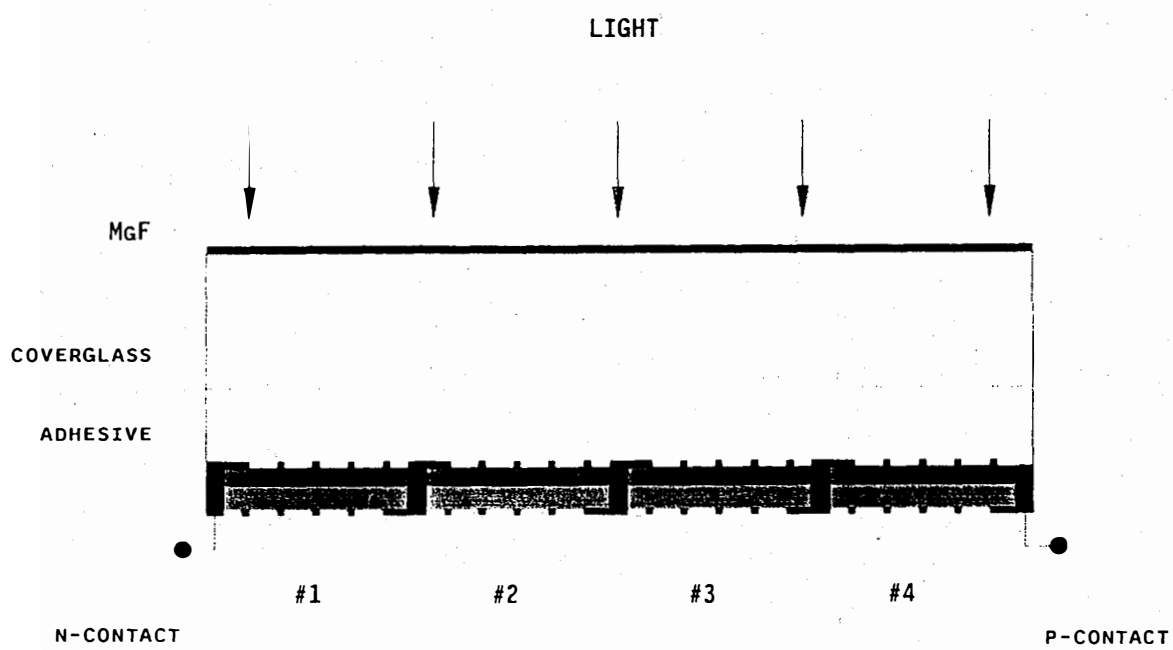

Figure 1. Schematic of monolithically interconnected thin-film cell.

Kopin, Cleft,monolithic submodule,global

Sample: 50965 Temperature = 25.0°C

Apr. 16, 1990 3:47 pm Area = 16.00 cm²

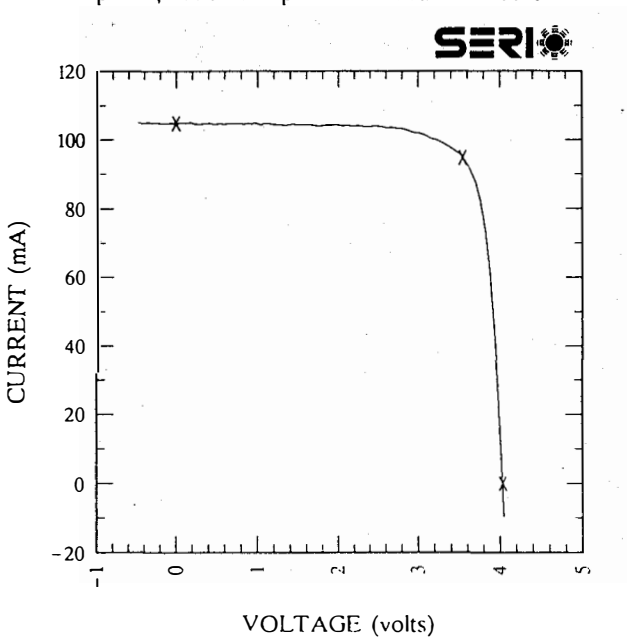

V_{oc} = 4.034 volts I_{sc} = 104.8 mA

J_{sc} = 6.550 mA/cm² P_{max} 336.3 mW

Fill factor = 79.55 % I_{max} = 94.9 mA

Efficiency = 21.0 % V_{max} = 3.545 V

Figure 2. Illuminated I-V curve for the 16 cm^2, four-cell submodule.

Kopin, 8 monolithic GaAs cleft, global

Sample: 50964 Temperature = 25.0°C

May. 15, 1990 1:48 pm Area = 2.006 cm²

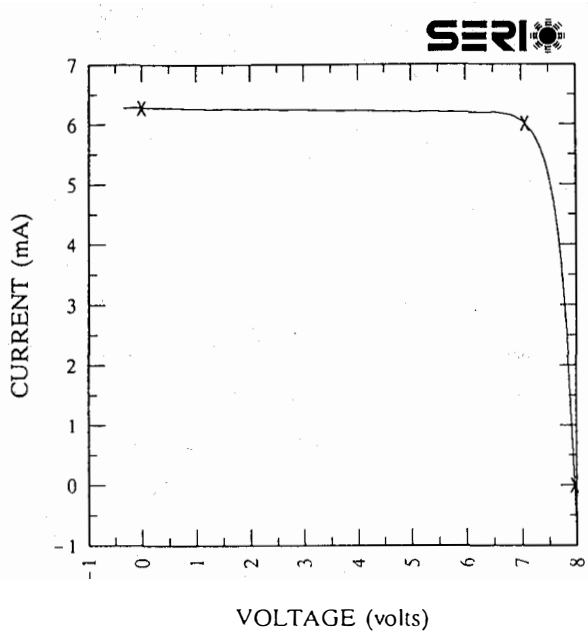

V_{oc} = 7.963 volts I_{sc} = 6.283 mA

J_{sc} = 3.132 mA/cm² P_{max} = 42.446 mW

Fill factor = 84.84 % I_{max} = 6.006 mA

Efficiency = 21.2 % V_{max} = 7.067 V

Figure 3. Illuminated I-V curve for the 2 cm^2, eight-cell submodule.

Title: **Basic Studies of III-V High-Efficiency Cell Components**

Organization: Purdue University, School of Electrical Engineering, W. Lafayette, IN 47907

Contributors: M. S. Lundstrom and M. R. Melloch, principal investigators, R. F. Pierret, faculty associate, M. S. Carpenter, H. L Chuang, P. E. Dodd, A. Keshavarzi, M. E. Klausmeier-Brown, G. B. Lush, and T. B. Stellwag, research assistants

Solar cell efficiency is determined both by material quality and by device design. As the efficiencies of both single and multiple junction III-V solar cells continue to rise, it has become increasingly important to carefully examine the internal device physics of solar cells so that cell designs can be tailored to the material constraints. Our work is directed at meeting this need for an improved understanding of the internal device physics and material parameters of compound semiconductor solar cells. The goal is to identify the internal recombination losses that control the performance of state-of-the-art, high-efficiency GaAs-based solar cells and to develop characterization methodologies and approaches that are broadly applicable to compound semiconductor cells. Another aim is to measure for the first time some of the fundamental parameters (such as the effective intrinsic carrier concentration and minority carrier mobility) which control the performance of solar cells. Finally, we aim to apply this evolving device physics knowledge in order to explore new approaches for enhancing solar cell efficiency.

During the past year, the specific project objectives were to:

- develop a quantitative understanding of perimeter and surface recombination along with a predictive numerical model to simulate such effects
- explore chemical techniques to permanently passivate GaAs surfaces
- assess the photovoltaic potential of pseudomorphic, ZnSe/GaAs heterostructures
- demonstrate high efficiency GaAs and AlGaAs cells using films grown in our MBE facility.

The perimeter and surface recombination studies concluded a long-term effort to understand such effects as well as their implications for III-V solar cells. As a result of this work, we now have a detailed, numerical model which has been verified experimentally.

Earlier work by our group demonstrated that ammonium sulfide treatments suppress perimeter recombination — but only temporarily. During the past year, we have demonstrated that a new arsenic glass treatment, developed by E. Yablonovitch at Bellcore, results in a permanent

reduction of perimeter recombination.

In collaboration with R.L. Gunshor at Purdue, we have successfully grown pseudomorphic ZnSe on a GaAs solar cell film. Measurements to assess the photovoltaic quality of the ZnSe/GaAs interface are underway.

In last year's report, we described a 23.8% efficient (1-sun, AM1.5) 0.5 cm by 0.5 cm heteroface cell fabricated at Spire Corporation using a Purdue-grown MBE film. This year Spire also fabricated a 16.1% efficient (1-sun, AM1.5) $Al_{0.2}Ga_{0.8}As$ solar cell using Purdue-grown material. This result is a record for MBE-grown AlGaAs, but since it was grown at a temperature lower than optimum we expect that much higher efficiencies can be achieved. Finally, we collaborated with Applied Solar Energy Corporation to fabricate large area (2cm by 4 cm) GaAs solar cells. The MBE-grown film had an average cell efficiency of 18.8% (1-sun, AM0) which is comparable to results obtained for similar size cells fabricated from MOCVD material and demonstrates that MBE-grown films are suitable for high-efficiency cell research.

Surface and Perimeter Recombination in GaAs Diodes: An Experimental and Theoretical Investigation

Gallium arsenide surfaces contain high densities of charge states and recombination centers which degrade the performance of electronic devices [1]. Recombination at the illuminated surface reduces a solar cell's photocurrent, and recombination along the cell's perimeter increases its dark current [2]. Perimeter recombination similarly degrades the performance of heterojunction bipolar transistors by producing a size effect which reduces the gain of small devices [3,4]. To suppress surface and perimeter recombination, a variety of novel device designs and surface treatments are being explored [5,6]. A quantitative understanding of surface recombination must be developed in order to analyze and design GaAs bipolar devices.

We have studied experimentally and with numerical modeling GaAs heteroface diodes in order to determine the mechanisms responsible for surface and perimeter recombination. An experimental technique was developed which allows extraction of the perimeter and bulk current components. A surface model which treats Fermi level pinning by SRH recombination through deep level traps was used and extensively compared to the experimental data for the purpose of verifying the model and quantifying the model parameters. A density of 5×10^{12} cm^{-2} traps located at midgap with surface recombination velocities of 4×10^{5} cm/s were found to reproduce the experimental data very well. Both the dark current *versus* voltage and the internal quantum efficiency *versus* wavelength are well described by this simple model.

For the GaAs homojunction diodes investigated, we found that the diode current under moderate forward bias was controlled by recombination along the perimeter. Most of the

recombination occurs where the junction space-charge region intersects the perimeter, and it results in an ideality factor of ≈ 2. Both the measured data and the computer model show that the ideality factor of the perimeter current decreases under high forward bias. The computer modeling results demonstrate that the decrease in ideality factor is caused by carriers injected in the bulk regions diffusing to the perimeter. For these devices, there appears to be little injection of carriers into the surface channel induced by Fermi level pinning. Computer modeling experiments uncovered no distinctive features in the current-voltage characteristic which could be attributed to Fermi level pinning. We found that the dark and illuminated characteristics could even be modeled by ignoring the charge on the surface states and employing an effective surface recombination velocity of $\approx 10^7$ cm/s.

Large Area GaAs Solar Cells Fabricated from MBE Material

Last year we demonstrated that GaAs solar cells fabricated from MBE material can have performance comparable to those fabricated from MOCVD material [7,8]. We attributed these improvements in performance to MBE system conditioning, higher purity of source materials, and possibly a reduction in defect density [8]. Solar cells are large area devices and therefore require high material uniformity and low defect densities. The largest previously reported GaAs solar cells fabricated from MBE material have an area of 0.25 cm^2 [7-9]. This year we had GaAs solar cells of area 2x4 cm^2 fabricated from our MBE material at Applied Solar Energy Corporation. The cell was a p on n heteroface design with a 0.4 μm emitter and a 3 μm base. The cell was measured under 1-sun AM1.5 conditions at the Solar Energy Research Institute and exhibited an efficiency of 21.7% at a temperature of 25°C. The cell was also measured under 1-sun AM0 conditions at Applied Solar Energy Corporation and exhibited an efficiency of 18.8% at a temperature of 28°C. These results are comparable to those obtained for 2x4 cm^2 cells which have been grown by MOCVD [10].

As_2S_3 Passivation of GaAs Surfaces

In the last few years it has been shown that chemical treatments of GaAs surfaces with inorganic sulfides can produce dramatic improvements in the surface electrical properties [11-16]. The chemical nature of one of these inorganic sulfide treatments, ammonium sulfide, has been investigated with X-ray photoelectron spectroscopy (XPS) [18-20], which shows that the ammonium sulfide treatment removes surface oxides and terminates the GaAs surface with about a monolayer of sulfur. Since the GaAs surface is terminated with just a monolayer of sulfur, it is not surprising that the surface eventually degrades back to its initial electrical characteristics due to reoxidation of the underlying GaAs [19]. Recently, Yablonovitch et al. [21]

have developed a sulfide chemical treatment which leaves the GaAs surface coated with an amorphous As_2S_3 layer. This As_2S_3 layer prevents oxygen from diffusing to the GaAs surface and results in a permanent modification of the surface electrical characteristics. We have investigationed the passivation of pn homojunction GaAs diodes and self-aligned HBTs with this As_2S_3 chemical treatment.

After fabrication, the diodes were electrically characterized after which they underwent the As_2S_3 chemical treatment. The As_2S_3 chemical treatment consisted of an oxide removal etch in 1:10 NH_4OH:H_2O followed by a 5 minute soak in ammonium sulfide. The sample was then rinsed in deionized water and placed in a solution of 0.16M As_2S_3 dissolved in a 1:1 solution of NH_4OH:MeOH. The sample was then spun dry under flowing nitrogen. Following the As_2S_3 chemical treatment, the diodes were again electrically characterized. Shown in Fig. 1 is the forward current voltage characteristic for a square diode of 50μm on a side before and after the As_2S_3 chemical treatment [22]. At high current levels the device characteristics are dominated by series resistance of the top contact and are not shown. As can readily be seen in Fig. 1, there is more than an order of magnitude reduction in current after the As_2S_3 chemical treatment at biases above where the shunt leakage dominates. The shunt leakage observed on the treated devices can be eliminated when the sample is annealed in nitrogen at 280°C. The annealing step is also necessary to make the As_2S_3 film impenetrable to oxygen and permanent. We have not performed this anneal on GaAs pn junctions but have on HBTs.

Following the initial electrical characterization, the HBTs underwent the As_2S_3 chemical treatment. In addition, the As_2S_3 treated HBTs were annealed at 280°C on a graphite strip heater in flowing nitrogen. This final anneal step makes the As_2S_3 film impermeable to oxygen and results in a permanent passivation. Following the As_2S_3 chemical treatment, the HBTs were again electrically characterized. Shown in Fig. 2 is the collector (IC) and base (IB) currents as a function of the base-emitter (VBE) voltage with the base collector junction shorted for an HBT with an emitter size of 14 μm x 14 μm before and after the As_2S_3 chemical treatment. No change was observed in the collector current except for a difference in roll-off at high current levels due to a difference in series resistance. (This difference in series resistance is probably a consequence of the probe contact.) In contrast, there is over an order of magnitude reduction in the base current at biases of VBE= 0.6 to 0.7 V following the As_2S_3 chemical treatment. Also seen in Fig. 2 is that the leakage current initially observed in the base current has been eliminated by the As_2S_3 chemical treatment. Similar behavior was observed with all the treated HBTs and no degradation has been observed after two months exposure to room temperature and atmospheric conditions.

References

[1] W.E. Spicer and S.J. Eglash, "Fundamental Studies of Interfaces: The Unified Defect Model and its Application to GaAs Integrated Circuits," in VLSI Electronics Microstructures, Volume 10, Einspuch and Bauer, Eds.: Academic Press, Inc., 1985.

[2] P.D. Demoulin, S.P. Tobin, M.S. Lundstrom, M.S. Carpenter, and M.R. Melloch, "Influence of Perimeter Recombination on High-Efficiency GaAs p/n Heteroface Solar Cells," IEEE Electron Device Lett. EDL-9, 368(1988).

[3] P.M. Asbeck, et al., "Nonthreshold Logic Ring Oscillators Implemented With GaAs/(GaAl)As Heterojunction Bipolar Transistors," IEEE Elect. Dev. Lett. EDL-5, 181(1984).

[4] Y.S. Hiraoka, et al., "Two-Dimensional Analysis of Emitter-Size Effect on Current Gain for GaAlAs/GaAs HBT's," IEEE Trans. Elec. Dev. ED-34, 721(1987).

[5] M.T. Schmidt, Q.Y. Ma, D.V. Podlesnik, R.M. Osgood, and E.S. Yang, "Chemically Modified GaAs Schotkky Barrier Variation," J. Vac. Sci. and Technol. B7, 980(1989).

[6] E. Yablonovitch, C.J. Sandroff, R. Bhat, and T.J. Gmitter, "Nearly Ideal Electronic Properties of Sulfide Coated GaAs Surfaces," Appl. Phys. Lett. 51, 439(1987).

[7] S.P. Tobin, S.M. Vernon, C. Bajgar, S.J. Wojtczuk, M.R. Melloch, A. Keshavarzi, T.B. Stellwag, S. Venkatesan, M.S. Lundstrom, and K.A. Emery, "Assessment of MOCVD- and MBE-Grown GaAs for High-Efficiency Solar Cell Applications," IEEE Trans. Electron Devices, vol.37, no. 2, p.469, 1990.

[8] M.R. Melloch, S.P. Tobin, T.B. Stellwag, C. Bajgar, A. Keshavarzi, M.S. Lundstrom, and K. Emery, "High- efficiency GaAs Solar Cells Grown by Molecular-Beam Epitaxy," J. Vac. Sci. Technol. B, vol 8, no. 2, p. 379, 1990.

[9] D.L. Miller and J.S. Harris, Jr., "Molecular Beam Epitaxial GaAs Heteroface Solar Cell Grown on Ge," Appl. Phys. Lett., vol. 37, no. 12, p. 1104, 1980.

[10] P.A. Iles, et al., "High-Efficiency (>20%AM0) GaAs Solar Cells Grown on Inactive-Ge Substrates," IEEE Elec. Dev. Lett., vol. 11, no. 4, p.140, 1990.

[11] C. J. Sandroff, et al., Appl. Phys. Lett. 51, 33 (1987).

[12] R.N. Nottenburg, et al., Appl. Phys. Lett. 52, 218(1988).

[13] M.S. Carpenter, M.R. Melloch, M.S. Lundstrom, and S.P. Tobin, Appl. Phys. Lett. 52, 2157(1988).

[14] M.S. Carpenter, M.R. Melloch, and T.E. Dungan, Appl. Phys. Lett. 53, 66(1988).

[5] J.F. Fan, H. Oigawa, and Y. Nannichi, Jpn. J. Appl. Phys. 27, L2125(1988).

[16] E. Yablonovitch, C.J. Sandroff, R. Bhat, and T.J. Gmitter, Appl. Phys. Lett 51, 439(1987).

[17] E. Yablonovitch, H.M. Cox, and T.J. Gmitter, Appl. Phys. Lett. 52,1002(1988).

[18] C.J. Sandroff, et al., Appl. Phys. Lett. 54, 362(1989).

[19] B.A. Cowans, Z. Dardas, W.N. Delgass, M.S. Carpenter, and M.R. Melloch, Appl. Phys. Lett. 54, 365(1989).

[20] M.S. Carpenter, M.R. Melloch, B.A. Cowans, Z. Dardas, and W.N. Delgass, J. Vac. Sci. Technol. B7, 845(1989).

[21] E. Yablonovitch, T.J. Gmitter, and B.G. Bagley, submitted to Appl. Phys. Lett.

[22] T.B. Stellwag, P.E. Dodd, M.S. Carpenter, M.S. Lundstrom, R.F. Pierret, M.R. Melloch, E. Yablonovitch, and T.J. Gmitter, Conference Record of the 21st IEEE Photovoltaic Specialists Conference (IEEE, New York, 1990).

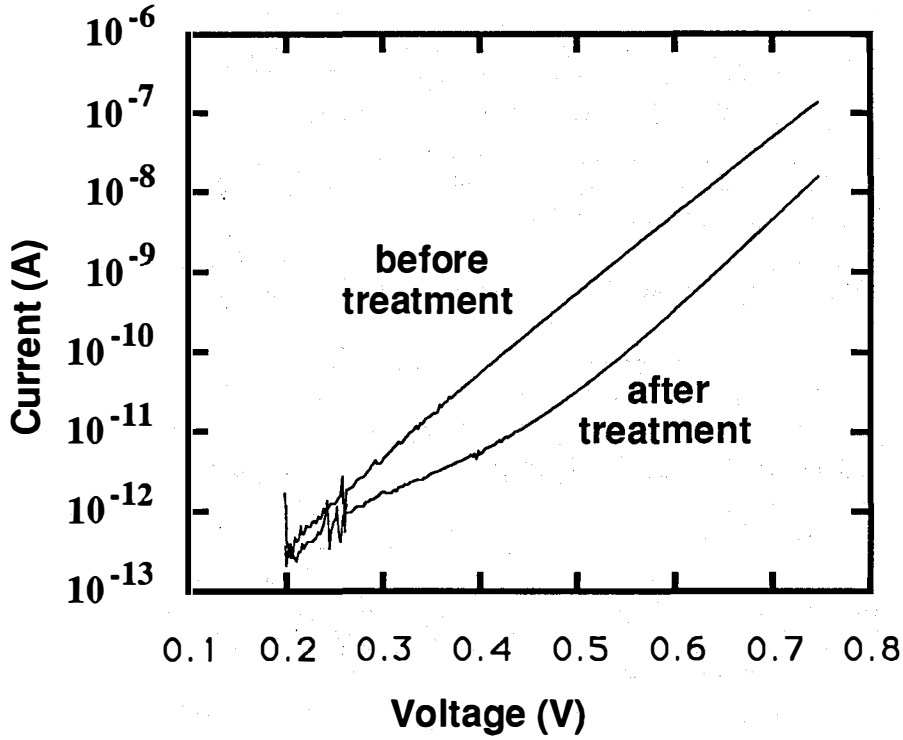

Fig. 1 Forward-bias current-voltage characteristics for a square diode of 50 μm on a side before and after the arsenic sulfide treatment.

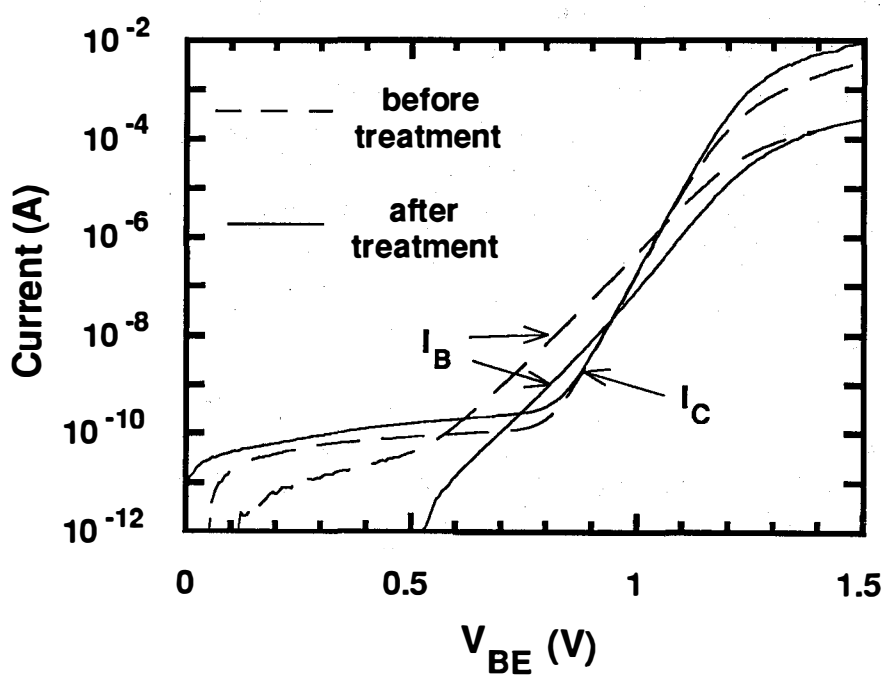

Fig. 2 Collector and base currents as a function of base-emitter voltage with the base collector junction shorted. Characteristics before and after the arsenic sulfide chemical treatment of the emitter-base perimeter are shown.

Title: **Research on Semiconductors for High Efficiency Solar Cells**

Organization: Department of Electrical, Computer and Systems Engineering, Rensselaer Polytechnic Institute, Troy, New York

Contributors: J.M. Borrego and S.K. Ghandhi, Co-Principal Investigators

The program objective is to investigate problems which are encountered in the development of high efficiency single and multi-junction solar cells. These problems involve issues of materials growth and characterization. Three of our tasks on this program are outlined below.

GROWTH MODELS AND NEW REACTOR CONCEPTS: This task involves the development of computer programs which are directed to OMVPE in practical growth situations, and are capable of experimental verification. A computer program, which gives a direct solution of the Navier Stokes equations in two-dimensional form, has been developed to study the effects of convection in epitaxial reactors, and on methods for the elimination of circulation effects. A unique feature of this program is that it allows all wall temperatures to be calculated. Thus, it is not necessary to use arbitrary boundary values for this parameter.

Application of the computer program to stagnation point reactors has resulted in the design of a new reaction chamber for the growth of solar cell materials with high chemical usage efficiency. A vertical stagnation flow reactor was designed since this configuration has demonstrated a potential for large area growth uniformity. The reactor has an inverted configuration to eliminate recirculation problems. The susceptor and gas inlet nozzle are closely spaced (about 1cm) in order to achieve improvements in deposition efficiency, layer uniformity and abruptness of interfaces. The simulated velocity field is shown for this situation in Fig. 1, and indicates a complete absence of circulation effects within the growth region. A specially designed water-cooled inlet nozzle is used to maintain the nozzle surface at relatively low temperatures (below 100°C) under all operating conditions. This nozzle consists of a repeated hexagonal pattern of tubes welded at both ends to perforated discs. Its top face is cooled by the circulation of water in the enclosed space of the nozzle outside the tubes. A closed-loop, cooling water circuit that includes a reservoir, heat exchanger and gear pump is used to cool the nozzle. The gear pump supplies a constant flow rate of water of about 1.3 l/min.

An alternative approach for improving the efficiency (as well as uniformity) in stagnation flow reactors is to use susceptor rotation rates of 100-1500 rpm. This causes a centrifugal pumping action that pulls the gases axially towards the susceptor and pushes them out radially along the susceptor surface. A disadvantage of this approach is in system complexity and cost. In addition, high susceptor rotation rates necessitate the use of high V-III ratios of (typically 100-400). For these ratios, the cost of Column V hydride becomes comparable and often exceeds that of the Column III alkyl. Waste disposal of the highly toxic Column V hydride presents an additional problem. The cost would further increase if these hydrides were substituted by lower toxicity alkyls such as tertiarybutylarsenic (TBAs).

Since OMVPE growth involves pyrolysis of the reactants (as in GaAs growth by OMVPE), an excessively large nozzle temperature will lead to a large amount of reactants cracking and depositing on it. The success of this novel reactor design depends critically on the ability of the cooling system to maintain the nozzle at a relatively low temperature, even for small nozzle-susceptor distances. Hence, the different thermal processes in the reactor were studied in detail, using computer simulations, before the reactor was fabricated. Figure 2 shows the simulations of nozzle temperature (T_n) vs. susceptor temperature (T_s) for $F =$ 6 slm, $P = 380$ Torr and $d = 0.5$, 1 and 2 cm, together with the experimental data points. As expected, T_n increases with increasing T_s, due to increased radiative and convective heat transfer to the nozzle. As d is reduced, T_n increases due to increased radiative heating (higher view factors) as well as convective heating (higher temperature gradients).

The difference between experimental and computed nozzle temperatures in Fig. 2 range from +14°C to -5°C. Although small, this error is at least partially due to misalignment of the nozzle with respect to the susceptor, which results in 10% to 20% errors in the value of d for $d = 1$ to 0.5 cm, respectively.

Figure 3 shows simulations and experimental data of T_n vs. T_s for $d = 1$ cm, $P = 380$ Torr and $F = 6$ and 10 slm. Note that the nozzle temperatures are lower for higher gas flow rates. This comes about because convective heating of the susceptor involves the successive transfer of heat from the susceptor to the flowing gases, and from the gases to the nozzle. At higher flow rates, the lower residence time of the gases allows less heat transfer to the nozzle and more rapid removal of heat from the susceptor-nozzle region.

We are now in the process of carrying out growth runs on this system. The layer morphology in preliminary samples is excellent with undoped carrier concentrations of 1×10^{15} cm^{-3}. The thickness uniformity is ±3% over 1 cm × 1 cm sample sizes.

LATTICE MISMATCHED EPITAXY: Modern solar cell design indicates that the heteroepitaxial growth of materials will give an increased photovoltaic conversion efficiency, provided that the resulting layers are of good electrical quality. Thus, there is considerable merit to understanding the problems if mismatched systems.

One very important consideration in the growth of mismatched heteroepitaxial layers is the density of threading dislocations. These act as non-radiative recombination centers in compound semiconductors, and degrade the performance of minority carrier devices. Dislocations and strain also cause rapid degradation in injection lasers. In our own research, we have developed a model for the high threading dislocation densities in mismatched heteroepitaxial materials, based on a half-loop model for the annihilation of misfit dislocations. This model begins with the following assumptions. Threading dislocations are introduced in the growth process by lattice relaxation. Neighboring threading dislocations will often have opposing Burgers vectors; they will therefore attract one another and coalesce. Upon coalescence, a half-loop such as the one shown in Fig. 4 will be formed. The forces acting on this half-loop will determine whether it glides back to the interface, preserving the two original threading dislocations, or glides to the surface and disappears.

Critical to our theory is the length of the misfit segment, L, of this half-loop, and calculations have been made for this parameter. Our model predicts that, for thick, highly-

mismatched layers with equilibrium strain, the threading dislocation density should be proportional to f/h, where f is the lattice mismatch and h is the film thickness. These predictions are in good agreement with experimental results on many systems. In particular, the observed dislocation densities in annealed GaAs on Si (001) suggest that an equilibrium limitation such as this one is at work.

There are several important implications of this theory. First, there are inherent limitations in the reduction of dislocation densities in the planar heteroepitaxy of highly mismatched semiconductors such as GaAs on Si, and novel architectures may be required to achieve further improvements. Second, closely matched material systems such as ZnSe on GaAs may see much improvement in the dislocation density through higher growth temperatures or thermal annealing. In the particular case of ZnSe on GaAs, the best grown material contains dislocation densities similar to those in GaAs on Si, despite an order of magnitude lower lattice mismatch. It thus seems that an order of magnitude improvement should be readily achieved in ZnSe on GaAs. A paper based on our studies is in preparation.

DIAGNOSTICS: A knowledge of resistivity, mobility and minority carrier lifetime is important in the study of semiconductor materials. Ideally, this should be done without destruction of the material. We have developed a microwave reflection technique as the nondestructive determination of these important material parameters.

We have also developed a lifetime measurement technique based on the open circuit voltage decay (OCVD) of solar cells. This method has been routinely applied to silicon devices, but presents special problems with direct gap materials such as GaAs, where minority carrier lifetimes in the base are typically on the order of a few nanoseconds. The time duration of signal waveforms in pulsed measurements are therefore very short, necessitating measurement equipment with extremely large bandwidth, to accurately measure the rise times or fall times. Furthermore, impedance matching of the device to the measuring equipment must be very precise, to prevent reflections that distort the signal. Specifically, any impedance mismatch between the source and the oscilloscope causes ringing at the rising and falling edges.

OCVD measurements were performed on p^+n diodes made on n^+ GaAs substrates. A pulse generator with a rise and fall time of approximately 6 ns, when terminated into 50 ohms was used for this purpose. The pulse shape deteriorated considerably when terminated directly into a forward biased diode necessitating the use of a resistance in series with it. A Schottky diode in the circuit prevents the leakage of the charge stored in the n^+p junction through the series resistance of the pulse generator.

Diodes under test were mounted at the center of a specially fabricated microstrip fixture which minimizes impedance mismatch in the circuit. The fixture consists of an input and an output port which are connected to a microstrip line via OSM launchers; the diode under test appears as a shunt element in the microstrip line. The pulse generator with Schottky diode and resistor in series is connected to the input port and the oscilloscope is connected to the output port. An HP1110A current probe is used to measure the current through the diode during the pulse. Using this system the effective lifetime in GaAs p^+n diodes was determined to be 6 ns and agrees well with a value of 5.7 ns measured by microwave transient photoconductivity.

REFERENCES:

1. P.D. Agnello and S.K. Ghandhi, J. Crys. Growth, 97, 551 (1989).
2. P.D. Agnello, P.B. Chinoy and S.K. Ghandhi, J. Crys. Growth, 102, 775 (1990).
3. P.D. Agnello, P.B. Chinoy and S.K. Ghandhi, Mater. Res. Soc., 161, 271 (1990).
4. S. Bothra, J.M. Borrego and S.K. Ghandhi, Solar Cells, 27, 437 (1989).
5. R. Venkatasubramanian and S.K. Ghandhi, J. Crys. Growth, 97, 827 (1989).
6. R. Venkatasubramanian, S. Bothra, S.K. Ghandhi and J.M. Borrego, Proc. 20th Photovoltaic Specialists Conf., pp. 689-694 (1989).
7. L.J. Schowalter, J.E. Ayers, S.K. Ghandhi, S. Hashimoto, W.M. Gibson, F.K. LeGoues and P.A. Claxton, Mater. Res. Soc., 160, 527 (1990).
8. P.B. Chinoy, D.A. Kaminski and S.K. Ghandhi, J. Heat Transfer, Part A, 19, 73 (1991).
9. P.B. Chinoy and S.K. Ghandhi, J. Crys. Growth (accepted).
10. P.B. Chinoy and S.K. Ghandhi, J. Electrochem. Soc. (submitted).
11. L.M. Smith, D.J. Wolford, R. Venkatasubramanian and S.K. Ghandhi, J. Vac. Sci. Tech., 138 (1990).
12. L.M. Smith, D.J. Wolford, R. Venkatasubramanian and S.K. Ghandhi, Proc. Mater. Res. Soc., 163, 95 (1990).
13. L.M. Smith, D.J. Wolford, R. Venkatasubramanian and S.K. Ghandhi, Appl. Phys. Lett. (accepted).
14. S. Bothra and J.M. Borrego, Solar Cells, 28, 95 (1990).
15. J.M. Borrego and S.K. Ghandhi, Solid State Electron., 33, 773 (1990).

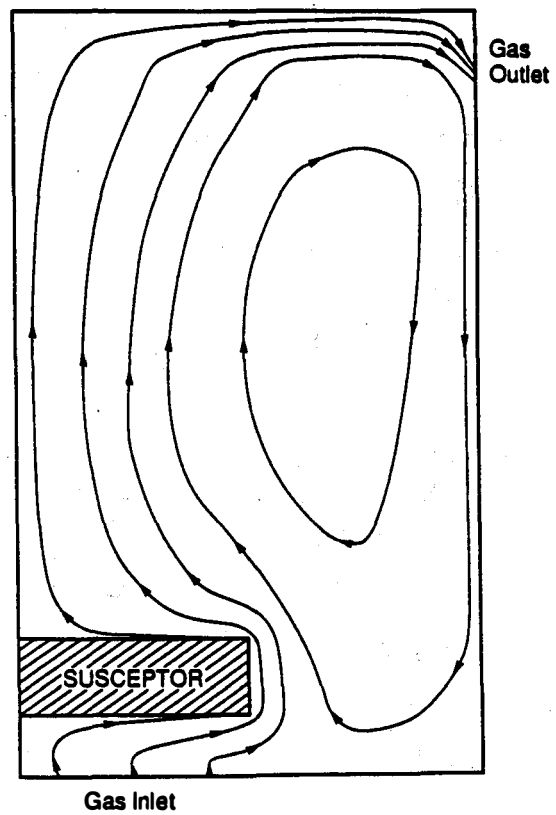

Figure 1: Simulated velocity field for $T_s = 700°C$, $d = 1$ cm, $F = 6$ slm and $P = 380$ Torr.

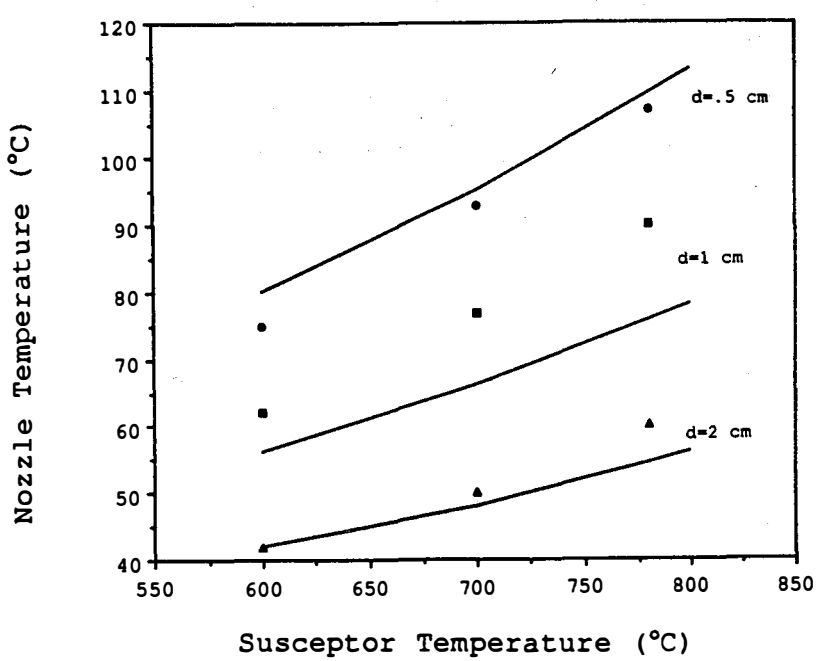

Figure 2. Simulation results and experimental data for $F = 6$ slm, $P = 380$ Torr and $d = 0.5$, 1 and 2 cm.

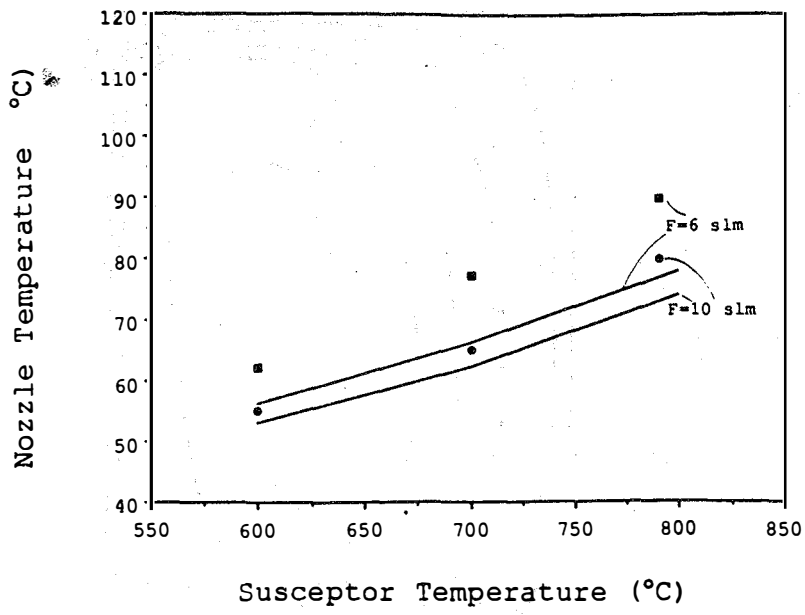

Figure 3: Simulation results and experimental data for $d = 1$ cm, $P = 380$ Torr and $F = 6$ and 10 slm.

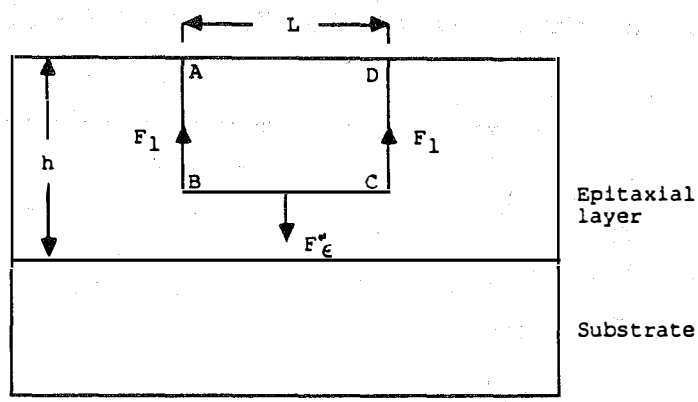

Figure 4: Dislocation half-loop in a strained heterostructure.

Title:	**Low-Cost, High-Efficiency Solar Cells Utilizing GaAs-on Si Technology**
Organization:	Spire Corporation, Bedford, Mass. 01730
Contributors:	S.M. Vernon and S.P. Tobin, Co-principal Investigators

Introduction

The overall goal of this research is to establish a technology to produce very-high-efficiency solar cells for terrestrial photovoltaic applications, using either multijunction or single-junction concepts. The approach pursued in this program involves the growth of GaAs and/or $GaInP_2$ materials onto Si substrates by the metalorganic chemical vapor deposition (MOCVD) technique. The program has only recently begun, and our efforts to date have been devoted to establishing a technology for producing Bragg-reflector structures for improved-efficiency solar cells having a reduced base thickness. Efforts of our prior SERI contracts have resulted in the achievement of a GaAs-on-Si solar cell having a terrestrial efficiency of 20% at 200 suns.

Efficiency Calculations

The primary objective of this contract is to develop high-efficiency photovoltaic devices on inexpensive, large-area Si substrates, utilizing GaAs substrates to first develop the necessary high-efficiency cell components. Maximum-efficiency calculations for the GaAs-$GaInP_2$ tandem-cell structures being developed here (see Figure 1) are as follows:

- On GaAs substrates: 34% at concentration
  30% at 1-sun
- On Si substrates: 31% at concentration
  27% at 1-sun

GaAs on Si Material Improvement

A number of techniques to reduce the dislocation density of our GaAs on Si films are being explored; these include optimization of our TCG process, use of strained layers of $In_xGa_{1-x}As$ to deflect threading dislocations, and the use of atomic-layer epitaxy for improved, 2-D film nucleation. These techniques are expected to result in a dislocation density of $\sim 1 \times 10^6$ cm^{-2}. Our prior studies have shown that material of this quality should yield solar cells of comparable efficiency to those fabricated on bulk GaAs substrates.

Bragg Reflector Development

Bragg reflector structures are being developed in order to reduce the thickness of the GaAs-on-Si solar cell layers without reducing the optical pathlength of the incoming radiation. For solar cell layers

with a fairly short diffusion length, as is typical for GaAs on Si, a thinner base region leads to higher efficiency. Use of a Bragg reflector at the back of the base region allows the cell thickness to be cut in half while still absorbing all the useful light by reflecting the long-wavelength portion of the spectrum back through the cell for a second pass. Important design parameters of this structure include the following: lattice matched to GaAs for permitting subsequent growth of high-quality GaAs layers, high reflectivity at the band edge of GaAs, transparent to light usable by GaAs solar cell, minimum total thickness, highly conducting, and alternating layers with indices of refraction as different from each other as possible.

A solution to these criteria is a structure consisting of alternating pairs of $Al_xGa_{1-x}As$ (x = 0.10 , 600Å thick) and $Al_xGa_{1-x}As$ (x = 0.85, 700Å thick). For 8 periods (1μm total thickness), a reflectivity at 850nm of 90% is possible; more periods improve performance as shown in Figure 2. A number of such Bragg reflector structures have been grown and characterized. Figure 3 shows the measured reflectance spectrum of one 15-period device grown in our lab by LP-MOCVD. The solid line shows the calculated fit to the data, using only the layer thicknesses as parameters. Figure 4 is a cross-section TEM of the same structure, showing that the interfaces are smooth and abrupt. The position of the reflectance peak is very sensitive to the exact layer thickness, so several structures have been characterized by optical reflectance modelling with the following results: uniformity over a full 2" wafer is typically about 3%, and reproducibility (run-to-run) is better than 2%.

Future Directions

Our continuing research interests include improving the efficiency of GaAs solar cells as well as reducing the defect level of our GaAs-on-Si "substrates". High-efficiency cell studies will include the development of $GaInP_2$ windows and of GaAs-$GaInP_2$ monolithic tandems. GaAs-on-Si material improvements will be accomplished by continued optimization of thermal-annealing. strained-layer, and two-dimensional-nucleation techniques.

Publications

Seri-funded research has resulted in a number of articles being published in the scientific literature over the course of this past year. They are listed below:

"Photoreflectance Study of Gallium Arsenide Grown on Si, "M.Dutta, H. Shen, S.M. Vernon, and T.M. Dixon, Appl. Phys. Lett. 57, 1775 (1990).

"Biaxial and Uniaxial Stress in Gallium Arsenide on Silicon: A Linear Polarized Photoluminescence Study," H. Shen, M. Dutta, D.W. Eckart. K.A. Jones, S.M. Vernon, and T.M. Dixon, J. Appl. Phys. 68, 369 (1990).

"Electrical Properties of Mesa Diodes on Epitaxial GaAs/Si," K.L. Jiao, A.J. Soltyka, W.A. Anderson, and S.M. Vernon, Mat. Res. Soc. Symp. Proc. 160, 481 (1990).

"Lattice-Mismatch Effects in GaAsP/GaAs and GaAs/GaAsP/GaAs Heterostructures," Y.W. Choi, C.R. Wie, and S.M. Vernon, Mat. Res. Soc. Symp. Proc. 160, 789 (1990).

"High-Efficiency $Al_{0.22}Ga_{0.78}As$ Solar Cells Grown by Molecular Beam Epitaxy," M.R. Melloch, S.P. Tobin, C. Bajgar, A. Keshavarzi, T.B. Stellwag, G.B. Lush, M.S. Lundstrom, and K. Emergy, Appl. Phys. Lett. 57, 52-54 (1990).

"Advances in High-Efficiency GaAs Solar Cells," S.P. Tobin, S.M. Vernon, S.J. Wojtczuk, C. Bajgar, M.M. Sanfacon, and T.M. Dixon, Conf. Record of the 21st IEEE Photovoltaic Specialists Conf. - 1990.

"Design of High Efficiency GaAs Solar Cells by Photoluminescence Studies," R.K. Ahrenkiel, D.J. Dunlavy, B. Keyes, S.M. Vernon, S.P. Tobin, and T.M. Dixon, Conf. Record of the 21st IEEE Photovoltaic Specialists Conf. - 1990.

"High-Efficiency GaAs and AlGaAs Solar Cells Grown by Molecular Beam Epitaxy," M.R. Melloch,S.P. Tobin, C. Bajgar, T.B. Stellwag, A. Keshavarzi, and M.S. Lundstrom, Conf. Record of the 21st IEEE Photovoltaic Specialists Conf. - 1990.

"Experimental Study of Solar Cell Performance Versus Dislocation Density," S.M. Vernon, S.P. Tobin, and M.M. Al-Jassim, Conf. Record of the 21st IEEE Photovoltaic Specialists Conf. - 1990.

"Assessment of MOCVD- and MBE-Grown GaAs for High-Efficiency Solar Cell Applications," S.P. Tobin, S.M. Vernon, C. Bajgar, S.J. Wojtczuk, M.R. Melloch, A. Keshavarzi, T.B. Stellwag, S. Venkatensan, M.S. Lundstrom, and K.A. Emery, IEEE Trans. Electron Dev. 37, 469-477 (1990).

"Analysis of AlGaAs/GaAs Solar Cell Structures by Optical Reflectance Spectroscopy," M.M. Sanfacon and S.P. Tobin, IEEE Trans. Electron Dev. 37, 450-454 (1990).

"Correlation of Material Properties and Recombination Losses in $Al_{0.2}Ga_{0.8}As$ Solar Cells," G.B. Lush, T.B. Stellwag, A. Keshavarzi, S. Venkatesan, M.R. Melloch, M.S. Lundstrom, R.F. Pierret, S.P. Tobin, and S.M. Vernon, Solar Cells 27, 363-372 (1989).

"High-Efficiency Heteroepitaxial Solar Cells for Space Power Applications," S.M. Vernon, S.P. Tobin, C.J. Keavney, and S.J. Wojtczuk, Proc. of 24th Intersociety Energy Conversion Engineering Conference, August 1989, pp. 799-803.

"An Approach Toward 25-Percent Efficient GaAs Heteroface Solar Cells," S.A. Ringel, A. Rohatgi, and S.P. Tobin, IEEE Trans. Electron Dev. 36, 1230-1237 (1989).

"Experimental Comparison of Light-Trapping Structures for Silicon Solar Cells," S.P. Tobi, C.J. Keavney, L.M. Geoffroy, and M.M. Sanfacon, Conf. Record of the 20th IEEE Photovolatic Specialists Conf. - 1988. (IEEE, New York), p. 545.

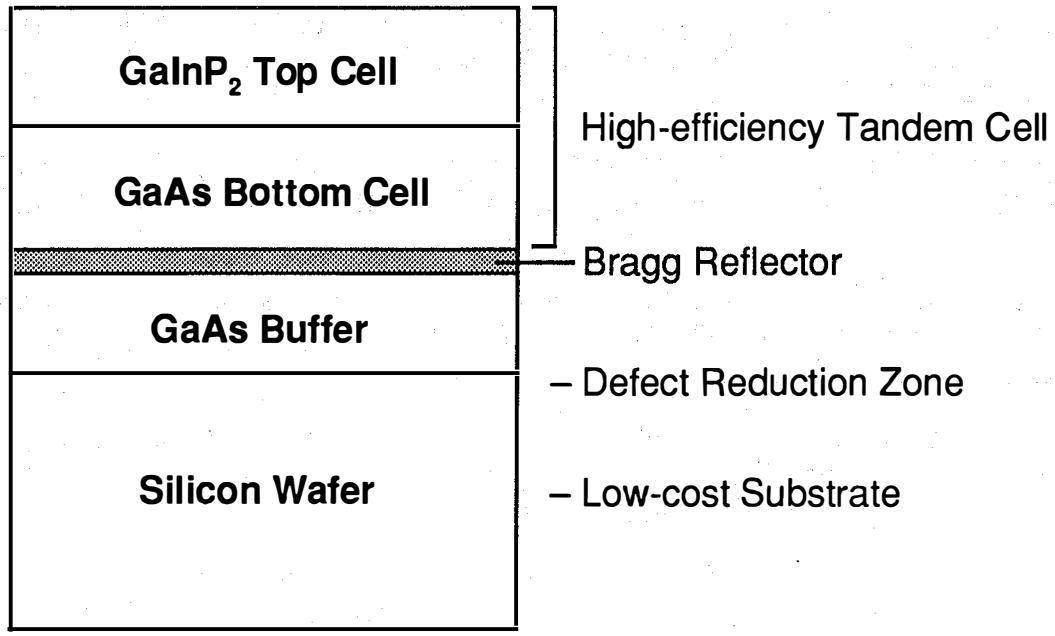

Figure 1: Simplified schematic of the high-efficiency cell structure being developed in this program.

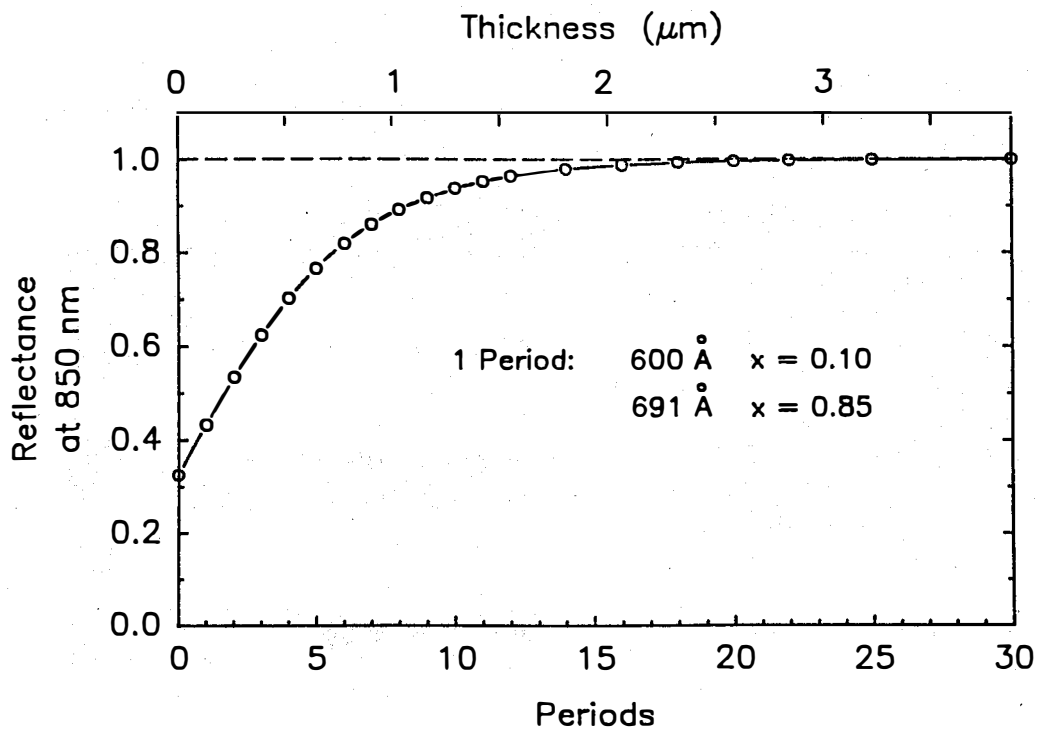

Figure 2: Calculated peak reflectance (at 850nm) versus the number of periods for an $Al_xGa_{1-x}As$ Bragg reflector.

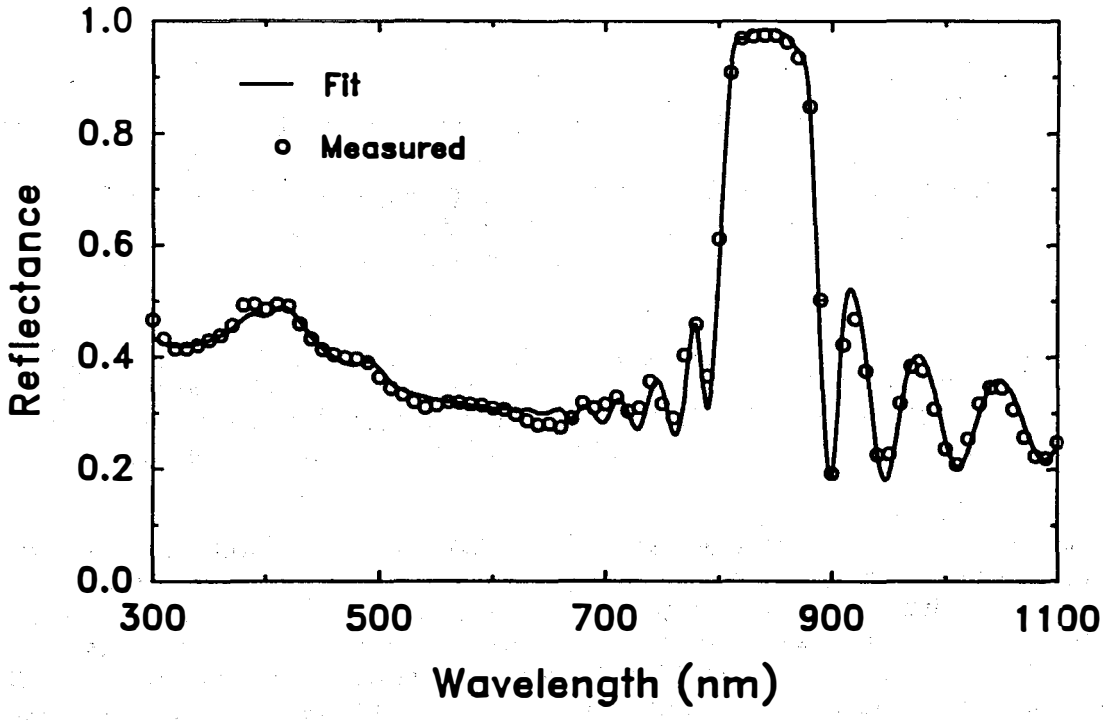

Figure 3: Reflectance versus wavelength for a 15-period $Al_xGa_{1-x}As$ Bragg reflector grown by LP-MOCVD.

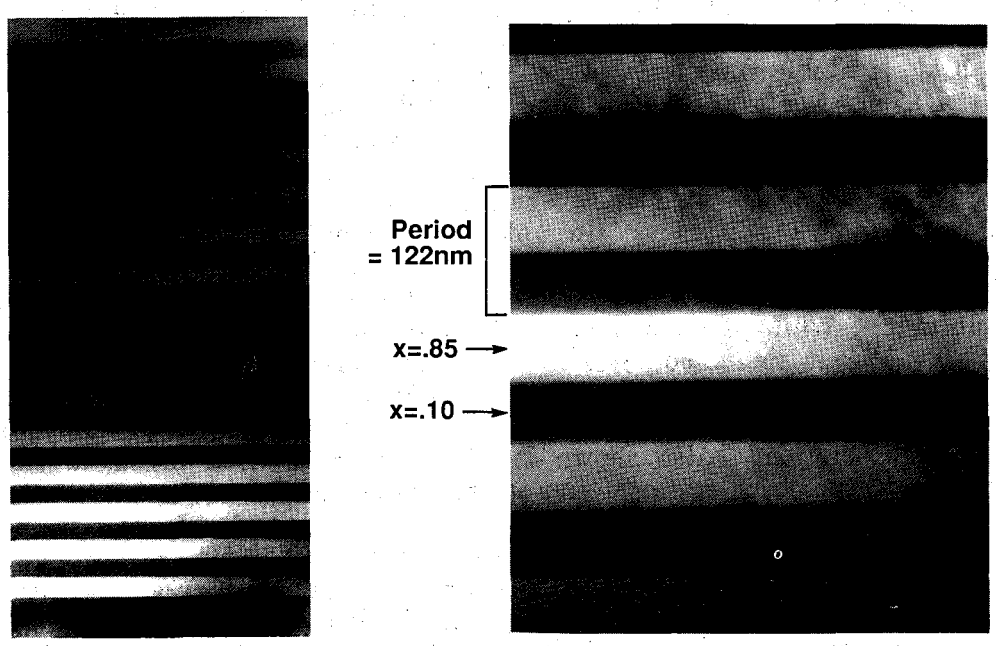

Figure 4: Cross-sectional transmission electron micrograph of a 15-period $Al_xGa_{1-x}As$ Bragg reflector grown by LP-MOCVD

Title: **Advanced High-Efficiency Concentrator Cells**

Organization: Varian Research Center, Palo Alto, California 94303

Contributors: H. F. MacMillan, principal investigator; B-C. Chung, M. S. Kuryla, M. Ladle Ristow, L. D. Partain, J. C. Schultz, G. F. Virshup and J. G. Werthen

The objective of this research program is the development of a multijunction solar cell with a terrestrial power conversion efficiency of 35-40% at solar concentrations of 400 to 1000 AM1.5D. In order to meet the cost goals for utility-scale photovoltaic power systems, the multijunction cells are designed to be monolithic two-terminal cells.

The approach of this cell development effort encompasses the following key features. First, development strategy and device performance evaluation have been guided by our detailed, realistic computer model [1]. The model predicts total cascade and component cell performance parameters from experimentally established input parameters, i.e., materials properties, device structure and operating conditions. Second, the III-V monolithic multijunction cells and interconnect materials are grown by computer-controlled organometallic vapor phase epitaxy on GaAs substrates. Third, the device fabrication utilizes standard wafer processing procedures for metallization and etching, which can be adapted to high-throughput manufacturing. Finally, the development sequence has been to first demonstrate the performance of the component cells and cell interconnects, and then to integrate these into a monolithic multijunction cell, initially for one-sun operation and then for operation under concentrated sunlight. As an important aspect of this strategy, we have also developed high-efficiency single-junction GaAs concentrator cells.

Using the best available materials data, the modeling of a three-junction cascade predicts an efficiency of 46% under high concentration, as shown in Fig. 1. The efficiencies of the AlGaAs, GaAs and InGaAs component cells are 22%, 15% and 9%, respectively. The modeling predicts that a 1.93-eV AlGaAs/GaAs two-junction cascade can achieve close to 35% efficiency, but a third junction will be necessary to approach or exceed 40% efficiency. In order to minimize the problems due to lattice mismatch and to develop this multijunction in stages, we have adapted the structure shown in Fig. 2. The upper 1.93-eV AlGaAs and GaAs cells are grown on one side of the GaAs substrate. While the upper two cells are lattice matched to the substrate, the lower cell is 3% mismatched, which requires development of a high-quality transparent grading layer. The lower 1.0-eV InGaAs cell is grown on the reverse side of the substrate in a second growth step [2]. The substrate is lightly doped to minimize optical absorption. Also shown in Fig. 2 is an Entech prismatic cover slide, which greatly reduces obscuration of the metal interconnect and permits its use up to 100X concentration [3].

During the past year, we have concentrated on the following areas of development: (1) continued growth and fabrication of high-efficiency component cells, 1.93-eV AlGaAs, GaAs and especially 1.0-eV InGaAs; (2) continued growth and fabrication of 1.93-eV AlGaAs/GaAs metal-interconnected cascade cells; and (3) improved manufacturability of GaAs concentrator cells for the purpose of streamlining all of our growth and processing steps for single and multijunction cells.

Summaries of the most significant results of the past year follow.

1. A 1.0-eV InGaAs cell has been fabricated on the reverse side of a low-doped GaAs substrate with a one-sun efficiency of 2.5% AM1.5D. The spectral response and cell performance parameters at one sun are shown in Fig. 3. Testing has not been done under concentrated sunlight, but open-circuit voltage and fill factor are expected to increase significantly with high photo-injection. The most significant aspect of the latest results is that the spectral response has been increased sufficiently that the lower cell is able to current match the upper 1.93-eV AlGaAs and middle GaAs cells for the first time. The highest photocurrent achieved thus far in a cascade of the upper two junctions is 13.8 mA/cm^2 [4]. The improved spectral response has been accomplished by utilizing a n-i-p structure in the InGaAs cell wherein photogenerated carrier drift in the intrinsic region overcomes the defect-reduced diffusion lengths in lattice-mismatched material.

2. Small-scale manufacturing of GaAs p/n concentrator cells has been attempted with excellent yield of high-efficiency cells. Cell structures were grown on two different OMVPE reactors and processed with an all-evaporated thick metallization to reduce front gridline obscuration below 5% [5]. Efficiency histograms of all the fabricated cells are shown in Fig. 4. The results imply that approximately 90% of all cells fabricated have efficiencies of 24 to 26% under concentrated sunlight. Minor improvements in the antireflection coating process, which was plagued with problems during this effort, should raise the efficiencies to the 26 to 28% range.

In preceding years, the focus has been on developing component and cascade cells for one-sun operation. In future work, the emphasis will be on integrating the components for operation at 100X and then higher concentrations. The potential for using Ge substrates for GaAs and AlGaAs/GaAs multijunction concentrator cells will also be developed. Portions of this work were supported by the Air Force Wright Aeronautical Laboratories.

References

1. H. C. Hamaker, J. Appl. Phys. **58**, 2344 (1985).
2. S. Kamath and R. Loo at Hughes Research Laboratories first proposed the idea of placing the lattice-mismatched InGaAs on the reverse side of the substrate.
3. Prismatic cover slide developed by Entech, Inc., Dallas/Fort Worth Airport, TX.
4. B-C. Chung et al., Appl. Phys. Lett. **55**, 15 (1989).
5. M. Ladle Ristow et al., "Aluminum Metallizaions for p/n GaAs Solar Cells", 21st IEEE Photovoltaic Specialists Conference, Orlando, FL (May 1990).

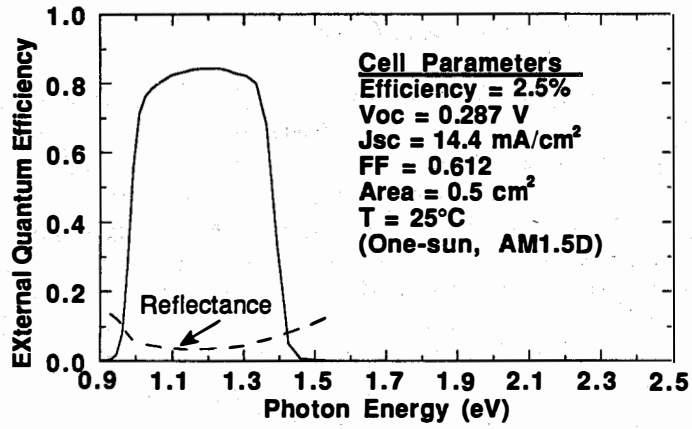

Fig. 3 Spectral response and cell performance parameters for 1.0-eV InGaAs cell on reverse side of GaAs substrate.

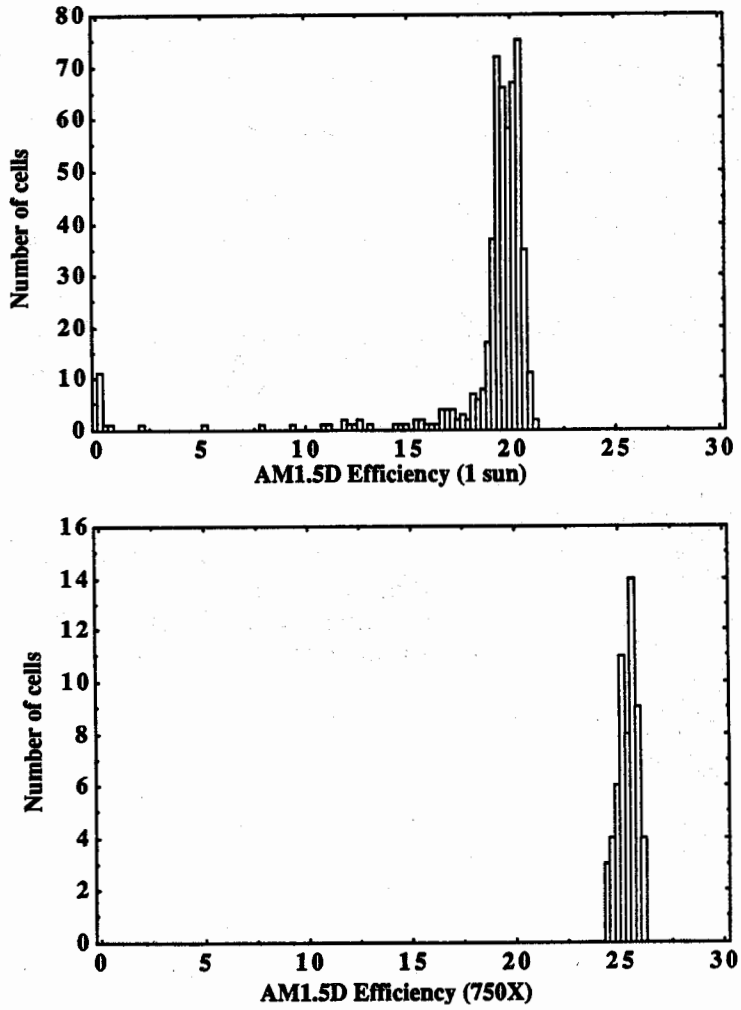

Fig. 4 Efficiency histograms of GaAs p/n concentrator cells. Upper 1-sun histogram is for all 516 cells fabricated from 14 wafers. Lower histogram is for 59 cells chosen randomly from the 19-21% range of 1-sun results and flash tested at 750X, 25°C.

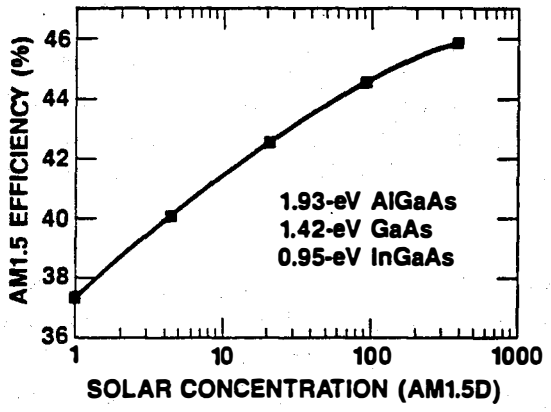

Fig. 1 Predicted efficiency of 1.93-eV AlGaAs-GaAs/0.95-eV InGaAs two-terminal cascade cell under concentrated terrestrial sunlight (25°C).

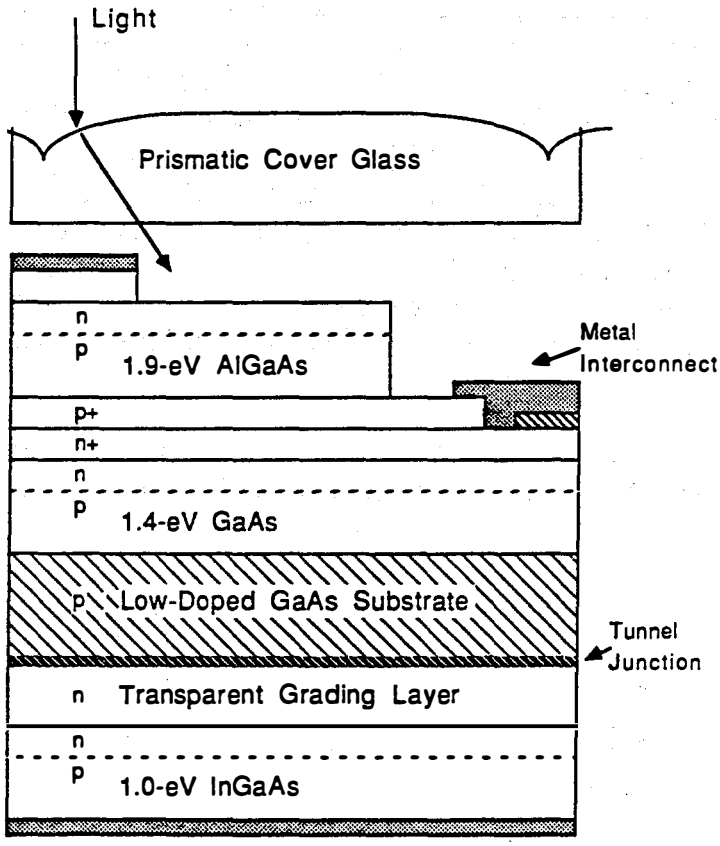

Fig. 2 Three-junction, two-terminal cascade cell structure.

6.0 NEW IDEAS FOR PHOTOVOLTAIC CONVERSION PROGRAM

Richard Mitchell[a], (Manager)

The objective of the New Ideas Task is to identify new photovoltaic materials, device configurations, and concepts and to conduct preliminary research and development in the areas that show the most promise. Subcontracted research in this task that shows significant potential is transferred into the appropriate major task area within the DOE Photovoltaic Program for continued support.

The New Ideas Task issues public solicitations for new and innovative research ideas that are relevant under the DOE National PV Program guidelines to perform high-risk, long-term, and potentially high-payoff research and development. These solicitations for new and innovative research ideas are submitted by universities, business, and nonprofit organizations. Subcontracts are awarded to study the most promising concepts associated with these solicitations. These subcontracts are reviewed, and successful concepts are selected for renewal with a second year of funding.

During FY 1990 work was concluded on these concepts: the avalanche heterostructure and superlattice solar cell developed by Georgia Tech Research Institute; the low-cost techniques for producing CdZnTe devices for cascade cell applications, researched by International Solar Electric Technology; and hydrogen radical enhanced growth of solar cells, at Rensselaer Polytechnic Institute. Also in FY 1990, three new subcontract awards were initiated: novel ways of depositing ZnTe films by solution, researched by the Institute of Energy Conversion (IEC) at the University of Maryland; development of an inverted AlGaAs/GaAs patterned tunnel junction cascade concentrator cell, at the Research Triangle Institute (RTI), and; development of high efficiency epitaxial optical reflector cells, at the University of Southern California (USC). These awards were based on the FY 1988 solicitation for New Ideas for Photovoltaic Conversion. That solicitation received almost 100 responses to the request for letters of interest (LOI). Evaluation of those LOI responses had identified several promising concepts for further evaluation, and during FY 1989, expanded proposals from 24 LOI finalists were evaluated and the three above awards were funded in FY 1990.

The ongoing New Ideas subcontracts will be reviewed in FY 1991 for a potential second year of funding. Additionally in FY 1991, another LOI solicitation is planned for FY 1992 awards, based on DOE approval.

[a]FY 1991 -- Thomas S. Basso (Manager)

Title: **The Avalanche Heterostructure and Superlattice Solar Cell**

Organization: Physical Sciences Laboratory, Georgia Tech Research Institute, Atlanta, Georgia

Contributors: C. J. Summers, A. Rohatgi, A. Torabi, D. Rajavel, B. K. Wagner, and R. G. Benz II

Introduction:

The objective of this program was to assess the potential of new material structures for enhanced solar cell performance, and to develop the technology of semiconductor material systems for testing these concepts. Device structures studied include the avalanche heterostructure and variably spaced superlattice photovoltaic device[1], modulation doped (nipi) superlattices[2] and heterointerface GaAs solar cells.[3] Although these concepts have been tested in the AlGaInAs system they ideally require the range of bandgap energies that can only be achieved under lattice-matched conditions in the HgCdTe and closely related alloy systems. A chemical beam epitaxy system was, therefore, developed to grow advanced material structures in these alloys. Recent progress in new solar device designs and materials growth are described below.

Device Modeling Studies:

During this and related programs computer models were developed for the structures described above. In this phase of the program considerable progress was made in developing new injector designs for the variably spaced superlattice photovoltaic device and the heterointerface solar cell.

The GaAs solar cell investigated in this study is a p-n heterointerface design which utilizes a two-step n-type GaAs base with back-surface AlGaAs passivation.[3] This design was chosen to optimize the tradeoff between the absorption of incident photons in the base and the subsequent collection of the photogenerated carriers by the p-n junction. Model calculations show that in a conventional cell an L_D/W (diffusion length, base width ratio) of at least 3 is necessary to collect all on the photogenerated carriers. Thus for a base width of 3 um, which is required to insure ~97% absorption within a cell using a 0.5 um emitter, a diffusion length of ~9 um is required. This is unrealistically high for the doping levels of interest in GaAs solar cells. The advantage of the two-step base design is that it allows maximum carrier collection for the lower-doped thin top base layer (which is where most of the absorption below the emitter occurs) by increasing the L_D/W ratio, and then utilizes the doping step as a back-surface-field enhancement. This more than offsets the decrease of both J_{SC} and V_{OC} resulting from greater carrier collection and lower saturation current, respectively. Thus, a

higher cell efficiency is predicted compared to uniformly-doped conventional base designs.

Model calculations predict that this cell design could achieve cell efficiencies as high as 25%. A schematic of the structure is shown in Figure 1. The range of base thicknesses was chosen to allow the base width to be as thick as possible without allowing L_D/W to fall below ~3 to maximize both absorption and collection in this region. The doping was varied to investigate the tradeoff between enhanced collection due to the back-surface-field effect as the doping is decreased, and lower saturation currents as the doping is increased. Therefore, the cell configurations investigated to optimize the efficiency of the concept included variations in the widths of the active n^--, and n^+-regions, and also slight changes in their doping levels. Because these cell designs require accurate doping of the n- and p-type contact regions and precise control of the thickness and alloy concentration of each layer they were grown by MBE and later fabricated into 1 cm square solar cells. Preliminary evaluations show that the best cells have very high open circuit voltages (0.977 0.997 V) and an overall efficiency of 14%. No anti-reflection coatings were used in this study, which are estimated to increase the total efficiency to ~20%. In fact by obtaining optimum valves for the open circuit voltage, V_{OC}, short circuit current, J_{SC}, and the fill factor, FF, efficiencies approaching or exceeding the best published valves for a single junction GaAs cell are predicted. These results, strongly suggest that with slight variations in design and improved fabrication, the theoretical goal of a 25% efficient GaAs solar cell is possible.

For the variably spaced superlattice photovoltaic cell injector energies of ~1 eV are required. We have, therefore, studied resonant tunneling in AlAs/GaAs VSSEF structures where the conduction band off-set between the Γ_1 -points for AlAs and GaAs is ~ 1.0 eV. For AlAs barriers less than 23Å in thickness, electron scattering into the lower-energy X-point in the barrier has been inferred to be small from photoluminescence studies. If this result also applies to resonant tunneling electrons, then higher electron injection energies can be obtained. Calculations have been performed for 1-, 2- and 3-well AlAs/GaAs VSSEF structures designed for injection energies of 0.5 and 0.8 eV. As shown in Figure 2 for the three-well 0.5eV injector the calculated transmittance for low incident electron energies is very high and drops rapidly at higher energies, or voltages. Similar results were also obtained for the 0.8 eV injector, but the cut-off characteristics are not so abrupt because the quantum states are higher in the well where the wavefunctions spread further into the barriers and provide more interaction between the quantum states. This interaction and the stronger dependence of the confined energy states on well width makes it more difficult to achieve close alignment between the QW states and, therefore, to obtain a very high peak transmission features.

These calculations were confirmed experimentally. As shown in

Figure 3 the 3-well 4-barrier structure exhibited a well pronounced tunneling resonance at 0.6 V when forward biased. This is in very good agreement with the theoretical curve shown in Figure 2. Also the peak resonant tunneling current was equal to other single- and multiple-well devices investigated in previous studies which suggests that the tunneling efficiency is high. For the 0.8 eV injection devices no clear resonant tunneling feature was observed which is in agreement with the calculated transmission curves. To achieve similar results slightly thicker AlAs barriers and longer devices are being investigated.

Material Growth Studies:

During this phase of the program the CBE system described previously for HgCdTe growth was completed and characterized for CdTe, HgTe, and HgCdTe growth.[1-6] As shown schematically in Figure 4 the system has operational gas sources for the host elements tellurium, cadmium and zinc, and also arsenic and iodine for p- and n-type doping.[7] Mercury flux was provided by a Hg-Pressure Controlled Vapor Source (Hg-PCVS) reported previously and solid sources of Cd, Te, Zn and CdTe are available for MBE growth. For CdTe and HgCdTe growth, the diisopropyltelluride (DipTe) and diethylcadmium (DeCd) flow rates were controlled by MKS Instruments 1150B pressure flow controllers, which do not require the use of carrier gases. The DeCd and DipTe were then directly injected into group II or group VI gas injectors, respectively, where they were cracked and directed onto the substrate.

Analysis of the cracking efficiency of the group II and VI injectors showed that DeCd was completely cracked to Cd at 500°C for flow rates up to 5 sccm. In contrast, as shown in Figure 5, for injector temperatures above 700°C the cracking efficiency of DipTe into monomer Te was ~ 80% at low flow rates, but dropped to 50% at the highest flow rate of 6 sccm.[7] Fortunately, for growth rates < 1μm the Te-flux is below the 2 sccm range and thus most of the alloys were grown with a high percentage of monomer Te.

Using this system epitaxial layers of CdTe, HgTe, and HgCdTe were grown on (001)-oriented CdTe, ZnCdTe and GaAs substrates using CdTe buffer layers either deposited by CBE or from the binary CdTe source. The Hg-based layers were grown at a substrate temperature of 165-185°C and the CdTe layers between 185-320°C. Substrate surface temperatures below 230°C were calibrated by the Te-condensation technique.[8] Growth rates for all layers were ~0.5-0.6 μm/m and layer thickness varied from 2-6 μm. The Hg-based materials were capped by a thin CdTe layer to prevent surface degradation.

The CdTe layers grown by CBE were examined by photoluminescence and showed strong bound exciton emission lines with LO-phonon replicas at lower energies. Both the PL and electrical data depended strongly on the Cd/Te ratio as expected from its influence on crystal stoichiometry. These effects are currently being examined in conjunction with the doping studies. The HgTe layers showed no

twinning from RHEED studies and were specular to the eye, although slight surface texturing was observed by optical microscopy.

Figure 6 shows a plot of Hall mobility versus temperature for two HgTe layers. The CBE grown layer has a peak mobility of 109,000 cm^2/Vs at 24K and compares well with the highest values quoted by Feldman et al.[9] The MBE grown layer had a peak mobility of 54,000 cm^2/Vs, and was the highest mobility obtained for a MBE HgTe layer grown in the system, although no efforts were made to optimize the layers. These results illustrate the benefits of precise flux control and monomer Te for growing high mobility HgTe layers.

HgCdTe layers have also been grown by CBE. RHEED analysis confirmed the absence of twinning for layers grown under the proper flux and substrate temperature conditions. Evaluations of the optical and electrical properties of the HgCdTe layers indicate that x-values between 0.16 and 0.35 have been grown. For the best samples low-temperature electron concentrations between 3×10^{14} and 1×10^{15} cm^{-3} were obtained with peak mobility values has high as 3.2×10^5 cm^2/Vs. These values were obtained on unannealed samples and are very competitive with published MBE results.

Conclusions:

In this explority program new heterointerface GaAs solar cell designs were grown, fabricated and demonstrated to have the potential for producing energy conversion efficiencies greater than 20%. An investigation of AlAs/GaAs variably spaced superlattice structures also showed their effectiveness as high-energy (0.5 - 0.8 eV) injectors with potential applications in avalanche heterostructure solar cells and high-speed transistors. The development of a chemical beam epitaxial system for growing advanced material structures in the HgCdZnTe alloy system was completed and high quality CdTe, HgTe, and HgCdTe layers were successfully grown.

References:

1. T.P. Pearsall, Electronics Lett. 18, 1982, p. 512.
2. G.H. Dolher, Phys. Stat. Sol. (b) 52, 1972, p. 79.
3. S.A. Ringel, A. Rohatgi and Tobin, S.P., IEEE Trans. Elect. Devices 36, 1989, p. 1230.
4. C.J. Summers, R.G. Benz II, B.K. Wagner, J.D. Benson and D. Rajavel, SPIE 1106, 1989, p. 2.
5. B.K. Wagner, R.G. Benz II and C.J. Summers, J. Vac. Sci & Technol. A7, 1988, p. 295.
6. R.G. Benz II, B.K. Wagner, and C.J. Summers, J. Vac. Sci. Technol. A8, 1990, 1020.
7. R.G. Benz II, B.K. Wagner, D. Rajavel and C.J. Summers, Proc. of Sixth Int. Conf. on MBE, La Jolla, CA, 26-31 August, 1990.
8. D. Rajavel, F. Mueller, J.D. Benson, B.K. Wagner, R.G. Benz II and C.J. Summers, J. Vac. Sci. Technol. B8, 1990, 192.
9. R.D. Feldman, M. Oron, R.E. Austin and R.L. Opila, J. Appl. Phy. 63, 1988, 2872.

1.	p^+- GaAs; d = 0.3μm; p = $3\times10^{19}cm^{-3}$
2.	p^+ $Al_{0.9}Ga_{0.1}As$, d = 0.04μm, p = $1\times10^{18}cm^{-3}$
3.	p^+- GaAs; d = 0.5μm; n = $2\times10^{18}cm^{-3}$
4.	n- GaAs
5.	n- GaAs
6.	n^+- $Al_{0.2}Ga_{0.8}As$; d = 0.2μm; n = $1\times10^{18}cm^{-3}$
7.	n^+- buffer GaAs; d = 0.2μm; n = $2\times10^{18}cm^{-3}$
8.	n^+- substrate GaAs

Figure 1. Heterointerface GaAs Solar Cell Design.

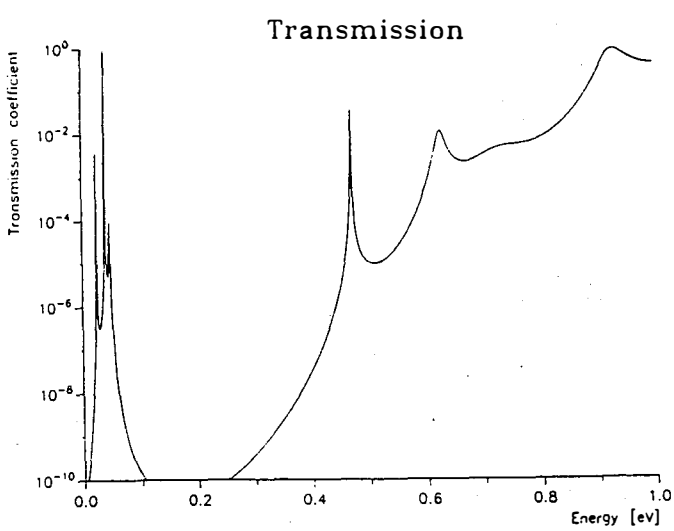

Figure 2. Calculated Transmissivity of three-well 0.5eV AlAs/GaAs VSSEF structure.

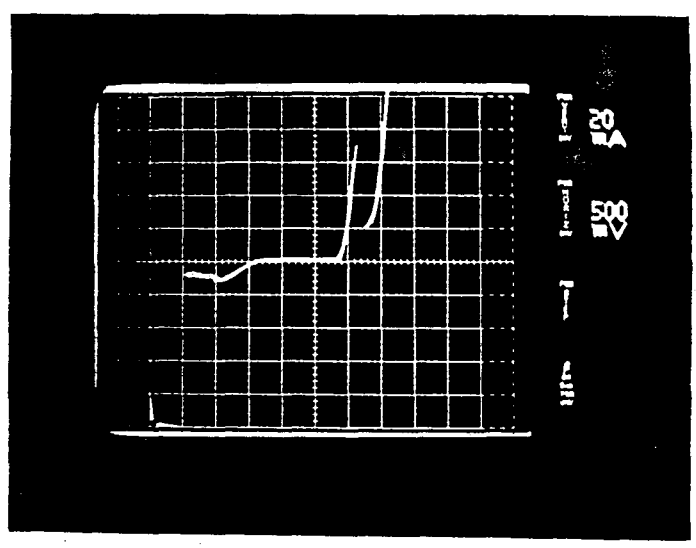

Figure 3. I-V Characteristics at 77k of three-well 0.5eV AlAs/GaAs VSSEF structure.

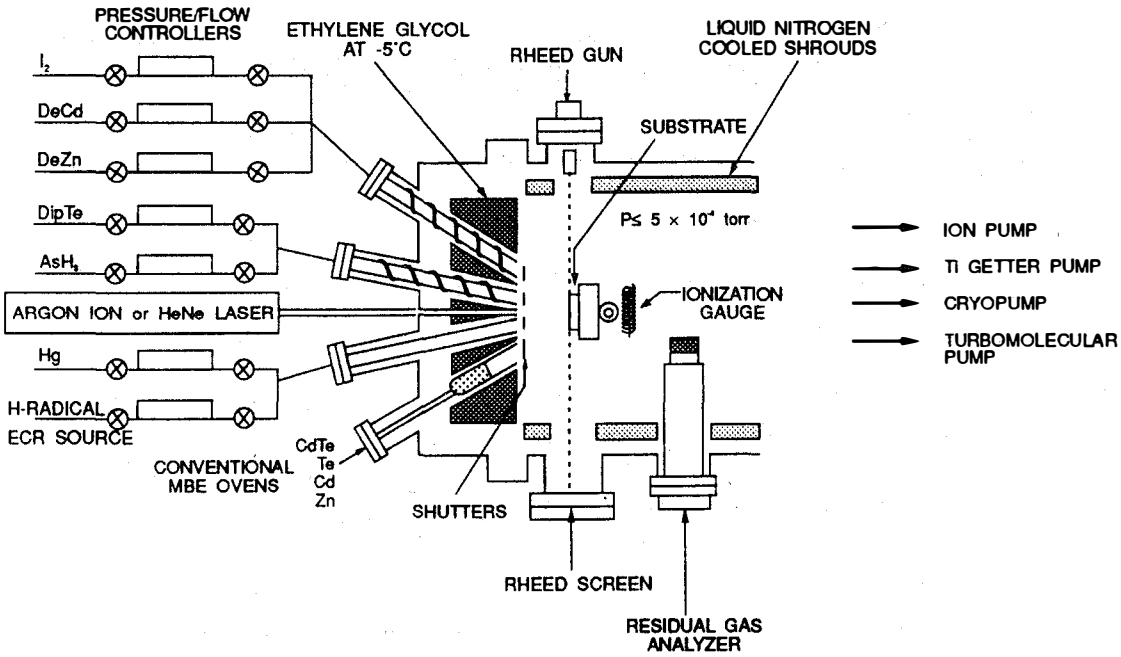

Figure 4. Schematic of Chemical Beam Epitaxy Systems.

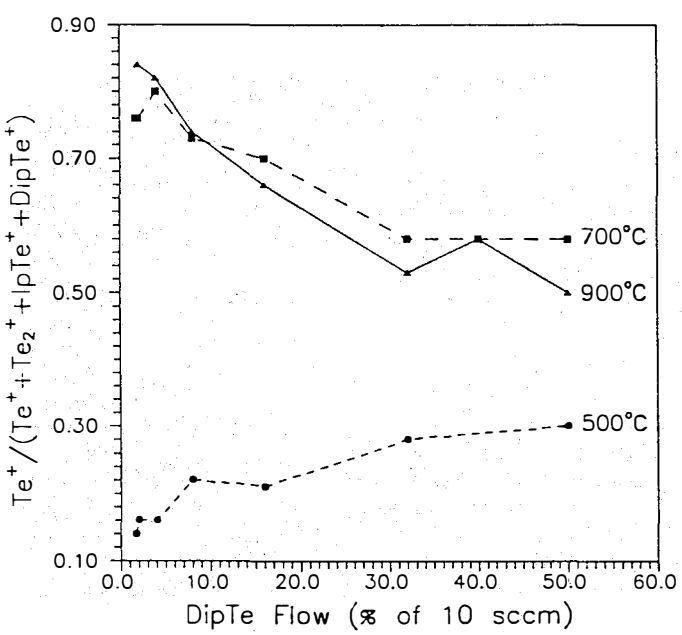

Figure 5. Monomer Te Production Ratio Versus DipTe Flow as Function of Injector Temperature.

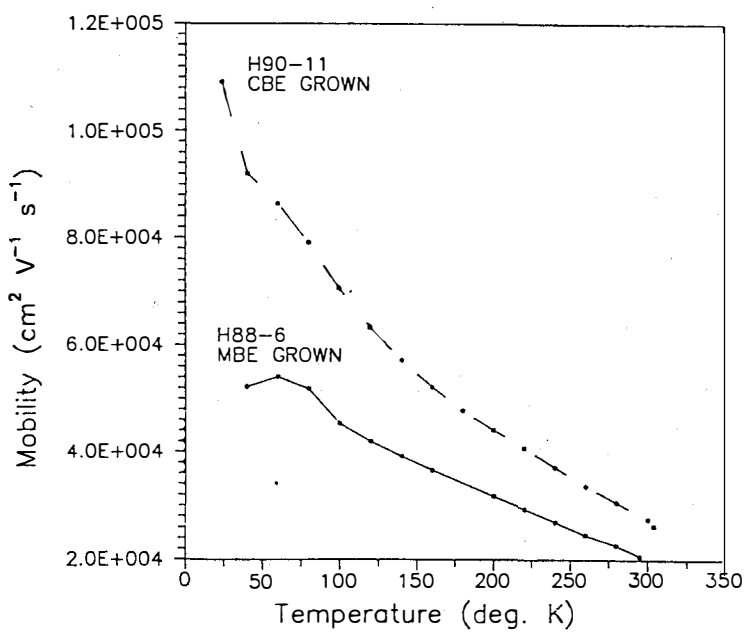

Figure 6. Hall Mobilities Versus Temperature for MBE and CBE Grown HgTe Layers.

Title : **Novel Ways of Depositing ZnTe Films by a Solution Growth Technique**

Organization: Institute of Energy Conversion
University of Delaware
Newark, Delaware 19716

Contributors: Robert W. Birkmire, Principal Investigator; Anup Mondal and Tracey Yokimcus, Research Contributors

Objectives

The objective of the research is to develop a low temperature process using solution growth techniques to deposit thin (<500Å) ZnTe films suitable as a transparent ohmic contact for CdS/CdTe solar cells.

Technical Approach

Methods for depositing ZnTe films from aqueous solution that were investigated included: ion exchange reaction between Zn^{+2} ions and CdTe; reaction of Zn^{+2} with modified Te rich CdTe surfaces and galvanic deposition. The structural, optical and electrical properties of the ZnTe films are characterized using established techniques of x-ray diffraction, four-point probe and total reflection and transmission measurements. CdS/CdTe/ZnTe solar cells are fabricated to characterize the contact properties of the ZnTe films on working devices. Properties of devices using the ZnTe contact are compared to devices using Au or Cu/ITO as the CdTe contact.

Significant Results

Uniform films of ZnTe have been deposited on 7059 glass/ITO/CdS/CdTe substrates using an electrochemical method. The approach has the advantage of simplicity in that it does not require instrumentation for external potentiostatic or galvanostatic control and is based on short-circuiting the substrate to an easily oxidizable electrode (e.g. Zn).

The electrolytic bath contained $1x10^{-1}$M $ZnCl_2$ and approximately $10x10^{-4}$M TeO_2 dissolved in NaOH. The pH of the solution was adjusted to 3-4 using dilute HCl and the bath temperature was 50-60°C during the deposition. A 7059 glass/ITO/CdS/CdTe substrate and a zinc strip were then dipped into the solution, and connected externally through a metal wire. The Zn is electropositive and goes into solution as Zn^{+2} ions:

$$Zn \rightarrow Zn^{2+} + 2e^{-}.$$

The electrons travel through the metal wire to the substrate and reduce the Zn^{+2} and Te^{+4} ions to form ZnTe on the CdTe surface. The Zn strip thus acts both as a source of Zn as well as of electrons for the cathodic deposition reaction. Figure 1 shows the thickness of the ZnTe film as a function of time on a 7059/ITO/CdS/CdTe substrate. A linear growth rate is observed until about 1

hour of deposition after which it tends to saturate due to the depletion of the Te^{+4} ions in solution.

Controlling both the pH and Te^{+4} ion concentration in the solution are vital for the formation of the ZnTe films. A pH range of 3 to 4 and a Te concentration of 10^{-4}M or less resulted in uniform film growth. At lower pH, free Te tends to deposit and above pH=5, the solution turns cloudy, probably due to the formation of $Zn(OH)_2$. Increasing the Te^{+4} ion concentration in solution increases the deposition rate, however again, Te was found to deposit instead of ZnTe. The X-ray diffraction pattern of a ZnTe film deposited on 7059/ITO/CdS/CdTe shows a sharp (111) peak at 2θ=25.19°, which establishes formation of a highly oriented ZnTe film.

CdTe cells with the ZnTe contact were made by first coating the 7059/ITO/CdS/CdTe sample with $CdCl_2$ and heating at 400°C in air for 30 minutes. The ZnTe film was then deposited followed by a Cu/Au contact. The device was optimized with a 150°C air heat treatment and a Br_2-MeOH dip. The I-V characteristic of the best CdS/CdTe/ZnTe cell are shown in Figure 2. The cell has an efficiency of 6.5% with a fill factor of ~52%. This is an extremely encouraging result since the ZnTe was not doped with Cu. Methods for doping the ZnTe with Cu are currently being developed.

Conclusion

An electrochemical method has been developed to deposit ZnTe on CdTe. The film deposition depends on the pH of the solution and the concentration of the Te^{+4} ions. A 7059/ITO/CdS/CdTe/ZnTe/Cu/Au solar cell with efficiencies over 6% was achieved using undoped ZnTe as the contact to the CdTe. Future work will focus on doping the ZnTe p-type with Cu and optimization of the ZnTe contact in high efficiency CdTe solar cells. The approach is also being extended to deposition of ZnSe on $CuInSe_2$.

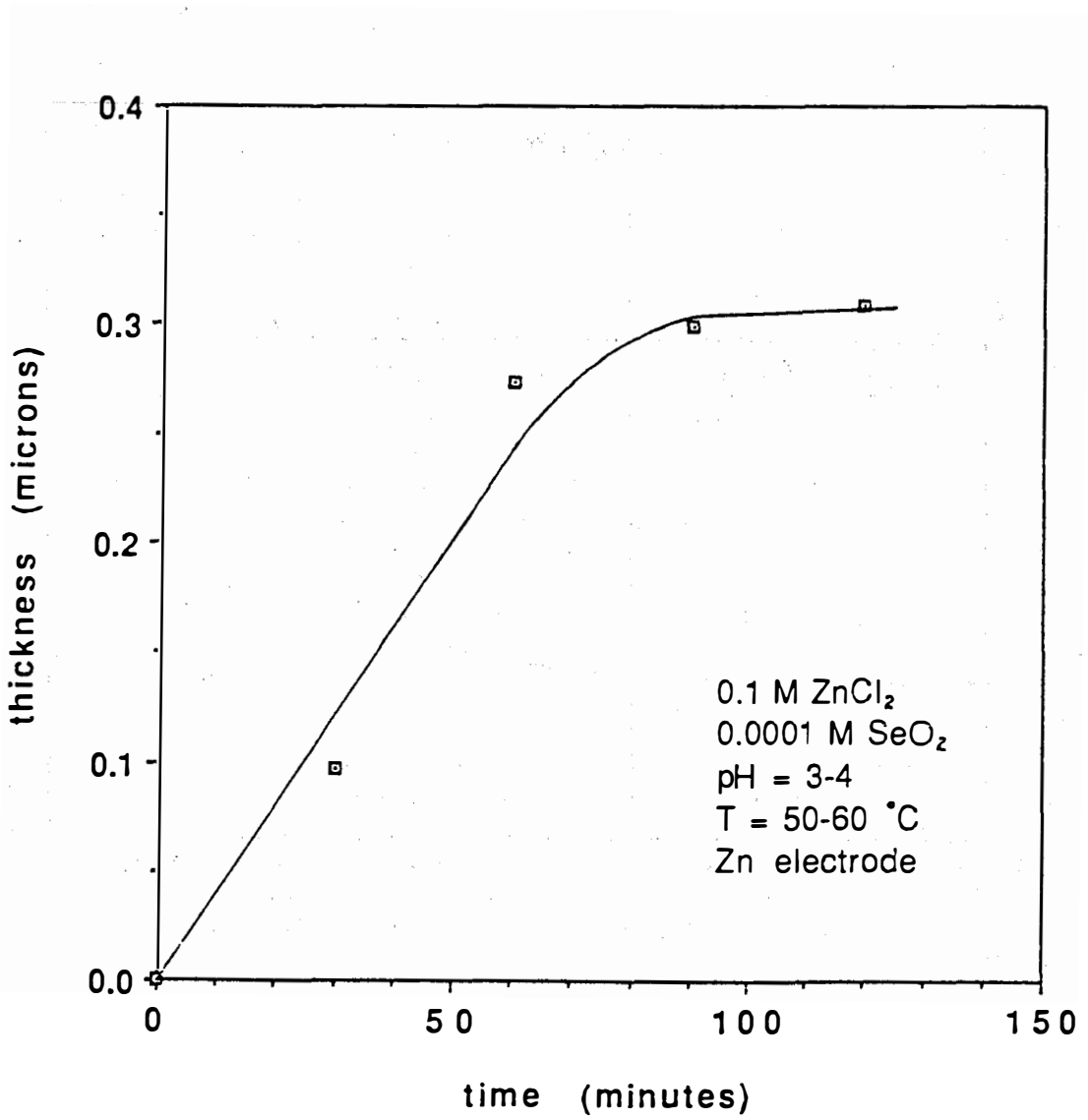

Figure 1. Thickness of ZnTe film grown on a 7059/ITO/CdS/CdTe substrate as a function of time.

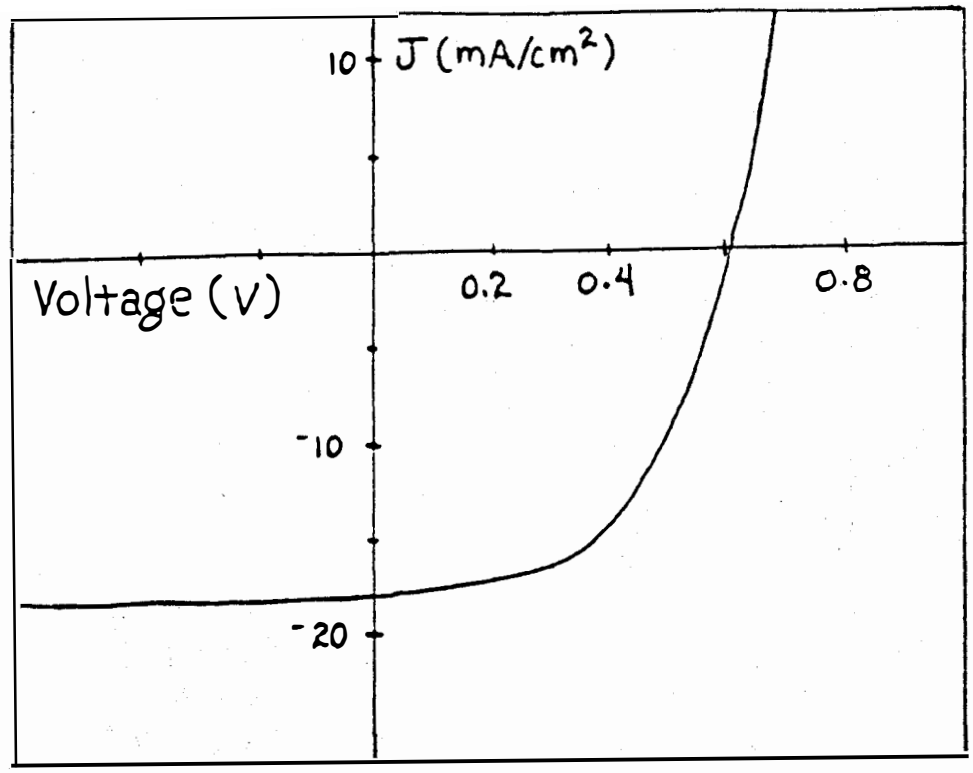

Figure 2. I-V characteristics of the best CdS/CdTe/ZnTe cell.

Title: **Low Cost Technique for Producing CdZnTe Devices for Cascade Cell Application**

Organization: International Solar Electric Technology (ISET), 8635 Aviation Blvd., Inglewood, CA 90301

Contributors: B.M. Basol, principal investigator; and V.K. Kapur

The objective of this program is to develop a two-stage process for the fabrication of large bandgap, transparent $Cd_{1-x}Zn_xTe$ (CdZnTe) solar cells for cascade cell application. The two-stage process consists of depositing elemental layers of Cd, Zn and Te on a substrate and then reacting these elemental layers to form the compound. During the first year of this program we had successfully demonstrated the use of the electroplating techniques for elemental layer deposition. During this period we concentrated on the evaporated Cd,Zn and Te layers.

Film Growth

ITO coated glass and CdS/ITO/glass substrates were used in this work. CdS films were chemically deposited on the ITO layers and they were typically 0.1-0.2 um thick. Layers of Te, Cd and Zn were sequentially deposited onto selected substrates by vacuum evaporation. The thicknesses of these layers were adjusted to yield the compound film of desired stoichiometry. The relationships between the thicknesses of the elemental layers and the resulting compound films after the reaction step are as follows:

a) A 100 Å thick Cd layer reacting with a 157 Å thick Te film is expected to yield a 298 Å thick layer of CdTe.
b) A 100 Å thick Zn layer reacting with a 223 Å thick Te film is expected to yield a 331 Å thick layer of ZnTe.
c) In a $Cd_{1-x}Zn_xTe$ alloy film the composition parameter, x, is related to the individual thicknesses of the CdTe (t_{CdTe}) and the ZnTe (t_{ZnTe}) components of the film by the equation,

$$t_{CdTe}/t_{ZnTe}=1.27\ (1-x)^{-1}x$$

where t_{CdTe} and t_{ZnTe} can be calculated using the relationships given in a) and b).

The reaction of the Te, Cd and Zn layers was carried out in a tube furnace. Reaction temperatures varied from 350 to 600 °C with reaction times changing from 15 minutes to 2 hours.

Device Processing

The device processing steps included; the deposition of Te, Cd

and Zn layers over CdS/ITO/glass substrates, the reaction of these layers to form CdZnTe, and the completion of the devices by evaporating gold contacts after a mild Br-methanol etch. Some of the films were annealed in air at 400 °C before the etching and contact evaporation steps.

Results

CdTe Films

CdTe films obtained by reacting evaporated Cd and Te layers were shiny, adherent and compact on both ITO/glass and CdS/ITO/glass substrates. Auger depth profile of a 0.8 um thick CdTe film grown on a CdS/ITO/glass substrate at 500 °C is shown in Fig. 1. It is observed that the distribution of Cd and Te through this film is quite uniform except for the oxidized surface region which is estimated to be less than 500 Å thick. The CdTe/CdS interface is clearly marked by a sharp sulfur peak in Fig.1. This is due to the fact that the Te film deposited directly over the CdS layer does not react with CdS. The reaction of elemental layers of Te and Cd, on the other hand, does get initiated for temperatures higher than 350 °C.

CdTe Devices

Solar cells were fabricated by evaporating gold contacts over CdTe films grown on CdS/ITO/glass substrates. Devices made on as-deposited films yielded low current density values (1.0-2.0 mA/cm^2) and low open circuit voltages (0.3-0.4 V). Spectral response measurements made on these cells revealed that they were Au/CdTe Schottky barriers rather than the intended CdTe/CdS heterojunctions. Curve A in Fig. 2 shows the spectral response data taken through the glass substrate of such a device. It is clear from the high long-wavelength response that the carrier collection in this cell takes place at the Au/CdTe interface.

This finding is similar to the results previously reported on electrodeposited CdTe solar cells. In the electrodeposited CdTe device fabrication process, a "type-conversion, junction-formation" step was developed that involved heat treatment of the as-deposited n-type CdTe films at around 400 °C in air. This annealing step was shown to convert the n-CdTe films into high resistivity p-type material, and thus allow fabrication of high efficiency CdTe/CdS solar cells. We have applied the same approach to the CdTe films of the present work. Curve B of Fig. 2 shows the spectral response data for a Au/CdTe/CdS device fabricated on a CdTe film which was annealed in air for 15 minutes at 400 °C. It is observed that, as a result of the annealing step, the rectifying junction of the device has moved from the Au/CdTe interface to the CdTe/CdS interface. The short circuit current density and the open circuit voltage values of the device have also improved. By using this approach and

optimizing the heat treatment step, we fabricated cells with J_{sc} and V_{oc} values as high as 15 mA/cm^2 and 0.65 V respectively.

CdZnTe Films and Devices

Fabrication steps for the CdTe/CdS devices could not be directly applied to the CdZnTe cells. Presence of a strong reducing agent, Zn, in the CdZnTe films changed the nature of the CdZnTe/CdS interface and also caused compositional non-uniformities in the annealed films.

Unlike the relatively sharp CdTe/CdS interface, the nature of the CdZnTe/CdS interface was found to depend on the composition, x. Higher values of x promoted more intermixing between the CdZnTe and the CdS layers during the reaction step. Fig. 3 is an Auger depth profile of a CdZnTe/CdS/ITO structure that was heat treated in air at 400 °C after the reaction step which was carried out in nitrogen at 500 °C. The intended x value for this $Cd_{1-x}Zn_xTe$ film was 0.3. The following observations can be made from the Auger data of Fig. 3:

a) Zn distribution through the film is non-uniform. A high concentration of Zn and O is observed within the top 2000 Å thick surface layer.

b) CdZnTe/CdS interface is highly diffused compared to the CdTe/CdS interface of Fig. 1. A Zn peak is also observed near the ITO contact.

The diffused CdZnTe/CdS interface and the Zn pile-up near the ITO surface are due to the exchange reaction between the CdS film and Zn. Zn, being a strong reducing agent, replaces Cd in the CdS layer at the elevated growth temperatures. As a result of this reaction the sharp interface observed between the CdTe layer and the CdS film of a CdTe/CdS structure is lost in a CdZnTe/CdS junction.

Efficient CdZnTe/CdS solar cells could not be fabricated using films with x>0.25. The main reason for this was the reaction of Zn with CdS giving rise to a highly diffused CdZnTe/CdS interface and poor morphology. Devices made on films with x<0.2 yielded efficiency values of 3-4%.

Conclusions

A two-stage process has been successfully developed and used to grow CdZnTe films of all stoichiometries on inert substrates. There are two key processing steps for CdZnTe device fabrication. The first step is the deposition of a CdZnTe film over a CdS coated transparent substrate. The CdS layer in such a structure needs to be thin (ideally <1000 Å) to maximize the J_{sc} values. Thin CdS films, on the other hand, get reduced by Zn, a strong reducing agent, during the high temperature growth process. This

difficulty may be somewhat alleviated by replacing the thin CdS window layer of the present device structure with a thicker and more transparent CdZnS film. The second step in the fabrication process for a CdZnTe/CdS device is the "type-conversion, junction-formation" step which involves heat treating the structure in an oxygen containing atmosphere. High reactivity of Zn with oxygen causes this element to diffuse to the surface of the film during the annealing step and, therefore, the composition of the absorber layer changes. This difficulty may be overcome by including excess Zn into the film and etching away the Zn-rich surface before contact deposition. It should be noted the above mentioned difficulties do not apply to the CdTe/CdS junctions and the two-stage technique is a promising low-cost approach for the fabrication of high efficiency CdTe solar cells.

List of the publications concerning this project are given below.

References

1. B.M. Basol, V.K. Kapur, R.C. Kullberg and R.L. Mitchell, 20th PVSC Conf., IEEE, New York, 1988, p. 1500.

2. B.M. Basol and V.K. Kapur, Thin Solid Films, 165 (1988) 237.

3. B.M. Basol, V.K. Kapur and M.L. Ferris, J. Appl. Phys., 66 (1989) 1816.

4. B.M. Basol, V.K. Kapur and R.L. Mitchell, 21st PVSC Conf., IEEE, New York, 1990, p. 509.

5. B.M. Basol and V.K. Kapur, Solar Cells, 1990 (in press).

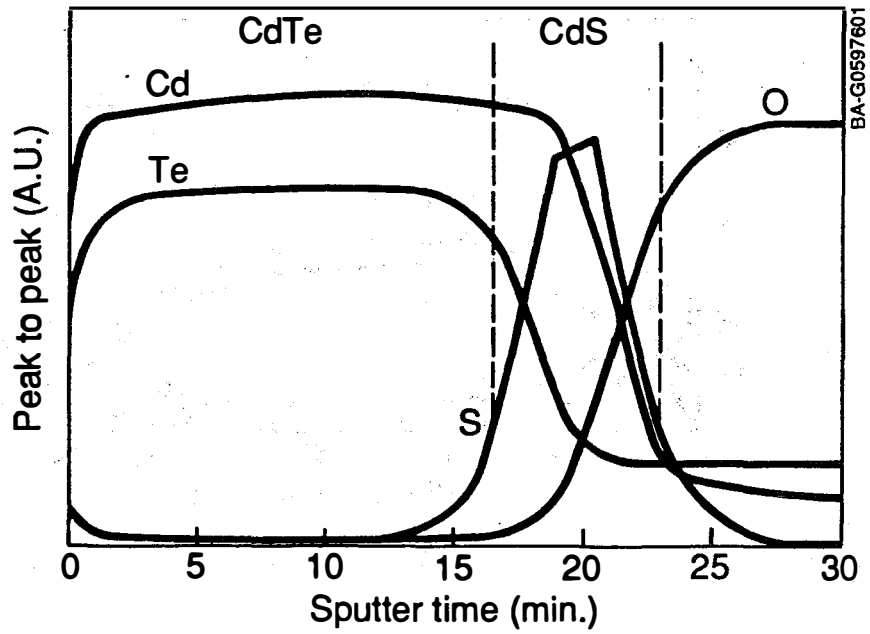

Fig. 1. Auger depth profile of a CdTe/CdS/ITO/glass structure.

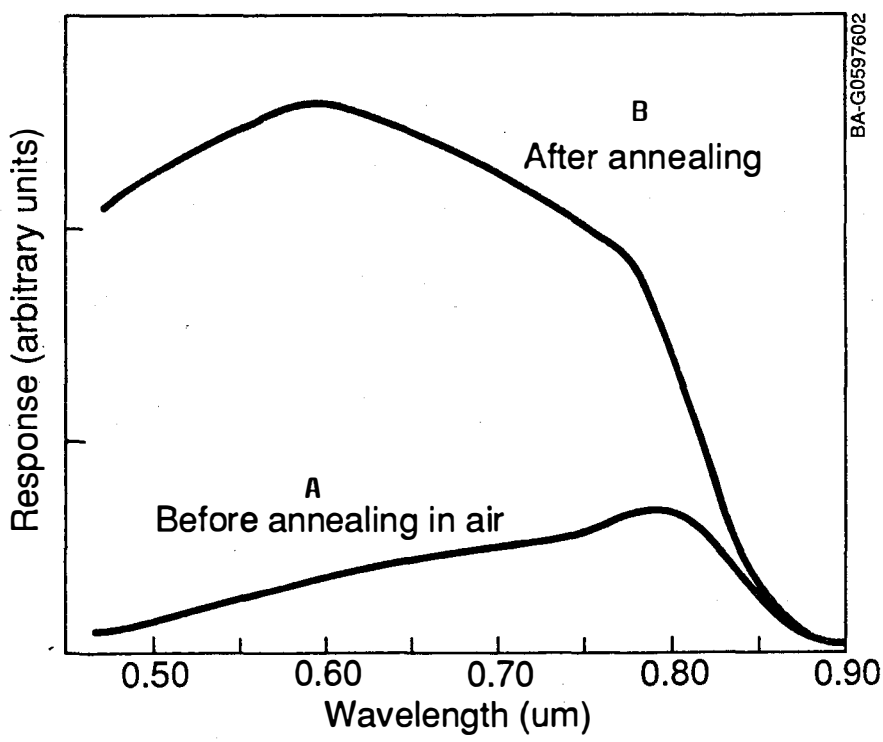

Fig. 2. Spectral response of a Au/CdTe/CdS/ITO/glass device.

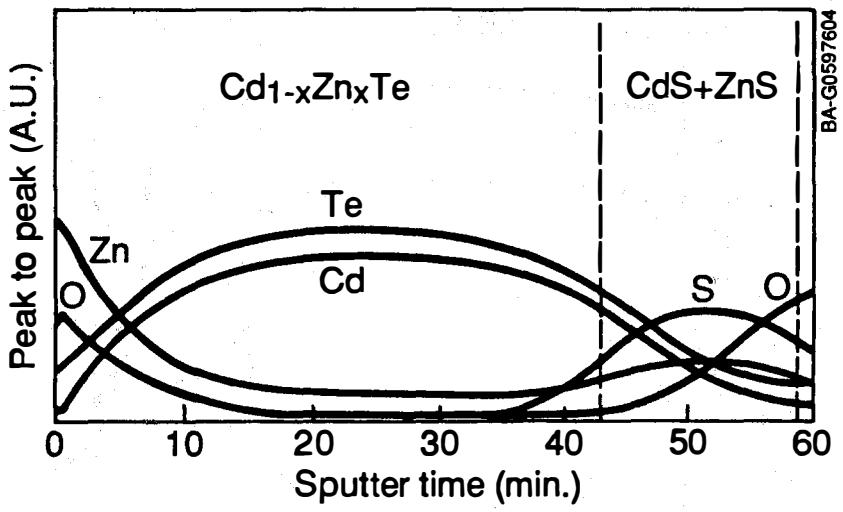

Fig. 3. Auger depth profile of a $Cd_{1-x}Zn_xTe$/CdS/ITO/glass structure. Intended composition, x, was 0.3.

Title: Advanced Studies of Solar Photovoltaic/ Electrolytic Hydrogen Systems

Organization: Center for Energy and Environmental Studies
Princeton University
Princeton, NJ 08544

Contributors: Joan M. Ogden, principal investigator

Hydrogen is a high quality, clean-burning fuel, which could replace oil and natural gas for transportation, heating and power. If hydrogen is made via solar photovoltaic (PV) powered water electrolysis (Figure 1), it would be possible, in principle, to provide energy on a global scale, with essentially no greenhouse gas emissions and very low local pollution.

In previous work [1-4], we have investigated the implications of projected advances in thin film solar cell technology for producing electrolytic hydrogen from photovoltaic (PV) electricity. These studies indicate that if year 2000 cost and efficiency goals for thin film solar cells are achieved, PV hydrogen produced in the Southwestern US could become roughly cost competitive with other synthetic fuels for applications such as automotive transport and residential heating, if efficient energy use is stressed. This suggests that PV hydrogen could potentially play a significant role in future energy supply.

Our current research examines the design and economics of PV hydrogen systems in more detail, addressing a number of unresolved cost and design issues. In the first phase of this work (described below) we have investigated the sensitivity of PV hydrogen production costs to changes in the assumed performance and cost of various system components [5]. The aim is to identify key conditions for low cost PV hydrogen production.

Our base case "year 2000" PV hydrogen system described in Table 1 and Figure 1. A large (>10 MW) tilted, fixed, flat plate PV array using thin film solar modules is coupled directly to an electrolyzer, which splits water to produce hydrogen and oxygen. Hydrogen is generated during the daylight hours and compressed for storage, onsite use or pipeline transmission to distant users. Both the PV array and the electrolyzer operate on DC power, so that no inverter or other AC equipment is needed in the PV system, and the electrolyzer requires no rectifier.

We assume that year 2000 goals for thin film solar cells are achieved, e.g., PV modules are 12-18% efficient and cost \$0.2-0.4 per peak Watt (Wp) (\$36-72/m^2). Drawing on recent low cost designs, the area-related balance of system costs are assumed to be \$33/m^2. The electrolyzer cost and performance estimates are for large scale (>10 MW) commercially available unipolar electrolyzer technology, assuming that the system is operated with a PV power source.

For the assumptions in Table 1, the levelized cost of DC electricity produced in the Southwestern US (assuming annual average insolation of 271 Watts/m^2, which is the value in El Paso, Texas) would be \$0.020-0.035/kWhDC. The cost of PV hydrogen (exclusive of compression, storage and transmission

costs) would then be $9-14/GJ.

Figure 2 illustrates the dependence of the PV hydrogen cost on PV module cost (in $/m^2) and PV module efficiency. Let us assume that we want to reduce the cost of PV hydrogen produced in the Southwest to less than $15/GJ so that it starts to become competitive with other synthetic fuels.

With present technology in 10 MWp/year factories, 6% efficient thin film PV modules would cost about $70/m^2 to manufacture. A recent study by Solarex indicates that costs of about $55/m^2 for thin film PV modules should be acheivable in 100 MWp/yr plants. If the efficiency were also increased to 12%, the cost of PV hydrogen would be about $15/GJ. In the longer term, with process improvements and maturing technology, the PV module cost could drop to $30/m^2. At module costs of $30/m^2, it would be possible to produce PV hydrogen costing less than $15/GJ even at efficiencies of 9%. Clearly, it is important to improve thin film manufacturing techniques to bring costs down, especially if the module efficiency reaches only the lower end of the projected range.

The sensitivity of PV hydrogen costs to changes in other PV system parameters and electrolyzer parameters are summarized in Figure 3. Several goals are particularly important for low cost PV hydrogen production.

For PV system lifetimes of less than about 30 years, the PV hydrogen cost rises sharply. Development of stable thin film solar cell materials and long lived modules is a high priority for PV hydrogen systems.

Low cost balance of system (BOS) designs could significantly reduce PV hydrogen costs. To reduce BOS costs it may be important to look at system designs which use automated factory assembly and wiring of PV panels rather than more expensive field construction, as well as low cost support structures and electrical design to minimize wiring costs.

Electrolyzer capital costs are an important contributor to the cost of PV hydrogen. At present there is limited experience with PV electrolysis systems. While experiments to date show no undue problems, questions of electrode lifetime with a diurnally varying PV power source remain to be answered. Continued research on PV powered electrolyzers is needed to address these issues.

Electrolysis efficiencies on the order of 75-85% would be required for low cost hydrogen production. These efficiencies could be reached in large electrolyzers using present technology.

CONCLUSIONS

In order to reach PV hydrogen costs of less than $15/GJ, the efficiency of thin film modules would have to be at least 9%. Reducing the module manufacturing cost to $30-70/m^2, acheiving PV system lifetime of 30 years, employing low cost balance of system designs, and optimizing electrolyzers for PV operation are also important goals for low cost PV hydrogen production. In future research we plan to examine low cost designs for PV hydrogen systems, with emphasis on reducing balance of system costs.

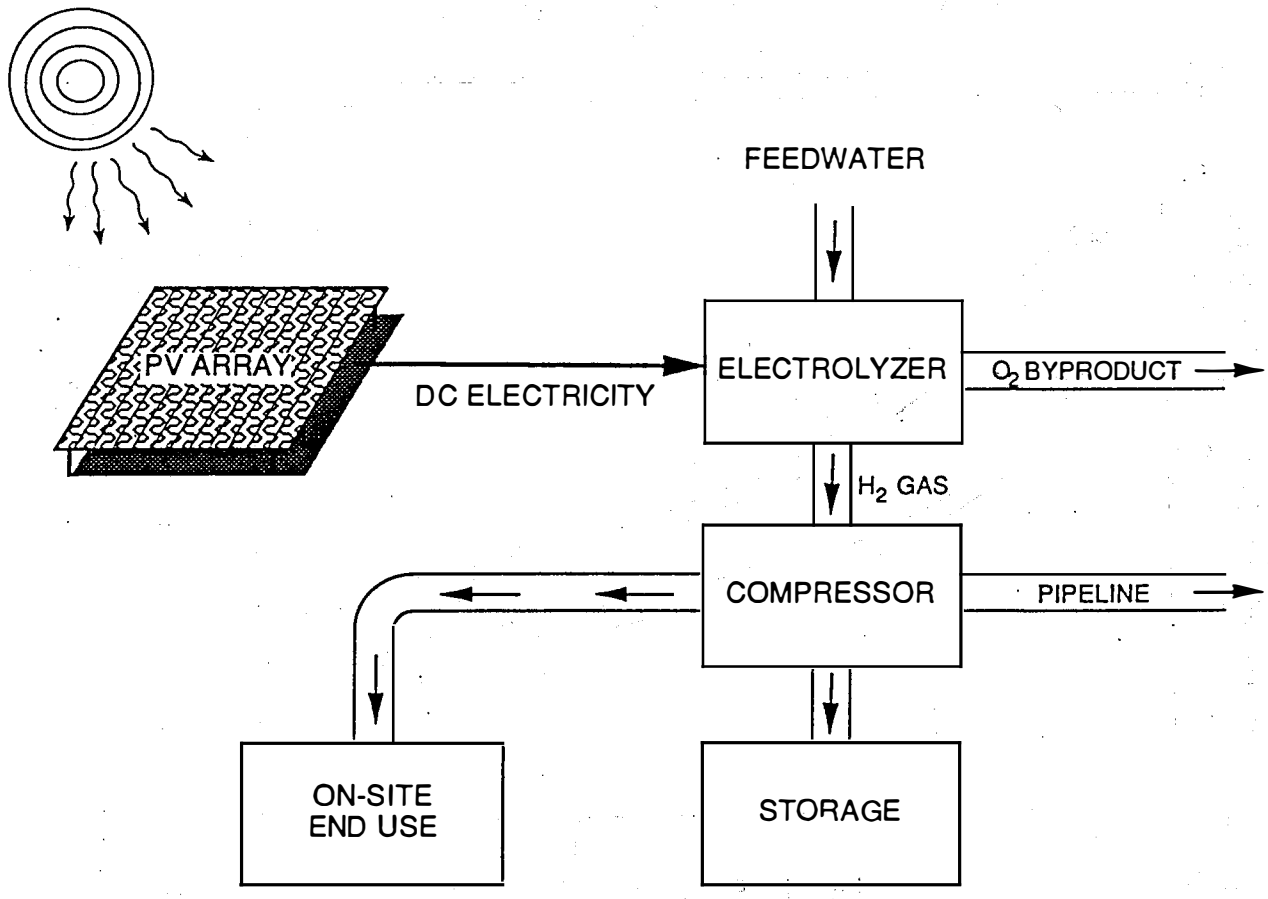

Figure 1. A solar photovoltaic electrolytic hydrogen system. A fixed, flat plate thin film PV array is connected directly to an electrolyzer, which splits water to produce hydrogen and oxygen. A compressor pressurizes the hydrogen for storage, onsite use or pipeline transmission to distant users.

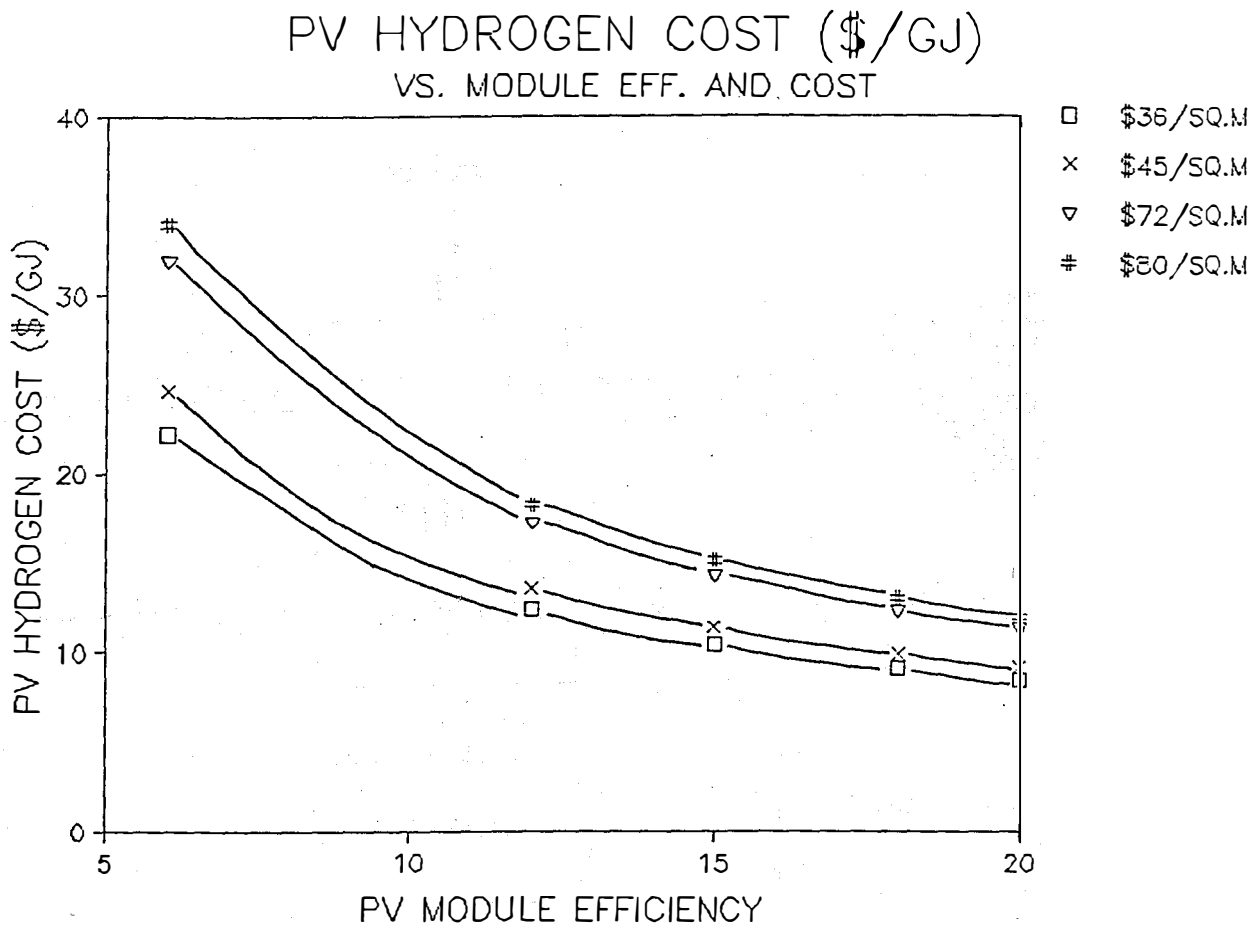

Figure 2. Production cost of PV hydrogen (in $/Gigajoule) as a function of PV module manufacturing cost (in $/square meter) and PV module efficiency. It is assumed that the average annual insolation is 271 Watts/square meter, the value measured in El Paso, Texas. The other PV system values are taken from Table 1. The cost of PV hydrogen can be determined from the graph, given the PV module efficiency and cost. For example, for the base case assumptions used in this study (12-18% efficiency, cost $36-72/m^2), the cost of PV hydrogen would be about $9-14/GJ. If year 2000 USDOE goals for thin film PV modules are used (efficiencies of 15-20% and costs of $45-80/m^2), the cost of PV hydrogen would be about $14/GJ. For 1990s thin film technology (6% efficiency, module cost of $70/m^2), the cost of PV hydrogen would be about $30/GJ.

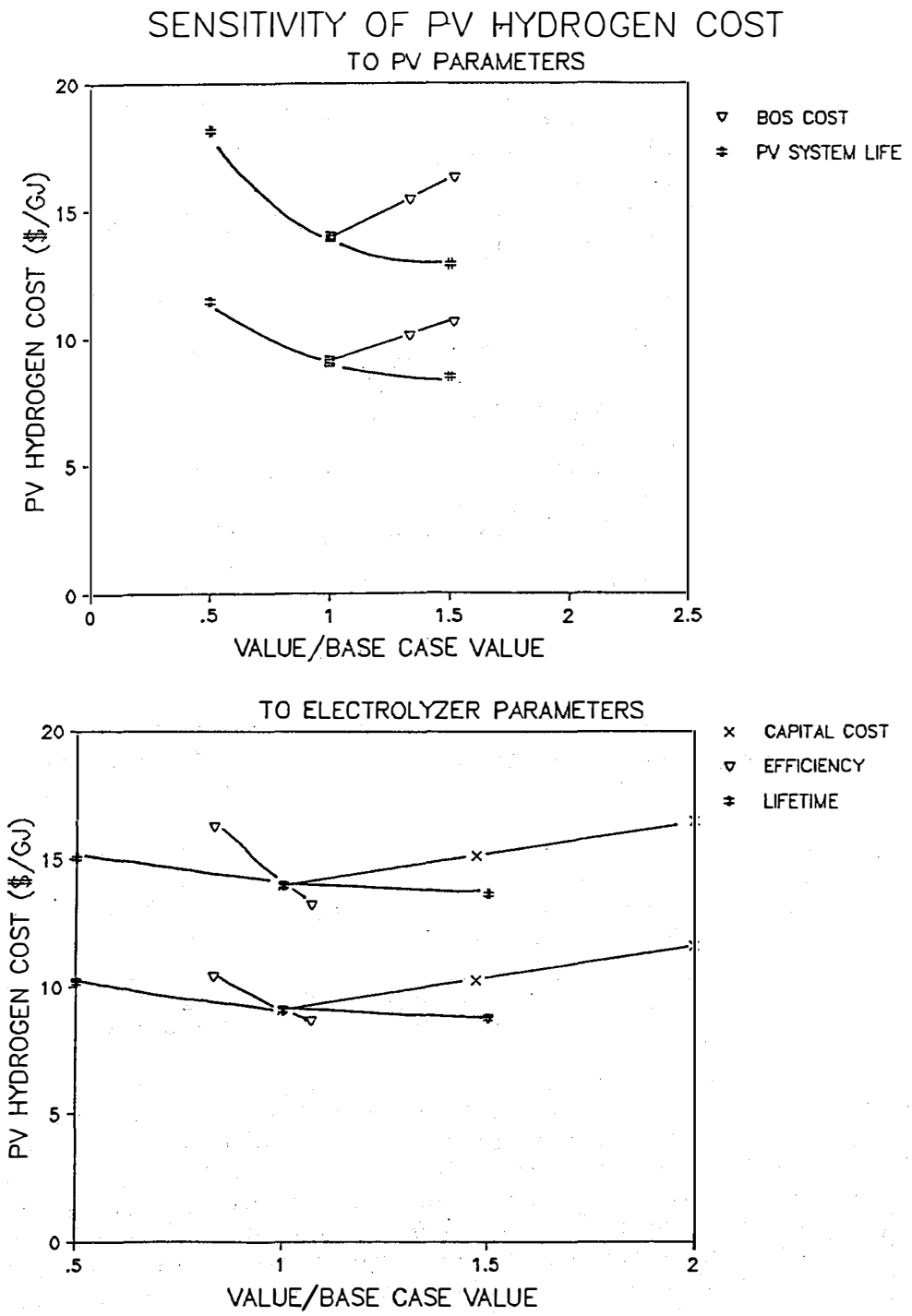

Figure 3. Sensitivity of PV hydrogen production costs to changes in PV parameters (upper graph) and electrolyzer parameters (lower graph). In each graph the cost of PV hydrogen is shown as a function of various system parameters. The variation of each parameter is expressed as its ratio to the base case value.

TABLE 1. BASE CASE SOLAR PHOTOVOLTAIC/ELECTROLYTIC HYDROGEN SYSTEM PARAMETERS[a]

PV SYSTEM:	THIN FILM PV MODULES	
	TILTED, FIXED FLAT-PLATE ARRAY	
	PV MODULE EFFICIENCY	12-18%
	PV MODULE COST	$0.2-$0.4/W_p
	AREA-RELATED BALANCE OF SYSTEM COST	$33/m2
	BALANCE OF SYSTEM EFFICIENCY	85%
	PV ANNUAL O&M COST	$0.45/$m^2$/YR[b]
	PV SYSTEM LIFETIME	30 YEARS
	PV SYSTEM INDIRECT COST FACTOR	25%
PV/ELECTROLYZER COUPLING:	DIRECT CONNECTION	
	COUPLING EFFICIENCY	93%[c]
	COUPLING EQUIPMENT COST	neglible
ELECTROLYZER:	ATMOSPHERIC PRESSURE UNIPOLAR ELECTROLYZER[d]	
	RATED VOLTAGE	1.74 Volts
	RATED CURRENT DENSITY	134 mA/cm^2
	OPERATING CURRENT DENSITY	268 mA/cm^2
	EFFICIENCY AT OPERATING VOLTAGE	84%
	INSTALLED PLANT CAPITAL COST	
	(NO RECTIFIER)@RATED CURRENT DENSITY	$247/kWDCIN
	@ TWICE RATED CURRENT DENSITY	$151/kWDCin
	ELECTROLYZER ANNUAL O&M COST	2% OF CAPITAL COST
	ELECTROLYZER LIFETIME	20 YEARS
ECONOMIC ASSUMPTIONS:	ALL COSTS EXPRESSED IN 1986 US DOLLARS	
	DISCOUNT RATE	6.1%[e]
	ANNUAL INSURANCE RATE	0.5% OF CAPITAL COST[e]
	INCOME AND PROPERTY TAXES	0

---

a From J.M. Ogden and R.H. Williams, Solar Hydrogen Moving Beyond Fossil Fuels, World Resources Institute, 1989. For systems larger than 10 MW_p.

b Suggested by field data from large PV arrays. G.J. Shusnar, J.H. Caldwell, R.F. Reinoehl and J.H. Wilson, "ARCO Solar Field Data for Flat Plate PV Arrays," 18th IEEE PV Specialists' Conference, Las Vegas, Oct.1985.

c C. Carpetis, International Journal of Hydrogen Energy, v. 7, p. 287, 1982; C. Carpetis, IJHE, v. 9, p. 969, 1984; R.W. Leigh, P.D. Metz and K. Michalek, Brookhaven National Laboratory Report BNL-34081, December 1983; P.D. Metz and M. Piraino, BNL-51940, July 1985.

d Electrolyzer operating characteristics and costs are based on currently available unipolar technology. We have assumed that no rectifier is needed. R.L. Leroy and A.K. Stuart, "Advanced Unipolar Electrolysis," and M. Hammerli, "When Will Electrolytic Hydrogen Become Competitive?" IJHE, v. 9, pp.25-51, 1984.

e For utility scale power production facilities (EPRI, Technical Assessment Guide, Vol.1: Electricity Supply, EPRI P-4463-SR, 1986).

REFERENCES

1. J.M. Ogden and R.H. Williams, "Hydrogen and the Revolution in Amorphous Silicon Solar Cell Technology," Center for Energy and Environmental Studies Report No. 231, Princeton University, Princeton, NJ, February, 1989.

2. J.M. Ogden and R.H. Williams, "New Prospects for Solar Hydrogen Energy: Implications of Recent Advances in Thin Film Solar Cell Technology," Proceedings of the IEA/OECD Expert Seminar on Energy Technologies to Reduce Emissions of Greenhouse Gases, Paris, France, April 12-14, 1989.

3. J.M. Ogden and R.H. Williams, "Electrolytic Hydrogen from Thin Film Solar Cells," International Journal of Hydrogen Energy, 15 (1990) 155.

4. J.M. Ogden and R.H. Williams, Solar Hydrogen: Moving Beyond Fossil Fuels, World Resources Institute, Washington, DC, October 1989.

5. J.M. Ogden, "Cost and Performance Sensitivity Studies for Solar Photovoltaic/ Electrolytic Hydrogen Systems," Proceedings of the 10th SERI PV Advanced Research and Development Meeting, October 23-25, 1990, Lakewood, Colorado, to appear in Solar Cells, 1991.

Title: **Hydrogen Radical Enhanced Growth of Solar Cells**

Organization: Department of Electrical, Computer and Systems Engineering, Rensselaer Polytechnic Institute, Troy, New York

Contributors: J.M. Borrego and S.K. Ghandhi, Co-Principal Investigators

The objective of this research is to grow InP in the presence of active radical species, and to characterize this material for solar cell applications. Here, we proposed the use of hydrogen radicals to aid in the organometallic vapor phase epitaxial (OMVPE) growth process, in two ways. First, energy transferred to the alkyl and hydride species would provide a high electron temperature, allowing growth at a reduced thermal temperature. Second, these active species can be used to enhance substrate cleaning prior to growth, and so allow growth at reduced temperatures.

During the first phase of this program, a special purpose reactor, operating in the 0.5 to 2 Torr range, was designed and put into operation for this purpose. Work with this reactor showed that active H species caused substrate damage during the cleaning process. On the other hand, active He species could be used to clean the substrate prior to InP growth, without damaging it. We believe that etching of the substrate with active H results in the formation of volatile PH_x species, with excess In on the surface. As a consequence, emphasis was placed on the use of He species, after consultations with our program monitor. System modifications were made to allow all-He or all-H_2 operation.
MICROWAVE CAVITY DESIGN: The purpose of this task is to be able to predict the electron concentration in the plasma. The approach we have taken is to combine the theory of microwave breakdown in gases with the known microwave cavity characteristics. Using measurements in the cold cavity, i.e., without the plasma, we have determine the fringe capacitance of the region where the plasma is generated. This capacitance, which is on the order of a few femtofarads, is related to the plasma conductance by the ratio of plasma conductivity to electric permittivity of free space.

A possible way to determine the plasma conductance is to calculate the voltage of the resonant cavity during operation. This is related to the electric field for producing breakdown and depends upon the dimensions of the tube in which the plasma is generated and on the partial pressure. With this voltage we can determine the plasma conductance, since we know the power given by the generator to the cavity in order to generate the plasma. Once the conductance is known, the electron concentration in the plasma can be calculated by using the mobility of the electrons at the partial pressure of the gas. We have used the data available in the literature in order to carry out these calculations, and the results obtained agree reasonably well with the measurements carried out in the plasma.

PLASMA STUDIES: During the reporting period, a series of tests were made to characterize the He plasma, by using a Langmuir probe which is located just above the substrate. V-I characteristics of this probe have been taken for a number of different bias conditions. Probe measurements were carried out at 1.5 Torr total pressure, and 150 sccm total gas flow (all He), with 20 sccm through the microwave cavity. These are the same flows as during typical growth runs, but with the 20 sccm PH_3 replaced by He and no TMI flowing.

The microwave power was set at 50W and the cavity kept tuned to reduce the reflected power to a minimum.

The probe consisted of a stainless steel wire, encased in a glass sheath, and positioned about 0.5 cm above the unheated susceptor, which is grounded. This was used because the plasma at the sample is of the most interest. (We are using the term plasma here loosely, as there is some uncertainty whether a true plasma exists due to the very low degree of ionization.)

Figure 1 shows a series of probe characteristics. Here, while the probe bias was varied from -60 to +60V, the top plate bias was kept constant at +70 V, 0 V, and -70 V. When the probe is biased -ve, it acts to collect positive ions and repel electrons, so the current collected is essentially the He^+ current. When the probe is biased +ve, it acts to collect only electrons and repel positive ions.

Consider negative probe bias conditions, which repel ions from the top plate, thereby providing more ions in the vicinity of the probe. Here, as expected, the ion current increases with negative probe bias. Moreover, for any given probe bias, the ion current will be larger for larger +ve plate bias. When the top plate bias is changed to -70V, it attracts ions and depletes them from the plasma region. The ion current collected is therefore very close to zero.

Now consider a positive probe bias. Here, if the top plate is grounded, a significant electron current is collected as the probe bias is increased. If the top plate is biased to +70V, the electron current collected by the probe near the grounded susceptor is decreased to near zero. The logical explanation for this is that the top plate attracts electrons and depletes the plasma region of them. Anomalous behavior is observed if the top plate is biased to -70V. To help explain this, the data of Fig. 2 were gathered. Here, the probe bias was kept at +70V (and collected electrons), while the top plate bias was varied continuously from -50 to +50V, with respect to ground. The magnitude of the electron current went through a maximum at about -15V, tended quickly towards zero as the top plate was more negatively biased, and dropped off to a low minimum as the top plate bias was increased to +15V. In the region >0V, the probe current drops to zero since the top plate attracts electrons and depletes them from the plasma. At biases more negative than -20V, we believe that the electric field established between the top plate and the ground acts to push all electrons out of the plasma region so that there are progressively fewer to be collected by the probe, and the electron current falls. The perturbations due to the biased top plate and biased probe probably act to destroy the quasi-neutral quality of the lightly ionized gas.

MATERIALS GROWTH: A series of runs were made with the all-Helium system. Our results can be summarized as follows: at $T \geq 535°C$, the samples behave reasonably well electronically, with $\mu_{77} > \mu_{300}$ and an n-type carrier concentration in the low to mid 10^{16} range. At growth temperatures of $\leq 500°C$, μ_{77} is always less than μ_{300}, and the carrier concentration is in the mid 10^{17} range, a decade higher than for layers grown at 525°C. This behavior is true even when the PH_3 pressure is increased to 0.30 Torr. We believe that ionized impurity scattering is the cause for this behavior. This is probably

due to a phosphorous related defect, as the cracking of PH_3 decreases rapidly with reduced temperature.

Our results have established that plasma cleaning of the substrate is beneficial since it removes surface oxides and hydrocarbons, and reduces the dependence on time, temperature and PH_3 pressure on the subsequent growth. Low temperature materials growth, after a plasma substrate clean, resulted in consistent deposition from run to run, and the absence of an induction period. While both plasmas can be used for this purpose, the H plasma was more effective than He. However, considerable care was required to control its process schedule in order to prevent indium droplets from forming on the substrate. It is possible that a H plasma (chemically active) can be used for the cleaning step if this control can be obtained. An end point detector, such as a residual gas analyser, would be ideal for this purpose.

Work during this period also involved the growth of InP in a He plasma, with the usual growth conditions: 1.5 Torr, 550°C, all He flow. With the plasma on during growth, the top plate of the reactor was biased to influence the charged particles, electrons and $He^{\bullet}$ ions. This influence is seen from the Langmuir probe curves described earlier. A bias of $\pm 70V$ has a very strong influence on the type of charged particles are present. Assuming a "plasma" density at the substrate of about 10^5 cm^{-3}, the Debye length (the length over which charged particles are affected by local electric fields) is about equal to the dimensions of the chamber. Since the gas is weakly ionized (the gas density is 10^{16} cm^{-3} at 1.5 Torr), it no longer strictly qualifies as a plasma, but we will continue to use this term for convenience.

Runs were made with and without plasmas, with the top plate biased successively to ground, -20V and $\pm 70V$ with respect to the substrate. The results can be summarized as follows: whenever the sample is grown with the plasma, the mobility of the layer is deteriorated (compared to the no plasma run), no matter what bias is applied to the top plate. As usual, $\mu_{77} < \mu_{300}$, for all plasma runs. These results leads us to the conclusion that the damage to the layers is probably due to energetic neutral He or He* species, where the star denotes a He atom raised to an excited state about 20 eV above the ground state, while an energetic He atom may only have gained kinetic energy. This is not unreasonable, since the predominant species in a low density-low temperature He plasma is expected to be excited neutrals. These uncharged species cannot be influenced by an applied electric field. It is unclear as of yet whether the damage is caused merely by incorporation of He into the InP, by energetic damage to the InP layer, or by effecting the chemistry of growth.

We have also repeated our growth experiments, using $H^{\bullet}$ as the active species. For these experiments, layers were first grown in hydrogen gas without active species. Next, these layers were exposed to the H plasma, with PH_3 but no TMI flowing, in order to prevent thermal decomposition. In a series of growth runs, the top plate of the reactor was biased +70V, -20V and grounded. The plasma power was 50W, with a duration of 30 minutes. In each case, two samples were grown, one serving as the control. Sample mobilities were measured by van der Pauw methods, and compared to layers which were not plasma treated. Our data showed that neither the room temperature mobility nor the low temperature value varied with the post growth plasma treatment. Together, the results indicate that

the H plasma does not change the electrical properties of the layer, once it has been grown. From these data (both He and H plasma treatment), it is clear that the damage is caused by the interaction of the plasma with the reactant species during the growth process.

CHARACTERIZATION: This is an important component of any program of research which involves materials growth, since it provides feedback for effecting improvements on the growth process. Our characterization effort concentrated on conventional methods which includes Optical and Scanning Electron Microscopy, Hall Effect, Double Crystal X-ray Diffraction and Photoluminescence. In addition, we have been using a microwave reflectance technique to characterize the InP material grown in the presence of a plasma. This technique involves determining the direct recombination lifetime as well as detecting the presence of trapping levels. The measurements technique consists of increasing the conductivity of the material by using a 50 nsec light pulse from a GaAs laser emitting at 904 nm. The laser pulse creates hole-electron pairs which increase the conductivity of the material. This photo-induced conductivity is observed by measuring the reflected signal from an incident microwave beam, which decreases as the conductivity of the material increases. Using a microwave detector and a digital oscilloscope, we can record the photo-conductivity decay transient. This transient consists of a fast decay of a few nanoseconds of duration which corresponds to the lifetime due to direct recombination, plus a long decay with time constant of the order of milliseconds. This long time constant is caused by carriers which are emitted from trapping levels which were filled during the light pulse. We are in the process of establishing a relationship between the growth conditions and the amplitude and duration of this long time constant.

Photoluminescence data, taken on samples grown with and without a remote He plasma, are now described. Figures 3 and 4 show PL scans from two layers, about 0.5 μm thick, grown at 550°C, with a V/III = 225. Figure 3 is for a sample grown with no plasma, and Fig. 4 is for 50W plasma. The layers grown with no plasma show a typical PL scan, with an acceptor peak (Zn) at 1.377 eV. The plasma-grown layer has two drastically different features. First is the presence of a large peak at 1.384 eV. This appears to be an acceptor which we have not identified. The second feature is the broad peak around 1.342 eV. The position indicates that it is a replica while its breadth indicates that it is likely a deep level, as deep levels interact with a wide range of phonons. We believe that the 1.384 eV peak may actually be a peak from a lower energy due to an acceptor-deep donor complex, shifted by the coulombic interaction energy between the two. Phosphorous vacancies are thought to act as deep donors and they are very mobile. Nearest neighbor or second nearest neighbor interaction with Zn would also cause a shift in the peak value.

CONCLUSION: This report represents the second, and concluding year of this program. Our work in the area has not been terminated, however, and a number of papers are currently being written on different aspects of our work. One Masters degree has been awarded on the design and characterization of the plasma-enhanced CVD system. A PhD will also be awarded, emphasizing the growth and characterization aspects of our work.

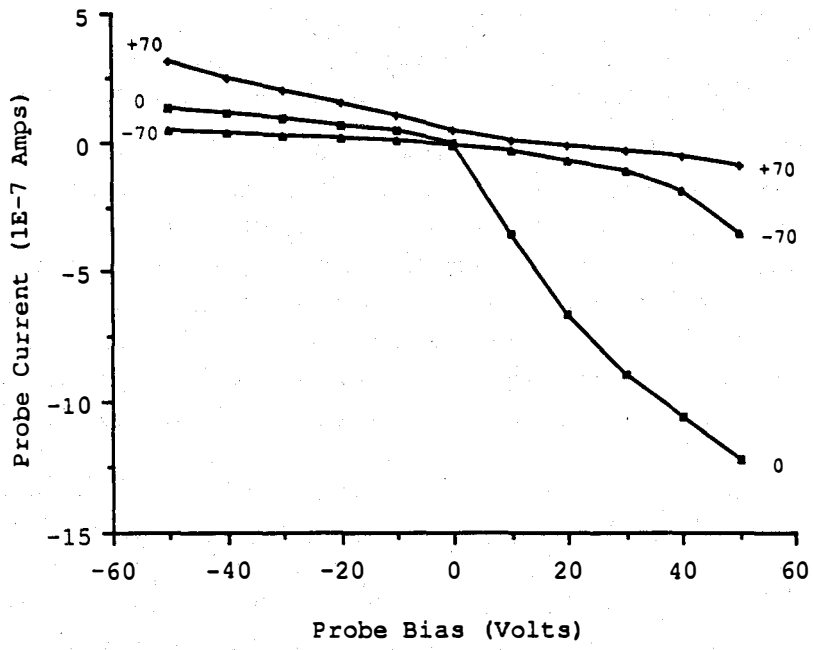

Figure 1. Probe current-voltage characteristics.

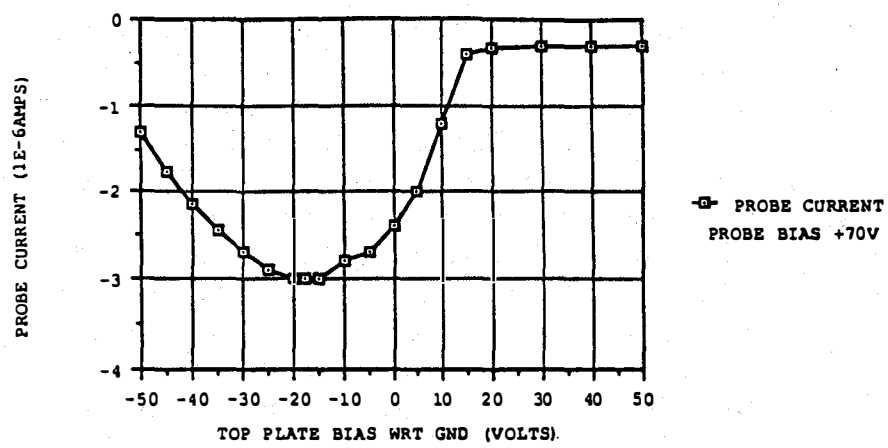

Figure 2. Probe current vs top plate bias (probe bias = +70 V).

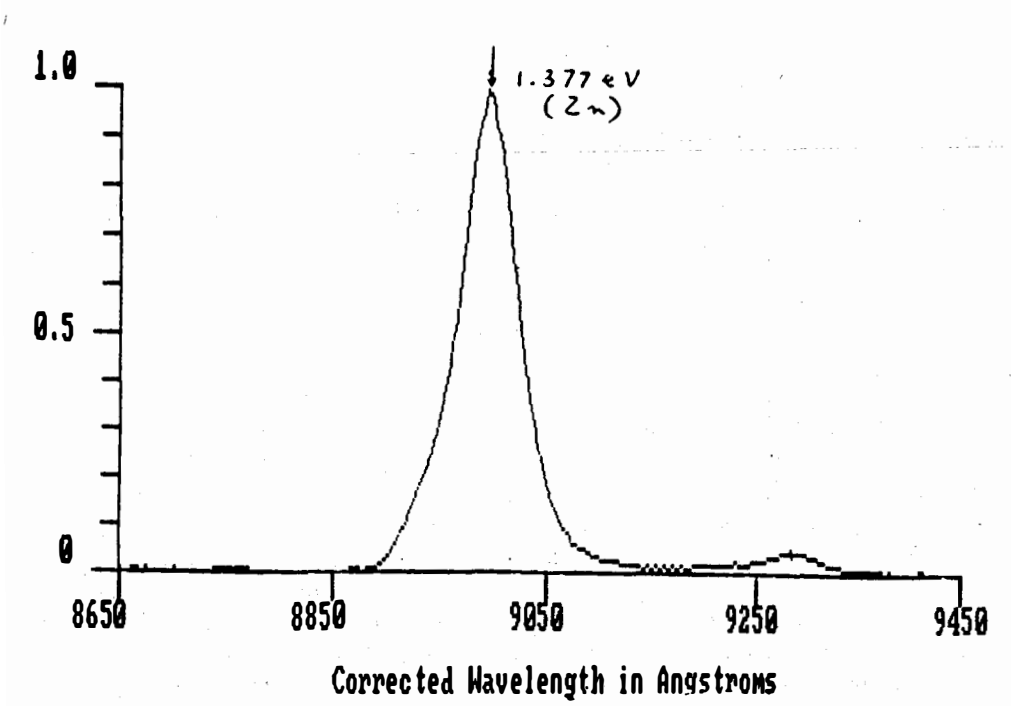

Figure 3. PL of InP grown at 550°C - no plasma.

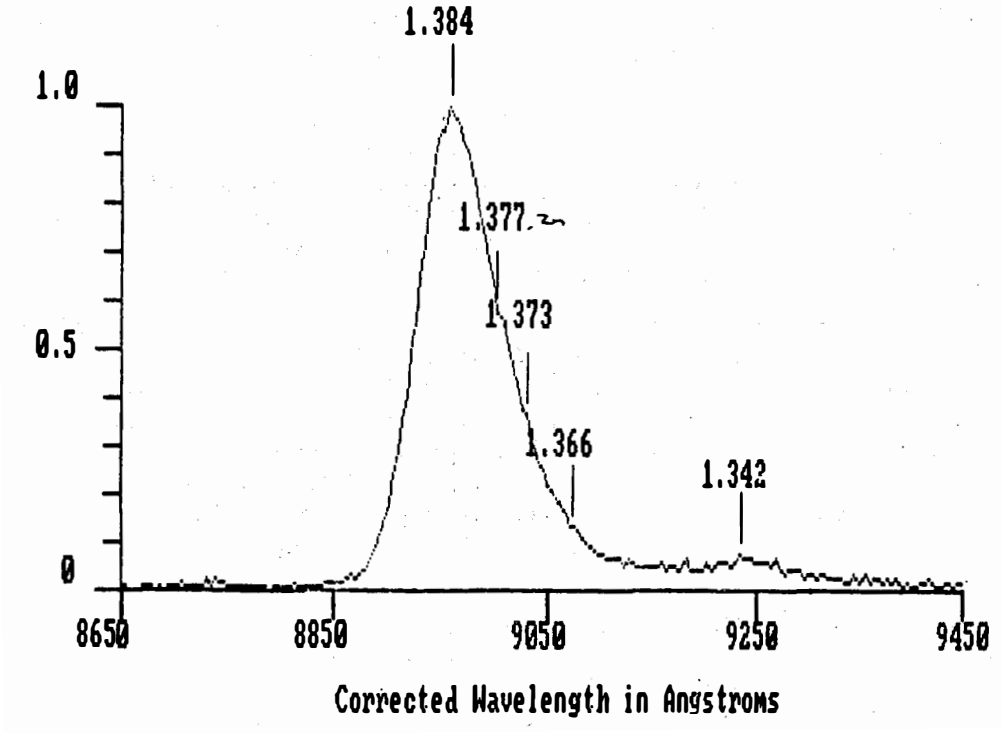

Figure 4. PL of InP grown at 550°C - 50 W plasma.

Title: **An Inverted AlGaAs/GaAs Patterned Tunnel Junction Cascade Concentrator Solar Cell**

Organization: Research Triangle Institute, RTP, NC 27709

Contributors: R. Venkatasubramanian, M.L. Timmons (Principal Investigators), T.S. Colpitts, J.S. Hills and R.T. Pickett

Introduction

Monolithic $GaInP_2$/GaAs [1] and AlGaAs/GaAs [2] cascade solar cells offer the promise of high efficiency conversion for concentrator-based terrestrial photovoltaic power systems. AlGaAs/GaAs materials system with a mature growth technology is attractive in spite of the high growth temperatures that are required for high-performance AlGaAs cells. Successful performance of such a cascade at high-current levels ($\sim$ 7.5 A/cm^2 at 500 suns, AM1.5) depends on the intercell ohmic connection (IOC) that must have simultaneously low resistivity ($\sim$ 2-3 $\times$ 10^{-3} ohm-cm^2) and high optical transparency. Research Triangle Institute originated the concept of a patterned-tunnel-junction (PTJ) cell in which a Ge tunnel junction is patterned to lie approximately beneath front-surface metallization in the complete AlGaAs/GaAs cascade structure [3]. Although such a PTJ is capable of handling the current levels at high concentration, it is rendered much less useful after the high temperature growth (800 ° C) of the top AlGaAs cell. However, the PTJ has been found stable enough at growth temperatures of 700 ° C [4].

Development Approach

Based on the PTJ's stability at 700 ° C and the ability to grow high quality AlGaAs top cells at 780 - 800 ° C [2], the approach suggested here involves the following three significant features. First, the AlGaAs/GaAs cascade structure will be grown inverted (see Figure 1). The AlGaAs top cell will be grown first at high temperatures, placing the surface that is to be illuminated nearest to the substrate. After the growth of the top cell, the PTJ will be fabricated, and then the GaAs bottom cell will be grown at lower temperatures (650 -700 ° C). This manner of inverted-structure growth allows the top AlGaAs cell to be grown under the most favorable conditions and the GaAs cell (whose efficiency can be very high, even at lower growth temperatures) to be grown without increasing the resistivity of the PTJ significantly.

After the inverted growth, the AlGaAs/GaAs cascade structure is selectively removed from the parent substrate. Originally we planned to use an electrochemical etching [5] to selectively and quickly remove p-type GaAs substrates. However, during the course of this work we have developed selective plasma etching of Ge with a CF_4/O_2 mixture to produce free-standing GaAs/AlGaAs structures. The etch rate of Ge substrates is as high as 220 μm/hr at temperatures of 175 ° C, and the etch-rate for GaAs or AlGaAs materials is negligible. This plasma etching technique, combined with a lattice-matched growth of GaAs/AlGaAs cascades on Ge substrates, makes the scheme of inverted growth followed by substrate removal a production-compatible process.

Two interesting developments as a consequence of the inverted-growth approach to AlGaAs/GaAs cascades have been considered. One involves a planar GaAs tunnel junction as an interconnect in the cascade that meets the specific resistivity requirements after the bottom-cell growth at 650-700 ° C. This would avoid PTJ using Ge chemical vapor deposition and allow a single, continuous growth of the AlGaAs/GaAs cascade in a III-V growth system. Hence we considered the development of a high-conductance planar GaAs tunnel junction in this effort. The second aspect is the optical transparency of the AlGaAs/GaAs cascade after Ge substrate-removal. The cascade cell can be mechanically stacked with a low cost Si or CIS cell to obtain an overall efficiency approaching 40% at 500-sun concentration. This second aspect has not

been addressed in this effort as we are in the process of optimizing the various components of the AlGaAs/GaAs cascade.

In the following sections, we discuss factors for achieving high-efficiency AlGaAs/GaAs cascades. These include the $Al_{0.37}Ga_{0.63}As$ cell development, the GaAs tunnel junction development, the optimization of the selective epitaxy of Ge for the PTJ, the GaAs bottom-cell nucleation on a patterned Ge structure, and the Ge substrate-removal scheme.

$Al_{0.37}Ga_{0.63}As$ Material and Top Cell Development

The top cell optimization involved the growth of best quality $Al_{0.37}Ga_{0.63}As$ layers at high growth temperatures (780-800 °C), both n- and p-type doping of these layers, optimization of cell structure, and development of ohmic contacts and anti-reflection coatings. The details of this development have been discussed elsewhere [6]. AsH_3 was purified on-line by passing it over chilled ($\sim$ 0 °C) molecular sieves and a gettering compound supplied by Advanced Technology Materials, Inc., and organometallic sources such as trimethylaluminum (TMA) and trimethylgallium (TMG) were chosen, based on lifetime measurements in AlGaAs by photoluminescence decay. Prelayers (AlGaAs layers of high Al-composition) were grown prior to the growth of the active-junction layers of the $Al_{0.37}Ga_{0.63}As$ top cell to getter any residual moisture in the growth chamber. Shown in Table 1 is the result of the influence of incorporation of an $Al_{0.85}Ga_{0.15}As/Al_{0.37}Ga_{0.63}As/Al_{0.85}Ga_{0.15}As$ getter structure prior to the growth of active junction in $Al_{0.37}Ga_{0.63}As$. The cell with the getter structure has an improved minority-carrier lifetime, measured by open-circuit voltage decay [7], as well as a better solar cell performance.

Diethylzinc was used to obtain p-type doping in $Al_{0.37}Ga_{0.63}As$ layers, to about 3×10^{17} cm^{-3}. N-type doping of $Al_{0.37}Ga_{0.63}As$ to about 1-2 $\times$ 10^{18} cm^{-3} is desirable in an optimum solar cell structure designed for concentrator applications. A key problem in this area arises from the well known DX-center effects [8] in AlGaAs. Our doping results with H_2Se as the Se dopant for $Al_{0.37}Ga_{0.63}As$ has indicated that the maximum free electron concentration obtainable at a growth temperature of 800 °C is about 6.8×10^{17} cm^{-3}. The carrier concentration does not saturate, but decreases with increased mole fraction of H_2Se in the growth ambient. The use of an AsH_3 source with a reduced GeH_4-impurity level leads to improved carrier mobilities. This is attributed to reduced Ge-acceptor compensation since a significant fraction of Ge is expected to go into acceptor sites at a growth temperature of 800 °C.

Silicon doping in $Al_{0.37}Ga_{0.63}As$, using both SiH_4 and Si_2H_6 as dopant sources, indicates that the free electron concentration in $Al_{0.37}Ga_{0.63}As$ with Si doping is limited to about 4.0×10^{17} cm^{-3}. This lower free-electron concentration limit, compared with that of Se-doped samples, is consistent with the deeper DX-center nature of Si. Similar to doping with Se, increasing the Si-dopant partial pressure beyond the point of highest free-electron concentration causes the concentration to fall.

The near-bandedge absorption coefficient in AlGaAs materials increases with the aluminum content in the alloy, increasing from about 1×10^4 cm^{-1} in GaAs to about 2.3×10^4 cm^{-1} in $Al_{0.37}Ga_{0.63}As$. Further, the reduced valence-band offset between $Al_{0.37}Ga_{0.63}As$ and $Al_{0.85}Ga_{0.15}As$, compared to GaAs and $Al_{0.85}Ga_{0.15}As$ in a GaAs cell, makes the surface passivation difficult. Therefore, shallow emitters about 0.2 μm deep were used, even though these cells were intended for concentrators where lateral spreading resistance is an important consideration. Another important consideration in the surface passivation is the heavy n-type doping in the $Al_{0.85}Ga_{0.15}As$ window layer. Since the incorporation rate of Se increases at lower growth temperatures, the window and GaAs-cap layers have been grown at 700 °C. In addition to the lower growth temperatures, the H_2Se flow is maintained in the reactor after the growth of emitter at 800 °C until the window-layer growth is initiated at 700 °C. The influence of some of these various surface-passivation techniques on the solar cell performance is shown in Table 2.

As part of this program, a new concentrator mask was designed. The emitter-grid lines are equally spaced about a $\sim$ 125 μm center-to-center spacing. The width of the grid fingers decreases from $\sim$ 25 μm at center to $\sim$ 2 μm at the very edge. This design provides an equal current density in all the fingers based on the variation of collected current from the center of the cell to the edge. This design is intended to be compatible with the Entech coverglass, which can be applied to a linear grid for the reduction of shadow losses in concentrator systems.

High-Conductance GaAs Tunnel Junctions

GaAs p^{++}-n^{+} tunnel diodes have been grown by atmospheric-pressure organometallic vapor phase epitaxy (OMVPE) using zinc as the dopant for the p^{+} regions and either Se or Si as the dopant for the n^{+} regions. Growth temperatures between 600-700 °C, compatible with the GaAs bottom-cell growth temperature in an inverted-growth structure, have been investigated. At a growth temperature of 700 °C, using a "cycled" growth for the Zn-doped p^{++}-GaAs layer, both the conductance and the peak-current of the tunnel diode have been increased by a factor of $\sim$ 65 compared to a tunnel diode with a conventionally-grown p^{++} GaAs layer (Fig. 2). The conductance of the tunnel diode is enhanced at a growth temperature of 650 °C where the benefits of cycled growths appear to be optimum. GaAs tunnel diodes with specific resistivities (3.3×10^{-3} ohm-cm^2) comparable to the lowest-reported values by MBE [10] have been obtained. Cycled growths for the n^{+} Se-doped regions are found detrimental to the tunnel-diode performance; the conductance is reduced by more than two orders of magnitude. Conductance degradation is not observed with Si doping for the n^{+} GaAs region. A model for these observations based on Zn diffusion at various doping levels in the n^{+} regions and on dopant incorporation of Zn, Se and Si in GaAs during OMVPE will be presented elsewhere [11].

Ge Selective Epitaxy for PTJ and GaAs Bottom Cell Regrowth

Two approaches have been used for the fabrication of the PTJ. One involves selective epitaxy of Ge on GaAs with nitride masks. The other approach involves selective removal of Ge from GaAs after planar growth. The newly-developed selective-etching of Ge, discussed in the next section, has been used to selectively remove Ge with better results.

Shown in Figure 3 is a scanning electron micrograph of a GaAs wafer on which Ge was selectively grown in openings in a silicon nitride (Si_3N_4) mask. The growth conditions and the thickness of Si_3N_4 control the selective deposition. Lower Ge growth rates ($\sim$ 10 Å/min) and higher Ge growth temperatures ($\sim$ 590 °C) lead to better selective growth. Also, the selectivity is improved with lower H_2-carrier gas flow rates. In addition, the selectivity is excellent to good on n^{+} GaAs and n-type $Al_{0.85}Ga_{0.15}As$ samples, compared to either poor or no selectivity on p^{+}-GaAs surfaces. All the above observations can be related to a mechanism in which H_2 adsorption on GaAs surfaces, i.e., where Si_3N_4 is absent, inhibits the rapid transport of Ge species from the dielectric surfaces. When the transport is inhibited, one obtains a poor selective epitaxy of Ge on GaAs. With a smaller H_2 adsorption, Ge transport from dielectric surfaces increases and selectively improves [12].

Another consideration following the selective deposition of Ge for PTJ is the ability to grow high quality GaAs bottom cells on patterned Ge. Shown in Figure 4 is a scanning electron micrograph of a GaAs cell grown over a patterned Ge structure. The contrast is the result of the growth of a p-GaAs layer on top of a p^{++}-Ge pattern on an n^{+}-GaAs substrate. The n^{+}-GaAs substrate with patterned Ge was given an etch in 1:1:5 $=H_2O:H_2O_2:H_2SO_4$ prior to regrowth. This etch does not attack Ge and therefore, can preserve the PTJ while preparing the GaAs substrate for high quality growth. This etch-step helps to quickly identify the PTJ after the regrowth, for alignment of the top emitter grid to coincide with the patterned Ge.

Selective Plasma Etching of Ge Substrates for Thin AlGaAs/GaAs Structures

Selective plasma etching of Ge has been developed to produce thin, free-standing GaAs-AlGaAs structures after growth on lattice-matched Ge substrates. This approach, besides being very rapid, can also take advantage of potentially cheaper, large area Ge substrates.

A CF_4/O_2 gas mixture is used as the etchant in this plasma etch process. The etch rate of Ge increases from about 78 μm/hr at 75 °C to about 220 μm/hr at 175 °C with no observable etching of GaAs and $Al_xGa_{1-x}As$ (x up to $\sim$ 0.85 has been studied). The etching of Ge with the CF_4/O_2 plasma is isotropic. The etch leaves no microscopic residues on the surfaces. The surface morphologies of the GaAs and $Al_xGa_{1-x}As$ layers remaining after the removal of the Ge substrate are specular. More details on this process will be presented elsewhere [12].

The development of this etch process (which is production-compatible) as part of the inverted growth of high-efficiency AlGaAs/GaAs cascade also permits high transmission of photons with energies below the GaAs bandgap. This could be used advantageously in mechanically stacking an inexpensive Si or CIS cell below an AlGaAs/GaAs monolithic cell to form a 3-junction, 4-terminal cascade cell with a potential efficiency approaching 40%.

Highlights

- $Al_{0.37}Ga_{0.63}As$ top cell efficiency was quickly improved from about 4% to 11% at 1-sun AM1.5. Further progress in this top cell efficiency to about 17% at 500-sun AM1.5 is necessary.
- Baseline GaAs bottom cells with active-area AM1.5 1-sun efficiencies around 24% were demonstrated.
- Planar GaAs tunnel junctions, with specific resistivities of 3.3×10^{-3} ohm-cm^2, were obtained using a novel "cycled" growth for the p^{++} GaAs layer.
- Selective Ge deposition for PTJ was optimized and GaAs bottom cell overgrowth on patterned-Ge was examined.
- A new plasma-etch technique for the selective and rapid removal of the inverted-grown AlGaAs/GaAs cascades from Ge substrates was demonstrated, which has potentially useful implications for many high-efficiency mechanically-stacked cascades employing III-V single- or multi-junction cells grown lattice-matched to Ge.

References

1. J.M. Olson, S.R. Kurtz, A.E. Kibbler, and P. Faine, Appl. Phys. Lett.**56**, (1990) 623.
2. B.-C. Chung, G.F. Virshup, S. Hikido, and N.R. Kaminar, Appl. Phys. Lett.**55**, (1989) 1741.
3. P.K. Chiang, M.L. Timmons, and J.A. Hutchby, Solar Cells **21**, (1987) 241.
4. M.L. Timmons, "An AlGaAs-GaAs Patterned Ge Tunnel Junction Cascade Concentrator Solar Cell", Final Technical Progress Report, prepared for the Solar Energy Research Institute, Golden, CO, under Subcontract No. XL-4-03032, May 1988.
5. M.L. Timmons, "A High-Efficiency, Single-Junction, Back-Surface GaAs Concentrator Solar Cell", Final Technical Report, prepared for the Solar Energy Research Institute, Golden, CO, under Subcontract No. XL-5-04074, May 1988.
6. R. Venkatasubramanian, M.L. Timmons, T.S. Colpitts and J.S. Hills, Proc. of the SERI PVAR&D 10th Review Meeting at Lakewood, Colorado, October 23-25, 1990, to be published in Solar Cells.
7. H.G. Bhimnathwala, S.D. Tyagi, S. Bothra, S.K. Ghandhi, and J.M. Borrego, Proc. of the 21st IEEE Photovoltaic Specialists Conf., Kissimmee, Florida, (1990) 394.

8. N. Chand, J. Klem, T. Henderson, and H. Morkoc, J. Appl. Phys.**59**, (1986) 3601.

9. T. Fujisawa, J. Yoshino, and H. Kukimoto, J. Cryst. Growth **98**, (1989) 243.

10. D.L. Miller, S.W. Zehr, and J.S. Harris, Jr., J. Appl. Phys. **53**, (1982) 744.

11. R. Venkatasubramanian, M.L. Timmons, and T.S. Colpitts, submitted for presentation at 1991 MRS Spring Symposium on Atomic Layer Growth and Processing, Anaheim, California.

12. R. Venkatasubramanian, M.L. Timmons, T.S. Colpitts, and D.P. Malta, submitted for presentation at 1991 MRS Spring Symposium on Atomic Layer Growth and Processing, Anaheim, California.

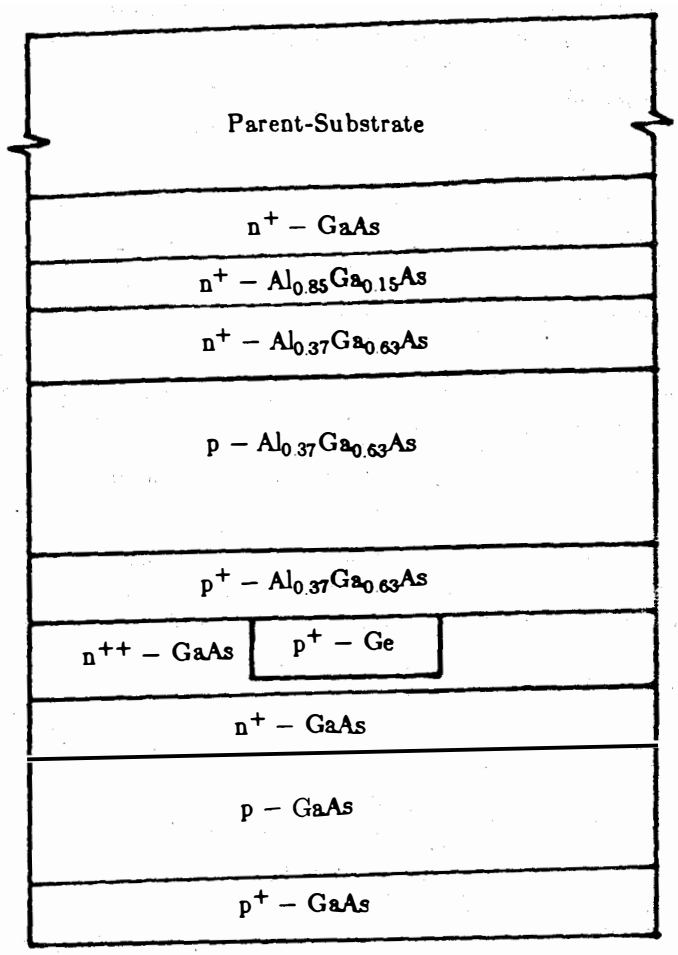

Figure 1. Schematic cross-section of the inverted grown AlGaAs/GaAs cascade with a Ge PTJ

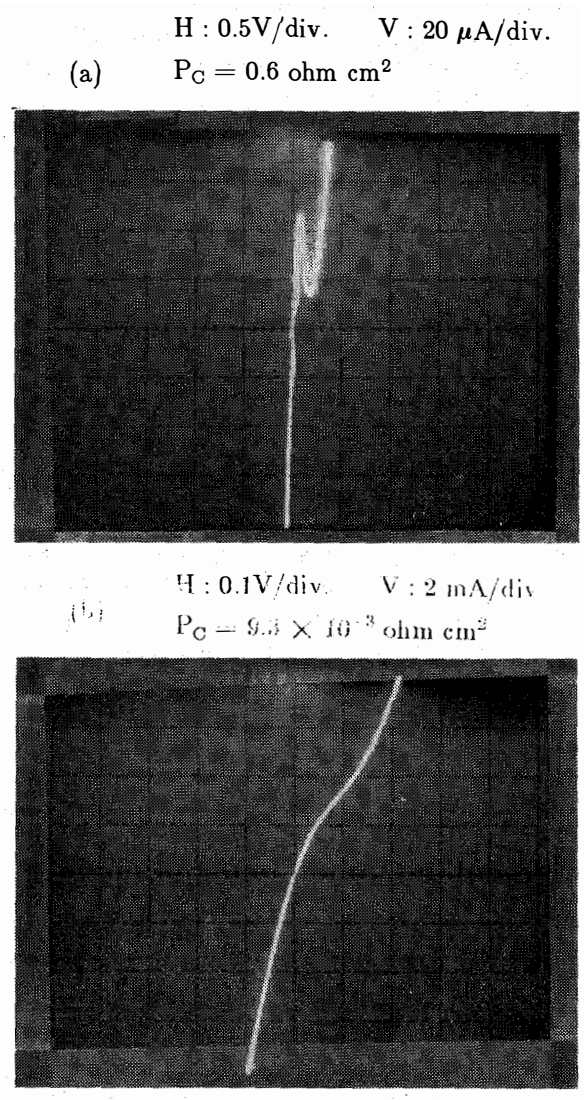

Figure 2. GaAs tunnel diode characteristic with (a)regular growth and (b)cycled growth for p^{++} GaAs

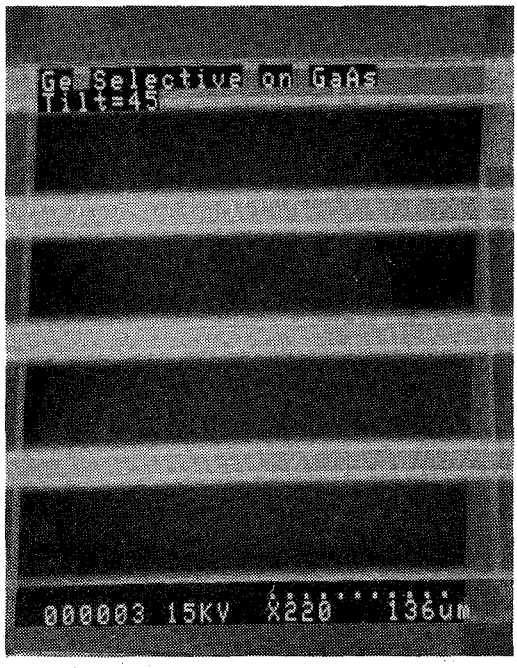

Figure 3. Selective epitaxy of Ge on GaAs

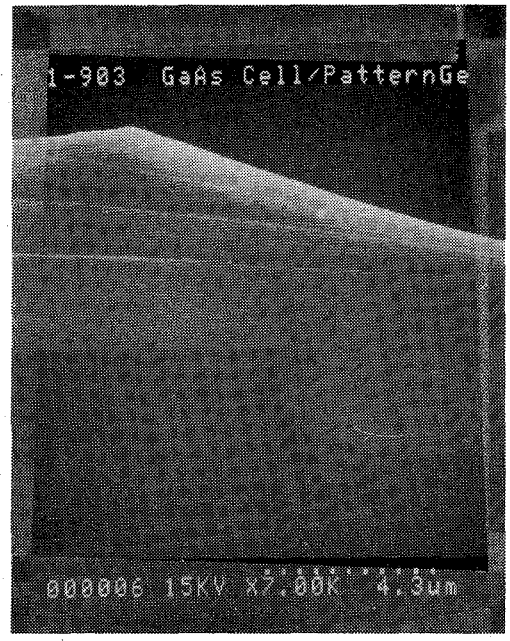

Figure 4. GaAs cell overgrowth on patterned-Ge

Sample Number	Prelayer Getter Structure	V_{oc}-Decay Lifetime	Solar Cell Data		
		(ns)	V_{oc}	J_{sc}(mA/cm^2)	η(%)
1-732	Yes	18	1.306	13.7	10.8
1-733	No	15	1.295	12.6	10.0

Table 1. Lifetime and I-V data showing the value of a getter structure

Sample Number	Emitter Thickness (μm)	Temperature for Window (°C)	H_2Se On During Ramp	Solar Cell Data		
				J_{sc}(mA/cm^2)	V_{oc}(V)	η(%)
1-691	0.4	800	No	4.8	1.221	4.2
1-680	0.2	800	No	6.2	1.251	6.2
1-704	0.2	725	Yes	8.6	1.272	8.7
1-714	0.2	675	Yes	9.1	1.275	9.3
1-733	0.2	650	Yes	12.6	1.295	10.0

Table 2. Effects of various surface passivation schemes on $Al_{0.37}Ga_{0.63}As$ cell performance

Title: **High Efficiency Epitaxial Optical Reflector Solar Cells**

Organization: Departments of Electrical Engineering and Materials Science
University of Southern California
Los Angeles, CA

Contributors: P. D. Dapkus, principal investigator,
S. G. Hummel, N. Frateschi (USC)
M. Klausmeier-Brown (Varian)

The objective of this program is to examine the epitaxial optical reflector (EOR) solar cell which alters current designs for high efficiency cells by changing the optical absorption efficiency of single cells. This change is introduced by the use of an epitaxial multilayer reflector as an integral part of the cell to increase the optical path length of certain wavelengths in the cell. The reflector is introduced at the rear of the cell and is designed to reflect those wavelengths that are weakly absorbed in the emitter and base layers of the cell. Fig. 1 shows a schematic diagram of the cell structure. The addition of the epitaxial optical reflector allows the base layer to be decreased, a heterojunction minority carrier reflector to be employed and the cell design to be further optimized. These changes are expected to increase the open circuit voltage at which power is extracted from the cell.

During the first year, efforts have focussed on the design of an epitaxial reflector with adequate reflectivity, R, to be used as part of an EOR cell but which requires the minimum total epitaxial thickness, the realistic modelling of cell performance and the growth of cell structures.

The goal of the reflector design is to achieve R>0.90 in the spectral region from 0.72 μm to 0.86 μm - the wavelength regions in which GaAs has absorption coefficient less than 10^4 cm^{-1} - with the minimum total growth thickness. Bragg reflectors using AlGaAs (x=0.2) and AlAs as the high and low index pairs of the reflector and employing a few sections with different periods have been modelled that allow the fabrication of the desired reflectors with a total growth thickness less than 4 μm. The wavelengths near the bandedge of GaAs with the longest wavelength and lowest absorption coefficient require the highest reflectance and thus the most periods. This sets some lower limit on how thin the reflector can be. We are also investigating the possibility of using GaAlAs/air reflectors using a newly conceived process in which the AlAs layers of the reflector are selectively removed. This approach if successful would most easily applied to a thin film peeled film cell.

Modelling of cell performance has been undertaken at Varian by Martin Klausmeier-Brown using Varian's CELLOPT program and PC-1D (Paul Basore). The initial results of this modelling suggest that EOR cells with total active layer

thicknesses in the range 1.3 - 1.5 μm are possible. Our assumption that R_b~0.90 is adequate for the EOR cell has been verified by the initial modelling. PC1D estimates a reduction of 0.1% in the cell efficiency for R_b=0.9 compared to R_b=1.0.

Modelling of both n on p and p on n solar cells to determine the optimum efficiency and structure has been completed. It has been determined that based upon CELLOPT parameters there is little difference between the structures and that the same conclusions with respect to insensitivity of efficiency upon cell parameters prevails for both designs. The efficiency of concentrator cells for AM1.5 applications shows that EOR cells have higher efficiency than conventional cells over an order of magnitude in doping. These data are summarized in Fig 2 shows the predicted performance of the EOR cell under concentration as a function of the doping of the base layer. These data suggest that efficiencies as high as 31.5% can be expected from these designs. It has been further shown that this design will be less sensitive to bulk degradation and, as a result, will be suitable for space applications.

The Bragg reflectors required for the construction of this cell require the growth of as many as one hundred layers with precisely controlled layer thickness. We have found that the growth rate during a run is stable enough to be able to grow reflectors with R~1.0 for 30 period reflectors. However, we have observed less than adequate reproducibility in the center wavelength of the reflectors. To overcome this lack of reproducibility we have developed an *in situ* growth rate monitoring technique that has permitted us to adjust and control the growth thickness of individual to an accuracy of ~1%[1]. The technique is based HeNe laser reflectometry. The reflection at near normal incidence of this wavelength from the growing surface exhibits maxima and minima corresponding to constructive and destructive interference owing to the growth of layers material with different index of refraction than the underlying layers. The choice of 6328Å radiation, that is heavily absorbed in GaAs, insures that each period of the Bragg reflector is optically isolated from previous ones. Using a measured value for the indices of refraction the oscillation in reflection can be used to measure the layer thickness or growth rate. This technique has been applied to the growth of Bragg reflectors in the GaAs/AlAs system with the results of Table I showing the comparative improvement in the reproducibility of the Bragg reflector center wavelength with the use of the in situ monitor. Work is now underway to grow solar cell structures with this technique.

References

1. N. C. Frateschi, S. G. Hummel, and P. D. Dapkus, Submitted to Electronics Letters.

Normal Base Solar Cell

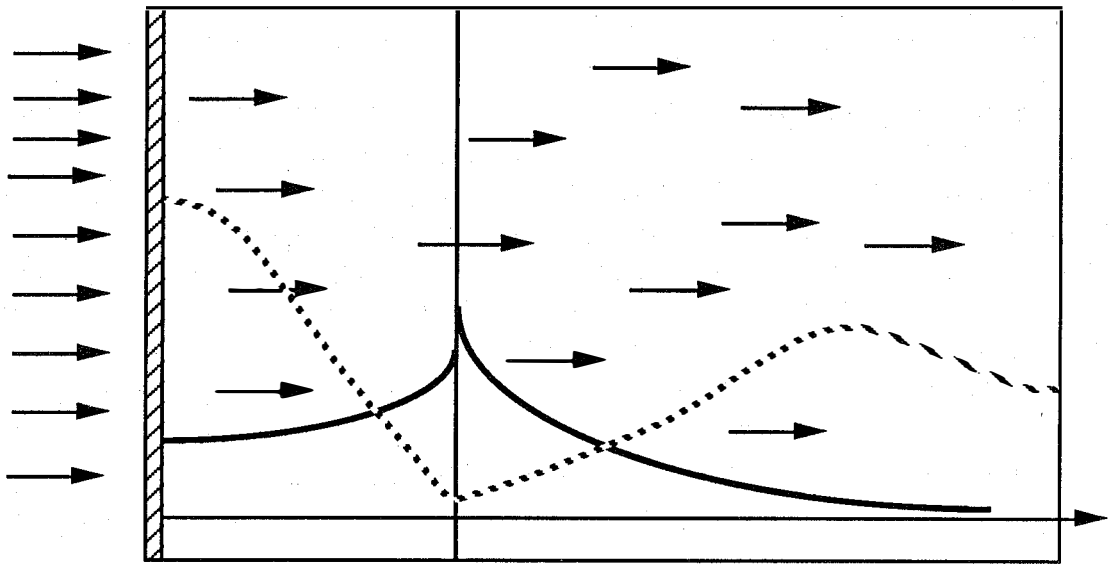

Window **Emitter** **Base**

Narrow Base, Bragg Reflector Solar Cell

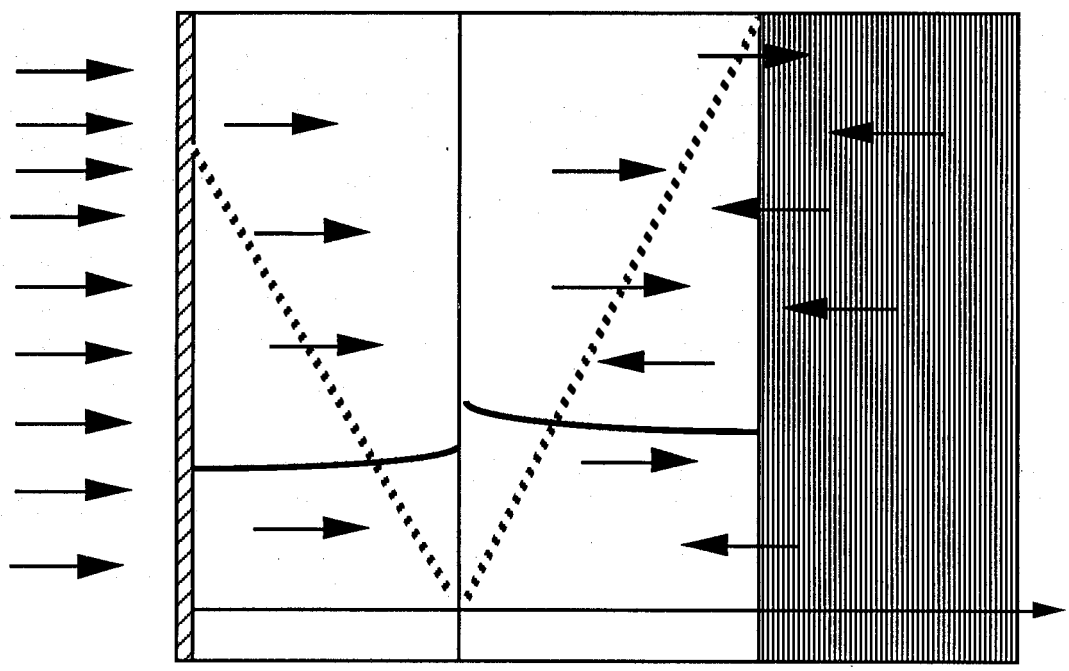

Window **Emitter** **Base** **Bragg Reflector**

Fig. 1

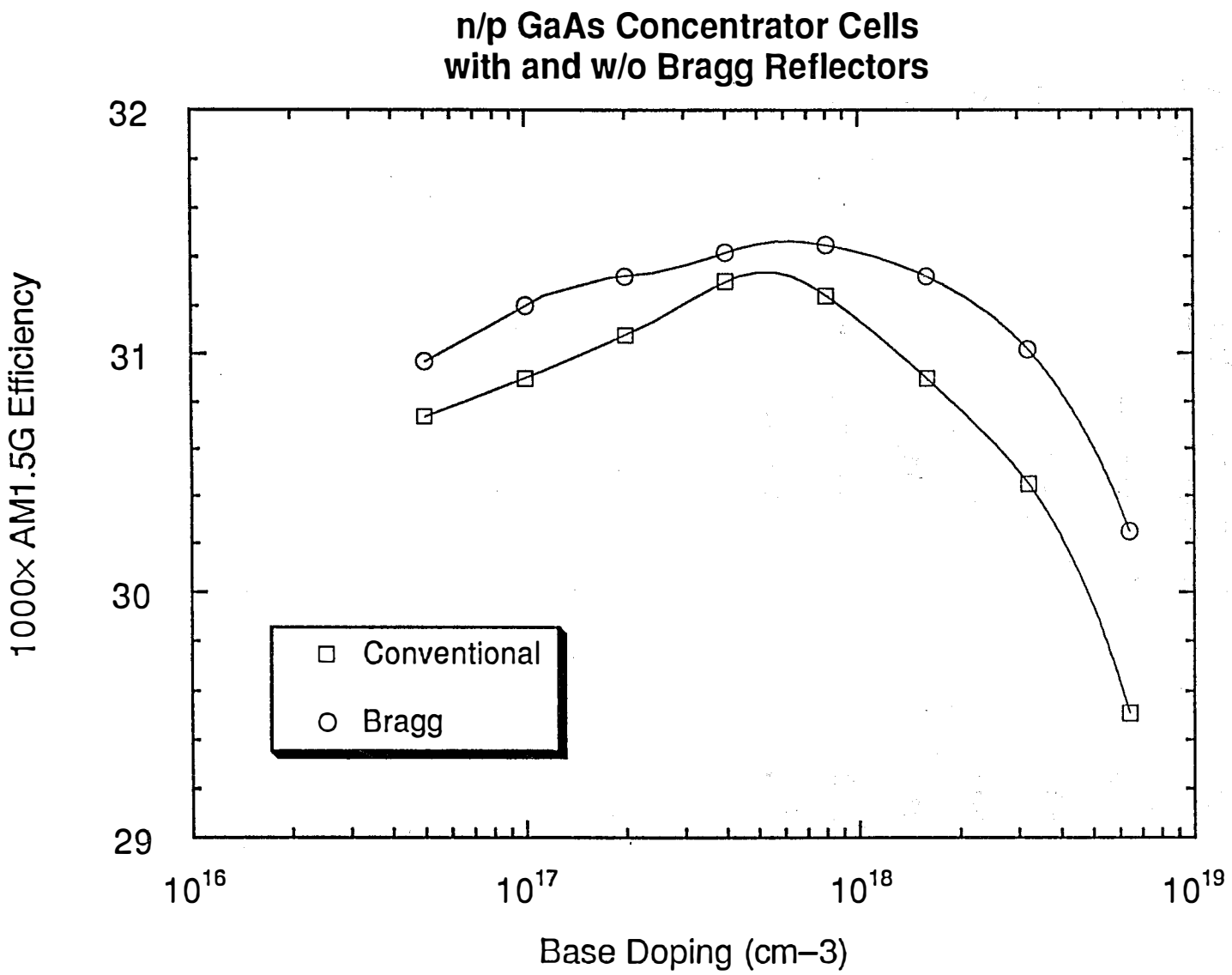
n/p GaAs Concentrator Cells
with and w/o Bragg Reflectors
1000x AM1.5G Efficiency
32
31
30
29
Conventional
Bragg
10^{16}
10^{17}
10^{18}
10^{19}
Base Doping (cm−3)

Table I

Sample #	Center of Stop Band for Design at 980 nm	Use of Laser Reflectometry?
1635	880 nm	No
1637	980 nm	No
1638	1040 nm	No
1686	976 nm	Yes
1692	976 nm	Yes
1696	976 nm	Yes

7.0 UNIVERSITY PARTICIPATION PROGRAM

John Benner (Manager), and Cecile Leboeuf

The objective of this program is to maximize the contribution of universities to the future of photovoltaic technology by focussing on the traditional needs and strengths of that community. Thus, it provides a forum in which the university researchers identify research topics critical to the advancement of photovoltaic technology with minimal influence from current programmatic interests. The selected participants are then permitted to pursue the proposed basic and applied research ideas in an environment designed to foster creativity by limiting requirements for delivery of reports, samples and achievement of specific goals. Reporting is limited to annual reports and journal publications. Research Symposia organized by the participants, are held periodically and are open to all students, program participants, and outside researchers. The intent of the initiative is to provide continuity of funding over a minimum three-year period which will allow universities to build and support interdisciplinary teams with specialized expertise which can be applied to furthering the technology base of photovoltaics. Such a program is expected to attract the most highly qualified university research teams to the DOE National Photovoltaics Program. The University Participation Program also supports photovoltaic industry through the technology transfer which occurs not only by publication of research results in the technical literature, but also through enhanced student awareness of photovoltaic technology and eduction of future professionals.

Title: **Improvement of Bulk and Epitaxial III-V Semiconductors for Solar Cells by Creation of Denuded Recombination Zones**

Organization: Department of Electrical and Computer Engineering, Carnegie Mellon University, Pittsburgh, Pennsylvania 15213

Contributors: A. G. Milnes and T. E. Schlesinger, principal investigators; D. Wong.

1. Objective

The aim of the research was to establish methods by which the hole diffusion lengths in bulk n type GaAs could be increased from 1 μm to about 3 μm so that efficient solar cells could be fabricated on wafers from ingots without the need for epitaxy.

Annealing Studies

Increases in hole diffusion lengths of up to a factor of three were obtained in commercially grown liquid encapsulated Czochralski (Te-doped) and Si-doped horizontal Bridgman GaAs. This was achieved by application of a technique involving proximity annealing of the material in sealed silica ampoules, Fig. 1. The beneficial effect of annealing is associated with the proximity protected surfaces, but extends several tens of microns into the bulk of the material, Fig. 2. The improvement depends on the achievement of a desired arsenic pressure at the proximity protected surface and therefore on the ampoule size in relation to the GaAs load [1, 2].

Similar results but not quite as impressive were obtained for Si doped horizontal Bridgman material.

In the Te-doped material studied, only two deep level defects were observed to be present in appreciable concentrations (> 10^{14} cm^{-3}) in control and proximity annealed material: the electron trap EL2 and a hole trap HCX at 0.29 eV above the valence band edge. If the hole lifetime τ_p in the material was being controlled by a single defect species with concentration N_t it would be expected (assuming hole capture to be the rate limiting step in the recombination process) that

$$\tau_p = \frac{L_p^2}{D_p} = 1/(\sigma_p N_t v_p) \qquad (1)$$

where D_p is the diffusion coefficient for holes, σ_p the hole capture cross section and v_p the thermal velocity of holes. This equation predicts that the plot of τ_p and the inverse of the concentration of the dominant recombination center will be a straight line passing through the origin. Such a relationship was found to exist between τ_p and the concentration of HCX in a

set of specimens which were proximity annealed at 950°C for a variety of anneal times. The concentration of EL2 appears to be associated with τ_p in a similar fashion. By application of eqn. 1 to the data it was inferred that if HCX is the dominant recombination center in the material it must have a hole capture cross section $\sigma_{p(HCX)} = 8x10^{-15}$ cm^2. Conversely, if EL2 is the dominant recombination center in the material, $\sigma_{p(EL2)} = 8x10^{-16}$ cm^2. The hole capture cross section of EL2 has been measured by other workers and found to be substantially smaller than $8x10^{-16}$ cm^2. From this, and other work in which a substantial increase of EL2 does not result in decrease of hole lifetime, we conclude that HCX rather than EL2 is the dominant recombination center [3-7].

3. Demonstration of improved solar cell performance

In order to ensure that in p^+n solar cells the efficiency is not severely degraded by poor carrier collection due to a small L_p in the base region of the cell, it is necessary to have L_p between 3 and 4 μm. Only a marginal advantage in terms of cell efficiency may be expected by further increasing L_p from 4 μm to the fundamental limits imposed by band-to-band radiative recombination (about 7 μm in $1x10^{17}$ cm^{-3} doped material). The results obtained in the present work show that proximity annealing is a technique which can be used to raise L_p in commercial GaAs material to the 3 to 4 μm level. An L_p of this magnitude in the base region of a solar cell is compatible with 1 sun AMO efficiencies in excess of 20% without the need for epitaxially grown layers.

To demonstrate that improvements in the material could be translated into enhanced device performance Zn diffused p^+n solar cells were fabricated in proximity annealed (L_p = 2.7 μm) and control (L_p = 1 μm) material. Spectral response measurements made on the cells with a junction depth of approximately 0.2 μm showed that cells fabricated in the anneal improved material had a larger long wavelength photoresponse than the cells fabricated in the control material, Fig 3. The enhancement in integrated photocurrent over a wavelength range 5500-8500 Å was about 15%. Passivation of the surface of the cells with an $(NH_4)_2S$ treatment was shown to be effective in raising the short wavelength response in the devices. The sulfide treatment was found to further increase the integrated short circuit photocurrent of a cell fabricated in improved material. Comparison of the photocurrent of this cell with the photocurrent of a control cell showed that increases in photocurrent of more than 16% (averaged over the wavelength range 4000-8500Å) could be achieved by the combination of the proximity annealing and sulfide passivation treatments [2].

4. Discussion

Extensive trap and photoluminescence studies have been made for a range of anneal conditions. From these studies we propose the following model to explain the effect of annealing on the defect structure close to the surface of the specimens. In the early stages of the anneal, the specimens are in a vacuum. As the temperature within the ampoule rises there will be As loss from the surfaces of the GaAs in order to build up the equilibrium As overpressure in the ampoule. Arsenic loss will be not only from exposed surfaces but also from proximity surfaces since the positive gradient of the arsenic partial pressure will force the arsenic (vapor) from between the proximity faces. It is this arsenic loss which results in the suppression of the defects HCX and EL2.

Once the arsenic overpressure in the ampoule has reached its equilibrium value at the anneal temperature, there will no longer be any pressure gradient in the ampoule. Interaction between the surface and the As vapor in the ampoule will be very much reduced at proximity surfaces but not at exposed surfaces. Chiang and Pearson [8] have pointed out that the flux of As atoms constantly leaving and returning to GaAs surfaces in dynamic equilibrium with the As vapor result in the creation of both As and Ga vacancies. Thus V_{Ga} will be generated rapidly at exposed surfaces and slowly at proximity surfaces during annealing. This is consistent with the experimental observations of a high concentration of another hole trap HCZ(at E_v + 0.57eV) found close to the exposed surface of a 16 hour 950°C annealed specimen. The presence of HCZ was observed to reduce the hole diffusion length in the unprotected surface.

The increases in L_p which result from proximity annealing of n-type GaAs are associated with the loss of As from the specimen surfaces in the early stages of the annealing [9]. This As loss is driven by the equilibrium requirements of As vapor pressure over GaAs at the anneal temperature. Since the sealed ampoules are of finite size, a limited amount of arsenic is removed from the specimen surfaces and as a result L_p versus depth profiles close to the proximity surfaces are characteristic of a limited source diffusion process.

The dominant recombination center in the material has been identified as a hole trap HCX (E_v + 0.29 eV). HCX is a native defect, probably associated with the excess arsenic in the substrates. Proximity annealing results in the suppression of both HCX and EL2 with similar characteristic diffusion coefficients of about 4×10^{-11} cm^{-3} at 950°C.

Annealing without proximity protection of the specimen surface results in the generation of a hole trap HCZ (E_v + 0.57 eV) at the exposed surface. This defect is associated with Ga vacancies and indiffuses into the material with a diffusion coefficient of about 3×10^{-11} cm^{-3} at 950°C.

Our studies were presented in part at the International Conference on the Science and Technology of Defect Control in Semiconductors, Yokahama, Japan September 1989. At the 17th International Symposium on Gallium Arsenide and Related Compounds in the UK, September 1990, Dr. Oda of the Nippon Mining Company presented a paper on multiple wafer-annealing LEC GaAs in relation to MOSFETs. The GaAs industry is now realizing the benefit of wafer-annealing and we believe our studies may have contributed to the move in this direction.

5. Acknowledgements

This work was supported by the Solar Energy Research Institute under Contract No. XB-6-06005-3. One of us (T.E.S.) acknowledges the support of the National Science Foundation through the Presidential Young Investigator Program.

References

[1] D. Wong, T. E. Schlesinger and A. G. Milnes, Solar Cells **27**, 419 (1989).

[2] D. Wong, T. E. Schlesinger and A. G. Milnes, IEEE Electron Device Lett., EDL 11, 321 (1990).

[3] A. Mitonneau, A. Mircea, G. M. Martin and D. Pons, Rev. Phys. Appl. **14**, 853 (1979).

[4] V. Ya. Prinz and S. N. Rechkunov, Phys. Stat. Sol. (b) **118**, 159 (1983).

[5] Liang Bingwen, Zou Yuanxi, Zhou Binglin and A. G. Milnes, J. Electron. Mater. **16**, 177 (1987).

[6] A. T. Hunter, in *Defect Recognition and Image Processing in III-IV Compounds II*, edited by E. T. Weber (Elsevier, Amsterdam, 1987), pp 137-145.

[7] R. Zucca, in *GaAs and Related Compounds*, St. Louis, 1976, (Institute of Physics, London, 1976), p. 228.

[8] S. Y. Chiang and G. L. Pearson, J. Appl. Phys. **46**, 2986 (1975).

[9] "Suppression of the dominant recombination center in n-type GaAs by proximity annealing of wafers," D. Wong, T. E. Schlesinger and A. G. Milnes, J. Appl. Phys., 1990, in press.

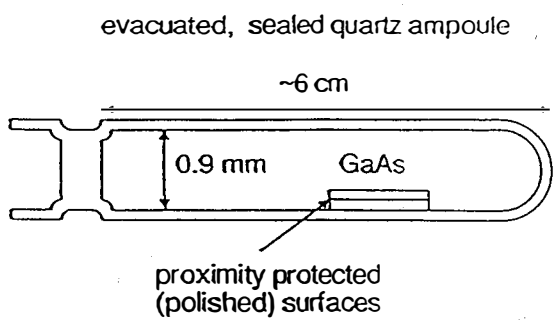

Figure 1. Proximity annealing arrangement.

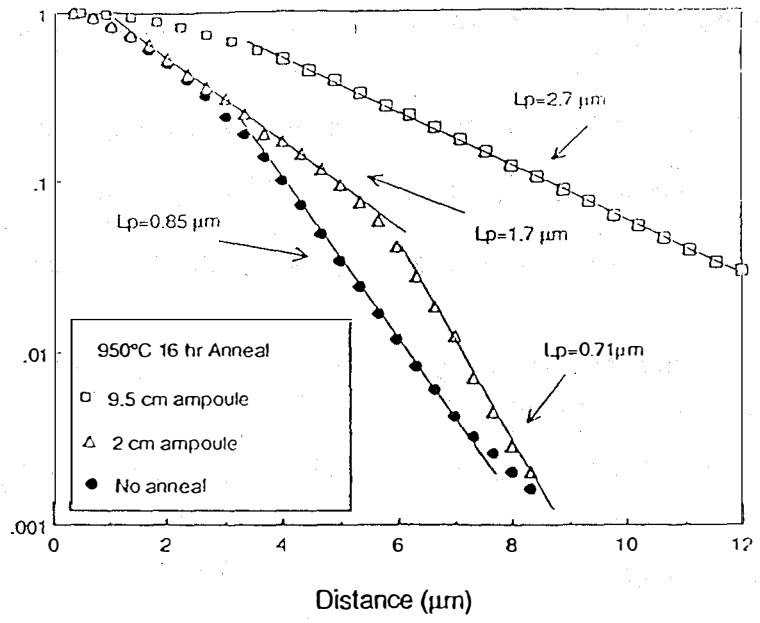

Figure 2. EBIC plots from Te-doped LEC specimens proximity annealed for 16 hrs. at 950°C in ampoules of different sizes (lengths). The control specimen was not proximity annealed.

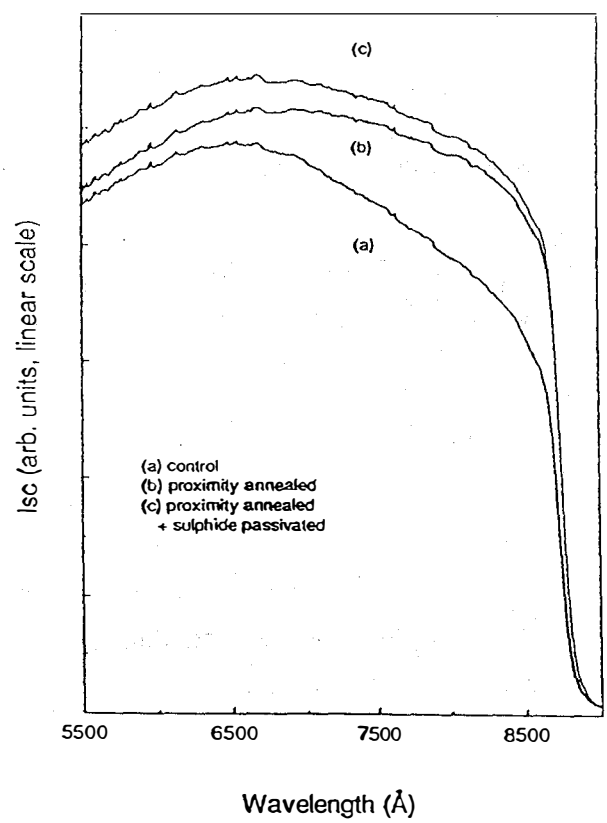

Figure 3. Short circuit photocurrent (I_{SC}) as a function of wavelength for Zn diffused solar cells with a junction depth of about 0.2 μm.

Title: **New Approaches for High Efficiency Solar Cell: Role of Strained Layer Superlattices**

Organization: Electrical and Computer Engineering Department
North Carolina State University
Raleigh, North Carolina

Contributors: S.M. Bedair and N.A. El-Masry

Objective

The object of the research program is to address current problems that are hindering progress toward achieving high efficiency cascade solar cell. During the last year our efforts were directed towards issues dealing with the quality and the growth conditions for the top high bandgap cell. Two material systems were studies, AlGaAs and GaInP, and atomic layer epitaxy (ALE) was used as the growth approach.

a) Low temperature growth of AlGaAs by Atomic Layer Epitaxy

The ALE growth approach in our laboratory relies on a specially designed growth chamber and susceptor. The substrate rotates between column III and column V streams of organometallic and hydride precursors. Trimethylgallium (TMG), trimethylaluminum (TMA), and arsine were the source materials. The ALE cycle consisted of the simultaneous exposure of the substrate to the TMG and TMA fluxes followed by rotation to the AsH_3 side to complete one cycle. The substrate makes one rotation in 2.6 s, allowing exposure time of about 0.3 s for each gas stream and yielding a growth rate of about 0.4 μm/h. The composition of the ALE-grown $Al_xGa_{1-x}As$ is controlled by the TMA/TMA + TMG molar ratio in the column III stream. We have also used the same reactor to grow AlGaAs films by the conventional MOCVD approach. In this case, the substrate is stationary and is exposed simultaneously to TMG, TMA, and AsH_3 fluxes. AlGaAs films with thicknesses of about 0.8 and 3 μm for ALE and MOCVD, respectively, were grown. Film thickness was determined by optical microscopy and the film compositions were obtained from photoluminescence measurements at 77 K. Carrier concentrations and their mobility were determined by the Hall technique. The growth conditions that allow the deposition of a monolayer of AlGaAs in a self-limiting fashion in the temperature range 550-700°C were determined[1].

Figure 1 shows the photoluminescence spectra for $Al_xGa_{1-x}As$ for difference values of x grown by ALE and MOCVD. The MOCVD film grown at 700°C showed very weak emission, as shown in Fig.(1a). The fairly broad PL emission from MOCVD material indicates that the MOCVD-grown AlGaAs at 700°C had additional defects and impurities which deteriorate the optical properties of the material. There were no PL signals observed from MOCVD films grown below 700°C. However, ALE-grown films showed fairly strong PL peaks for growth temperatures as low as 600° and a weaker emission at 550°C, as shown in Figs. 1(b) and 1(c), respectively. This is considered one of the lowest temperatures where AlGaAs was grown with good optical properties. AlGaAs ALE layers grown at 600 and 700°C have a comparable PL intensity to 4 μm MOCVD films grown at 800°C. The ALE process allows an improvement

in the PL properties that can be related to enhancement in the surface migration of column III adsorbed atoms. It has been shown that Al and Ga species have high surface diffusion coefficient in the absence of AsH_3 or As_2 exposure. This may result in improving the quality of ALE films, but it would not explain the difference in the incorporation mechanism of oxygen in these two techniques. It may be possible that TMA is the source of oxygen, and low TMA flux in the ALE growth is accompanied by reduced oxygen incorporation in the grown films.

ALE films have also better composition uniformity across 1.8 cm wafers than the MOCVD sample. The distribution of the PL peak corresponds to solid composition variation Δx of 0.2% and 4% for the ALE and MOCVD films, respectively[2], as shown in Fig. 2. This is another indication that the $Al_xGa_{1-x}As$ ternary alloys are grown in a self-limiting fashion. Thus ALE grown AlGaAs can have potential applications in the low temperature growth of the top cell.

b) Atomic Layer Epitaxy of $Ga_{0.5}In_{0.5}P$

InGaP has attracted wide interest as a high band-gap (E_g) material nearly lattice matched to GaAs. A large valence-band discontinuity, with direct E_g in the visible operating range, low surface recombination with GaAs, and smooth inverted heterointerfaces, make InGaP an attractive alternative to AlGaAs in optoelectronic devices generates. InGaP was deposited directly on GaAs substrate using TMGa, TEI, and phosphine as source material. During growth, PH_3 flowed continuously on the column V side. While the substrate was under the PH_3 flow, TMGa was turned on and allowed to stabilize and the substrate was rotated one cycle through the TMGa flux back to PH_3 to deposit near a monolayer of GaP. TMGa was then turned off and TEI was turned on and stabilized, while traces of TMGa were purged out. The substrate was rotated through the TEI flux back to PH_3 to deposit near a monolayer of InP, and thus a Ga-P-In-P structure was deposited. The structure was deposited at substrate temperatures in the range 480-700°C. The grown layers were characterized by x-ray diffraction, photoluminescence, photoreflectance, and transmission electron microscope techniques[3].

GaInP grown films at 500 and 550°C showed high quality, smooth surface morphology when examined by Nomarski interference contrast microscopy. Samples grown at 600-700°C showed increasing opacity. This may be due to the rapid surface depletion of P while the substrate is not PH_3 stabilized during the ALE rotation cycle. Double-crystal x-ray diffraction rocking curves shown in Fig. 3 have the (311) peaks of the GaAs substrate and $In_xGa_{1-x}P$ epilayer. The sample has $x \approx 49\%$ and a mismatch of $<0.1\%$. It should be mentioned that the TEI and TMGa fluxes for these epitaxial films were chosen arbitrarily.

ALE, with its self-limiting monolayer growth, is expected to have excellent large area uniformity in comparison to conventional MOCVD. Our typical ALE sample size (1.75 cm x 1.75) was cleaved into strips approximately 3mm wide, and double-crystal X-ray was used to determine the lattice-mismatch of each strip[4]. $\Delta a_x/a_o$ maximum variation, point-to-point, was equal to 0.000054 which corresponded to a maximum In fluctuation in the alloy of 0.0084%.

Cross-sectional transmission electron microscope (TEM) was performed on samples grown on (100) GaAs substrates oriented 2° off towards [110]. Electron diffraction pattern for the [110] zone axis showed superlattice spots that are distinct and well defined indicating the CuPt type of ordering. Ideally, with the ALE deposition regime for this alloy, we would expect the column III sublattice to be ordered in the [001] growth direction. However, we found no evidence of a (001) superlattice from our diffraction studies and preferential ordering is taking place in (111) alternating planes. Ordering was not observed in samples grown on (100) oriented substrates.

PL was used to detect the bandgaps of ordered and disordered structures. Misoriented sample showed a 4K peak at 1.857 eV with a full-width half maximum of 30meV, while a (100) ± 0.5 grown sample showed 2.01 eV with a slightly wider width. The ordered alloy bandgap is lower than any values detected to date to our knowledge. These results confirmed the TEM diffraction patterns with regards to ordering and the resultant bandgap suppression.

Photoreflectance was also used to look at the bandgap of the ALE GaInP[3], as shown in Figure 4. This was measured by F.H. Pollak and associates at CUNY Brooklyn. It gave a room temperature E_g of 1.77 eV. This matches rather closely the photoluminescence value.

Thus in conclusion ALE offers a low temperature growth technique of the growth of AlGaAs and InGaP films with good optical and compositional uniformity on GaAs substrate.

References

1. J.R. Gong, D. Jung, N.A. El-Masry and S.M. Bedair, Appl. Phys. Lett. 57, 400 (1990).

2. J.R. Gong, P.C. Colter, A. Dip, W. Duncan and S.M. Bedair, J. Cryst. Growth (accepted).

3. B.T. McDermotte, K.G. Reed, N.A. El-Masry, S.M. Bedair and F. Pollak, Appl. Phys. Lett. 56, 1172 (1990).

4. B.T. McDermott, N. El-Masry, W. Duncan, and S.M. Bedair, J. Cryst. Growth (accepted).

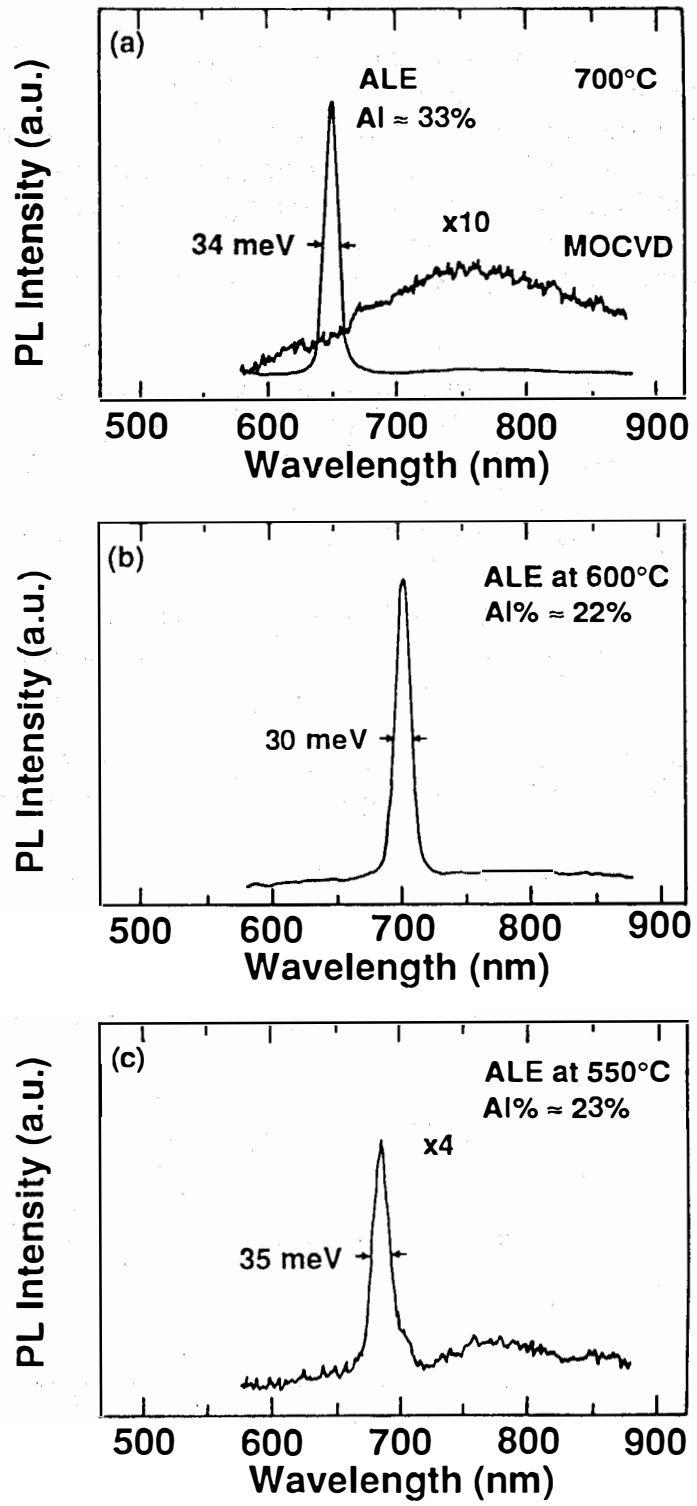

Figure 1: Photoluminscence at 77K˚ of AlGaAs grown by ALE and MOCVD

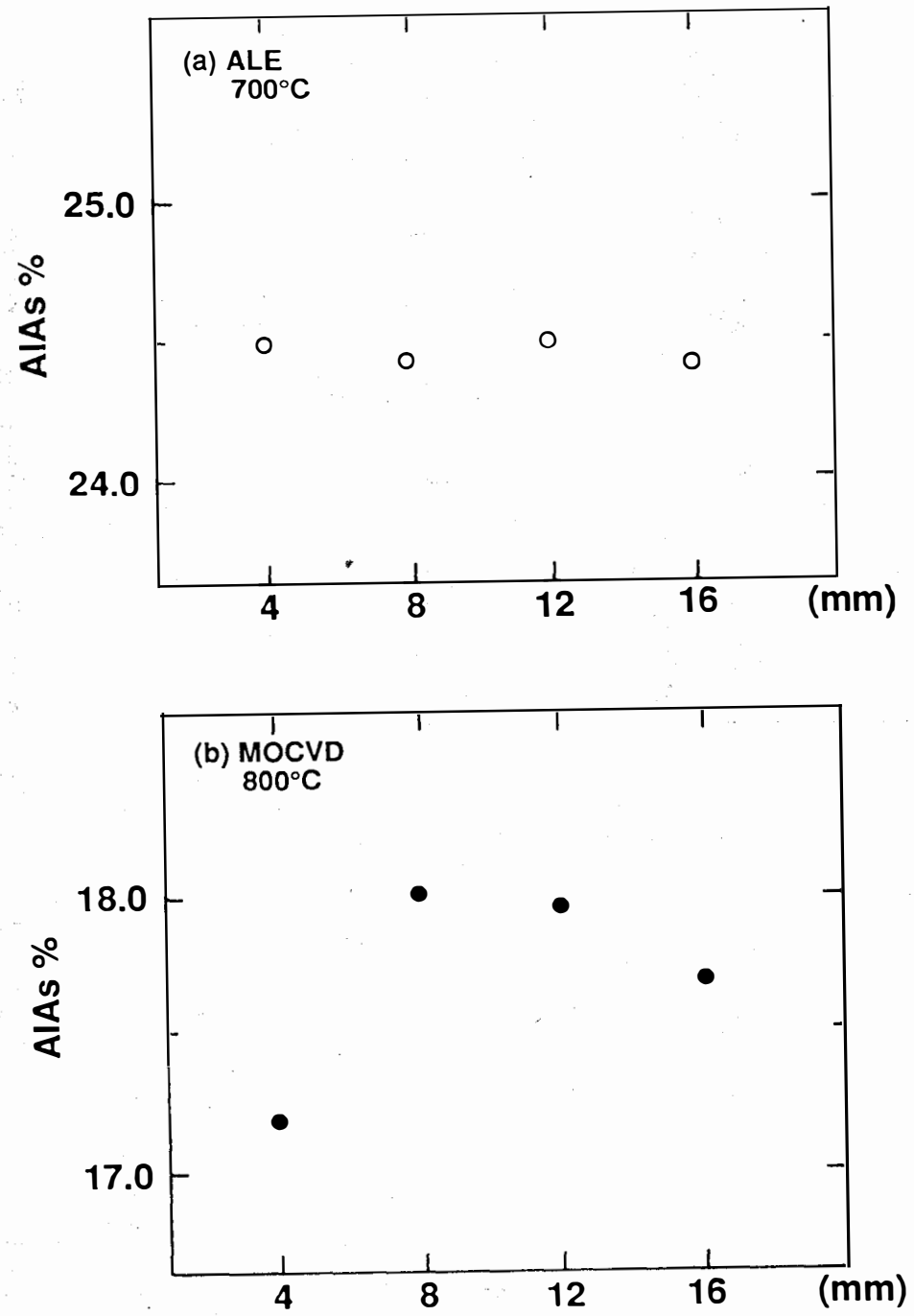

Figure 2: Composition Uniformity of AlGaAs films grown by ALE and MOCVD

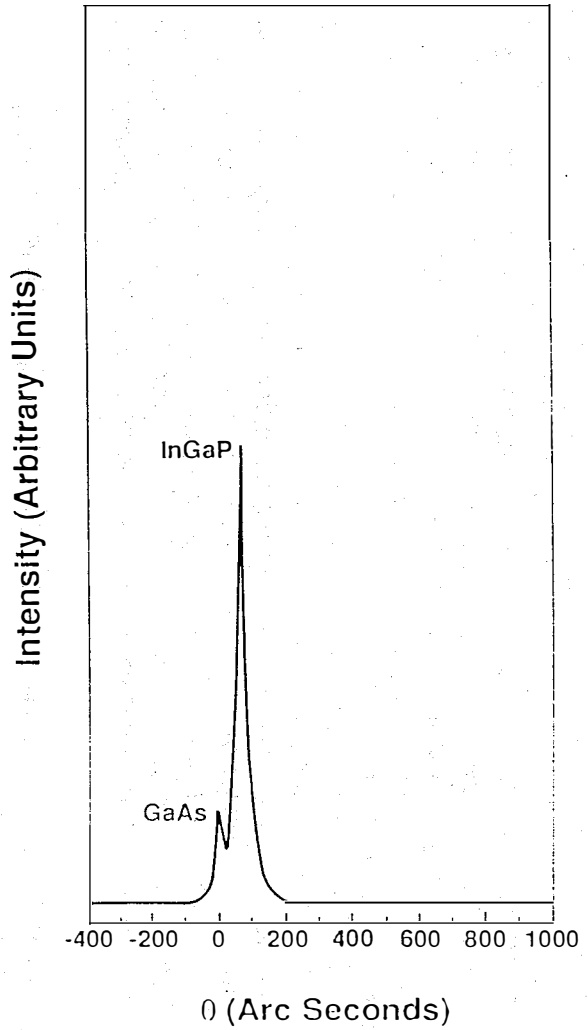

Figure 3: Double-crystal x-ray diffraction rocking curve for InGaP grown on GaAs substrate

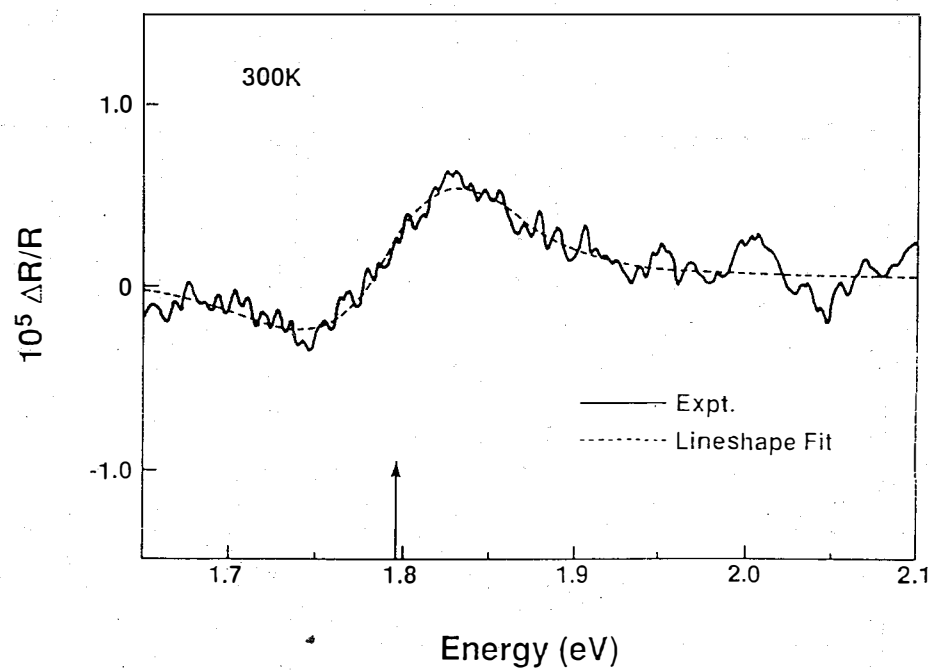

Figure 4: Photoreflectance spectrum at 300K of InGaP on GaAs substrate

Title: **Fundamental Studies of Defect Generation in Amorphous Silicon Alloys Grown by Remote Plasma-Enhanced Chemical-Vapor Deposition (Remote PECVD)**

Organization: Departments of Physics, and Materials Science and Engineering,
North Carolina State University
Raleigh, North Carolina 27695-8202

Contributors: Professor Gerald Lucovsky, Principal Investigator;
Professors Robert J Nemanich and Jerzy Bernholc, Faculty Contributors;
Greg Parsons, Cheng Wang, Brian Davidson and Meredeth Williams, Graduate Students

Introduction

Research under this sub-contract, XM-9-18141-2, was begun on 01 July 1989. This report addresses the research issues relevant to tasks that are defined in portions of Phases I and II of this three-year research program.

Process Definition for Device Quality a-Si:H by Remote PECVD

(a) Film Deposition

We have shown that the relative concentrations of monohydride, SiH, and polyhydride, $\{SiH_2\}_n$, bonding groups in hydrogenated amorphous silicon, a-Si:H, are determined by the total bonded hydrogen concentration, [H], and therefore are not intrinsically dependent on any deposition parameter, e.g., the substrate temperature. We have shown that there are two independent requirements for the formation of electronic grade a-Si:H: a) it should contain a bonded hydrogen concentration, [H], that is in the range of [H] ≈ 5-15 at.%, thereby promoting silicon-hydrogen bonding predominantly in monohydride arrangements; and b) the material must be annealed for a sufficient, and temperature-dependent time either during or after film deposition, in order to reduce the density of deposition process induced defects. This annealing is a thermally activated process with an activation energy of the order of 1 eV or more, and therefore, in order to be accomplished in reasonable times, the annealing requires temperatures in excess of about 150°C.

For T_s in the range between about 100°C and 300°C, Remote PECVD films have about one-half of the bonded-H relative to GD films. This is a result of the different ways the silane reactant contributes to film deposition, and in particular to the availability of hydrogen for incorporation in the growing film. In the GD process, the silane molecule, SiH_4, is fragmented in the gas phase, and all four hydrogen atoms are available for film incorporation. In Remote PECVD, the first step involves the excitation of a silane molecule by electrons derived from a remote He plasma. The next step is the fragmentation of the vibrationally excited silane molecule, SiH_4^*, at the deposition surface into SiH_2 and H_2, so that only half of the total hydrogen of the SiH_4 molecule is available for film incorporation. a-Si:H produced by Remote PECVD between about 150 and 200°C is superior to GD material deposited in the same range of T_s, primarily because it contains less polyhydride material, and therefore has fewer "polyhydride-induced" defects. a-Si:H deposited by Remote PECVD between about

225°C and 250°C has essentially the same electronic properties as the GD material deposited at the same temperatures: i) the same dark conductivity, and dark conductivity activation energy; ii) the same photoconductivity; and iii) the same defect density, as determined by CPM, but, it has a lower bonded hydrogen concentration.

(b) Annealing Kinetics

We have compared the kinetics of defect relaxation in films deposited by Reactive Magnetron Sputtering, RMS, and with defect relaxation in light-soaked RMS and Remote PECVD films. i.e., in films initially deposited at high temperatures, 220°C to 250°C, with bonded hydrogen in the range of 8 to 15 at.%, that have been exposed to high intensity illumination, ~50 mW of white light for periods of about 6-10 hours. We have determined the conductivity changes as a function of time, and have investigated different ways of characterizing the kinetics of the relaxation process. The main issue is an accurate determination of a characteristic relaxation time, τ. We have tried several approaches, and have converged on a procedure that is unambiguous and consistent with the prevailing model of characterizing the relaxation process with a stretched exponential function, s exp $\{-(t/\tau)^b\}$. The problem that we have encountered is that there is usually insufficient experimental data, at both long and short observation times, to determine an unambiguous three-parameter fit, i.e., s, τ and b. To get around this limitation for τ, we rely on the analysis of Crandall, which showed that the rate of change of the stretched exponential function is greatest at a time which is equal to the relaxation time, τ. We then use these analytically-determined times to calculate the activation energy. For the RMS films, we find an activation energy of 1.6 eV for relaxation of deposition process induced defects, and 1.3 eV for relaxation of light-soaking induced defects, whereas for light-soaked induced defects in Remote PECVD films, we find a significantly lower activation energy of 0.6 eV. We have not been able to correlate this difference with any other property difference between the RMS and Remote PECVD films.

Doping of Remote PECVD a-Si:H Thin Films

We have been able to dope a-Si:H films both n-type and p-type by exciting mixtures of SiH_4, and PH_3 or B_2H_6, respectively, with active species extracted from a remote He plasma. We find the same relationship between the conductivities of these doped Remote PECVD films and the gas phase ratio of the doping gas to silane, as had been previously established for film deposition by the GD process.

Electrical Properties of a-Si:H by Remote PECVD

Gas Phase Ratio	Dark Conductivity (S/cm) = $(\Omega cm)^{-1}$	Activation Energy eV
$PH_3/SiH_4 = 10^{-2}$	2.0×10^{-3}	0.25
undoped	2.4×10^{-10}	0.80
$B_2H_6/SiH_4 = 10^{-1}$	2.3×10^{-3}	0.31

Deposition of Microcrystalline Si by Remote PECVD

We have deposited intrinsic and doped thin films of μc-Si by Remote PECVD at temperatures in the range of 150°C to 400°C. We have achieved conductivities as high as 40 S/cm in the n-type material, and 6 S/cm in the p-type material, with activation energies of 0.018 eV and 0.040 eV, respectively. In addition, we have made a break-through in the deposition of a low-conductivity, ~6×10^{-8} S/cm, lightly boron-

doped near-"intrinsic" μc-Si material, (source gas ratio of $B_2H_6/SiH_4 = 10^{-5}$), that displays photoconductivity comparable to device grade a-Si:H. This material shows no Stabler-Wronski effect, so far measured for a light flux of 50 mW/cm^2 for 6-10 hours.

We have deposited μc-Si films by Remote PECVD using two different techniques with respect the addition of hydrogen to the process gas mixture: i) a He/H_2 mixture was plasma excited, and the SiH_4 and doping gases were added downstream; and ii) He was plasma excited, and all other process gases, SiH_4, H_2 and the dopant atom source gases were added downstream. H_2/SiH_4 ratios were varied from 5:1 to 80:1, and μc-films, were obtained for all ratios of 10:1 and greater. Microcrystallinity was determined by Raman scattering, TEM imaging and electron diffraction. An H_2/SiH_4 ratio of 30:1, coupled with downstream injection of hydrogen gave: i) the strongest and sharpest microcrystalline feature in the Raman spectrum; ii) crystallite sizes of about 100Å in the TEM images; and iii) no non-crystalline silicon transition regions between c-Si and SiO_2 substrates, and the onset of the μc-Si deposit. The same conditions were used to deposit the n-type and p-type μc-Si.

Doped films were deposited by remotely exciting mixtures of PH_3/SiH_4 and B_2H_6/SiH_4. Undoped μc-Si has a dark conductivity of $6x10^{-4}$ S/cm and a dark conductivity activation energy of 0.3 eV. The conductivity increased monotonically with the addition of PH_3 to the SiH_4; at the same time the dark conductivity activation energy decreased. The highest value of dark conductivity, obtained for a ratio of $PH_3/SiH_4 = 10^{-2}$, was 40 S/cm, with a dark conductivity activation energy of 0.018 eV. The addition of a relatively small amount of the p-type doping gas, $B_2H_6/SiH_4 = 10^{-5}$, caused a significant decrease in the dark conductivity to $6x10^{-8}$ S/cm, paralleling a similar behavior previously reported for boron doped a-Si. The activation energy increased to 0.7 eV, very nearly one-half of the optical gap, 1.44 eV, as defined by E_{04}. Higher concentrations of B_2H_6 to SiH_4, between 10^{-5} and $1x10^{-3}$, produced increases in the dark conductivity, accompanied by decreases in the dark conductivity activation energy. The highest level of dark conductivity obtained was 6 S/cm, with an activation energy of 0.04 eV. Further increases in the doping gas ratio, resulted in decreases in the dark conductivity, and increases in the dark conductivity activation energy. Raman scattering studies showed that these decreases in the dark conductivity resulted from the deposited films being amorphous rather than microcrystalline.

Electrical Properties of μc-Si:H by Remote PECVD

Gas Phase Ratio	Dark Conductivity (S/cm) = $(\Omega cm)^{-1}$	Activation Energy eV
$PH_3/SiH_4 = 10^{-2}$	40	0.018
undoped	$6x10^{-4}$	0.30
$B_2H_6/SiH_4 = 10^{-5}$	$6x10^{-8}$	0.70
$B_2H_6/SiH_4 = 10^{-3}$	6	0.040

We have conducted a comprehensive study of the most-resistive μc-Si, the films grown from the $B_2H_6/SiH_4 = 10^{-5}$ mixture. For these films we find: i) a dark conductivity of $6x10^{-8}$ S/cm with an activation energy of 0.70 eV; ii) an effective band-gap as defined by E_{04} of 1.44 eV; iii) a monochromatic photoconductivity of $4x10^{-5}$ S/cm for a generation rate of about $1x10^{19}$/cm^3; iv) a flat spectral response between 500 nm and

750 nm; iv) a photocoductivity of ~$1x10^{-4}$ S/cm for 0.5 AM1 light; and v) no detectable Stabler-Wronski effect for light exposures to 50 mW/cm^2 for up to 6 hours.

Deposition of a-Si,C:H and μc-Si,C by Remote PECVD

(a) a-Si:H

We have deposited a-Si,C:H alloy films at a substrate temperature of 250°C using remote excitation of SiH_4/CH_4 source gas mixtures. We have varied the methane fraction, and studied source gas ratios, R, defined as $R = SiH_4/(SiH_4 + CH_4)$ from 1 to 0.33. The properties of these films are essentially the same as those produced by the GD process for the same source gas ratio. As R decreases from 1 for a-Si:H, the E_{04} band-gap increases and the photoconductivity decreases. The main features in the IR spectra of this series of films are: i) a shift of the SiH stretching frequency from about 2000 cm^{-1} in a-Si:H to about 2075 cm^{-1} in all of the a-Si,C:H alloy films; 2) the appearance of features associated with CH_3, at about 1250-1400 cm^{-1}, and 2800-3000 cm^{-1} in all of the a-Si,C:H alloys; and 3) the appearance of sharp feature at about 750 cm^{-1} associated with Si-C vibrations, and in a local bonding environment in which the C-atom is part of a methyl group, i.e., an $Si-CH_3$ structure.

We have added B_2H_6 downstream to the SiH_4/CH_4 source gas mixture and produce p-type alloy films. These studies were restricted to films prepared with R equal to 0.67. For the highest doping gas ratio used, the conductivity is about a factor of 500 hundred less than in a-Si:H, and the activation energy is about 0.15 eV higher. These changes are consistent with the conductivity prefactor, the product of a band density of states and a band mobility, being about the same in the a-Si:H and a-Si,C:H films.

Electrical Properties of a-Si,C:H and μc-Si,C Alloys

Gas Phase Ratio	Dark Conductivity (S/cm) = $(\Omega cm)^{-1}$	Activation Energy eV
(a) a-Si,C:H		
undoped	$2.3x10^{-13}$	0.99
$B_2H_6/SiH_4 = 10^{-3}$	$2x10^{-9}$	0.69
$B_2H_6/SiH_4 = 10^{-2}$	$1.4x10^{-6}$	0.46
(b) μc-Si,C		
$B_2H_6/SiH_4 = 10^{-3}$	$6.3x10^{-4}$	0.18
*$B_2H_6/SiH_4 = 10^{-2}$	$1.4x10^{-7}$	0.56
*this film is		

(b) μc-Si,C

We have deposited films of μc-Si,C by Remote PECVD by adding hydrogen to the downstream injected SiH_4/CH_4 source gas mixture (R=0.67). Raman spectra indicate: i) that the fraction of microcrystallinity, estimated from the ratio of the scattering at 475 and 520 cm^{-1} is lower in the Si,C alloy material than in a material with no carbon added; and ii) that adding diborane further reduces the fraction of microcrystallinity; i.e., a film grown from a source gas mixture that includes 0.1% diborane shows evidence for microcrystallinity, whereas a film grown from 1% diborane shows no evidence in the Raman spectrum for a detectable microcrystalline component. The table above includes conductivity data for these samples grown with hydrogen added downstream, where we note that the films deposited with 1% diborane with and without hydrogen dilution have similar electrical properties. The

effect of adding hydrogen to this particular downstream mixture is then to increase the dark conductivity activation energy and to reduce the conductivity. In this instance the changes in activation energy and conductivity can not be accounted for with the same value of the conductivity prefactor. The main regions that exhibit changes in the IR absorption are: i) the spectral region of the SiH stretching vibration, 2000-2100 cm^{-1}; and ii) the spectral range between 1200 and 1500 cm^{-1}, which is associated with CH_3 groups. For the samples grown with hydrogen injected downstream, there are nearly equal IR absorption strengths at about 2000 and 2075 cm^{-1}; these are associated respectively with SiH vibrations in which the SiH group has only Si neighbors, and with SiH groups where there are one or more carbon atoms back bonded to the SiH group. For the three samples grown without hydrogen dilution, the 2075 cm^{-1} mode dominates. In addition, the three samples grown without hydrogen dilution show stronger features associated with the CH_3 groups. This means: i) that hydrogen dilution influences the local bonding environments of SiH groups, and that this is independent of the microcrystalline or amorphous nature of the film; and ii) that addition of hydrogen also effects the concentration of methyl groups. Additional studies of local bonding in doped a-Si,C and μc-Si,C alloy films are necessary before all of these effects can be explained.

Applications of μc-Si and μc-Si,C in Device Structures

We have formed p-i-n junctions that are fabricated using only μc-Si. These p-i-n structures have the following layer dimensions: the p-layer, and n-layers are 300Å thick and the i-layer is 2800Å thick. The i-layer is grown from the boron-compensated material discussed above, The p-i-n diodes exhibit: i) rectification ratios of about 10^4 at a 0.5 V bias level and have ii) short circuit current densities of about 4 mA/cm^2, and open circuit voltages of 0.4 V. These structures are "non-optimized" PV devices, i.e., i) they are devices with "poor" contact geometries; and ii) they are illuminated through absorbing μc-Si p-layers that were deposited onto the ITO-coated glass substrates.

We have also fabricated p-i-n structures with μc-Si,C p-layers grown from 0.1% diborane source gas mixtures, using an $SiH_4/(SiH_4 + CH_4)$ ratio = 0.67. These structures employed heavily doped μc-Si n-layers, and had a-Si:H i-layers. The n and p-layer thicknesses were 150 and 300Å, respectively, and the i-layer thicknesses were 3000Å and 4000Å. The structures were deposited onto ITO-coated glass substrates and illuminated through the p-regions. Open circuit voltages were 0.6 eV, and the short circuit current density, under approximately 0.5 AM1 illumination - 50 mW/cm^2 from quartz halogen lamp, were respectively 5.2 and 8.1 mA/cm^2 for the devices with the 3000Å and 4000Å thick i-layers.

Modelling of the Electronic States of a-Si

We have employed two different tight-binding models to Si-Bethe lattice structures in order to investigate the effects of bond-angle, and/or dihedral angle disorder on the band edge density of electronic states. We find that a Hamiltonian with: i) only nearest neighbor interactions; and ii) using the "empirically-constructed" sp^3s^* basis set of Dow and co-workers, yields qualitatively different results than using a Hamiltonian with: i) nearest and second-nearest neighbor interactions; and ii) a set of tight-binding parameters that generate a proper band-structure for crystalline Si with an sp^3 basis set.

We have studied electronic states associated with bond-angle deviations from an ideal tetrahedral geometry. Our objective is to determine whether bonding configurations with large bond-angle deviations are the origin of the weak bonds that eventually contribute to defect generation via light-soaking or stress bias. Our initial calculations used nearest neighbor interactions, an sp^3s^* basis set, and averaged over Bethe lattices in which all bonds were distorted. These calculations indicated that as the average bond-angle deviation is increased, the gap narrows with the major contribution to the narrowing being a broadening, and tailing into the gap at the valence band edge. There is very little movement or change in the conduction band edge in this model calculation. We have also performed calculations for isolated clusters with bond-angle distortions; these are terminated with ideal Si Bethe Lattices. These calculations indicate that bond-angle deviations greater than about 20 degrees can lead to the generation of localized states that emerge from the valence band edge.

We have also studied the effects of bond-angle distortions using a Hamiltonian that includes second neighbor interactions, and have used an sp^3 basis set for these calculations. The parameters for this calculation are obtained from the application of the same Hamiltonian to crystalline silicon, where it yields excellent results for both the valence and conduction bands. The application of this Hamiltonian to a Bethe Lattice structure with no bond angle distortions, and a single "idealized" dihedral angle, gives an excellent representation of both the valence and conduction band structures for a-Si. This is the same result we found for the sp^3s^* basis set and nearest neighbor interactions, indicating the "non-uniqueness" of these model calculations.

We have also used the second-neighbor Hamiltonian to calculate the band structure for Bethe Lattices that included statistical distributions of bond-angle distortions. There are two important results that we have found: i) the effective band-gap decreases as the average bond angle distortion increases; and ii) the band-gap penetration at the conduction and valence band edges are about the same. The first of these results is similar to what has been found in the tight-binding calculations that used only nearest neighbor interactions, and the sp^3s^* basis set. However, the second observation is qualitatively and and quantitatively different. In particular we find that as the valence band edge moves into the forbidden gap, the edge softens, whereas as the conduction band edge moves into the gap, the edge sharpens.

Therefore the results of both models support the idea that the slope of the absorption edge in the exponential region is determined primarily by the valence band edge. Both models also support the interpretations of transport data which indicate the dispersion at the conduction band edge is less than at the valence band edge. In this instance, the nearest neighbor interaction model, using the sp^3s^* basis set, over-estimates the ratio of band tailing effects; i.e., the calculated ratios are about three to one, whilst the experimentally estimated ratios are less than two to one. Overall, it appears that a Hamiltonian with second neighbor interactions and an sp^3 basis set provides a better starting point for model calculations of weak bonds, and other types of defects, e.g., dangling bonds as well.

Title: **Photon and Ion Assisted Doping and Growth of II-VI Compound Thin Films**

Organization: Department of Materials Science and Engineering, Stanford University, Stanford, CA 94305-2205

Contributors: R.H.Bube (Principal Investigator), A. L. Fahrenbruch, S-G.Huang, D. Kim, A. Lopez-Otero, and P. Sharps

The purpose of this work is to investigate the doping and growth of II-VI compound films, especially p-CdTe, by physical vapor deposition with co-evaporation of the dopant. Two methods of dopant incorporation, photon-assisted doping (PAD) and ion-assisted doping (IAD), are compared with respect to the growth, structural, and photoelectronic properties of the deposited films.

Methods of Approach

Control of p-type doping in polycrystalline CdTe solar cells is a promising tool for minimizing series resistance loss and maximizing V_{oc} [1]. Our previous work, using IAD [2-7], focused on the incorporation of the dopants and yielded carrier densities up to 2×10^{17} cm^{-3} in homoepitaxial films with P, but gave films with low minority carrier diffusion length L_d. We are investigating PAD as a gentler alternative that would enable doping, but yield good L_d and crystalline quality.

Schetzina *et al.* [8-9] and his students [10-11] have reported PAD doping of CdTe epitaxial layers deposited by MBE to levels as high as $p = 6 \times 10^{18}$ cm^{-3} with As, and good crystalline quality, as evidenced by photoluminescence (PL), double crystal rocking curves (DCRC), and excellent carrier mobility μ. Although their data suggest long L_d, it was not measured.

Other workers [12-13], including ourselves, have not been able to reproduce the PAD results of Schetzina *et al.*, but there appears to be a consensus that illumination during deposition does enhance the crystalline quality. Arias *et al.* [12] found that illumination had little or no effect on doping, but that a Cd/Te flux ratio = 1.1-1.3 was necessary to incorporate As during the MBE growth of p-CdTe and to activate it electrically, regardless of whether the sample was illuminated or not.

Our deposition system is now capable of deposition in the IAD mode [e.g., 7], plus blue green illumination of the substrate using an Ar ion laser and control of the Cd/Te ratio in the vapor flux using separate Cd (or Te) and CdTe sources Fig. 1. During deposition the vacuum is 10^{-8} to low 10^{-7} Torr.

Significant Results

IAD results during this period include a refined p vs. ion dose relationship and correlation with SIMS data indicating that self compensation limits the hole densities p to 2×10^{17} cm^{-3}, Fig. 2, and the fabrication of a series of solar cells, e.g., Figs. 3, 4 Preliminary work on the IAD growth of polycrystalline films unexpectedly showed through-the-film resistivity ρ increased with increased ion dose N_i, rather than decreasing [6, pp. 58, 66]. Carrier densities in the films were 10^{15} to 10^{16} cm^{-3} (by C-V), but ρ vs. T data indicated that the cause for the increase in ρ with N_i was an increase in the grain boundary potential barrier height, resulting in drastically lowered mobilities.

Although we have grown more than 160 homoepitaxial films using various combinations of illumination, Cd/Te flux ratio, dopants (Sb, P, As, none), and substrate temperature (in some cases duplicating the conditions of Schetzina *et al.* and Arias *et al.*, except for vacuum level), we have been unable to reproduce the reported PAD results of Schetzina *et al.* [8-11]. Most of our

PAD films appear to be semi-insulating, and, although some films showed measurable conductivity, the effect is modest, and there appears to be little or no correlation between illumination and doping at this stage of our research. The use of a Cd/Te flux ratio > 1, however, shows a strong effect on the electrical properties of In/p-CdTe diodes (Fig. 5), whether light and/or the dopant (As) are/is present or not. PL and structural measurements are in progress.

Conclusions

Up to this time we have been unable to reproduce the PAD results of Schetzina *et al.* The use of Cd/Te flux ratios > 1 is promising, however, judging from the large increase in the rectification ratio we observed and the consensus of the results of other workers. In addition the IAD approach remains a fertile ground for research, particularly using Cd/Te flux ratios >1.

We intend to pursue the PAD approach for a short additional period using improved technique (recently improved vacuum level, advanced diagnostics, etc.) in order to reach a more definitive conclusion about whether it works for our system.

If we can achieve enhanced dopant incorporation by PAD, we will extend the PAD results by investigating dependences of film properties on photon flux, Cd/Te ratio, and photon energy. Both the electrical and structural characterization will be then be expanded.

If, however, we are unable to obtain positive results with PAD, we will extend the IAD results to include:

(i) The effects of Cd/Te flux ratios > 1 during IAD film growth on doping, self-compensation, crystalline quality, and, especially, L_d.
(ii) N and/or group I dopants.
(iii) Post-annealing the films in Cd vapor to anneal out ion damage, if present, and to drive the stoichiometry to Cd-rich to determine whether the L_d of IAD samples can be improved.

Using the most promising technique(s) from the studies above, our ultimate goal is to test the properties of CdS/CdTe heterojunction solar cells based on these PAD and/or IAD doped single-crystal and polycrystalline CdTe films.

A portion of our program is being diverted to investigation of ZnTe films, both single crystal and polycrystalline, grown by CSVT, for low-resistance Ohmic contacts to p-CdTe and as an active component in tandem cells.

References

1. C.M. Fortmann, A.L. Fahrenbruch, and R.H. Bube, J. Appl. Phys. **61**, 2038 (1987).
2. A. Fahrenbruch, A. Lopez-Otero, P. Sharps, and R.H. Bube, Proc. 19th IEEE Photovoltaic Spec. Conf. (1987) p. 1309.
3. P. Sharps, A. Fahrenbruch, A. Lopez-Otero, and R.H. Bube, Proc. 20th IEEE Photovoltaic Spec. Conf. (1988).
4. A.L. Fahrenbruch, K-F. Chien, D. Kim, A. Lopez-Otero, P. Sharps, and R.H. Bube, Solar Cells **27**, 137 (1989).
5. P. Sharps, A. Fahrenbruch, A. Lopez-Otero, and R. H. Bube, Proc. 21st IEEE Photovoltaic Spec. Conf. (1990), p. 493.
6. SERI Final Report, "Ion-Assisted Doping of II-VI Compounds During Physical Vapor Deposition," 9/1/85 to 8/30/89, dated 6/12/90.
7. P. Sharps, A.L. Fahrenbruch, A. Lopez-Otero, and R.H. Bube, to be published J. Appl. Phys. Dec. 15, 1990.
8. R.N. Bicknell, N.C. Giles, and J.F. Schetzina and C. Hitzman, J. Vac. Sci. Technol., **A5**, 3059 (1987).
9. R.L. Harper Jr., S. Hwang, N.C. Giles, and J.F. Schetzina, D.L. Dreifus, and T.H. Myers, Appl. Phys. Lett., **54** (2), 170 (1989).

10. R.N. Bicknell-Tassius *et al.*, J. Cryst. Growth **101**, 33 (1990).
11. T.H. Myers *et al.*, Proc. 1990 U.S. Workshop on Phys. and Chem. of HgCdTe and Related II-VI Compounds, to be published.
12. J.M. Arias et al., Proc. 1989 U.S. Workshop on Phys. and Chem. of HgCdTe and Related II-VI Compounds, 1025 (1989). Also J. Vac. Sci. Technol. **A8**, 1025 (1990).
13. C.J. Summers, private communication, 1990 workshop on Phys. and Chem. of HgCdTe and Related II-IV Compounds, October,1990, San Francisco.

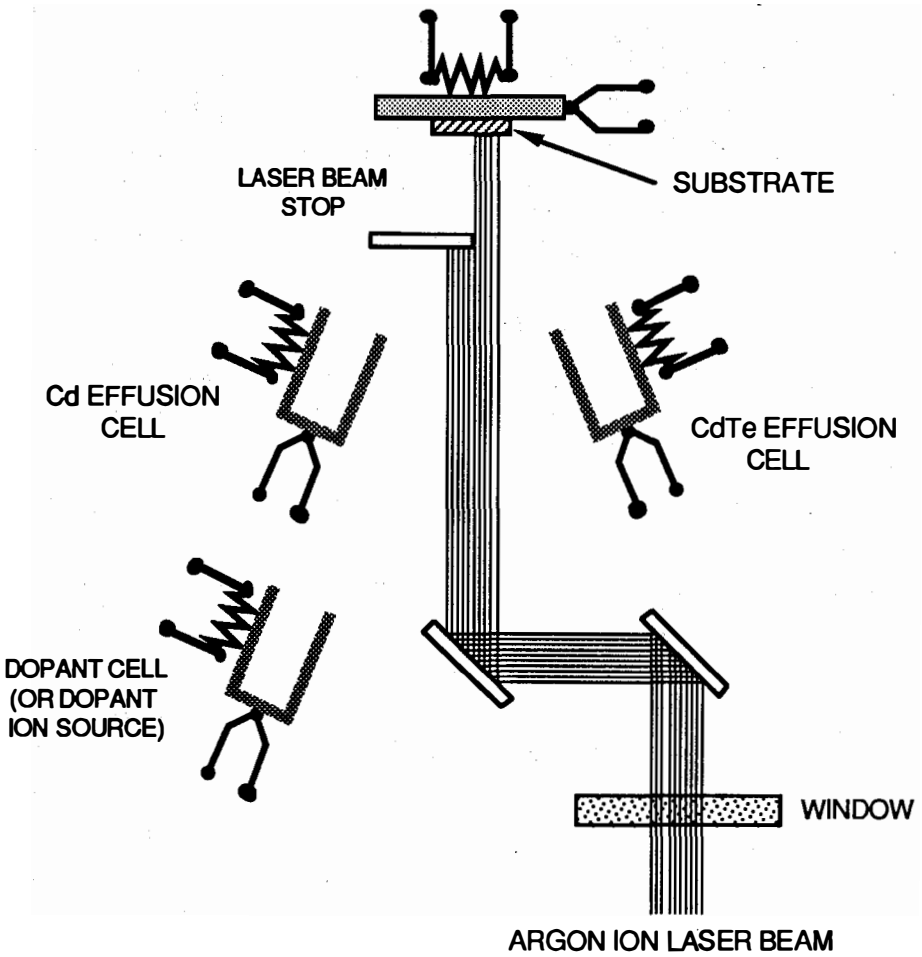

Fig. 1. Experimental setup. Laser beam intensity at substrate is typically 50-100 mW/cm^2.

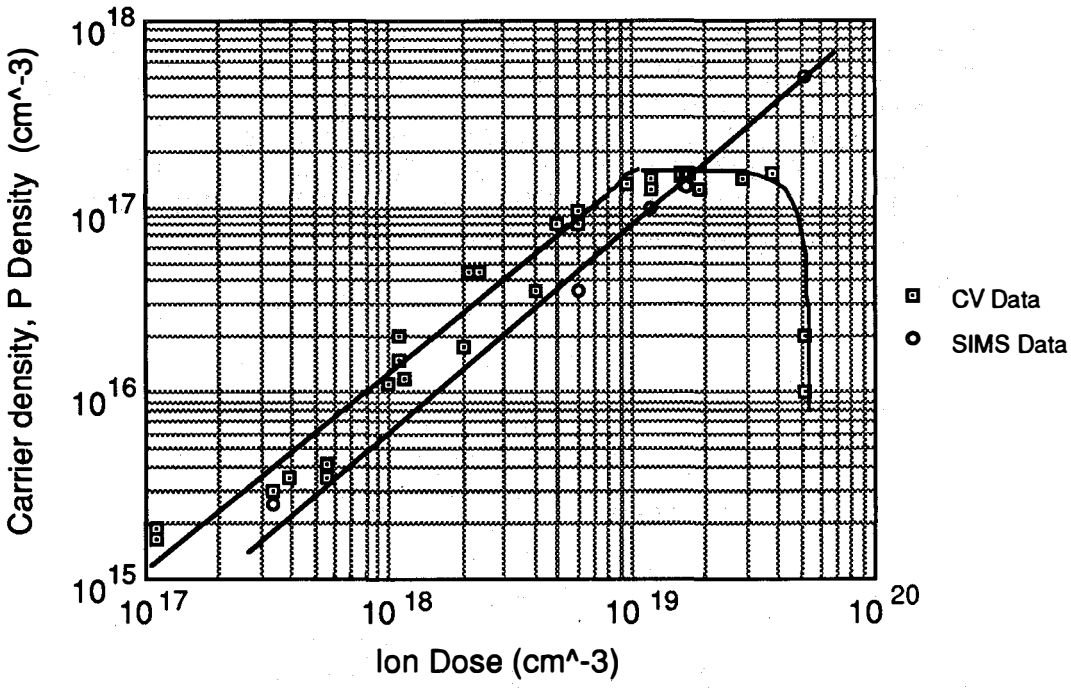

Fig. 2. Carrier density and P density (measured by SIMS) vs. ion dose. Ion dose is the density of P that would be in the layer if all the incident ions were incorporated. Ion energy = 60 eV, T_{sub} = 400°C, growth rate = 10 μm/hr, and film thickness ≈ 10 μm.

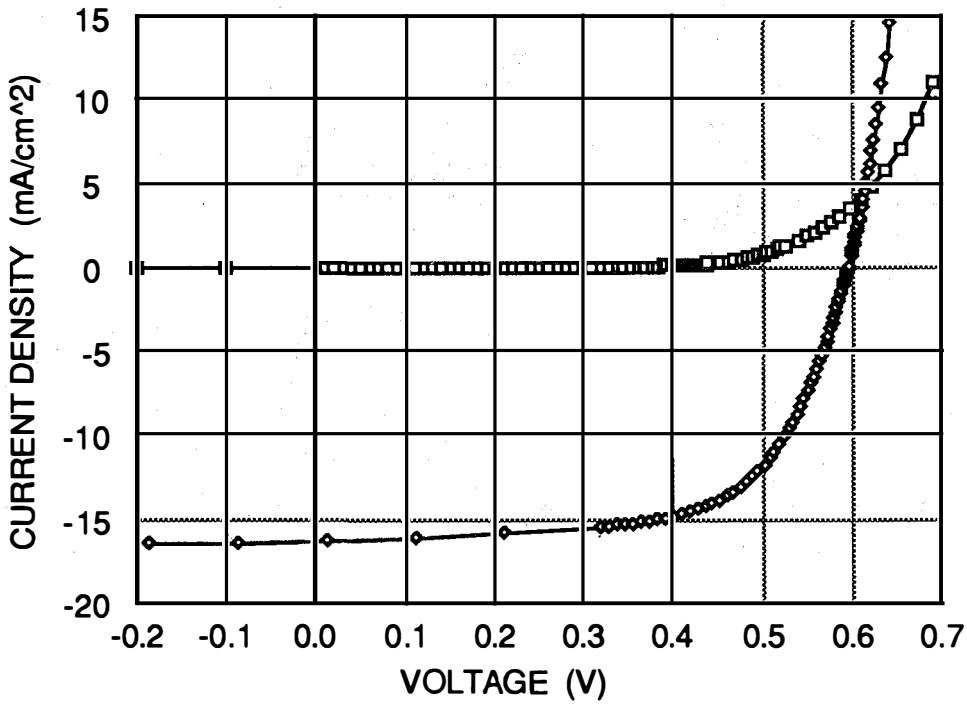

Fig. 3. Dark and light J-V curves for In/n-CdS/i-CdTe/p-CdTe/Au cell #SC-37. This cell has two layers of CdTe: a thin layer of undoped CdTe next to the CdS and a layer of IAD p-CdTe:P.

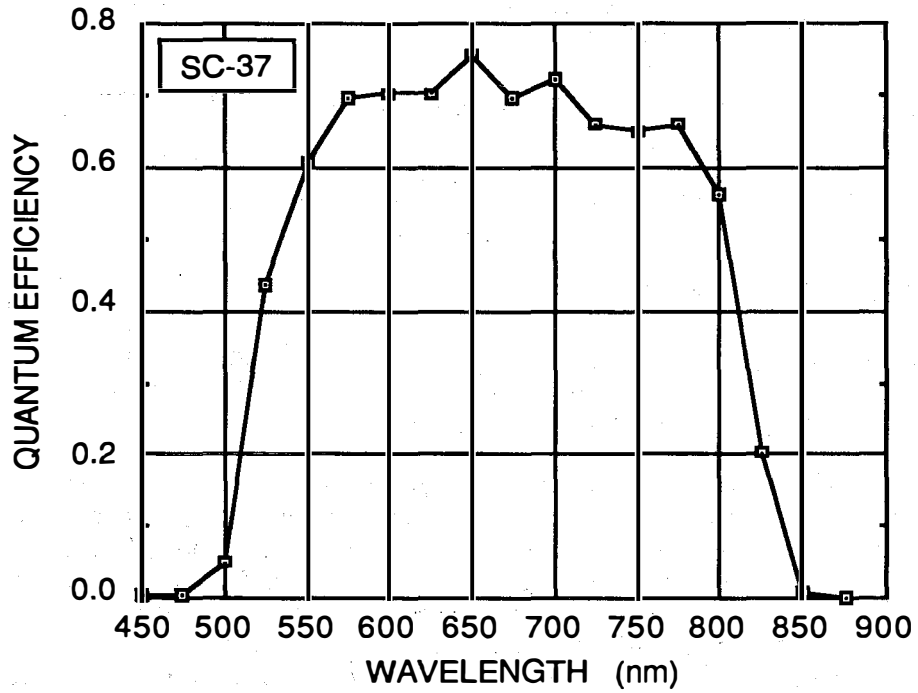

Fig. 4. Quantum efficiency for cell #SC-37.

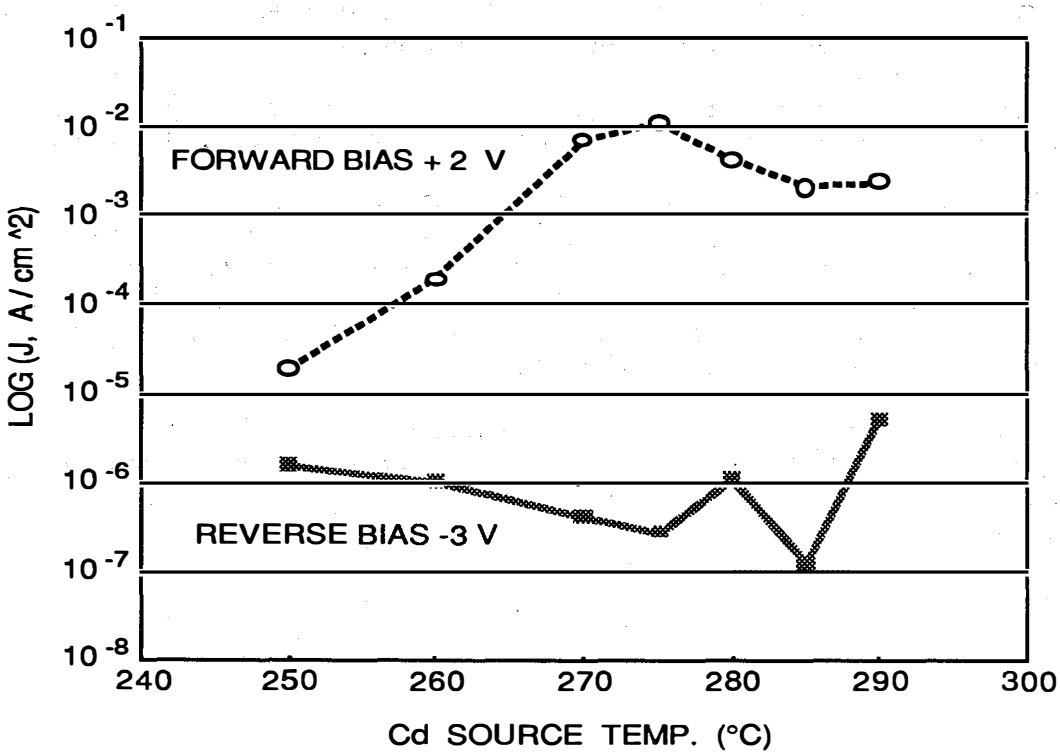

Fig. 5. Current density at +2 V and -3 V bias for In p-CdTe Schottky barriers, as a function of Cd source temperature T_{Cd}. A source temperature of 275°C corresponds to a Cd/Te ratio in the vapor flux at the substrate of ≈ 1.8 and the Cd/Te ratio varies from 1.2 to 3.6 for 240°C ≤ T_{Cd} ≤ 300°C. The As dopant source temperature was 200°C, illumination was 100 mW/cm^2, and T_{sub} = 230°C. These data show a remarkable increase in the rectification ratio for Cd/Te > 1, compared to stoichiometric flux ratios.

Title: **Defects and Photocarrier Processes in Hydrogenated Amorphous Silicon Alloys**

Organization: Department of Physics, Syracuse University, Syracuse, NY 13244

Contributors: Eric A. Schiff, principal investigator; Homer Antoniadis, Jung–Keun Lee, Qi Wang, and Sufi Zafar.

Projects and Research Approaches

The materials studied in this project are hydrogenated amorphous silicon–germanium alloys. In this annual report we shall describe the status of three of the research projects with results most closely associated with solar cells:

Deep Center Generation in a–Si:H: Four important processes leading to generation of deep centers and to degradation of the electronic properties of a–Si:H may be distinguished: deposition, thermal, dehydrogenation, and illumination. In this project we use electron spin resonance to measure the defect density, and in the last year we have primarily studied the interrelationship of thermal and hydrogenation effects. The deposition and illumination effects are more directly related to solar cells but also more complex to understand. We feel that understanding the simpler effects will suggest solutions to the more complex problems.

Deep Center Charge States in a–Si:H: The electronic effects of deep centers are dramatically changed by their equilibrium charge states. The standard model for a–Si:H is that most deep centers are neutral, but several recent experiments and models have challenged this view. We have performed research on the temperature-dependence of the electron spin resonance signal which addresses this issue.

Photocarrier Drift in a–$Si_{1-x}Ge_x$:H: We are completing a survey of electron and hole drift mobilities in hydrogenated amorphous silicon–germanium alloys prepared by Energy Conversion Devices, Inc.. One important feature of this collaboration is that single–junction solar cells based on the same material are also being studied. In addition we have developed a technique to permit more direct comparison of drift mobility information between laboratories.

In addition, we have been performed experiments in the last year upon plasma hydrogenation and dehydrogenation of amorphous silicon and upon nonlinear, high electric field transport of electrons and holes.

Deep Center Generation in a–Si:H

The pioneering work of Biegelsen, *et al* [1] showed that, on average, between one hundred and one thousand hydrogen atoms need to be removed from a–Si:H to create a single deep center detectible by electron spin resonance (the *D*–center). This measurement challenges the possibility of a establishing a direct connection between deep levels and the structures to which the hydrogen in a–Si:H is bonded. More recently, defect "equilibration" experiments have once again suggested that there may be linkage between deep centers and hydrogen, but a quantitative model has not been established.

In the last year we have found two new experimental effects on hydrogen–depleted a–Si:H which significantly clarify the relationship of hydrogen to the spin density in a–Si:H. From measurements of Jackson, *et al* [2] we find that the "efficiency" of hydrogen in creating or destroying spins rises dramatically when the spin density exceeds 10^{18} cm^{-3}. In a second experiment conducted at Syracuse we found that the thermally activated behavior of the spin density characteristic of low spin densities is lost in hydrogen–depleted samples with spin densities greater than 10^{19} cm^{-3} (Zafar and Schiff, unpublished; see also [3]). We illustrate the latter experiment in Fig. 1, where we have plotted the activation energy of the spin density against the spin density itself (at 350 C). The various points to the left of the figure represent several as–deposited specimens [3]. The two points to the right correspond to one of the specimens at the left which had been partially depleted of hydrogen by high–temperature baking.

Both of these new effects are predictions of a hydrogen–mediated model for deep centers published in 1989 [4]; the solid curve of Fig. 1 illustrates the predicted behavior. The model was based on the principle that changes in spin density reflect the transfer of hydrogen between sites of the clustered and dilute phases of hydrogen in a–Si:H. These sites are almost all hydrogenated in as–deposited a–Si:H; the density of such sites varies rather little between specimens. The large variations in defect density between a–Si:H specimens reflect variations in the *hydrogen deficits*, which is the density of unhydrogenated sites in the material.

The model also has an important (and as yet untested) consequence for the density of defects created by illumination. In this model an increase of specimen temperature creates spins by the following process. Hydrogen atoms on the dilute phase are transferred to form hydrogen pairs on formerly empty, "weak bond" sites of the clustered phase. Each pair which forms creates two dangling bonds. A similar process may also account for metastable defects. In particular excess carriers might drive a process similar to the thermal process, causing isolated hydrogen atoms from the dilute phase to shift and form pairs on the clustered phase.

Deep Level Charge States in a–Si:H

The simplest possible model – a "standard model" – for defect effects in undoped a–Si:H is that the dominant deep center is the *D*–center observed by electron spin resonance, and that this center is predominantly neutral. If most *D*–centers were charged, the observed spin density would grossly underestimate the true density of *D*–centers. This issue is of the utmost importance in constructing a satisfactory description of the photoelectronic properties of a–Si:H.

For a variety of reasons many workers in a–Si:H have supported the simpler view that most *D*–centers are neutral in undoped a–Si:H such as are used solar cells. Recently several experiments have suggested that most of the *D*–centers are in fact charged. Our

own work is most closely related to the experiment of Essick and Cohen [5]. These authors found in their specimens of a–Si:H that electrical charging of the specimen in a Shottky diode structure produced far fewer spins than expected from the standard model. They interpreted their effect by proposing that the *D*–centers have a rather small electronic correlation energy compared with the intrinsic energy variations of the corresponding gap states. Most defects in such a model are charged – about half with each sign. Assuming an intrinsic energy broadening of about 300 meV, Essick and Cohen suggested a correlation energy of less than 50 meV.

The same model predicts that the spin density in a–Si:H should exhibit a substantial temperature–dependence even near room–temperature. We found that the temperature-dependence of the spin density in a–Si:H had not been carefully measured before; most authors have stated that their data supported negligible temperature–dependence.

Our own data (Lee and Schiff, unpublished) are presented in Fig. 2 for a–Si:H. We have graphed the spin density (normalized to its value at 77 K) as a function of the temperature. For very defective specimens there is a substantial increase in the density with temperature (upper curve, corresponding to a spin density of order 10^{19} cm^{-3}). In specimens closer to device–grade a–Si:H the temperature dependence is much reduced. We can compare these data with the predictions of simple models such as that suggested by Essick and Cohen. Assuming an energy broadening of 300 meV, we estimate that the correlation energy is about 300meV in device quality a–Si:H – about six times larger than the value estimated by Essick and Cohen. One possible explanation for this difference is the differing role of interface or near–interface states in the two experiments, but the issue is not yet resolved.

Photocarrier Drift in a–$Si_{1-x}Ge_x$:H

We have been conducting photocarrier drift–mobility measurements in specimens deposited at Energy Conversion Devices, Inc.. There are two important aspects of this collaboration. First, Dr. Guha (formerly at Energy Conversion Devices, Inc., and presently at United Solar Systems, Inc.) is studying the properties of solar cells prepared from material comparable to that used in the drift mobility measurements. We shall not report on these results here. Second, we have developed conventions and interpolation procedures which permit a more direct comparison of the photoelectronic properties of specimens in different laboratories.

In Fig. 3 we have graphed the correlation of the electron drift mobility μ_e with the germanium concentration x for the present work (ECD/SU) (Wang, Antoniadis, Schiff, and Guha, unpublished) and for earlier work at the University of Stuttgart [6]. An additional point for an a–Si:H specimen prepared at Xerox Palo Alto Research Center is also shown [7]. The drift mobility estimates correspond to a 200 K sample temperature and to a nominal ratio of specimen thickness and drift field $d/E = 10^{-9}$ cm^2/V. In practice μ_e is estimated from drift–mobilities for thicker specimens and smaller fields than the value suggests. The choice of the value of d/E is crucial. Standard time–of–flight techniques for measuring drift mobilities depend strongly on d/E because of "dispersion" effects, and thus estimates of μ_e from different laboratories must be adjusted to correspond to the same d/E ratio. In addition, in order to compare specimens of widely varying electronic quality such as the germanium–silicon alloys d/E must be chosen smaller than the electron "deep–trapping" mobility–lifetime products for the range of alloys studied.

The data confirm the well–known effect that Ge alloying reduces the electron drift mobility; the effect is usually attributed to a broadening of the conduction bandtail as more Ge is incorporated. The data suggest that the electron drift mobility in the alloys

is determined primarily by the alloy parameter x, in which case further improvements in μ_e would appear unlikely. However, the effect needs better confirmation.

In Fig. 4 we have presented a plot of the correlation between the hole deep–trapping mobility lifetime product $\mu\tau_h$ and the alloy parameter x. Measurements published by the Princeton [8], Siemens [9], and ECD/Syracuse groups are shown. These mobility–lifetime products are also obtained from time–of–flight measurements. They reflect hole motion only up to some experimental drift time. This time was about 1 ms for the SU/ECD measurements. Drift–times were not reported by the Princeton and Siemens groups, although we consider it unlikely that this ambiguity contributes substantially to the differences between specimens indicated by the figure.

The measurements of Fig. 3 and 4 are primarily useful for comparing materials prepared in different laboratories; they are very incomplete descriptions of photoelectronic properties. In particular we emphasize that deep–trapping mobility–lifetime products are only very rough guides to recombination effects. For electrons in silicon–germanium alloys the steady state mobility–lifetime products (corresponding to indefinite drift times) are about 100 times larger than the deep–trapping values measured in the microsecond domain [10–12]. Less has been established for holes. The data in Fig. 4 indicate a decrease of $\mu\tau_h$ of nearly two decades for the ECD specimens when the alloy parameter reaches 0.5. We consider it very unlikely that the steady–state values for $\mu\tau_h$, as might be estimated using the steady–state photocarrier grating or other techniques, decreased this dramatically. The issue needs further exploration.

References

1. D. K. Biegelsen, R. A. Street, C. C. Tsai, and J. C. Knights, *Phys. Rev.* **B20**, 4839 (1979).
2. W. B. Jackson, C. C. Tsai, and R. Thompson, *Phys. Rev. Lett.* **64**, 56 (1990).
3. Sufi Zafar and E. A. Schiff, *J. Non–Cryst. Solids* **114**, 618 (1989).
4. Sufi Zafar and E. A. Schiff, *Phys. Rev. B* **40**, 5235 (1989).
5. J. M. Essick and J. D. Cohen, *Phys. Rev. Lett.* **64**, 3062 (1990).
6. C. E. Nebel, H. C. Weller, and G. H. Bauer, collected in *Amorphous Silicon Technology*, edited by A. Madan, *et al* (Materials Research Society, Pittsburgh, 1988), p. 507; C. E. Nebel, *Ladungsträgertransport und Rekombination in a–SiGe:H*, Ph. D. thesis (unpublished), Universität Stuttgart, 1990.
7. J. M. Marshall, R. A. Street, and M. Thompson, *Phil. Mag. B* **54**, 51 (1986).
8. S. Aljishi, Z. E. Smith, D. Slobodin, J. Kolodzey, V. Chu, R. Schwarz, and S. Wagner, collected in *Materials Issues in Amorphous Semiconductor Technology*, edited by D. Adler, *et al* (Materials Research Society, Pittsburgh, 1986), p. 269.
9. F. Karg, W. Krühler, M. Möller, and K. v. Klitzing, *J. Appl. Phys.* **60**, 2016 (1986).
10. E. A. Schiff, *Phil. Mag. Lett.* **55**, 87 (1987).
11. K. D. MacKenzie and W. Paul, *J. Non–Cryst. Solids* **97&98**, 1055 (1987).
12. H. Antoniadis and E. A. Schiff, collected in *Amorphous Silicon Technology – 1990*, edited by P. C. Taylor, *et al* (Materials Research Society, Pittsburgh, 1990), p. 293.

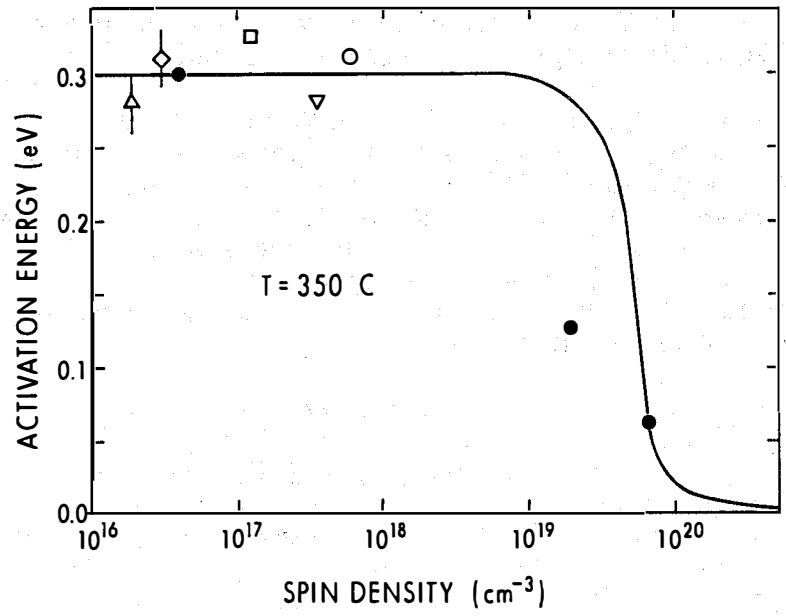

Fig. 1: Correlation of the thermal activation energy of the spin density in a–Si:H at 350 C with the spin density at 350 C. The open symbols represent several specimens of undoped a–Si:H in their as–deposited state (after Zafar and Schiff, [3]). The solid symbols represent a study of a thickness series of specimens in the as–deposited state as well as two hydrogen–depleted states created by heating the specimens to 550 C. The solid line represents a calculation based on the model of ref. [4]. the calculation was fitted to the data for low spin densities, but no other parameters were fitted.

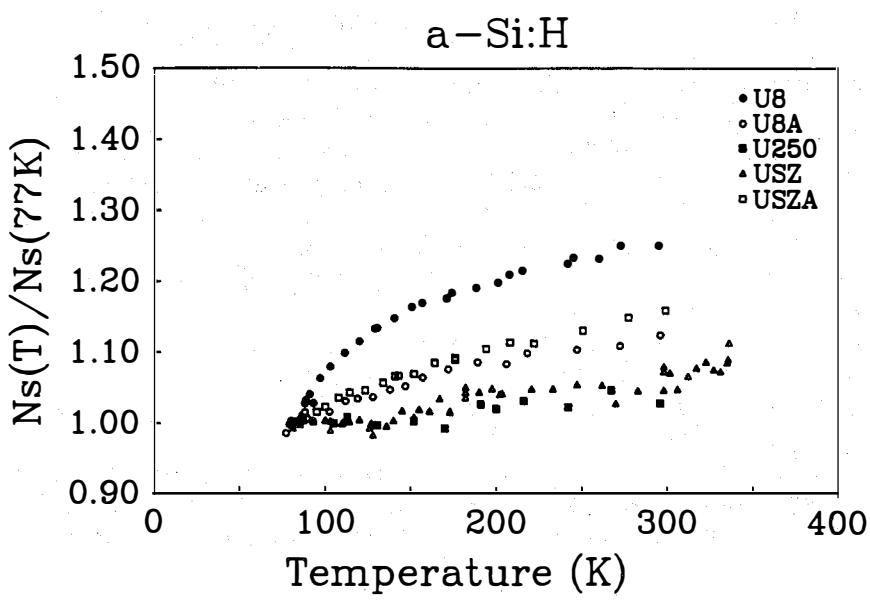

Fig. 2: Spin density as a function of temperature for several undoped specimens of a–Si:H. All densities were normalized to unity at 77 K. Electron transfer between defects is believed to be the mechanism for this effect, in which case the data permit the effective electronic correlation energy of the *D*–center to be estimated.

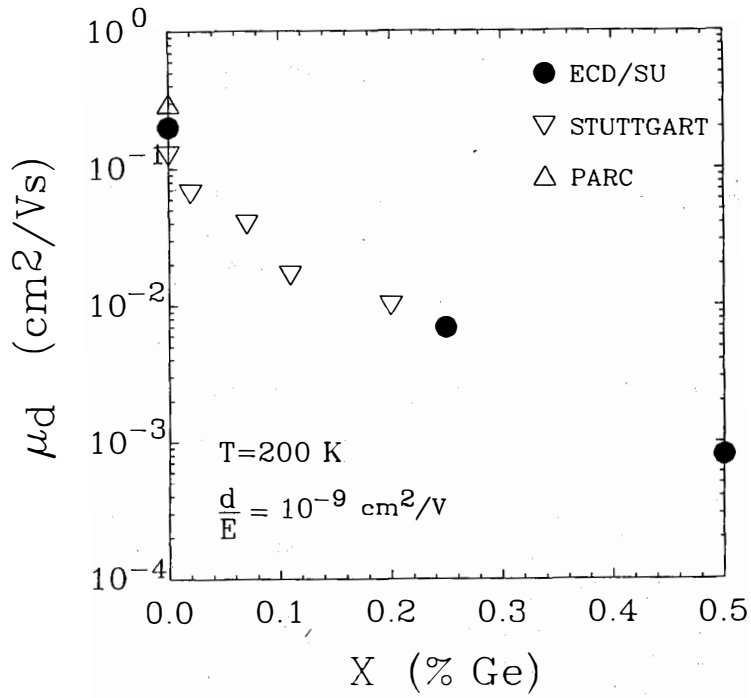

Fig. 3: Average electron drift mobility μ_e determined by time–of–flight experiments at 200 K in a–$Si_{1-x}Ge_x$:H alloys for several alloy parameters x. The drift mobilities correspond to a nominal ratio of the specimen thickness d and the electric field E of $d/E = 10^{-9}$ cm²/V. References: Stuttgart [6], PARC [7], ECD/SU – unpublished.

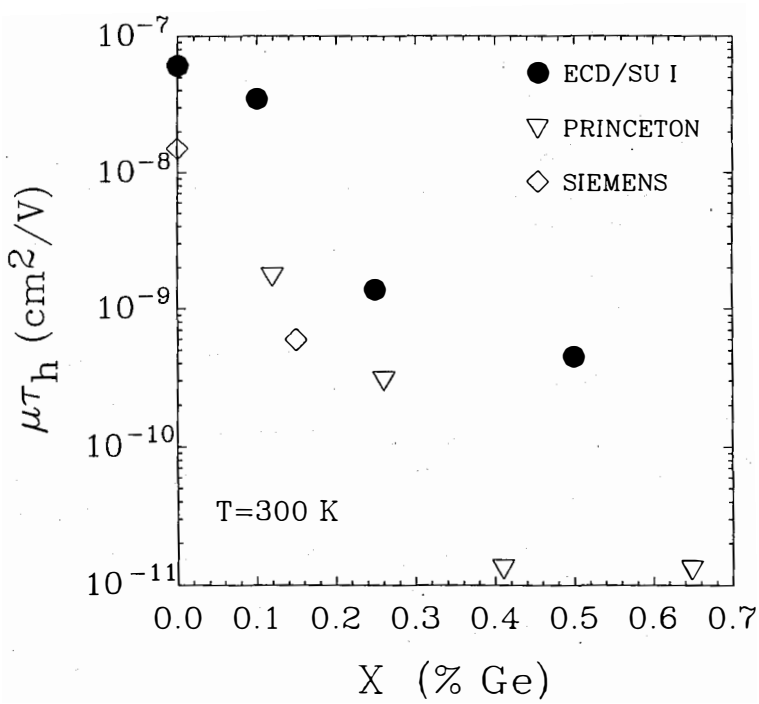

Fig. 4: Hole deep–trapping mobility lifetime product $\mu\tau_h$ measured near room–temperature in a–$Si_{1-x}Ge_x$:H alloy specimens for various alloy parameters x. The data reflect hole drift measured in time–of–flight experiments up to about 1.0 ms. References: ECD/SU – unpublished, Princeton [8], Siemens [9].

Title: **Atomic Layer Epitaxy for High Efficiency Solar Cells**

Organization: Departments of Electrical Engineering and Materials Science
University of Southern California
Los Angeles, CA

Contributors: P. D. Dapkus, principal investigator, B. Y. Maa, and M.Jow

The objective of this program is to explore and develop a low temperature, large scale epitaxial process for high efficiency solar cells based upon atomic layer epitaxy (ALE). ALE has the potential for high throughput, layer thickness control and uniformity based upon the inherent saturated surface reactions involved in the process. We have previously shown that the growth rate in atmospheric pressure, thermally driven ALE is limited by the maximum temperature attainable before homogeneous gas phase reactions dominate the process and preclude the achievement of saturated monolayer growth[1]. In this program we will be exploring the use of photoassisted ALE and vacuum ALE as alternative approaches for achieving usable growth rates and high throughput. The program is structured in two phases. In the current phase, we are measuring the fundamental thermal and photoassisted surface reaction rates involved in the growth of GaAs using TMGa and a variety of As sources. Based upon these results a decision will be made as to the viability of either approach and the second phase will concentrate upon developing one of these approaches for the growth of high efficiency solar cells. In this phase issues such as materials quality, reactant utilization, and throughput will be examined.

The fundamental surface reactions and reaction rates are being assessed by a combination of tools that allows us to study the surface chemistry that results from reaction of Ga and As sources on the GaAs surface (XPS), the structural properties of the surface (RHEED), and the rates of the surface ordering (reflection difference spectroscopy-RDS). Previous work has shown that the fundamental reaction between TMGa and an As-stabilized GaAs surface saturates at one monolayer of Ga as soon as a Ga-stabilized surface reconstruction is formed[2,3]. Similarly, this surface can be readily converted to an As-stabilized surface by exposure to As_4, tertiarybutylarsine, or monoethylarsine[2,4,5]. Our work under this program has focussed on the assessment of the *kinetics* of the surface reactions using RDS measurements. We have successfully built an RDS system and are in the process of taking data at wavelengths resonant with absorption by As dimers and Ga dimers on the GaAs surface. The data of Fig. 1 shows the RDS response at 6328Å of an As-stabilized GaAs (100) surface to exposure with TMGa for various exposure

times at temperatures of 450°C and 500°C. The total change in reflectivity indicated in each of the curves represents a transition from an As-stabilized surface to a Ga-stabilized. The slope of the transition is related top the surface reactions rates. From data such as these we have been able to ascertain the temperature dependence of the TMGa surface reaction rate and the rate of desorption of reaction by-products from the surface. Based upon our initial assessment of these rates, it appears that growth temperatures in the range of 550°C and 600°C are suitable for practical ALE growth rates. Work is focussing on the rates of reaction and by-product desorption operative under photoexcitation in the visible portion of the spectrum. We have already determined that the rates of desorption are significantly enhanced by photoexcitation at 5145Å at a power density of 200 W/cm^2. We are now assessing the relative roles of thermal and photolytic processes in the fundamental surface reactions.

References:

1. P. D. Dapkus, B.Y. Maa, Q. Chen, W. G. Jeong and S. P. DenBaars, to be published J. Crystal Growth (1991).

2. B. Y. Maa and P. D. Dapkus, J. Electron. Mater. **19**, 289 (1990).

3. B. Y. Maa and P. D. Dapkus, J. Crystal Growth **105**, 213 (1990).

4. B. Y. Maa and P. D. Dapkus, Appl. Phys. Letters (submitted for publication).

5. B. Y. Maa and p. D. Dapkus, unpublished data.

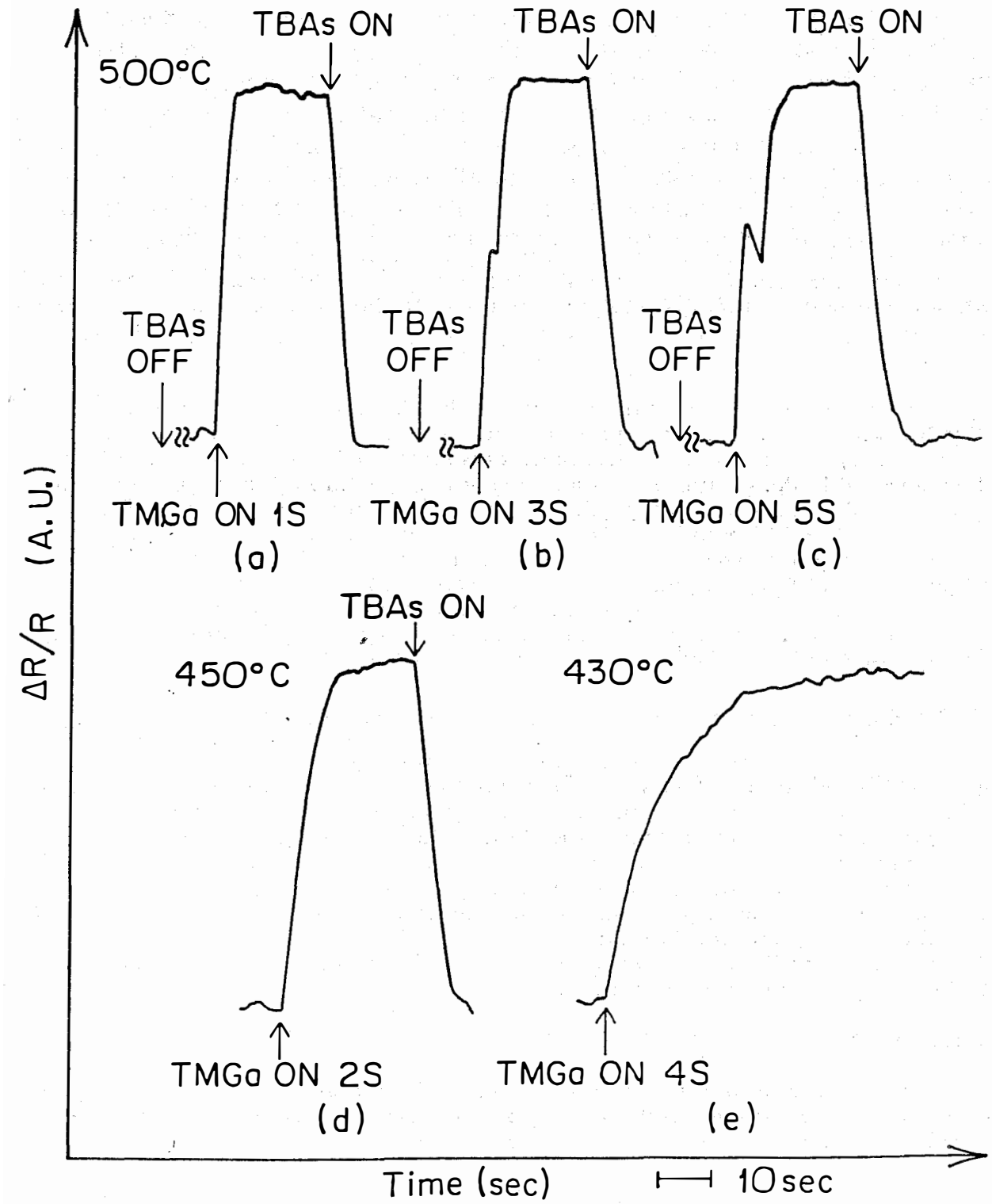
TBAs ON
TBAs ON
TBAs ON
500°C
TBAs OFF
TBAs OFF
TBAs OFF
TMGa ON 1S
(a)
TMGa ON 3S
(b)
TMGa ON 5S
(c)
ΔR/R (A.U.)
TBAs ON
450°C
430°C
TMGa ON 2S
(d)
TMGa ON 4S
(e)
Time (sec)
10sec

Fig. 1

Title: Electronic Processes in Thin Film PV Materials

Organization: Department of Physics, University of Utah, Salt Lake City, Utah

Contributors: P.C. Taylor, principal investigator, G.A. Williams, W.D. Ohlsen, S. Gu, I. Viohl, K. Gaughan, S. Hershgold, D. Chen

One important class of materials for PV conversion of solar energy is the group of thin film amorphous semiconductors based on hydrogenated amorphous silicon (a-Si:H). Important alloys include a-Si_xGe_{1-x}:H, a-Si_xC_{1-x}:H and a-Si_xN_{1-x}:H which are used to produce narrower gaps for tandem cells, and wider band gaps for top-surface p-layers, respectively. Also of interest are artificially layered structures, such as a-Si:H/a-Si_xC_{1-x}:H, where the individual layers may be only 10-1000 Å thick.

Defects and impurities in these films create enhanced densities of electronic states in the gap which are deleterious to the performance of PV devices. In addition, both the alloy systems and a-Si:H itself are plagued by electronically- and optically-induced metastabilities (Staebler-Wronski effect) and by metastable departures from equilibrium below a "freezing in" temperature. These metastabilities adversely affect device performance and make projections of useful device lifetimes difficult. Recently some improvements in device performance have been accomplished by using artificially layered structures, as for example, in the p-layer in p-i-n devices. However, there is still no detailed understanding of the electronic and optical properties or of any quantum mechanical effects due to confinement of the electrons in these multilayers.

Objectives

The major objectives of this subcontract are (1) to grow and characterize high quality of a-Si:H and related alloys and multilayers using the glow discharge technique, (2) to characterize by optical and magnetic resonance techniques the roles of defects and impurities in amorphous tetrahedrally-coordinated thin films, (3) to determine the quality of the interfaces and junctions which occur in PV devices by employing surface-sensitive optical and magnetic resonance techniques, and (4) to understand the recombination-induced metastabilities (Staebler-Wronski effect) and the frozen-in departures from equilibrium (as mediated by hydrogen diffusion or defect motion) in amorphous tetrahedrally-coordinated thin films.

Discussion

Several techniques have been employed to accomplish these objectives. Samples are grown in a state-of-the-art glow discharge deposition system and characterized using infrared and Raman spectroscopy, electrical conductivity, electron microprobe, and photothermal deflection spectroscopy (PDS). Other important experimental techniques include nuclear magnetic resonance (NMR), electron spin resonance (ESR), various optical spectroscopies, and double spectroscopies such as optically detected magnetic resonance (ODMR).

The subcontract is divided into seven tasks. The first task is the growth and characterization of doped and undoped a-Si:H. We have performed the first measurements[1] on the use of a liquid organic source for n-type doping in hydrogenated amorphous silicon (a-Si:H). Tertiarybutylphosphine (TBP) vapor is added to silane in an r.f. glow discharge process to produce doped a-Si:H thin films. Impurity levels from parts per million to about 1% phosphorus have been incorporated into the film with this method. Measurements of dark conductivity, photoconductivity, conductivity activation energy, electron spin resonance and subgap optical absorption of the TBP doped films are comparable to those published for films doped with phosphine. Figure 1 shows the room temperature electrical conductivity for TBP-doped (closed symbols) and PH_3-doped (dashed line)[2,3] a-Si:H films.

The second task concerns non-equilibrium phenomena in a-Si:H and related alloys. Rapid quenching of thin ($\leq 1\ \mu m$) device-quality i-layers of a-Si:H have shown interface-driven decreases in ESR which are more important than the well-known increases in bulk spin densities on rapid quenching. Recent measurements on P-doped samples of a-Si:H using both TBP and phosphine have shown that there may be differences in the freeze-in temperatures depending on the dopant gas which is used.

The third task involves the study of recombination-induced metastabilities in a-Si:H and related alloys. We have employed photoluminescence absorption spectroscopy (PLAS) to measure light traveling down the length of a film in a waveguide mode. The basic idea of the PLAS technique is to measure self-absorption of that portion of the PL which is totally internally reflected within the film because the larger dielectric constant of the film produces a dielectric waveguide. If α is the absorption coefficient, then the optical path length αd is greatly increased because d is the length of the film and not its thickness. The PLAS technique is sensitive to surface effects just as are PDS and PAS. The surface effects in PLAS result from the fact that the waveguide modes have intensities which "leak" into the boundary regions, which have lower index of refraction.

Measurements have shown[4,5] that the peak in the absorption near 1.15 eV can be increased in magnitude after irradiation at 300 K with above-gap light. There is thus a connection between this feature and the Staebler-Wronski effect in these alloys. The explanation for this peak is still controversial.

The investigation of interfacial effects in a-Si:H and related alloys constitutes the fourth task. Comparative studies of low-temperature ($T \sim 30$ K) optically induced ESR using above gap red (633 nm) and below gap i.r. (1060 nm) light have been performed on several samples of a-Si:H. Experiments were performed on both films on quartz substrates and on powdered samples which were removed from the substrates. Excitation with red light always yields the well-known light induced ESR (LESR) spectrum which is ascribed to a superposition of two resonances: electrons trapped in conduction band-tail states and holes trapped in valence band tail states in a 1:1 ratio. On the other hand, excitation with i.r. light results in a different LESR spectrum with an enhanced feature overlapping with the signal attributed to trapped band-tail electrons. Typical results are shown in Fig. 2. Although observed on all films studied on quartz substrates, this asymmetry is not observed in a powdered sample where only the band tail electron and hole resonances are observed in the ratio 1:1. This result suggests that interface states are responsible for the excess LESR

spin density in the films on quartz substrates. Experiments performed as a function of film thickness confirm this interpretation.

The fifth task concerns investigations of defects and impurities in a-Si:H and related alloys. We have recently employed excitation spectroscopy of PL (PLE) to probe defects which produce absorption below the gap in a-Si:H. The PLE spectrum (intensity of PL as a function of the wavelength of the exciting light) has been measured over the range 1.0 - 1.25 eV for PL at 0.79 eV using a free electron laser (FEL) as the excitation source.[7] At all wavelengths, the PL intensity varies with incident laser power, I, as $I^{0.9}$ independent of wavelength. The resulting PL excitation spectrum has two distinguishing features,[8] an exponential rise at lower energies followed by a leveling-off above about 1.15 eV. Although the precise functional form of the data at low energies is not uniquely determined, the data are consistent with an exponential rise whose slope is the same as that measured in optical absorption at higher energies.

Recently PLE spectra at 77 K have been measured over the range 1.20 -1.75 eV using the Ti sapphire cw tunable laser as the excitation source.[9] Two undoped a-Si:H samples on rough substrates have been investigated. The first sample has a very high dangling bond (DB) density; the second one has low DB density. The PLE spectrum of photoluminescence (PL) at 0.8 eV for the first sample follows the shape of the absorption spectrum measured by photothermal deflection spectroscopy (PDS) at room temperature. This behavior can be understood within the context of the existing models as due to recombination through defects which produces PL centered around 0.8 eV. However the PLE spectrum of PL at 0.8 eV for the second sample drops very rapidly with decreasing energy for energies less than about 1.3 eV. This behavior, which differs dramatically from that of the absorption spectrum, is consistent with the earlier results[7,8] and suggests that the PL measured at 0.8 eV for the second sample may be largely due to a contribution of the tail of the PL band which peaks near 1.3 eV The PLE spectrum for PL at 1.0 eV and 1.1 eV for the second sample approach the PLE spectrum previously obtained using the integrated PL intensities.

In addition to these PLE studies, ^{1}H NMR has been employed to study the local environments of bonded hydrogen and trapped molecular hydrogen (H_2) in a series of a-$Si_{1-x}Ge_x$:H alloys.[10]. There is a monotonic decrease of bonded hydrogen with increasing x from ~ 10 at. % at x = 0 (a-Si:H) to ~ 1 at. % at x = 1 (a-Ge:H). The amplitude of the broad ^{1}H NMR line, which is attributed to clustered bonded hydrogen, decreases continuously across the system. The amplitude of the narrow ^{1}H NMR line, which is attributed to bonded hydrogen essentially randomly distributed in the films, decreases as x increases from 0 to ~ 0.2. From $x \approx 0.2$ to $x \approx 0.6$ the amplitude of the narrow ^{1}H NMR line is essentially constant, and for $x \geq 0.6$ the amplitude decreases once again. The existence of trapped H_2 molecules is inferred indirectly by their influence on the temperature dependence of the spin-lattice relaxation times, T_1. Through T_1 measurements it is determined that the trapped H_2 concentration drops precipitously between x = 0.1 and x = 0.2, but is fairly constant for $0.2 \leq x \leq 0.6$. For a-Si:H (x = 0) the H_2 concentration is ~ 0.1 at. %, while for $x \geq 0.2$ the concentration of H_2 is ≤ 0.02 at. %.

In a separate series or NMR experiments the proton NMR spectra, spin lattice relaxation times T_1 and free induction decay times T_2^* were measured in various a-Si:H films deposited by rf-sputtering.[11] All spectra exhibited broad and

narrow components, of $T_2^* \sim 20$ and 45 μsec, respectively. In samples deposited at high rf power, the ratio of the integrated intensities of the broad and narrow lines was ~ 1.5. These samples, which apparently contain mainly bulk monohydride bonds and a low volume fraction of microvoids, exhibit long-range H motion. In a sample deposited at low rf power, this ratio was ~ 3. These samples, which contain significant dihydride and microvoid content, show a dramatic suppression of the long-range H motion. The T_1 of both types of samples exhibits a clear minimum at ~ 30 K, indicative of relaxation by H_2 trapped in microvoids. The absolute values of T_1, however, are smaller in the sample deposited at low rf power (0.1 sec at the minimum as opposed to 0.3 to 1.0 sec at the minimum), apparently due to a larger ratio of molecular hydrogen to bonded hydrogen. After annealing for 24 hours at 294°C, the ratio of broad-to-narrow components increases to > 10 in all samples, and the magnitudes of the T_1 minima increase to about 1 sec in all samples.

Studies of states in the gap constitute the sixth task of this subcontract. We have recently used PDS to study the states in the gap in films of a-Si:H doped with TBP. Electronic states in the pseudogap affect the electronic properties of doped a-Si:H just as they do intrinsic a-Si:H. These defects have been successfully studied by PDS which is based on measuring the thermal energy deposited in the material as electromagnetic radiation is absorbed. We have measured[1] the absorption coefficient vs. energy for various TBP-doped films. The subgap absorption is lowest for the lightly doped material. Samples with TBP show absorption spectra as a function of impurity concentration which are similar to those obtained using phosphine.[12]

Task seven is the training of graduate students and postdoctoral research associates. Three students are currently being trained under partial support of this subcontract. In addition, one postdoctoral research associate is benefiting from training received under this program. We currently have active collaborative efforts with Solarex Corp., Plasma Technology, North Carolina State University, University of Delaware, Iowa State University, Gifu University and the University of Marburg. All of these institutions have provided well characterized samples to use for various research purposes.

Although they do not fall directly under any of the tasks of the present subcontract, measurements of optical bistability in a-Si:H are being pursued because of the potential of this material as a bistable optical switch.[12,13]

Conclusions

Major accomplishments of the previous year include (1) the first doping experiments using a liquid organic source (TBP) to produce n-type a-Si:H films, (2) the discovery of significant interface effects in intrinsic a-Si:H by below-gap optical excitation of ESR and the potential presence of charged defects in these interfacial regions, and (3) preliminary investigations of metastabilities in TBP-doped a-Si:H films. Future directions for the research include (1) studies of metastabilities in TBP-doped a-Si:H films, (2) growth of a-Si:H and related alloys using other liquid, less toxic sources, (3) continuation of below-gap spectroscopy of a-Si:H using PLE and PLAS, (4) measurements of local hydrogen diffusion in boron-doped a-Si:H using NMR techniques, and (5) investigations of optical properties of a-Si_xGe_{1-x}:H and a-Si_xN_{1-x}:H alloys.

References

1. K. Gaughan, S. Nitta, J.M. Viner, J. Hautala and P.C. Taylor, Appl. Phys. Lett. **57**, 2121 (1990).
2. W.E. Spear and P.G. LeComber, Solid State Commun. **17**, 1193 (1975).
3. H. Tarui, T. Matsuyama, S. Okamoto, Y. Mishikawa, M. Dohjo, N. Makamura, S. Tsuda, S. Nakano, M. Ohnishi and Y. Kuwano, Tech. Digest 3rd Int. PVSEC-3, Tokyo, **41** (1987).
4. R. Ranganathan and P.C. Taylor, in *Proc. 12th Int. Conf. on Amorphous and Liquid Semiconductors, Prague, 1987* (North-Holland, Amsterdam, 1987), p. 707.
5. P.C. Taylor, J. Ristein, J. Hautala and R. Ranganathan, *SERI Subcontractors Review Meeting Proceedings 1989*.
6. J. Ristein, J. Hautala and P.C. Taylor, in *Amorphous Silicon Technology - 1989* (Materials Research Society, 1989), 717.
7. J. Ristein, B. Hooper, S. Gu and P.C. Taylor, Solar Cells **27**, 403 (1989).
8. J. Ristein, J. Hautala and P.C. Taylor, J. Non-Crystal. Solids **114**, 444 (1989).
9. S.Q. Gu and P.C. Taylor, Solar Cells **27**, 403 (1989).
10. E.J. VanderHeiden, G.A. Williams, P.C. Taylor, F. Finger and W. Fuhs, in *Amorphous Silicon Technology - 1989* (Materials Research Society, 1989), 503.
11. M. Zheng, E.J. VanderHeiden, P.C. Taylor, R. Shinar, S. Mitra and J. Shinar, in *Amorphous Silicon Technology 1990* (Materials Research Society), 657.
12. N.M. Amer and W.B. Jackson, in *Semiconductors and Semimetals*, J.I. Pankove, Ed. (Academic, New York, 1984), vol 21b, p. 83.
13. Z.Y. Xu, J. Tann, M. Gal, K. Gaughan, I. Vioňl and P.C. Taylor, Int. J. of Optoelectronics, in press.

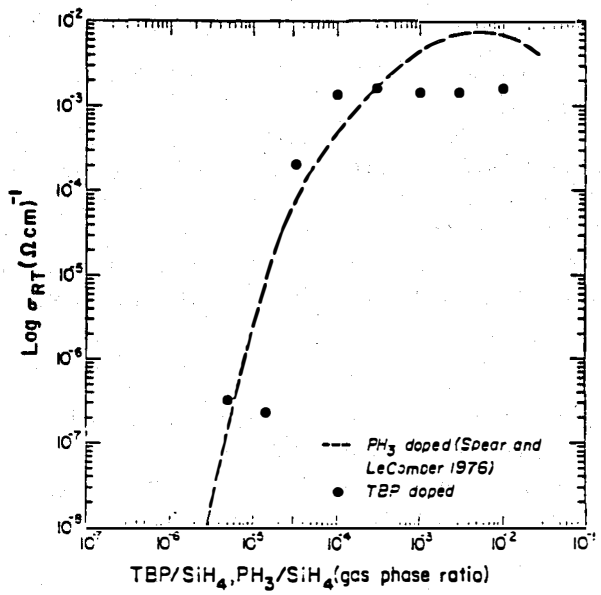

Fig. 1. Comparison of room temperature conductivity for TBP-(closed symbols) and PH_3-(dashed line) doped a-Si:H films. PH_3 data taken from W.E. Spear and P.G. LeComber.[2,3]

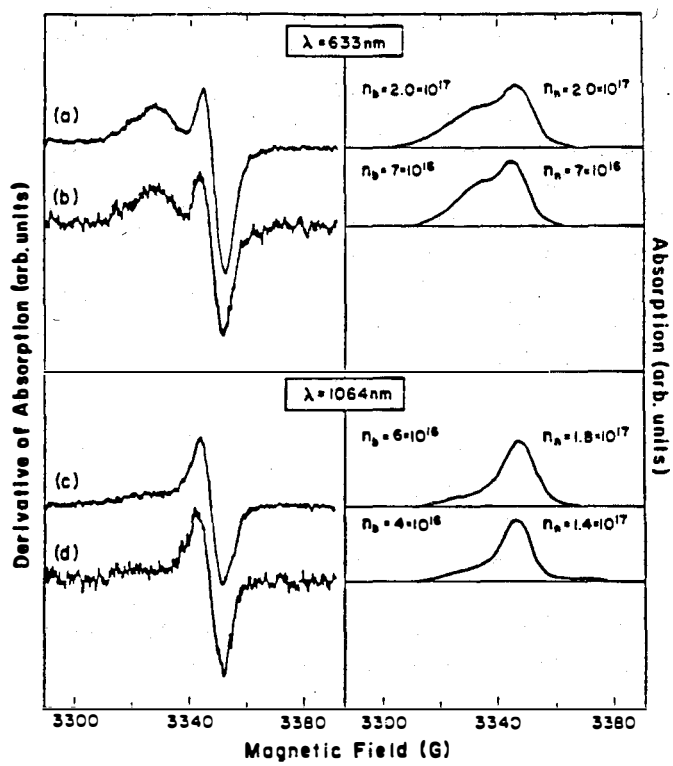

Fig. 2. LESR derivative spectra for above-gap and below-gap light excitation (left-hand side) along with the first integrals (right-hand side) for an 8 μm thick undoped a-Si:H film on a roughened quartz substrate. Exciting light power densities j and microwave power p were (a) j 0.14 W cm^{-2}, p = 200 μW; (b) j = 0.41 mW cm^{-2}, p = 20 μW; (c) j = 53 W cm^{-2}, p = 200 μW; (d) j = 39 W cm^{-2}, p = 20 μW.

8.0 PHOTOVOLTAIC MANUFACTURING TECHNOLOGY (PVMaT) PROJECT

The Photovoltaic Manufacturing Technology (PVMaT) Project is being developed as a group of government/industry partnerships between the Federal government (through the U.S. Department of Energy) and U.S. industry. The project's planned major impacts over a five-year period are to improve manufacturing processes, accelerate manufacturing cost reductions for PV modules, increase commercial product performance, and lay the groundwork for substantial scale-up of U.S.-based manufacturing plant capabilities.

The project goal is to ensure that U.S. industry retains and extends a world leadership role in the manufacture and commercial development of PV components and systems. Most of the R&D will be done by industrial participants that will be selected through competitive procurements and that have strong commitments to improve their manufacturing lines and products, reduce manufacturing costs, and increase their manufacturing capacities.

In addition to establishing government/industry partnerships to pursue the objectives of this project, the integration of utility interests and needs into the project will be strongly encouraged. It is possible that some utilities will want to be directly involved in developing manufacturing technology capabilities either as a principal or as an associate with an industrial company. In particular, utilities will be encouraged to join with industry in various cooperative arrangements for future deployment of cost-effective PV technology.

PVMAT's basic approach is focused on advancing company-specific manufacturing processes (technology) through cooperative, cost-shared R&D activities with industry. These R&D activities are to be identified by industrial companies as most important to their manufacturing and commercialization needs and are to be performed largely by the companies themselves. In parallel with the company-specific R&D activities, there will be efforts to identify and solve generic PV problems common to the PV industry or to groups of companies.

PVMaT is being implemented in two phases. Phase 1 is a problem identification phase of about three months duration. Phase 1 subcontracts were being negotiated as of the end of FY90. In this phase the Department of Energy (DOE) is seeking to characterize the status and needs of the U.S. photovoltaic manufacturing industry. Phase 2 is the solution phase expected to be initiated shortly after the Phase 1 subcontracts are underway.

In addition to the Phase 1 and Phase 2 procurements described above, it is expected that at least one procurement associated with generic manufacturing R&D will be undertaken under this project.

Phase 1

In Phase 1, approximately 20 subcontracts of up to $50,000 each will be issued. The Statement of Work (SOW) will require industry participants to identify and characterize (1) their current PV module manufacturing capabilities and costs of producing commercial modules; (2) important manufacturing improvements, problems to be resolved, and projected impact on their manufacturing capabilities; and (3) technology-specific and generic manufacturing technology

R&D that will enable them to meet their cost reduction, module performance, and production goals.

Successful bidders for Phase 1 subcontracts were chosen based upon the offerors' qualifications to perform the tasks outlined in the solicitation's statement of work. Criteria for this determination are given in the Phase 1 solicitation. Cost-sharing by participants is not a requirement for winning an award in Phase 1.

Phase 2

Phase 2 is the solution phase with a five-year duration. It is expected that there will be two Phase 2 solicitations (Phases 2A and 2B) that address R&D on company-specific manufacturing technology during the 5-year period. Thus, organizations not yet ready for the Phase 2A procurement cycle will have a later chance to "ramp-on" to the solution phase of the five-year project. In addition, a separate solicitation for R&D on generic manufacturing technology will be issued after the completion of awards in the Phase 2A solicitation.

Substantial cost-sharing is a requirement for Phase 2 R&D subcontracts although no minimum level is expected to be designated. Instead, the evaluation criteria for Phase 2 proposals are expected to state that degree of cost-sharing will be one of the important factors in the final ranking of proposals for negotiation and R&D funding under the project.

The Phase 2A solicitation is expected to be released about midway through the performance period for the Phase 1 subcontracts. Only responses from those organizations receiving awards in the Phase 1 solicitation will be accepted. The Phase 2B solicitation to be released in the next year to two years after Phase 2A begins will be open to all organizations. There will not be a second Phase 1 solicitation preceding the Phase 2B solicitation.

PVMaT FEDERAL FUNDING

The Federal funding for the PVMaT project in DOE's FY91 budget is $9M. An initial estimate of Federal funding requirements for the entire 5-year project totals $55 million with industry cost-sharing expected to approximately match the government's contribution.

Cost-Sharing Requirements

Although a minimum level of cost-sharing will not be specified in the Phase 2 solicitations, the evaluation criteria for the proposals place a substantial weight on the level of cost-sharing provided in a given proposal.

Cost-sharing for the planning and problem identification under the Phase 1 procurement being done in partnership with industry is not required. For the generic research procurement expected after the completion of the Phase 2A procurement, cost-sharing by industry will be encouraged but not required.

FEDERAL PROCUREMENTS

Under the Phase 2A procurement, it is expected that multiple, cost-shared subcontracts of up to three years' duration will be negotiated. Though 3-year subcontracts will be negotiated, the projects will be funded on a year-to-year basis after subcontract reviews and subject to the availability of appropriated funds to the Department of Energy (DOE) for this project.

Each proposal submitted in response to PVMaT solicitations will be evaluated on its own merit. There is no SERI commitment to spread the awards among a number of technologies. The procurement awards will be based strictly upon the merits of the proposals in responding to the statements of work and in convincing the evaluation panels of the offerors' potential and commitment to meet the project goals and objectives.

Generic R&D

It is anticipated that at least one Request for Proposal (RFP) for generic R&D on various aspects of photovoltaic manufacturing technology will be issued in the first year after awards for the Phase 2A procurement have been completed. The generic R&D problems are defined as being relatively mutual problems in PV manufacturing and implementation associated with the industry as a whole, a number of companies, or the design and deployment of photovoltaic systems. Examples of generic problems in module manufacture might include encapsulation, robotics, stability, alternative materials, alternative processing equipment, on-line process or product monitoring, modeling, yield. etc. Generic problems in design and deployment of systems might include solar resource assessment, environmental reliability testing, improved balance-of-system components (e.g., power conditioning equipment), radiation resistance of materials, voltage isolation, etc.

Generic problems will be identified by the industry and other participants in this project both through industries' responses to the Phase 1 procurement and through evaluating Phase 2A proposals and overviewing the problems and trends in manufacturing technology and commercialization. Performers for generic research activities under an RFP may come from consortia of industrial companies, individual companies, a university or group of universities, combinations of company and university groups, and a variety of other organizations or groupings with special capabilities for solving a problem. If the industrial participants feel that DOE laboratories can provide special capabilities in generic problem areas, it is anticipated that methods of involving them in group or specific activities can be developed. SERI and Sandia staff will be permitted to help or join industry groups in generic problem areas.

Cost-sharing on generic R&D proposals can be relatively flexible to encourage collaboration among industrial companies with common needs for information. It is encouraged but is not expected to be required. However, the proposals for generic R&D will be evaluated on a competitive basis and cost-sharing could have a bearing on the final procurement rankings.

ELIGIBILITY OF U.S.-BASED COMPANIES

The PVMaT project has been established to assist U.S.-owned companies (organizations). Furthermore, the procurement is intended to assist those companies with commercial photovoltaic manufacturing facilities in place, or proposed for near-term placement, in the United States.

In order to be eligible to participate in the Phase 2 procurements of this project, each participating company is expected to commit to conducting the subject research in the U.S. and to implementing the manufacturing advances solely in the United States for at least a five-year period after completion of the subcontract. All participating companies must have their research facilities and staff located and functioning as a dedicated PV R&D group in a U.S. location. In addition, all participating companies must agree that the improved manufacturing technology developed under a PVMaT subcontract will be exclusively applied to production lines located in the United States for a minimum period of five years.

If no manufacturing facilities are built or improved after a subcontract completion, the participating company will be expected to license its results exclusively to U.S.-based companies for the first five years. The intent of the project is that the results of all R&D activities are to be implemented in the U.S. by the participating company. Evaluation criteria in the procurements will be used to maximize the fulfillment of this intent. The basic terms of contractual agreements will be negotiated with each company.

OTHER CONSIDERATIONS

A 25% small business set-aside of the total project funds has been established for the Phase 1 solicitation. The expectation is that the small business awards will exceed that percentage.

Proprietary information in the PVMaT project will be treated with the utmost care. Proposals will be distributed only on a need-to-know basis and only after confidentiality agreements have been put in place with the individual evaluators.

The evaluation of proposals will be done by ad hoc evaluation panels made up largely of independent (non-DOE) consultants with broad experience in manufacturing, business analysis, and PV technology, and chaired by an executive-level person with broad manufacturing and business experience. It is anticipated that one SERI and one Sandia photovoltaic expert will participate in the evaluation panels. All proposal evaluators will need to sign confidentiality agreements along with statements disavowing participation in any of the subcontracts arising from these procurements.

Standard government and SERI procurement procedures for evaluation, prioritization, and selection of proposals for negotiation will be in practice. These procedures involve use of a technical evaluation panel, a cost evaluation panel, a source evaluation board, and a source selection official. Following the approval of the source selection official, the SERI subcontracting group will begin the negotiation processes with the highest rated proposal sponsors to develop the conditions of a subcontract, including terms for cost-sharing, patents, reporting, auditing, and a number of other needs.

The applicable government patent policies will be applied by the SERI negotiation team in these project procurements. Patent rights for small businesses are readily negotiated to benefit the R&D performer, while patent rights for large companies become dependent on the amount of cost-sharing in relationship to any request for patent waivers, among other considerations. It is expected that in company-specific manufacturing technology R&D, in particular, suitable grounds for exclusive patent rights can be developed.

DOE and its laboratories will be responsible for the planning, administration, and implementation of the overall project. DOE, SERI, and Sandia managers and technical persons will be involved in evaluation and technical overview of the project activities, as required. The SERI subcontract office will be in charge of all subcontract administration and procurement matters. Once the prioritization and award activities are completed, the SERI subcontracts office will become the administrative focus for the selected projects and SERI, Sandia, DOE, and selected consultants will provide the technical support and technical overview functions.

9.0 LIST OF ACTIVE SUBCONTRACTS

Active Contract List

Contractor, Principal Investigator, Address	Work Title (Research Activity)	Contract Number	Total Funding ($K)	FY 1990 Funding ($K)	Start/ End Dates
AMORPHOUS SILICON FY1990					
ARCO Solar K. Mitchell Chatsworth, CA 91311	Res. on Stable Hi-Eff. Large Area a-Si Based Submodules	06003-3	2622.8	599.3	7/89 11/90
Chronar Corporation A. Delahoy Princeton, NJ 08542	Stable Hi-Eff. Large Area a-Si Based Submodules	06003-1	4193.0	1399.8	6/90 11/90
ECD S. Guha Troy, MI 48084	Hi-Eff. Multigap Multijunction a-Si Based Submodules	06003-4	4049.3	1350.0	3/87 5/90
Glass Tech Solar P. Bhat 6800 Joyce St. Golden, CO 80403	Material Properties & Device Quality a-Si Deposited at Hi-Deposition Rates Using Higher Order Silanes	06002	606.1	171.2	7/89 8/91
Harvard R. Gordon Cambridge, MA 02138	Optimization of Transparent & Reflecting Films for a-Si Solar Cells	19121	130.0	55.0	10/89 11/90
Harvard W. Paul 1350 Mass. Ave. Cambridge, MA 02138	Structural & Electronic a-SiGe:H Alloys	18131	229.5	164.5	7/88 1/90
National Institute of Standards & Tech. A. Gallagher Boulder, CO 80303	Diagnostics/Glow Discharges Used for a-SiGe:H Alloy Deposition	404078	631.7	99.9	4/88 11/90
Solarex Corp. A. Catalano Newtown, PA 18940	Stable Hi-Eff. a-Si Multijunction Modules	19033	999.7	999.7	5/90 6/93

Contractor, Principal Investigator, Address	Work Title (Research Activity)	Contract Number	Total Funding ($K)	FY 1990 Funding ($K)	Start/ End Dates
AMORPHOUS SILICON FY1990					
Univ. of Delaware J. Meaken Newark, DE 19716	Photo-CVD of a-Si Alloy Materials & Devices	18092-1	720.0	85.0	5/88 6/90
North Carolina Univ. M. Silver Chapel Hill, NC 27599	Relative Effects of Charged & Neutral Defects in a-Si:H Research	07183	106.9	45.0	10/87 7/91
Univ. of Oregon J. Cohen Eugene, OR 97403	Origin of Metastable Light-Induced Changes in a-Si:H	18061-1	193.9	75.0	4/89 5/91
Washington University R. Norberg St. Louis, MO 63130	Research into the Structures of a-Si Alloy Films	06055-1	224.8	60.0	1/87 3/91
Xerox Corporation R. Street 3333 Coyote Hill Rd. Palo Alto, CA 94304	Research on Electronic & Structural Properties of a-Si Silicon Alloys	06056-1	1717.8	173.0	11/86 8/90
POLYCRYSTALLINE THIN FILMS FY1990					
CA Inst. of Technology M. Nicholet Pasadena, CA 91025	Stable Contacts to a-Si Thin Film Contacts $CuInSe_2$ Thin Film Contacts	7133-1	105.0	45.0	9/87 1/91
Colorado State Univ. J. Sites Fort Collins, CO 80523	Role of Polycrystallinity in CdTe & $CuInSe_2$	10046-1	80.0	80.0	4/90 5/93

Contractor, Principal Investigator, Address	Work Title (Research Activity)	Contract Number	Total Funding ($K)	FY 1990 Funding ($K)	Start/ End Dates
POLYCRYSTALLINE THIN FILMS FY1990					
Georgia Tech. A. Rohatgi Atlanta, GA 30332	Hi-Eff. CdTe & ZnTe Thin Film Cells	06031-1	607.7	148.1	6/87 3/93
ISET V. Kapur Inglewood, CA 90301	Hi-Eff. $CuInSe_2$ & $CuInSe_2$-Alloy Films	06031-6	944.1	55.1	3/87 8/90
Photon Energy S. Albright El Paso, TX 79924	Hi-Eff. Large Area CdTe & CdHgTe Panels	06031-3	837.9	338.0	6/87 7/90
Univ. Colorado A. Hermann Boulder, CO 80309	Novel Thin Film $CuInSe_2$ Fabrication	10012-1	35.3	35.3	3/90 4/91
Univ. Delaware B. Baron Newark, DE 19716	Fundamentals Polycrystalline Thin Film Materials & Devices	19032-1	567.0	567.0	1/89 3/90
Univ. of Illinois A. Rockett 809 S. Wright St. Champaigne, IL 61820	Alternate Fabrication Tech-ques for Hi-Eff. $CuInSe_2$ & $CuInSe_2$	10017-1	190.1	59.5	3/90 5/91
Univ. of S. Florida T. & S. Chu Tampa, FL 33620	Thin Film CdTe, ZnTe, & $Hg_{1-x}Zn_xTe$ Solar Cells	18091-1	624.7	324.8	7/88 8/90
Purdue Univ. R. Schwartz W. Lafayette, IN 47907	Dev. of Computer Model For Poly Thin Film $CuInSe_2$ & CdTe Solar Cells	10013-1	50.0	50.0	1/90 10/90

Contractor, Principal Investigator, Address	Work Title (Research Activity)	Contract Number	Total Funding ($K)	FY 1990 Funding ($K)	Start/ End Dates
CRYSTALLINE SILICON MATERIALS RESEARCH FY1990					
Duke Univ. U. Göesele Dept. of Mech. Engin. Durham, NC 27706	Point Defects & Their Influence on Solar Cell Related Elec. Properties of Crystalline Silicon	18097-1	198.3	99.4	7/88 9/90
Georgia Tech G. Rohatgi Atlanta, GA 30332	Impurity Characterization Support for Silicon	19145-1	25.0	25.0	10/89 10/90
N. Carolina St. Univ. G. Rozgonyi Box 7214 Raleigh, NC 27695	Effectiveness & Stability of Impurity/Defect Interactions & Their Impact on Minority Carrier Lifetime	18097-2	280.0	140.0	6/88 7/91
Suny/Albany J. Corbett Albany, NY 12201	Passivation & Gettering in Solar Cell Silicon	18097-3	248.4	248.4	7/88 10/90
Univ. of Southern CA S. Forrest University Park Los Angeles, CA 90089	Electric Characterization Support for Crystalline Silicon	18154	50.6	50.6	10/88 10/90
ADVANCED HIGH EFFICIENCY FY1990					
Kopin Corp. J. Fan Taunton, MA 02980	Hi-Eff. Thin Film GaAs & Ternary III-V Solar Cells	18083-1	769.0	435.0	4/88 2/90
Rensselaer Ghandhi/Borrengo Troy, NY 12180	Research on Semiconductors for Hi-Eff. Solar Cells	5018-2	995.0	200.0	9/85 1/90

Contractor, Principal Investigator, Address	Work Title (Research Activity)	Contract Number	Total Funding ($K)	FY 1990 Funding ($K)	Start/ End Dates
ADVANCED HIGH EFFICIENCY FY1990					
Carnegie/Mellon U. A. Milnes Pittsburgh, PA	Improvement of Bulk Epitaxial III-V Semiconductors	6005-3	403.3	91.4	9/86 8/90
Spire Corp. S. Vernon Bedford, MA 01730	GaAs Based Ternary Compounds & Multibandgap Solar Cell Research	18063-1	651.2	359.9	4/88 2/90
NEW IDEAS FY1990					
Georgia Tech. C. Summers Atlanta, GA 30332	Avalanche Heterostructural & Superlattice Solar Cells	19056-1	100.0	100.0	5/89 5/90
ISET V. Kapur 8635 Aviation Blvd. Inglewood, CA 90301	Low Cost Technique for Producing CdZnTe Devices for Cascade Cells Application	6074-02	199.1	99.8	6/87 2/90
Res. Triangle Instit. M. Timmons R.T.I.	An Inverted AlGaAs/GaAs Patterned Tunnel Junction Cascade Concentrator Cell	18110-2	100.0	100.0	1/90 2/91
Rensselaer S. Ghandhi Troy, NY 12180	Hydrogen Radical Enhanced Growth of Solar Cells	06074-03	200.1	100.0	6/87 10/90
Univ. of Delaware R. Birkmire Newark, DE 19716	Novel Ways of Depositing ZnTe Films by a Solution Growth Technique	18110-1	100.0	100.0	1/90 1/91
Univ. of S. California D. Dapkus Los Angeles, CA 90089	High Efficiency Epitaxial Optical Reflector Cells	18110-3	92.8	92.8	1/90 2/91
UNIVERSITY PROGRAM FY1990					
No. Carolina St. Univ. S. Bedair Box 7003 Raleigh, NC 27695	New Approaches to Hi-Eff. Solar Cells by MOCVD	18141-1	238.9	79.4	7/87 8/92

Contractor, Principal Investigator, Address	Work Title (Research Activity)	Contract Number	Total Funding ($K)	FY 1990 Funding ($K)	Start/ End Dates
UNIVERSITY PARTICIPATION PROGRAM FY1990, (continued)					
No. Carolina St. Univ. G. Lucovsky Raleigh, NC 27695	Fundamental Studies of Defect Generation in a-Si Alloy Grown by Remote Plasma Enhanced CVD	18141-2	188.3	63.7	7/89 8/92
Stanford University R. Bube 660 Arguello Way Stanford, CA 94305	Ion Beam & Photo-Assisted Growth & Doping of II-VI Compounds	18141-4	254.9	85.0	7/89 8/92
Univ. of Utah C. Taylor 309 Park Bldg. Salt Lake City, UT 84112	Electronic Processes in Thin Film PV Materials	18141-3	254.3	86.0	7/89 8/92

10.0 PV SUBCONTRACTED RESEARCH
FY 1990 BIBLIOGRAPHY

Subcontractor Reports and Publications

Albright, S. P.; Ackerman, B. (October 1989). *High-Efficiency Large-Area CdTe Modules, Annual Subcontract Report, 1 July 1988 -30 June 1989.* SERI/STR-211-3585. 30 pp. Work performed by Photon Energy, Inc., El Paso, Texas. Available NTIS: Order No. DE89009498.

Ayra, R. A.; Bennett, M. S.; Dickson, C. R.; Fieselmann, B.; Fortmann, C.; Goldstein, B.; Morris, J. G.; O'Dowd, R. S.; Oswald, R. S.; Wiedeman, S.; Yang, L. (October 1989). *Research on High-Efficiency, Single-Junction, Monolithic, Thin-Film Amorphous Silicon Solar Cells, Phase II Semiannual Report, 1 February 1988 - 31 July 1989.* SERI/STR-211-3583. 119 pp. Work performed by Solarex Thin Film Division, Newtown, Pennsylvania. Available NTIS: Order No. DE89009496.

Baron, B. N.; Rocheleau, R. E.; Hegedus, S. S. (November 1989). *Chemical Vapor Deposition and Photochemical Vapor Deposition of Amorphous Silicon Photovoltaic Devices, Final Subcontract Report, 1 May 1984 - 30 April 1988.* SERI/STR-211-3601. 101 pp. Work performed by Institute of Energy Conversion, University of Delaware, Newark, Delaware. Available NTIS: Order No. DE89009510.

Baron, B. H.; Birkmire, R. W.; McCandless, B. E.; Roy, M.;Phillips, J. E.; Shafarman, W. N. (July 1990). *Materials Analysis and Device Optimization of CuInSe2 Solar Cells, Final Subcontract Report, 16 January 1987 - 15 January 1989.* SERI/TP-211-3896. 56 pp. Work performed by Institute of Energy Conversion, University of Delaware, Newark, Delaware. Available NTIS: Order No. DE90000365.

Baron, B. N.; Birkmire, R. W.; McCandless, B. E.; Phillips, J. E. (July 1990). *Two Terminal CuInSe2 Based Cascade Cells, Final Subcontract Report, 16 January 1987 - 15 January 1989.* SERI/TP-211-3914. 32 pp. Work performed by Institute of Energy Conversion, University of Delarare, Newark, Delaware. Available NTIS: Order No. DE90000363.

Book of Abstracts; SERI Workshop in the Role of Point Defects/Defect Complexes in Silicon Device Fabrication, (August 1990). SERI/CP-211-3976. 67 pp. Conference held 30-31 August 1990, Keystone, Colorado. Available NTIS: Order No. DE90000377.

Borrego, J. M.; Ghandi, S. K. (October 1989). *Hydrogen Radical Enhanced Growth of Solar Cells, Phase I, Annual Subcontract Report, 1 June 1987 - 31 March 1989.* SERI/STR-211-3584. 29 pp. Work performed by Rensselaer Polytechnic Institute, Troy, New York. Available NTIS: Order No. DE89009497.

Bube, R. H.; Fahrenbruch, A. L.; Lopez-Otero, A.; Chien, K.-F.; Grimbergen, M.; Kim, D.; Sharps, P. (July 1990). *Ion-Assisted Doping of II-VI Compounds During Physical Vapor Deposition, Final Subcontract Report, 1 September 1985 -30 August 1989.* SERI/TP-211-3907. 89 pp. Work performed by Department of Materials Science and Engineering, Stanford University, Stanford, California. Available NTIS: Order No. DE90000358.

Catalano, A. W.; Ayra, R. R.; Bennett, M. S.; Dickson, C. R.; Fieselmann, B.; Goldstein, B.; Morris, J.; Newton, J. L.; O'Dowd, J. G.; Oswald, R. S.; Twesme, E.; Wiedeman, S.; Yang, L. (October 1989). *Task B: Research on Stable High-Efficiency, Large Area, Amorphous Silicon Based Solar Cells, Phase II, Annual Subcontract Report, 1 February 1988 - 1 February 1989.* SERI/STR-211-3580. 114 pp. Work performed by Solarex Thin Film Division, Newtown, Pennsylvania. Available NTIS: Order No. DE89009491.

Catalano, A. W.; Carlson, D. E.; Ayra, R. R.; Bennett, M. S.; D'Aiello, R. V.; Dickson, C. R.; Fortmann, C. M.; Goldstein, B.; McVeigh, J.; Morris, J.; Newton, J. L.; Wiedeman, S. (October 1989). *Research on High-Efficiency, Single-Junction, Monolithic, Thin-Film Amorphous Silicon Solar Cells, Phase I Annual Subcontract Report, 1 February 1987 - 31 January 1988.* SERI/STR-211-3582. 161 pp. Work performed by Solarex Thin Film Division, Newtown, Pennsylvania. Available NTIS: Order No. DE89009495.

Catalano, A.; Arya, R. R.; Bennett, M.; Fieselmann, B.; Goldstein, B.; Morris, J.; Newton, J.; O'Dowd, J.; Oswald, R. S.; Podlesny, R.; Wiedeman, S.; Yang, L. (July 1990). *Research on Stable, Large-Area Amorphous Silicon Based Submodules, Phase III, Semi-Annual Subcontract Report, 1 February 1989 - 31 July 1989.* SERI/TP-211-3805. 94 pp. Work performed by Solarex Thin Film Division, Newtown, Pennsylvania. Available NTIS: Order No. DE90000339.

Catalano, A.; Arya, R. R.; Bennett, M.; Fieselmann, B.; Morris, J.; Newtown, J.; Podlesny, R.; Tawseme, E.; Wiedeman, S.; Yang, L.; Rothwarf, A.; Shapiro, F. (September 1990). *Research on High-Efficiency, Large-Area,Amorphous Silicon Based Solar Cells, Final Subcontract Report, 1 February 1989 - 28 February 1990.* SERI/TP-211-3906. 82 pp. Work performed by Solarex Thin Film Division, Newtown, Pennsylvania and Drexel University, Philadelphia, Pennsylvania. Available NTIS: Order No. DE90000356.

Chapple-Sokol, Jonathan D.; Gordon, Roy G. (1989) "Substrate-Dependent Growth of Atmospheric Pressure Chemically Vapor Deposited Silicon Dioxide from Dichlorosilane and Oxygen." *Thin Solid Films*, 171, pp. 291-305. Work performed by Harvard University, Cambridge, Massachusetts.

Chapple-Sokol, Jonathan D.; Giunta, Carmen J.; Gordon, Roy G. (October 1989) "A Kinetics Study of the Atmospheric Pressure CVD Reaction of Silane and Nitrous Oxide." *Journal of the Electrochemical Society*, Vol. 136, No. 10. Work performed by Harvard University, Cambridge, Massachusetts.

Crandall, Richard S.; Sadlon, Kyle; Kalina, Jeffrey; Delahoy, Alan E. (1989) "Direct Measurement of the Mobility-Lifetime Product of Holes and Electrons in an Amorphous Silicon p-i-n Cell." *Amorphous Silicon Technology - 1989, Materials Research Society Symposium Proceedings, Volume 149*, Madan, A. et al., eds. Pittsburgh, PA: Materials Research Society; p. 423. Presented at the MRS Spring Meeting, San Diego, California, April 25-28, 1989.

Chu, T. L. (October 1989). *Thin Film Cadmium Telluride, Zinc Telluride, and Mercury Zinc Telluride Solar Cells, Annual Subcontract Report, 1 July 1988 - 30 June 1989.* SERI/STR-211-3586. 37 pp. Work performed by the University of South Florida, Tampa, Florida. Available NTIS: Order No. DE89009499.

Delahoy, A. E.; Ellis, F. B., Jr.; Kampas, F. J.; Tonan, T.; Weakliem, H. A. (December 1989). *Research on Amorphous Silicon Based Thin Film Photovoltaic Devices, Task B: Research on Stable High-Efficiency Large Area Amorphous Silicon Based Submodules, Annual Subcontract Report, 16 March 1988 - 15 March 1989.* SERI/STR-211-3609. 51 pp. Work performed by Chronar Corporation, Princeton, New Jersey. Available NTIS: Order No. DE89009515.

Delahoy, A.E. (1989) "Recent Developments in Amorphous Silicon Photovoltaic Research and Manufacturing at Chronar Corporation." *Solar Cells*, 27, pp. 39-57. Work performed by Chronar Corporation, Princeton, New Jersey.

Delong, M. C.; Taylor, P. C.; Olson, J. M. (6 August 1990). "Excitation Intensity Dependence of Photoluminescence in Ga0.52In0.48P." *Applied Physics Letters* (57:6); pp. 620-622. Work performed by Department of Physics, University of Utah, Salt Lake City, Utah; and Solar Energy Research Institute, Golden, Colorado.

DeLong, M. C.; Taylor, P. C.; Olson, J. M. (July/August 1990). "Growth Temperature and Substrate Orientation Dependences of Moving Emission and Ordering in Ga0.52In0.48P." *Journal of Vacuum Science and Technology. B, Microelectronics, Processing and Phenomena* (8:4); pp. 948-954. Work performed by Department of Physics, University of Utah, Salt Lake City, Utah; and Solar Energy Research Institute, Golden, Colorado.

Devaney, W. E.; Chen, W. S.; Stewart, J. M.; Gillette, R. B. (July 1990). *High Efficiency CuInSe2 and CuInGaSe2 Cells and Materials Research, Final Subcontract Report, 1 November 1987 - 31 October 1989.* SERI/TP-211-3909. 73 pp. Work performed by Boeing Electronics High Technology Center, Seattle, Washington. Available NTIS: Order No. DE90000362.

Doughty, D.A.; Gallagher, A. (January 1990) "Spatial distribution of a-Si:H film-producing radicals in silane rf glow discharges." *Journal of Applied Physics* **67** (1).

Giunta, Carmen J.; McCurdy, Richard J. (January 1990) "Gas-phase kinetics in the atmospheric pressure chemical vapor deposition of silicon from silane and disilane." *Journal of Applied Physics*, **67** (2), p. 1062. Work performed by Harvard University, Cambridge, Massachusetts.

Gallagher, A.; Doughty, D.A.; Doyle, J. (May 1990). *Diagnostics of Glow Discharges Used to Produce Hydrogenated Amorphous Silicon Films, Annual Subcontract Report, 1 December 1988 - 30 November 1989.* SERI/TRP-211-3747. 40 pp. Work performed by National Institute of Standards and Technology, Boulder, Colorado, and University of Colorado, Boulder, Colorado. Available NTIS: Order No. DE90000329.

Gillette, R.B.; Devaney, W.E.; Chen, W.S.; Stewart, J.M. (July 1990) *High Efficiency $CuInSe_2$ and $CuInGaSe_2$ Cells and Materials Research, Final Subcontract Report, 1 November 1987 - 31 October 1989.* Work performed by Boeing Electronics High Technology Center, Seattle, Washington. Available NTIS: Order No. DE90000362.

Guha, S. (August 1990). *Research on High-Efficiency, Multiple-Gap, Multi-Junction Amorphous Silicon-Based Alloy Thin-Film Solar Cells, Final Subcontract Report, 1 March 1987 - 28 February 1990.* SERI/TP-211-3918. 157 pp. Work performed by Energy Conversion Devices, Inc., Troy, Michigan. Available NTIS: Order No. DE90000364.

Hanak, T. R.; Bakry, A. M.; Ahrenkiel, R. K.; Timmons, M. L. (1990). "DX-Center in Se-Doped AlxGa1-xAs." *Impurities, Defects and Diffusion in Semiconductors: Bulk and Layered Structures, Materials Research Society Symposium Proceedings, Volume 163*, Wolford, D. J.; Bernholc, J.; and Haller, E. E. Pittsburgh, PA: Materials Research Society; pp. 781-784. Presented at the MSR Fall Meeting, November 27-December 1, 1989, Boston, Massachusetts. Work performed by Department of Physics, University of Denver, Denver, Colorado; Solar Energy Research Institute, Golden, Colorado; Research Triangle Institute, Research Triangle Park, North Carolina.

Hanak, T.R.; Ahrenkiel, R.K.; Dunlavy, D.J.; Bakry, A.M.; Timmons, M.L. (1 May 1990) "New Method to Analyze Multiexponential Transients for Deep-Level Transient Spectroscopy." *Journal of Applied Physics* (67:9). Work performed by Department of Physics, University of Denver, Denver, Colorado; Solar Energy Research Institute, Golden, Colorado; and Research Triangle Institute, Research Triangle Park, North Carolina.

Kalina, J.; Schade, H.; Delahoy, A.E. (1989) "Correlation Between Fill Factors of Amorphous Silicon Solar Cells and Their i Layer Densities of States as Determined by DLTS." *Solar Cells*, 27, pp. 341-346. Work performed by Chronar Corporation, Princeton, New Jersey.

Kisilev, A.; Marcu, V.; Cahen, D.; Schock, H. W.; Noufi, R. (January 1990). "Photoelectrochemical Characterization of $CuGaSe_2$ and $Cu(Ga,In)Se_2$ Films." Solar Cells (28:1); pp. 57-67. Work performed by Department of Structural Chemistry and Centre for Energy Research, The Weizmann Institute of Science, Rehovot, Israel; Institute for Physical Electronics, University of Stuttgart, Stuttgart, West Germany; and Solar Energy Research Institute, Golden, Colorado.

Lundstrom, M. S.; Melloch, M. R.; Pierret, R. F.; Carpenter, M. S.; Chuang, H. L.; Keshavarzl, A.; Klausmeier-Brown, M. E.; Lush, G. B.; Morgan, J. M.; Stellwag, T. B. (July 1990). *Basic Studies of III-V High Efficienty Cell Components, Annual Subcontract Report, 15 August 1988 - 14 August 1989.* SERI/TP-211-3904. 120 pp. Available NTIS: Order No. DE90000360.

Melloch, M.R.; Tobin, S.P.; Stellwag, T.B.; Bajgar, C.; Keshavarzi, A.; Lundstrom, M.S.; Emery, K. (1990) "High-Efficiency GaAs Solar Cells Grown by Molecular-Beam Epitaxy." *Journal of Vacuum Science & Technology. B, Microelectronics, Processing and Phenomena* (8:2); pp. 379-383. Presented at the Tenth Molecular-Beam Epitaxy Workshop, 13-15 September 1989, Raleigh, North Carolina. Work performed by School of Electrical Engineering, Purdue University, West Lafayette, Indiana; Spire Corporation, Bedford, Massachusetts; and Solar Energy Research Institute, Golden, Colorado.

Meyers, P.V. (June 1990) "Polycrystalline Thin Film Cadmium Telluride n-i-p Solar Cells. Final Subcontract Report September 1988 - August 1989." SERI/TP-211-3873. Work performed by Ametek, Inc., Harleysville, Pennsylvania, under Subcontract No. ZL-7-06031-2.

Melloch, M. R.; Tobin, S. P.; Bajgar, C.; Keshavarzi, A.; Stellwag, T. B.; Lush, G. B.; Lundstrom, M. S.; Emery, K. (2 July 1990). "High Efficiency $Al_{0.22}Ga_{0.78}As$ Solar Cells Grown by Molecular Beam Epitaxy." *Applied Physics Letters* (57:1); pp. 52-54. Work performed by School of Electrical Engineering, Purdue University, West Lafayette, Indiana; Spire Corporation, Bedford, Massachusetts; and Solar Energy Research Institute, Golden, Colorado.

Mooney, G. David; Hermann, Allen M. (September 1990) *Novel Thin-Film $CuInSe_2$ Fabrication, Final Subcontract Report.* SERI/TP-211-3864. Work performed by University of Arkansas, Fayetteville, Arkansas and University of Colorado, Boulder, Colorado. Available NTIS: Order No. DE90000345.

Moskowitz, P.D.; Zweibel, K.; Fthenakis, V.M. (January 1990) *Health, Safety and Environmental Issues Relating to Cadmium Usage in Photovoltaic Energy Systems.* SERI/TR-211-3621. 34 pp. Work performed by Solar Energy Research Institute, Golden, Colorado and Brookhaven National Laboratories, Upton, New York. Available NTIS: Order No. DE90000310.

Nicolet, M-A. (January 1990). *Investigations of CuInSe2 Thin Films and Contacts, Annual Subcontract Report, September 1988 - October 1989.* SERI/STR-211-3612. 14 pp. Work performed by California Institute of Technology, Pasadena, California. Available NTIS: Order No. DE90000301.

Norberg, R. E.; Fedders, P. A. (August 1990). *Structure of Amorphous Silicon and Germanium Alloy Films, Annual Subcontract Report, 15 January 1989 - 14 January 1990.* SERI/TP-211-3908. 31 pp. Work performed by Department of Physics, Washington University, St. Louis, Missouri. Available NTIS: Order No. DE9000355.

Olson, J.M.; DeLong, M.C.; and Taylor, P.C. (July/August 1990) "Growth Temperature and Substrate Orientation Dependences of Moving emission and ordering in $Ga_{0.52}In_{0.48}P$", *J. Vac. Sci. Technol.* B 8 (4), p. 948-954.

Palmer, Bruce J.; Gordon, Roy. (December 1989) "Frequency-dependent conductivity in polycrystalline metals and semiconductors." *Physical Review B*, Vol. 40, No. 17.

Photovoltaic Advanced Research and Development Project, Technical Summary Report, February 1990. (February 1990). SERI/MP-210-3722. 26 pp.

Photovoltaic Advanced Research and Development Project Technical Summary Report. (January 1990). SERI/MP-210-3665. 24 pp.

Research on High-Efficiency, Multiple-Gap, Multi-Junction Amorphous Silicon-Based Alloy Thin-Film Solar Cells, Phase III, Semi-Annual Subcontract Report, 1 March 1989 - 31 August 1989. (July 1990). SERI/TP-211-3804. 53 pp. Work performed by Energy Conversion Devices, Inc., Troy, Michigan. Available NTIS: Order No. DE90000338.

Shen, D. S.; Bhat, P. K. (August 1990). *Amorphous Silicon Solar Cells Prepared at High Deposition Rates, Annual Subcontract Report, 1 July 1989 - 30 June 1990.* SERI/TP-211-3949. 30 pp. Work performed by Glasstech Solar, Inc., Golden, Colorado. Available NTIS: Order No. DE90000371.

Singh, R.; Kumar, A.; Thakur, R.P.S.; Chou, P.; Narayan, J.; Srivatsa, A.R.; Nelson, A.J.; Ullal H.S. (1990) "Solid phase epitaxial growth of IIDA fluorides on InP by in-situ rapid isothermal processing". *Materials Research Society Symposium Proceedings* Volume 149 (MRS, Pittsburgh).

Singh, R.; Sinha, S.; Chou, P.; Hsu, N. J.; Radpour, F.; Ullal, H. S.; Nelson, A. J. (15 December 1989). "Preparation of BaF2 Films by Metalorganic Chemical Vapor Deposition." *Journal of Applied Physics* (66:12); pp. 6179-6181.

Singh, R.; Kumar, A.; Thakur, R.P.S.; Chou, P.; Narayan, J.; Nelson, A.J.; Ullal, H.S. (1990) "Solid Phase Epitaxial Growth of IIDA Fluorides on Semiconductors by in-situ Rapid Isothermal Processing", *J. Electronic Materials* 19(5), p. 481.

Singh, R.; Thakur, R. P. S.; Katz, A.; Nelson, A. J.; Gebhard, S. C.; Swartzlander, A. B. (17 September 1990). "Relationship between Thermal Stress and Structural Properties of SrF2 Films on (100)InP." *Applied Physics Letters* (57:12); pp. 1239-1241. Work performed by School of Electrical Engineering and Computer Science, University of Oklahoma, Norman, Oklahoma; AT&T Bell Laboratories, Murray Hill, New Jersey; and Solar Energy Research Institute, Golden, Colorado.

Sites, J. R. (August 1990). *Analysis of Loss Mechanisms in Polycrystalline Thin Film Solar Cells, Final Subcontract Report, 1 April 1988 - 31 March 1990.* SERI/TP-211-3950. 39 pp. Work performed at Colorado State University, Fort Collins, Colorado. Available NTIS: Order No. DE90000372.

Taylor, P. C.; Williams, G. A.; Ohlsen, W. D. (August 1990). *Electronic Processes in Thin Film PV Materials, Final Report, 1 September 1986 - 31 May 1989.* SERI/TP-211-3905. 40 pp. Work performed by Department of Physics, University of Utah, Salt Lake City, Utah. Available NTIS: Order No. DE90000359.

Technical Summary Report, August, 1990, Solar Electric Research Division. (August 1990). SERI/MP-210-4004. 25 pp.

Technical Summary Report, July 1990, Solar Electric Research Division. (July 1990). SERI/MP-210-3970. 25 pp.

Thornton, J.P.; DeBlasio, R.; Zweibel, K. (1990) "Photovoltaics - Today's Reality, Tomorrow's Promise," *Energy Engineering*, Journal of the Association of Energy Engineers, Vol. 87, No. 3, pp. 63-70.

Tobin, S.P.; Vernon, S.M.; Bajgar, C., Wojtczuk, S.J.; Melloch, M.R.; Keshavarzi, A.; Stell Wag, T.B.; Venkatensan, S.; Lundstrom, M.S.; Emery, K.E. (1990) "Assessment of MOCVD- and MBE-Grown GaAs for High-Efficiency Solar Cell Applications," *IEEE Transactions on Electron Devices.* Vol. 37, No. 2, February, p. 469.

Tsuo, Y.S.; Xu, Y.; Crandall, Richard S.; Ullal, H.S.; Emery, K. (1989) "Hydrogen-Plasma Reactive Flushing for a-Si:H P-I-N Solar Cell Fabrication." *Amorphous Silicon Technology - 1989, Materials Research Society Symposium Proceedings, Volume 149*, Madan, A. et al., eds. Pittsburgh, PA: Materials Research Society, p. 471. Presented at the MRS Spring Meeting, San Diego, California, April 25-28, 1989.

Turner, W.A.; Jones, S.J.; Pang, D.; Bateman, B.F.; Chen, J.H.; Li, Y.-M.; Marques, F.C.; Wetsel, A.E.; Wickboldt, P.; Paul, W.; Bodart, J.; Norberg, R.E.; El Zawawi, I.; Theye, M.L. (1990) "Structural, Optical, and Electrical Characterization of Improved Amorphous Hydrogenated Germanium." *Journal of Applied Physics* **67** (12), p. 7430. Work performed by Harvard University, Cambridge, Massachusetts, Washington University, St. Louis, Missouri, and Universite P. et M. Curie, Paris, France.

Weber, M. F. (February 1990). *Improvement of Small-Area, Amorphous-Silicon Thin-Film Photovoltaics on Polymer Substrate, Final Subcontract Report, 1 March 1988 - 30 June 1989.* SERI/TP-211-3656. 37 pp. Work performed by 3M Laboratories, St. Paul, Minnesota. Available NTIS: Order No. DE90000314.

Wiesmann, H. J. (January 1990). *Hydrogenated Amorphous Silicon Films Prepared by Glow Discharge of Disilane, Final Subcontract Report, 16 December 1987 - 28 February 1988.* SERI/STR-211-3620. 52 pp. Work performed by UHT Corporation, Dobbs Ferry, New York. Available NTIS: Order No. DE90000309.

PV Program Branch Reports and Publications

Luft, W. (1990) "Research in the U.S. on High-Efficiency Amorphous Silicon Photovoltaic Devices." *International Journal of Solar Energy*, Volume 8.

Luft, W. (1989). "Characteristics of Hydrogenated Amorphous Silicon-Germanium Alloys." *Applied Physics Communications* (9:1&2); pp. 43-63.

Luft, W. (1990) "Photovoltaic Application for Silicon Carbon Films and Microcrystalline Silicon Films." *Applied Physics Letters.*

Securing Our Future. (1990) Brochure distributed at the 21st IEEE Photovoltaic Specialists Conference, Orlando, Florida, May 21-25, 1990.

SERI Photovoltaic Subcontract Reports: 1989 Abstracts and Document Control Information. (April 1990). SERI/TP-211-3678. 57 pp. Available NTIS: Order No. DE90000336.

Tsuo, Y. S.; Luft, W. (1990). "Alternative Deposition Processes for Hydrogenated Amorphous Silicon and Related Alloys." *Applied Physics Communications* (10:1&2); pp. 71-141.

Ullal, H. S.; Zweibel, K. (December 1989). *Progress in Thin Film Solar Photovoltaic Technologies.* SERI/TP-211-3604. 12 pp. Prepared for the 9th Miami International Congress on Energy and Environment, Miami Beach, Florida, 11-13 December 1989. Available NTIS: Order No. DE89009513.

Ullal, H. S.; Zweibel, K.; Mitchell, R. L. (November 1989). *U.S. Polycrystalline Thin Film Solar Cell Program.* SERI/TP-211-3595. 6 pp. Prepared for the Materials Research Society 1989 Fall Meeting, 27 November - 2 December 1989, Boston, Massachusetts. Available NTIS: Order No. DE89009506.

Ullal, H. S.; Zweibel, K.; Surek, T. (March 1990). *Recent Technological Advances in Thin Film Solar Cells.* SERI/TP-211-3679. 5 pp. Prepared for the World Renewable Energy Congress, 23-28 September 1990, Reading, United Kingdom. Available NTIS: Order No. DE90000321.

Ullal, Harin S.; Zweibel, Kenneth. (1990) "Progress in Thin Film Solar Photovoltaic Technologies." *9th Miami International Congress on Energy and Environment, Volume 1.* Proceedings of Condensed Papers, T. Nejat Veziroglu, Editor.

Ullal, Harin S.; Zweibel, Kenneth; Mitchell, Richard. (1990) "U.S. Polycrystalline Thin Film Solar Cells Program." *Properties of II-VI Semiconductors: Bulk Crystals, Epitaxial Films, Quantum Well Structures, and Dilute Magnetic Systems.* Materials Research Society Symposium Proceedings, Vol. 161, F.J. Bartoli, Jr., H.F. Schaake, J.F. Schetzina, Eds., November 27-December 2, 1989, Boston, Massachusetts.

Ullal, Harin S.; Zweibel, Kenneth; Surek, Thomas. (1990) "Recent Technological Advances in Thin Film Solar Cells." *Energy and the Environment Into the 1990s*, Proceedings of the 1st World Renewable Energy Congress, Vol. 1, p. 195, Pergamon Press.

Zweibel, K. (1990). *Harnessing Solar Power: the Photovoltaics Challenge.* New York: Plenum Press; 330 pp.

Zweibel, Ken; Mitchell, Richard. (December 1989) *$CuInSe_2$ and CdTe: Scale-Up for Manufacturing.* SERI/TR-211-3571.

Document Control Page	1. SERI Report No. SERI/TP-214-4135	2. NTIS Accession No. DE91002149	3. Recipient's Accession No.

4. Title and Subtitle	5. Publication Date
Annual Report, Photovoltaic Subcontract Program, FY 1990	March 1991
	6.
7. Author(s) Photovoltaic Program Branch, SERI	8. Performing Organization Rept. No.
9. Performing Organization Name and Address Solar Energy Research Institute 1617 Cole Boulevard Golden, Colorado 80401-3393	10. Project/Task/Work Unit No. PV040101
	11. Contract (C) or Grant (G) No. (C) (G)
12. Sponsoring Organization Name and Address Solar Energy Research Institute 1617 Cole Blvd. Golden, CO 80401	13. Type of Report & Period Covered Annual Progress Report
	14.

15. Supplementary Notes

16. Abstract (Limit: 200 words)

This report summarizes the progress of the Photovoltaic (PV) Subcontract Program of the Solar Energy Research Institute (SERI) from October 1, 1989 through September 30, 1990. The PV Subcontract Program is responsible for managing the subcontracted portion of SERI's PV Advanced Research and Development Project. In fiscal year 1990, this included more than 54 subcontracts with a total annualized funding of approximately $11.9 million. Approximately two-thirds of the subcontracts were with universities at a total funding of nearly $3.3 million. The six technical sections of the report cover the main areas of the subcontract program: the Amorphous Silicon Research Project, Polycrystalline Thin Films, Crystalline Silicon Materials Research, High-Efficiency Concepts, the New Ideas Program, and the University Participation Program. Technical summaries of each of the subcontracted programs provide a discussion of approaches, major accomplishments in FY 1990, and future research directions. Another section introduces the PVMaT project and reports on its progress.

17. Document Analysis

a. Descriptors

photovoltaic cells, amorphous materials, solar cells, silicon, thin films, deposition, copper selenide, cadmium telluride, gallium arsenide, efficiency, semiconductor materials

b. Identifiers/Open-Ended Terms

Solar Energy Research Institute

c. UC Categories

270

18. Availability Statement	19. No. of Pages
National Technical Information Service U.S. Department of Commerce 5285 Port Royal Road Springfield, VA 22161	314
	20. Price A14

Form No. 0069E (6-30-87)

U.S. GOVERNMENT PRINTING OFFICE 1991/573-110/44000